MCEER
EARTHQUAKE ENGINEERING TO EXTREME EVENTS

ISSN 1520-295X

Shake Table Testing of Triple Friction Pendulum Isolators under Extreme Conditions

by
Apostolos A. Sarlis, Michael C. Constantinou
and Andrei M. Reinhorn

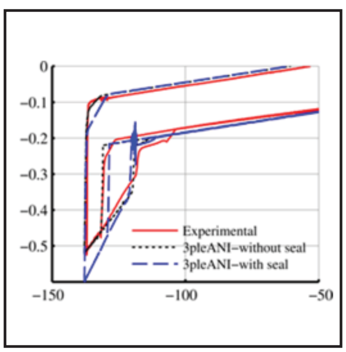

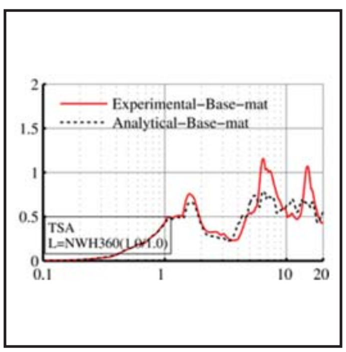

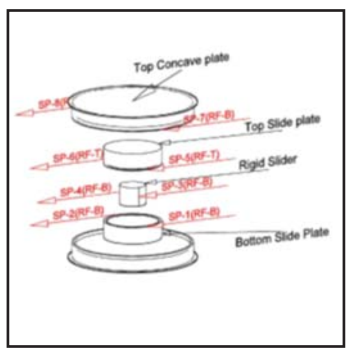

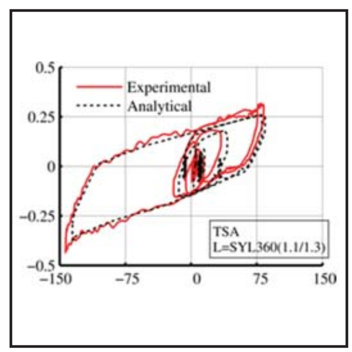

Technical Report MCEER-13-0011

July 2, 2013

This research was conducted at the University at Buffalo, State University of New York, and was supported by MCEER Thrust Area 3, Innovative Technologies.

Shake Table Testing of Triple Friction Pendulum Isolators under Extreme Conditions

by

Apostolos A. Sarlis[1] Michael Constantinou[2] and Andrei M. Reinhorn[3]

Publication Date: July 2, 2013
Submittal Date: June 27, 2013

Technical Report MCEER-13-0011

MCEER Thrust Area 3, Innovative Technologies

1 Ph.D. Candidate, Department of Civil, Structural and Environmental Engineering, University at Buffalo, State University of New York
2 Professor, Department of Civil, Structural and Environmental Engineering, Univesity at Buffalo, State University of New York
3 Emeritus Professor, Department of Civil, Structural and Environmental Engineering, University at Buffalo, State University of New York

MCEER
University at Buffalo, State University of New York
133A Ketter Hall, Buffalo, NY 14260
E-mail: mceer@buffalo.edu; WWW Site: http://mceer.buffalo.edu

Preface

MCEER is a national center of excellence dedicated to the discovery and development of new knowledge, tools and technologies that equip communities to become more disaster resilient in the face of earthquakes and other extreme events. MCEER accomplishes this through a system of multidisciplinary, multi-hazard research, in tandem with complimentary education and outreach initiatives.

Headquartered at the University at Buffalo, The State University of New York, MCEER was originally established by the National Science Foundation in 1986, as the first National Center for Earthquake Engineering Research (NCEER). In 1998, it became known as the Multidisciplinary Center for Earthquake Engineering Research (MCEER), from which the current name, MCEER, evolved.

Comprising a consortium of researchers and industry partners from numerous disciplines and institutions throughout the United States, MCEER's mission has expanded from its original focus on earthquake engineering to one which addresses the technical and socio-economic impacts of a variety of hazards, both natural and man-made, on critical infrastructure, facilities, and society.

The Center derives support from several Federal agencies, including the National Science Foundation, Federal Highway Administration, National Institute of Standards and Technology, Department of Homeland Security/Federal Emergency Management Agency, and the State of New York, other state governments, academic institutions, foreign governments and private industry.

This report describes an experimental program of a 3-story seismically isolated structure in which Triple Friction Pendulum (TFP) isolators were tested under extreme conditions, including uplift. This report presents information on (a) the performance of the TFP isolators and the isolated superstructure under strong excitation where the TFP isolators operate in all five regimes, including stiffening and deformation up to the displacement capacity, (b) the effect of the vertical component of earthquakes on the isolation system and superstructure response, (c) the behavior of TFP bearings of unusual configurations of which the behavior cannot be predicted by conventional models of TFP behavior, and (d) comparison of experimental results to analytical predictions of programs SAP2000 and 3pleANI in order to investigate the degree of accuracy of existing analysis models and newly developed formulations.

ABSTRACT

This report describes an experimental program of a 3-story seismically isolated structure in which Triple Friction Pendulum (TFP) isolators were tested under extreme conditions, including uplift.

This report presents information on (a) the performance of the TFP isolators and the isolated superstructure under strong excitation where the TFP isolators operate in all five regimes, including stiffening and deformation up to the displacement capacity, (b) the effect of the vertical component of earthquakes on the isolation system and superstructure response, (c) the behavior of TFP bearings of unusual configurations of which the behavior cannot be predicted by conventional models of TFP behavior, and (d) comparison of experimental results to analytical predictions of programs SAP2000 and 3pleANI in order to investigate the degree of accuracy of existing analysis models and newly developed formulations.

ACKNOWLEDGEMENTS

The authors would like to thank Dr. Daniel M. Fenz of ExxonMobil, Houston, TX for his invaluable input in the preparations of the experimental work. Partial financial support for this project was provided by the Multidisciplinary Center for Earthquake Engineering Research, Buffalo, NY and Earthquake Protection Systems, Inc., Vallejo, CA.

TABLE OF CONTENTS

LIST OF ILLUSTRATIONS

LIST OF TABLES

SECTION 1
INTRODUCTION

The behavior of the Triple Friction Pendulum (TFP) isolator has been previously described by Fenz and Constantinou (2008a to 2008e) and Morgan (2007). The TFP isolator exhibits multiple changes in stiffness and strength with increasing amplitude of displacement. The construction of the force-displacement loop is complex as it may contain several transition points which depend on the geometric and frictional properties. Figure 1-1 shows the geometry of a Triple FP bearing and its parameters. Its behavior is characterized by radii R_1, R_2, R_3 and R_4 (typically $R_1=R_4$ and $R_2=R_3$), heights h_1, h_2, h_3 and h_4 (typically $h_1=h_4$ and $h_2=h_3$, distances (related to displacement capacities) d_1, d_2, d_3 and d_4 (typically $d_2=d_3$ and $d_1=d_4$) and friction coefficients μ_1, μ_2, μ_3 and μ_4 (typically $\mu_2=\mu_3<\mu_1\le\mu_4$).

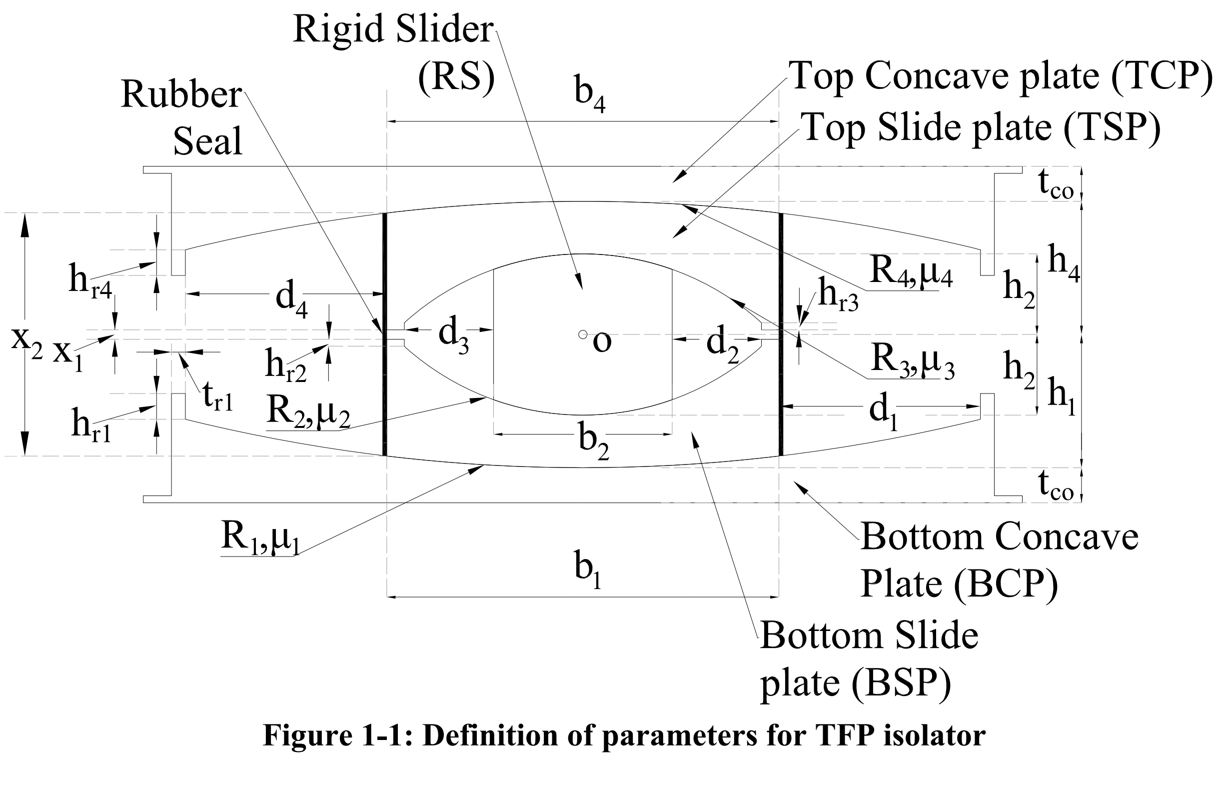

Figure 1-1: Definition of parameters for TFP isolator

The lateral force-displacement relation of the isolation system is illustrated in Figure 1-2. Five different loops are shown in Figure 1-2, each one valid in one of five different regimes of displacement. The parameters in the loops relate to the geometry of the bearing, the friction coefficient values and total weight W carried by the isolation system as described in Fenz and Constantinou (2008a and 2008b). Triple FP isolators are designed to operate in regimes I to IV, whereas regime V is reserved for providing displacement restraint in earthquakes beyond the maximum considered earthquake. In regime V, the isolator has consumed its displacement capacities d_1 and d_4 and only slides on surfaces 2 and 3 (see Figure 1-1).

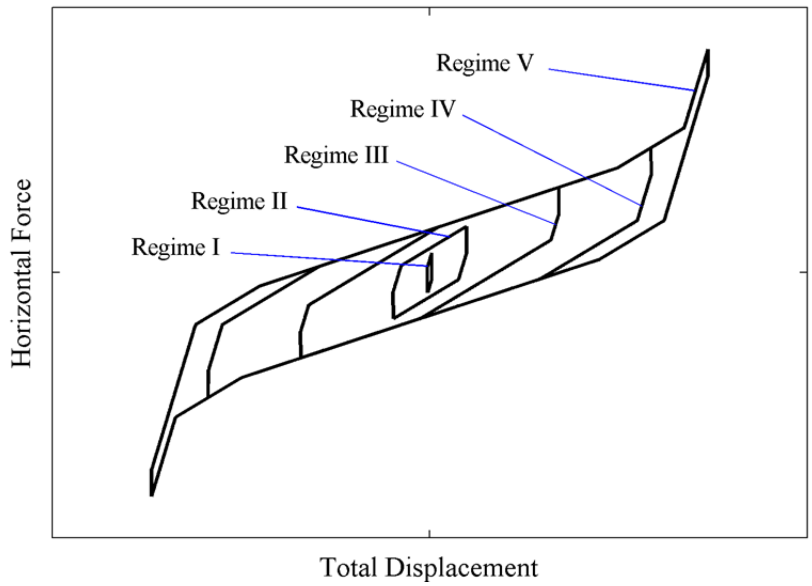

Figure 1-2: Force-displacement loops of Triple FP bearing (Fenz and Constantinou, 2008)

For response history analysis, the TFP can be modeled using the Series Model described in Fenz and Constantinou (2008d) provided that d_2=d_3, d_1=d_4 and $\mu_2 = \mu_3 < \mu_1 \leq \mu_4$. A simpler model (Parallel Model) for the special case of $\mu_2 = \mu_3 < \mu_1 = \mu_4$ and provided that stiffening does not occur was presented by Sarlis et al. (2010). Recently, Becker and Mahin (2011), Ray et al. (2013) and Dao et al. (2013) have developed formulations that can model the TFP behavior. All the formulations are based on satisfaction of horizontal force equilibrium and are restricted to the same constraints as the Series Model: d_2=d_3 and d_1=d_4, $\mu_2 = \mu_3 < \mu_1 \leq \mu_4$. Under such conditions, these models produce nearly identical results.

The TFP behavior for any random combination of geometric and frictional properties is described on the basis of a more advanced theory in Sarlis and Constantinou (2013). The theory is based on consideration of equilibrium of moments in addition to equilibrium of forces and requires use of eight degrees-of-freedom to describe the displacements and rotations of the parts of the bearing in each principal direction. The new model was implemented in the newly developed program 3pleANI that calculates and animates the TFP motion under extreme conditions, including uplift, landing and impact of components.

The frictional parameters that describe the behavior of the Triple FP bearing in the models of Fenz and Constantinou (2008a to 2008e) (denoted now as $\bar{\mu}_1, \bar{\mu}_2, \bar{\mu}_3, \bar{\mu}_4$, with the following constraints $\bar{\mu}_2 = \bar{\mu}_3 \leq \bar{\mu}_1 \leq \bar{\mu}_4$) utilize the values extracted from experiments of the Triple FP bearings and are not fundamental properties of the interfaces. Sarlis and Constantinou (2013) have shown that the true frictional values ($\mu_1, \mu_2, \mu_3, \mu_4$ without any constraints) are related to those in the models of Fenz and Constantinou (2008a to 2008e) by the following equations:

$$\bar{\mu}_2 = \mu_2 \frac{R_2}{R_{eff\,2}}$$
$$\bar{\mu}_1 = \frac{\mu_1 R_1 - \mu_2 R_2}{R_{eff\,1} - R_{eff\,2}} \qquad (1\text{-}1)$$
$$\bar{\mu}_4 = \frac{\mu_4 R_4 - \mu_2 R_2}{R_{eff\,1} - R_{eff\,2}}$$

Program 3pleANI makes use of friction values $\mu_1, \mu_2, \mu_3, \mu_4$.

This report describes an experimental program of a 3-story seismically isolated structure in which TFP isolators were tested under extreme conditions, including uplift. Analytical predictions of the response of the tested structure are made using the advanced theory model of Sarlis and Constantinou (2013).

The 3-story model structure is a modification of the six-story structure extensively used in the past at the University at Buffalo (Reinhorn et al., 1989; Mokha et al., 1990; Wolff and Constantinou, 2004; Fenz and Constantinou, 2008e). The structure was isolated using three different configurations of TFP bearings, including one in which the frictional properties were such that it could not be modeled by any existing models based on horizontal force equilibrium alone. The main purpose of these tests was to:

1. Study the performance of the TFP isolators and the isolated superstructure under strong excitation where the TFP isolators operate in all five regimes, including stiffening and up to their displacement capacity. Earlier studies of Fenz and Constantinou (2008e) presented shake table results of testing of a six-story structure in which the TFP isolators reached displacements in Regime IV (see Figure 1-2) but were further limited due to uplift. Morgan (2007) presented experimental results where TFP isolators displaced in all five regimes of operation but the tests were conducted with sinusoidal excitation rather than random seismic motions. Also, the isolators uplifted prior to reaching their displacement capacity in similarity to the Fenz and Constantinou (2008e) tests. More recently, Becker and Mahin (2011) presented experimental results of TFP bearings in all five regimes of operation in the testing of an isolated rigid block. The tests presented in this report add to the body of experimental results on the TFP isolators by extending to flexible structure in which the TFP bearings are displaced to their displacement capacity and simultaneously undergo uplift.
2. Study the effect of the vertical component of earthquakes on the isolation system and superstructure response. Previous experimental work (Fenz and Constantinou, 2008e, Morgan, 2007 and Becker and Mahin, 2011) also reported on this issue and generally have shown small effect of the vertical component on the horizontal global response. The study

of vertical earthquake effects in this report adds to the existing body of knowledge and includes some data where the effects are important.

3. Study the re-centering capability and the effect of initial offsets on the response.
4. Study the behavior of TFP bearings of unusual configurations such as cases having higher friction in the inner sliding surfaces, which cannot be predicted by conventional models of TFP behavior. The behavior of these bearings is described in Sarlis and Constantinou (2013).
5. Collect data on response to compare with analytical predictions in programs SAP2000 and 3pleANI (Sarlis and Constantinou, 2013) in order to investigate the degree of accuracy of existing analysis models and newly developed formulations.

SECTION 2
EXPERIMENTAL SETUP

2.1 Specimen Description

The model structure used in the shake table testing is shown in the photographs of Figure 2-1 and Figure 2-2. Figure 2-3 shows schematics of the model structure on the shake table. The model structure is a quarter length scale three-story steel model. The superstructure is a portion of the 6-story model last used by Fenz and Constantinou (2008e) in testing of TFP isolators. The superstructure consists of moment resisting frames in the longitudinal direction and consists of braced frames in the transverse direction. Five concrete blocks, each weighing 8.9kN, were installed at each floor and two more at the base in order to achieve mass similitude. The total weight of the model (frame, base and added weight) on top of the isolators was 196kN (distributed as 53.2kN at the base and 47.6kN at each floor). All beams and columns are S3×5.7 (SI designation S75×8.5) and all braces are L1½×1½×¼ (SI designation L38×38×6.4). The beam to column connections are fully welded and stiffened so that they are rigid. Horizontal bracing of all floors at all bays achieves, together with the concrete blocks, rigid diaphragm behavior. The 3-story structure seats on a base-mat that consists of a grid of two longitudinal W14x90 (SI designation W360x134) beams and four transverse W12x35 (SI designation W310x52) beams which are located at the superstructure's column locations. Also, the model features two HSS16x8x5/16 (SI designation HSS406.4x203.2x7.9) beams in the transverse direction that are connected on the top of the W14 x90 beams.

Four isolators were placed below the W14x90 beams on a 122cmx244cm footprint as shown in Figure 2-2 and Figure 2-3. The yellow plates seen at the bottom of the isolator-load cell assembly in Figure 2-2 and Figure 2-3 were used to first level the bearings and then to raise them so that the gravity loads on each isolator were approximately equal. The leveling plates were also used for bearing alignment.

Testing was conducted with earthquake shaking in the longitudinal (or E-W direction in Figure 2-3) and vertical directions.

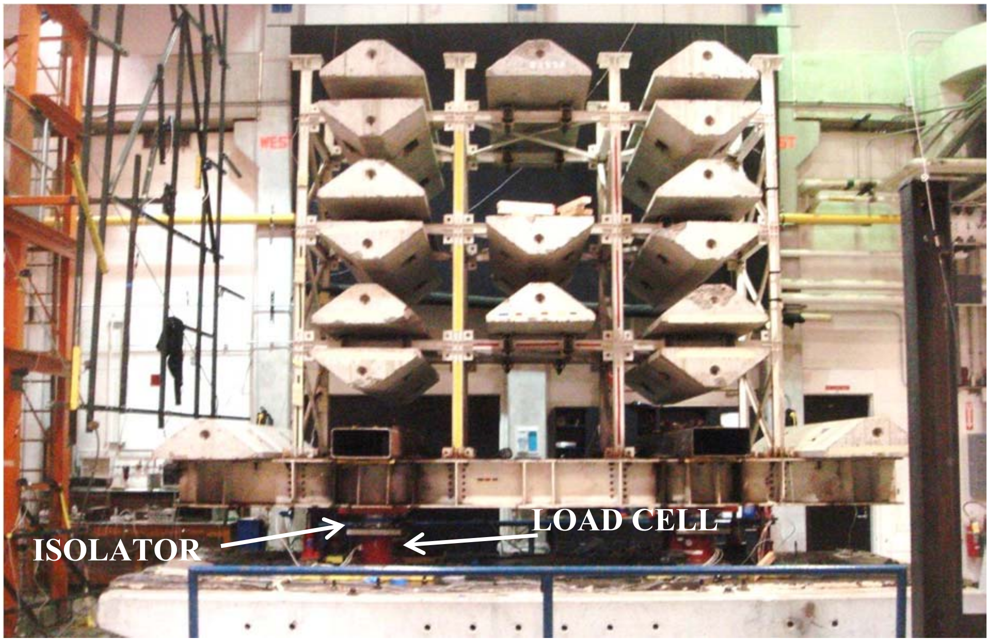

Figure 2-1: Front view of the tested structure

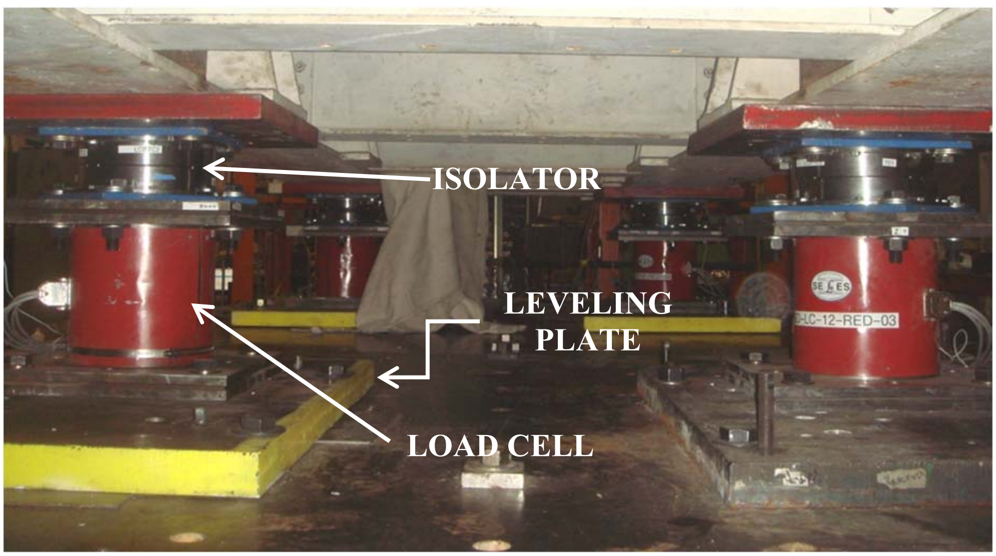

Figure 2-2: View of TFP isolators installed at the base of the tested structure

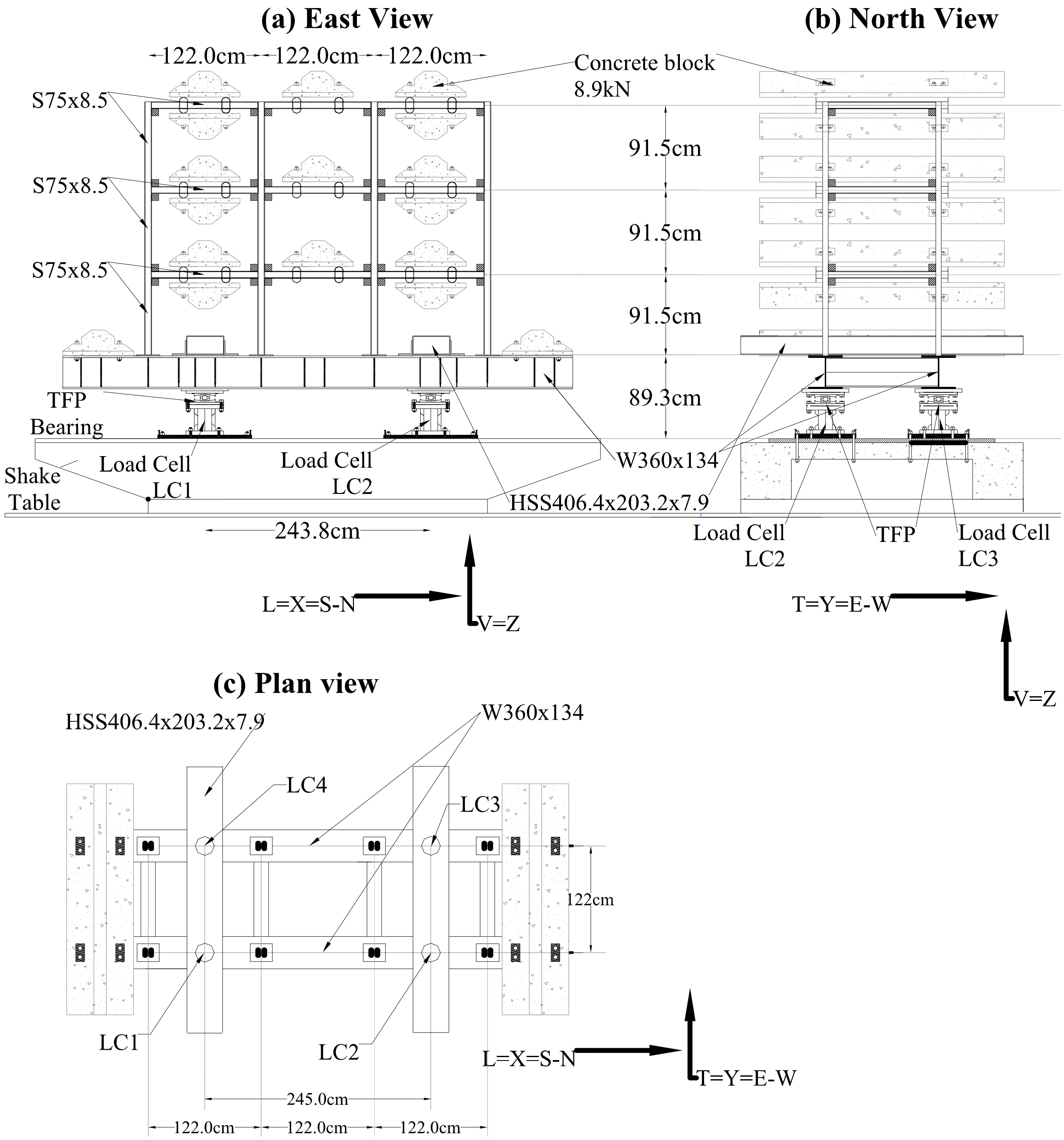

Figure 2-3: Schematics of tested structure

The techniques for the installation, leveling and alignment of the isolators have been described in Fenz and Constantinou (2008e). At the conclusion of a test, triple FP bearings may exhibit permanent displacements; particularly in the cases where the coefficient of friction at the inner sliding surfaces (2 and 3 in Figure 1-1) is large. Figure 2-4 shows a photograph of the TFP obtained at the end of a shake table test which shows two types of permanent displacements that may be exhibited by triple FP bearings:

a) Isolation system permanent displacement, which is the offset between the top and bottom concave plates of the bearings.
b) Internal component permanent displacements. These permanent displacements always occur even in the absence of isolation system permanent displacements.

Permanent displacements of either type affect the behavior of the bearings in subsequent earthquakes. This complicates the comparison of experimental results for various tested configurations as the initial conditions are different. Moreover, analytical prediction of the experimental response would have required measurement of the permanent displacements of the internal components, which is complex. Accordingly, the tested structure was re-centered when needed by use of the following procedure. First, a hydraulic jack was placed inclined with one edge supported on the shake table and the other on the base of the structure (see Figure 2-4(b)) in order to bring the structure to its zero position. Next, a hydraulic jack was placed vertically in order to remove the normal load from one bearing at a time and re-center the internal components.

(a) Example of permanent displacements (b) Re-centering procedure

Figure 2-4: Permanent displacements and TFP re-centering

2.2 Instrumentation

The complete list of the instruments used in the tests is presented in Table 2-1.

Table 2-1: List of instrumentation notation, location and direction of measurement

Name	Type	Location	Direction
1N	Load Cell	SE LC Normal Force	V
1SY	Load Cell	SE LC Shear Force	T
1SX	Load Cell	SE LC Shear Force	L
1MY	Load Cell	SE LC Moment	T
1MX	Load Cell	SE LC Moment	L
2N	Load Cell	NE LC Normal Force	V
2SY	Load Cell	NE LC Shear Force	T
2SX	Load Cell	NE LC Shear Force	L
2MY	Load Cell	NE LC Moment	T

2MX	Load Cell	NE LC Moment	L
3N	Load Cell	NW LC Normal Force	V
3SY	Load Cell	NW LC Shear Force	T
3SX	Load Cell	NW LC Shear Force	L
3MY	Load Cell	NW LC Moment	T
3MX	Load Cell	NW LC Moment	L
4N	Load Cell	SW LC Normal Force	V
4SY	Load Cell	SW LC Shear Force	T
4SX	Load Cell	SW LC Shear Force	L
4MY	Load Cell	SW LC Moment	T
4MX	Load Cell	SE LC Moment	L
SPSE-SL	String Pot	SE Table	L
SPSW-SL	String Pot	SW Table	L
SPSE-1L	String Pot	SE 1st floor	L
SPSW-1L	String Pot	SW 1st floor	L
SPSE-2L	String Pot	SE 2nd floor	L
SPSW-2L	String Pot	SW 2nd floor	L
SPSE-3L	String Pot	SE 3rdfloor	L
SPSW-3L	String Pot	SW 3rd floor	L
SPSE-BL	String Pot	SE Base	L
SPSW-BL	String Pot	SW Base	L
SPNE-BT	String Pot	NE Base	T
SPSE-TR-TC	String Pot	SE Bearing Top Concave plate	L
SPSE-TR-TS	String Pot	SE Bearing Top Slide plate	L
SPSE-TR-TR	String Pot	SE Bearing Rigid Slider	L
SPSE-TR-BS	String Pot	SE Bearing Bottom Slide plate	L
ASE-SL	Accelerometer	SE Table	L
ASW-SL	Accelerometer	SW Table	L
ASE-1L	Accelerometer	SE 1st floor	L
ASW-1L	Accelerometer	SW 1st floor	L
ASE-2L	Accelerometer	SE 2nd floor	L
ASW-2L	Accelerometer	SW 2nd floor	L
ASE-3L	Accelerometer	SE 3rdfloor	L
ASW-3L	Accelerometer	SW 3rd floor	L
ASE-BL	Accelerometer	SE Base	L
ASW-BL	Accelerometer	SW Base	L
ANE-BT	Accelerometer	NE Base	T
ANE-1T	Accelerometer	NE 1st floor	T
ANE-3T	Accelerometer	NE 3rd floor	T
ASW-BT	Accelerometer	SW Base	T
ASW-1T	Accelerometer	SW 1st floor	T
ASW-3T	Accelerometer	SW 3rd floor	T
AN-SV	Accelerometer	NW Table	V
AN-SV-2	Accelerometer	NE Table	V
AS-SV	Accelerometer	SW Table	V
AS-SV-2	Accelerometer	SE Table	V
AN-BV	Accelerometer	NW Base	V
AN-BV-2	Accelerometer	NE Base	V
AS-BV	Accelerometer	SW Base	V

AS-BV-2	Accelerometer	SE Base	V
ALC1-BV	Accelerometer	SE Load Cell 1	V
ALC1-BL	Accelerometer	SE Load Cell 1	L
ALC2-BV	Accelerometer	NE Load Cell 2	V
ALC2-BL	Accelerometer	NE Load Cell 2	L
ALC3-BL	Accelerometer	NW Load Cell 3	L
ALC4-BL	Accelerometer	SW Load Cell 4	L
L=Longitudinal direction, V= vertical direction, LC=load cell, SE=South-East, SW=South-West, NE=North-East, NW=North-West			

Figure 2-5 and Figure 2-6 show the location of the potentiometers (displacement transducers) and accelerometers installed on the superstructure and shake table. Two accelerometers and two displacement transducers were installed at each floor, base and the shake table in order to have redundancy in the measurements and to also measure torsional motion. Vertical accelerometers were installed on the shake table and the base at four opposite corners. Transverse accelerometers were also installed on the 1st and 3rd floors and at the base at the NE and SW corners of the model.

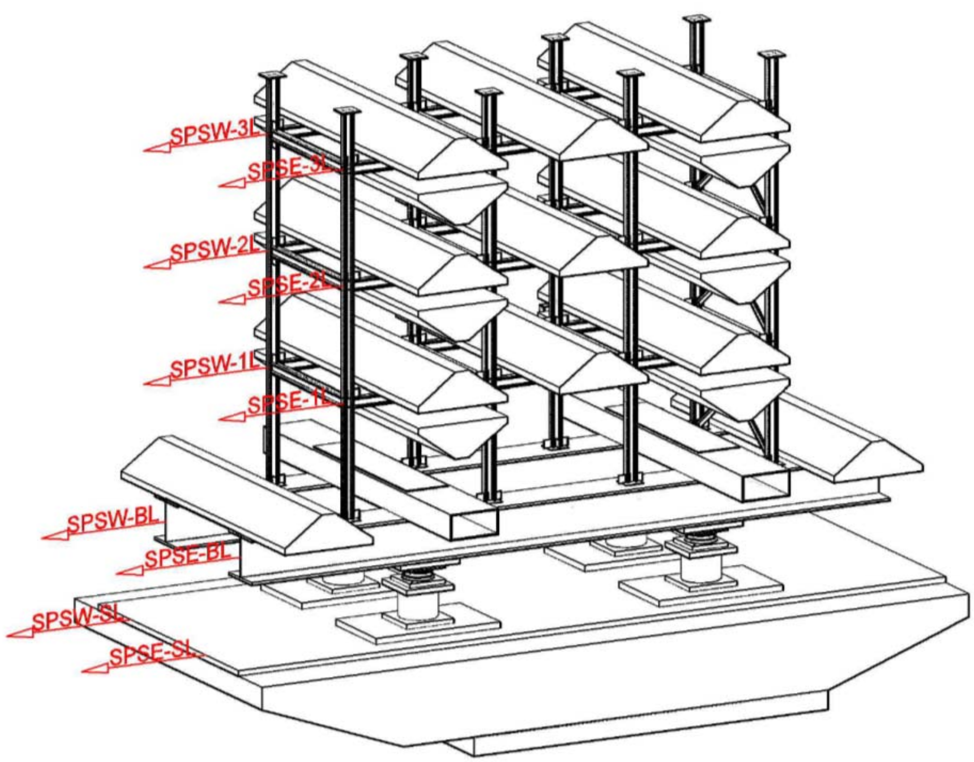

Figure 2-5: Location of displacement transducers on superstructure and shake table

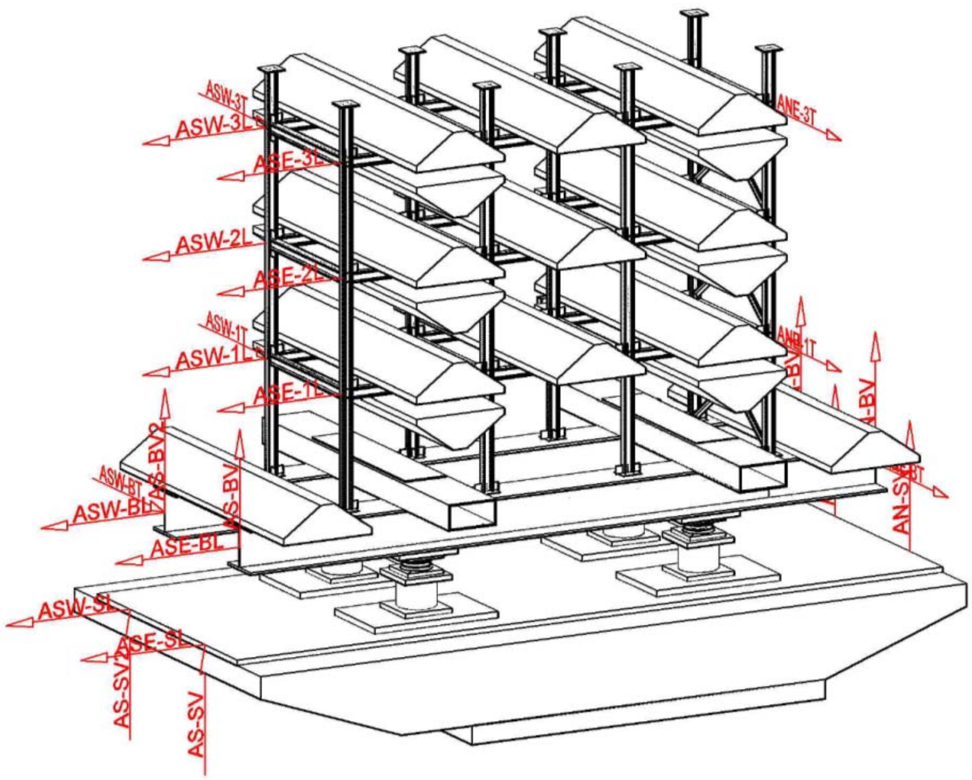

Figure 2-6: Location of accelerometers on superstructure and shake table

The TFP isolators were installed on top of four 5-component load cells. The load cells measured axial, shear forces in two orthogonal directions and moments about two horizontal axes. Details about the load cells and how they are calibrated can be found in Bracci et al. (1992). The list of all measured components (channels) is shown in Figure 2-7. The TFP isolator on Load Cell 1 was also instrumented with displacement transducers as shown in Figure 2-8 in order to measure the displacements of the inner components. It should be noted that the inner parts of the TFP isolators occasionally experience torsional motions due to uneven distribution of friction tractions. This leads to erroneous measurements by the string pots so that the displacements of the inner parts could not be measured.

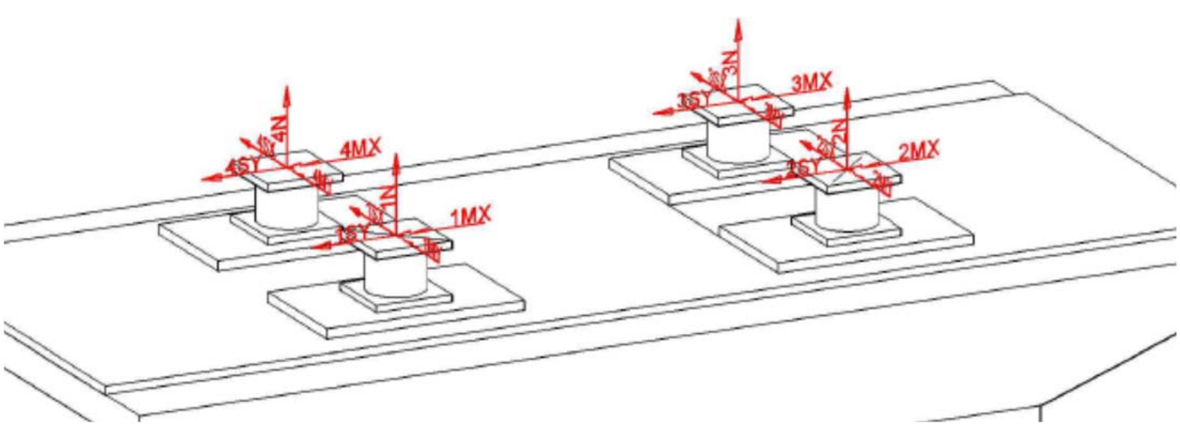

Figure 2-7: Five-component load cell channels

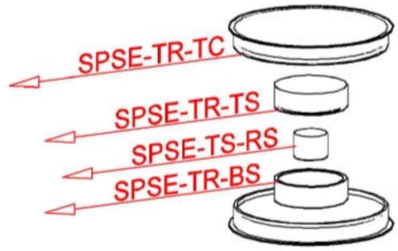

Figure 2-8: Displacement transducers installed at TFP inner components

An important part of any experimental study is to have redundancy in the measurements so that (a) the accuracy of measurements can be checked, and (b) sufficient data are acquired in case of failure of instrumentation. Although rarely reported, load cells often have measurement errors due to calibration errors (particularly for complex multichannel cells in which there is channel "cross-talk"), manufacturing errors (e.g., due imperfect placement of strain gages), installation errors in the test arrangement (e.g., leveling), condition of other supporting equipment (e.g., conditioners) and effects of the environmental conditions (e.g., temperature and humidity). Deviations of measured force of up to 20% of the actual forces are not uncommon. Figure 2-9 compares results for the base shear in shake tests of the tested isolated model obtained by direct measurement of the shear force (force F_{lc}) and by processing of the acceleration records obtained at each floor and the base-mat of the structure (force F_{acc}). Force F_{lc} was obtained as the sum of the shear forces recorded by the load cells supporting the isolators (sum of 1SX+2SX+3SX+4SX in Figure 2-7) and force F_{acc} was calculated as the sum of the floor and base-mat inertia forces:

$$F_{acc} = m_b \ddot{u}_b + m_f \left(\ddot{u}_1 + \ddot{u}_2 + \ddot{u}_3 \right) \tag{2-1}$$

where m_b is the mass of the base-mat (weight equal to 53.2kN), m_f is the mass of one floor (weight equal to 47.6kN), $\ddot{u}_b$ is the longitudinal acceleration of the center of mass of the base-mat and $\ddot{u}_1, \ddot{u}_2$ and $\ddot{u}_3$ are the center of mass accelerations of the 1st, 2nd and 3rd floors, respectively. The center of mass accelerations were calculated as the average of the two accelerometers recording on each floor. For example, $\ddot{u}_b$ is the average of the recordings of instruments ASE-BL and ASW-BL (see Figure 2-6), $\ddot{u}_1$ is the average of the recordings of instruments ASE-1L and ASW-1L, etc.

The two sets of results in Figure 2-9 are in very good agreement. However, to obtain this good agreement, the load cell measurement was multiplied by a correction factor of 1.055-a factor found to be needed as the load cell measurements were systematically lower than the results obtained from processing of the acceleration records, which were presumed to be accurate. It was discovered that the difference was due to load cell calibration. The load cell calibration procedure followed is described in Bracci et al. (1992) and utilizes the fixture shown in Figure 2-10. The load cells are bolted together and placed on top of two rollers at the edges of the two outermost load cells. A loading beam is placed on top of the load cells supported by two rollers placed on two of the load cells. A reference load cell is placed at the center and on top of the loading beam and load is applied on top of the reference load cell. The two outermost load cells are calibrated for half the load measured by the reference load cell. This however ignores the weight of the loading beam and the weight of the load cells. Each load cell has a weight of about1.8kN and the loading beam, reference load cell and other features weigh another 1.8kN for a total of about 9kN additional unaccountable load. The distribution of this load gives rise to shear forces of 4.5kN for the two outer cells which are calibrated for shear force. Given that load cells were calibrated to a shear of about 90kN, this leads to a calibration error of the order of 5%.

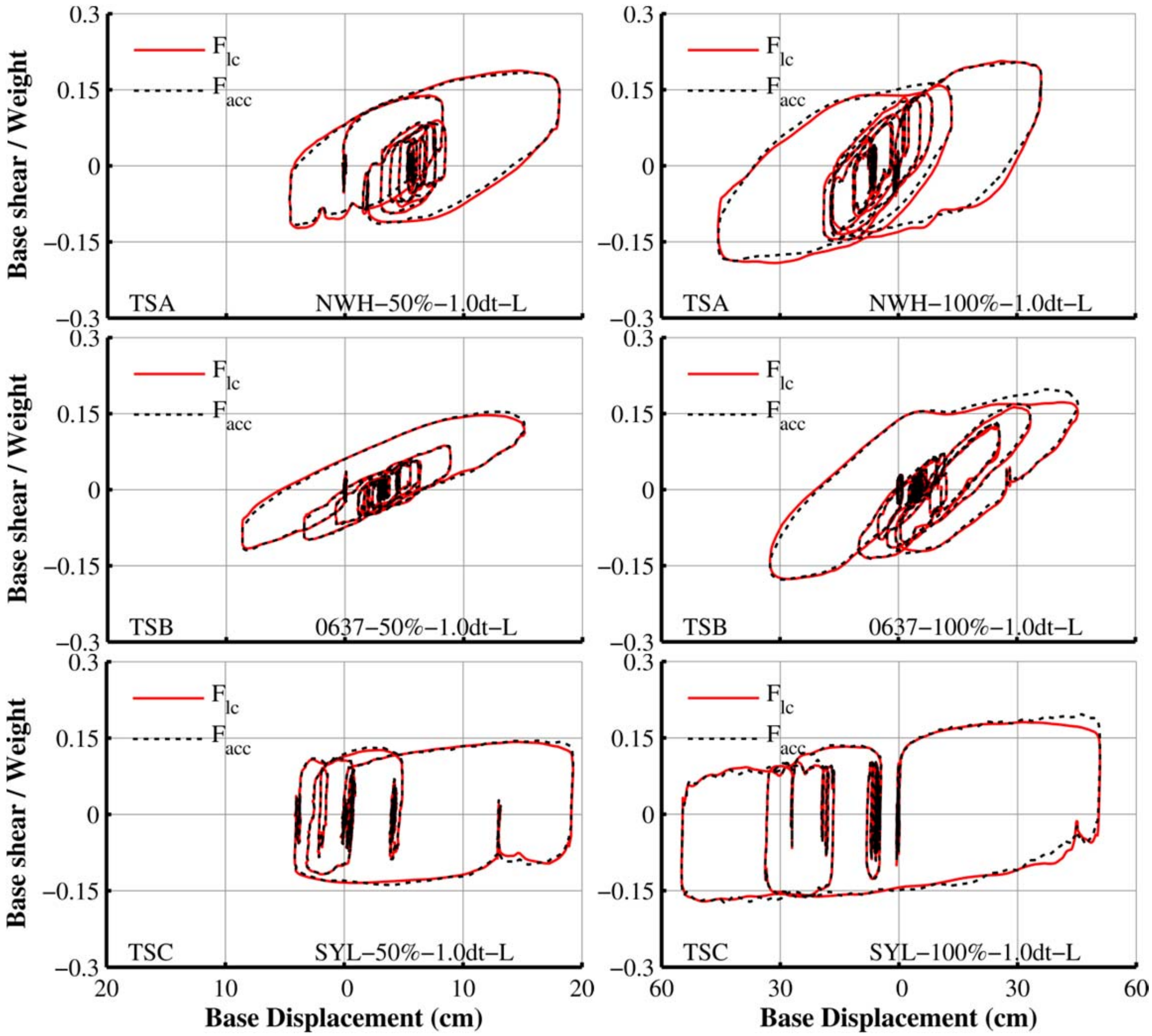

Figure 2-9: Comparison of base shear-base displacement loops obtained from processing of acceleration records (force F_{acc}) and directly measured by load cells (force F_{ld})

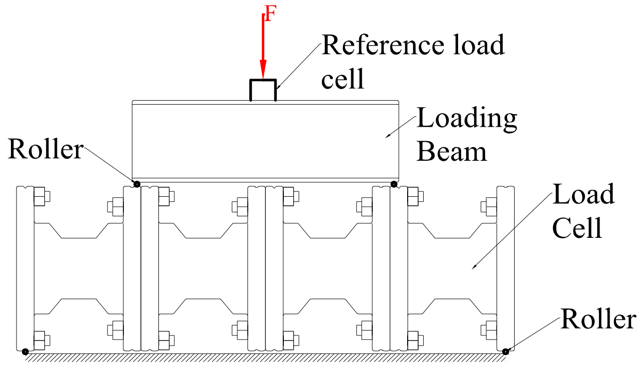

Figure 2-10: Load cell calibration fixture

An additional problem encountered in the tests was significant drifting of the load cell values with time due to environment temperature changes that affected the temperature of the load cell conditioners. The sensitivity of the conditioners is shown in Figure 2-11(a) for the vertical load on each of the four load cells when a fan was used to cool the conditioners. Load cell drifts of about 15kN can be observed when no additional load was applied on the structure. Figure 2-11(b) shows load cell drifting over a 12 hour period without the use of a fan to cool down the conditioners. In the latter case, the drift in measured load in two of the load cells is 50kN and 400kN which indicates the severity of the problem.

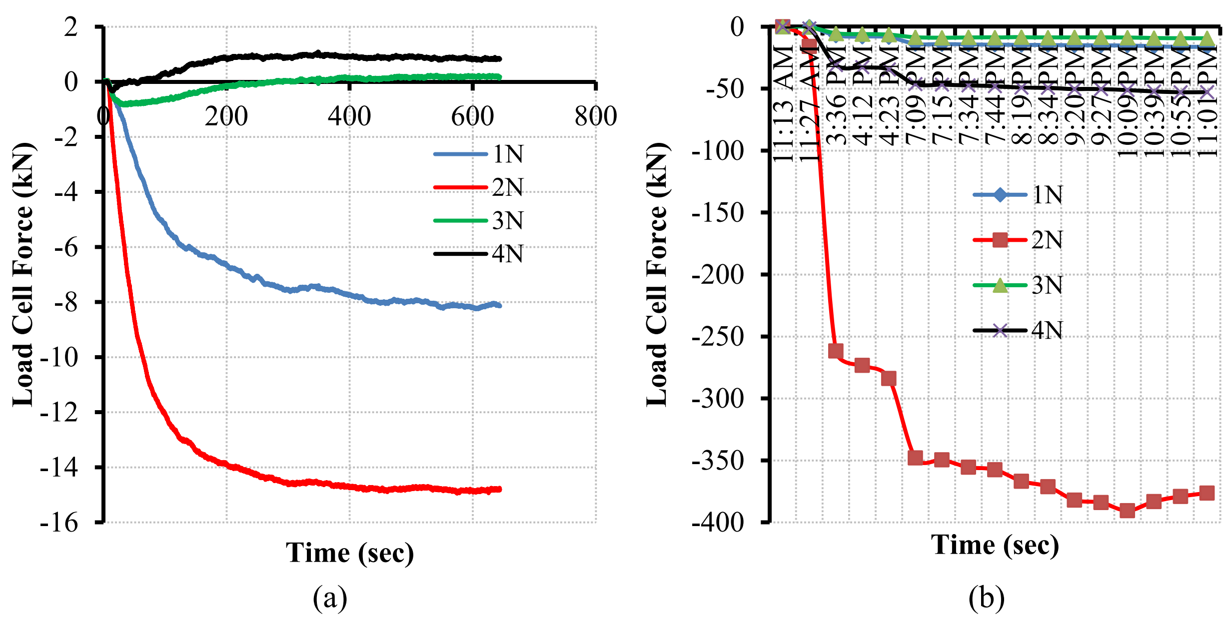

Figure 2-11: Load cell normal load variation for (a) with fan cooling the conditioners and (b) without fan cooling

It was determined that the problem of drifting values was negligible for short times of the order of one minute so that it did not affect the measurements in single dynamic tests. Accordingly, the procedure followed to obtain values of load on each isolator at the start of each test was as follows:

1. At the first test and when re-centering of the isolators was needed or whenever the isolators were replaced, the load cells were balanced by jacking the structure up and removing the normal load from each isolator at a time (see Section 2.1). The normal load values were recorded after normal load was reinstated at all isolators. These values then served as the initial normal load values for the subsequent test.
2. For subsequent tests, the changes in the normal loads from the beginning to the end of each test were added to the initial values until the next time the load cells were balanced.

Application of the procedure described above resulted in the evolution of the value of the sum of the measured normal load on the four isolators for the duration of testing (the value of the measurement should be constant and equal to weight of the structure). The evolution of the measured total load is shown in Figure 2-12. While the measured load still exhibits some small drift (by less than 3% in over 100 tests), the drift is far less than that depicted in Figure 2-11 and it does not affect the fidelity of the measured forces in the testing.

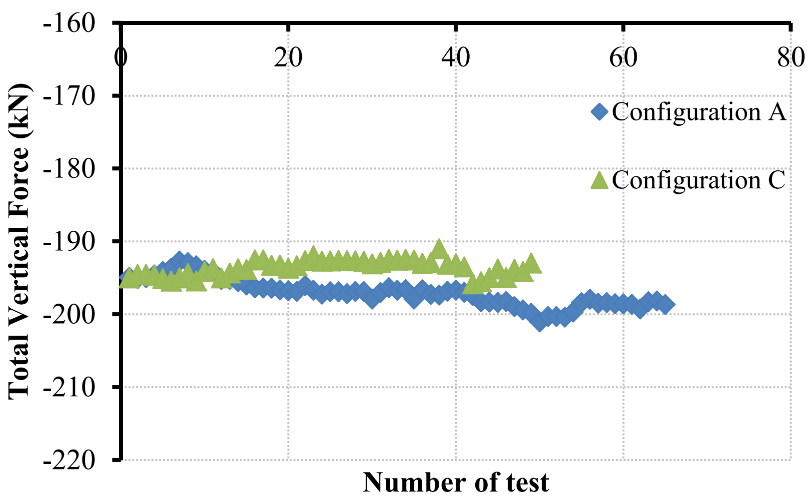

Figure 2-12: Evolution of measured total vertical load on four isolators during testing

SECTION 3
INDIVIDUAL TESTING OF TRIPLE FP ISOLATORS

This section presents experimental results on the behavior of the isolators that were used for the shake table testing. The isolators were tested in the single bearing testing machine at the University at Buffalo (Kasalanati and Constantinou, 1999). For the shake table tests, TFP isolators of three different configurations were used with the geometric characteristics presented in Table 3-1. From the three configurations, A and C had the exact same geometry while Configuration B had slightly different geometry (the rigid slider was slightly shorter). The values of the friction coefficients for Configurations A and B satisfied the condition $\mu_2=\mu_3<\mu_1<\mu_4$ for which standard models of TFP isolator behavior are valid. Configuration C satisfied the condition $\mu_1=\mu_4<\mu_2=\mu_3$, for which the behavior cannot be predicted with standard models. The tests revealed the frictional properties of the isolators.

Table 3-1: Geometric properties of Triple FP used in shake table tests (with reference to Figure 1-1)

Geometric Properties	Configuration A and C	Configuration B
$R_1 = R_4$ (mm)	473	473
$R_2 = R_3$ (mm)	76	76
$h_2 = h_3$ (mm)	23	18
$h_1 = h_4$ (mm)	38	33
$R_{eff1} = R_{eff4}$ (mm)	435	440
$R_{eff2} = R_{eff3}$ (mm)	55	58
$d_1 = d_4$ (mm)	64	64
$d_2 = d_3$ (mm)	19	19
$b_1 = b_4$ (mm)	101	101
$b_2 = b_3$ (mm)	51	51

3.1 Equipment and Instrumentation Used

A detailed description of the bearing testing machine can be found in Kasalanati and Constantinou (1999). The machine is depicted in Figure 3-1. The bearing sits on top of a five component load cell (the particular type of load cell used is denoted "5D-LC-12-BLU" in the University at Buffalo Structural Engineering and Earthquake Simulation Laboratory manual, http://nees.buffalo.edu/docs/labmanual/HTML/Chapter%203.htm#_Toc145756944). This load cell records forces in three directions and moments about two axes. The horizontal actuator shown in Figure 3-1 is also equipped with an axial-only load cell which allows for direct verification of force measurements for slow tests and indirect for dynamic tests (correction is needed for the inertia force effects of the loading beam in Figure 3-1).

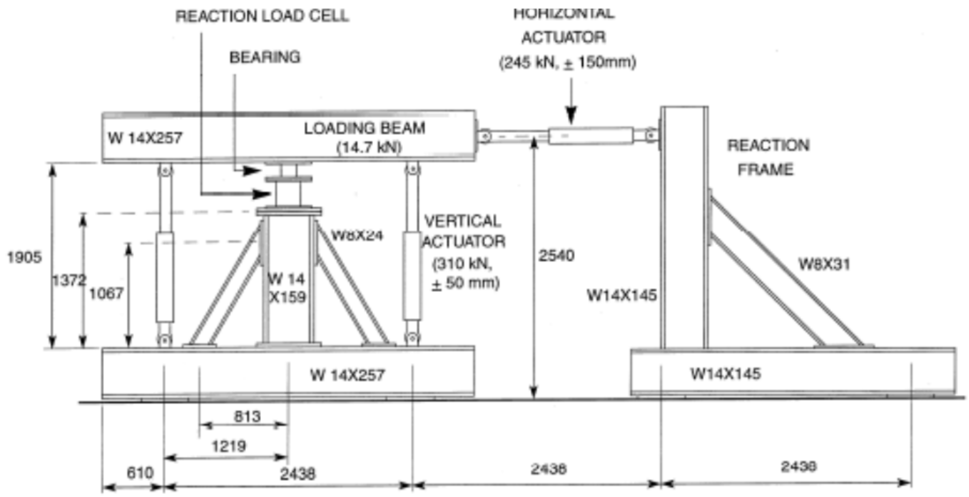

Figure 3-1: Schematic of single bearing testing machine (Kasalanati et al., 1999)

Figure 3-2 shows the instrumentation used to monitor the motion of the three internal components of the bearing. Note the two instruments that were needed for each component as the parts also exhibited torsion (Sarlis and Constantinou, 2013). This apparatus was used for the testing of only Configurations B and C.

Figure 3-2 shows string pots (potentiometers) SP-1, SP-2, SP-5 and SP-6 attached to the tip of the interior restrainer ring of the corresponding slide plates which are located at a distance z_{sp} from surface 1 for SP-1 and SP-2 and surface 4 for SP-5 and SP-6. SP-3 and SP-4 are attached at the mid-height of the rigid slider and directly measure the displacement of its center of mass (see Figure 1-1 for terminology). The measured displacements of the parts required post-processing on the basis of the geometry of the components and the location of the instruments in order to calculate displacements at each surface.

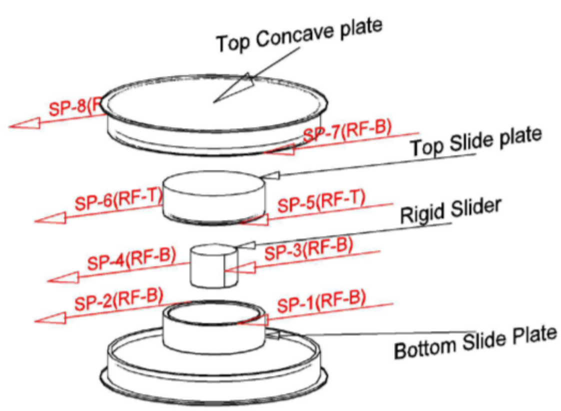

Figure 3-2: String-pot instrumentation of internal components for tested Triple FP bearing Configurations B and C

3.2 Configuration A Testing

Configuration A consisted of the isolators used for testing by Fenz and Constantinou (2008e). Surfaces 1, 2 and 3 of these isolators consisted of a material labeled as M1 and shown in Figure 3-3 on the right and Figure 3-4. Friction on surfaces 2 and 3 was much lower than on surface 1 due to the combination of higher pressure and the effect of some lubrication that was introduced in the 2008 tests. Surface 4 consisted of a high friction material labeled as M8 and shown in Figure 3-3. Experimental results for the isolators of Configuration A are presented in Figure 3-5. The left column of the graphs shows results for tests with imposed lateral motion at 0.01Hz frequency and the right column shows results for 0.3Hz frequency. The results are in the form of loops of the horizontal force normalized by the vertical force versus the displacement of the top concave plate with respect to the bottom concave plate. The notation used in the graphs is as follows for one of the four tested bearings: M1LC1-M1LC4 denotes the isolator that consisted of the bottom slide plate with material M1 used in the shake table testing in the bearing placed on top of load cell 1 (Figure 2-3), together with the bottom slide plate with material M1 used in the shake table testing in the bearing placed on top of load cell 4. These tests were conducted one month prior to the shake table tests.

Figure 3-3: Views of slide plates with material M8 (left row) and material M1 (right row) used in Configuration A isolators

Figure 3-4: Top view of rigid sliders with material M1 used for surfaces 2 and 3 in Configuration A isolators

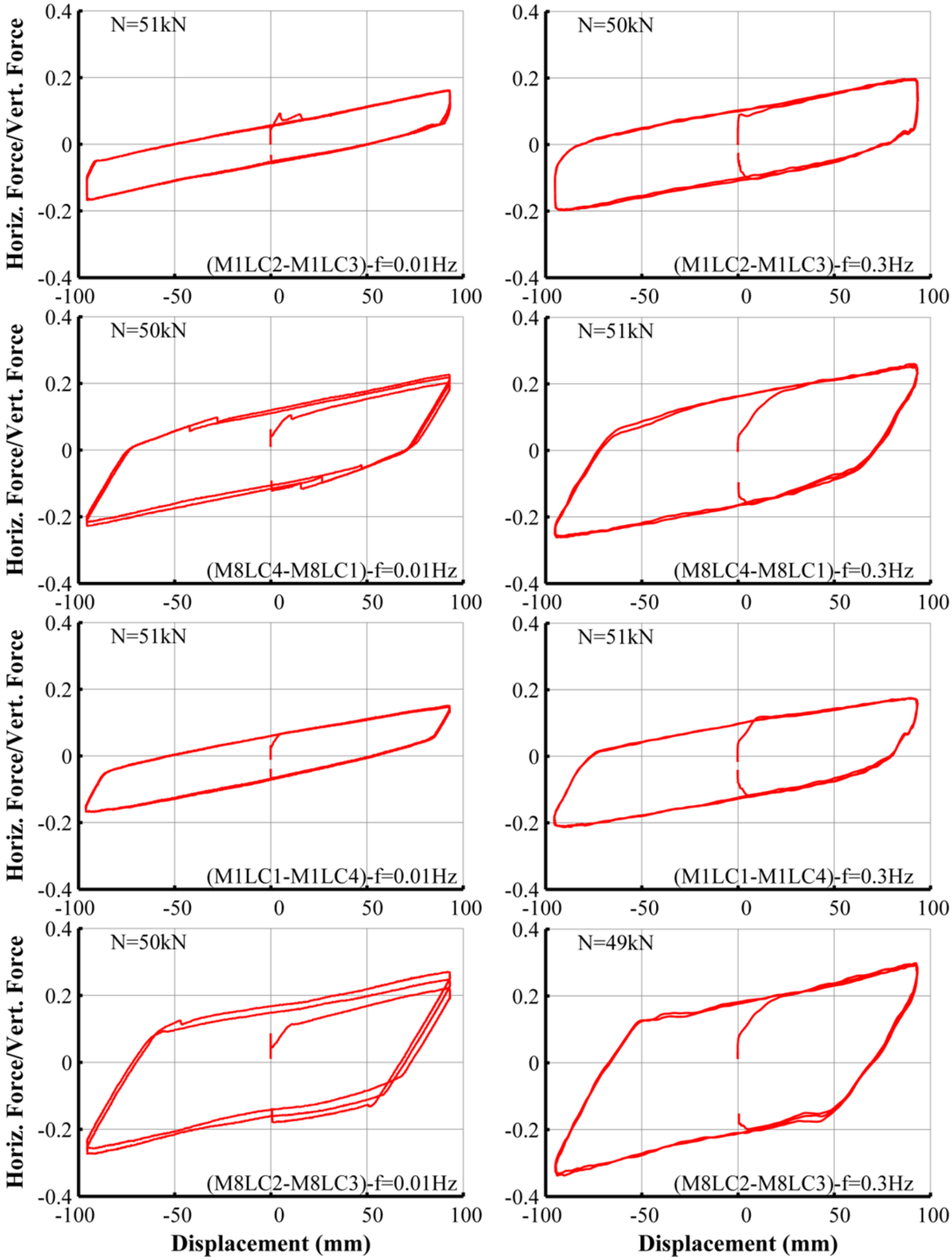

Figure 3-5: Normalized force-displacement loops of Configuration A TFP isolators

3.3 Configuration B Testing

The bearings for Configuration B consisted of the same materials as those of Configuration A and have not been tested prior to the shake table testing. Rather, they were tested five months after the completion of the shake table tests. The bearings have not been cleaned or conditioned in the period between the shake table and the bearing machine testing. Results are presented in Figure 3-6. For these tests, the bearings were placed in the bearing testing machine at an offset that led to un-symmetric displacement input. TSB1 denotes the isolator that was located on top of load cell 1 (see Figure 2-7), TSB2 on top of load cell 2, etc. in the shake table tests. Observations in the results of Configuration B are:

1. During testing, bearing TSB3 exhibited stick-slip phenomena on surface 4 that were pronounced in low velocity tests (f=0.02Hz). While the phenomenon of stick-slip may be artificial and created by the test apparatus and/or any corrections of errors due to inertia effects (see Section 4 of Constantinou et al., 2007), it is believed that it was real and the result of high breakaway friction coefficient. The phenomenon was not observed in the shake table testing and it was barely observed in the faster test machine tests because frictional heating eliminated the difference between breakaway and sliding friction values.
2. The internal bearing parts (BSP; bottom slide plate, RS; rigid slider and TSP; top slide plate) exhibited significant torsional rotations as indicated by the results of Figure 3-7 which presents recorded values of the torsion angle during the tests for which the loops are presented in Figure 3-6. The torsion angle was calculated from the difference between the measurements of the two displacement transducers of each part shown in Figure 3-2 and divided by the distance between the attachments of the two transducers to the parts. It can be seen that some components exhibited up to 70^{o} angle of rotation about the vertical axis. This behavior was also occasionally observed but not directly measured in the shake table tests in all configurations. It is caused by uneven distribution of traction forces on the sliding surfaces. The motion resulted in changes in the displacement capacities of the internal parts.
3. In test TSB4-f=0.1Hz, the tested bearings exhibited uplift so that the normalized force could not be obtained (division by zero). For this test the lateral force-displacement loop and the history of the vertical force on the bearing are shown in Figure 3-8. Uplift can be recognized when the lateral force is zero over a range of displacements. Uplift occurred because of inability to control the axial load on the tested bearings, particularly at high speed motion.

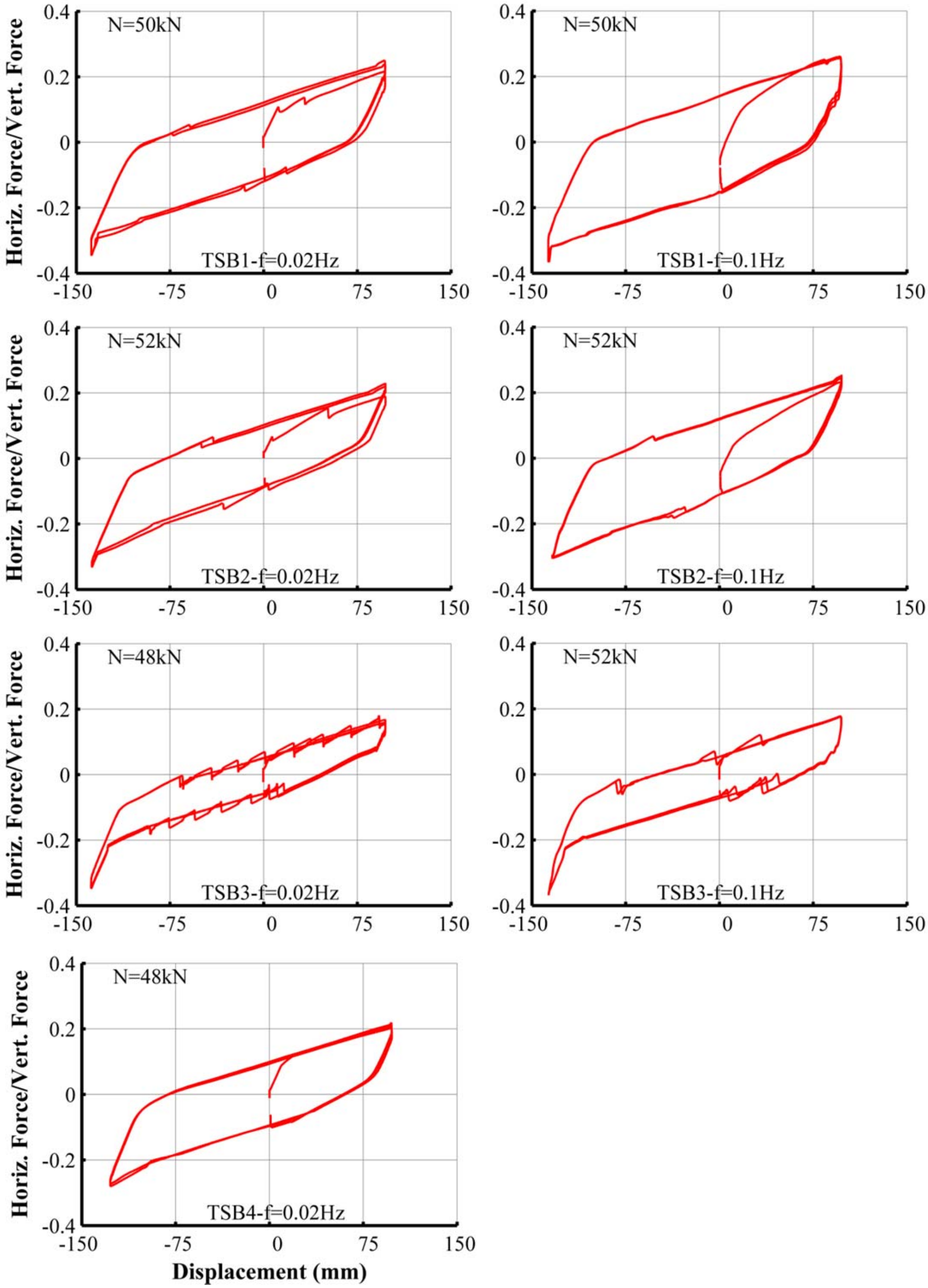

Figure 3-6: Normalized force-displacement loops of Configuration B TFP isolators

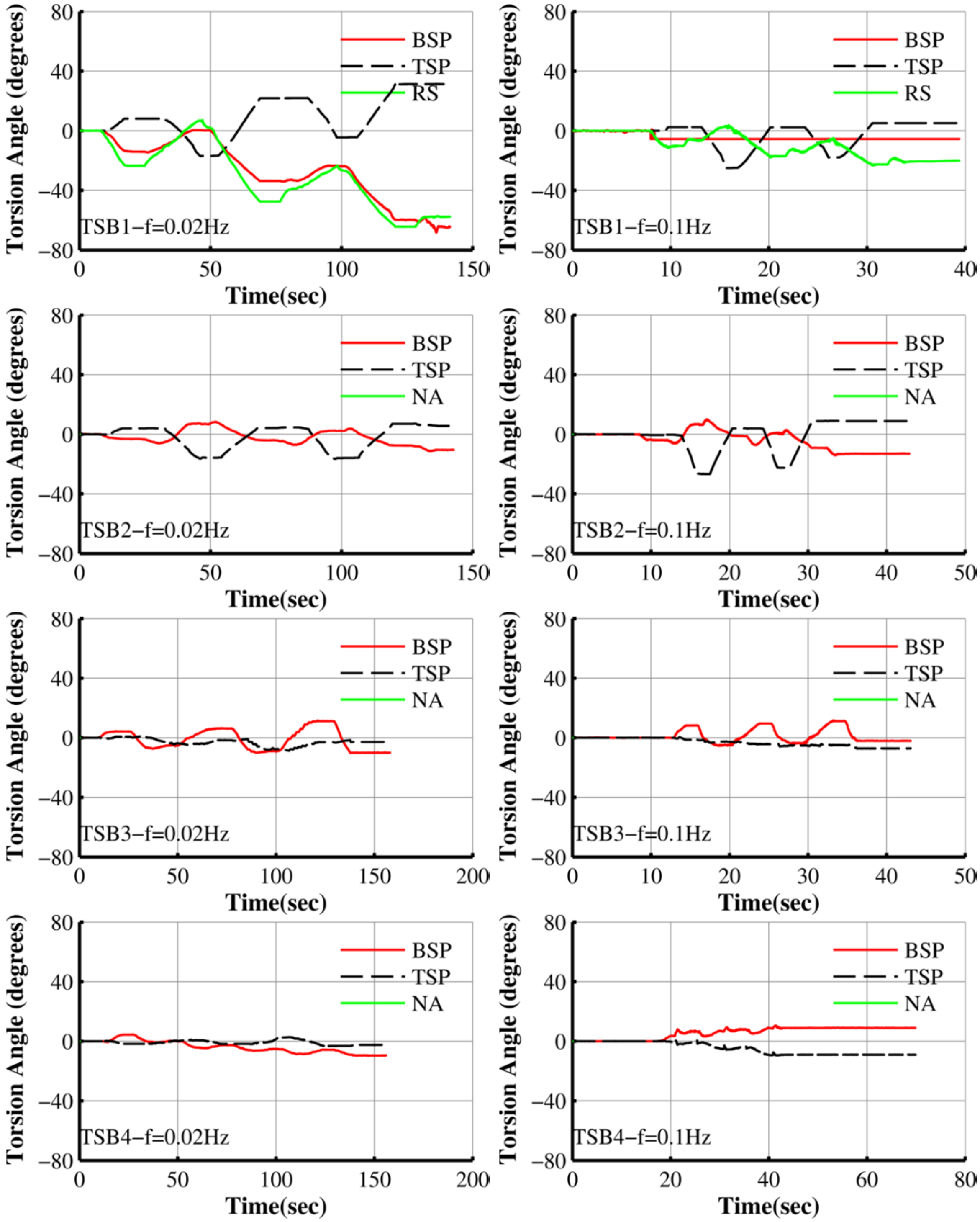

Figure 3-7: Torsion angle of internal components of TFP isolators of Configuration B

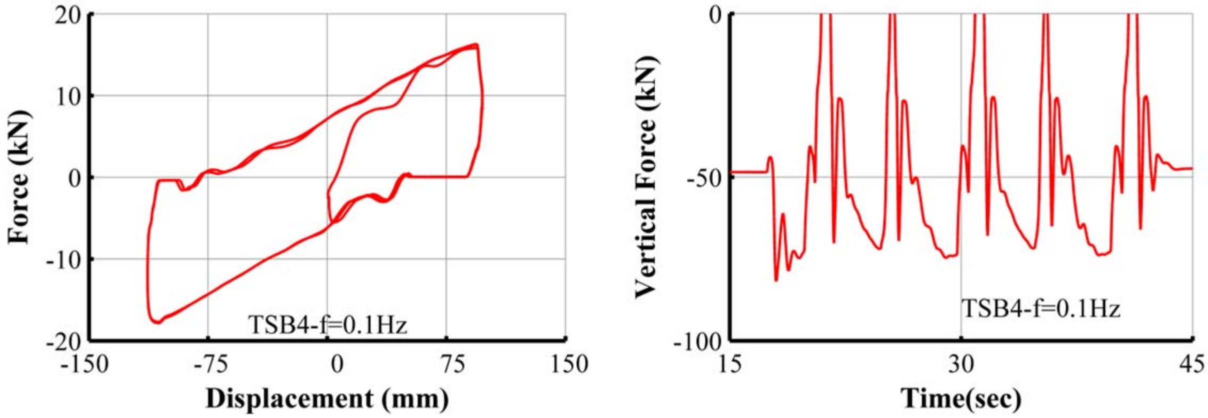

Figure 3-8: Force-displacement loops of isolators exhibiting uplift

3.4 Configuration C Testing

Experimental results for the isolators of Configuration C are presented in Figure 3-9. Testing was conducted after the shake table testing. The isolators were assembled with friction on surfaces 1 and 4 having a value that is much smaller than the value of friction on the inner surfaces 2 and 3. This is an unusual configuration of which the behavior cannot be predicted by the conventional models of TFP bearings. Rather, the more advanced theory in Sarlis and Constantinou (2013) is capable of describing their behavior. For these isolators, motion initiates simultaneously on surfaces 1 and 4 when the lateral force becomes equal to the highest friction force among the two surfaces 1 and 4. In theory, motion on surfaces 2 and 3 will not initiate until the following two incidents occur: a) the displacement capacity of surfaces 1 and 4 is consumed, and b) the lateral force becomes equal to the highest friction force among surfaces 2 and 3. Between incidents a) and b) above there is an abrupt increase in the isolator lateral force. Actually, the displacement capacity of surfaces 1 and 4 cannot be simultaneously consumed as a result of initial offsets of the TFP surfaces caused by misalignments in the top concave plate. Such complex cases can be analyzed using the theory presented in Sarlis and Constantinou (2013). For the results in Figure 3-9, the measurements of both the isolator and actuator load cells are shown as some small differences were observed in the two independent measurements. Also, Figure 3-10 presents results on the torsional motion exhibited by the internal components of the bearings of Configuration C.

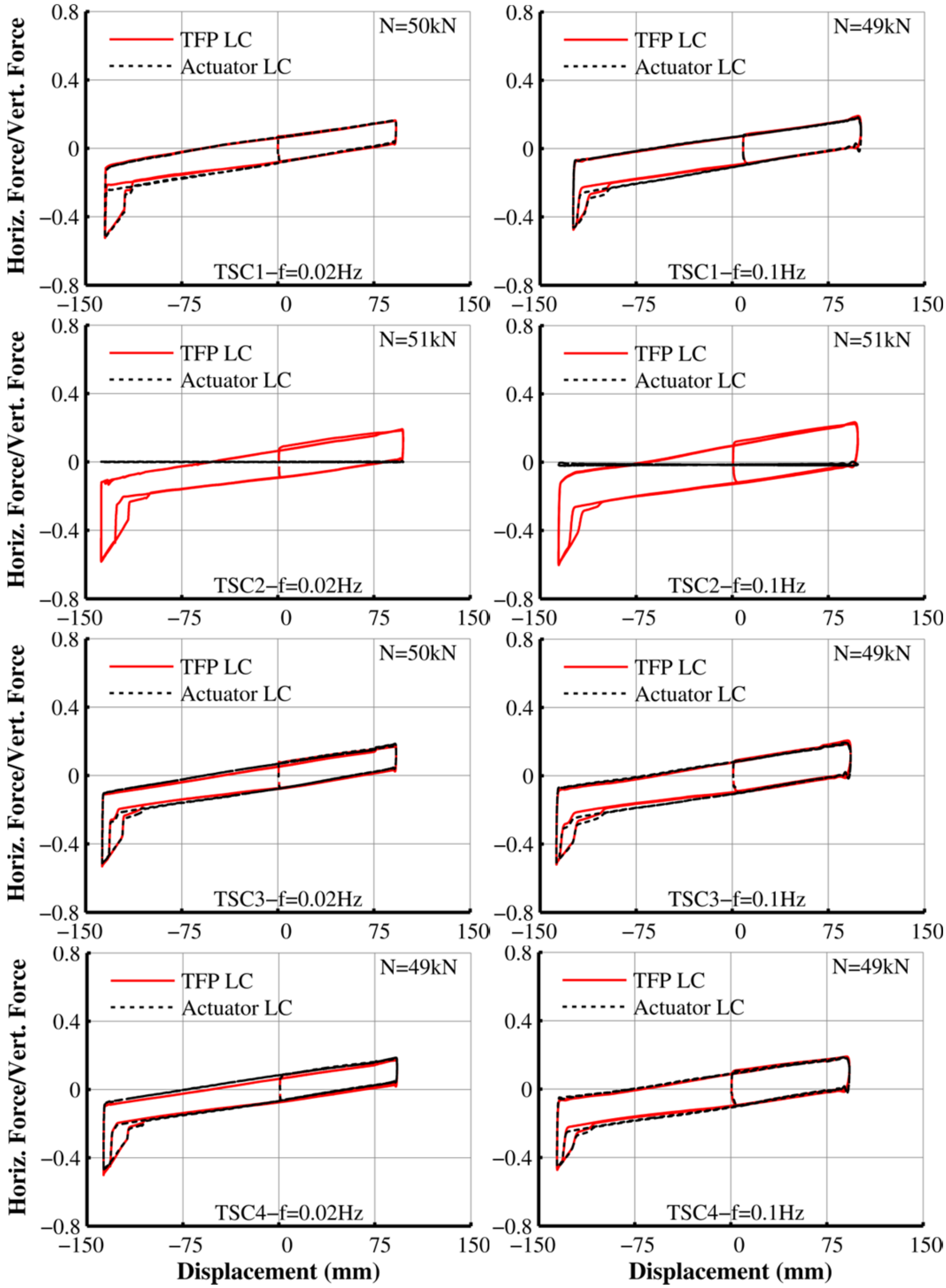

Figure 3-9: Normalized force-displacement loops of Configuration C TFP isolators

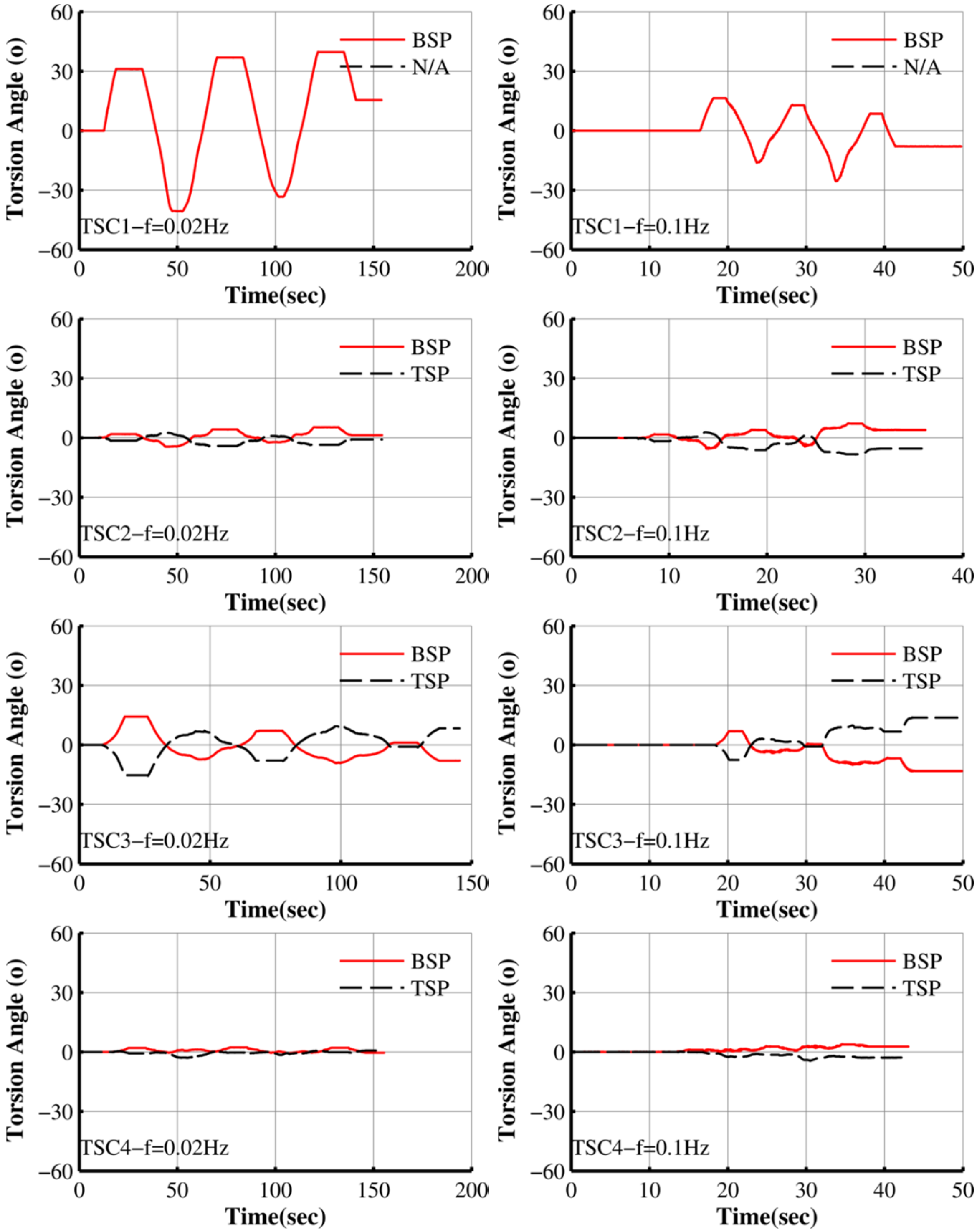

Figure 3-10: Torsion angle of internal TFP bearing components exhibited of the isolators of Configuration C

3.5 Additional Topics on the Testing of TFP Isolators

Figure 3-11 presents a comparison of experimental normalized force-displacement loops for a bearing of Configuration A under different axial loads. Figure 3-11 on the left shows results for an isolator having material M8 on surfaces 1 and 4 and subjected to a normal load of a) N=107kN and b) N=44kN. Figure 3-11 on the right shows results for the case in which the high friction material M8 was replaced by the low friction material M1. For both isolators, the inner surfaces 2 and 3 consist of material M1. Note that there is small effect of load on the behavior of the bearings due to the effect of pressure on the coefficient of friction at surface 1 and 4 where the apparent bearing pressure varies between 6.4 and 14.0MPa. In contrast, there is no effect on the friction coefficient of surfaces 2 and 3 where pressure varies between 25 and 55MPa-already large values for which pressure does not have significant effects (Constantinou et al, 2007).

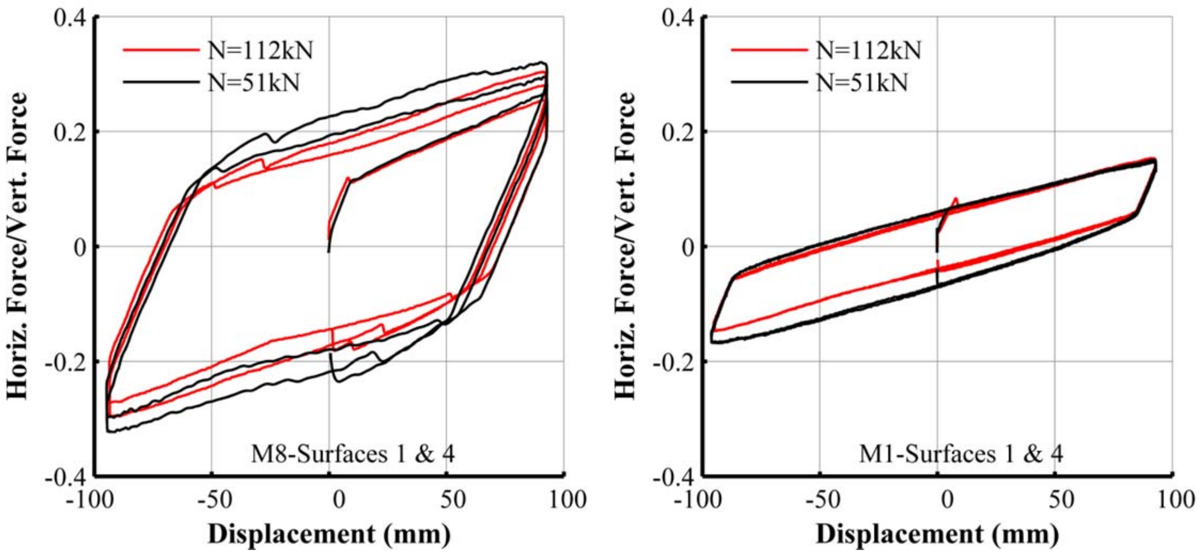

Figure 3-11: Normalized force-displacement loops of TFP isolators at different loads

A subject investigated in the testing arises when isolators exhibit differences in vertical displacements. This situation occurs when isolators of different geometric and frictional properties are combined in the isolation system. It also occurs when identical isolators are used but natural variability in frictional properties causes differential vertical displacements of the isolator parts. Differential vertical motion results in redistribution of the axial load on the isolators in addition to variations due to overturning moment and vertical earthquake effects. Figure 3-12 shows results from tests conducted at the single bearing machine for two isolators having the same geometry but different friction properties: a) one with material M8 (high friction) on surfaces 1 and 4 and b) one with material M1 (low friction) on surfaces 1 and 4 and subjected to identical displacement inputs. The two isolators exhibit different vertical displacements. This occurs because the isolator with the higher friction M8 material exhibits larger displacements on surfaces 2 and 3 prior to initiation of motion on surfaces 1 and 4 than the isolator with the lower friction M1 material (note that surfaces 2 and 3 have small radius of curvature which affects the vertical motion). Note in Figure 3-12 that there is permanent vertical displacement for the bearing of the higher friction material M8 despite the fact that the bearing has no permanent horizontal displacement. This is due to the fact that there is permanent displacement of the internal components of the bearing.

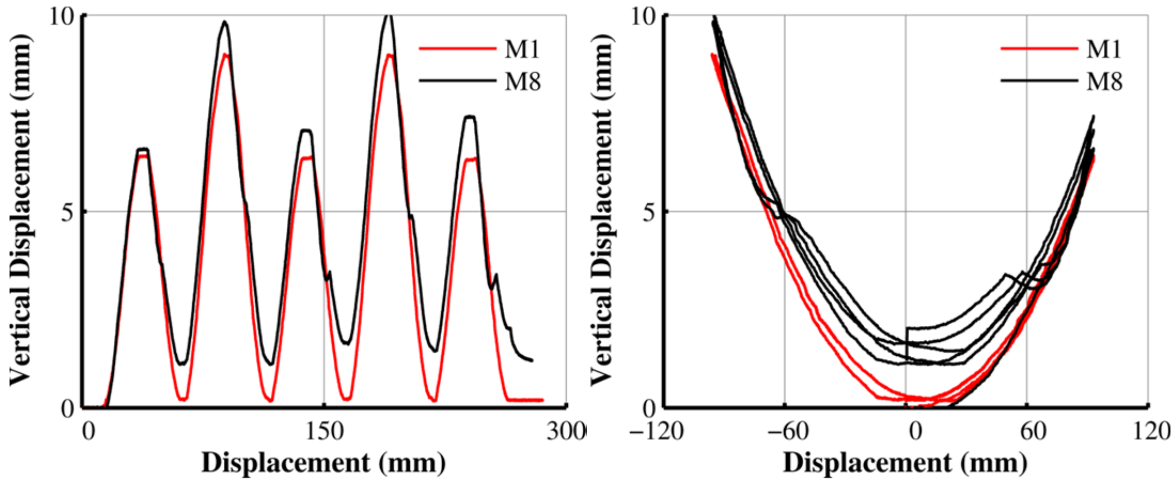

Figure 3-12: Vertical displacement histories of isolators with a) low friction material M1 on surfaces 1 and 4 and b) high friction material M8 on surfaces 1 and 4

Permanent vertical displacements such as those shown in Figure 3-12 can cause redistribution of the axial loads on the isolators after the seismic shaking ends. As an example, Figure 3-13 shows the vertical load on the four isolators (calculated using the procedure described in Section 2.2) at the start of consecutive shake table tests conducted for the three-story model structure. There is vertical load re-distribution at the conclusion of tests 2 and 13, 14 and again at 15, when the bearings returned to their original condition. Note that the load shifts so that more load is carried by the two bearings along the diagonal NE-SW and less load by the bearings on the diagonal NW-SE. Such shift in the load can easily occur due to the large vertical stiffness of the bearings and the large stiffness on the base-mat supporting the structure on top of the bearings. Under such conditions, small differences in the height of the bearings affect the distribution of load. These small differences in height are due to misalignments, small differences in friction values even for otherwise identical bearings and slightly different initial conditions for the bearings.

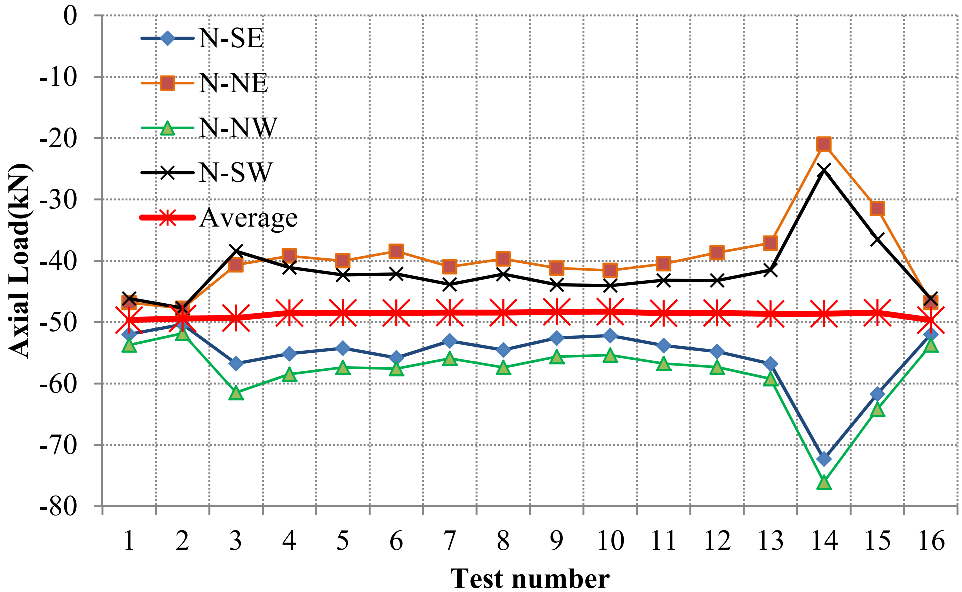

Figure 3-13: Normal load values recorded at the start of consecutive shake table tests

SECTION 4
SHAKE TABLE TESTING RESULTS

4.1 Introduction

This section presents experimental results of the shake table testing of the 3-story structure shown in Figure 2-1 to Figure 2-3 as follows:

1. Section 4.2 presents results for the fixed structure that are used to identify the superstructure properties.
2. Section 4.3 presents a testing summary and description of the ground motions used for the shake table tests of the isolated structure.
3. Section 4.4 presents results for the isolated structure for low (displacements <50mm) and moderate (displacements <100mm) amplitude ground motions.
4. Section 4.5 presents results for the isolated structure subjected to strong ground motions that result in stiffening of the isolators and in some cases contact with the restrainers.
5. Section 4.6 presents results that investigate the effect of the vertical component of ground motions on the horizontal response of the isolation system and superstructure.

4.2 Fixed-base Structure

Prior to testing the isolated structure, the superstructure was identified by directly connecting the base, without the isolators, on the load cells (see Figure 2-3) and subjecting it to shake table motion. For the identification of the superstructure properties, the shake table was driven in white noise motion with frequency content of 0 to 50Hz, amplitude of 0.1g and 60 second duration. The transfer functions were obtained (see Bracci et al., 1992 for a description of the process) using records of acceleration recorded at each floor and the shake table. They are shown in Figure 4-1. The mode shape, period and damping ratio of each of the three translational (testing direction) modes of the superstructure were derived from the transfer functions (see Bracci et al., 1992) and are presented in Table 4-1.

Table 4-1: Modal shape, period and damping ratio for three modes of vibration of superstructure obtained in low amplitude white noise testing

Mode No.	Period (sec)	Damping Ratio	Mode Shape		
			1st floor	2nd floor	3rd floor
1st	0.299	0.0862	0.415	0.753	1.000
2nd	0.077	0.0137	1.216	0.816	-1.000
3rd	0.046	0.0078	2.364	-2.199	1.000

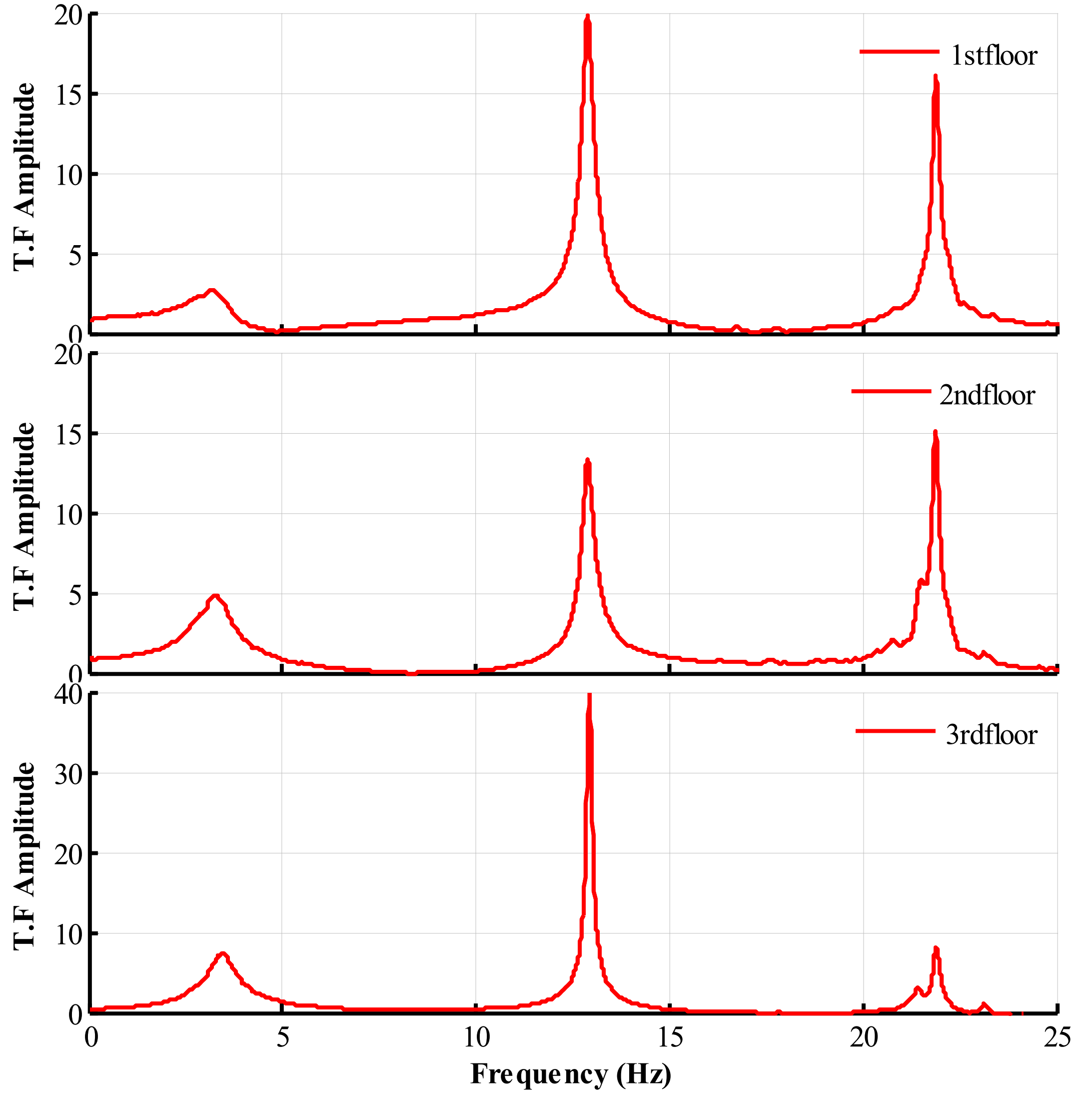

Figure 4-1: Amplitude of transfer functions of superstructure obtained in low amplitude white noise testing

The structure has a high damping ratio in the first mode, something also observed in previous identification of the complete 6-story model (Fenz and Constantinou, 2008e and Wolff and Constantinou, 2004). This is attributed to slippage in the connections of the concrete blocks to the steel frame. The damping is dependent on the amplitude of motion, hence excitation too. It is largest at small amplitude vibration with rich frequency content. The structure was also identified in low amplitude (to prevent yielding) seismic excitation using motion ATL 270 (see Table 4-3). Results are presented in Table 4-2 and Figure 4-2. There is some difference between the two sets of results, which is typical of the difficulties in the identification of models that are not exactly linear elastic and linear viscous.

Table 4-2: Modal shape, period and damping ratio for three modes of vibration of superstructure obtained in low amplitude seismic testing with motion ATL 270

Mode No.	Period (sec)	Damping Ratio	Mode Shape		
			1st floor	2nd floor	3rd floor
1st	0.277	0.0597	0.385	0.746	1.000
2nd	0.077	0.0135	1.217	0.803	-1.000
3rd	0.045	0.0060	2.528	-2.328	1.000

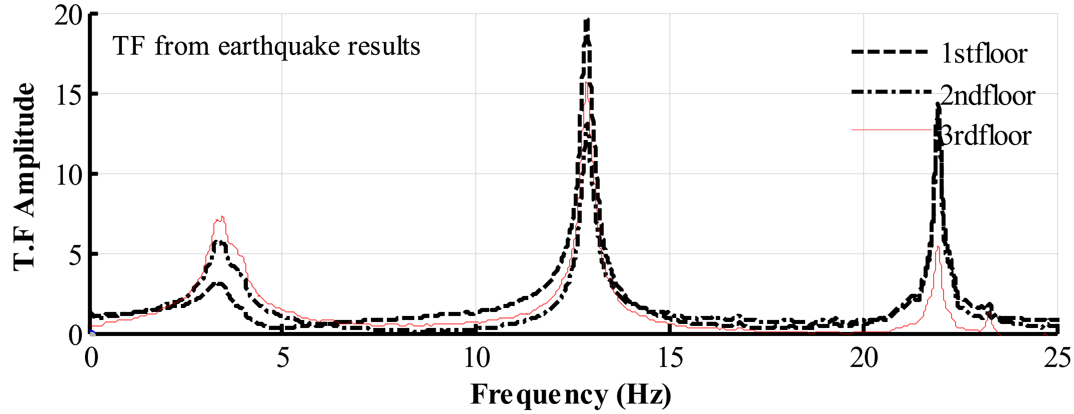

Figure 4-2: Amplitude of transfer functions of superstructure obtained in low amplitude seismic testing with motion ATL 270

4.3 Testing Summary and Selection of Ground Motions

Table 4-3 presents characteristics of the ground motions that were used for the shake table tests. The majority of the ground motions selected for this study have near fault characteristics since these typically impose large displacement demands on isolated structures. Due to similitude requirements, all the ground motions had to be scaled in time by a factor of 0.5. This scale factor alone was not sufficient to cause displacements in the stiffening regimes of the TFP bearings. In order to amplify the effect of the utilized ground motions and excite the structure in Regime V, scales in time larger than 0.5 and scales in accelerations larger than 1.0 were used, which distorted similitude.

The following should be noted about the results that are presented in Section 4:

1. Displacements and accelerations were directly measured by string pots and accelerometers, respectively. Relative displacements were calculated by subtracting the records of displacements at two points.
2. All results presented here are un-processed with the exception of a digital 50Hz low pass filter that was applied directly by the data acquisition system.
3. The vertical acceleration of the base-mat and shake table was calculated using the average of the measurements of four accelerometers that were located at the four opposite corners of the base-mat and shake table.

4. The normalized base shear was calculated from records of acceleration after multiplication by the effective masses and addition over the height of the model (F_{acc} as given by Equation (2-1)) and dividing by the sum of the instantaneous vertical load measured by the four load cells. Small fluctuations in the normalized base shear loops occur because of a) errors in measurements of the vertical force by the load cells, and b) variations of friction due to pressure changes. Large fluctuations typically occur because of uplift of the structure, which was observed in tests that included vertical excitation and are presented in Section 4.6. Note also that the normalized base shear loops are less accurate than the non-normalized loops since they are divided by the sum of the load cell measurements and thus are susceptible to load cell error measurements.

Table 4-3: Ground motions used for the Triple FP testing

Earthquake/ Date	Station	Component Notation	M_w	PGA (g)	PGV (cm/sec)	PGD (cm)
San Fernando 2/1971	CDMG 279 Pacoima Dam, Upper Left Abutment	PUL-164	6.6	1.16	75.6	18.1
Northridge-01 1/1994	CDMG 24514 Sylmar - Olive View Med FF	SYL-360	6.7	0.70	95.4	21.9
Northridge-01 1/1994	USGS/VA 637 LA - Sepulveda VA Hospital	0637-270	6.7	0.80	74.1	16.3
Chi-Chi, Taiwan 9/1999	CWB 9999936 TCU129	TCU-129-E	7.6	0.79	47.3	38.7
Kobe 1/1995	JMA 99999 KJMA	KJM-000	6.9	0.71	77.8	18.9
Northridge-01 1/1994	CDMG 24279 Newhall - Fire Station	NWH-360	6.7	0.70	81.8	26.1
N. Palm Springs 07/1986	USGS 5231 Anza - Tule Canyon	ATL-270	6.06	0.10	7.27	0.73
M_w: Moment Magnitude, PGA: Peak Ground Acceleration, PGV: Peak Ground Velocity, PGD: Peak Ground Displ.						

4.4 Isolated Structure Results for Low and Moderate Amplitude Excitations

This section presents results for configurations tested with selected ground motions of low and moderate amplitude so that the isolators did not exhibit stiffening. A complete set of results is presented in Appendix A. For this set of tests, there was no vertical component of earthquake applied to the structure apart from some unintentional high frequency vertical excitation that existed in all tests. Table 4-4 presents the recorded peak response quantities for selected ground motions and for Configurations A, B and C. The response quantities are: (a) Base (or Isolator) displacement, (b) Inter-story drift as percentage of story height, (c) Floor and base acceleration, and (d) Base shear force (BS).

Figure 4-3 to Figure 4-8 presents results on base shear-base displacement loops, drift histories and floor 5%-damped acceleration spectra for selected ground motions for each of the tested configurations. Additional results are presented in the appendices. Note that the time scale factors reported herein are applied to the time step of the model scaled ground motion. For example, the test designation SYL360 (0.5/1.3) denotes that ground motion SYL360 was applied in the longitudinal direction, the original acceleration values were multiplied by factor 0.5 and the duration of the motion scaled for similitude was additionally multiplied by factor 1.3 (that is, the original motion was first compressed in time by factor 2 for similitude and then the duration was further multiplied by factor 1.3).

Table 4-4: Peak response quantities in tests with low and moderate amplitude ground motions

Ground Motion	Multiplier		Base displacement (mm)[3]				Story drift (% of height)			Floor acceleration (g)				BS (kN)[4]
	A[1]	t[2]	In.	Max	Res	Ch.	1	2	3	Base	1	2	3	
Configuration A														
SYL360	1.0	1.0	2	86	-2	88	0.31	0.39	0.54	0.51	0.41	0.42	0.48	56
SYL360	0.5	1.3	-4	38	-12	33	0.22	0.33	0.32	0.36	0.39	0.42	0.43	34
PUL164	0.5	1.0	-7	26	-8	18	0.20	0.25	0.19	0.40	0.37	0.38	0.38	28
PUL164	1.0	1.0	-8	62	-9	57	0.28	0.41	0.27	0.48	0.44	0.50	0.55	42
PUL164	0.8	1.4	-8	95	10	103	0.32	0.54	0.29	0.47	0.46	0.45	0.54	63
NWH360	0.5	1.0	-8	19	0	27	0.20	0.23	0.18	0.21	0.26	0.23	0.28	34
NWH360	1.0	1.0	1	45	-5	46	0.24	0.38	0.27	0.34	0.33	0.33	0.38	38
NWH360	1.5	1.0	-2	82	-1	85	0.37	0.43	0.36	0.50	0.46	0.52	0.45	53
KJM000	0.5	1.0	-4	17	-2	15	0.26	0.26	0.19	0.27	0.28	0.33	0.35	31
KJM000	1.0	1.0	-2	40	0	38	0.33	0.41	0.24	0.35	0.34	0.39	0.43	37
KJM000	1.5	1.0	3	71	1	67	0.32	0.55	0.35	0.42	0.45	0.44	0.56	48
637270	0.5	1.0	0	22	5	22	0.23	0.33	0.16	0.24	0.26	0.27	0.32	35
637270	1.0	1.0	5	45	5	41	0.26	0.41	0.21	0.32	0.33	0.36	0.39	41
TCU129E	1.0	2.0	1	68	2	69	0.33	0.48	0.41	0.44	0.47	0.46	0.63	46
Configuration B														
SYL360	0.5	1.0	0	25	1	25	0.21	0.27	0.16	0.29	0.27	0.25	0.35	23
SYL360	1.0	1.0	1	76	-2	77	0.24	0.39	0.30	0.36	0.33	0.32	0.39	41
SYL360	0.5	1.3	-3	36	0	33	0.20	0.27	0.21	0.26	0.27	0.30	0.30	33
PUL164	1.0	1.0	-2	66	-3	64	0.24	0.36	0.25	0.36	0.37	0.36	0.48	39
PUL164	0.5	1.4	23	87	22	65	0.20	0.35	0.25	0.30	0.36	0.34	0.32	40
KJM000	0.5	1.5	0	42	1	42	0.21	0.28	0.17	0.26	0.23	0.24	0.28	35
KJM000	1.0	1.5	-5	88	-6	85	0.32	0.46	0.31	0.34	0.31	0.36	0.41	46
KJM000	1.0	1.0	15	52	18	56	0.26	0.36	0.23	0.36	0.29	0.31	0.42	39
TCU129E	1.0	1.0	22	46	24	23	0.26	0.36	0.22	0.41	0.42	0.36	0.47	28
NWH360	0.5	1.0	14	36	16	22	0.22	0.26	0.21	0.20	0.19	0.22	0.25	31
NWH360	1.0	1.0	16	64	9	50	0.22	0.35	0.24	0.31	0.27	0.27	0.34	39
637270	0.5	1.8	-1	82	5	83	0.19	0.40	0.19	0.27	0.26	0.29	0.31	44
637270	0.5	1.0	5	28	10	23	0.15	0.27	0.13	0.19	0.21	0.19	0.25	28
637270	1.0	1.0	10	55	14	45	0.22	0.39	0.17	0.26	0.28	0.35	0.31	38
Configuration C														
SYL360	0.5	1.0	0	19	4	19	0.26	0.40	0.26	0.58	0.31	0.42	0.53	28
SYL360	1.0	1.0	4	55	-1	55	0.27	0.36	0.29	0.50	0.40	0.40	0.61	38
SYL360	1.0	1.2	7	92	12	98	0.29	0.39	0.34	0.58	0.38	0.44	0.58	42
PUL164	0.5	1.4	-2	26	2	28	0.30	0.37	0.28	0.56	0.57	0.55	0.62	33
637270	0.5	1.8	9	66	3	56	0.23	0.43	0.24	0.32	0.27	0.30	0.42	37
NWH360	0.5	1.5	-3	34	4	37	0.29	0.36	0.25	0.31	0.28	0.34	0.43	34
KJM000	0.5	1.5	0	40	1	40	0.30	0.44	0.33	0.40	0.36	0.38	0.59	37
TCU129E	0.5	2.0	5	19	-2	20	0.40	0.41	0.31	0.45	0.37	0.42	0.64	32

1. **A** multiplies accelerations of original ground motion
2. **t** multiplies time step of the ground motion in addition to the 0.5 factor that is applied due to similitude
3. **In.** is the initial, **Res** is the residual and **Ch.** is the maximum change of the base displacement (with respect to In.)
4. Base Shear

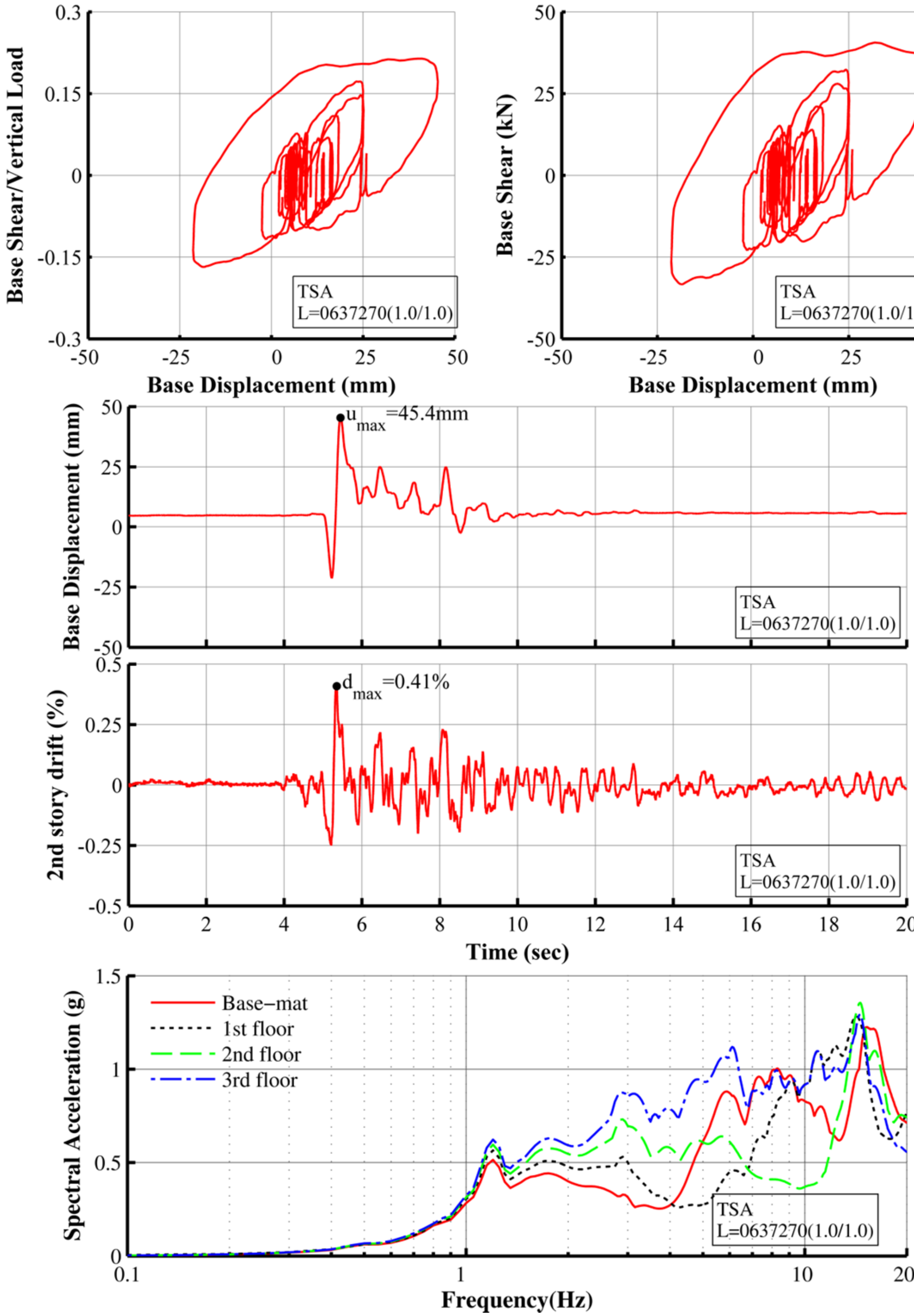

Figure 4-3: Experimental results for Configuration A and ground motion 0637-270 scaled by factors 1.0 in acceleration and 1.0 in time

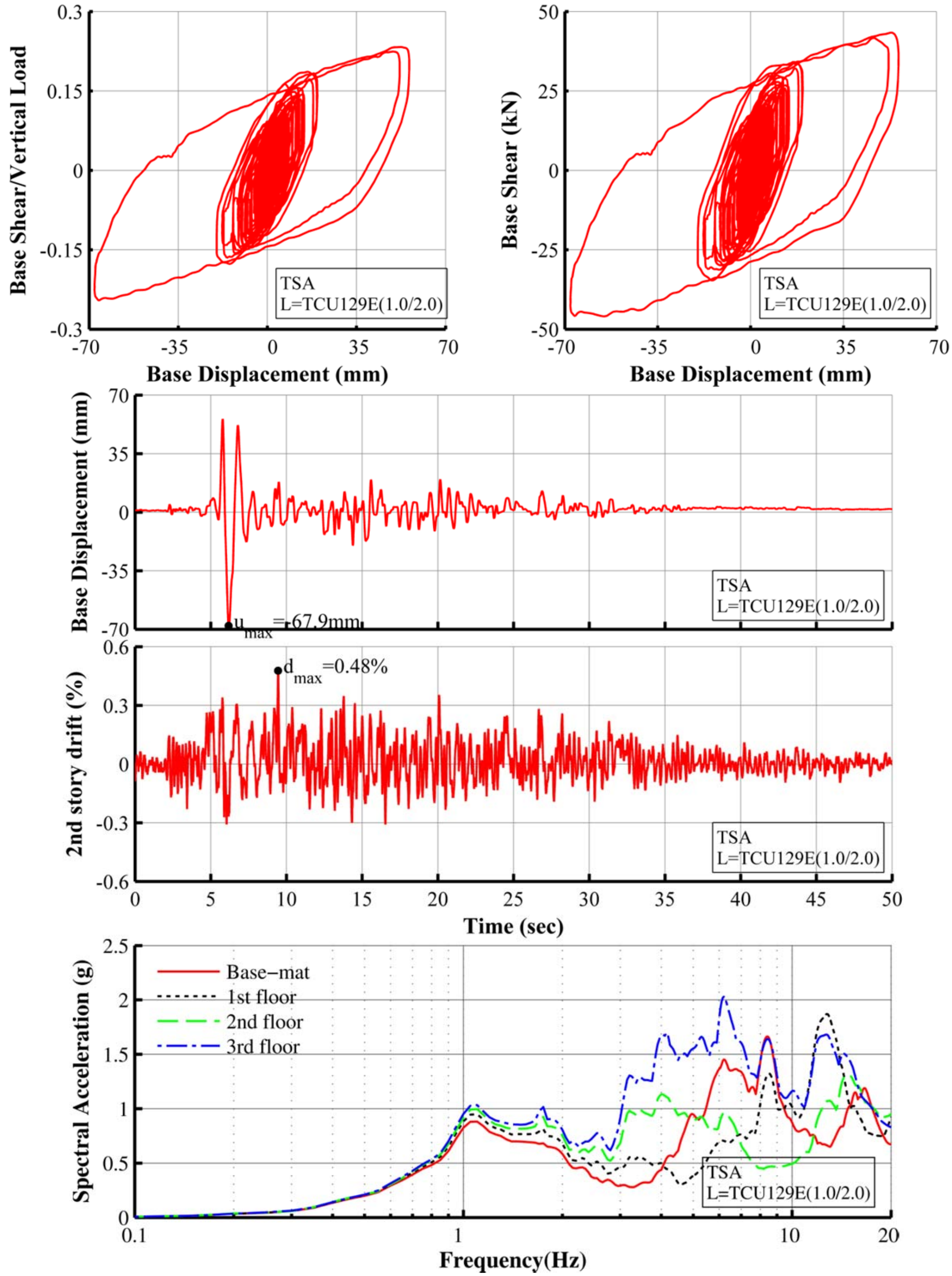

Figure 4-4: Experimental results for Configuration A and ground motion TCU-129-E scaled by factors 1.0 in acceleration and 2.0 in time

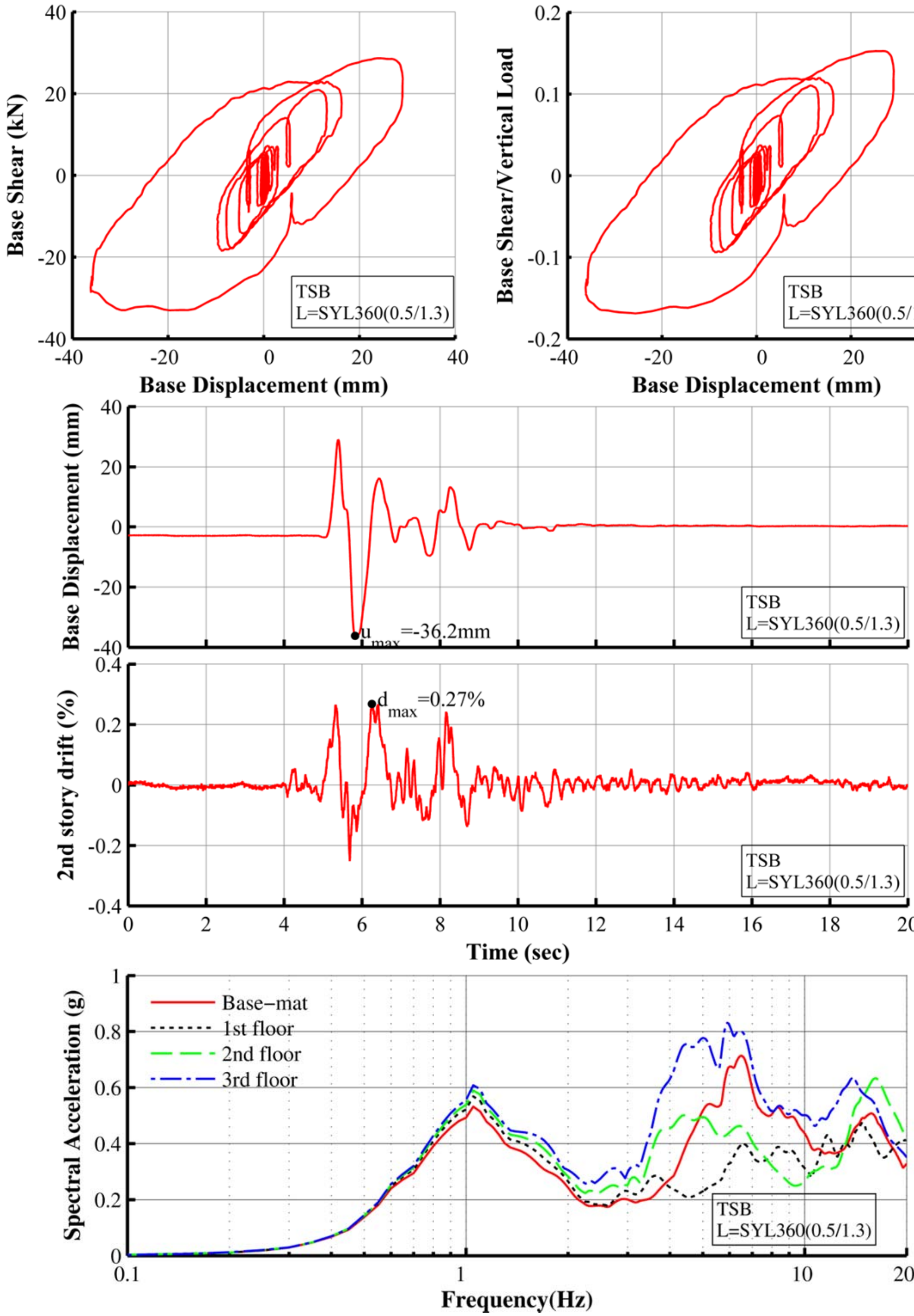

Figure 4-5: Experimental results for Configuration B and ground motion SYL-360 scaled by factors 0.5 in acceleration and 1.3 in time

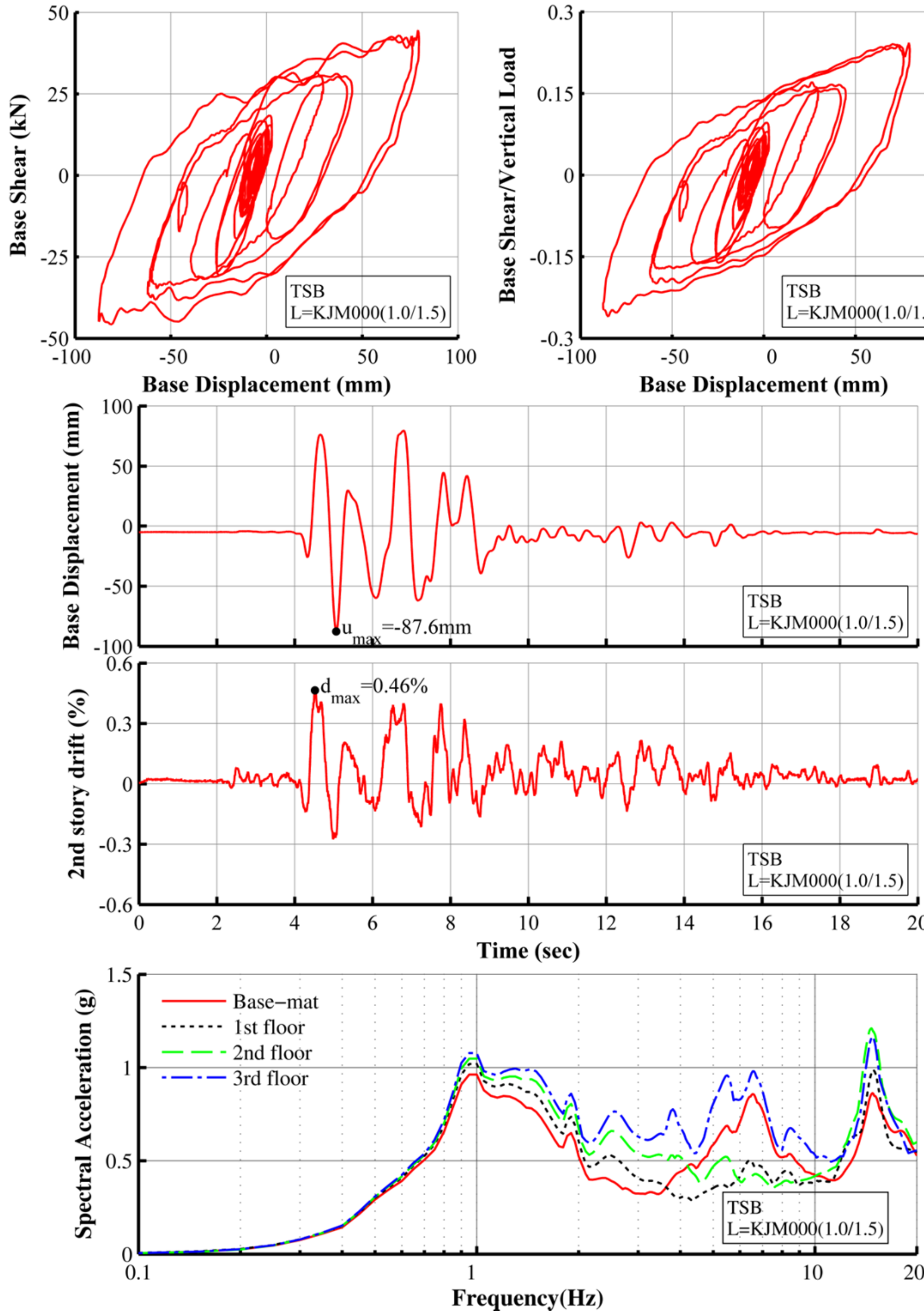

Figure 4-6: Experimental results for Configuration B and ground motion KJM-000 scaled by factors 1.0 in acceleration and 1.5 in time

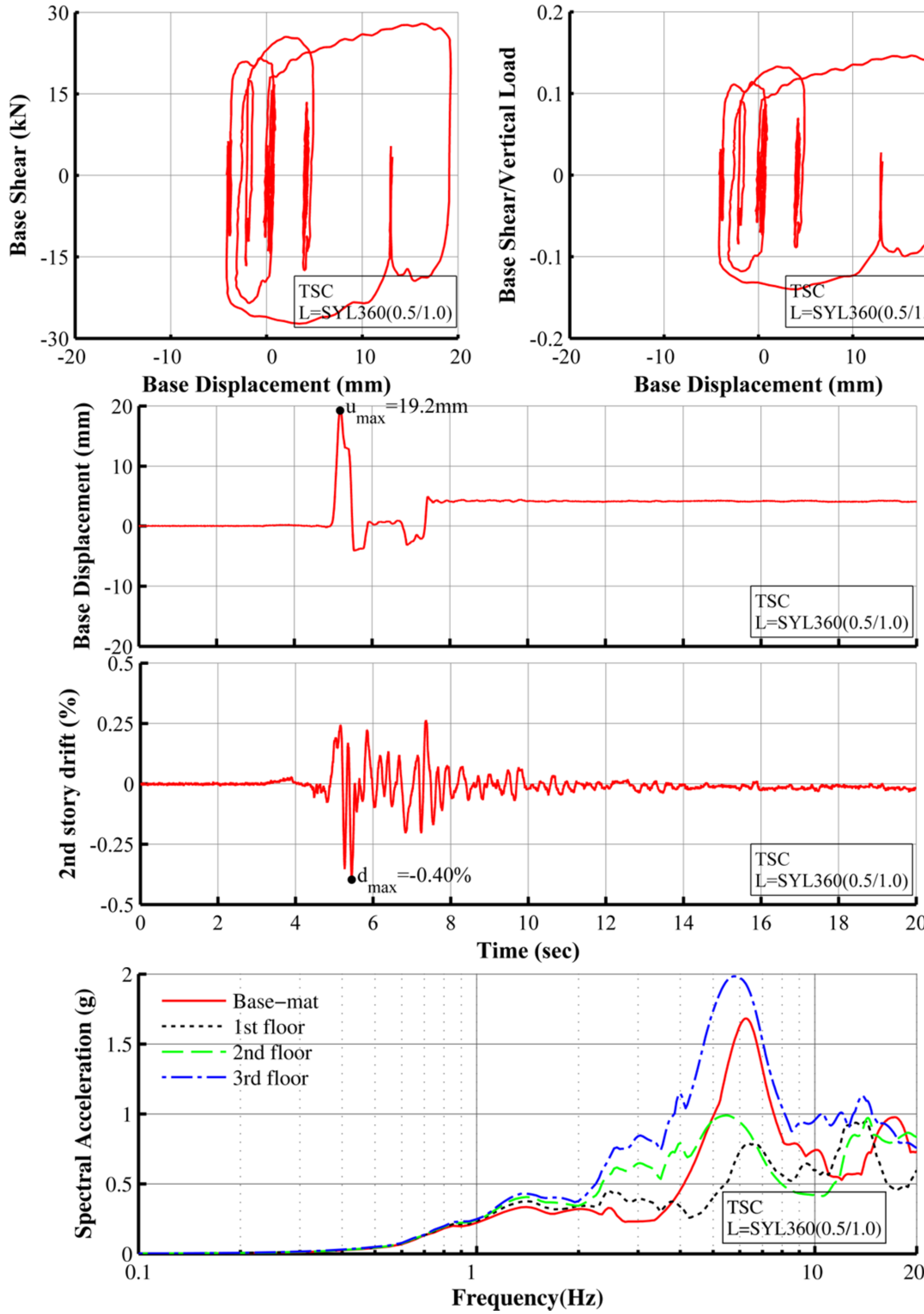

Figure 4-7: Experimental results for Configuration C and ground motion SYL-360 scaled by factors 0.5 in acceleration and 1.0 in time

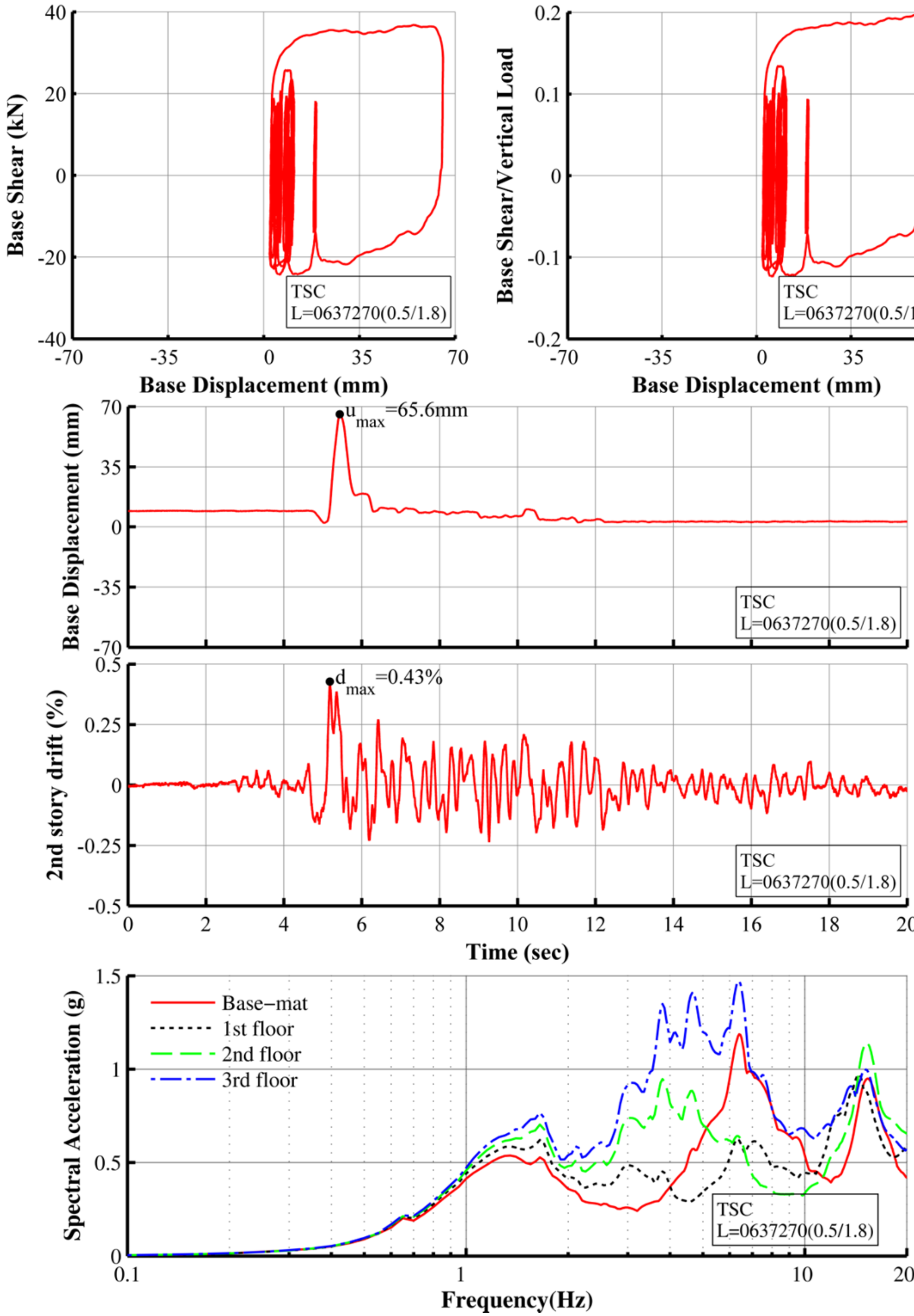

Figure 4-8: Experimental results for Configuration C and ground motion KJM-000 scaled by factors 0.5 in acceleration and 1.8 in time

4.5 Isolated Structure Results for High Amplitude Excitations

This section presents results of shake table tests with strong excitations so that the isolators exhibited stiffening (Regimes IV and V) and contact with the restrainer rings. There was no vertical excitation in this group of tests apart from some very high frequency parasitic vertical excitation. Table 4-5 presents experimental results of peak response quantities for all tested configurations for which the isolators exhibited stiffening.

Table 4-5: Peak response quantities for high amplitude motions

Ground Motion	Multiplier		Base displacement (mm)[3]				Story drift (% of height)			Floor acceleration (g)				BS[4] (kN)
	A[1]	t[2]	In.	Max	Res	Ch.	1	2	3	Base	1	2	3	
SYL360	1.1	1.3	-6	143	5	137	0.34	0.54	0.49	0.71	0.58	0.74	0.75	83
637270	1.0	1.5	9	111	25	102	0.33	0.52	0.31	0.53	0.49	0.50	0.60	70
TCU129E	1.2	2.0	2	102	-17	103	0.53	0.49	0.75	0.50	0.47	0.42	0.46	60
PUL164	1.0	1.4	10	154	31	143	0.44	0.70	0.58	0.66	0.63	0.64	0.72	103
Configuration B														
SYL360	1.0	1.3	-2	138	8	136	0.27	0.43	0.49	0.61	0.56	0.64	0.53	64
PUL164	1.0	1.3	1	135	17	134	0.43	0.57	0.35	0.44	0.41	0.45	0.51	62
PUL164	0.8	1.4	20	143	25	123	0.37	0.52	0.49	0.58	0.50	0.47	0.51	71
NWH360	0.7	1.8	4	117	13	113	0.38	0.49	0.33	0.35	0.38	0.39	0.40	58
NWH360	0.8	1.6	-1	115	24	117	0.33	0.52	0.32	0.47	0.45	0.54	0.56	61
KJM000	0.9	1.8	-3	123	-7	120	0.43	0.51	0.42	0.57	0.53	0.52	0.54	61
637270	1.0	1.5	10	124	22	114	0.30	0.46	0.26	0.48	0.40	0.46	0.46	60
637270	0.8	1.8	21	158	5	137	0.72	0.94	0.84	1.23	0.93	0.91	0.80	131
Configuration C														
637270	0.8	1.8	-4	140	-3	144	0.32	0.68	0.54	0.92	0.74	0.76	0.82	93
NWH360	1.2	1.5	2	113	0	115	0.38	0.44	0.38	0.37	0.42	0.44	0.56	47
KJM000	1.5	1.3	-7	104	-8	111	0.40	0.60	0.40	0.50	0.51	0.56	0.72	45
PUL164	0.5	2.0	1	107	5	107	0.34	0.44	0.37	0.64	0.64	0.68	0.77	47
PUL164	1.1	1.4	7	122	40	115	0.35	0.39	0.38	0.45	0.61	0.58	0.44	52

1. **A** multiplies accelerations of original ground motion
2. **t** multiplies time step of the ground motion in addition to the 0.5 factor that is applied due to similitude
3. **In.** is the initial, **Res** is the residual and **Ch.** is the maximum change of the base displacement (with respect to In.)
4. Base Shear

Figure 4-9 to Figure 4-11 present results on base shear-base displacement loops, drift histories, floor acceleration histories, bearing axial load histories and floor 5%-damped acceleration spectra for one ground motion for each of the tested configurations. Additional results are presented in the appendices. Note that the time scale factors reported herein are applied to the time step of the model scaled ground motion. For example, the test designation SYL360 (0.5/1.3) denotes that ground motion SYL360 was applied in the longitudinal direction, the original acceleration values were multiplied by factor 0.5 and the duration of the motion scaled for similitude was additionally multiplied by factor 1.3 (that is, the original motion was first compressed in time by factor 2 for similitude and then the duration was further multiplied by factor 1.3). Also, Figure 4-12 presents frames captured from the video of the motion of isolator TFP-1 (located on the SE corner; see Figure 2-7) where the isolator exhibits its maximum displacement for the test designated 0637270(0.8/1.8). Graphs of results for this test are shown in Figure 4-10. A complete set of results is presented in Appendix A.

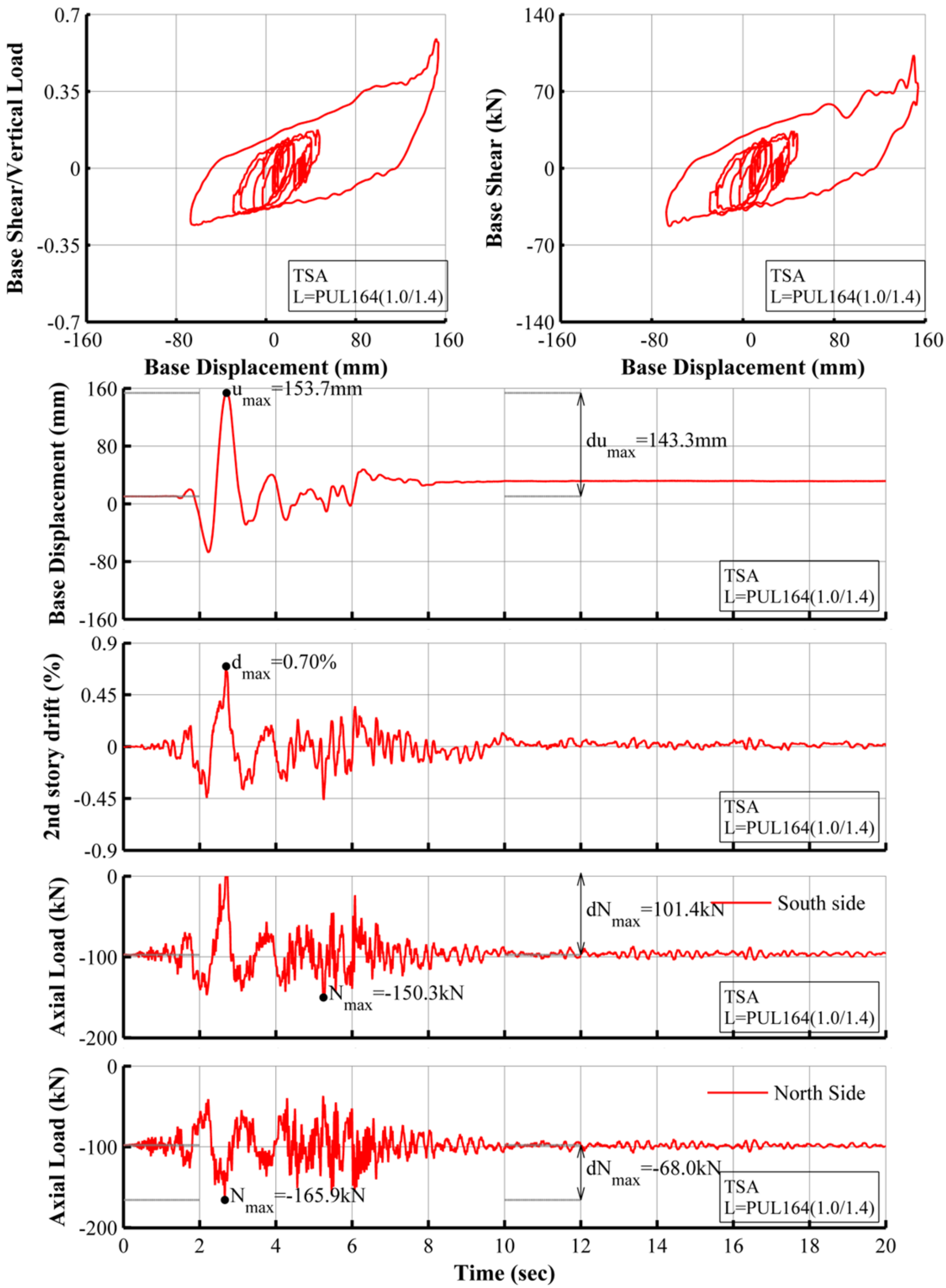

Figure 4-9: Experimental results for Configuration A and ground motion PUL-164 scaled by factors 1.0 in acceleration and 1.4 in time

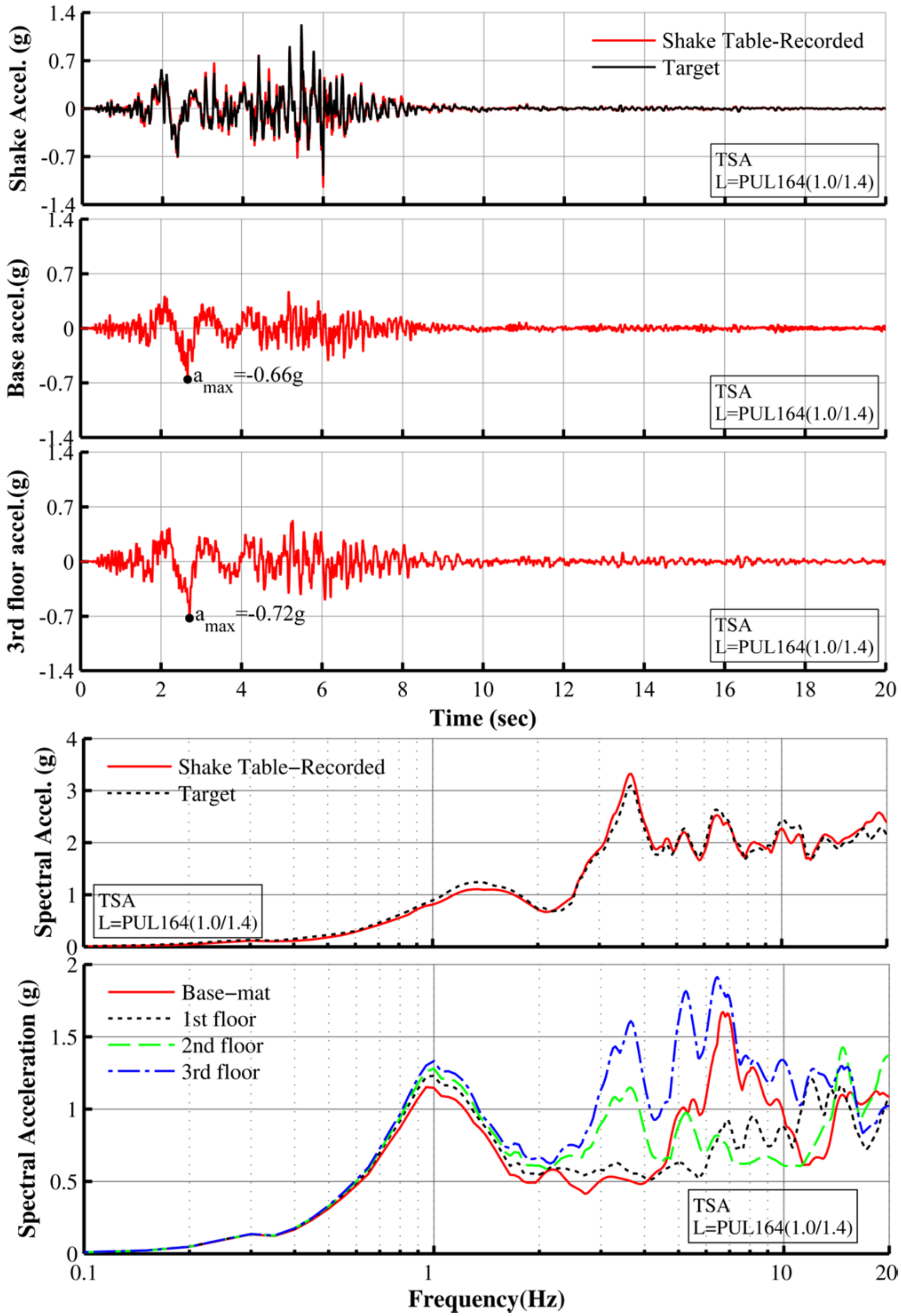

Figure 4-9 (cont'd): Experimental results for Configuration A and ground motion PUL-164 scaled by factors 1.0 in acceleration and 1.4 in time

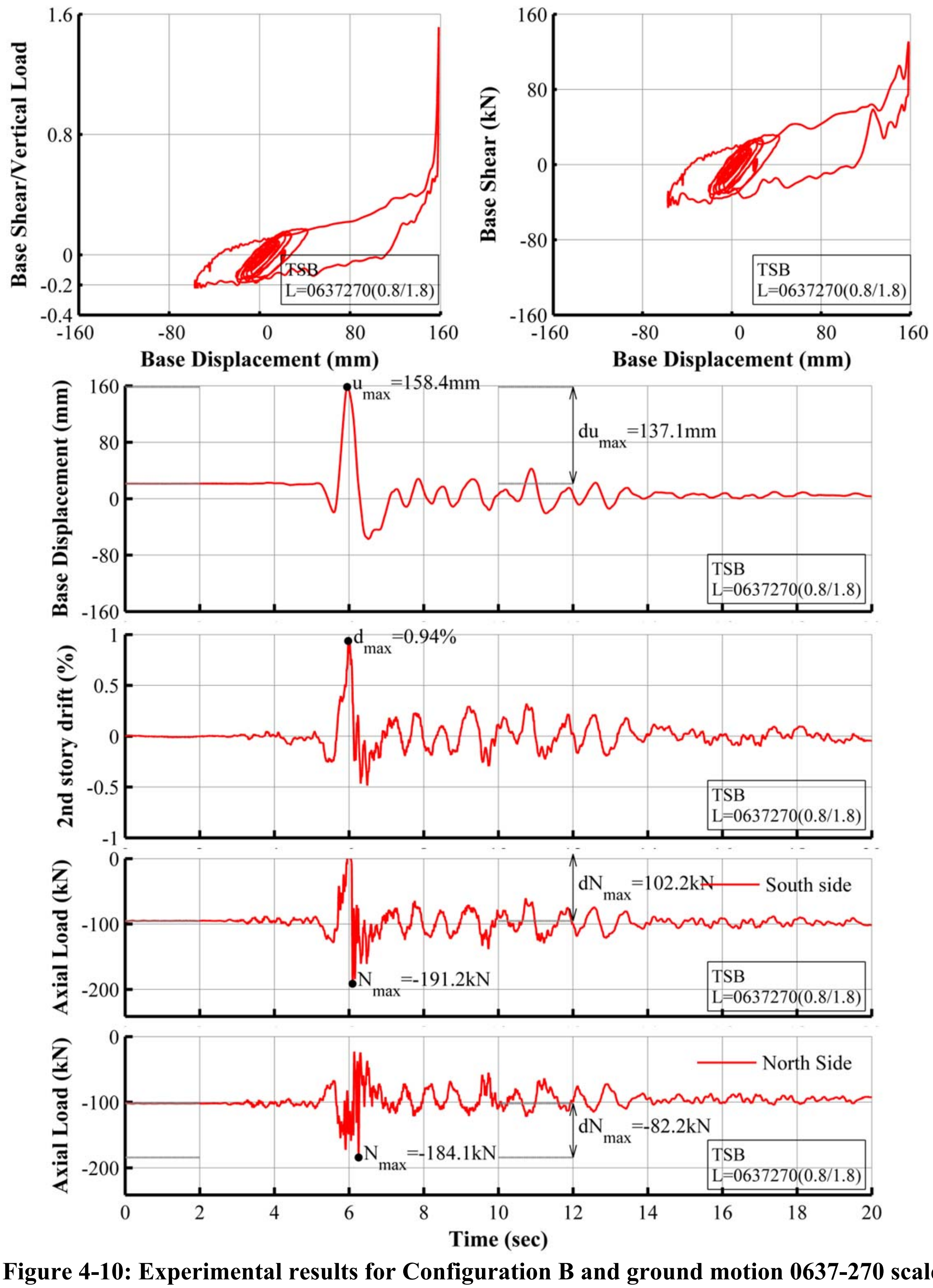

Figure 4-10: Experimental results for Configuration B and ground motion 0637-270 scaled by factors 0.8 in acceleration and 1.8 in time

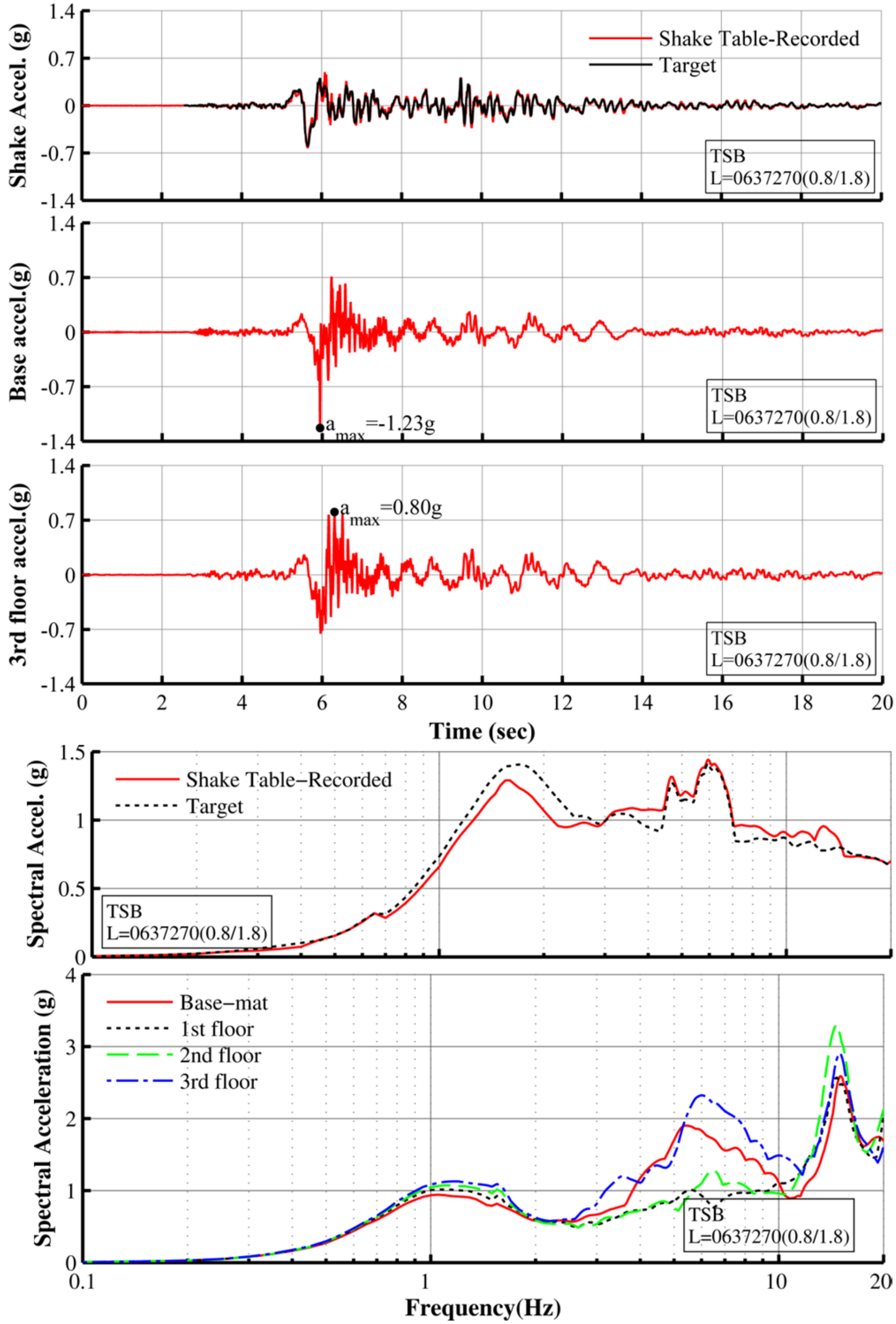

Figure 4-10 (cont'd): Experimental results for Configuration B and ground motion 0637-270 scaled by factors 0.8 in acceleration and 1.8 in time

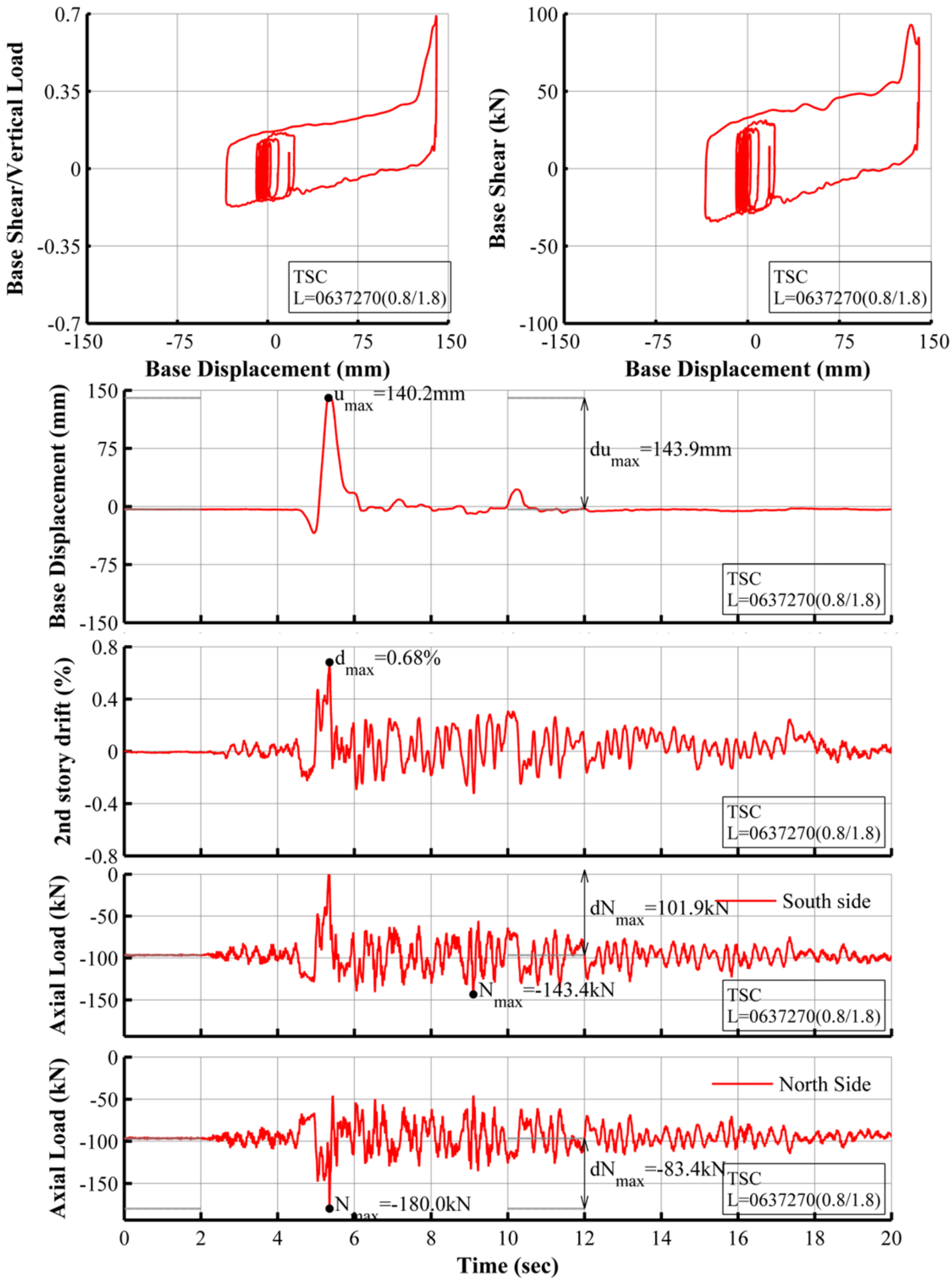

Figure 4-11: Experimental results for Configuration C and motion 0637-270 scaled factors 0.8 in acceleration and 1.8 in time

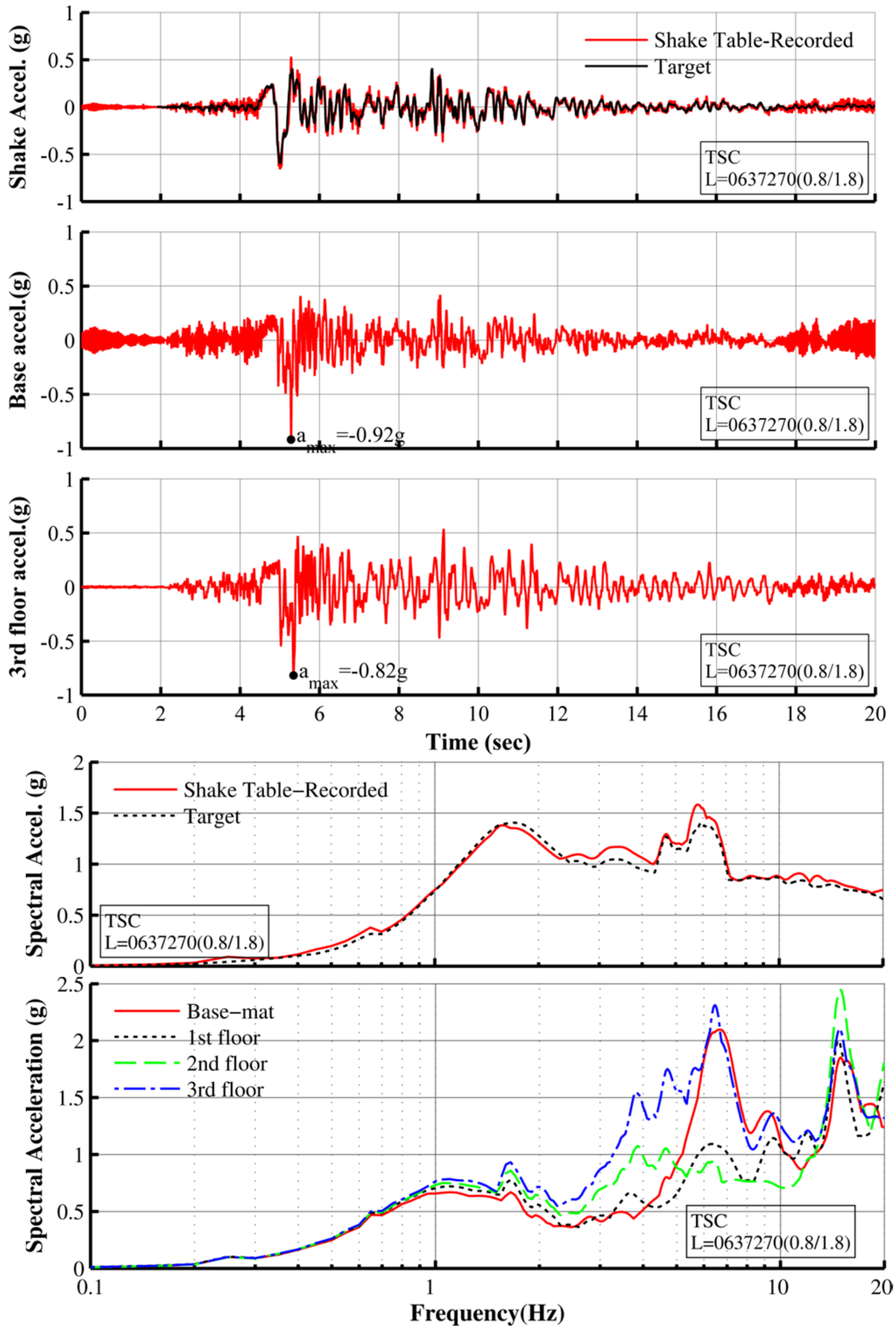

Figure 4-11 (cont'd): Experimental results for Configuration C and ground motion 0637-270 scaled factors 0.8 in acceleration and 1.8 in time

(a) t=0sec (b) t=0.04 (c) t=0.08

(d) t=0.12sec (e) t=0.16 (f) t=0.20

Figure 4-12: Captured frames of TFP isolator motion during maximum deformation for Configuration B and ground motion 0637-270 (results presented in Figure 4-10)

4.6 Isolated Structure Results for Tests with Vertical Component of Ground Motion

This section presents comparisons of experimental results with only horizontal excitation applied in the longitudinal direction (case L) and with combined horizontal and vertical excitation (case L+V).

Peak response results for all tested configurations are presented in Table 4-6. Figure 4-13 to Figure 4-15 present comparison of results (base shear loops, normalized base shear loops, drift histories, acceleration histories and floor spectra) for tests selected from Table 4-6 for one ground motion for each configuration. In Figure 4-13 to Figure 4-15, tests without a vertical component are denoted as “L” and tests with a vertical component are denoted as “L+V”. Graphical results from the remaining tests of Table 4-6 are presented in the Appendices.

Table 4-6: Peak response quantities obtained in horizontal and combined horizontal-vertical excitation

Gr. Motion	Scale		Base Displacement (mm)[3]				Story Drift (% of height)			Floor Acceleration (g)				BS[4] (kN)
	A[1]	t[2]	In.	Max	Res	Ch.	1	2	3	Base	1	2	3	
Configuration A														
L=PUL164	1.0	1.0	-8	62	-9	57	0.28	0.41	0.27	0.48	0.44	0.50	0.55	42
L=PUL164 V=PULUP			-4	61	-8	57	0.33	0.51	0.39	0.90	0.93	0.82	0.87	55
L=NWH360	1.0	1.0	1	45	-5	46	0.24	0.38	0.27	0.34	0.33	0.33	0.38	38
L=NWH360 V=NWHUP			3	45	-4	48	0.26	0.43	0.31	0.65	0.82	0.79	0.75	62
L=KJM000	1.0	1.0	-2	40	0	38	0.33	0.41	0.24	0.35	0.34	0.39	0.43	37
L=KJM000 V=KJMUP			-1	41	0	40	0.40	0.47	0.30	0.52	0.64	0.68	0.57	58
L=0637270	1.0	1.0	5	45	5	41	0.26	0.41	0.21	0.32	0.33	0.36	0.39	41
L=0637270 V=0637UP			7	45	6	38	0.32	0.51	0.27	0.59	0.62	0.62	0.65	49
Configuration B														
L=NWH360	1.0	1.0	16	64	9	50	0.22	0.35	0.24	0.31	0.27	0.27	0.34	39
NWH360 V=NWHUP			1	52	1	51	0.30	0.43	0.28	0.62	0.86	1.04	0.73	54
L=KJM000	1.0	1.0	15	52	18	56	0.26	0.36	0.23	0.36	0.29	0.31	0.42	39
L=KJM000 V=KJMUP			8	47	6	55	0.28	0.42	0.28	0.54	0.51	0.64	0.53	46
L=TCU129	1.0	1.0	22	46	24	23	0.26	0.36	0.22	0.41	0.42	0.36	0.47	28
L=TCU129 V=TCUUP			7	29	3	23	0.23	0.38	0.33	0.40	0.41	0.35	0.48	34
L=637270	1.0	1.0	10	55	14	45	0.22	0.39	0.17	0.26	0.28	0.35	0.31	38
L=637270 V=0637UP			9	54	10	44	0.25	0.35	0.26	0.47	0.76	0.73	0.59	49
L=637270	0.7	1.8	5	129	21	124	0.31	0.50	0.32	0.46	0.39	0.46	0.54	64
L=637270 V=0637UP			15	138	17	123	0.39	0.46	0.43	0.66	0.64	0.77	0.59	70
Configuration C														
L=637270	0.7	1.8	3	112	-3	109	0.30	0.49	0.32	0.40	0.34	0.36	0.54	46
L=637270 V=0637UP			1	98	-2	97	0.35	0.51	0.32	0.69	0.50	0.58	0.56	53
L=KJM000	1.0	1.5	1	68	-3	67	0.32	0.53	0.31	0.42	0.44	0.48	0.59	39
KJM000 V=KJMUP			0	61	-5	61	0.39	0.59	0.35	0.50	0.54	0.52	0.54	50

1. **A** multiplies accelerations of original ground motion
2. **t** multiplies time step of the ground motion in addition to the 0.5 factor that is applied due to similitude
3. **In.** is the initial, **Res** is the residual and **Ch.** is the maximum change of the base displacement (with respect to In.)
4. Base Shear

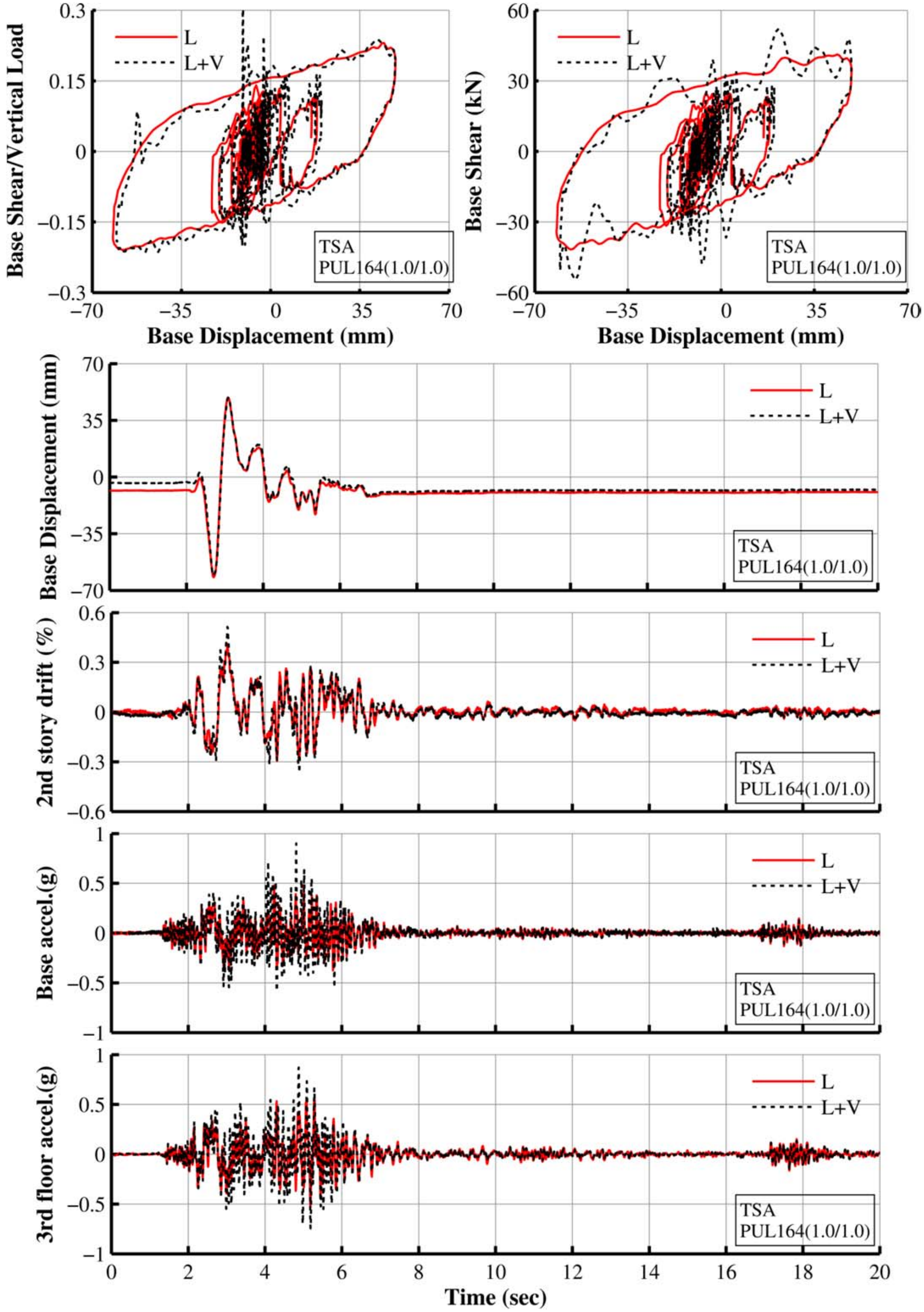

Figure 4-13: Experimental results for Configuration A and ground motion PUL-164 scaled by factors 1.0 in acceleration and 1.0 in time

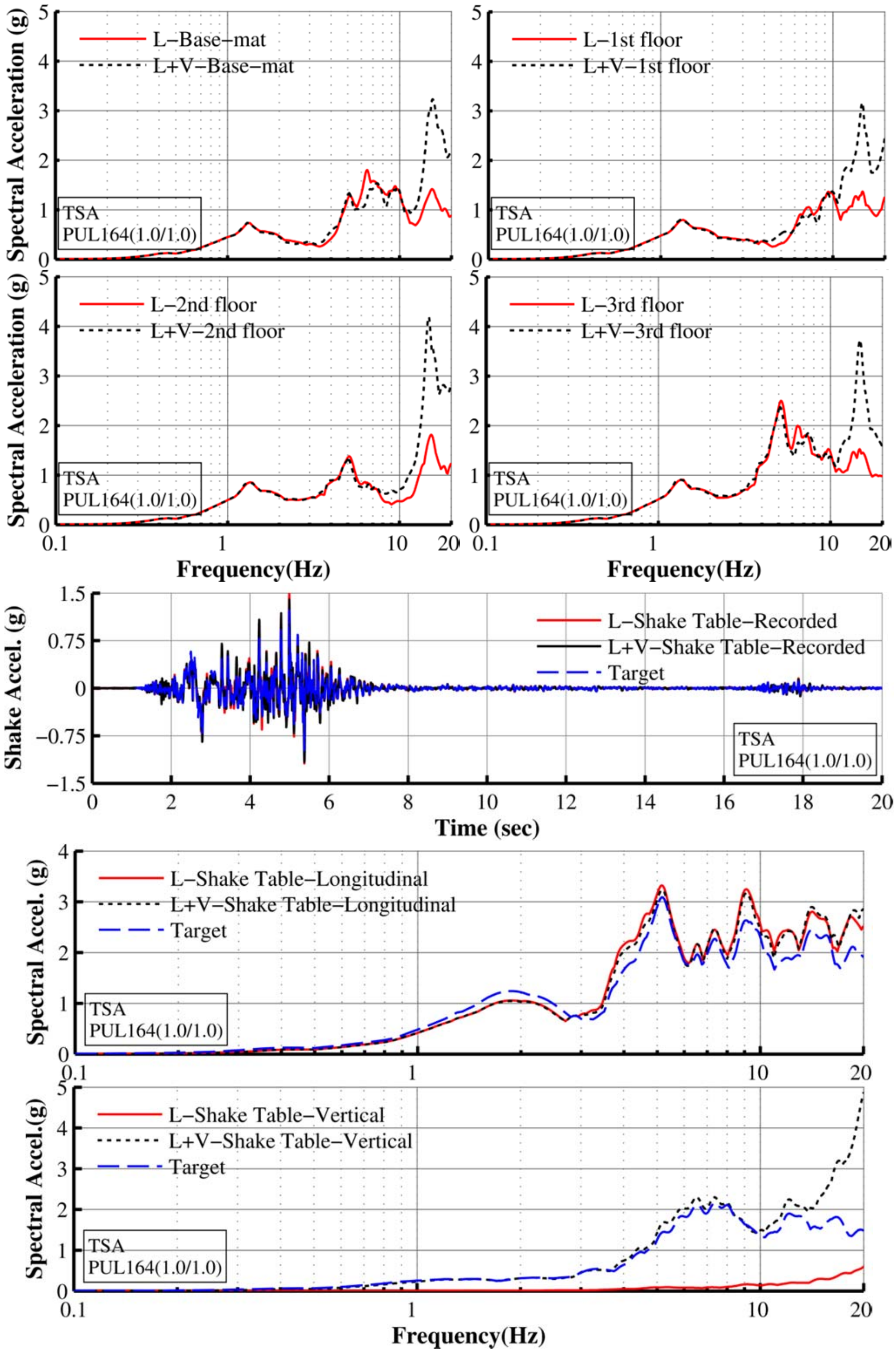

Figure 4-13 (cont'd): Experimental results for Configuration A and ground motion PUL-164 scaled by factors 1.0 in acceleration and 1.0 in time

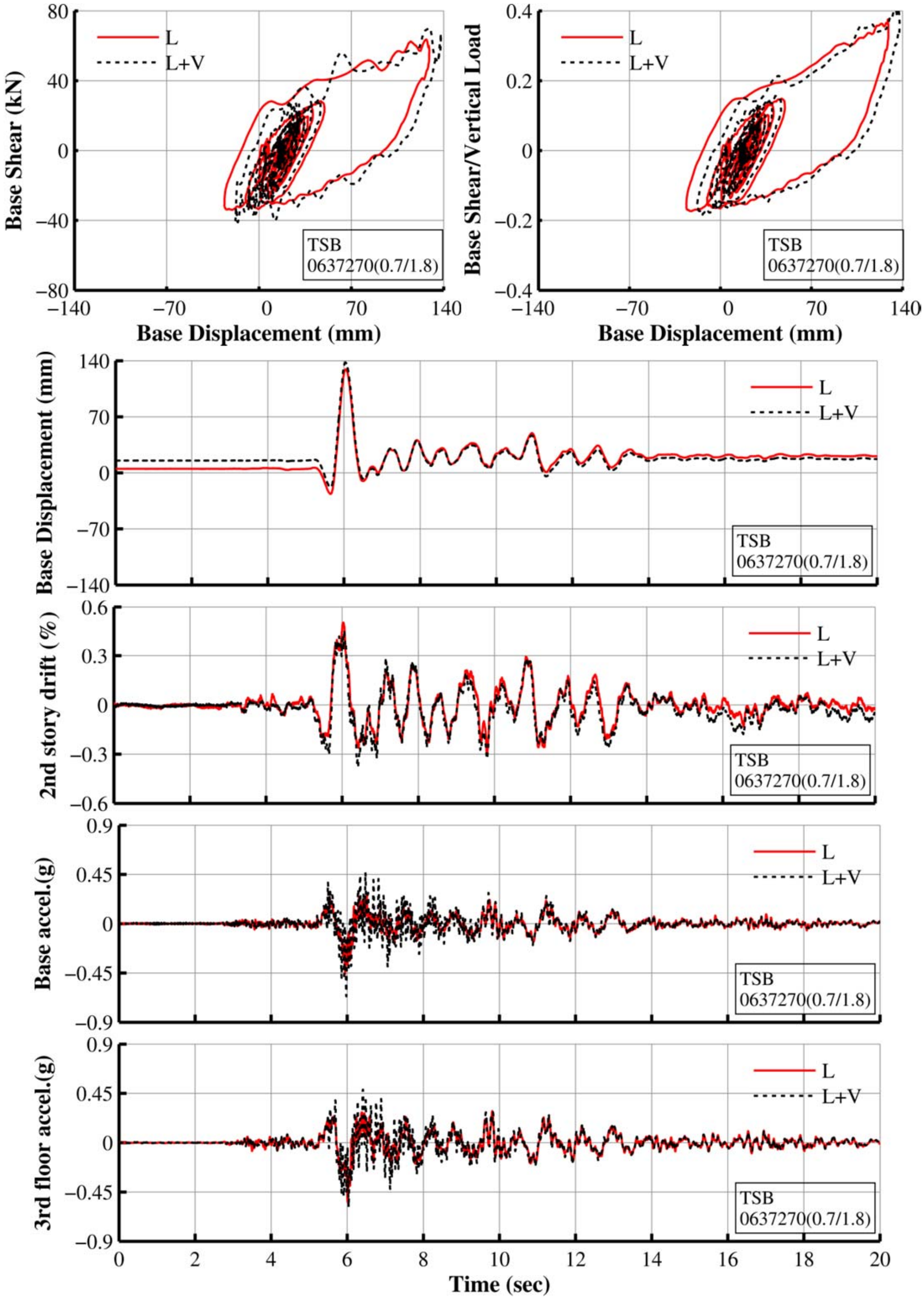

Figure 4-14: Experimental results for Configuration B and ground motion 0637-270 scaled by factors 0.7 in acceleration and 1.8 in time

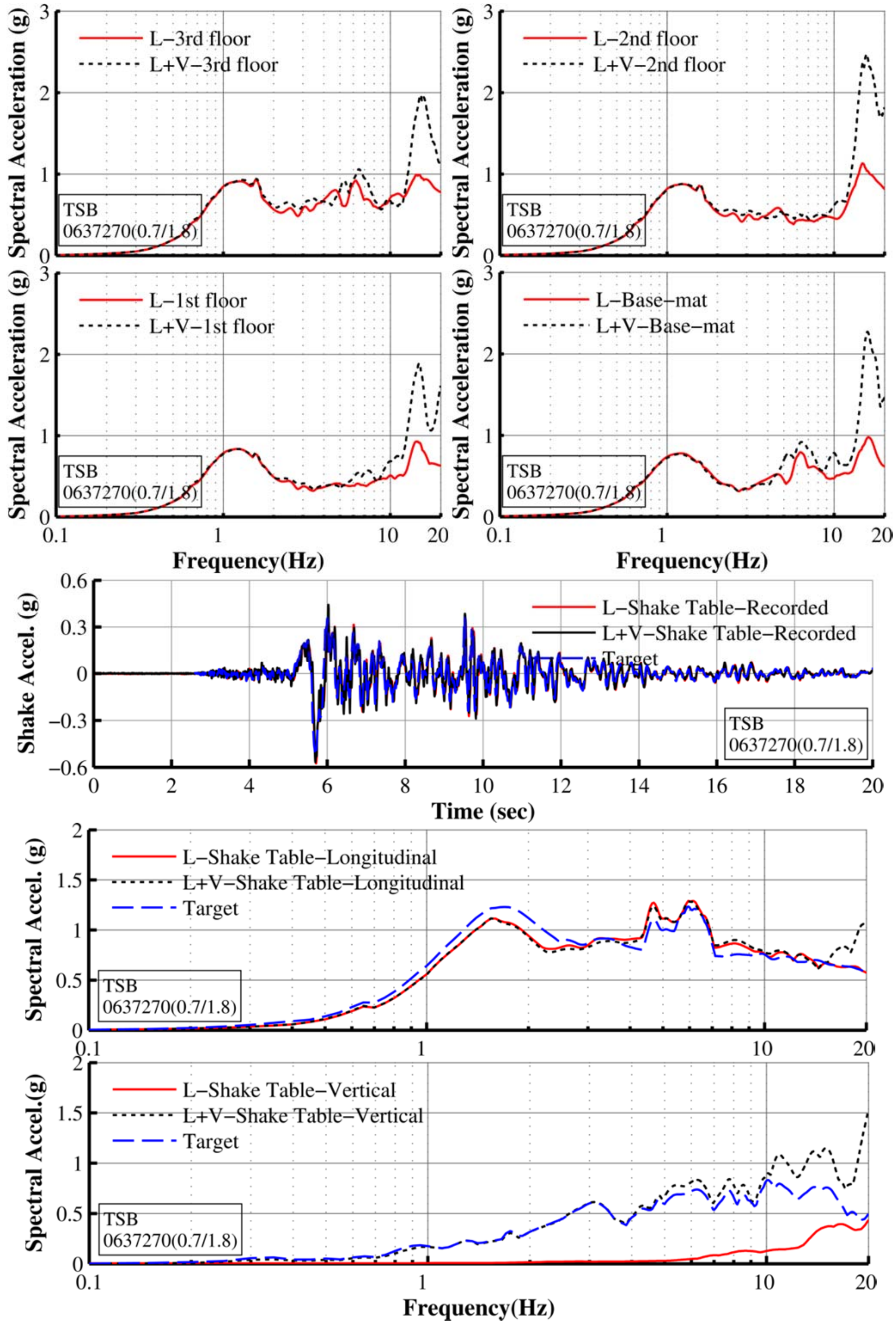

Figure 4-14 (cont'd): Experimental results for Configuration B and ground motion 0637-270 scaled by factors 0.7 in acceleration and 1.8 in time

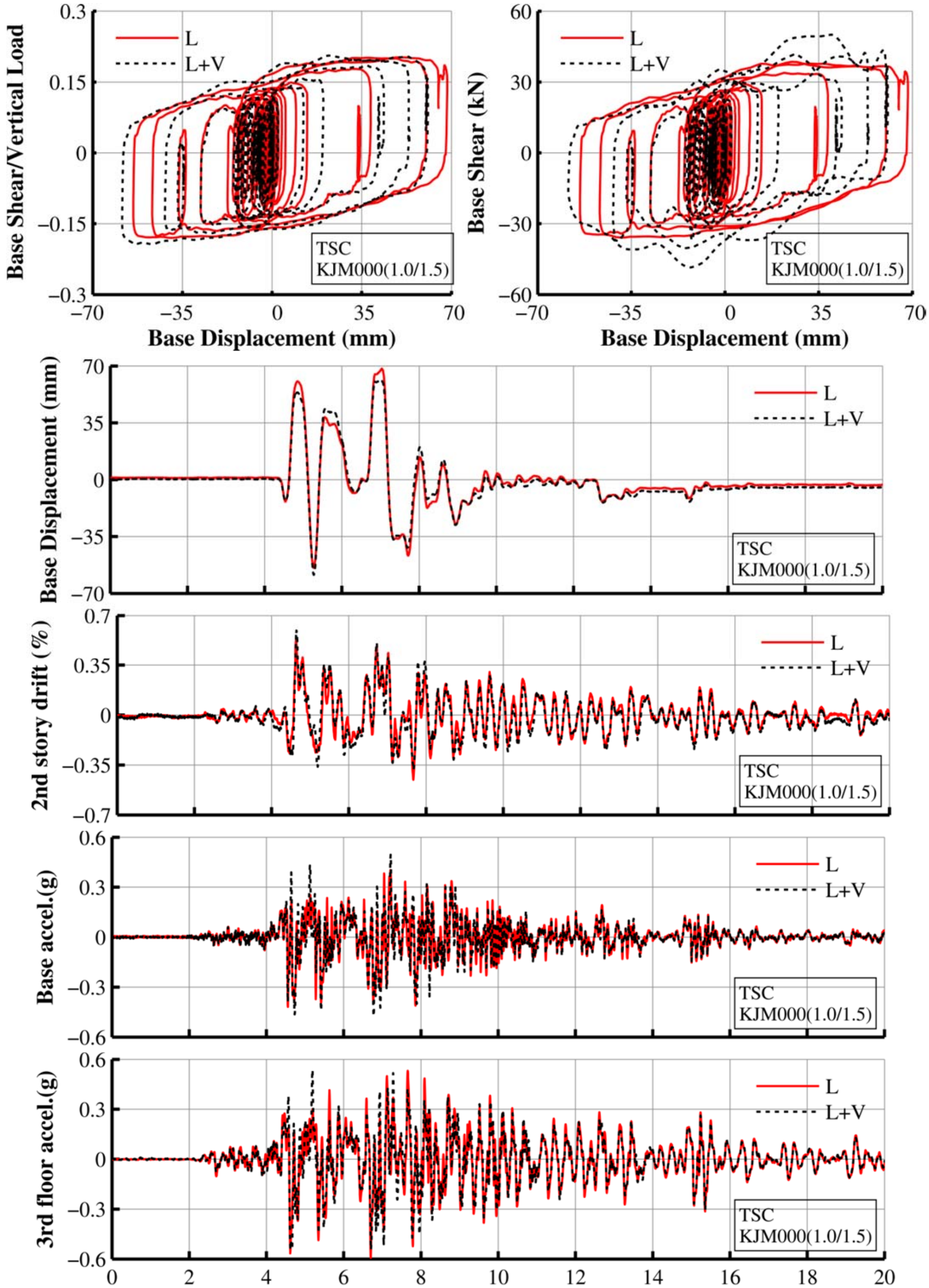

Figure 4-15: Experimental results for Configuration C and ground motion KJM-000 scaled by factors 1.0 in acceleration and 1.5 in time

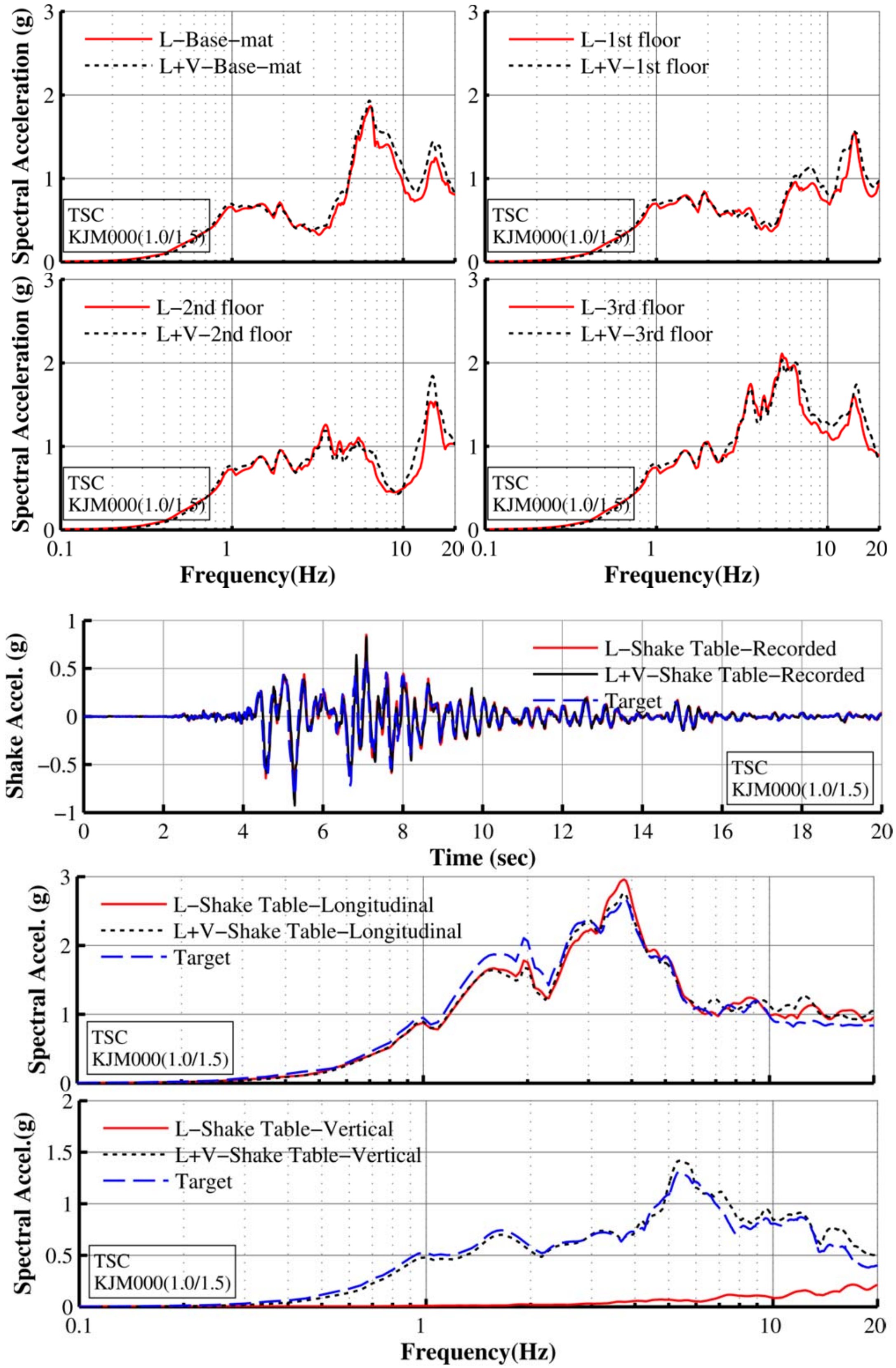

Figure 4-15 (cont'd): Experimental results for Configuration C and ground motion KJM-000 scaled by factors 1.0 in acceleration and 1.5 in time

4.7 Comments on Experimental Results of Sections 4.4 to 4.6

In discussing the experimental results of Sections 4.4 to 4.6, it is important to first comment on the behavior of the three tested Triple FP configurations. Section 5 presents details on the frictional properties of the configurations. In summary, the four isolators exhibited different frictional properties. However, for the discussion herein, the weighted average values for the entire isolation system were used. Table 4-7 presents representative weighted friction values at high velocity for the four sliding surfaces of each of the three tested configurations. They are based on the data in Table 5-1 of Section 5.

Table 4-7: Weighted average friction coefficient values for tested configurations

Friction coefficient	Configuration A	Configuration B	Configuration C
μ_1	0.102	0.108	0.128
μ_2	0.038	0.033	0.228
μ_3	0.038	0.033	0.228
μ_4	0.173	0.155	0.128

Evidently, Configurations A and B are very similar in frictional and geometric properties (see also Table 3-1), characterized by capability to exhibit all five regimes, and to take advantage of the adaptive nature of the Triple FP isolator. Configuration C lacks these attributes and behaves as a high friction (value of 0.128) single FP or a double FP (with equal friction on the two sliding surfaces) isolator but with a final stiffening regime. With this background, the following observations are made from the results reported in Sections 4.4 to 4.6:

1. The results of Section 4.4 show the advantages of the adaptive Configurations A and B over the non-adaptive Configuration C. The advantages are particularly obvious for ground motions KJM000(0.5/1.5), NWH360(0.5/1.0), SYL360(1.0/1.0) and0637270(0.5/1.8) in Table 4-4 where Configurations B and C have the same base shear and base displacements but Configuration B has much less inter-story drifts and floor accelerations. The advantages of adaptive systems over non-adaptive systems have been discussed by Fenz and Constantinou (2008a to e), Morgan (2007) and Morgan and Mahin (2010).

2. In the results of Section 4.5, the isolators experience impact on all restrainer rings (surfaces 1, 2, 3 and 4) in Figure 4-9 and Figure 4-10. Also, as seen in Figure 4-11, the isolators are excited in their Regime V. In all cases, the isolators exhibited stable behavior under these extreme conditions. Also, note that the large shear forces reached in these experiments depend on the strength of the restrainer rings of the triple FP bearings. In the tests, the rings had very high strength that is unlikely to be achieved (or is desirable) in full size bearings. Full size bearings will have limited strength of the rings so that impact, like those experienced in the tests, would have most likely resulted in fracture of the impacted rings of surfaces 2 or 3, which would have limited the shear

force, allowed for some additional displacement and, likely, cause some damage to the sliding material.

As evident in the figures, upon reaching the isolator displacement capacity, the south side of the model uplifted for a short duration as indicated by the vanishing axial load record for the south side. This caused rocking in the structure, which in turn limited the floor accelerations. Moreover, in Figure 4-10 and Figure 4-11, the isolator maximum displacement values are larger than the theoretical displacement capacity of the isolators. As discussed in Section 3.3, Item 2, this is most likely caused by uneven distribution of traction forces on the sliding surfaces that results in torsional motion of the inner parts, which in turn causes changes in the displacement capacities of the internal parts.

3. In some tests and particularly in tests of configuration TSA with motion PUL-164 (1.0/1.0) and TSB with motion 0637-270 (0.7/1.8) (see graphs in Figure 4-13 to Figure 4-15), the vertical ground excitation had an important effect on floor accelerations but insignificant effect on base displacements (consistent with the results of Fenz et al. 2008e, Morgan, 2007 and Becker and Mahin, 2011) and some small effect on inter-story drifts. The floor spectra were also affected but over a limited range of frequencies, larger than about 10Hz in the time scale of the tests. It should also be noted that in the tests with (L+V) and without (L), the vertical ground excitation is not directly comparable due to large differences in parasitic rocking shake table motion in the tests. The rocking motion of the shake table was systematically larger in tests with vertical motion than in tests without it due to limited ability to control the shake table.

SECTION 5
ANALYTICAL PREDICTION OF RESPONSE

5.1 Introduction

This section presents the data on the friction properties of the Triple FP isolators used in the shake table testing, and presents comparisons of experimental results of the tested 3-story model structure to analytical results obtained with programs 3pleANI (Sarlis and Constantinou, 2013) and SAP2000 (Computers and Structures, 2007).

5.2 Identification of Friction Properties

The friction coefficient values for each sliding interface of each bearing used in the testing have been identified. The coefficient of friction is considered to be velocity-dependent and assumed to follow the relation (Constantinou et al., 1990):

$$\mu_i = \mu_{fi} - \left(\mu_{fi} - \mu_{si}\right) e^{-a_i |v_i|} \tag{5-1}$$

In Equation (5-1), μ_{fi} and μ_{si} are the values of the friction coefficient at large velocities (called *fast* herein) and at zero velocity (called *slow* herein), respectively, α_i is a rate parameter that controls the variation with velocity and v_i is the sliding velocity of the *i-th* surface. For identification of the three parameters needed to describe the model of friction of Equation (5-1), the recorded force-displacement loops had to be decomposed to loops of force versus sliding displacement for each sliding interface for at least three different velocities. This enabled the identification of values of the friction coefficients, which were then used to construct analytical force-displacement loops for comparison to the experimentally recorded loops.

For example, Figure 5-1 shows comparisons of experimental results for the isolators of Configuration A and analytical results obtained by the model of Fenz and Constantinou (2008a to e) following identification of the friction coefficient values. The isolators consist of particular interfaces as identified in Section 3.2 of this report. Results are presented for a slow test at frequency of 0.01Hz on the left column and for a fast test at frequency of 0.3Hz on the right column. The friction coefficient values used to construct the analytical loops are presented in each graph. In these graphs, μ_1 denotes the least friction value and μ_4 denotes the largest friction value among the two main sliding interfaces.

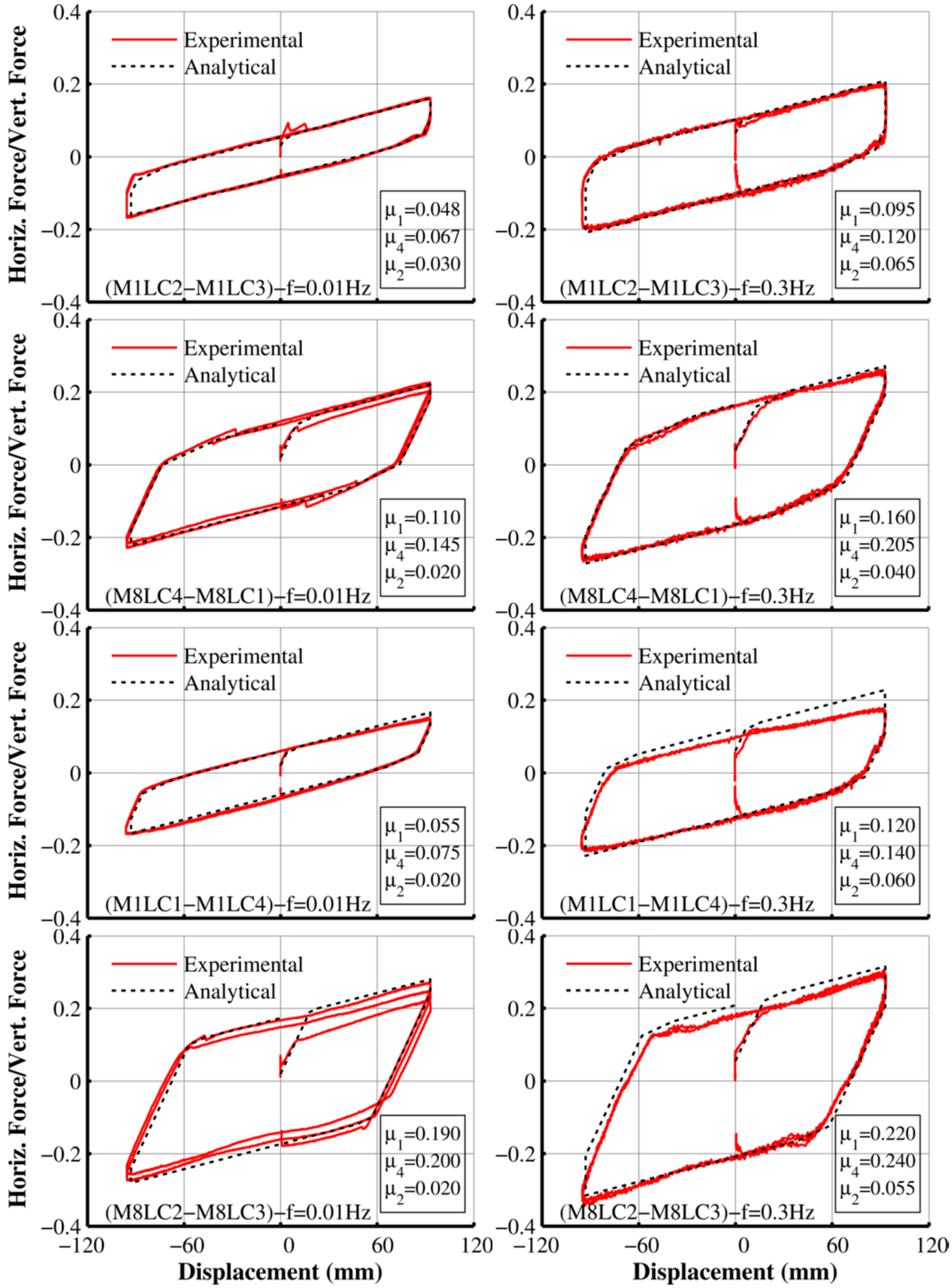

Figure 5-1: Comparison of experimental results obtained from testing of individual isolators and analytical results for Configuration A. Left column presents results at frequency of 0.01Hz; right column for frequency of 0.3Hz

Figure 5-2 presents theoretical force-displacement loops of the isolators of Configuration A using the identified slow and fast friction coefficients values in Figure 5-1. The four isolators are identified by the load cell number (LC1, LC2, LC3 and LC4) with reference to Figure 2-3 for the location of each load cell. The construction of these loops also requires values of the friction coefficient for the sliding interfaces 2 and 3 (see Figure 1-1), which were assumed to be equal. Values of the friction coefficient $\mu_2 = \mu_3$ were also identified from the experimental loops. The rate parameter could not be identified for the Configuration A bearings as there were insufficient test data at intermediate velocities for individual bearings. Rather, shake table test data were utilized. Values of the parameter are presented later in this report.

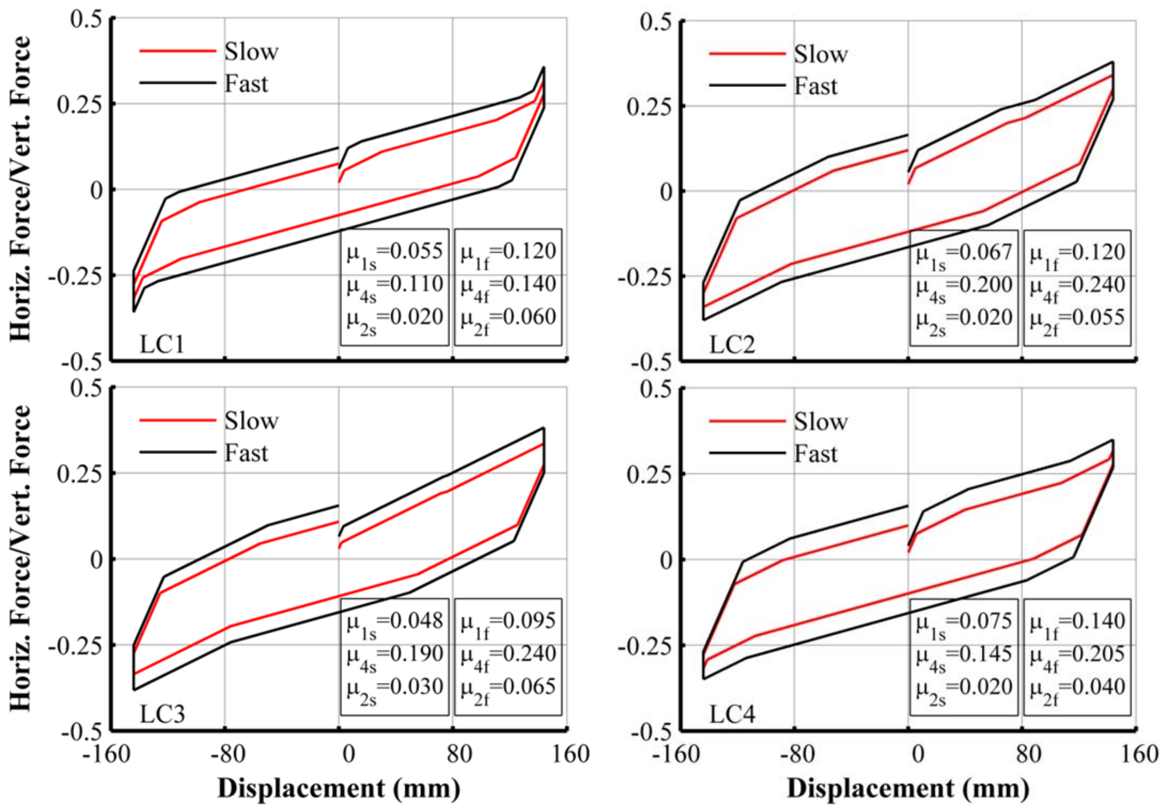

Figure 5-2: Analytical loops for Triple FP isolators of Configuration A

Figure 5-3 presents comparisons of experimental and analytical results for the isolators of Configuration B. TSB1 denotes the isolator that was placed on load cell LC1 (Figure 2-3), TSB2 is the isolator placed on load LC2, etc. Tests were conducted at 0.02Hz frequency (left column of graphs) for the identification of the slow friction coefficient values and at frequency of 0.5Hz (right column of graphs) for the identification of the fast friction coefficient values. The rate parameters were identified using an additional test conducted at 0.1Hz and shown in the center column of the graphs in Figure 5-3. All friction coefficient values were identified from the decomposed loops (force versus the sliding displacement of each surface) as shown in Figure 5-4 (for the same tests as those shown in Figure 5-3). The identified friction coefficient values are presented in each graph of Figure 5-3. Note that the abnormalities in the experimental loops of

TSB2 and TSB4 at frequency of 0.5Hz are caused by uplift of the bearings and therefore division by zero load in the normalization of the lateral force by the vertical load. The identification procedure was based on the decomposed loops of Figure 5-4 and the following considerations:

1. The slow friction coefficient was identified by matching the analytical loop with the minimum width of the experimental loop of each of sliding interfaces 1 and 4, measured at maximum displacement for the tests conducted at 0.02Hz frequency (essentially zero velocity).
2. The fast friction coefficient was identified by matching the analytical loop with the experimental loop at the zero displacement force intercept of each of sliding interfaces 1 and 4 (velocity is maximum) for the tests conducted at 0.5Hz frequency.
3. The slow friction of surfaces 2 and 3 was obtained from the isolator force-displacement loops of Figure 5-3 when velocity reverses sign. On unloading, the drop in force equals to twice the friction force on surfaces 2 and 3 at essentially zero velocity. The fast friction coefficient of surfaces 2 and 3 was difficult to determine so that approximate values were assigned based on a study of the loops of Figure 5-3.

The following are noted in the results of Figure 5-3:

1. The calibrated analytical model cannot capture the experimental behavior well during initial loading as a result of initial offsets of the Triple FP inner parts which existed in most of the tests.
2. Some of the isolators have different properties although they are composed from essentially the same materials. The only possible explanation for this behavior is the effect of contamination of the sliding interfaces with dust and lubricants during the numerous interchanges of parts in the conduction of testing.

Figure 5-5 shows comparisons of the analytical friction coefficient versus sliding velocity graphs to experimental results for surfaces 1 and 4 of the isolators of Configuration B. The experimental data on velocity were obtained by numerical differentiation of the surface displacement histories acquired by the instruments shown in Figure 3-2. The tests utilized in collecting the data in Figure 5-5 are those presented in Figure 5-4 and Figure 5-3. Note that the graphs of Figure 5-5 include information on the rate parameter a in units of sec/mm.

Figure 5-6 presents comparisons of experimental and analytical force-displacement loops for the isolators of Configuration C. Figure 5-7 shows the decomposed loops for the same tests whereas Figure 5-8 shows graphs of the friction coefficient as a function of the surface velocity. For these isolators, the friction coefficient for surfaces 1 and 4 had essentially the same value so that the calibrated model is based on the assumption of equal friction values. Note that in Figure 5-7 the displacements of surfaces 1 and 4 are not exactly equal as they should have been if the friction coefficient values were equal for the two surfaces. However, in this case, the difference is due to initial offsets in the internal components of the isolators at the start of each test. Note that the offset occurs naturally at the conclusion of a test even when the parts are centered at the start of the test. Accordingly, all tests but the first one started with initial offsets.

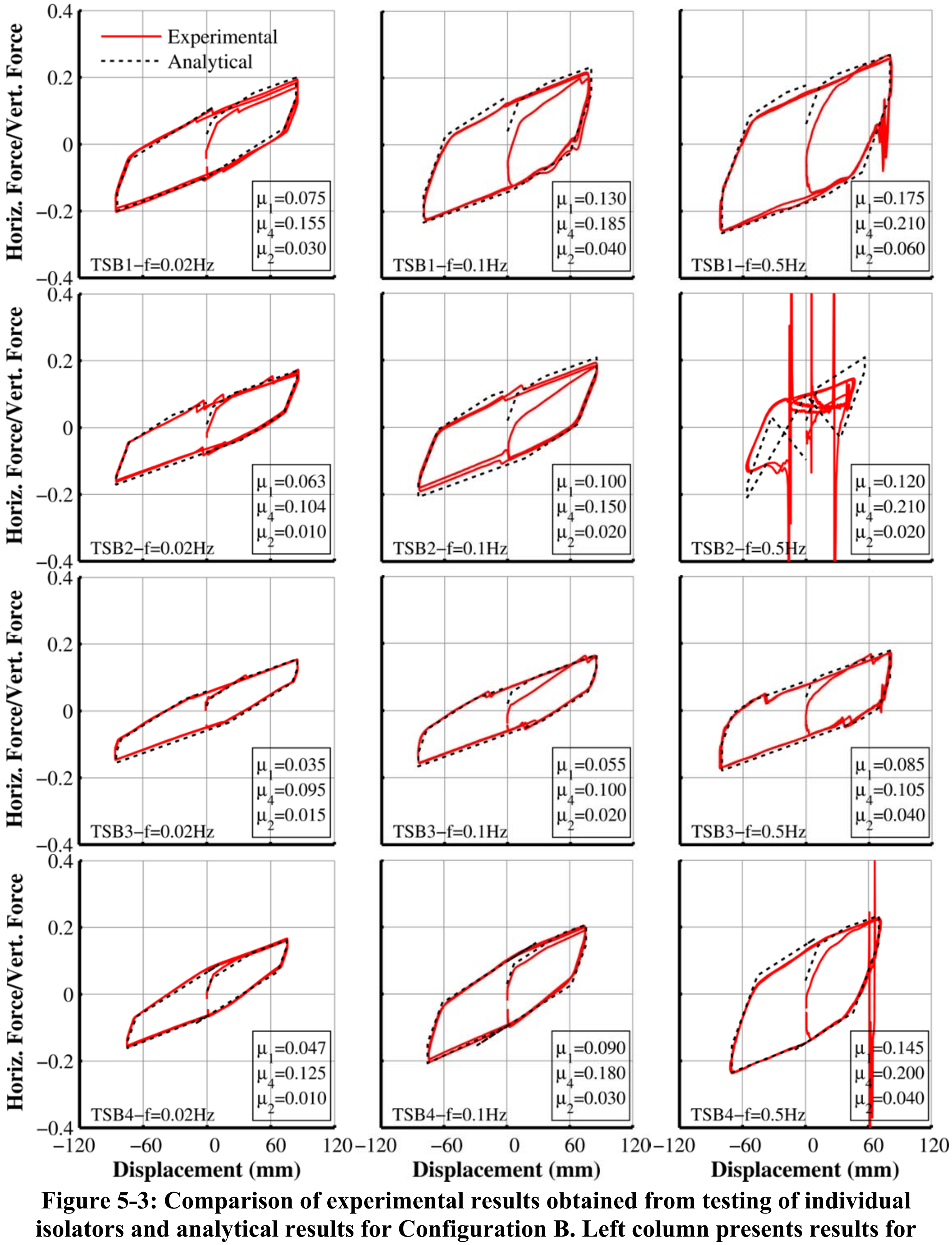

Figure 5-3: Comparison of experimental results obtained from testing of individual isolators and analytical results for Configuration B. Left column presents results for frequency of 0.02Hz; center column for 0.1Hz and right column for 0.5Hz

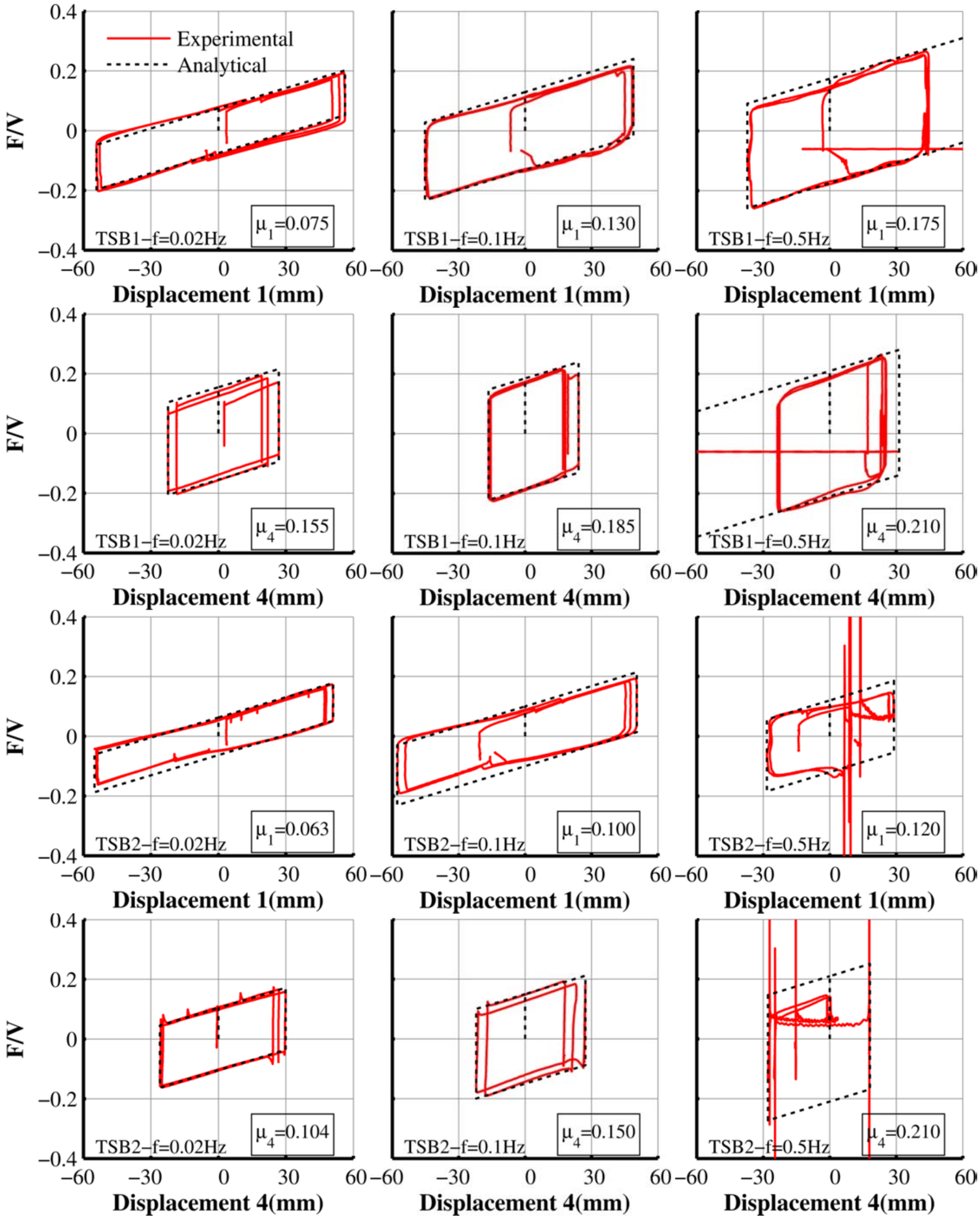

Figure 5-4: Decomposed normalized force versus sliding displacement loops for two isolators of Configuration B at three different excitation frequencies

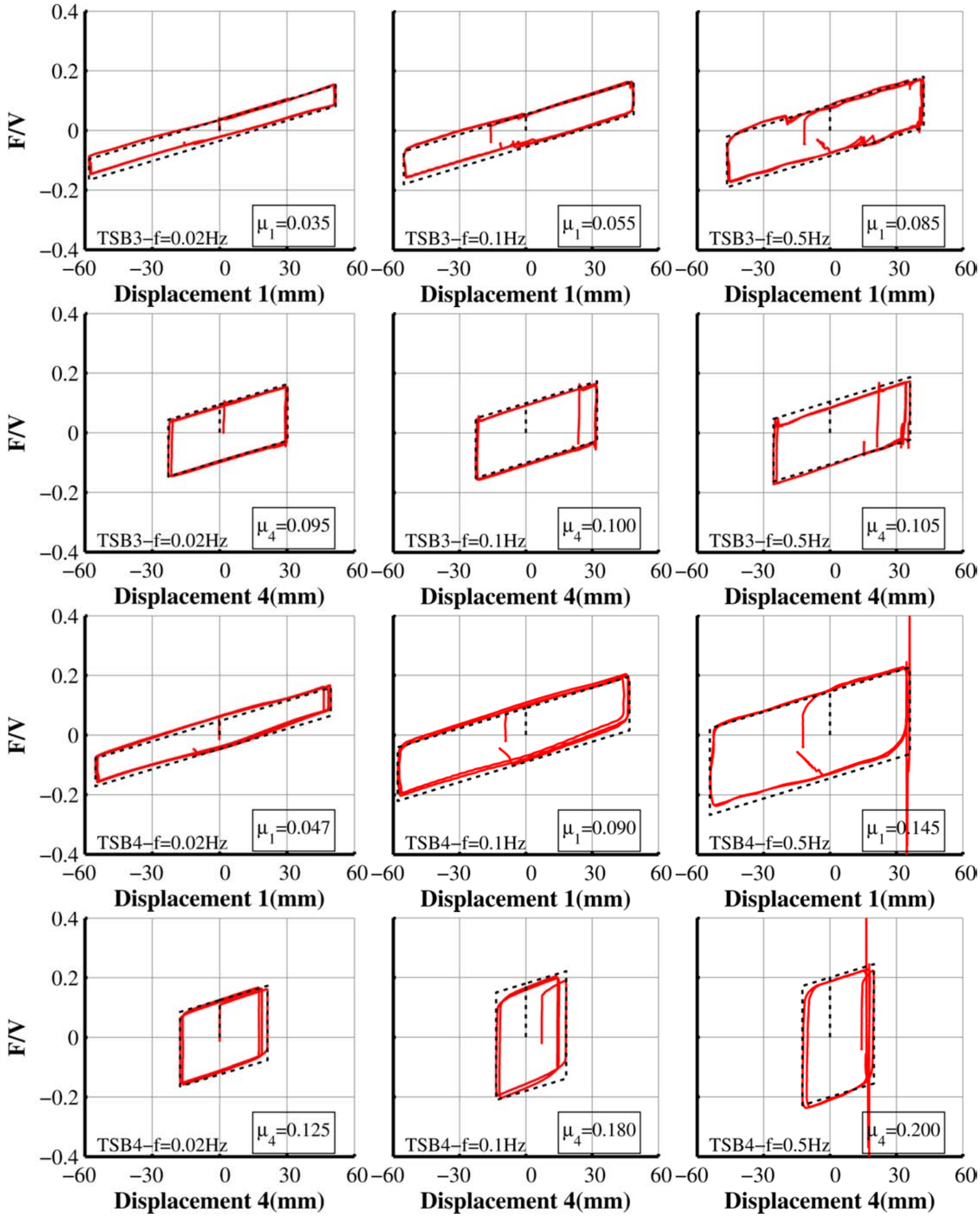

Figure 5-4 (cont'd): Decomposed normalized force versus sliding displacement loops for two isolators of Configuration B at three different excitation frequencies

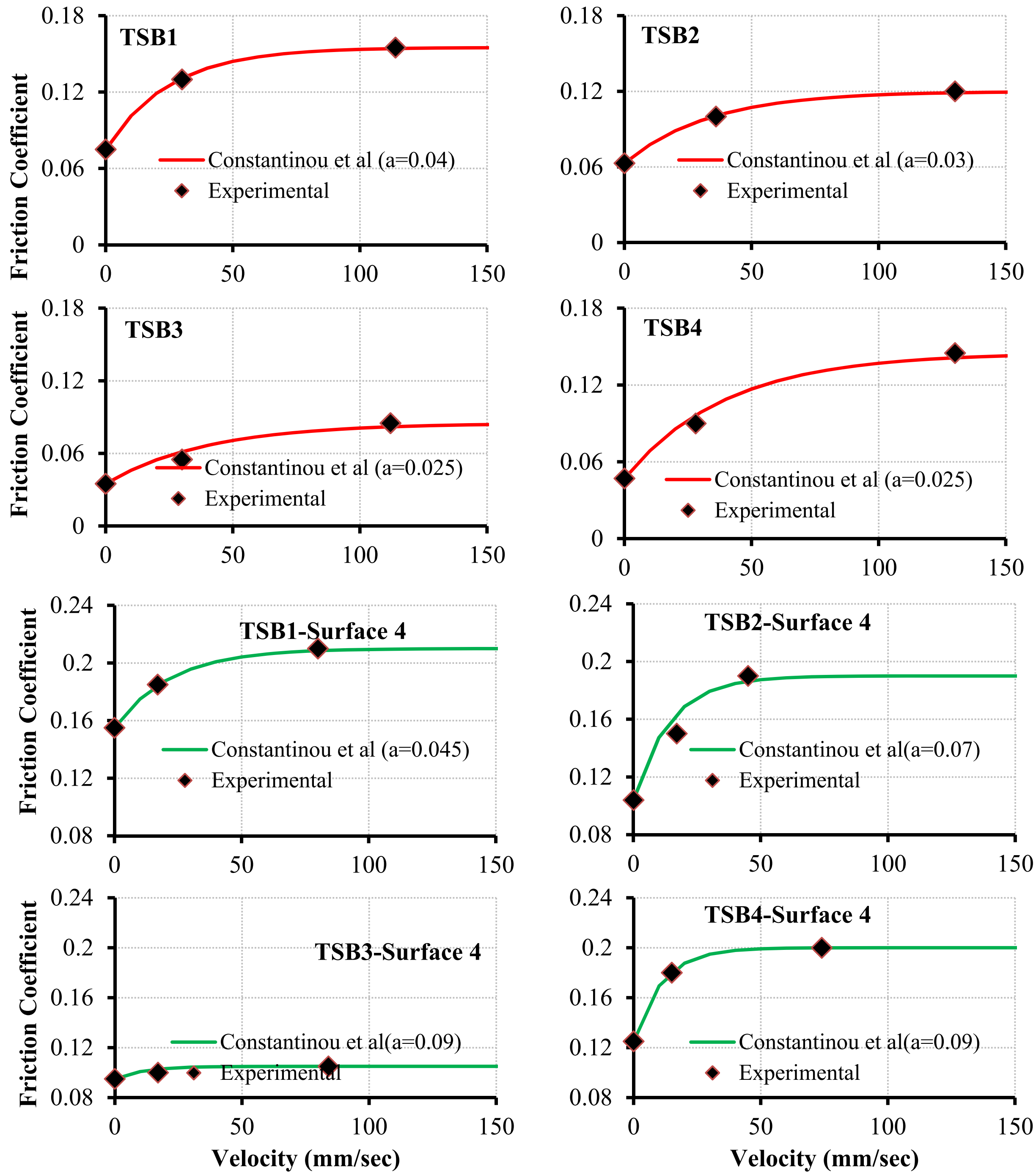

Figure 5-5: Friction coefficient as function of velocity for surfaces 1 and 4 of isolators of Configuration B (parameter *a* in units of sec/mm)

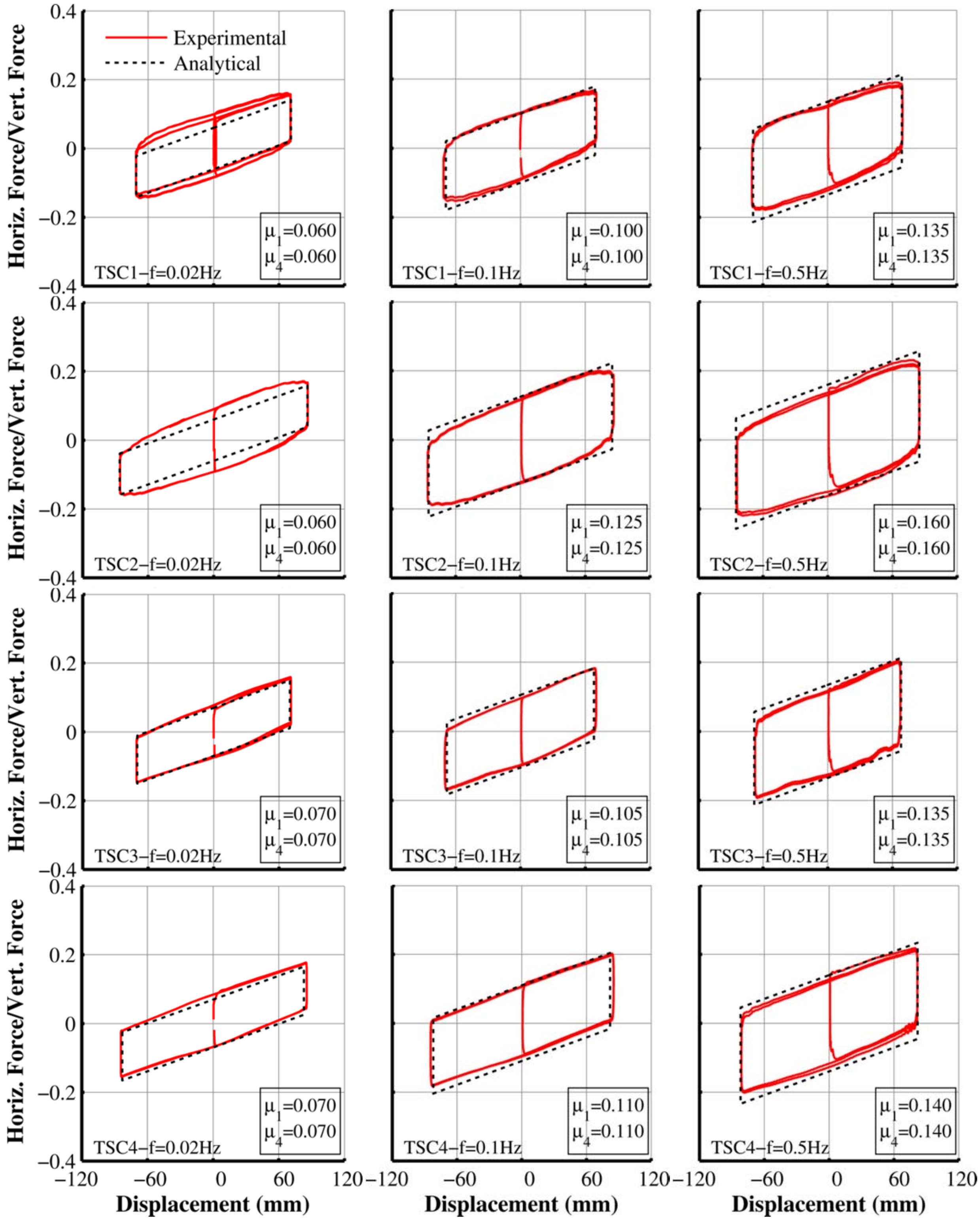

Figure 5-6: Comparison of experimental results obtained from testing of individual isolators and analytical results for Configuration C. Left column presents results for frequency of 0.02Hz; center column for 0.1Hz and right column for 0.5Hz

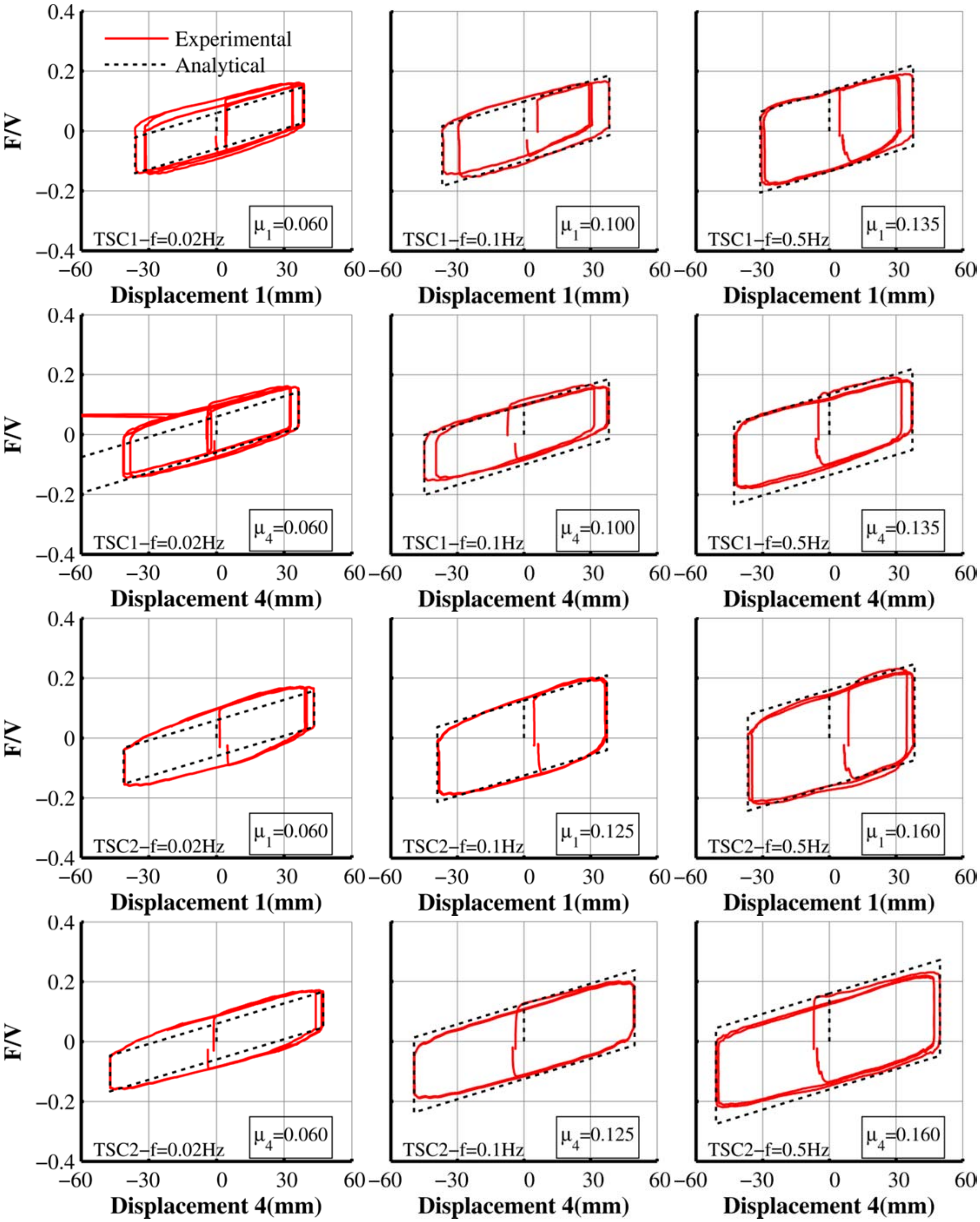

Figure 5-7: Decomposed normalized force versus sliding displacement loops for two isolators of Configuration C at three different excitation frequencies

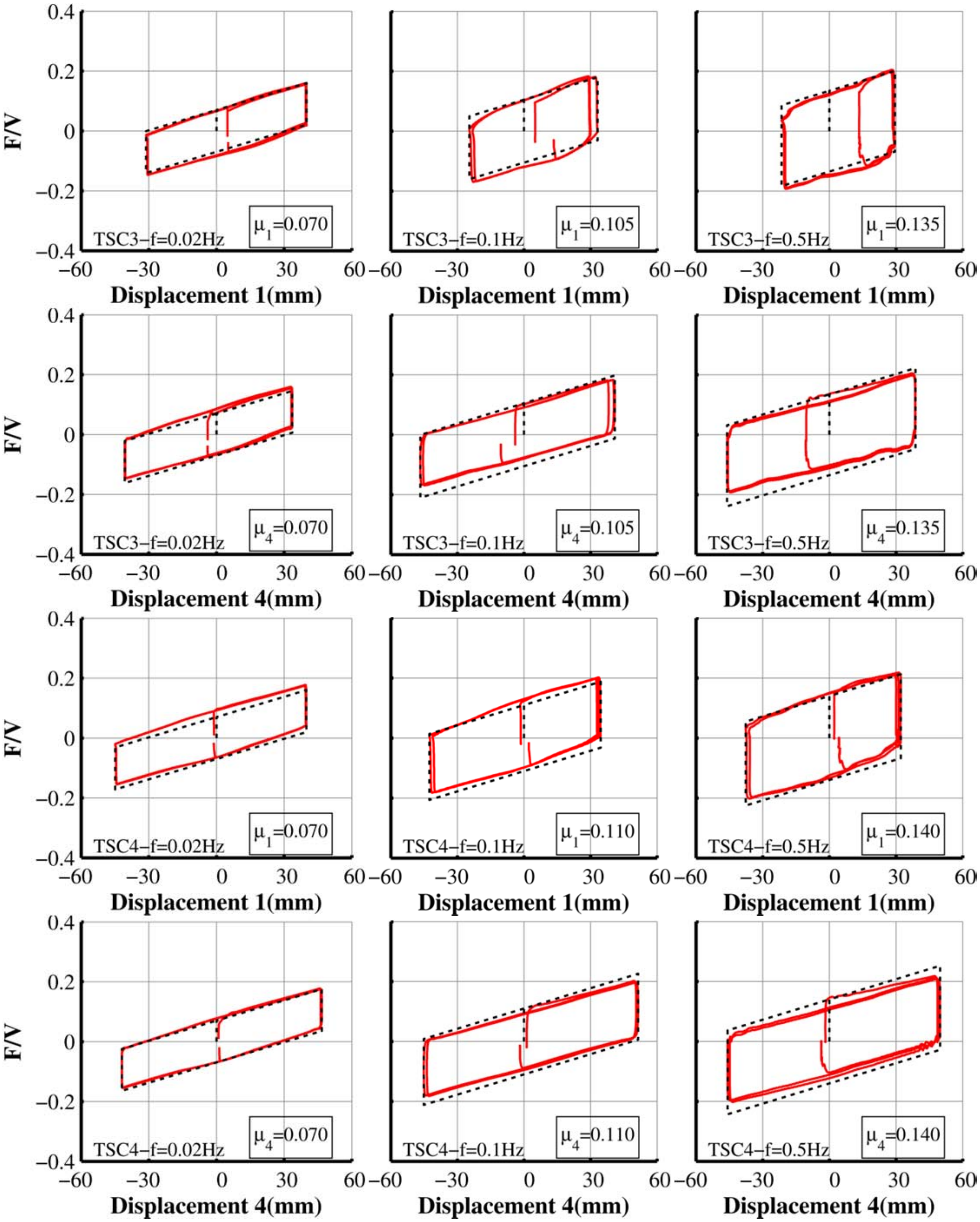

Figure 5-7 (cont'd): Decomposed normalized force versus sliding displacement loops for two isolators of Configuration C at three different excitation frequencies

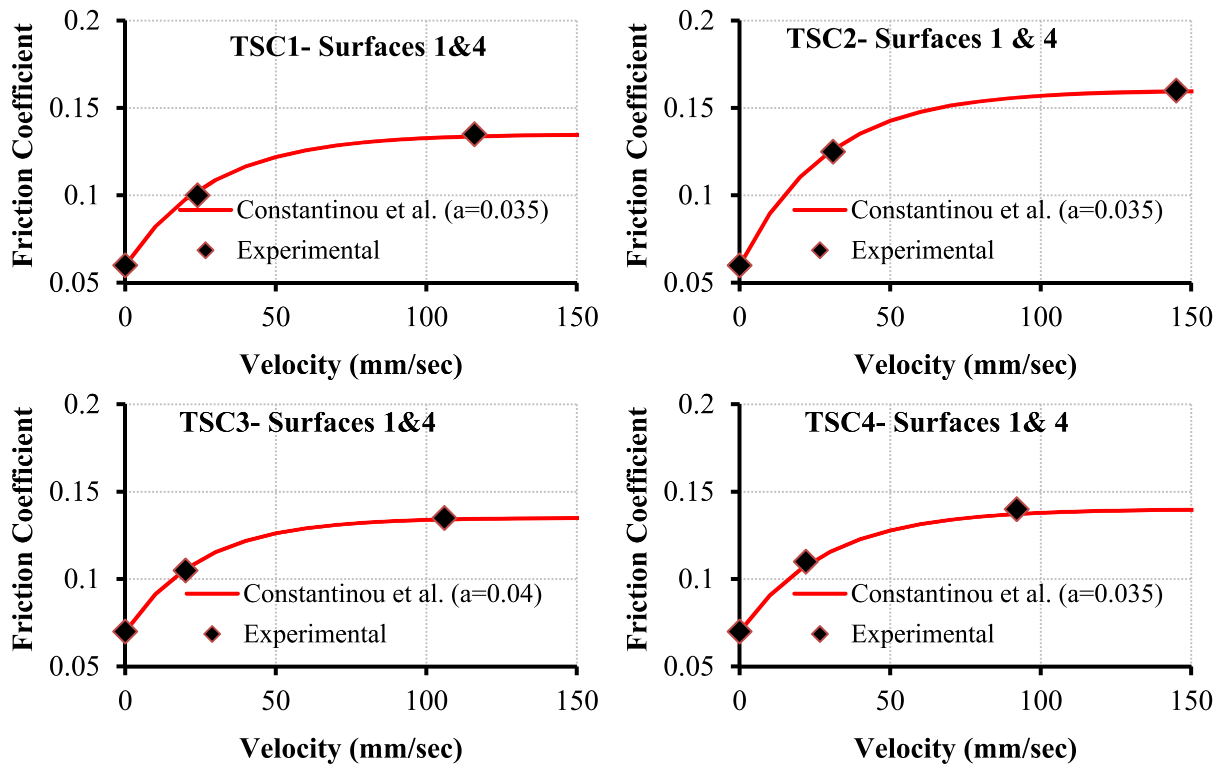

Figure 5-8: Friction coefficient as function of velocity for surfaces 1 and 4 of isolators of Configuration C (surfaces 1 and 4 are assumed to be identical) (parameter *a* in units of sec/mm)

5.3 Analytical Prediction Using Program 3pleANI

Analysis of the tested isolated model structure have been conducted in program 3pleANI (Sarlis and Constantinou, 2013). This program allows for:

1. Explicit modeling of the superstructure,
2. Use of an advanced model of the Triple FP isolator with unrestricted geometric and frictional parameters, and
3. Consideration of non-zero initial conditions.

Table 5-1 presents the identified fast and slow coefficient of friction values for the fours isolators in each of the three tested configurations on the shake table. These friction values are those used in program 3pleANI (denoted as $\mu_1, \mu_2, \mu_3, \mu_4$) which differ from the values in the theory of Fenz and Constantinou (2008a to 2008e) (denoted as $\bar{\mu}_1, \bar{\mu}_2, \bar{\mu}_3, \bar{\mu}_4$) as discussed in Section 1 herein. The two sets of friction coefficient values are related through Equation (1-1).

It should be noted that for the isolators of Configuration A, the friction coefficient values used for the analytical prediction of the experimental results are somewhat higher from the ones identified in the bearing machine tests (Section 5.2), whereas for Configurations B and C they are identical. This was actual behavior and was likely caused by contamination of the interfaces during multiple disassembly and reassembly of the bearings in the course of the test program.

Table 5-1: Friction coefficients values ($\mu_1, \mu_2, \mu_3, \mu_4$) used in program 3PLEANI for analytical prediction of response

	Isolator ID	Friction coefficient			
		Configuration A (TSA)			
		Surface 1	Surface 2	Surface 3	Surface 4
Fast	TSA1	0.104	0.042	0.042	0.120
	TSA2	0.103	0.038	0.038	0.200
	TSA3	0.084	0.045	0.045	0.201
	TSA4	0.118	0.028	0.028	0.170
Slow	TSA1	0.047	0.014	0.014	0.091
	TSA2	0.056	0.014	0.014	0.164
	TSA3	0.042	0.021	0.021	0.157
	TSA4	0.063	0.014	0.014	0.119
		Configuration B (TSB)			
Fast	TSB1	0.142	0.053	0.053	0.178
	TSB2	0.099	0.015	0.015	0.184
	TSB3	0.074	0.031	0.031	0.090
	TSB4	0.118	0.031	0.031	0.166
Slow	TSB1	0.078	0.031	0.031	0.134
	TSB2	0.052	0.008	0.008	0.101
	TSB3	0.030	0.011	0.011	0.079
	TSB4	0.039	0.008	0.008	0.102
		Configuration C (TSC)			
Fast	TSC1	0.124	0.258	0.258	0.124
	TSC2	0.138	0.248	0.248	0.138
	TSC3	0.124	0.212	0.212	0.124
	TSC4	0.124	0.193	0.193	0.124
Slow	TSC1	0.064	0.184	0.184	0.064
	TSC2	0.055	0.178	0.178	0.055
	TSC3	0.064	0.150	0.150	0.064
	TSC4	0.064	0.136	0.136	0.064

Comparisons of analytical results produced by 3pleANI and experimental results are presented in Figure 5-10 for Configuration B and Figure 5-11 for Configuration C with experimental results obtained in the testing of the isolators in the single bearing testing machine. For the simulation results in program 3pleANI, the top concave plate (TCP) was subjected to a prescribed displacement and varying axial load which were the ones recorded in the experiments. Also in the simulations, the initial offsets of the inner parts of the bearings as measured at the beginning of each test by the instrumentation shown in Figure 3-2 were included in the analysis. Isolator TSB4 in Figure 5-10 underwent uplift so that its normalized loop is not defined during the uplift duration. For this test, the non-normalized loop is shown in Figure 5-12. Note that program

3pleANI can analyze isolators exhibiting uplift. It can be seen that analytical and experimental results are in good agreement except for minor differences attributed to:

1. Load cell error measurements which were obvious in the comparisons between the actuator load cell and isolator load cells in Figure 3-9. In fact, the isolator load cell had to be repaired after these tests. In testing friction pendulum isolators, the measurements of the load cells can easily be verified by comparing the analytically predicted stiffness with the experimentally measured stiffness. Such comparisons led to the requirement of multiplying the experimental results with different scaled factors for each test
2. The presence of the rubber seal which was not accounted for in the analyses. The rubber seal has a more pronounced effect in the reduced size tested bearings than in full size isolators. The seal affects the stiffness of Regimes I, II, IV and V for bearings with $\mu_2 = \mu_3 < \mu_1 < \mu_4$ and the stiffness of Regime V for bearings with $\mu_1 = \mu_4 < \mu_2 = \mu_3$ (see Figure 1-2). It is noted that the seal was omitted here for simplicity. However, an example of an analysis in 3pleANI that shows the effect of the seal is shown in Figure 5-9. Note that in Figure 5-9 the analysis that includes the seal over-predicts the stiffness because the exact seal properties for the analysis were unknown. For more details the reader is referred to Sarlis and Constantinou (2013).

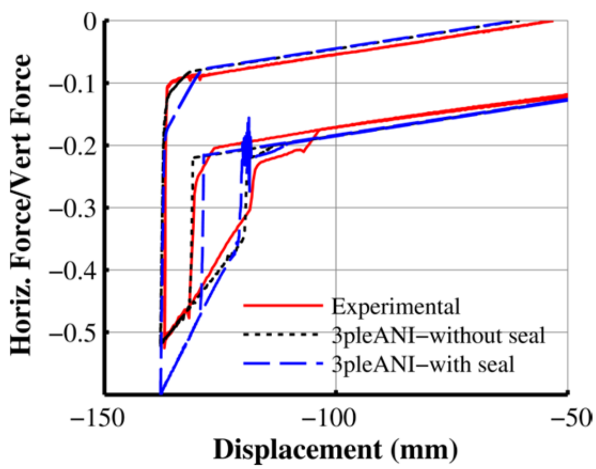

Figure 5-9: Rubber seal effect in the reduced size tested isolators

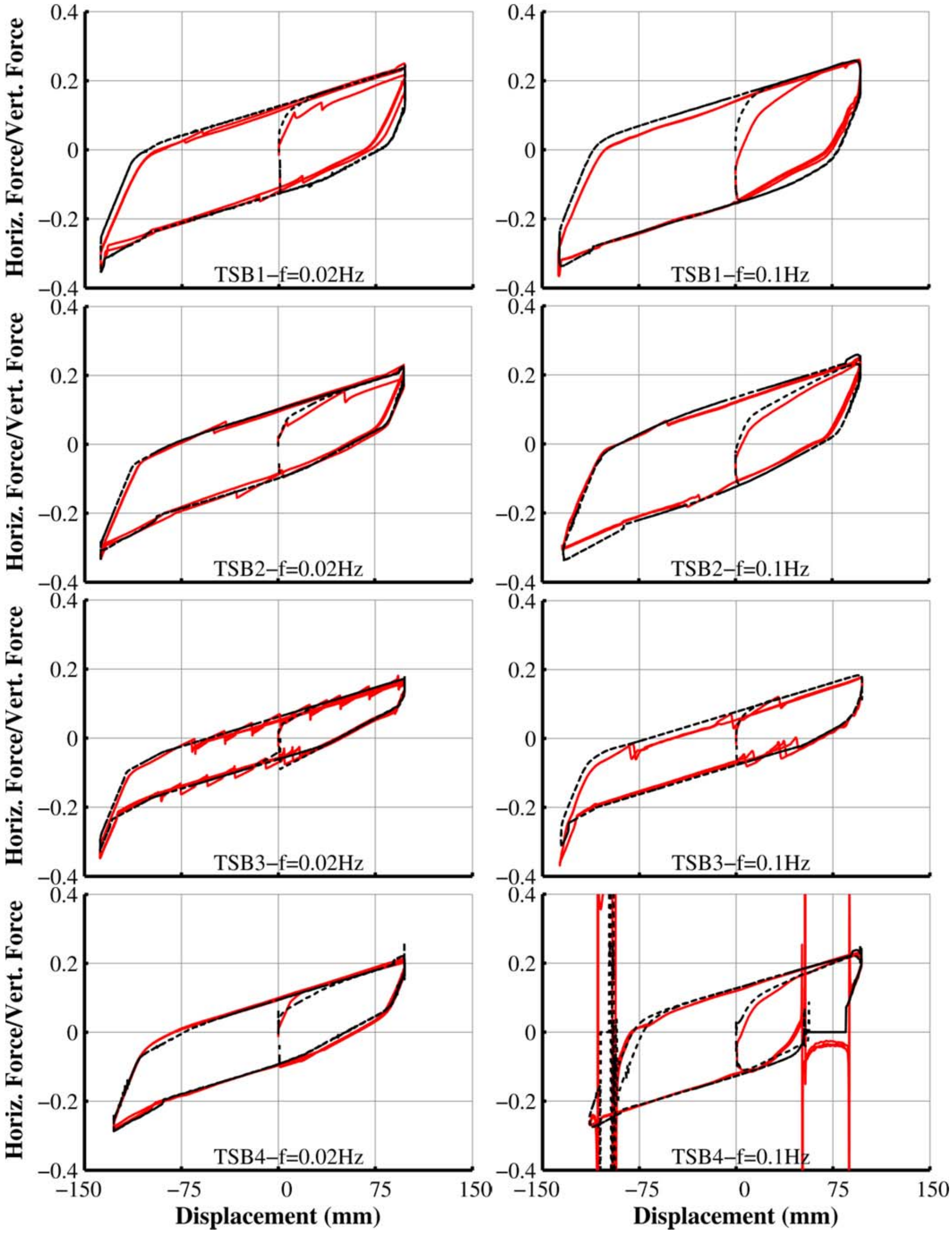

Figure 5-10: Comparison of experimental (bearing test machine) and analytical (red line-program 3pleANI) normalized force-displacement loops for Configuration B isolators

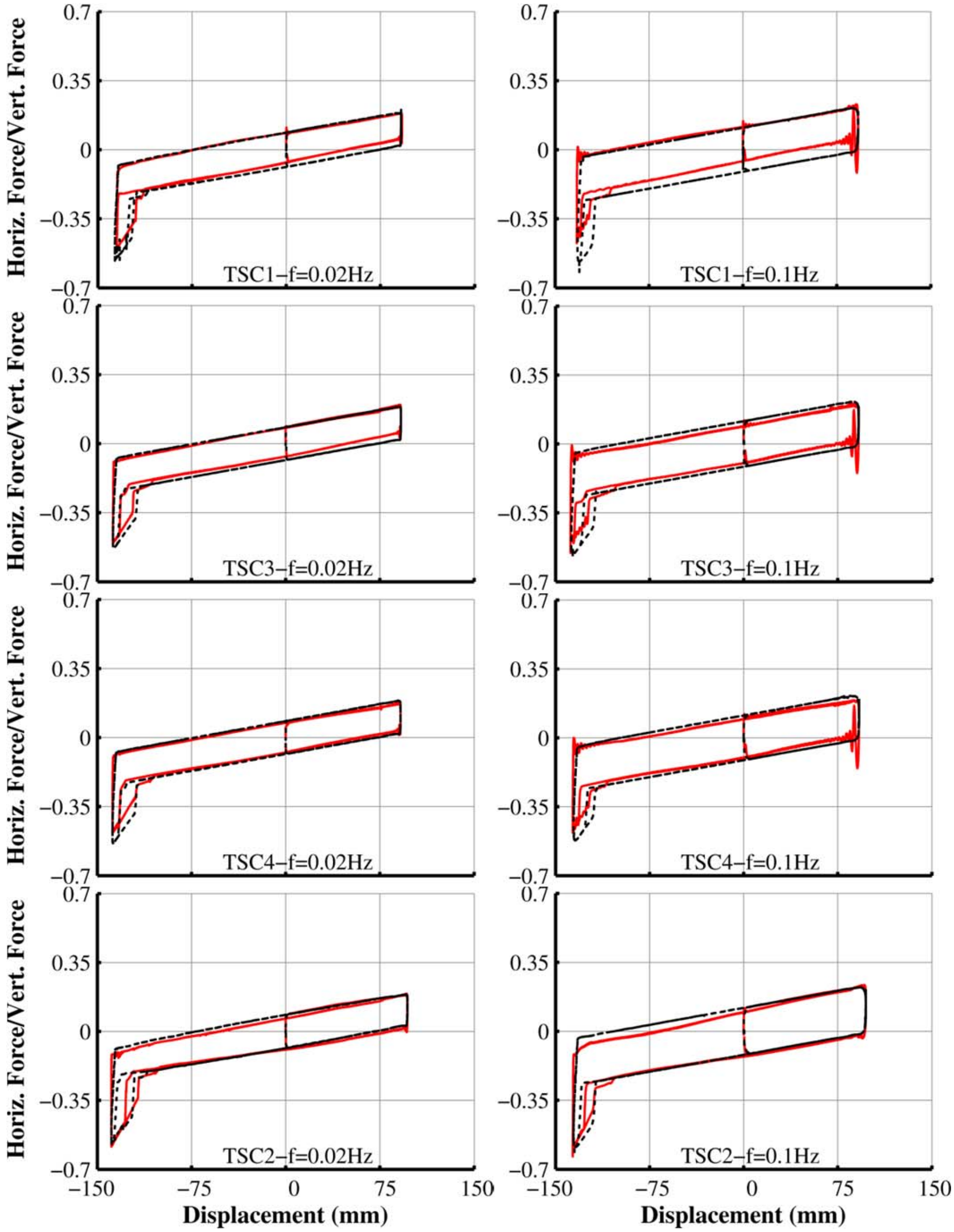

Figure 5-11: Comparison of experimental (bearing test machine) and analytical (red line-program 3pleANI) normalized force-displacement loops for Configuration C isolators

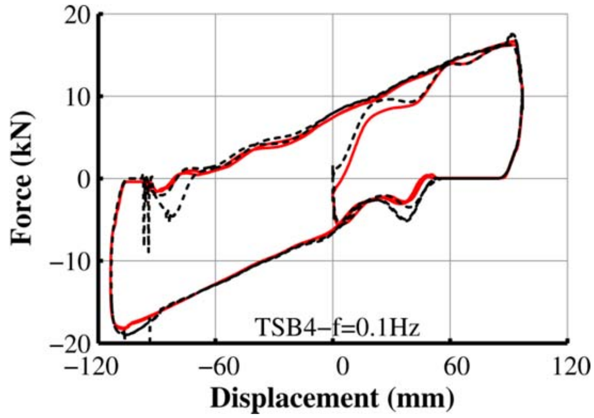

Figure 5-12: Comparison of experimental (bearing test machine) and analytical (red line-program 3pleANI) force-displacement loops of isolator TSB4 (with uplift)

5.3 Structural Model and Analytical Results of Fixed-base Superstructure using Program 3pleANI

The stiffness and damping matrices of the superstructure of the isolated model, fixed at the base, were constructed using the procedures presented in Bracci et al. (1992) and the identified mode shapes and periods (shown in Table 4-1 and Table 4-2). These matrices are presented in Table 5-2. Note that two sets of matrices are presented as based on data obtained in white noise and in seismic motion identification tests. In the analysis programs 3pleANI (and later program SAP2000), the stiffness matrix was derived from the white noise data. For the damping matrix, the mode shapes identified in the white noise tests were used (consistent with the construction of the stiffness matrix). However, the damping ratios obtained in the seismic identification tests were used as these tests resulted in more realistic values.

Analysis of the fixed-base superstructure with seismic motion ATL 270 at its base was conducted in 3pleANI and results are compared to experimental results in Figure 5-13 to 5-14. The figures show histories of inter-story drift and floor accelerations, and the 5%-damped floor acceleration spectra. The analytical results are in good agreement with the experimental results except for the peak values of response which are occasionally over-estimated or under-estimated by the analytical model. There are two reasons for this: a) the experimental response has not been filtered (except for a filter at 50Hz) so that it contains noise, and b) the analytical model is based on linear elastic and linear viscous behavior, whereas the fixed superstructure exhibits nonlinear behavior due to flexing and slipping of the concrete block connections.

Table 5-2: **Stiffness and damping matrices constructed from identified mode shapes and damping ratios**

Test No.	Stiffness matrix (*kN/cm*)	Damping Matrix (*kN-sec/cm*)
White Noise 0.1g, 0-50Hz	$K=\begin{bmatrix} 555.5 & -333.2 & 26.6 \\ -333.2 & 515.8 & -233.2 \\ 26.6 & -233.2 & 185.9 \end{bmatrix}$	$C=\begin{bmatrix} 0.118 & 0.018 & 0.021 \\ 0.018 & 0.123 & 0.028 \\ 0.021 & 0.028 & 0.143 \end{bmatrix}$
Ground motion ATL-270	$K=\begin{bmatrix} 558.9 & -330.2 & 40.3 \\ -330.2 & 520.9 & -242.5 \\ 40.3 & -242.5 & 190.1 \end{bmatrix}$	$C=\begin{bmatrix} 0.101 & 0.018 & 0.004 \\ 0.018 & 0.097 & 0.015 \\ 0.004 & 0.015 & 0.116 \end{bmatrix}$

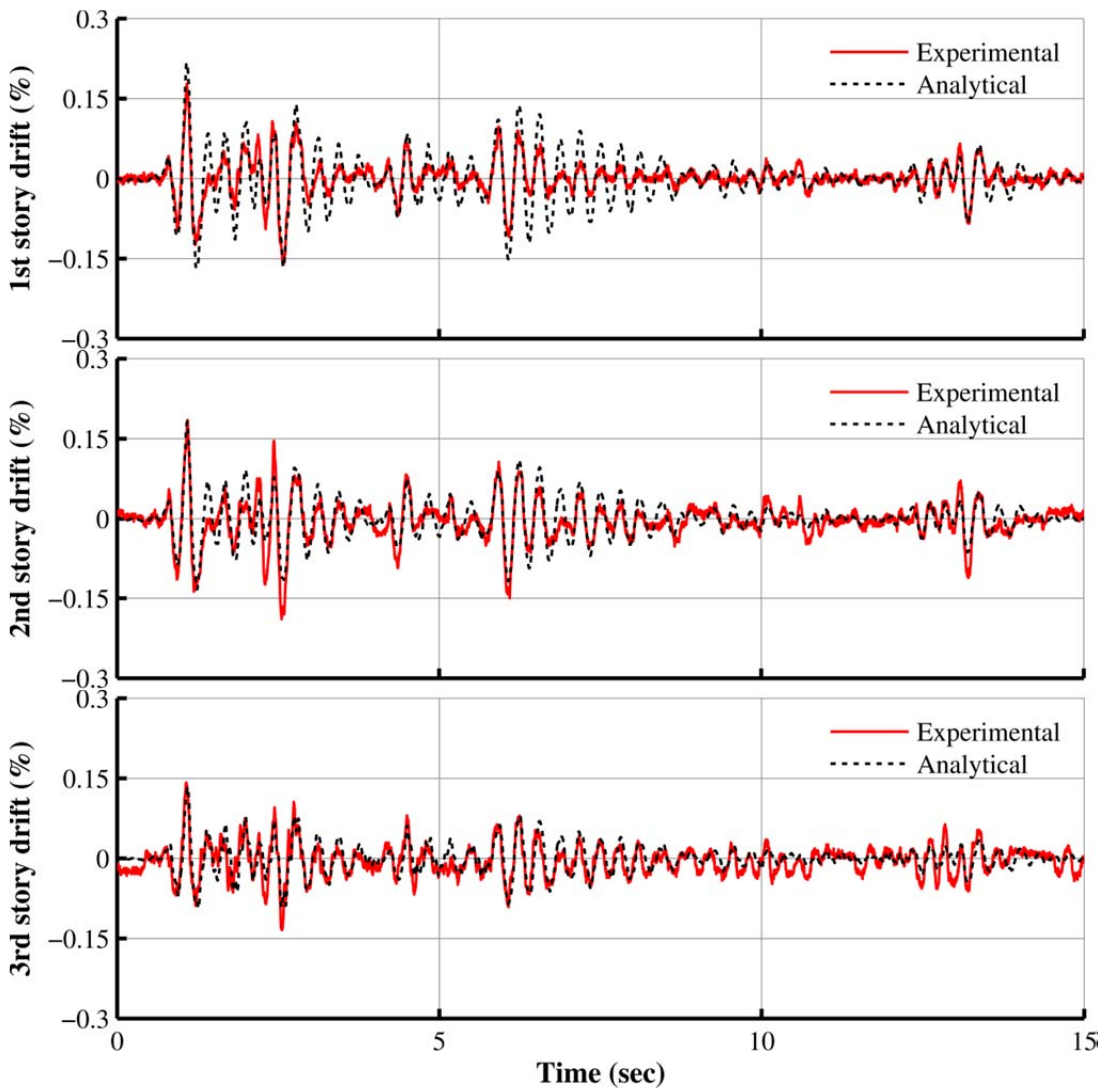

Figure 5-13: Comparison of analytical (program 3pleANI) and experimental results for inner-story drift of fixed structure for ground motion ATL-270

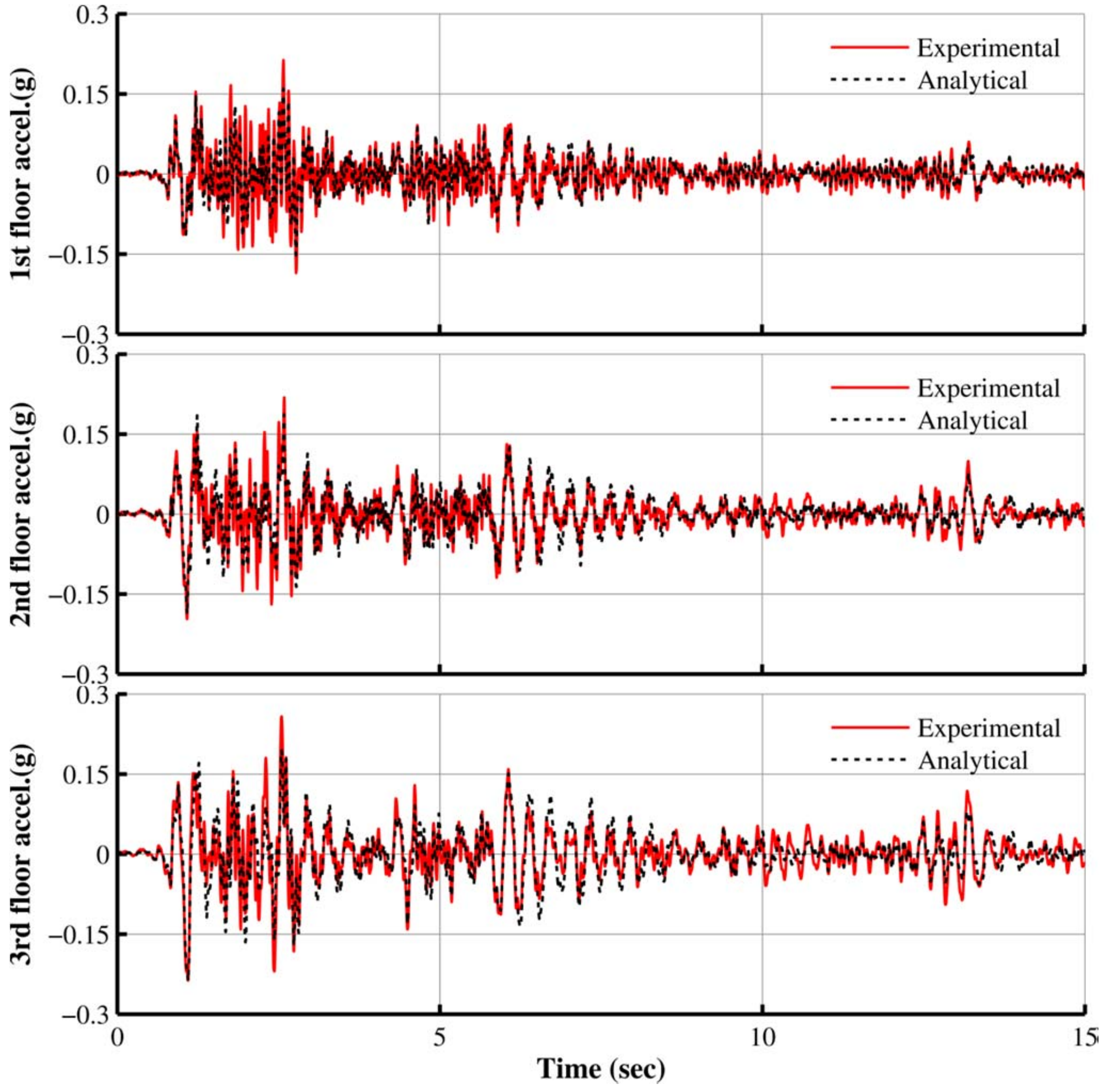

Figure 5-14: Comparison of analytical (program 3pleANI) and experimental results for floor acceleration of fixed structure for ground motion ATL-270

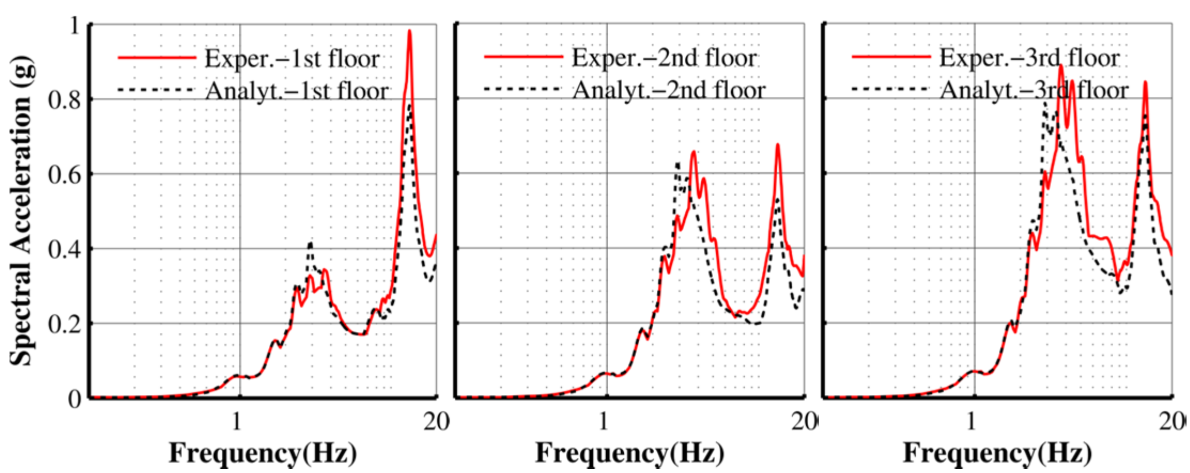

Figure 5-15: Comparison of analytical (program 3pleANI) and experimental results for 5%-damped floor response spectra of fixed structure for ground motion ATL-270

5.4 Analytical Results of Isolated Structure using Program 3pleANI

Comparisons of experimental and analytical results for the isolated structure are presented in Figure 5-16 to Figure 5-18. For each isolation system configuration, six ground motions are shown; two of small amplitude (displacements less than 50mm) two of moderate amplitude (displacements less than 100mm) and two of high amplitude (displacements greater than 100mm) ground motions. Additional comparisons of results are presented in Appendix B.

The superstructure was described in program 3PLEANI using the stiffness and damping matrices shown in Table 5-2 (case of seismic test identification) and the isolators using the friction coefficient values of Table 5-1. In the analysis, non-zero initial isolator displacements were used as the measured permanent isolator displacements at the conclusion of the preceding test. However, the isolator internal part offsets could not be accurately measured in the experiments since only one potentiometer was used for each part. Also, the internal bearing parts exhibited torsion (see Section 3), further complicating the extraction of data on the motion of the parts. Accordingly, analysis was used to approximately calculate the internal parts offsets and then use them as initial conditions, together with the experimentally measured permanent isolator displacement, for the analysis in the subsequent test. Note that the initial conditions so determined may contain errors and thus violate equilibrium and compatibility. To correct for this, analysis at the first integration step results in the calculation of the internal parts sliding displacements that satisfy equilibrium and compatibility.

The test results presented in Figure 5-16 to Figure 5-21 and in Appendix B do not include a vertical component of excitation. In all tests, however, there was parasitic vertical excitation, which was included in the analysis. In program 3pleANI, the vertical excitation is included by varying the axial load on each isolator as:

$$N = W(1 + \ddot{u}_{vg} / g) \tag{5-2}$$

In Equation (5-2), W is the starting (at time $t=0$) value of load on the isolator and $\ddot{u}_{vg}$ is the history of vertical acceleration taken as positive if in the downward direction. W was obtained at the beginning of each test for each isolator using the procedure described in Section 2.2 (see also Figure 3-13). In all simulations, the vertical excitation was imported directly into the program as obtained from the average of the measurements of the four shake table vertical accelerometer recordings (ASSV, ASSV2 ANSV, and ANSV2 as shown in Figure 2-6) after filtering them using a low pass 30Hz filter.

Note that the approach in program 3pleANI to account for the vertical acceleration effects ignores the damping and flexibility of the structure in the vertical direction. An approach for accounting for flexibility and damping in program 3pleANI (but not used in the analyses presented herein) is:

1. Analyze a Single-Degree-of-Freedom (SDOF) system with damping and stiffness representing the structure in the vertical direction and subjected to ground excitation $\ddot{u}_{vg}$.
2. Use the calculated total acceleration response history of the SDOF as input $\ddot{u}_{vg}$ in program 3pleANI.

Note that the procedure described above is similar to the procedure followed when analyzing a structure in program SAP2000. Accordingly, results that include the vertical excitation component (L+V tests) are presented only when analysis is performed in program SAP2000 in Section 5.4.

Figure 5-16 to Figure 5-21 demonstrate that the analytical model in program 3pleANI predicts well the experimental response in terms of frequency content of the response and shape of the loops but it occasionally over-predicts or under-predicts the experimental peak response. However, the predicted peak base displacement and peak base shear force are in very good agreement with the experimental peak values. The occasional over- or under-prediction of the peak structural response was also observed in the analysis of the structure without the isolation system (see Figure 5-13 to Figure 5-15). It is believed that this is due to inability of the analytical model of the superstructure to capture sliding and minor impact in the connections of the masses of the model to the floors and in the connections of the braces to beams and columns during strong shaking. Additional reasons for differences between analytical and experimental results are:

1. Uncertainty in the friction coefficient values, which certainly changed during testing due primarily to heating effects as the bearings were extensively tested without pausing to allow for return to ambient temperature conditions. Note also that the identification of friction coefficients was done under different heating conditions than those that existed in the shake table tests.
2. Effect of rubber seal in the tested reduced size bearings (see Figure 5-9).
3. Anisotropy in friction. Note that in some tests, the friction of surfaces 2 and 3 is direction dependent, with different values at positive displacements than at negative displacements. This is explained by the fact that the contact forces are applied away from the center of the sliding surface (Sarlis and Constantinou, 2013), resulting in uneven wear and variability in friction.
4. The accuracy of the analytical prediction deteriorates at small amplitude motions, due to inaccuracies in the friction-velocity relation at small velocities.
5. For the isolation system normalized force-displacement loops, the division by the instantaneous vertical load introduces error in the experimental results due to the addition of axial loads from four load cells, with the measurement of each one of these load cells containing some error.

In some tests, the analytically predicted floor response spectra are substantially higher than the experimental ones and in some others the analytically predicted floor response spectra are substantially lesser than the experimental ones. A notable example of the former case is test TSB 0637-270 (0.8/1/8) (see Figure 5-17 and Figure 5-20) where the analysis under-predicts the experimental floor spectra. In this case, there was impact on the restrainer rings which was not well captured in the analysis. Under conditions of impact with large restrainer stiffness and strength, small differences in the prediction of displacement result in large differences in force prediction, and thus floor response spectra as well.

Test TSC NWH-360 (1.2/1.5) (see Figure 5-18 and Figure 5-21) is an example of over-prediction of floor response spectral values by analysis. In this case, analysis predicted response in the stiffening isolator range, which did not occur. The result was over-prediction of acceleration response and floor spectral values.

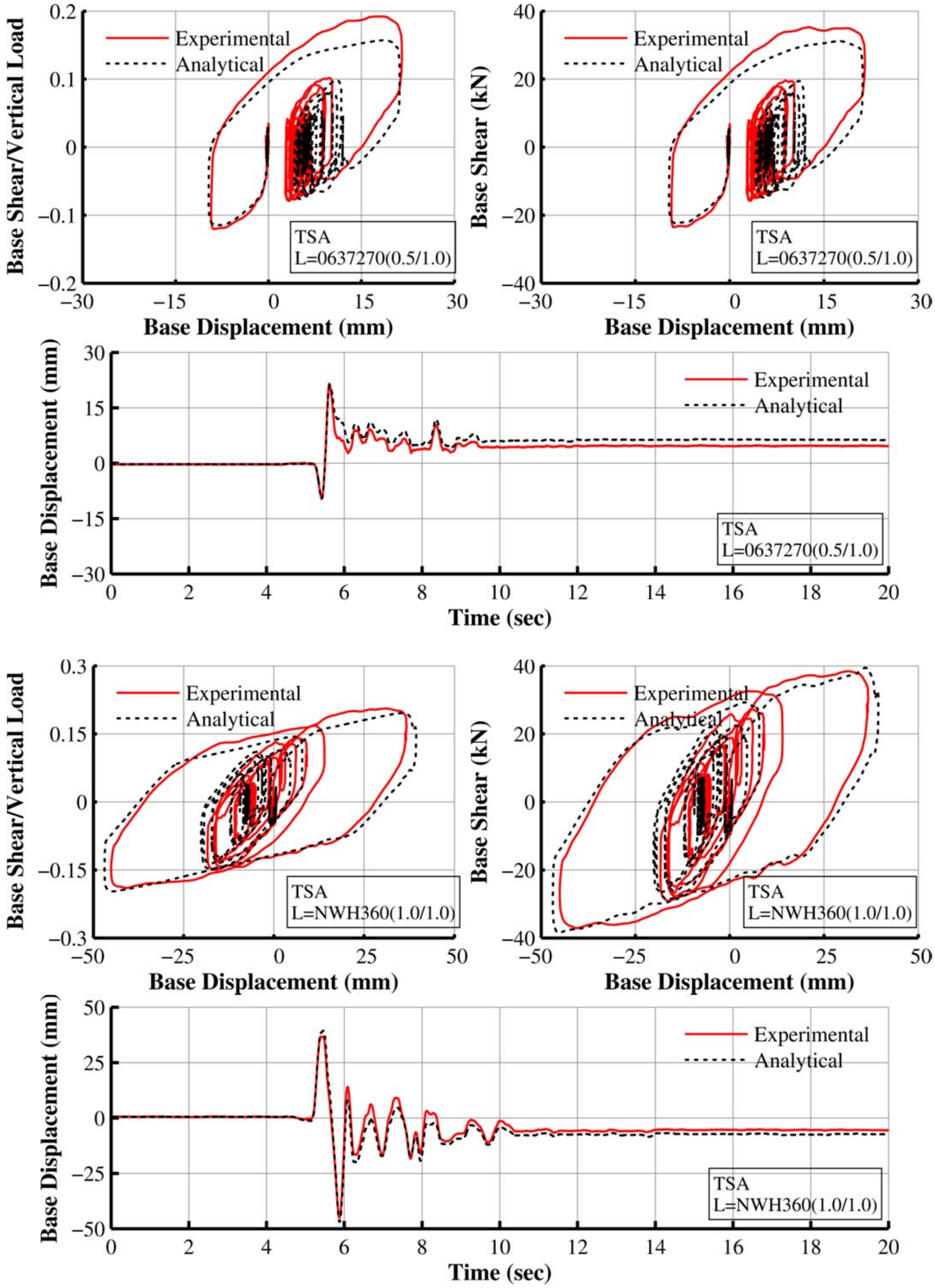

Figure 5-16: Comparison of analytical (program 3pleANI) and experimental results for isolated structure with Configuration A isolators

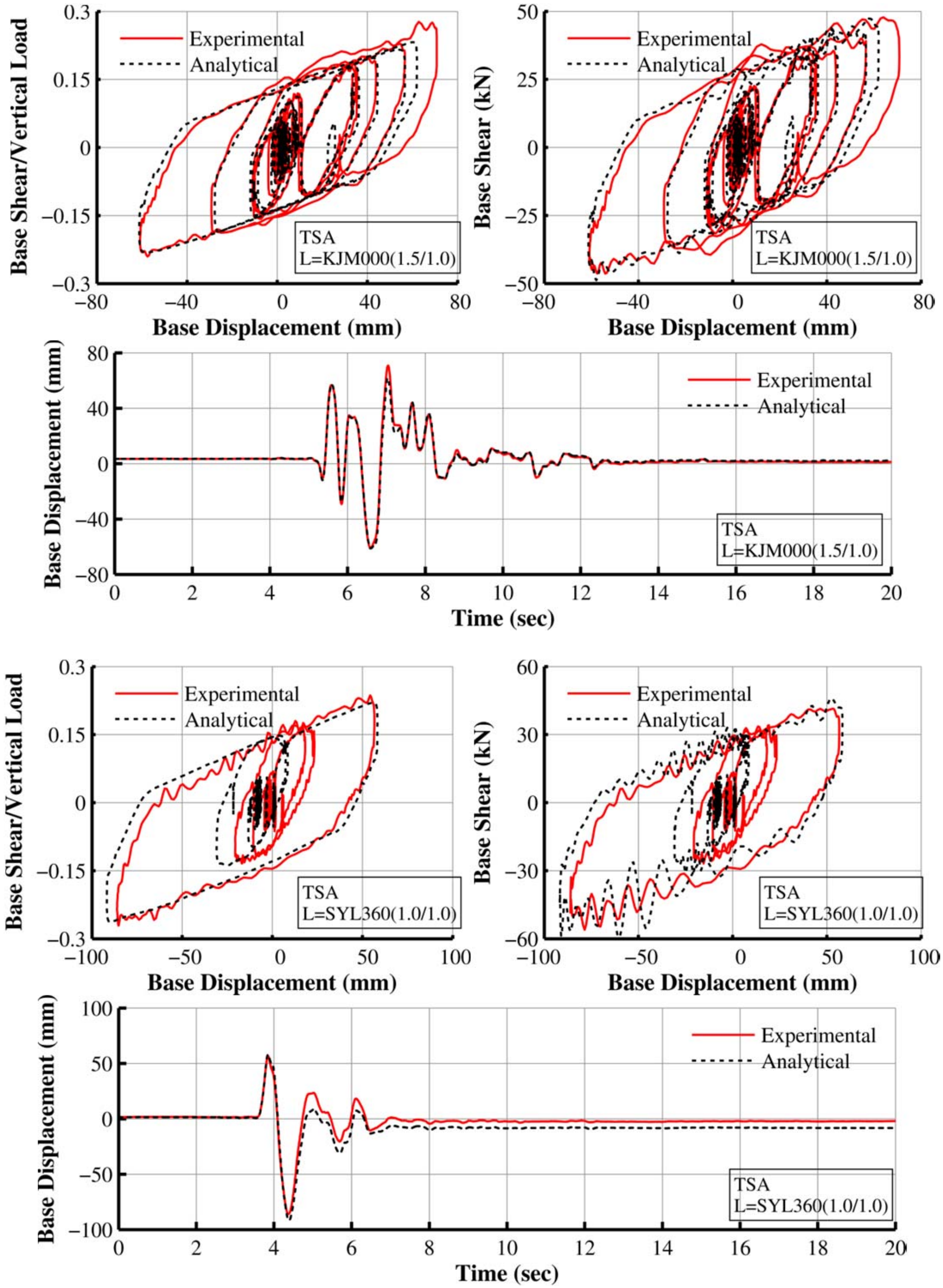

Figure 5-16 (cont'd): Comparison of analytical (program 3pleANI) and experimental results for isolated structure with Configuration A isolators

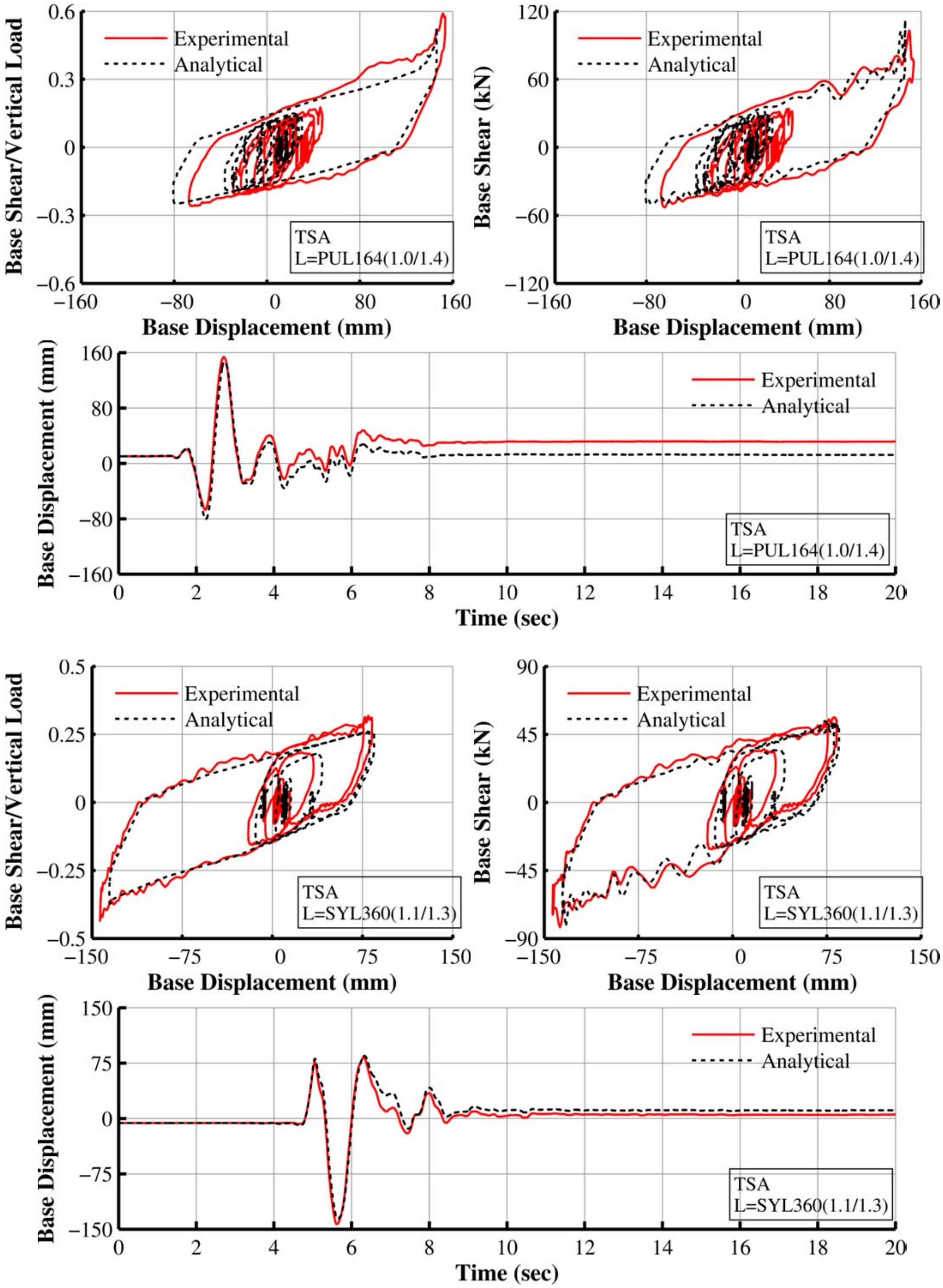

Figure 5-16 (cont'd): Comparison of analytical (program 3pleANI) and experimental results for isolated structure with Configuration A isolators

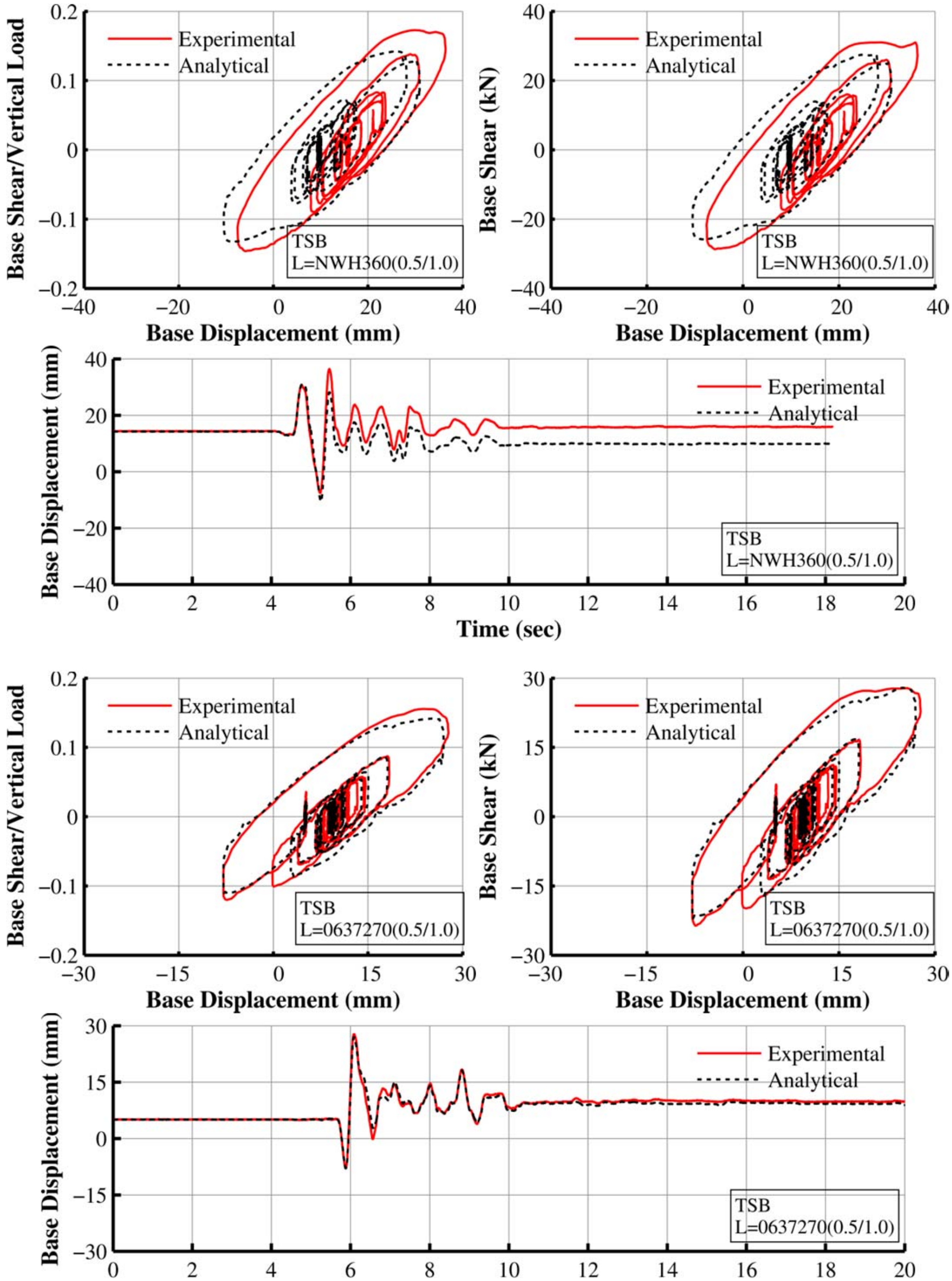

Figure 5-17: Comparison of analytical (program 3pleANI) and experimental results for isolated structure with Configuration B isolators

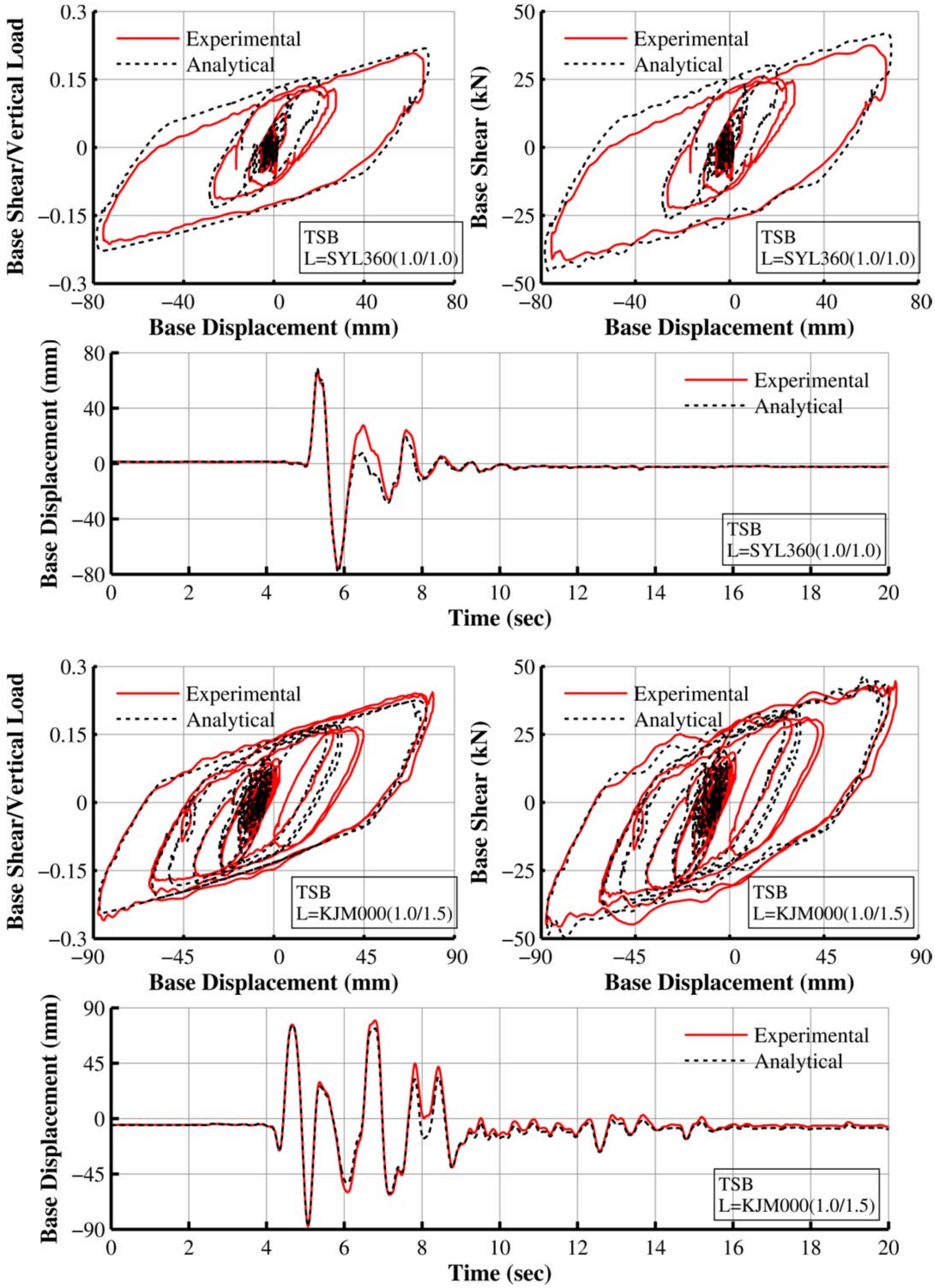

Figure 5-17 (cont'd): Comparison of analytical (program 3pleANI) and experimental results for isolated structure with Configuration B isolators

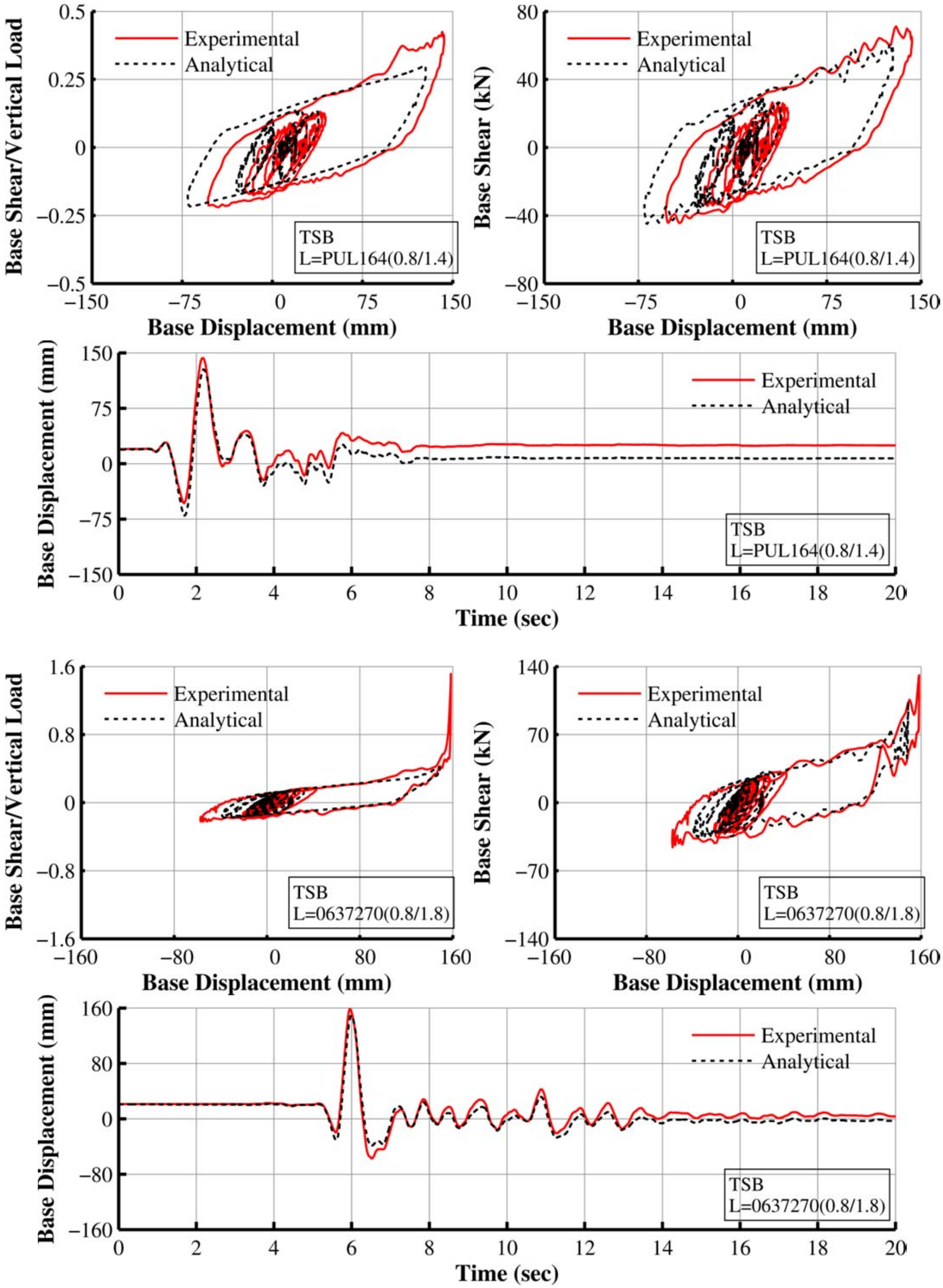

Figure 5-17 (cont'd): Comparison of analytical (program 3pleANI) and experimental results for isolated structure with Configuration B isolators

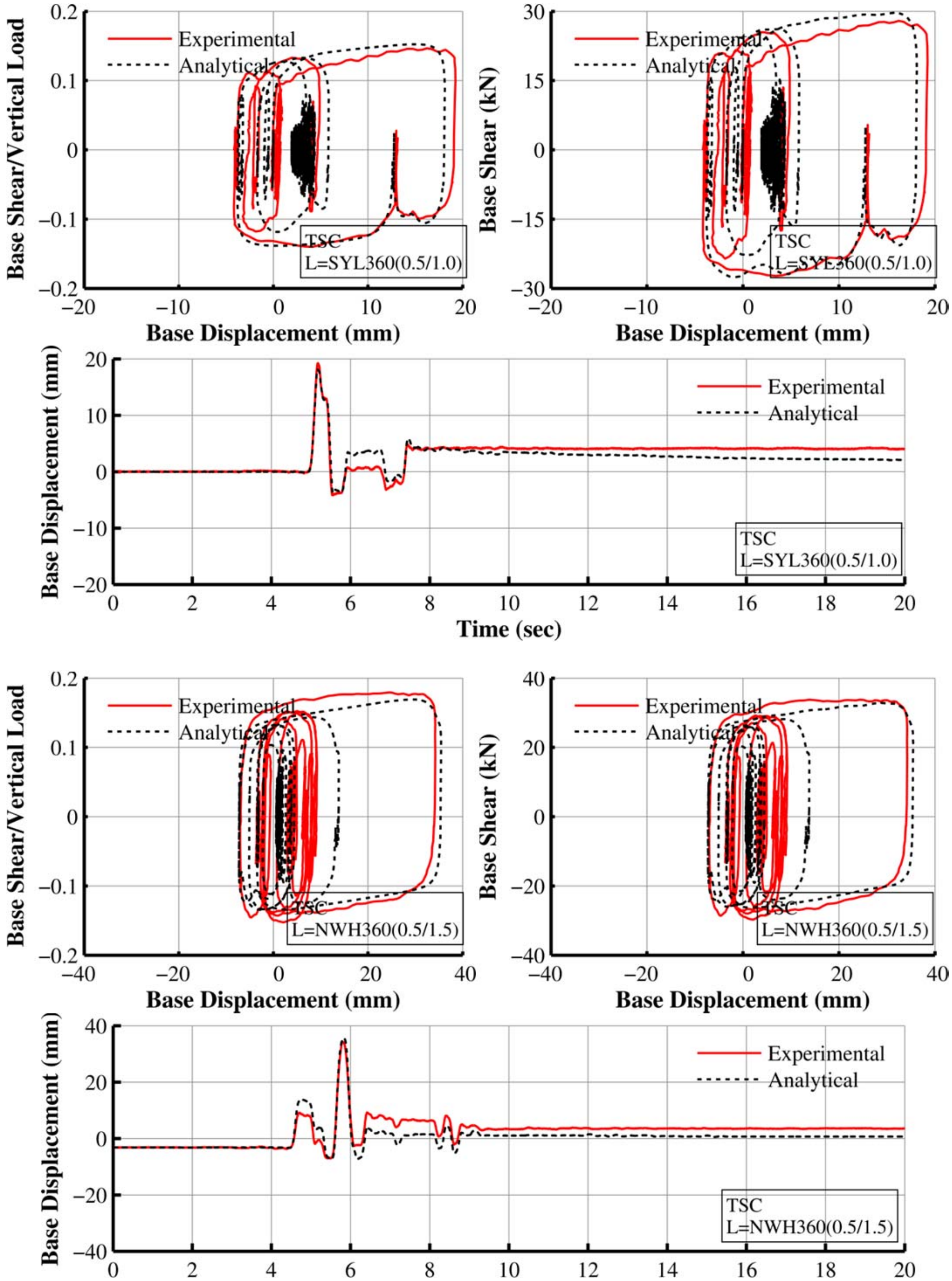

Figure 5-18: Comparison of analytical (program 3pleANI) and experimental results for isolated structure with Configuration C isolators

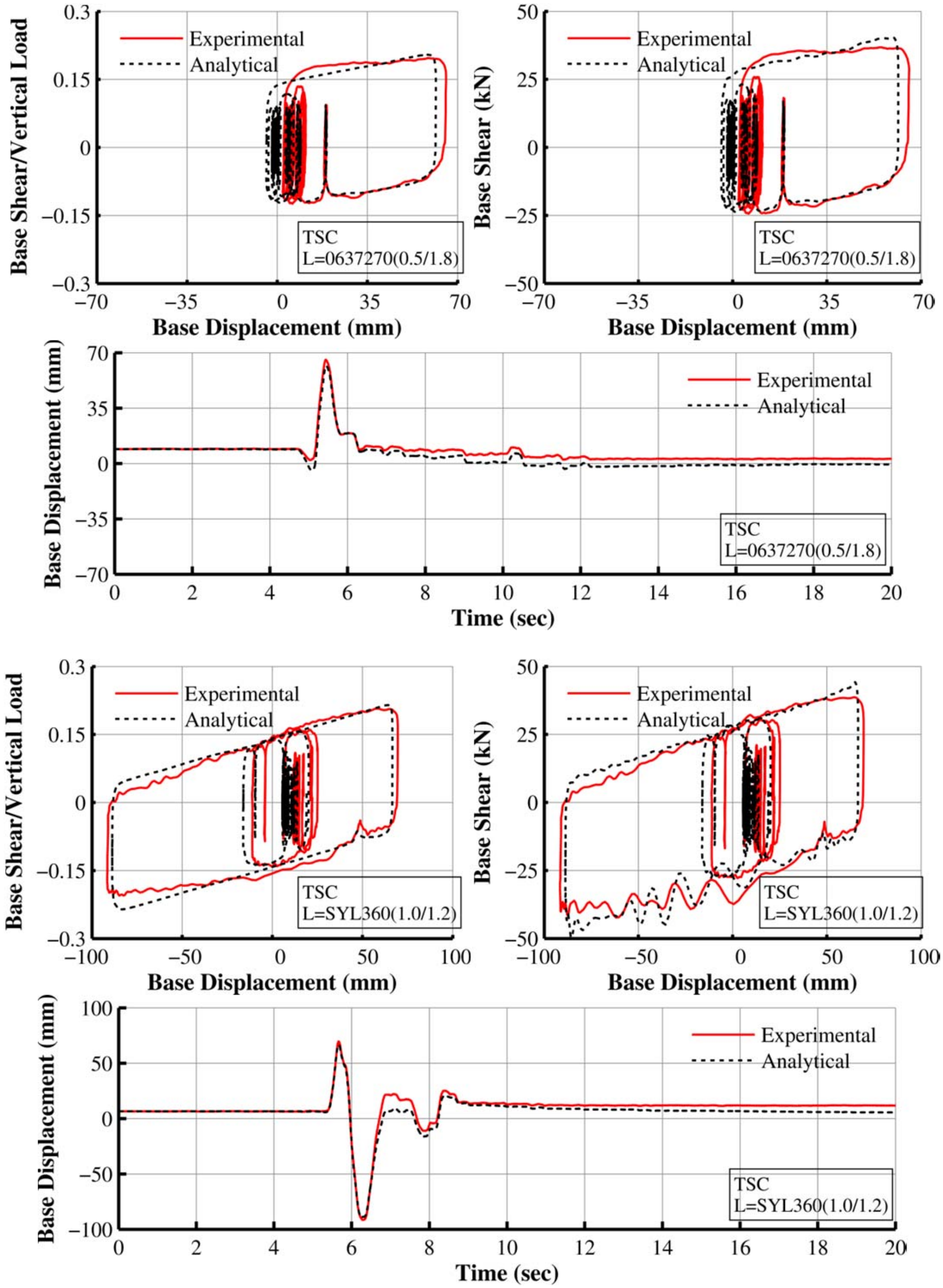

Figure 5-18 (cont'd): Comparison of analytical (program 3pleANI) and experimental results for isolated structure with Configuration C isolators

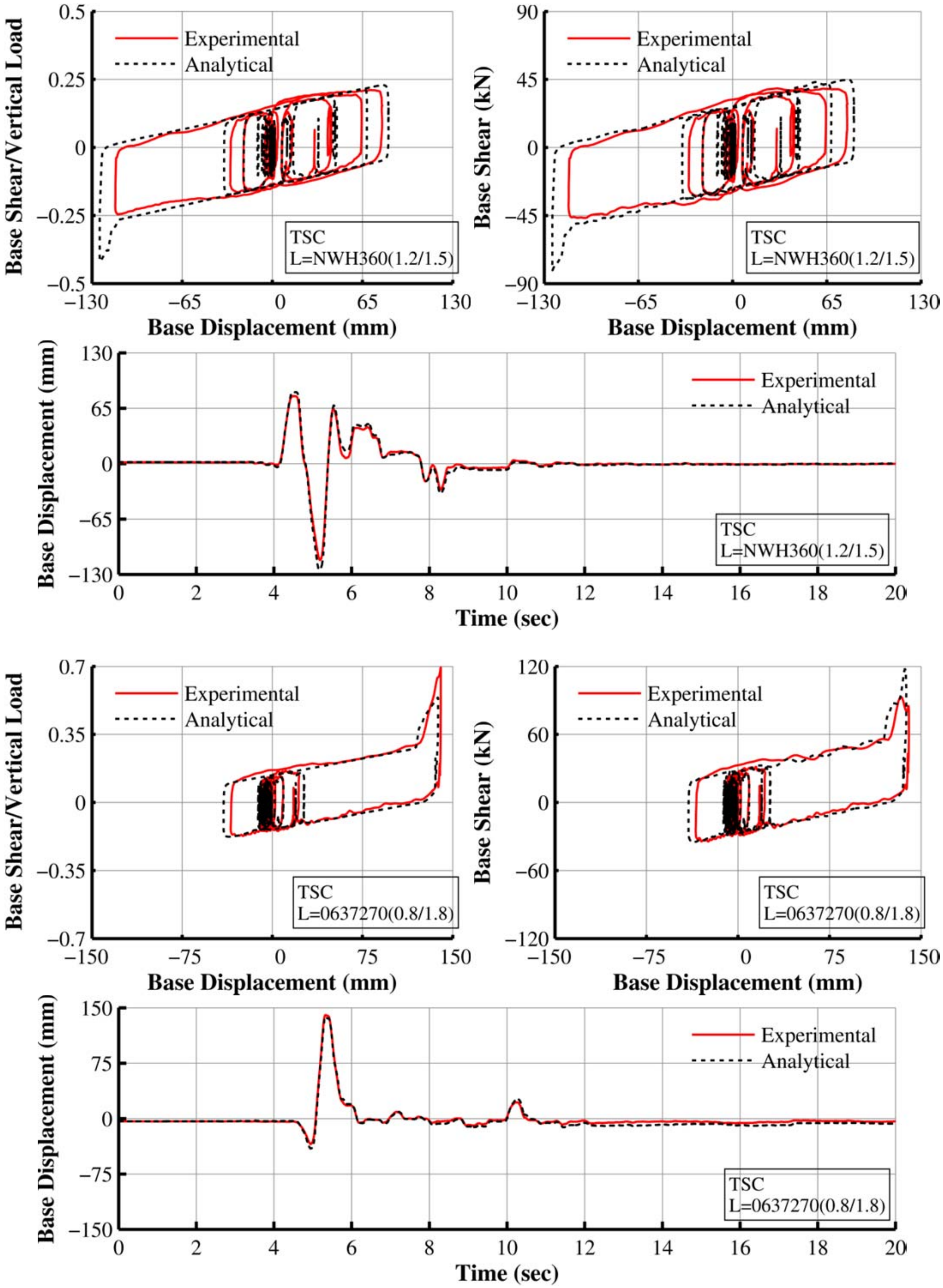

Figure 5-18 (cont'd): Comparison of analytical (program 3pleANI) and experimental results for isolated structure with Configuration C isolators

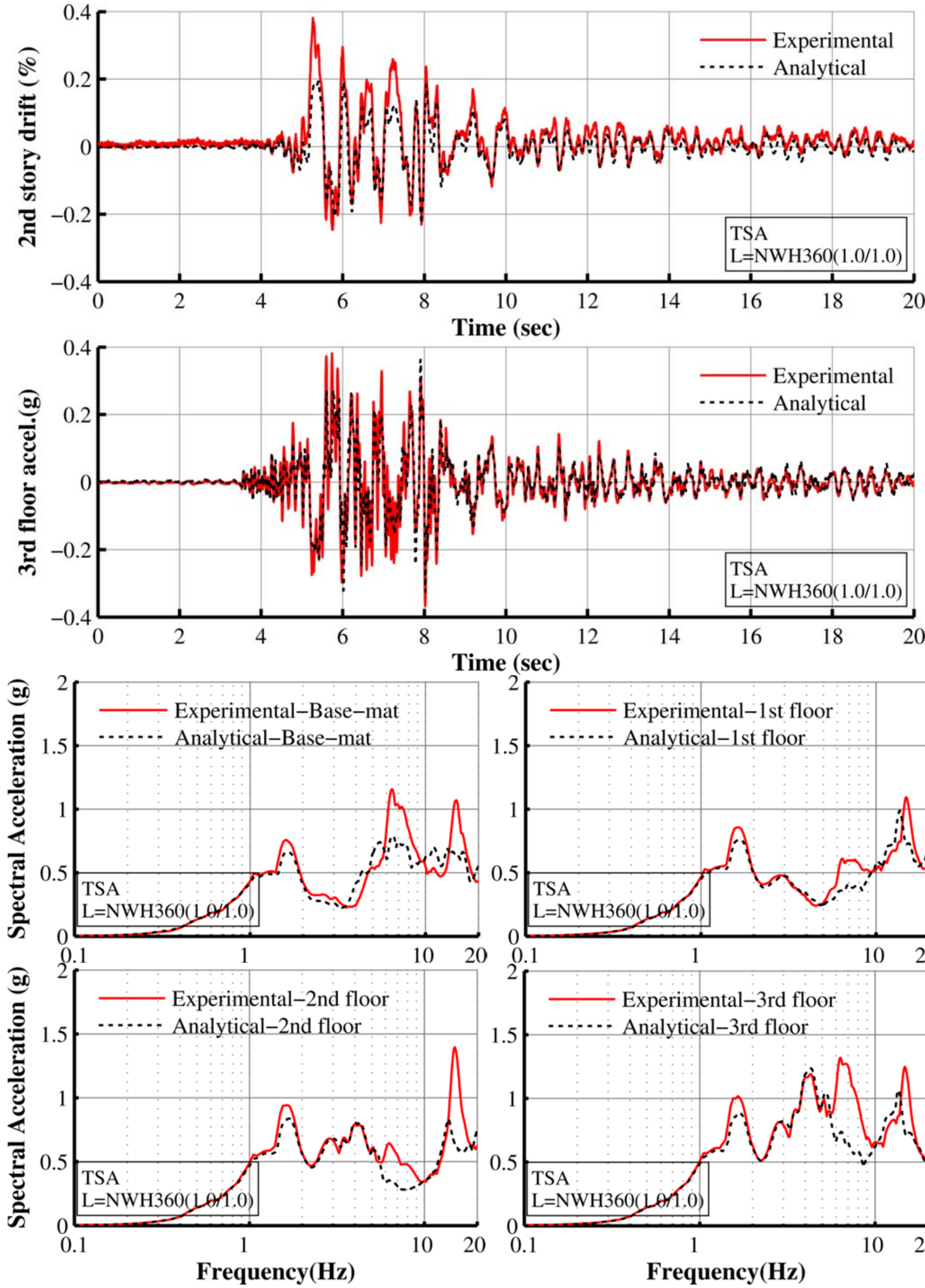

Figure 5-19: Comparison of analytical (program 3pleANI) and experimental results for isolated structure with Configuration A isolators for drift and acceleration histories and 5%-damped floor response spectra

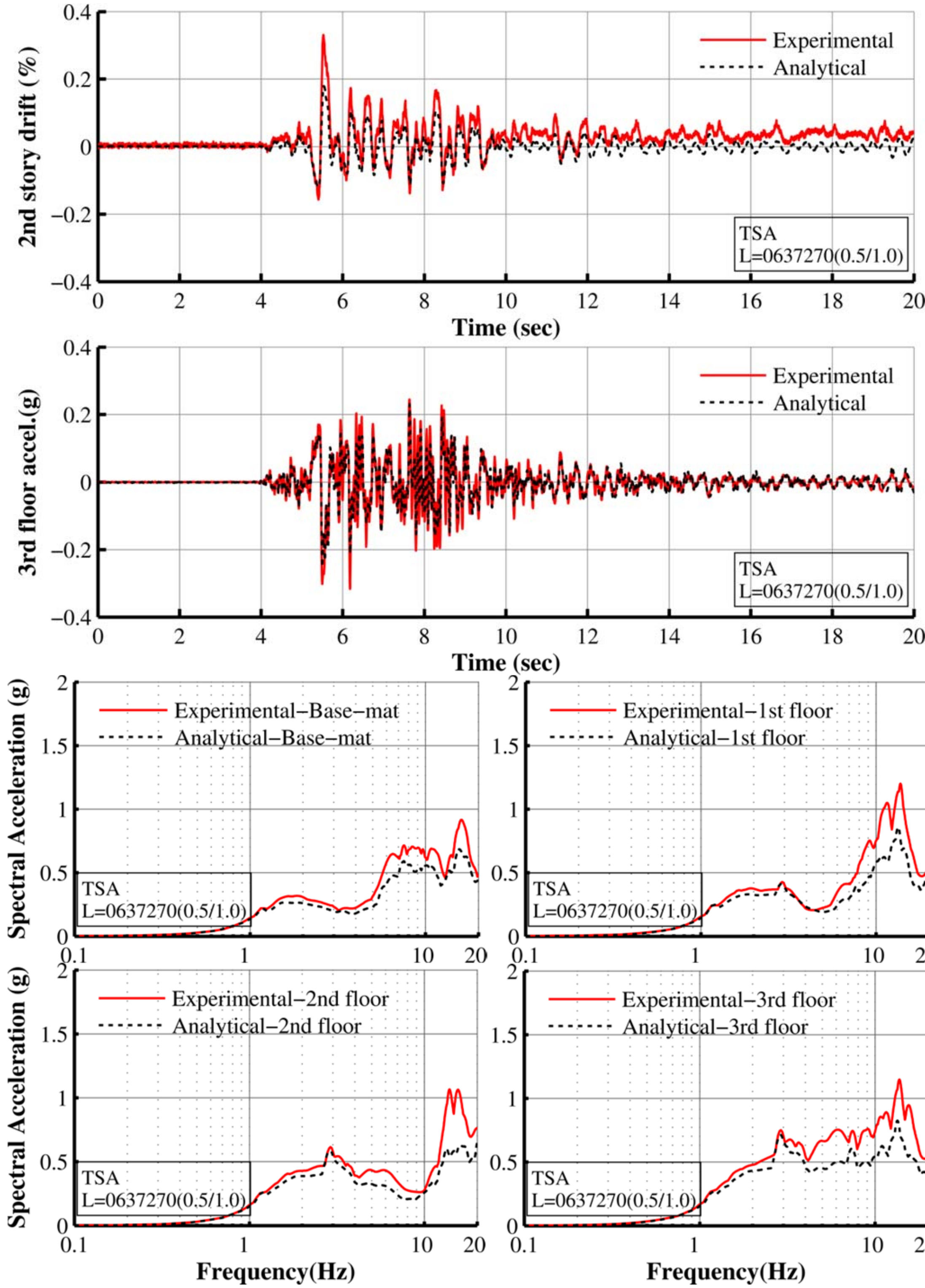

Figure 5-19 (cont'd): Comparison of analytical (program 3pleANI) and experimental results for isolated structure with Configuration A isolators for drift and acceleration histories and 5%-damped floor response spectra

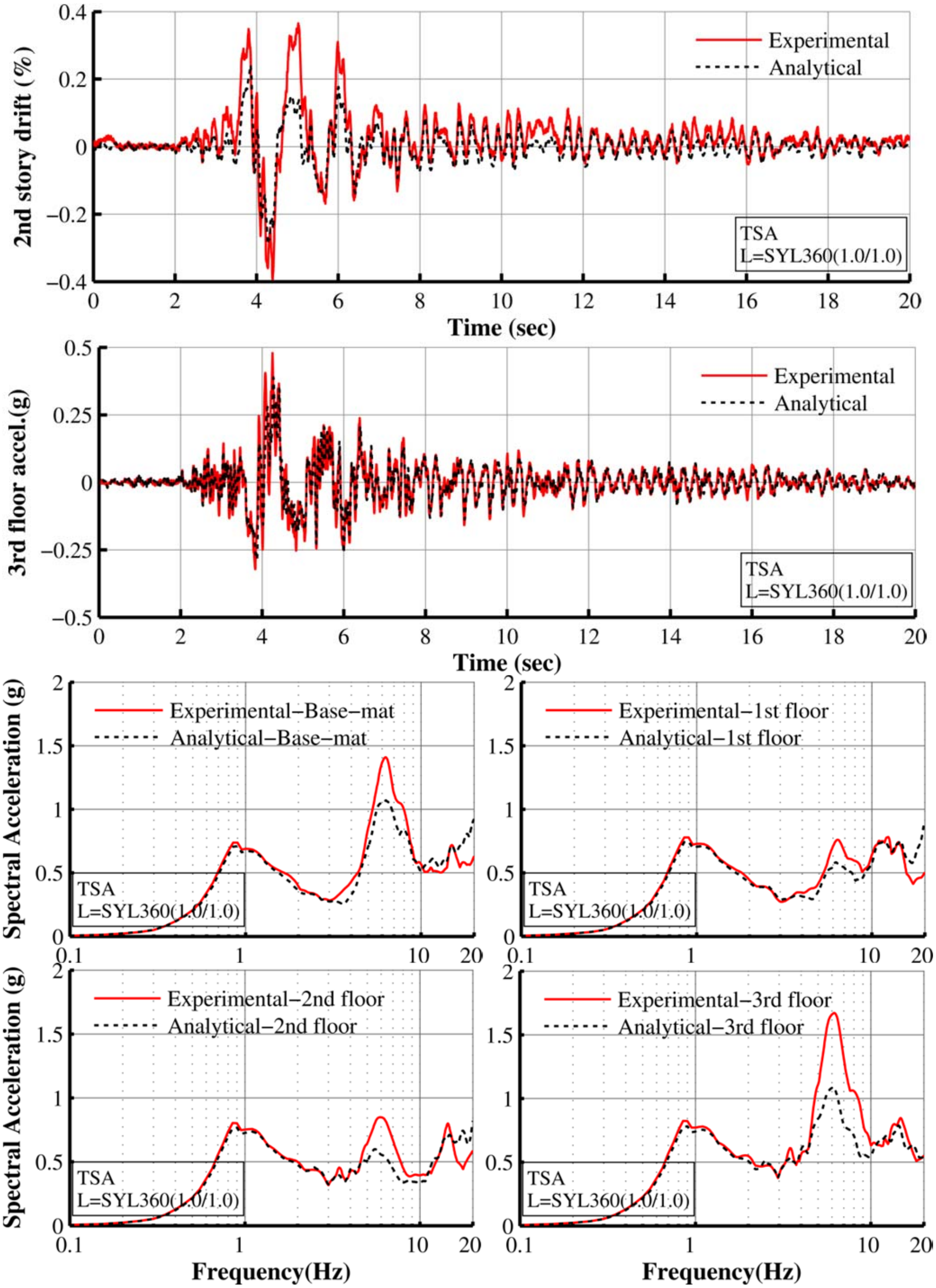

Figure 5-19 (cont'd): Comparison of analytical (program 3pleANI) and experimental results for isolated structure with Configuration A isolators for drift and acceleration histories and 5%-damped floor response spectra

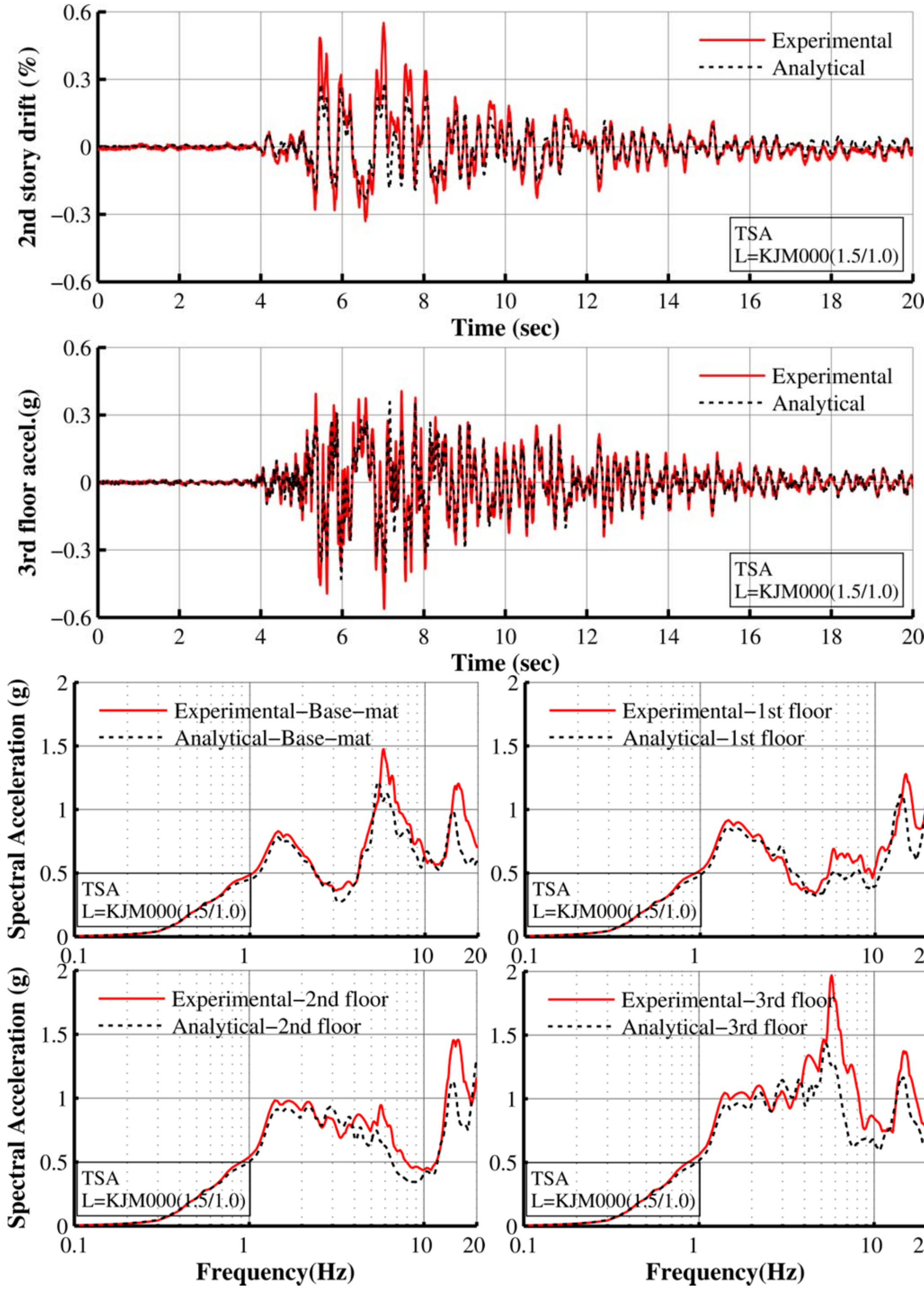

Figure 5-19 (cont'd): Comparison of analytical (program 3pleANI) and experimental results for isolated structure with Configuration A isolators for drift and acceleration histories and 5%-damped floor response spectra

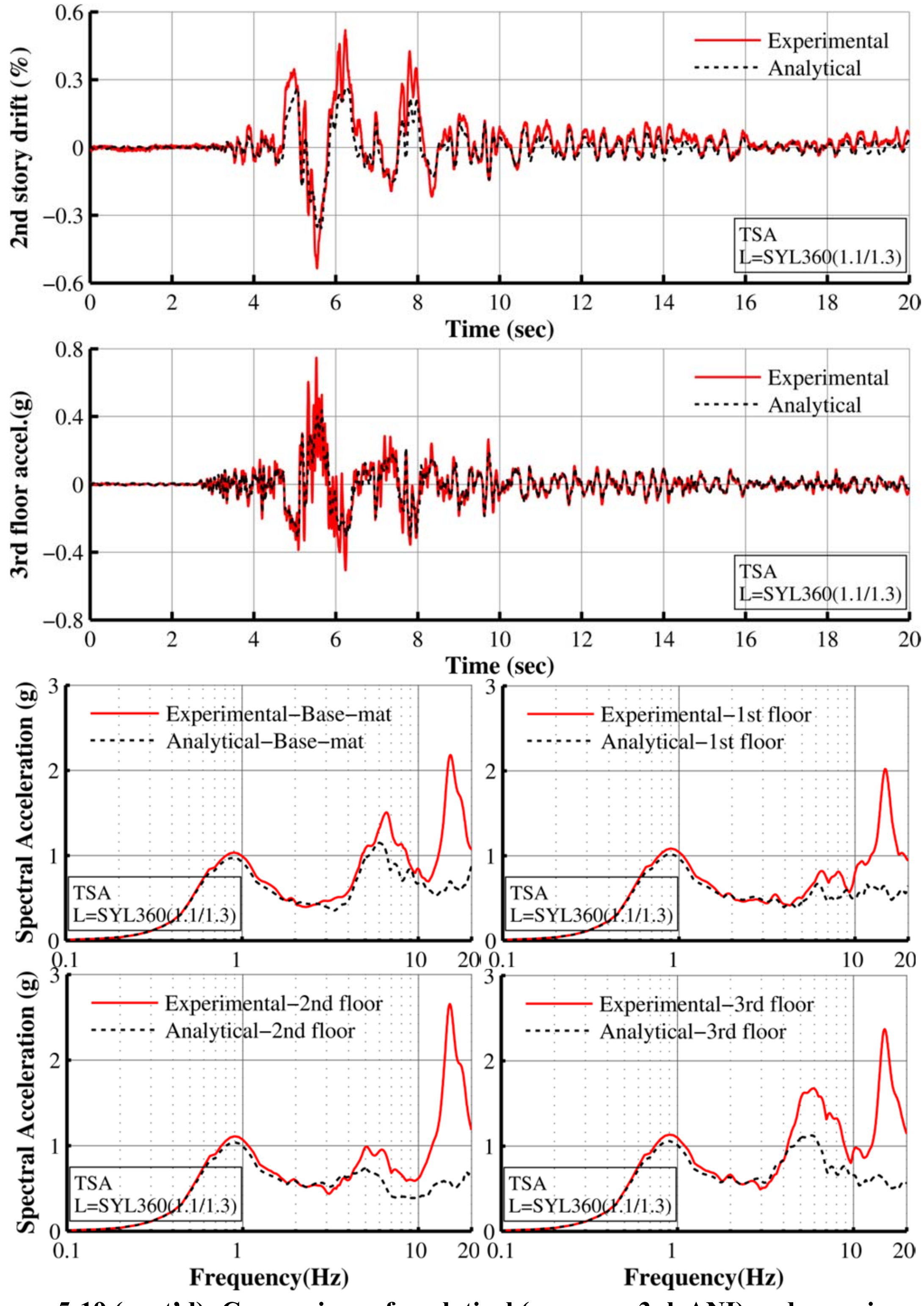

Figure 5-19 (cont'd): Comparison of analytical (program 3pleANI) and experimental results for isolated structure with Configuration A isolators for drift and acceleration histories and 5%-damped floor response spectra

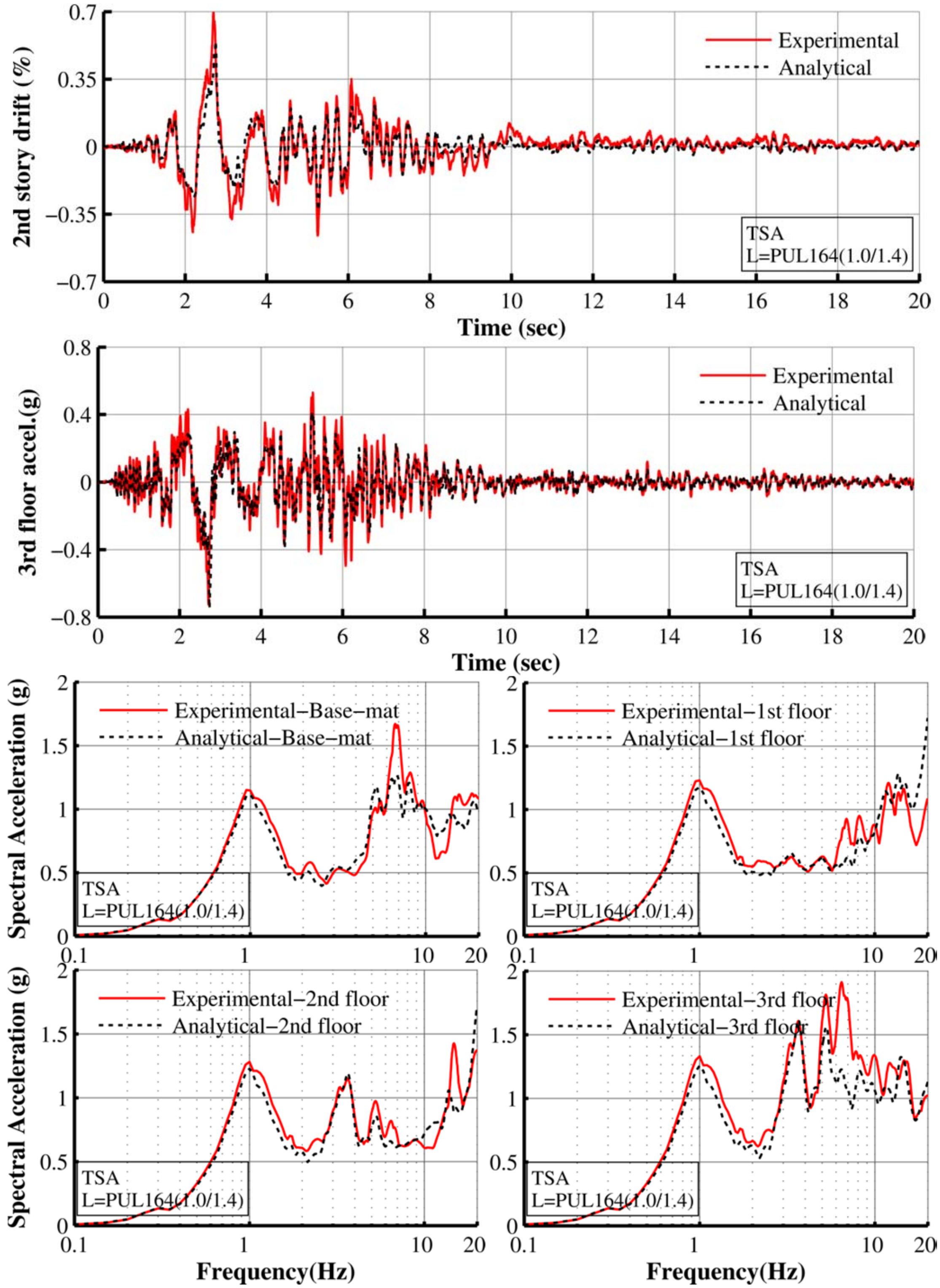

Figure 5-19 (cont'd): Comparison of analytical (program 3pleANI) and experimental results for isolated structure with Configuration A isolators for drift and acceleration histories and 5%-damped floor response spectra

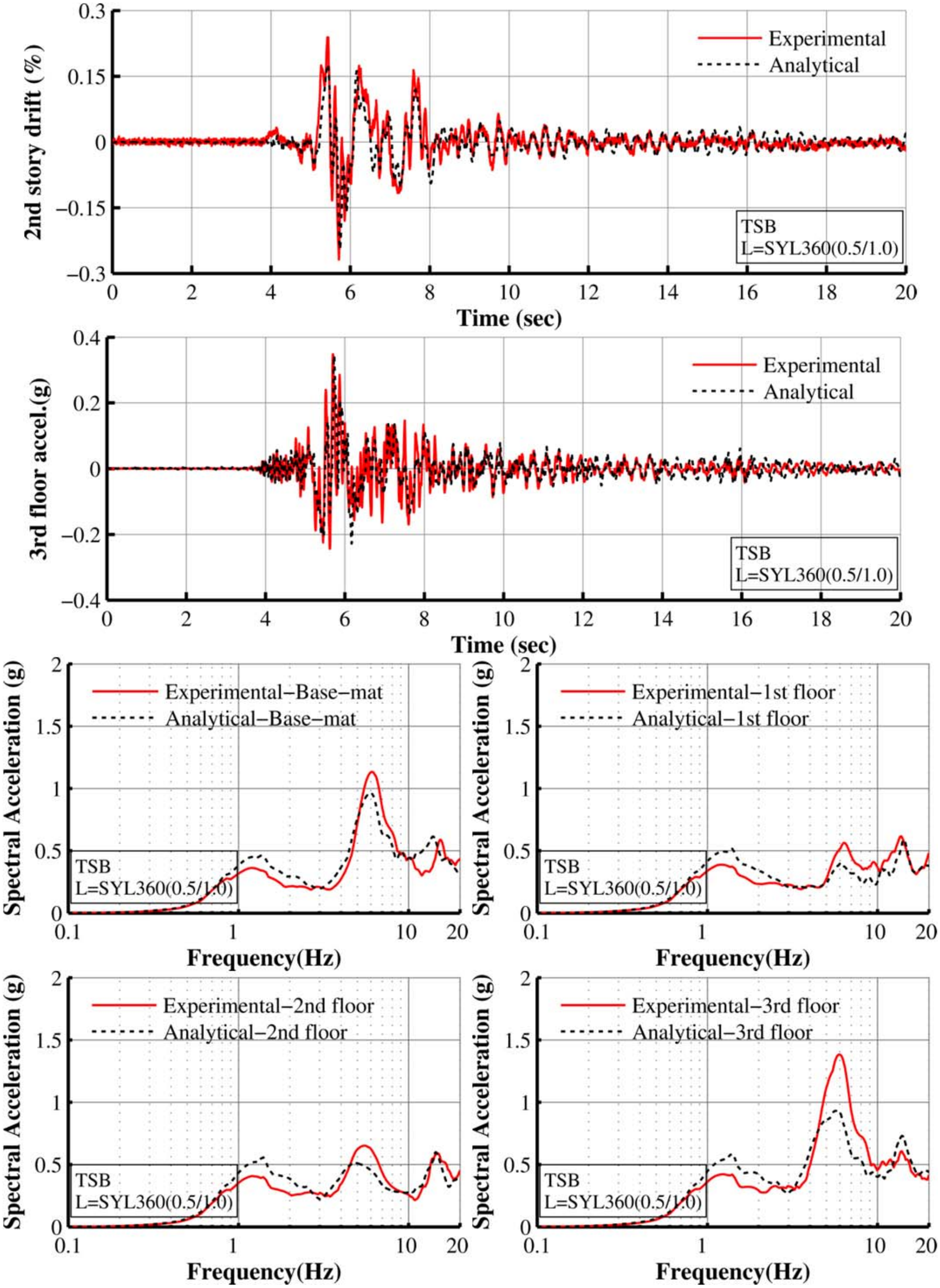

Figure 5-20: Comparison of analytical (program 3pleANI) and experimental results for isolated structure with Configuration A isolators for drift and acceleration histories and 5%-damped floor response spectra

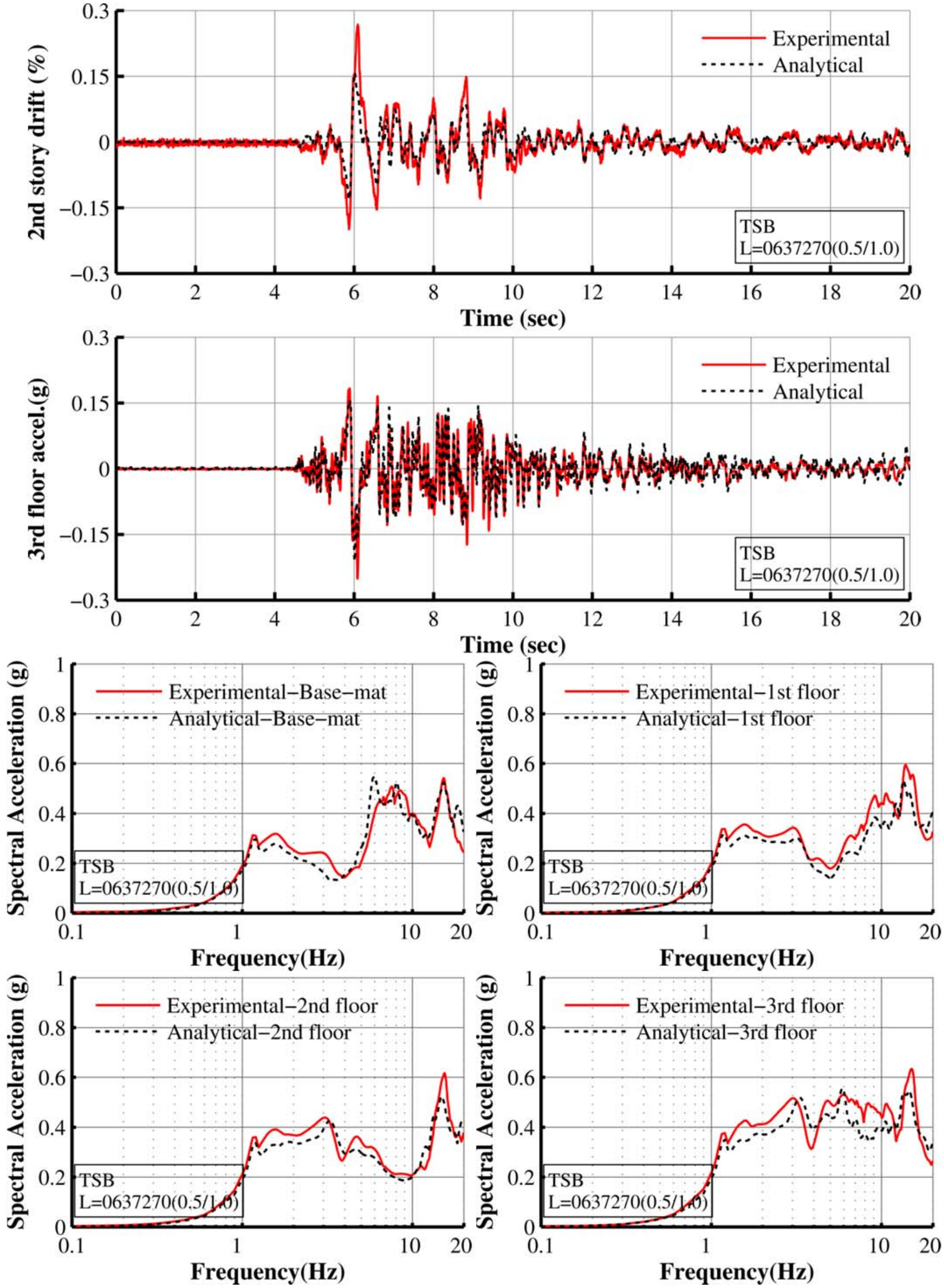

Figure 5-20 (cont'd): Comparison of analytical (program 3pleANI) and experimental results for isolated structure with Configuration B isolators for drift and acceleration histories and 5%-damped floor response spectra

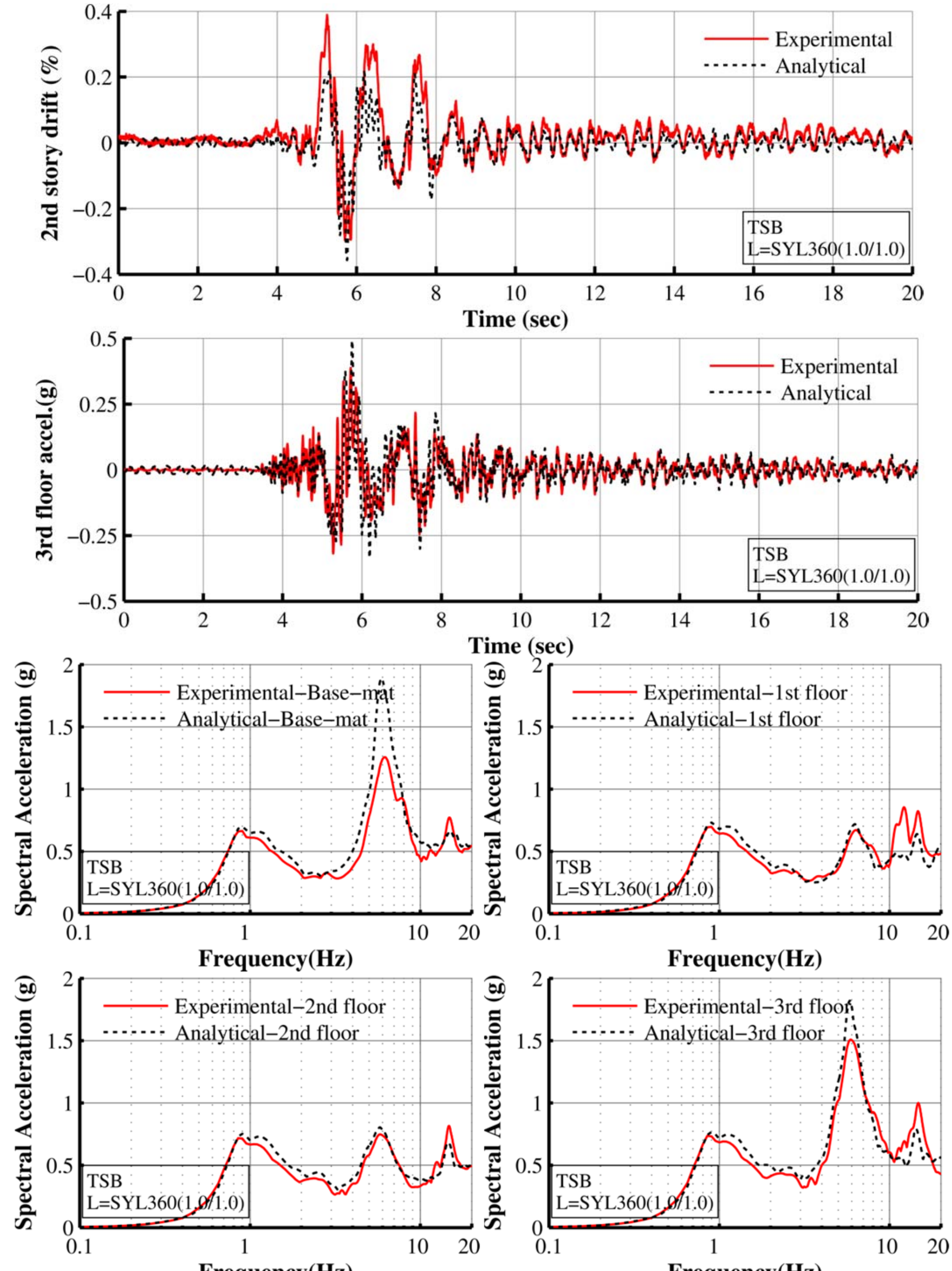

Figure 5-20 (cont'd): Comparison of analytical (program 3pleANI) and experimental results for isolated structure with Configuration B isolators for drift and acceleration histories and 5%-damped floor response spectra

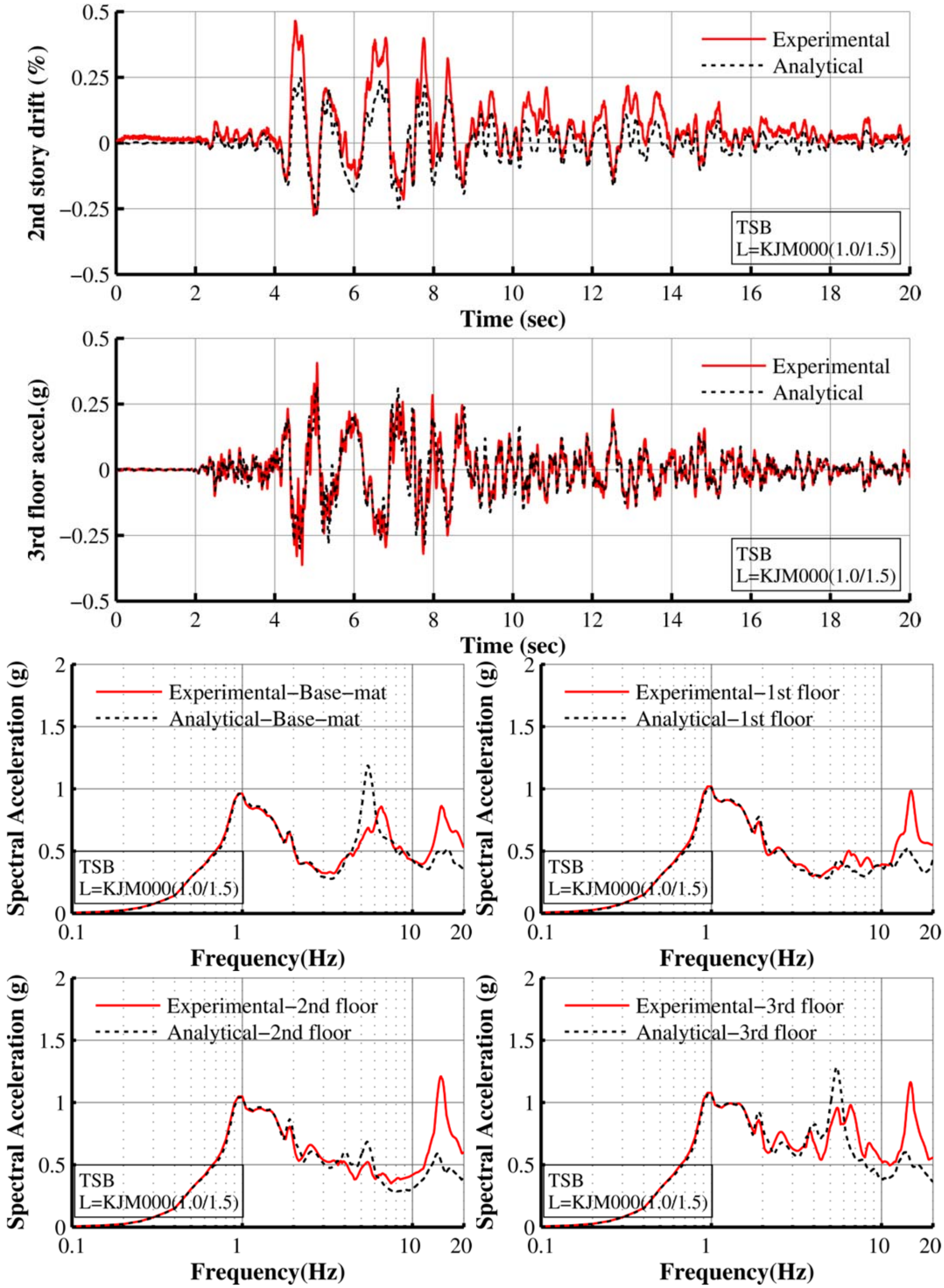

Figure 5-20 (cont'd): Comparison of analytical (program 3pleANI) and experimental results for isolated structure with Configuration B isolators for drift and acceleration histories and 5%-damped floor response spectra

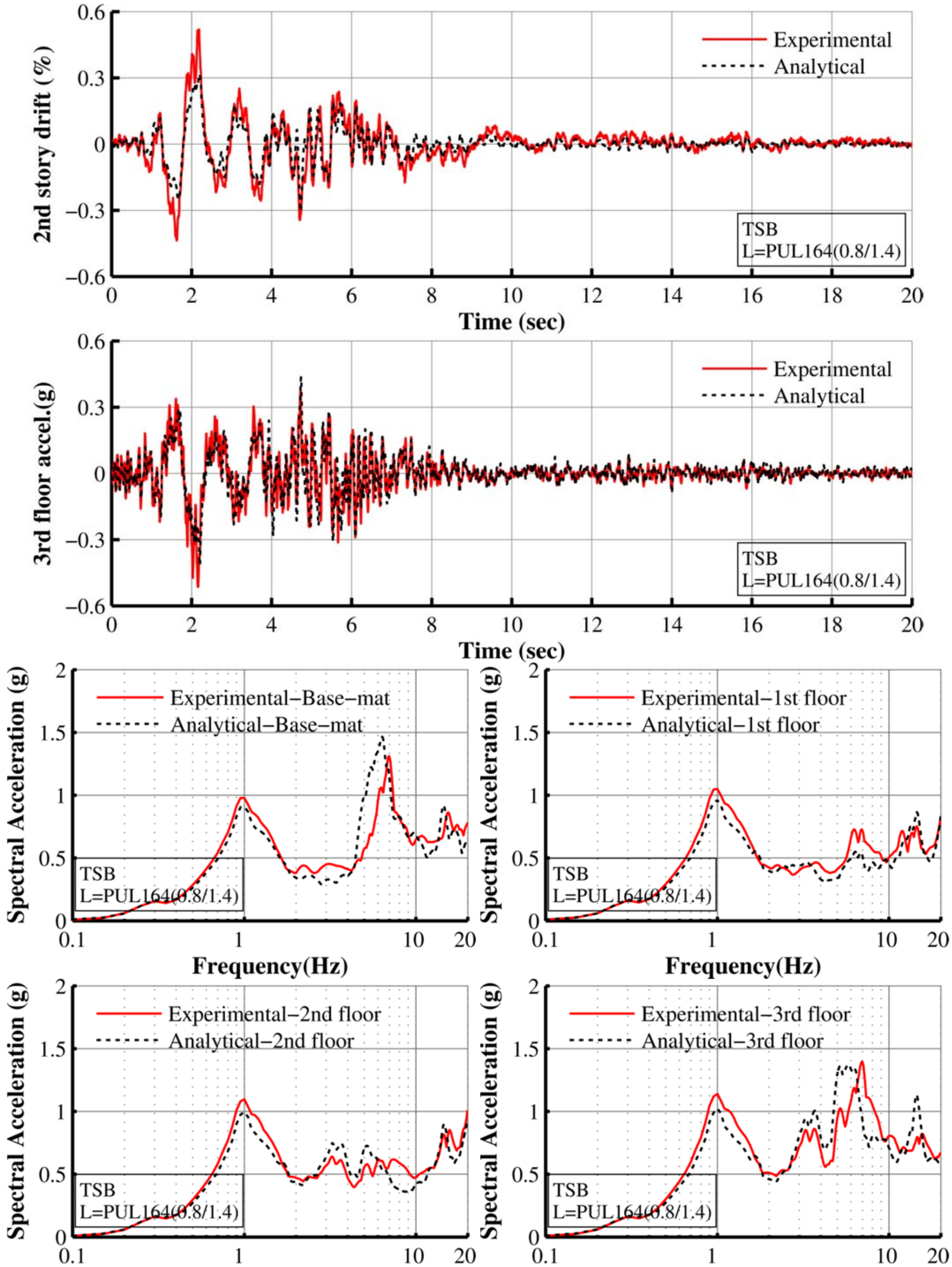

Figure 5-20 (cont'd): Comparison of analytical (program 3pleANI) and experimental results for isolated structure with Configuration B isolators for drift and acceleration histories and 5%-damped floor response spectra

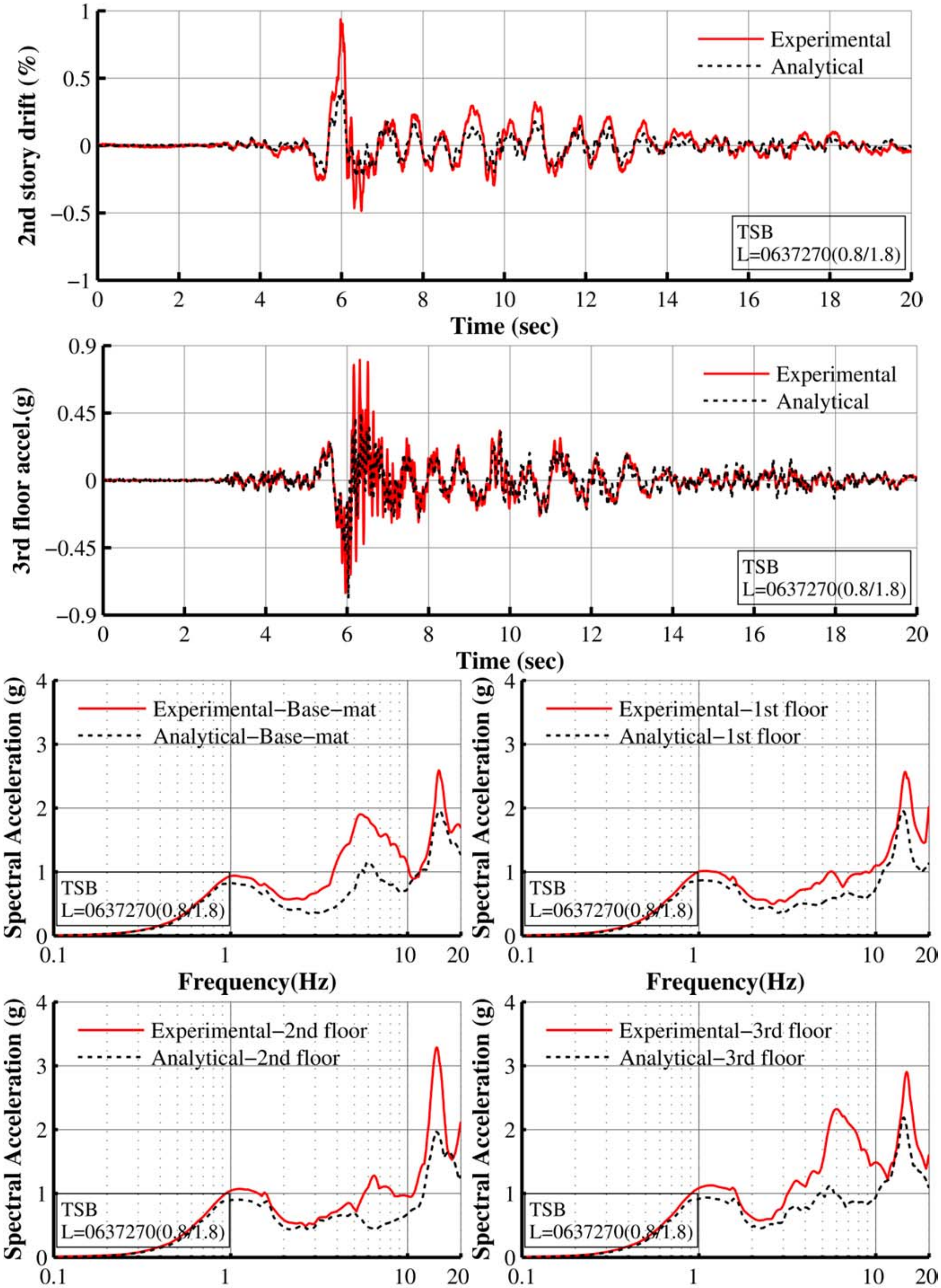

Figure 5-20 (cont'd): Comparison of analytical (program 3pleANI) and experimental results for isolated structure with Configuration B isolators for drift and acceleration histories and 5%-damped floor response spectra

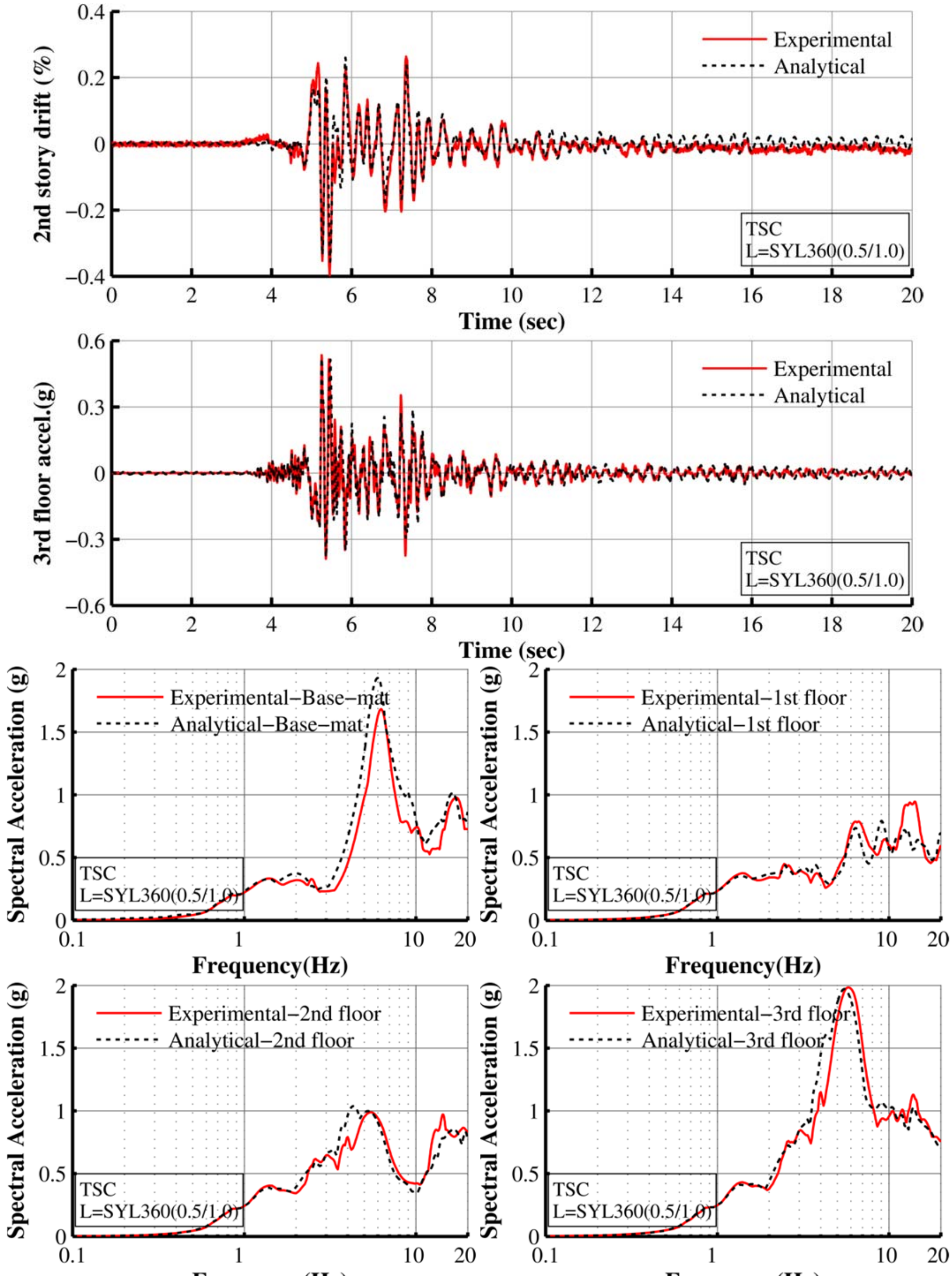

Figure 5-21: Comparison of analytical (program 3pleANI) and experimental results for isolated structure with Configuration C isolators for drift and acceleration histories and 5%-damped floor response spectra

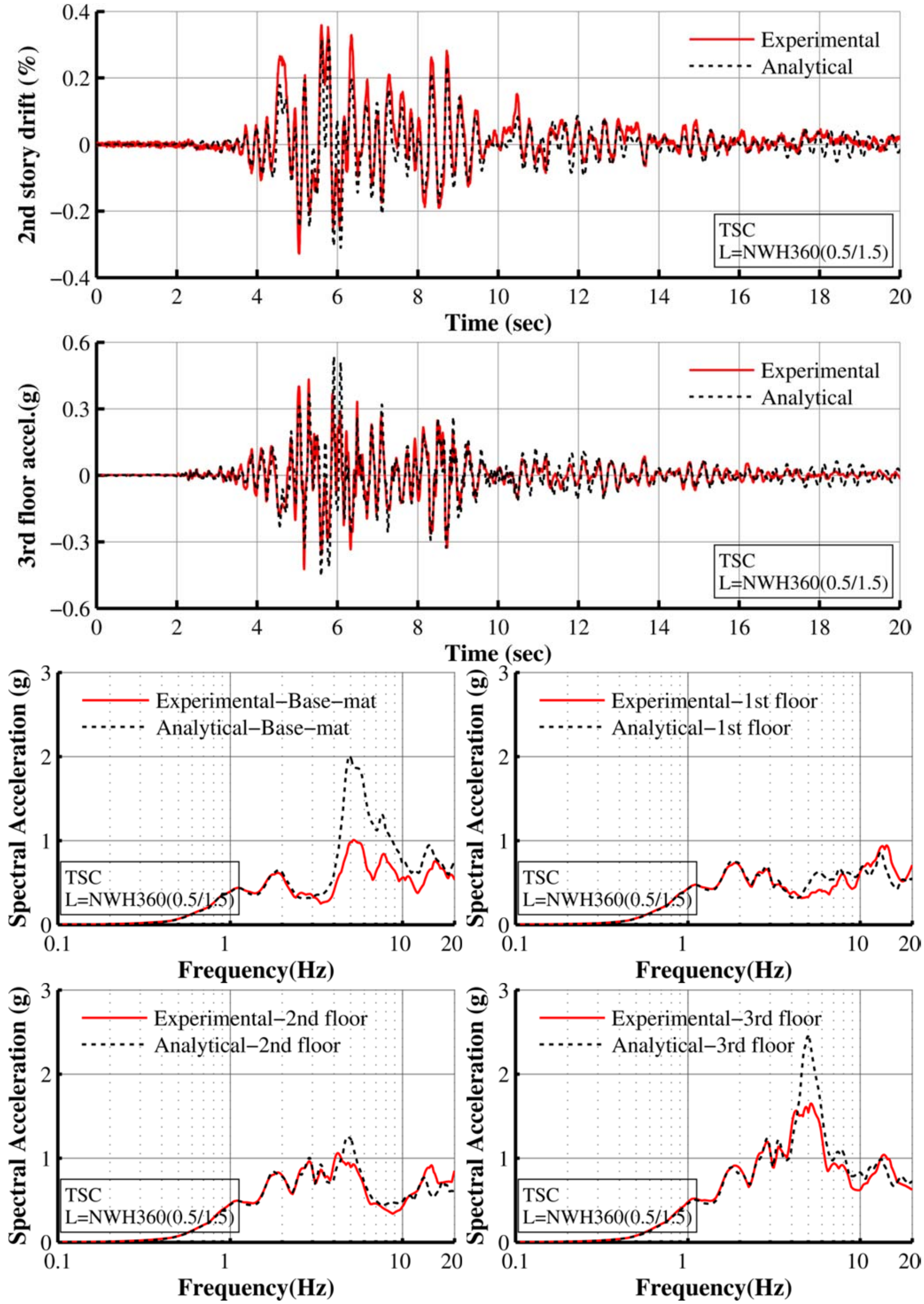

Figure 5-21 (cont'd): Comparison of analytical (program 3pleANI) and experimental results for isolated structure with Configuration C isolators for drift and acceleration histories and 5%-damped floor response spectra

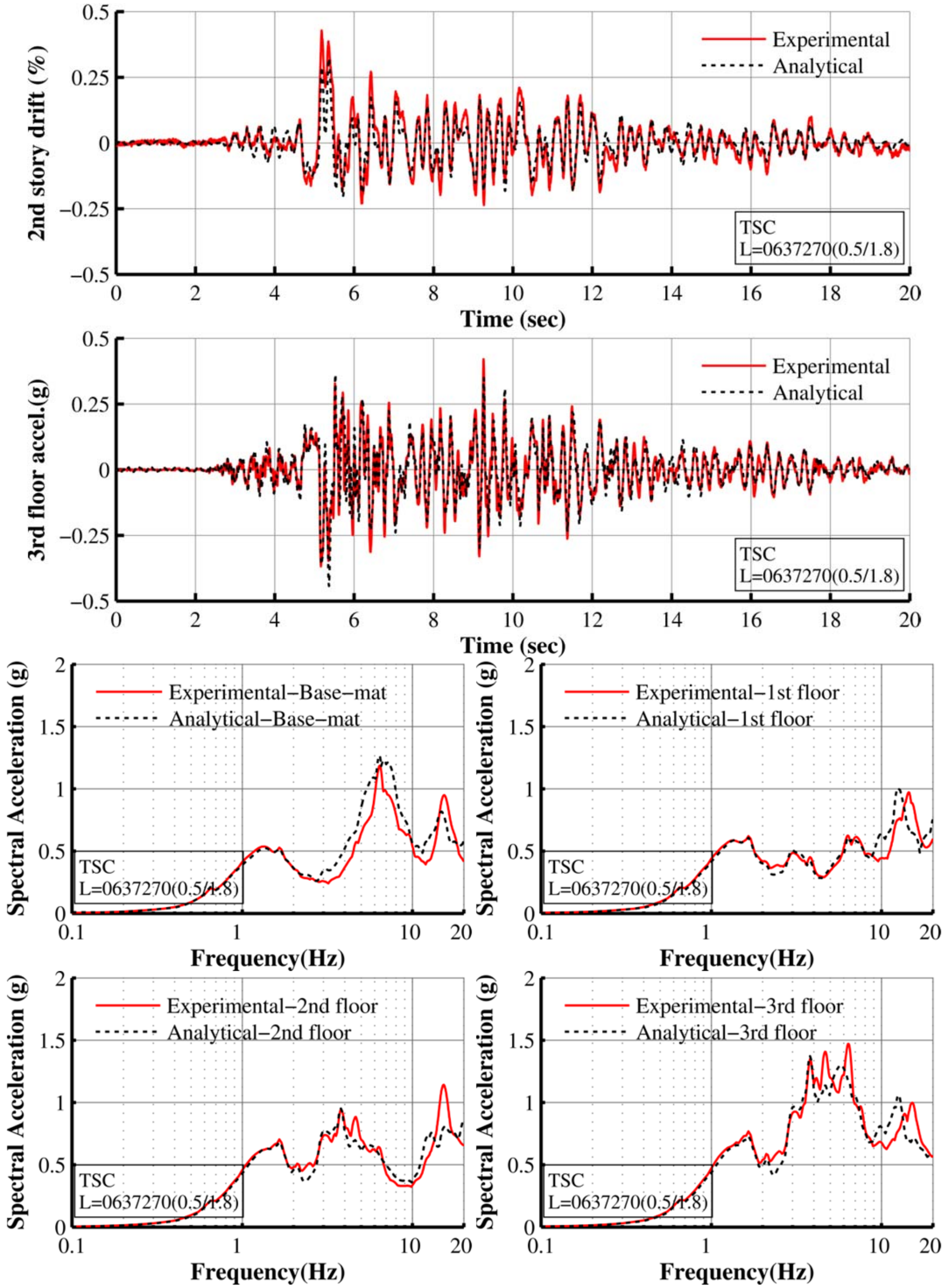

Figure 5-21 (cont'd): Comparison of analytical (program 3pleANI) and experimental results for isolated structure with Configuration C isolators for drift and acceleration histories and 5%-damped floor response spectra

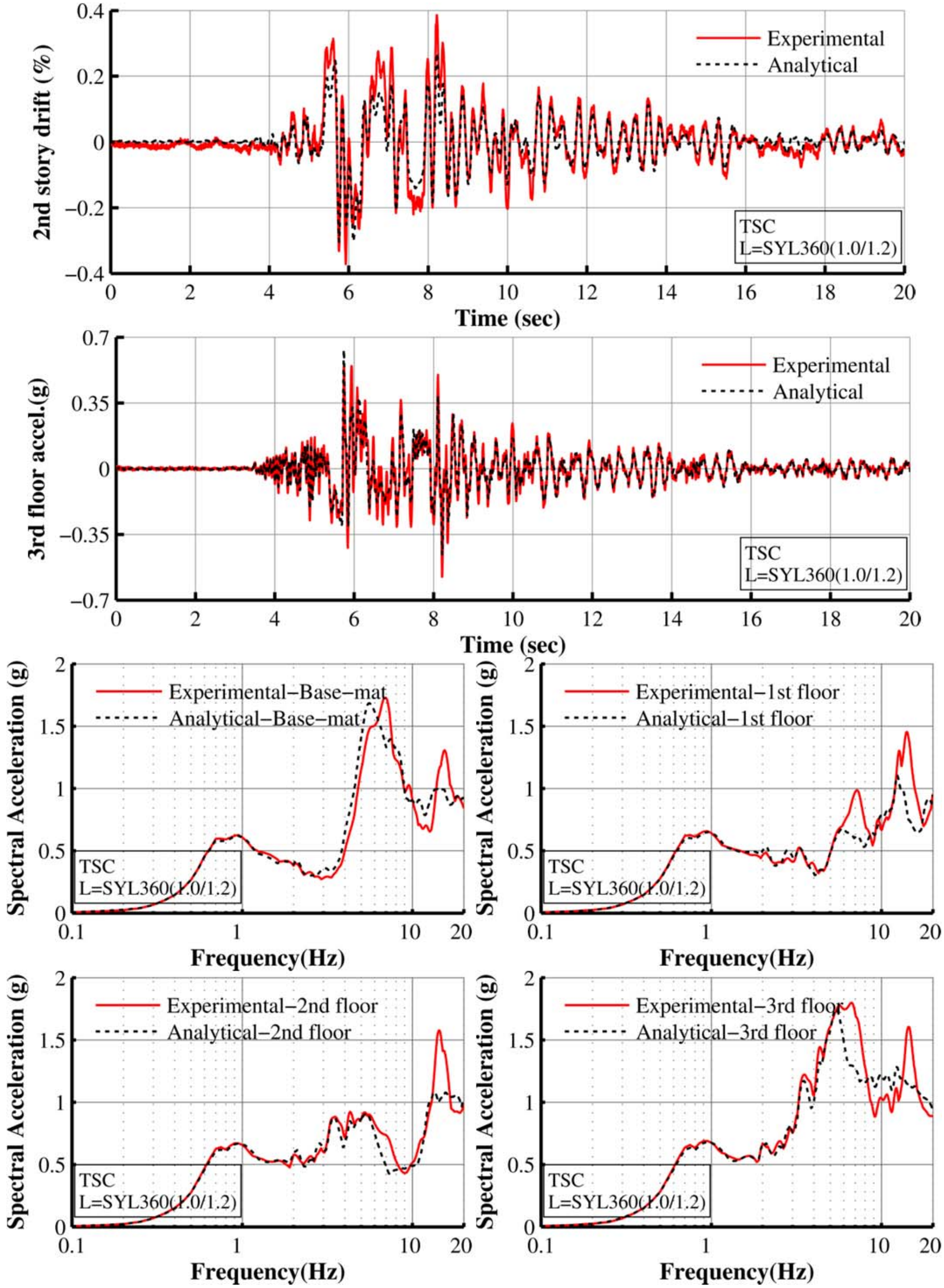

Figure 5-21 (cont'd): Comparison of analytical (program 3pleANI) and experimental results for isolated structure with Configuration C isolators for drift and acceleration histories and 5%-damped floor response spectra

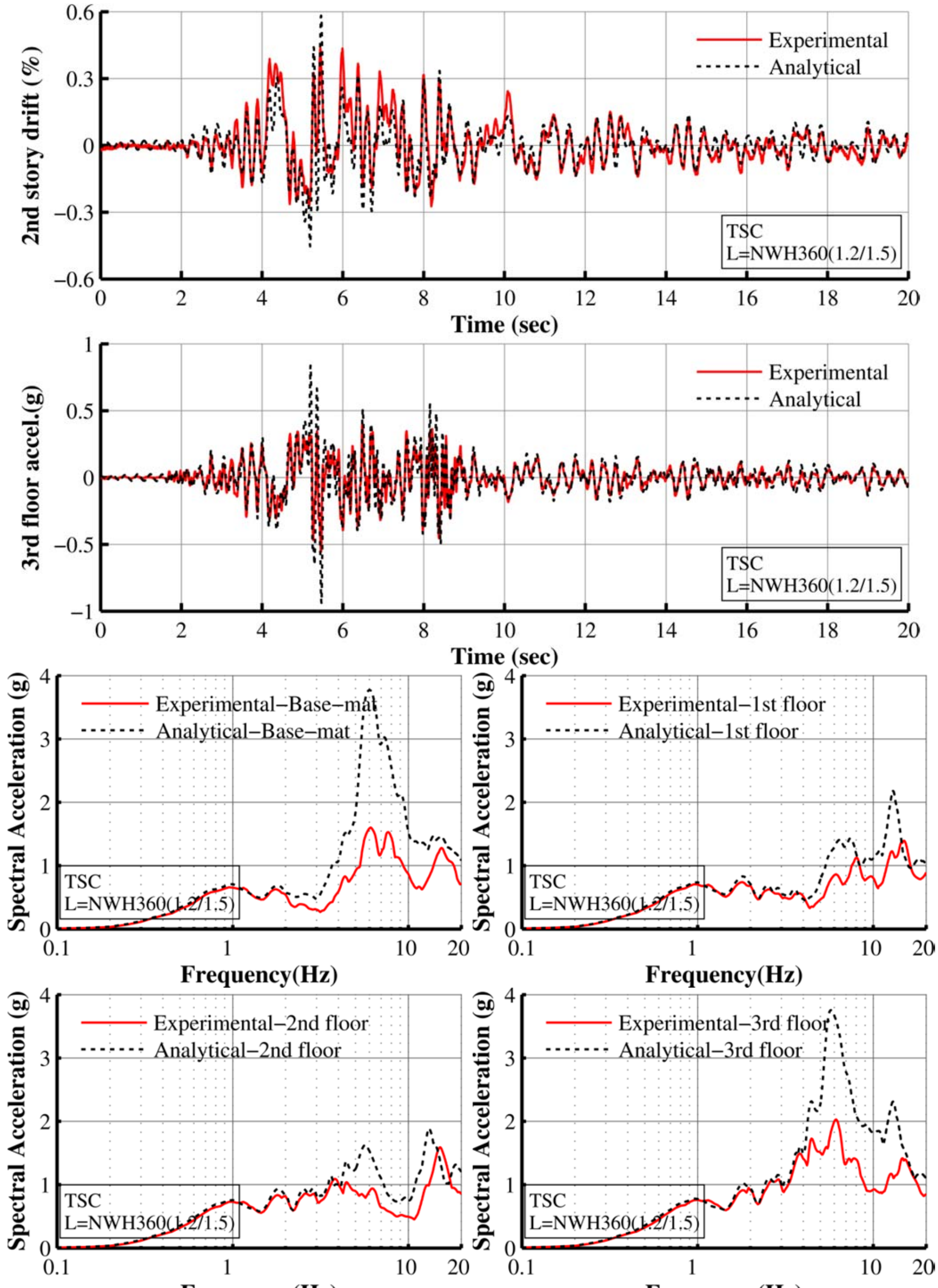

Figure 5-21 (cont'd): Comparison of analytical (program 3pleANI) and experimental results for isolated structure with Configuration C isolators for drift and acceleration histories and 5%-damped floor response spectra

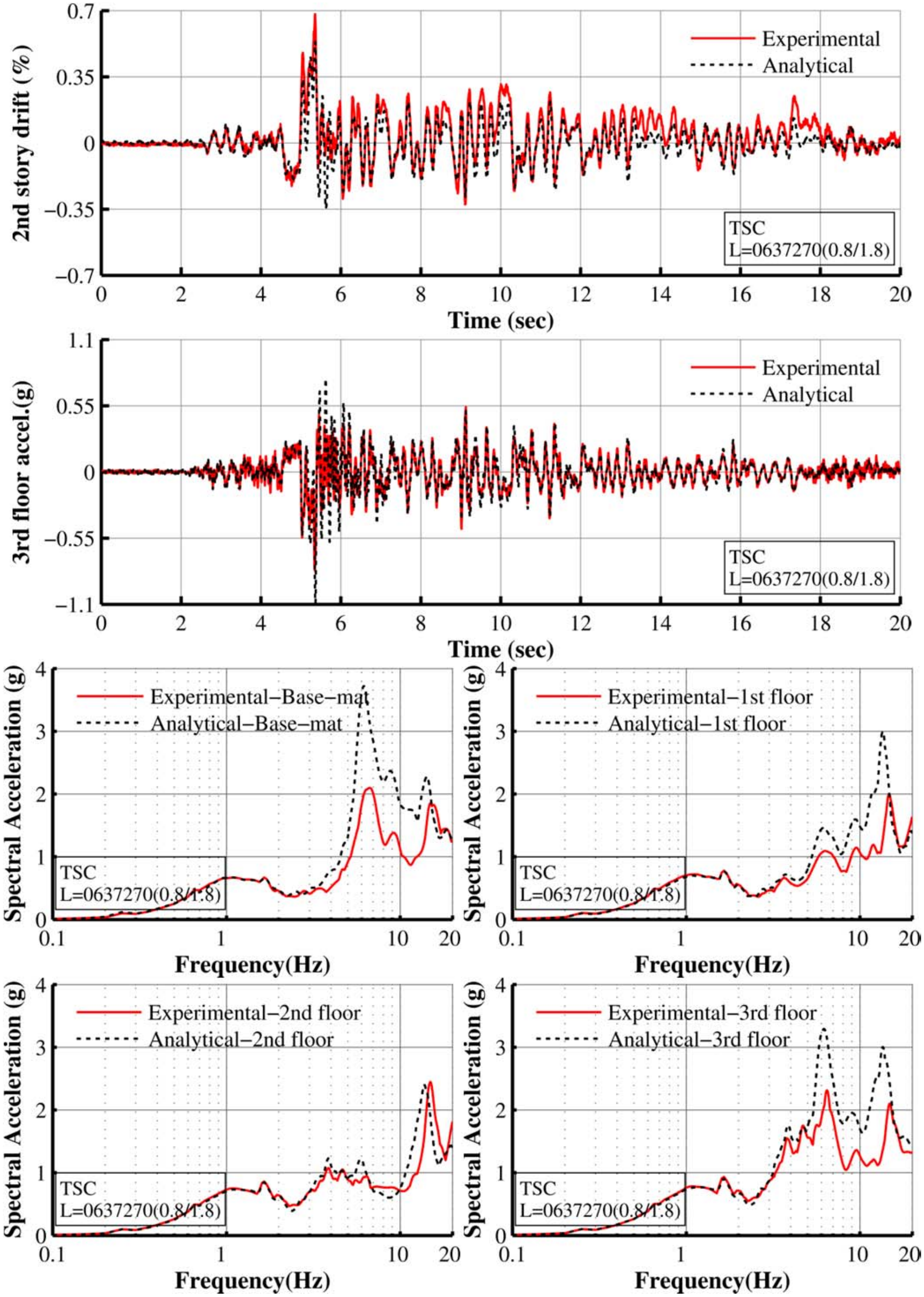

Figure 5-21 (cont'd): Comparison of analytical (program 3pleANI) and experimental results for isolated structure with Configuration C isolators for drift and acceleration histories and 5%-damped floor response spectra

5.5 Analytical Prediction Using Program SAP2000

The superstructure, fixed at its base, was modeled in program SAP2000 using linear elastic frame elements for all beams, columns and braces. The diaphragm bracing of the superstructure was explicitly modeled and no diaphragm constraints were assigned. The concrete blocks were modeled as lumped masses without mass moment of inertia. The self-weight of the frame was explicitly captured using the steel density value for the material in SAP2000. Additional small masses were added at the base-mat to capture the difference in the total weight calculated by the program and the one obtained from measurement by the load cells. This additional weight was contributed by the elements not accounted for in the model, such as steel connecting plates, stiffeners, bolts and connection angles. Due to the large dimensions of the base-mat beams compared to the superstructure elements, rigid beam elements have been used to connect the bottom of the columns to the centerline of the W360 beams of the base-mat. Rigid offsets have not been used for the beam-to-column connections of the structure. Table 5-3 presents results for the modal properties of the model, fixed at the base, as obtained by program SAP2000 for the first three modes. The damping ratio is the value assigned for each mode in SAP2000 for the construction of the inherent damping matrix. Note that the assigned damping ratio values are between the values identified in the two sets of experiments and presented in Table 4-1 and Table 4-2. There is good agreement between the mode shapes and period values obtained in the experimental identification (Table 4-1 and Table 4-2) and the results of the modal analysis in SAP2000.

Analysis of the fixed-base superstructure with seismic motion at its base was conducted and results are compared to experimental results in Figure 5-22 to Figure 5-24 in terms of histories of inter-story drift and floor acceleration, and 5%-damped floor acceleration spectra. Results are in good agreement but, as in the case of analysis with program 3pleANI, the peak values of response are occasionally over-estimated or under-estimated by the analytical model.

Table 5-3: Modal characteristics of analytical model in SAP2000

Mode	Period (sec)	Assigned Damping Ratio	Mode Shape		
			1st floor	2nd floor	3rd floor
1st	0.292	0.0650	0.331	0.741	1.000
2nd	0.092	0.0100	1.176	0.808	-1.000
3rd	0.053	0.0078	2.286	-2.397	1.000

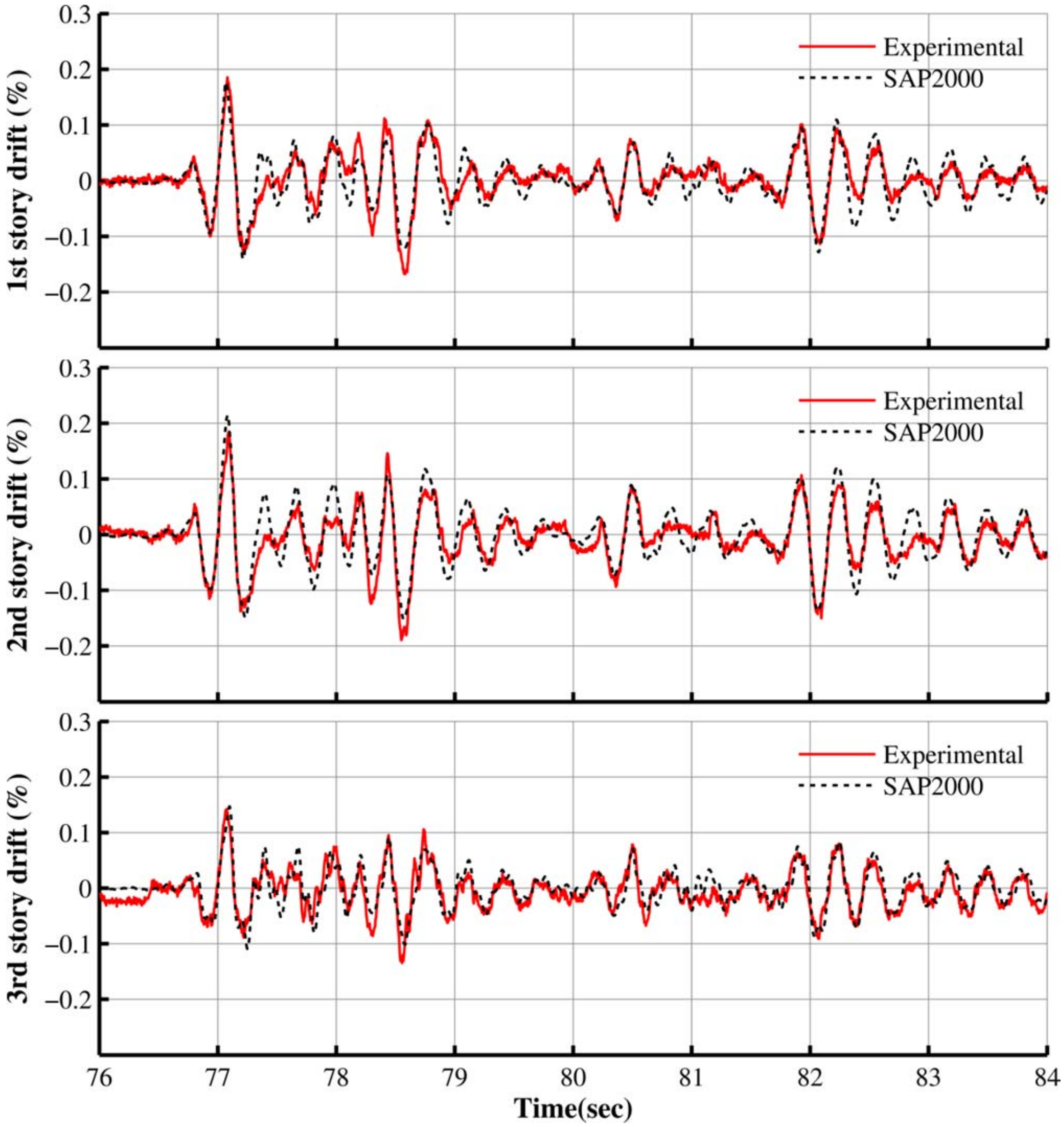

Figure 5-22: Comparison of analytical (program SAP2000) and experimental results for inner-story drift of fixed structure for ground motion ATL-270

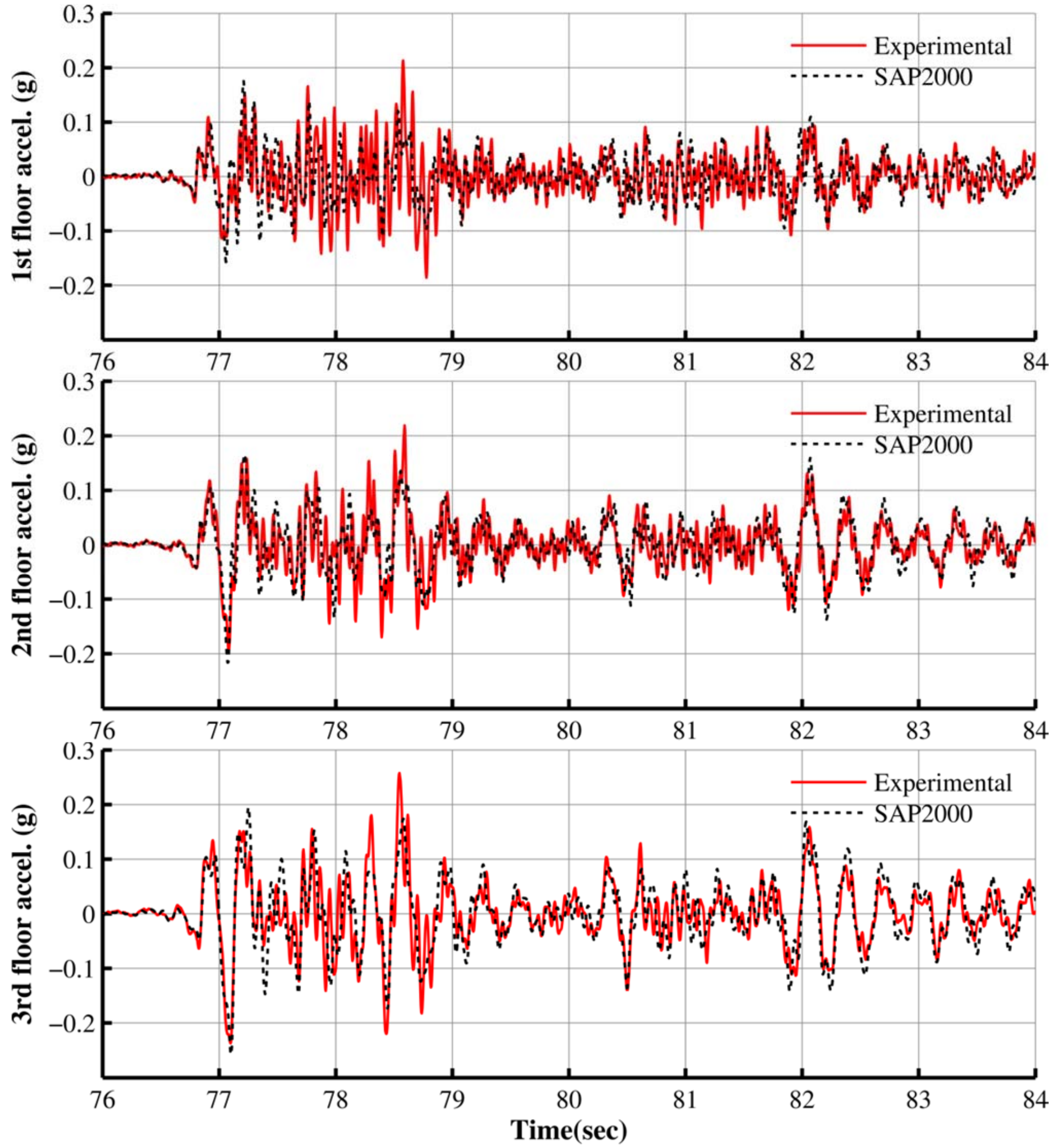

Figure 5-23: Comparison of analytical (program SAP2000) and experimental results for floor acceleration of fixed structure for ground motion ATL-270

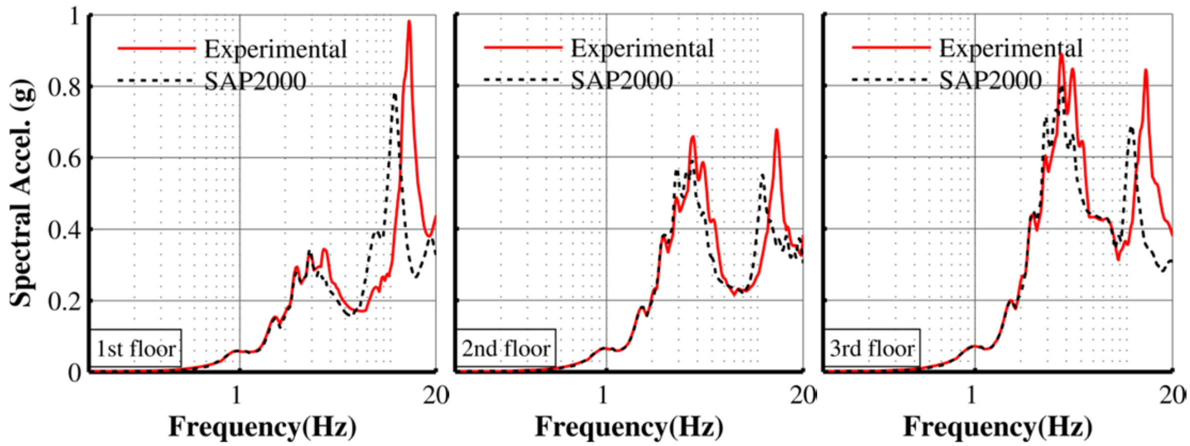

Figure 5-24: Comparison of analytical (program SAP2000) and experimental results for 5%-damped floor response spectra of fixed structure for ground motion ATL-270

In SAP2000, the Triple FP isolators were modeled using the series model described in Fenz and Constantinou (2008d and e). The series model consists of three friction pendulum elements arranged in series and denoted as FP1, FP2 and FP3. Gap elements are connected between the top and bottom joints of the FP2 element and the top and bottom joints of the FP3 element. The properties specified in program SAP2000 for the series model representation of the isolators are shown in Table 5-4. For more details on how these properties are selected, the reader is referred to Fenz and Constantinou (2008d and e) and Sarlis and Constantinou (2010). Note that the effective stiffness of element FP1 is assigned a small value so that "damping leakage" is minimized (Sarlis and Constantinou, 2010). Also, the effective stiffness of elements FP2 and FP3 is assigned a large value in order to reduce the execution time. Given that elements FP1, FP2 and FP3 are arranged in series, the high effective stiffness of elements FP2 and FP3 does not affect the total effective stiffness of the assembly (so that damping leakage is minimized). Also the vertical stiffness of the elements is selected such that the dominant mode of the structure in the vertical direction has the same frequency as the one measured in the experiments (as obtained from transfer functions of the base of the structure in the vertical direction from records of accelerations and for tests that included a vertical component).

Table 5-4: Series model properties of Triple FP isolators in program SAP2000

SAP2000 element ID	FP1			FP2			FP3		
Configuration	**A**	**B**	**C**	**A**	**B**	**C**	**A**	**B**	**C**
Element Height (mm)	25.4			38.1			38.1		
Shear Deformation Location from bottom (mm)	0			0			0		
Element Mass (kN-s^2/mm)	0.00002			0.1			0.1		
Yield Displacement (mm)	0.1			0.1			0.1		
Vertical Stiffness (kN/mm)	235			235			235		
Rotational/Torsional Stiffness (R1,R2,R3)	0			Fixed			Fixed		
Rotational Moment of Inertia (kN-mm-sec^2)	0.00113			0			0		
Isolator 1									
Effect. Stiffness (kN/mm)	0.0175			130	150	120	130	310	120
Elastic Stiffness (kN/mm)	30	60	528	130	150	120	240	310	120
Radius (mm)	106	116	106	382	382	382	382	382	382
Friction Slow	0.02	0.04	0.264	0.055	0.09	0.07	0.11	0.16	0.07
Friction Fast	0.06	0.07	0.28	0.12	0.165	0.135	0.14	0.21	0.135
Rate Parameter (sec/mm)	0.03	0.015	0.01	0.102	0.046	0.0175	0.0239	0.052	0.0175
Isolator 2									
Effect. Stiffness (kN/ mm)	0.0175			130	126	120	130	208	120
Elastic Stiffness(kN/ mm)	40	20	510	154	126	120	420	208	120
Radius (mm)	106	106	106	382	382	382	382	382	382
Friction Slow	0.02	0.01	0.255	0.067	0.063	0.06	0.20	0.124	0.06
Friction Fast	0.055	0.02	0.27	0.12	0.12	0.15	0.24	0.225	0.15
Rate Parameter (sec/mm)	0.03	0.015	0.01	0.102	0.035	0.0175	0.0239	0.081	0.0175
Isolator 3									
Effect. Stiffness (kN/mm)	0.0175			130	70	140	130	190	140
Elastic Stiffness (kN/mm)	40	30	430	136	70	140	400	190	140
Radius (mm)	106	116	106	382	382	382	382	382	382
Friction Slow	0.03	0.015	0.215	0.048	0.035	0.07	0.19	0.095	0.07
Friction Fast	0.065	0.04	0.23	0.095	0.085	0.135	0.24	0.105	0.135
Rate Parameter (sec/mm)	0.03	0.015	0.01	0.102	0.029	0.02	0.0239	0.1036	0.02
Isolator 4									
Effect. Stiffness (kN/mm)	0.0175			130	94	140	130	250	140
Elastic Stiffness (kN/mm)	50	20	390	130	94	140	330	250	140
Radius (mm)	106	116	106	382	382	382	382	382	382
Friction Slow	0.02	0.01	0.195	0.075	0.047	0.07	0.145	0.125	0.07
Friction Fast	0.04	0.04	0.21	0.14	0.14	0.135	0.205	0.20	0.135
Rate Parameter (sec/mm)	0.03	0.015	0.01	0.102	0.029	0.0175	0.0239	0.1036	0.0175

Comparisons of analytical results obtained in SAP2000 to experimental results are presented in Figure 5-25 to Figure 5-30 for tests without vertical component of excitation and in Figure 5-25 and 5-32 for tests with a vertical component of excitation. Six ground motions for each configuration are shown: two for small amplitudes (isolator displacement<50mm), two for moderate amplitude (isolator displacement<100mm) and two for high amplitudes (isolator displacement>100mm). The ground motions presented are the same as those presented in Section 5.3 for the analysis with program 3pleANI. Additional results are presented in Appendix C. The effect of the initial base displacement in the SAP2000 analysis was included by creating an additional analysis case where a force was applied at the base and then removed. The force value was such that a permanent displacement was achieved in the analytical model equal to the one measured in the experiments (the process required a trial and error approach in order to find the force vector).

An immediate observation in the results presented in Figure 5-25 to Figure 5-30 is that the fidelity of the analytical prediction by SAP2000 is similar to that of program 3pleANI (presented in Section 5.3), although the program 3pleANI results appear slightly better than those of SAP2000 likely due to (a) better modeling of the velocity dependence of the friction coefficient (it is approximate in the series model of the Triple FP), and (b) more accurate consideration of the non-zero initial conditions.

The comparison of analytical and experimental results in Figure 5-31 and Figure 5-32 with combined horizontal and vertical excitation is less favorable that in Figure 5-25 to Figure 5-30 without the vertical excitation. An important contributor to this problem is the effect of the specified vertical stiffness of the isolators in the analysis. Incorrect specification of the vertical stiffness, combined with vertical excitation, often results in numerical problems and incorrect or premature prediction of isolator uplift and/or incorrect fluctuation of vertical load on the isolators. These difficulties are evident in the results of Figure 5-31 and Figure 5-32.

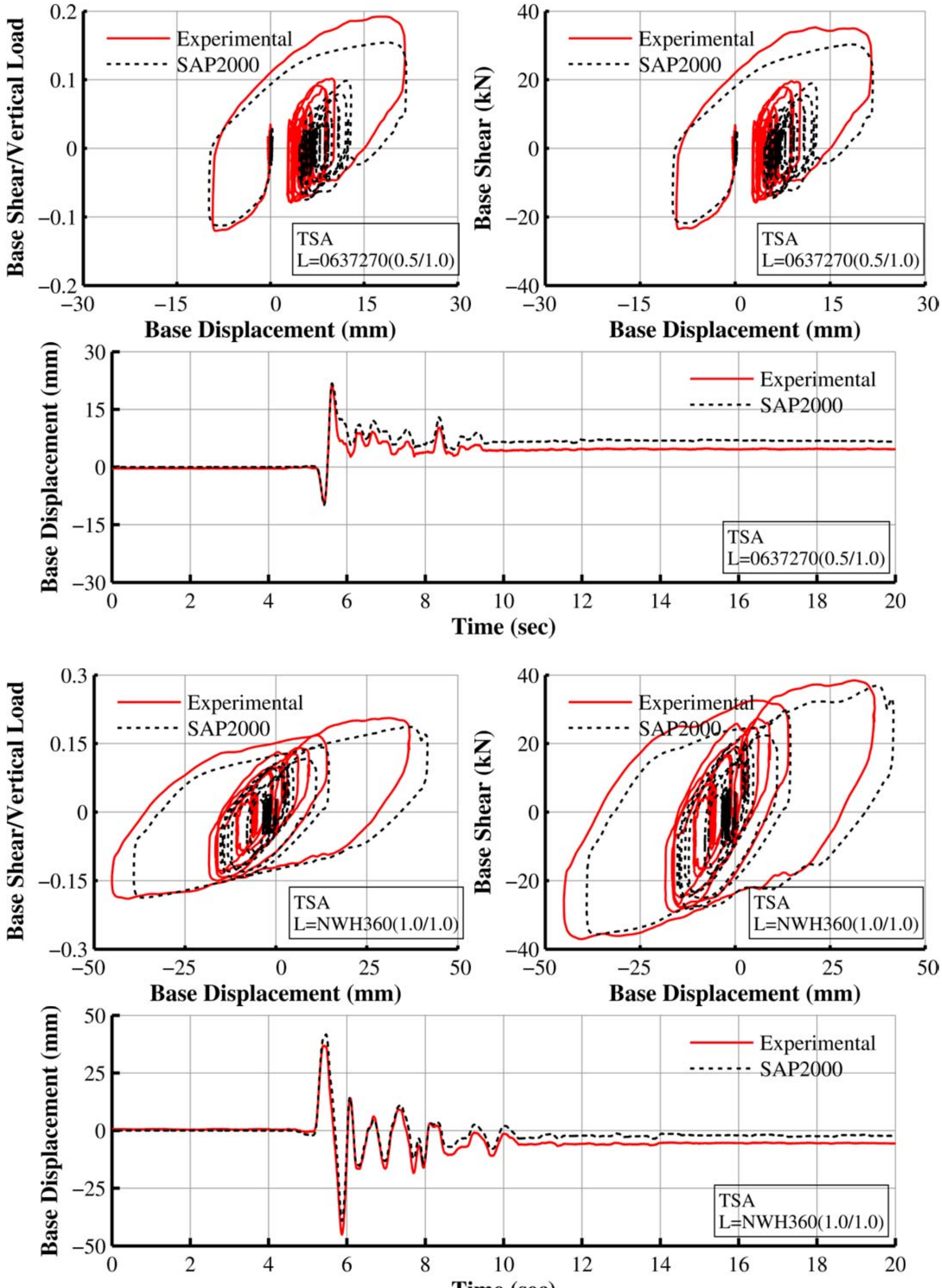

Figure 5-25: Comparison of analytical (program SAP2000) and experimental results for isolated structure with Configuration A isolators

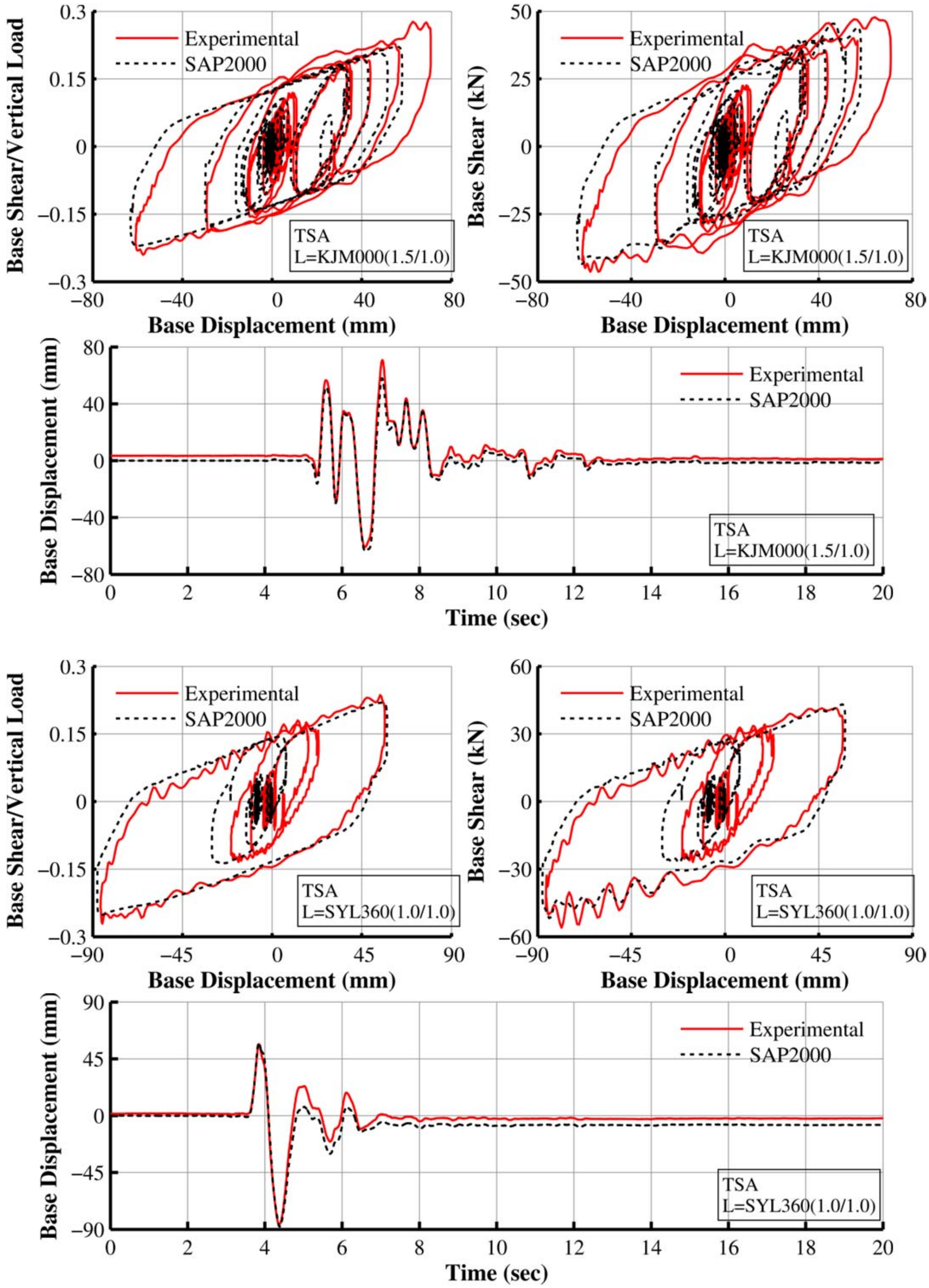

Figure 5-25 (cont'd): Comparison of analytical (program SAP2000) and experimental results for isolated structure with Configuration A isolators

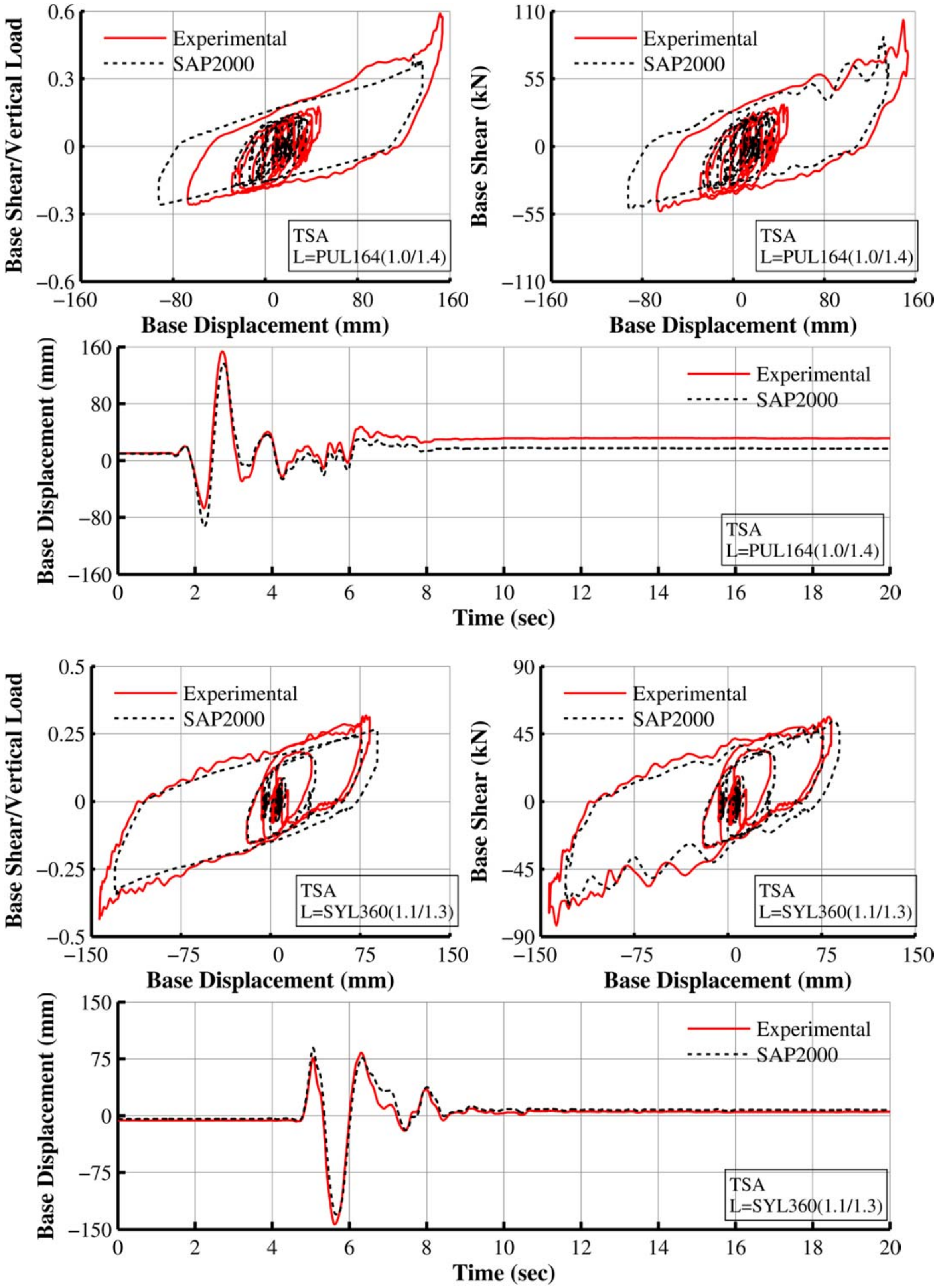

Figure 5-25 (cont'd): Comparison of analytical (program SAP2000) and experimental results for isolated structure with Configuration A isolators

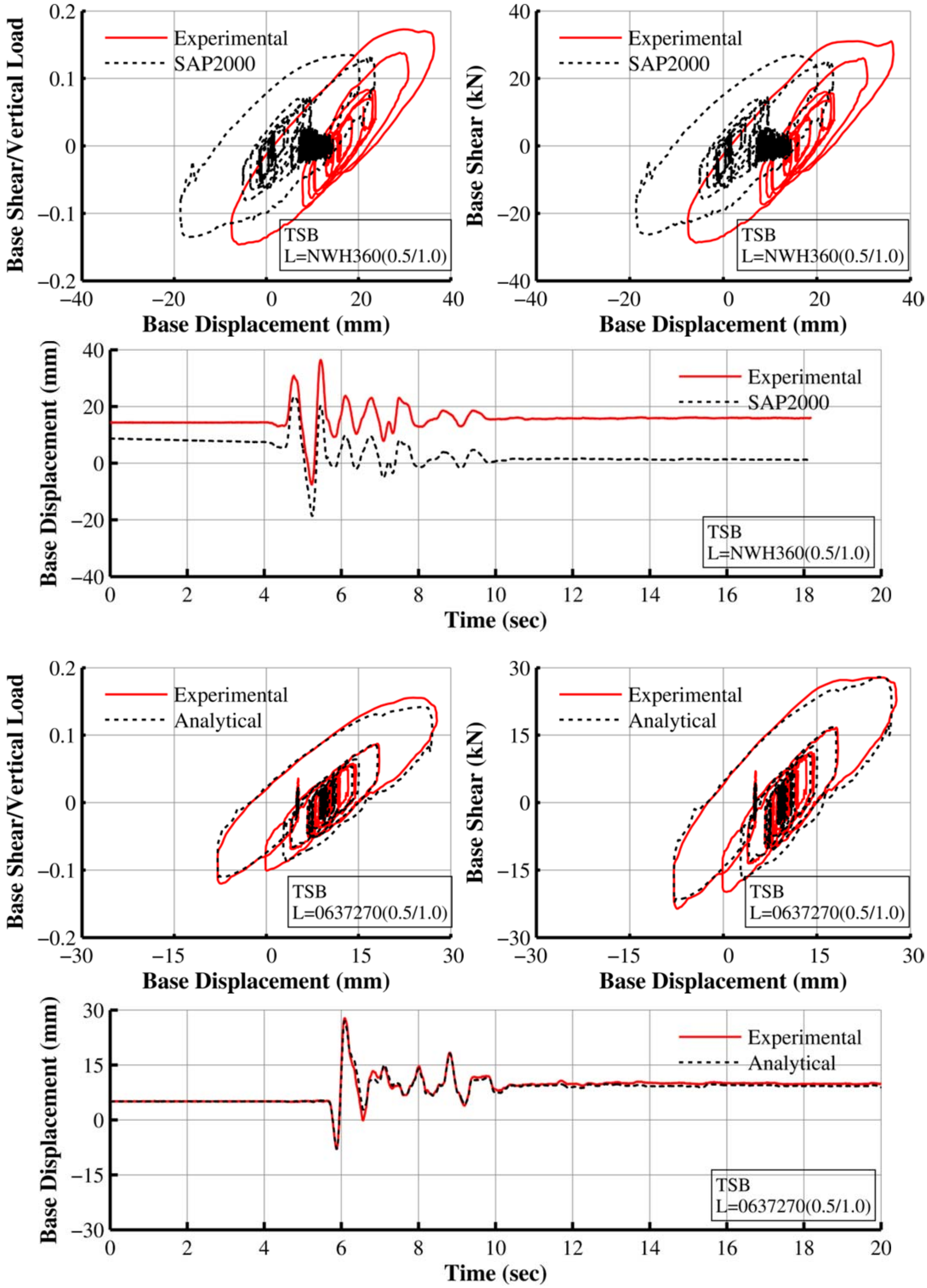

Figure 5-26: Comparison of analytical (program SAP2000) and experimental results for isolated structure with Configuration B isolators

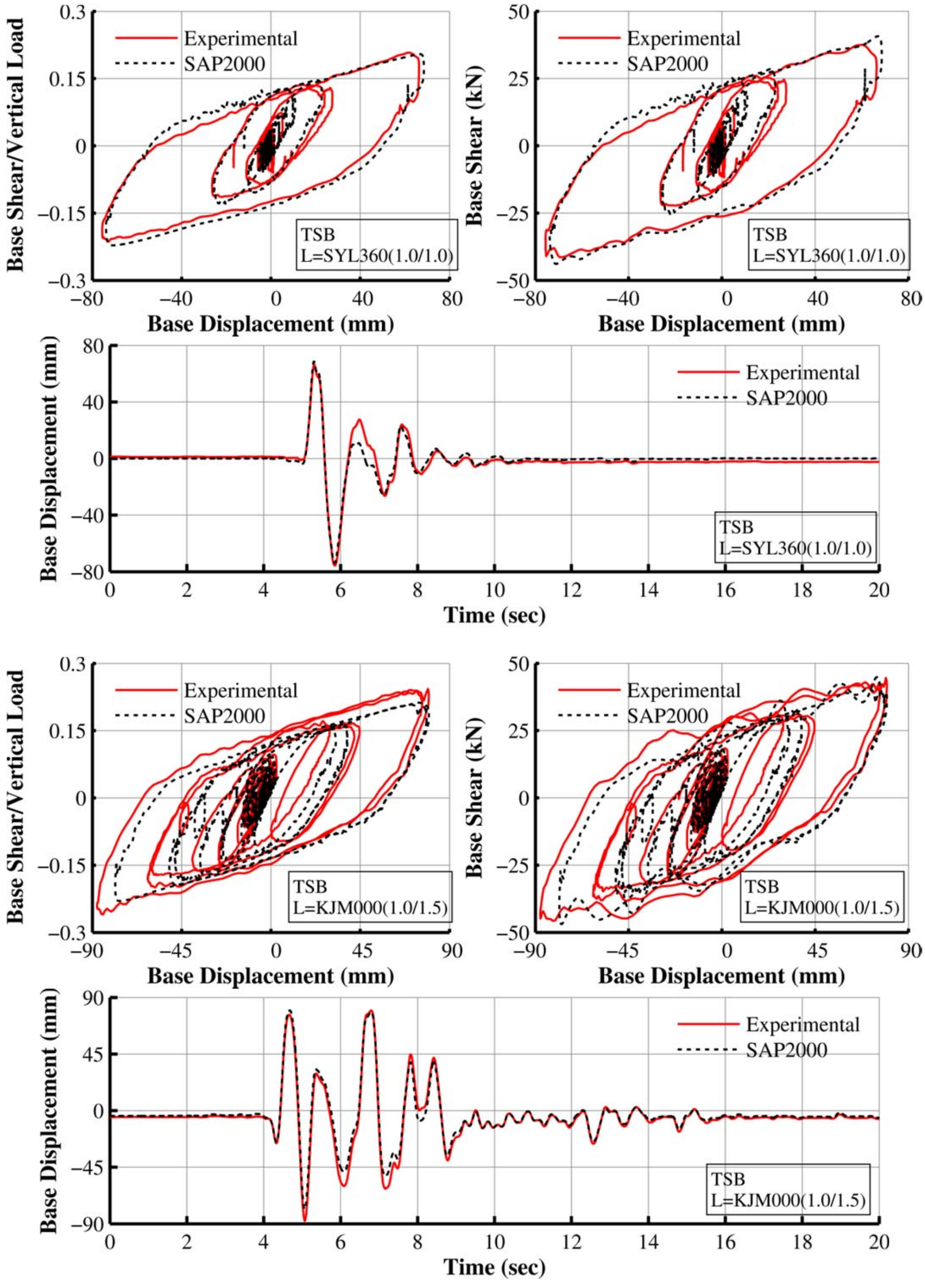

Figure 5-26 (cont'd): Comparison of analytical (program SAP2000) and experimental results for isolated structure with Configuration B isolators

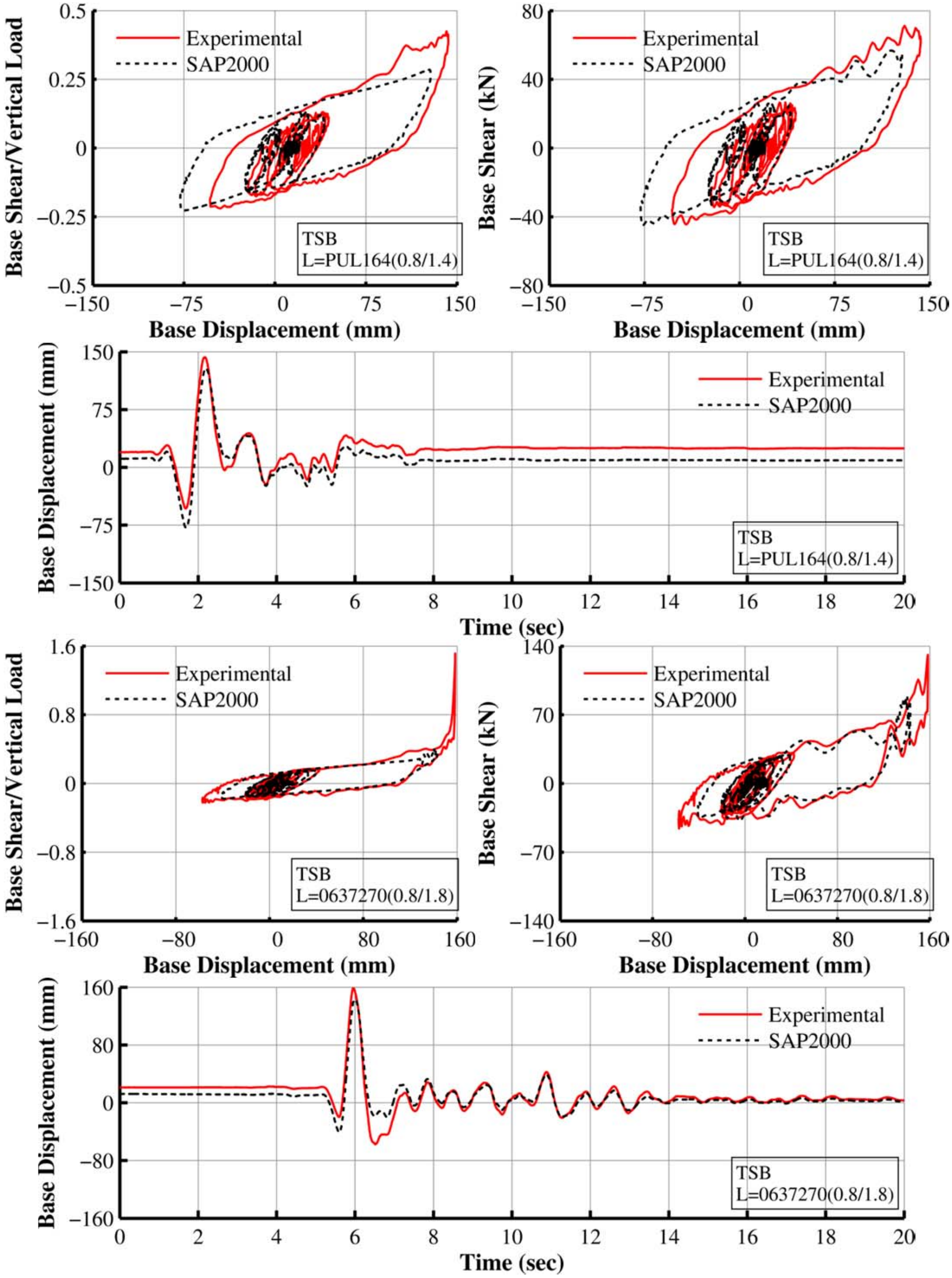

Figure 5-26 (cont'd): Comparison of analytical (program SAP2000) and experimental results for isolated structure with Configuration B isolators

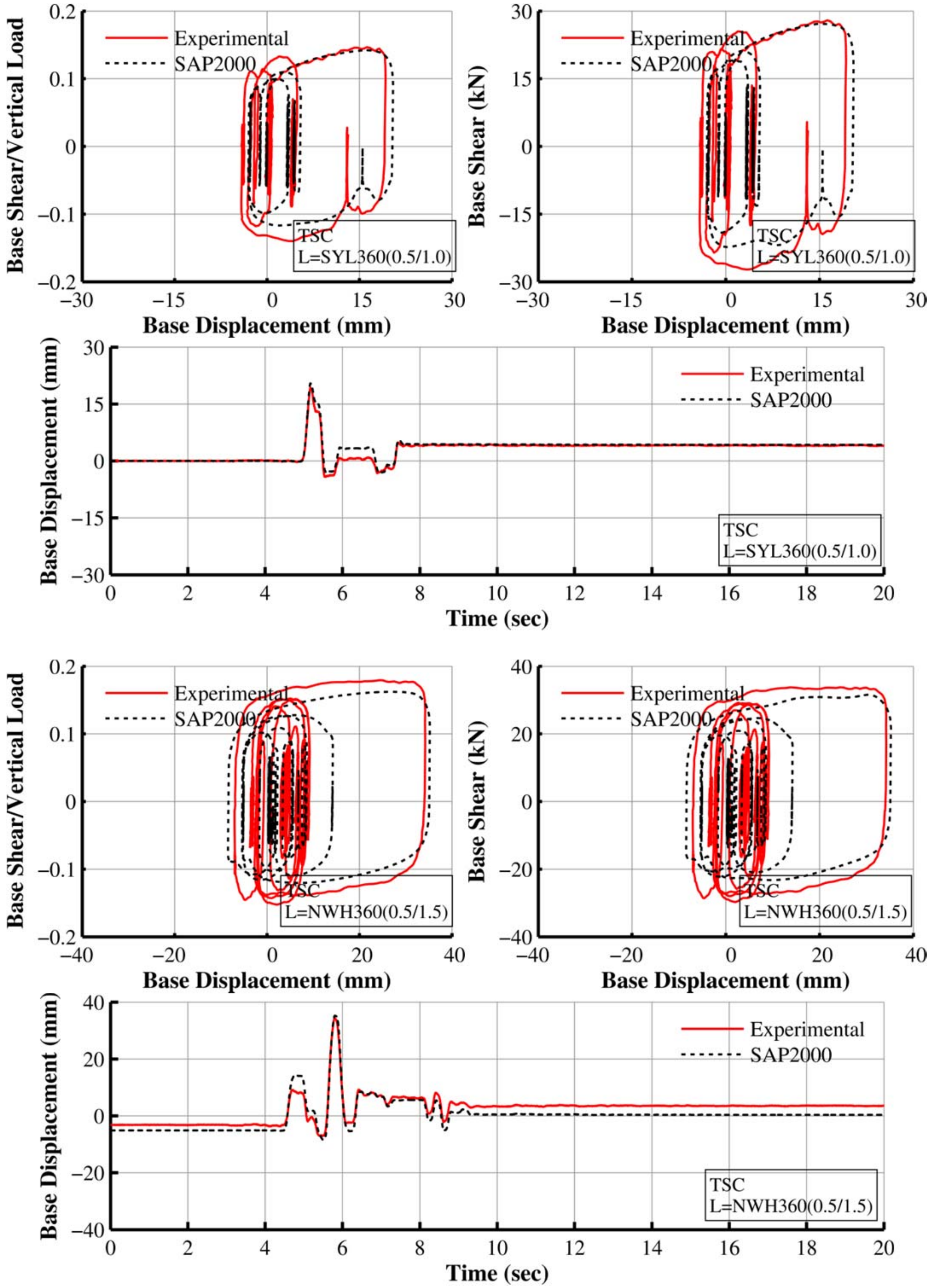

Figure 5-27: Comparison of analytical (program SAP2000) and experimental results for isolated structure with Configuration C isolators

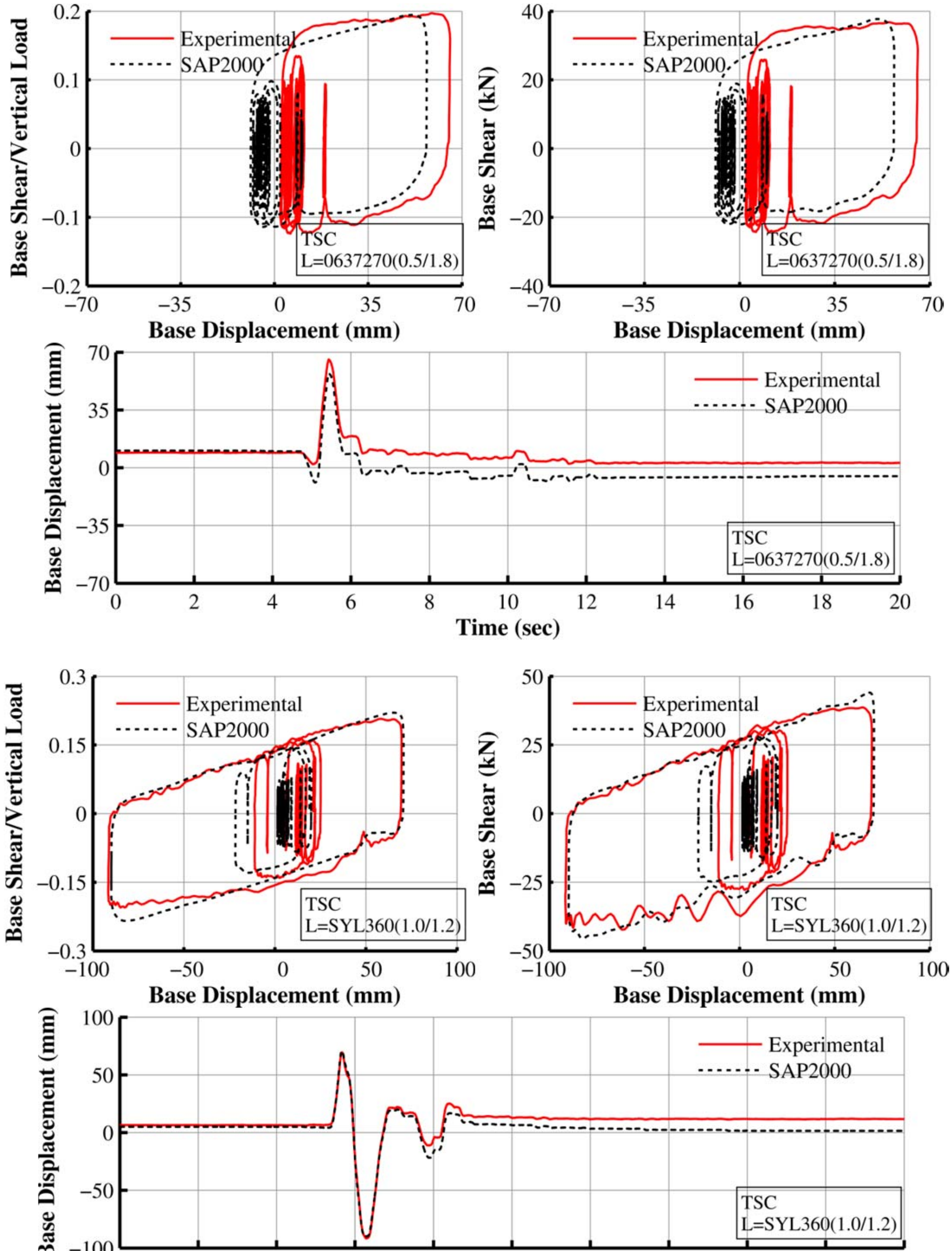

Figure 5-27 (cont'd): Comparison of analytical (program SAP2000) and experimental results for isolated structure with Configuration C isolators

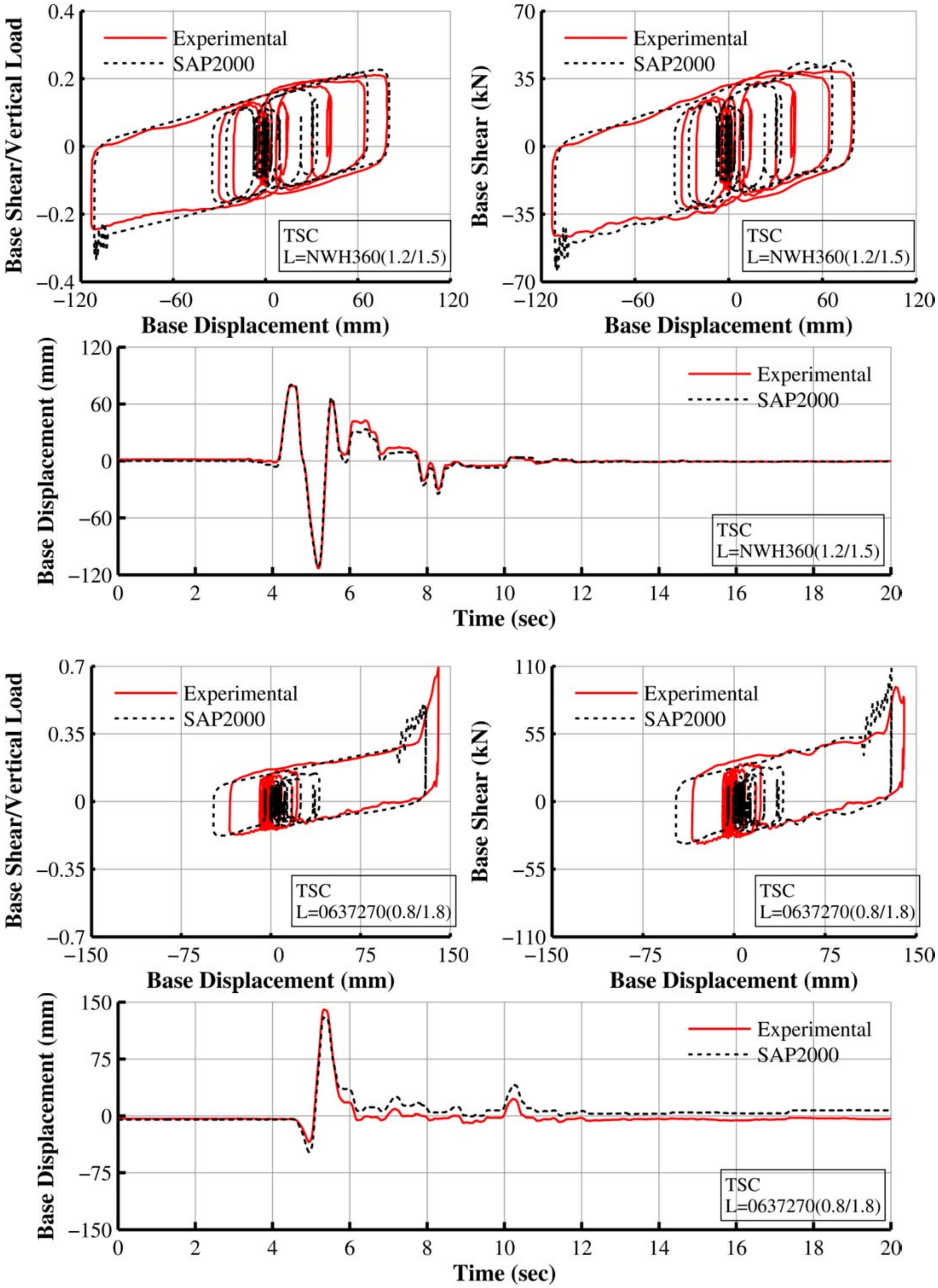

Figure 5-27 (cont'd): Comparison of analytical (program SAP2000) and experimental results for isolated structure with Configuration C isolators

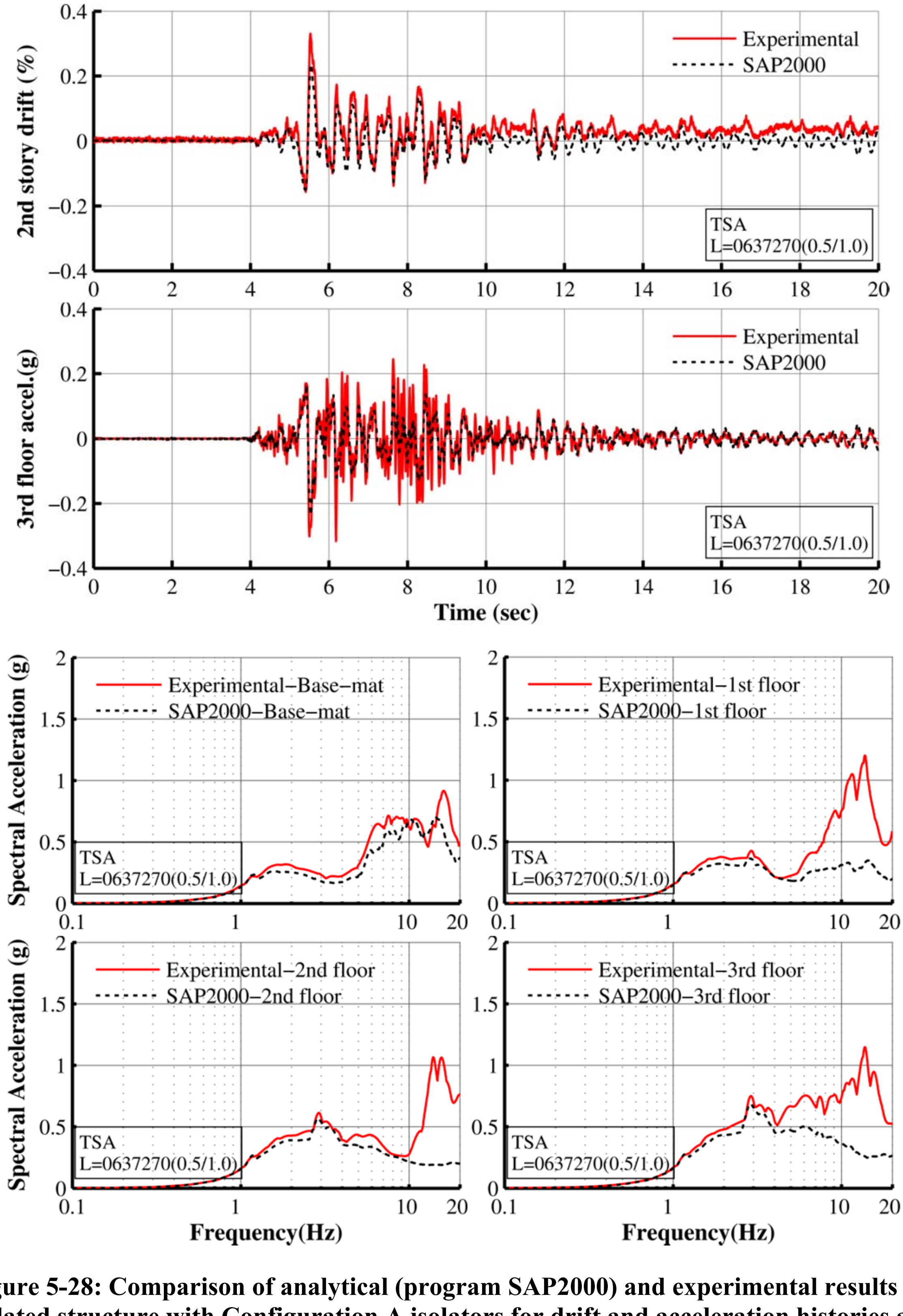

Figure 5-28: Comparison of analytical (program SAP2000) and experimental results for isolated structure with Configuration A isolators for drift and acceleration histories and 5%-damped floor response spectra

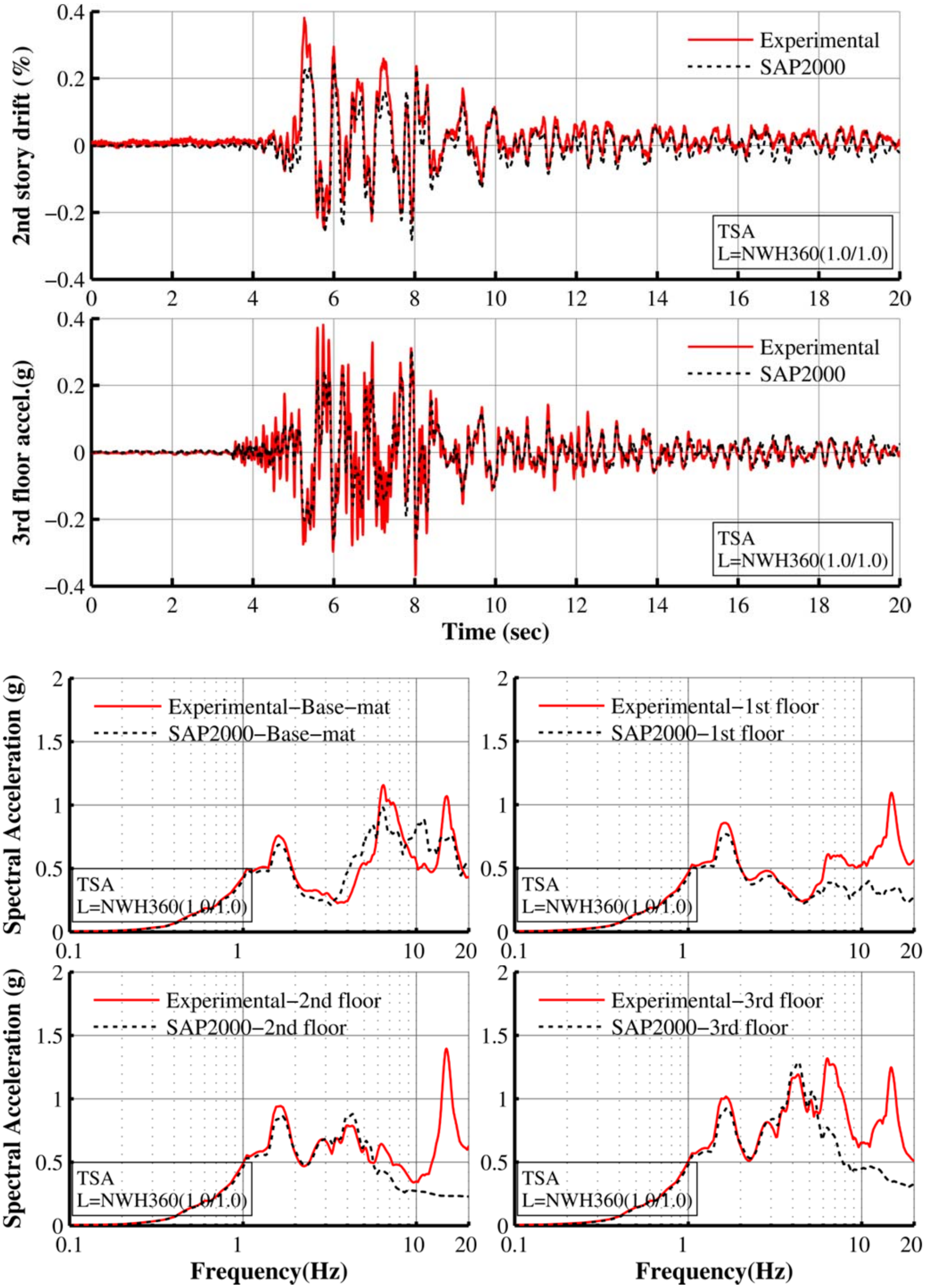

Figure 5-28 (cont'd): Comparison of analytical (program SAP2000) and experimental results for isolated structure with Configuration A isolators for drift and acceleration histories and 5%-damped floor response spectra

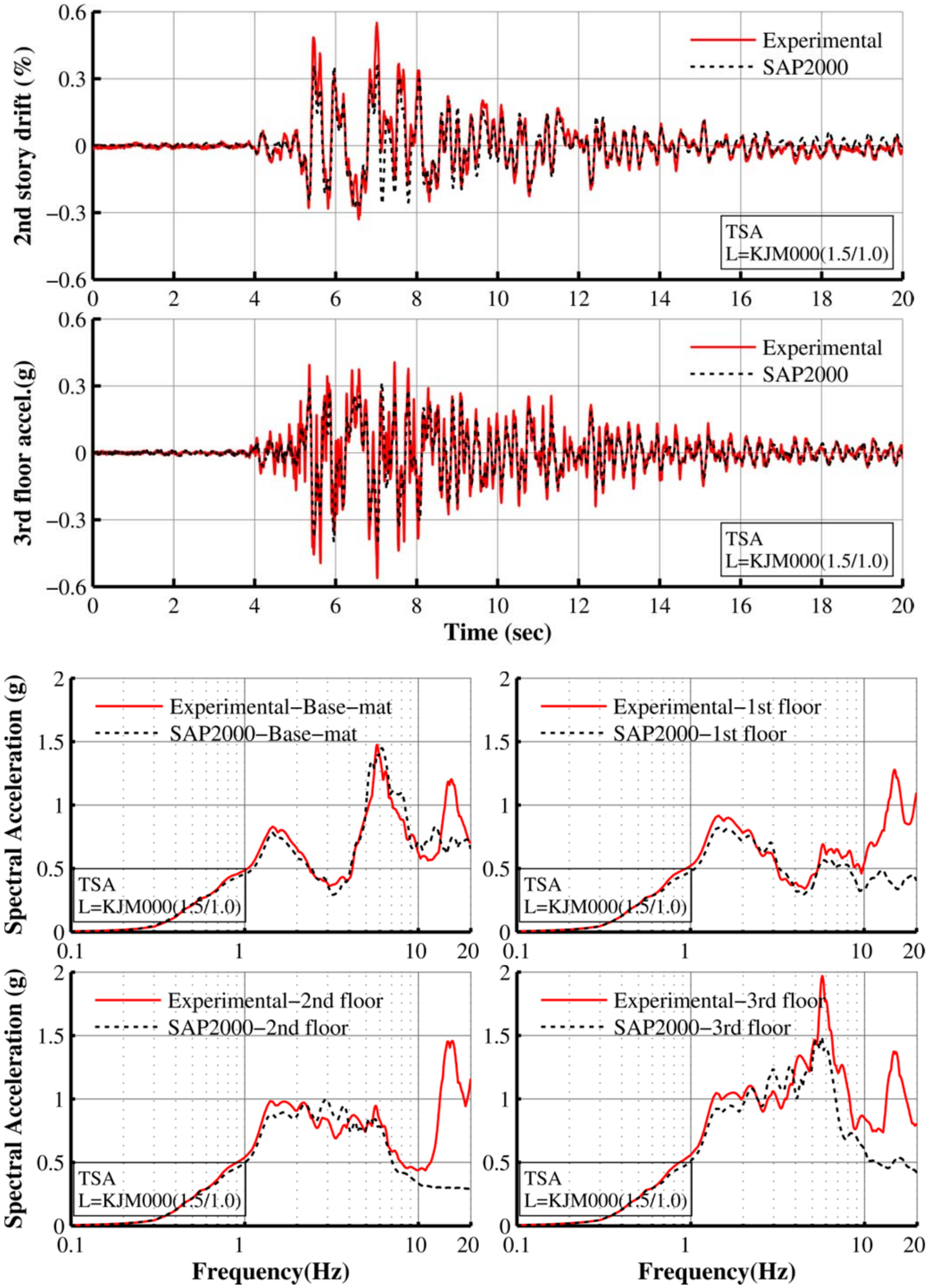

Figure 5-28 (cont'd): Comparison of analytical (program SAP2000) and experimental results for isolated structure with Configuration A isolators for drift and acceleration histories and 5%-damped floor response spectra

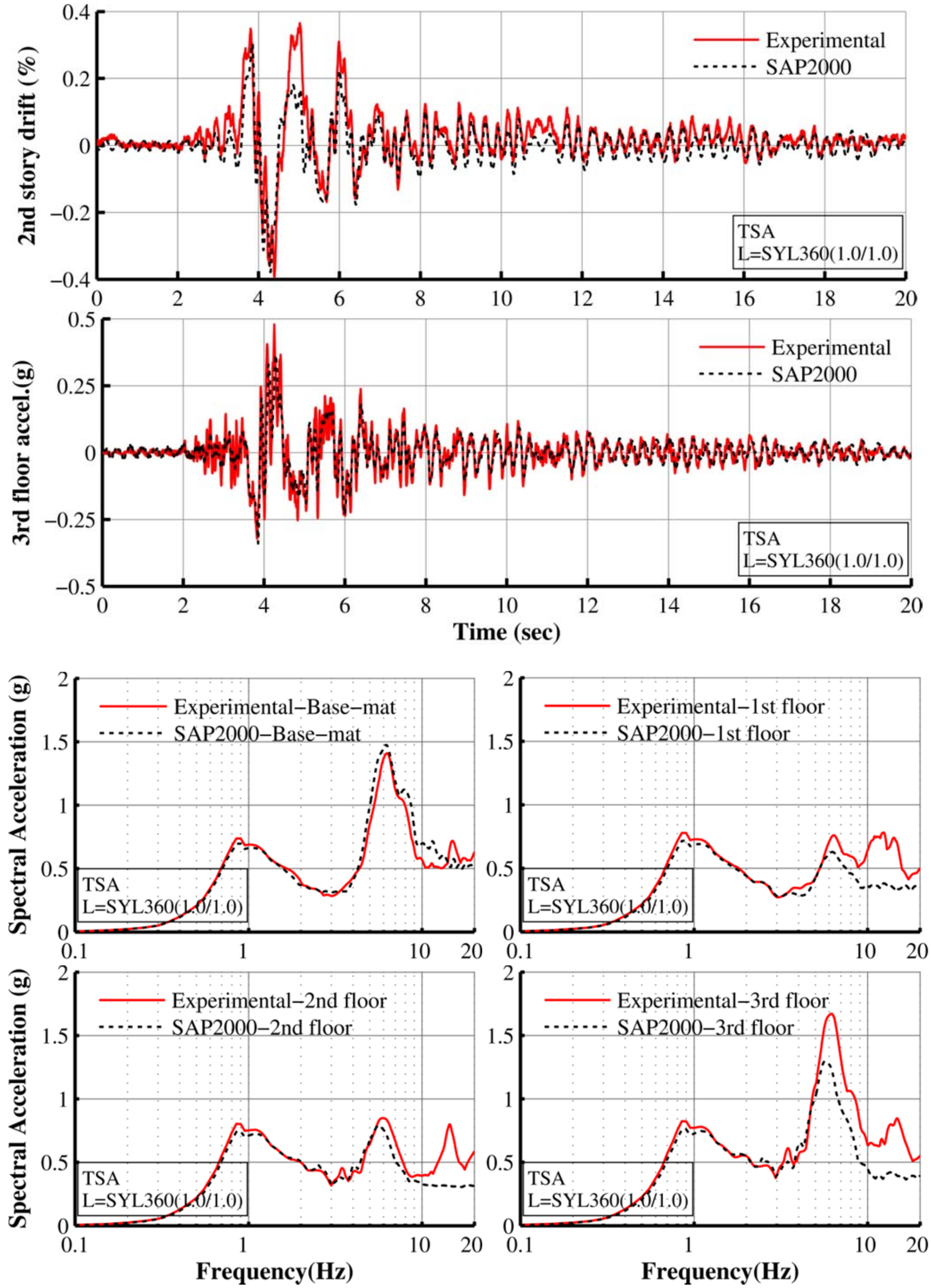

Figure 5-28 (cont'd): Comparison of analytical (program SAP2000) and experimental results for isolated structure with Configuration A isolators for drift and acceleration histories and 5%-damped floor response spectra

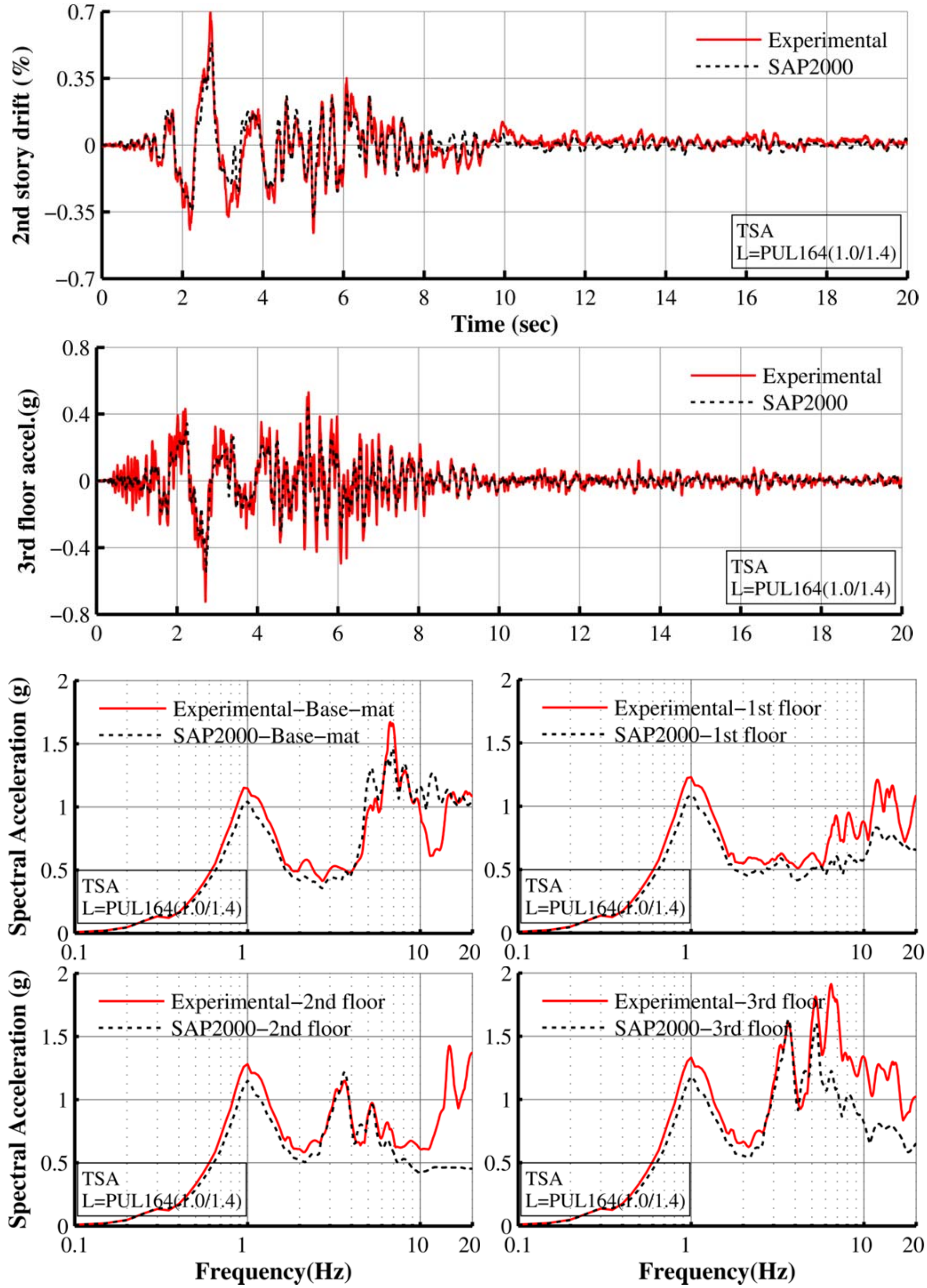

Figure 5-28 (cont'd): Comparison of analytical (program SAP2000) and experimental results for isolated structure with Configuration A isolators for drift and acceleration histories and 5%-damped floor response spectra

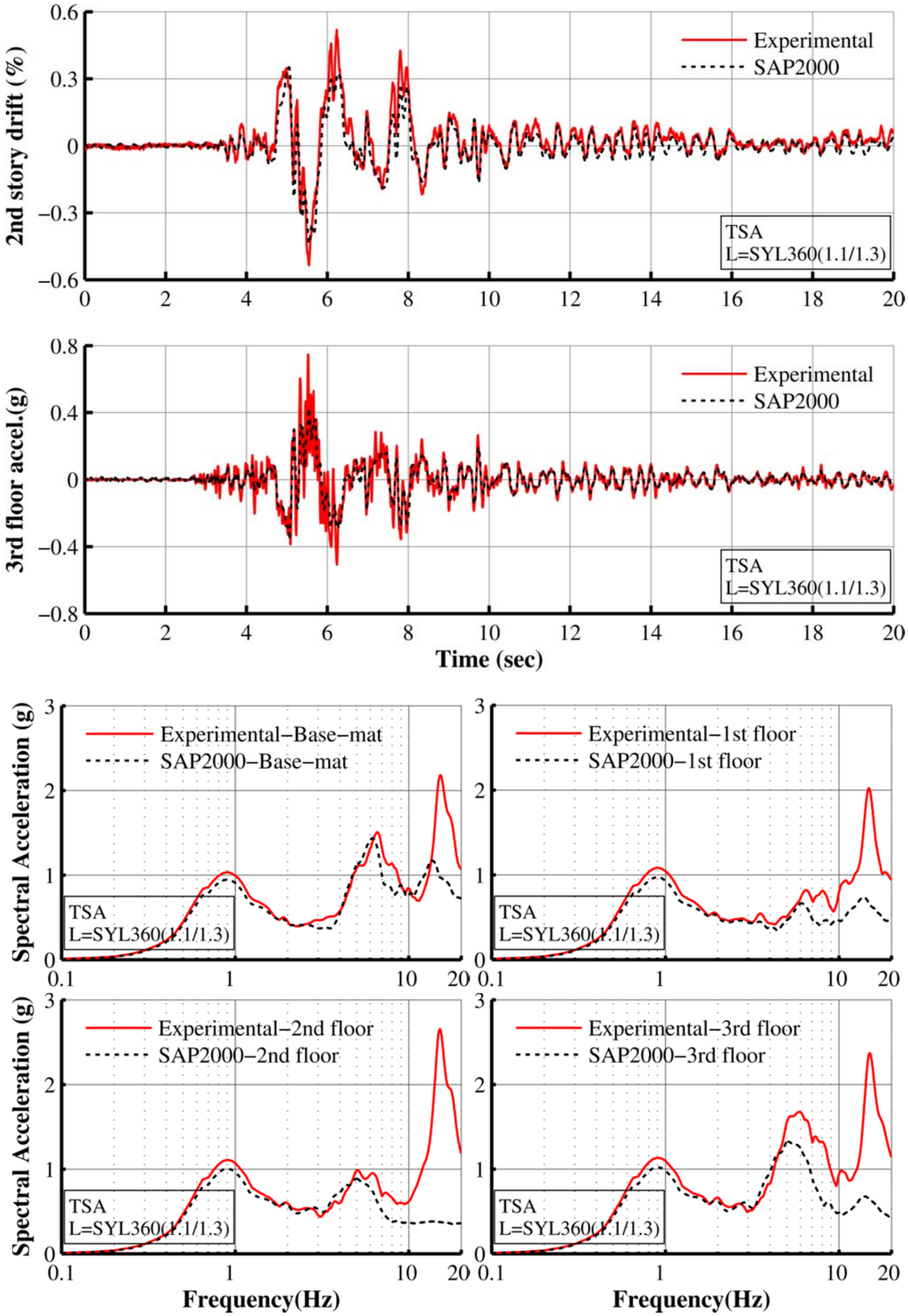

Figure 5-28 (cont'd): Comparison of analytical (program SAP2000) and experimental results for isolated structure with Configuration A isolators for drift and acceleration histories and 5%-damped floor response spectra

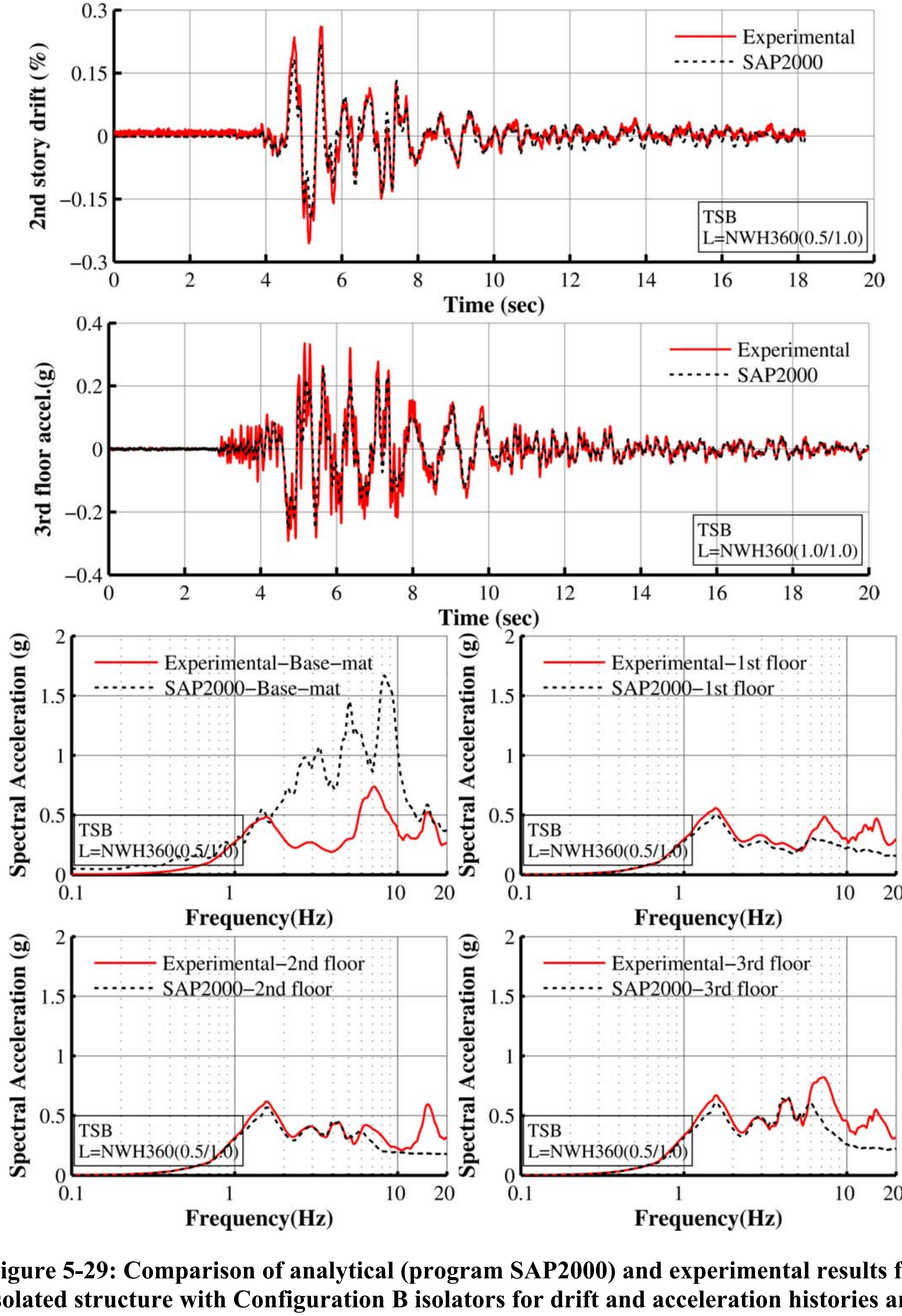

Figure 5-29: Comparison of analytical (program SAP2000) and experimental results for isolated structure with Configuration B isolators for drift and acceleration histories and 5%-damped floor response spectra

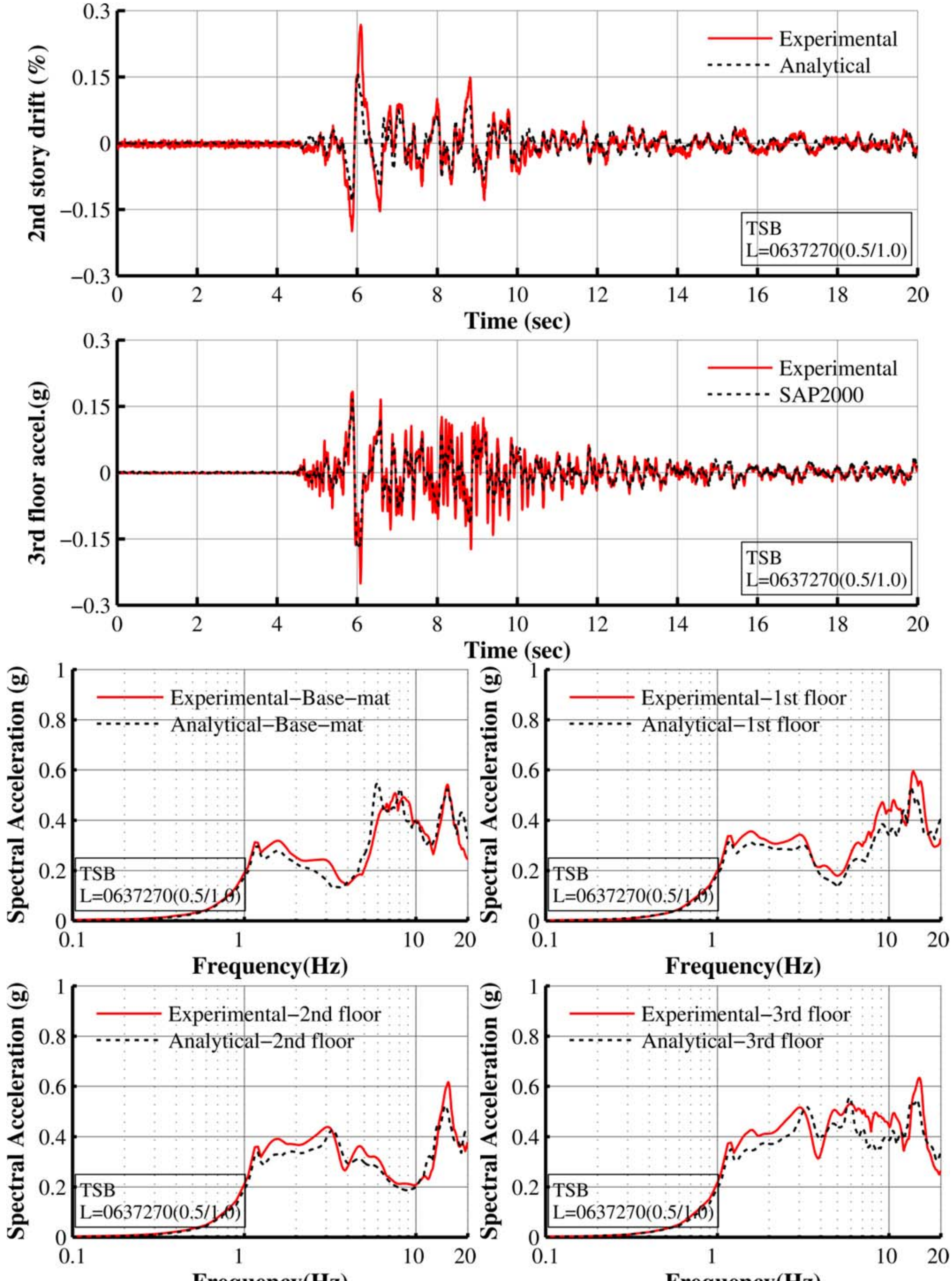

Figure 5-29 (cont'd): Comparison of analytical (program SAP2000) and experimental results for isolated structure with Configuration B isolators for drift and acceleration histories and 5%-damped floor response spectra

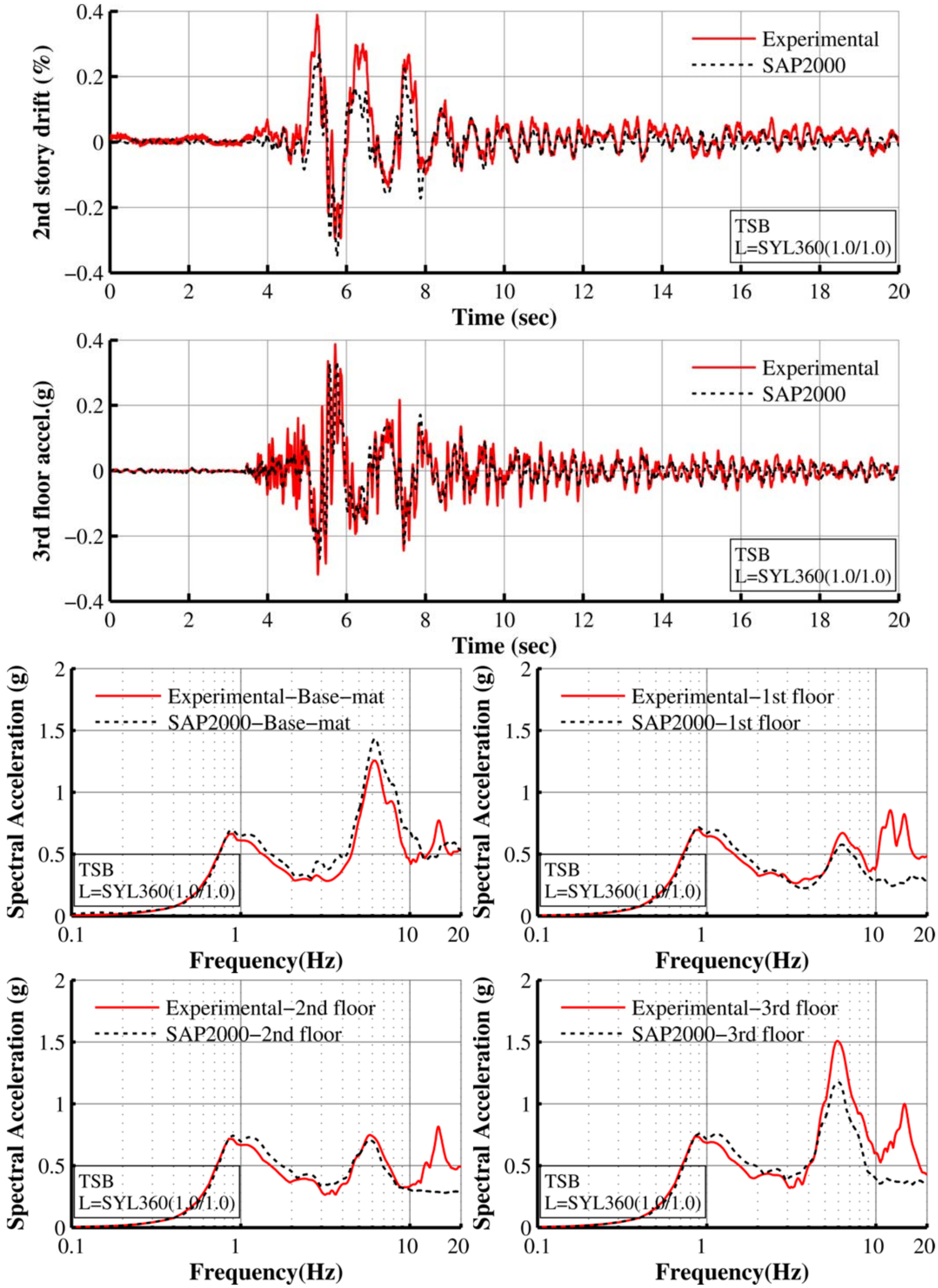

Figure 5-29 (cont'd): Comparison of analytical (program SAP2000) and experimental results for isolated structure with Configuration B isolators for drift and acceleration histories and 5%-damped floor response spectra

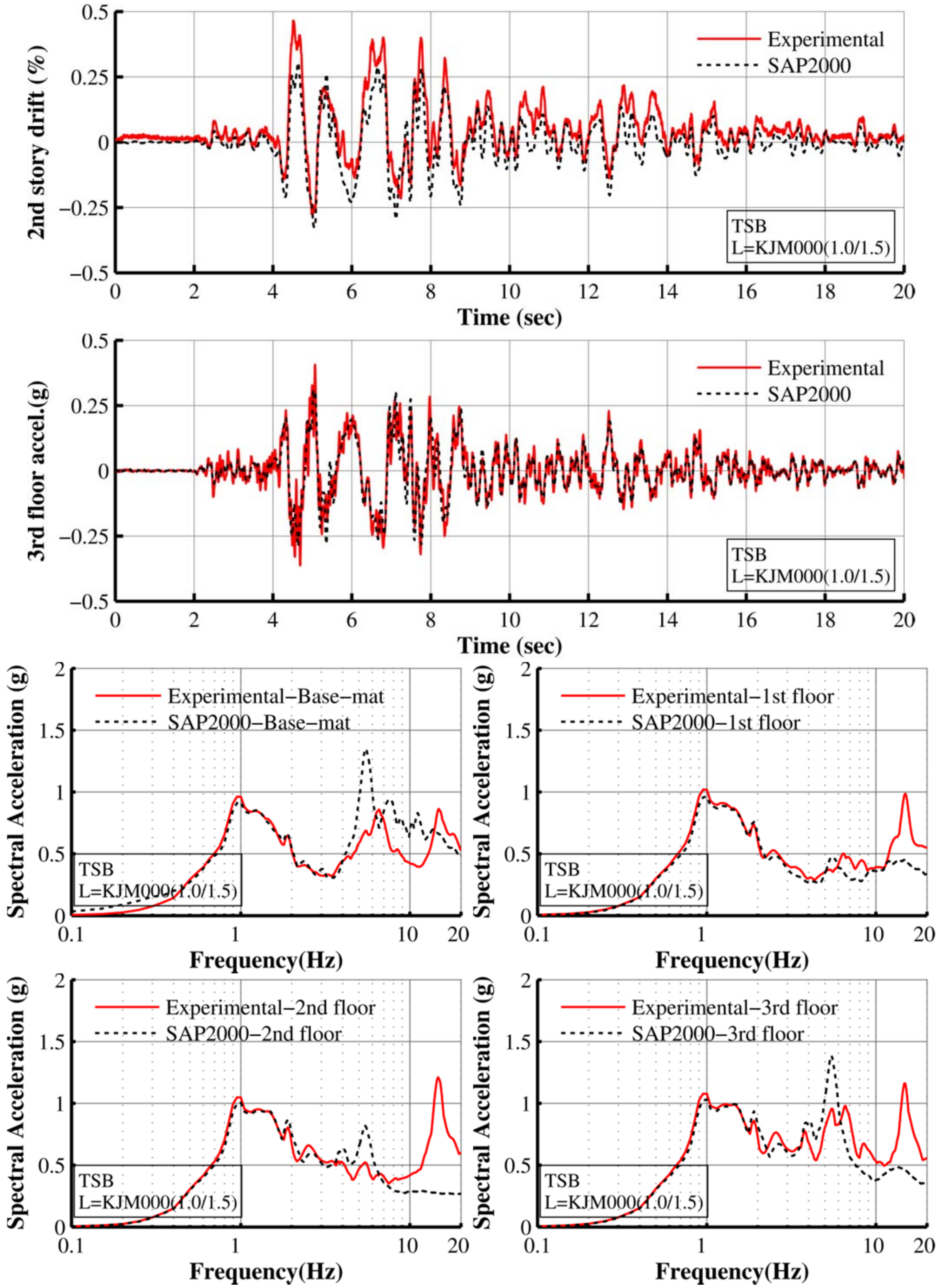

Figure 5-29 (cont'd): Comparison of analytical (program SAP2000) and experimental results for isolated structure with Configuration B isolators for drift and acceleration histories and 5%-damped floor response spectra

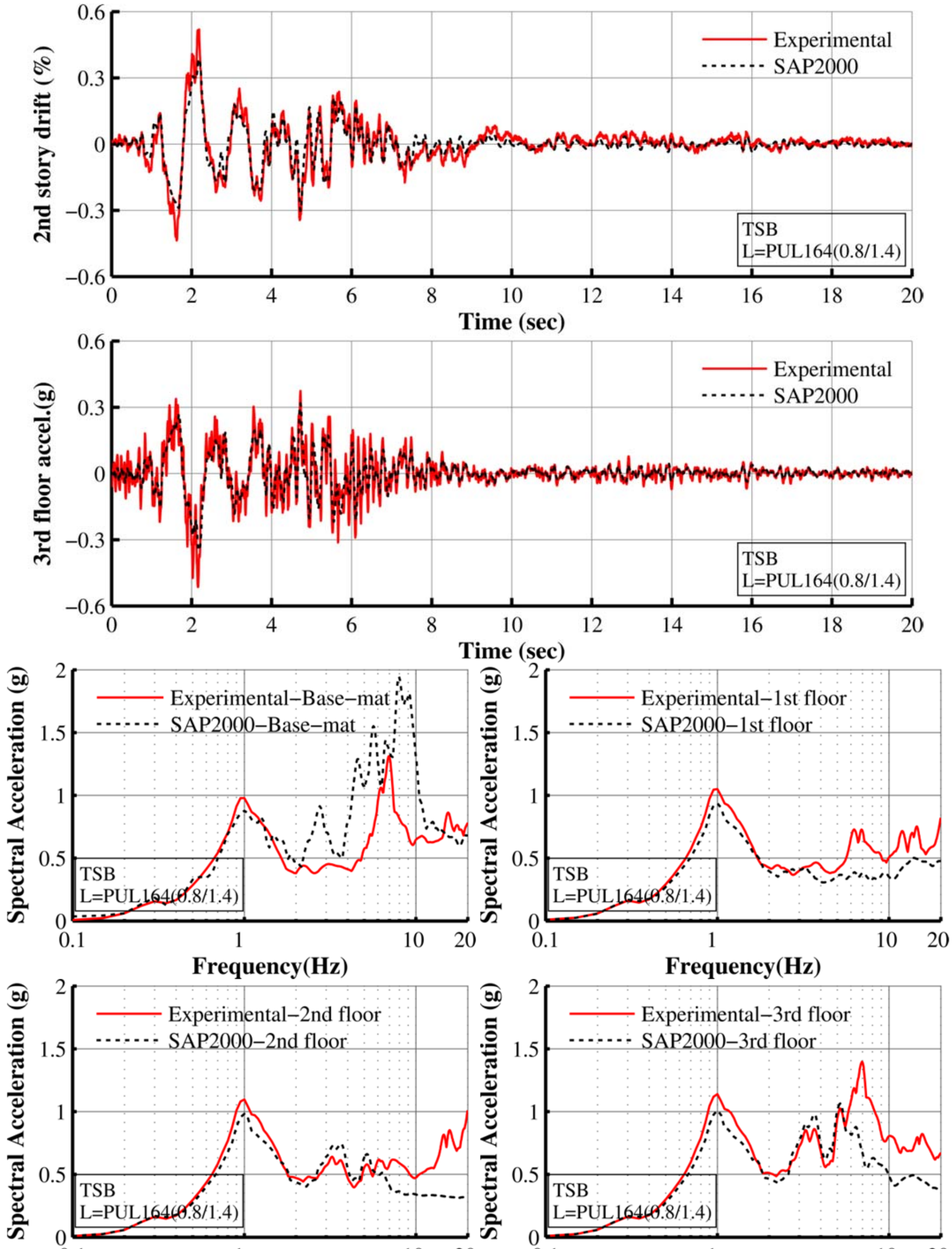

Figure 5-29 (cont'd): Comparison of analytical (program SAP2000) and experimental results for isolated structure with Configuration B isolators for drift and acceleration histories and 5%-damped floor response spectra

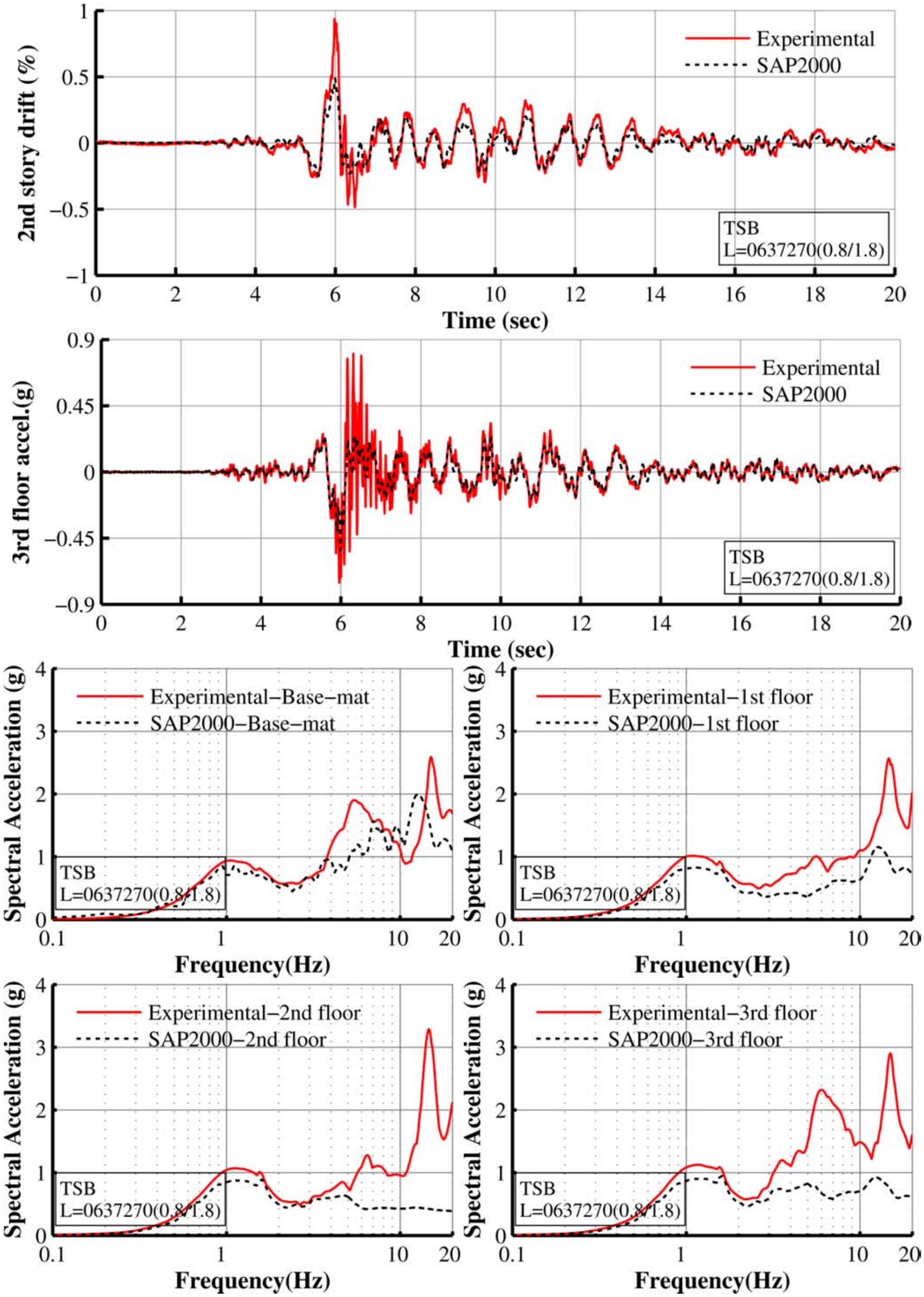

Figure 5-29 (cont'd): Comparison of analytical (program SAP2000) and experimental results for isolated structure with Configuration B isolators for drift and acceleration histories and 5%-damped floor response spectra

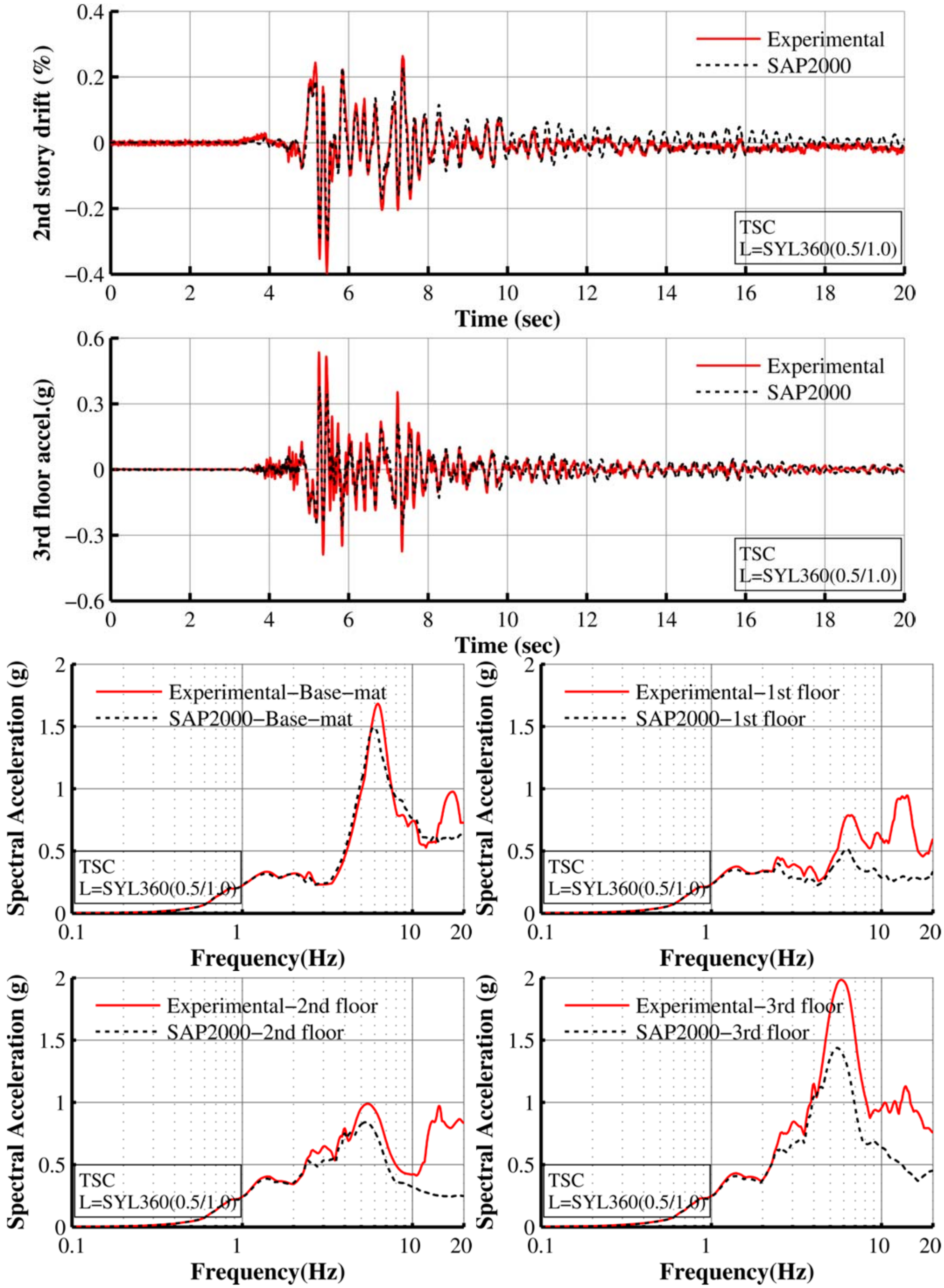

Figure 5-30: Comparison of analytical (program SAP2000) and experimental results for isolated structure with Configuration C isolators for drift and acceleration histories and 5%-damped floor response spectra

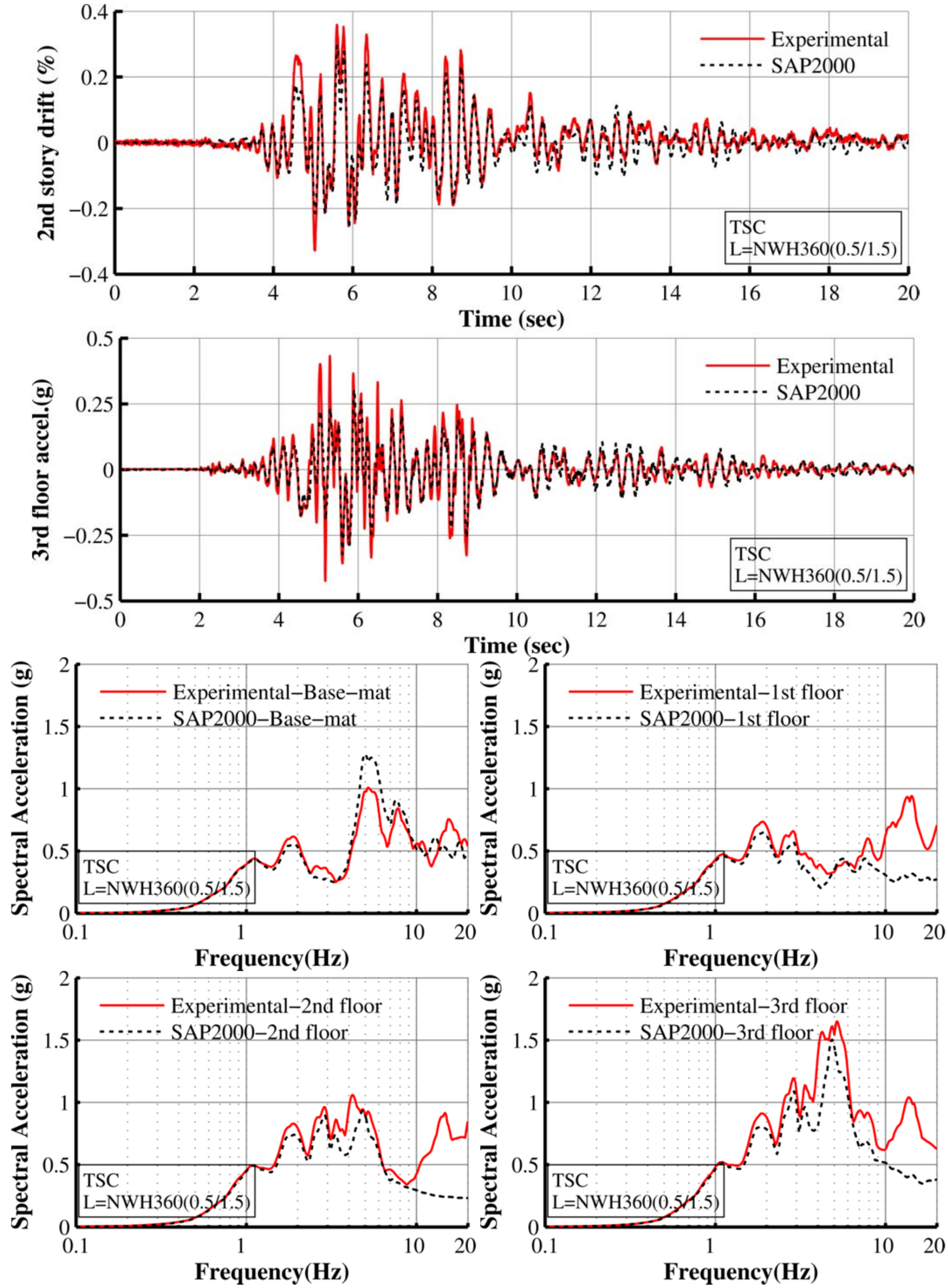

Figure 5-30 (cont'd): Comparison of analytical (program SAP2000) and experimental results for isolated structure with Configuration C isolators for drift and acceleration histories and 5%-damped floor response spectra

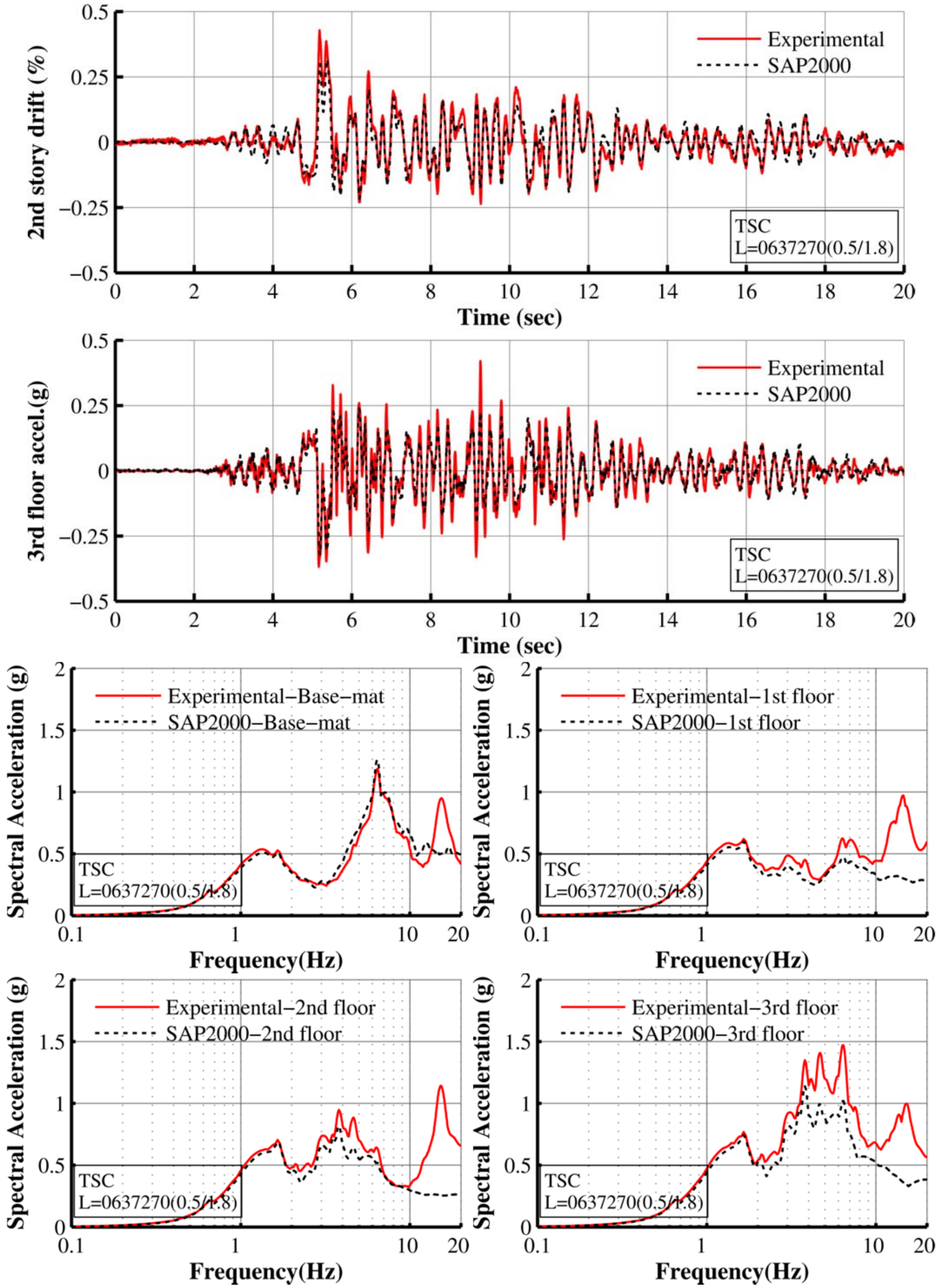

Figure 5-30 (cont'd): Comparison of analytical (program SAP2000) and experimental results for isolated structure with Configuration C isolators for drift and acceleration histories and 5%-damped floor response spectra

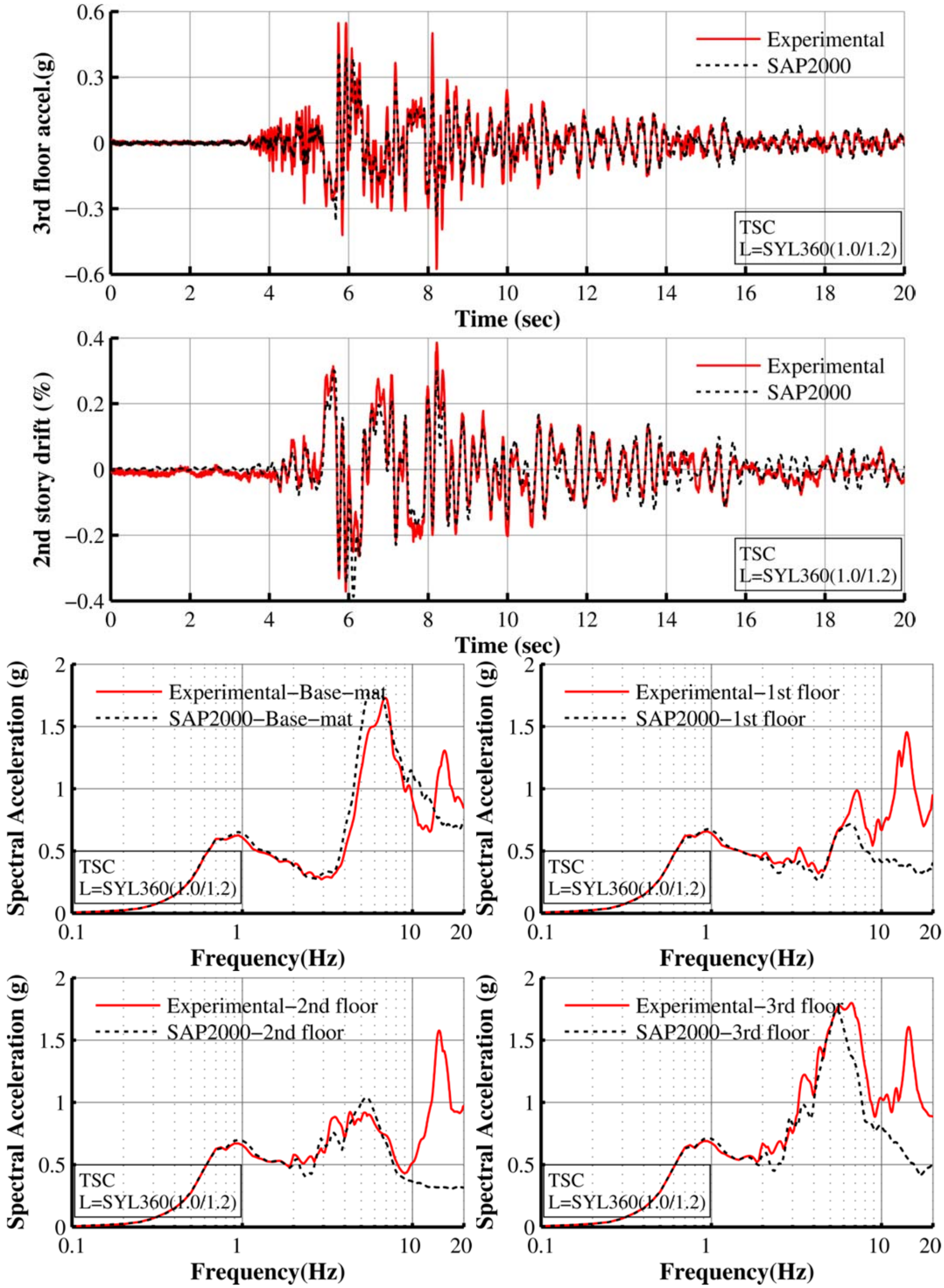

Figure 5-30 (cont'd): Comparison of analytical (program SAP2000) and experimental results for isolated structure with Configuration C isolators for drift and acceleration histories and 5%-damped floor response spectra

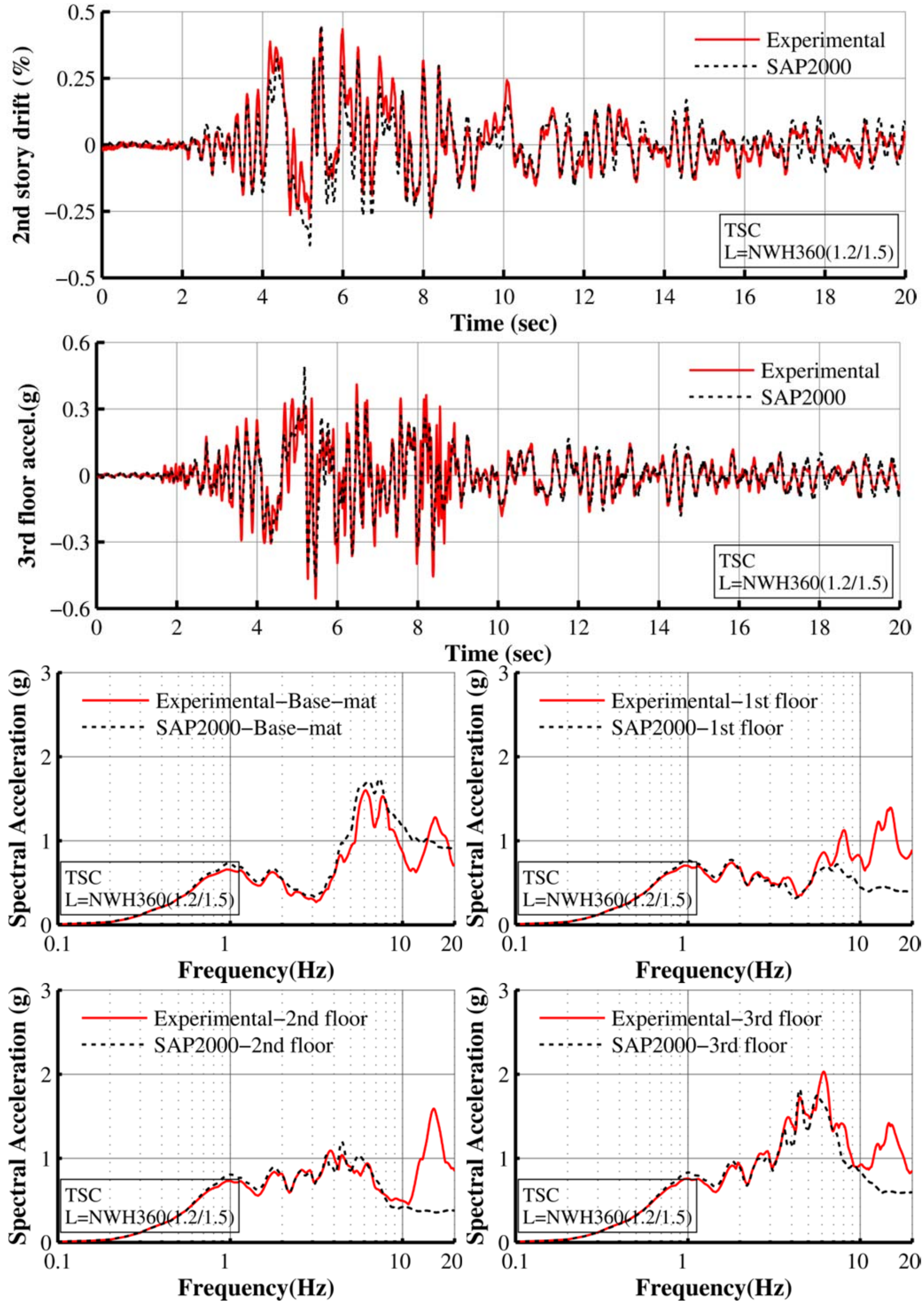

Figure 5-30 (cont'd): Comparison of analytical (program SAP2000) and experimental results for isolated structure with Configuration C isolators for drift and acceleration histories and 5%-damped floor response spectra

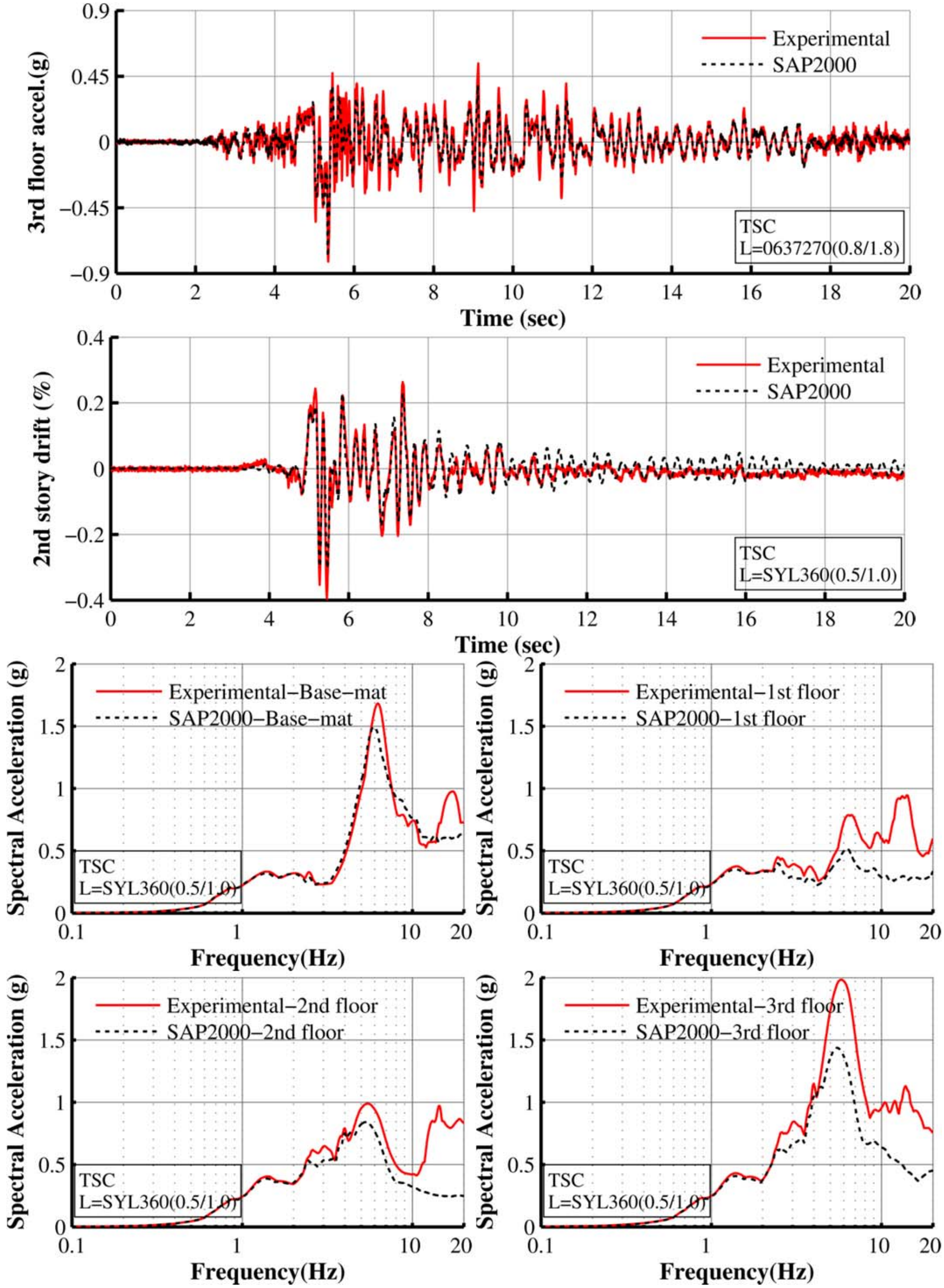

Figure 5-30 (cont'd): Comparison of analytical (program SAP2000) and experimental results for isolated structure with Configuration C isolators for drift and acceleration histories and 5%-damped floor response spectra

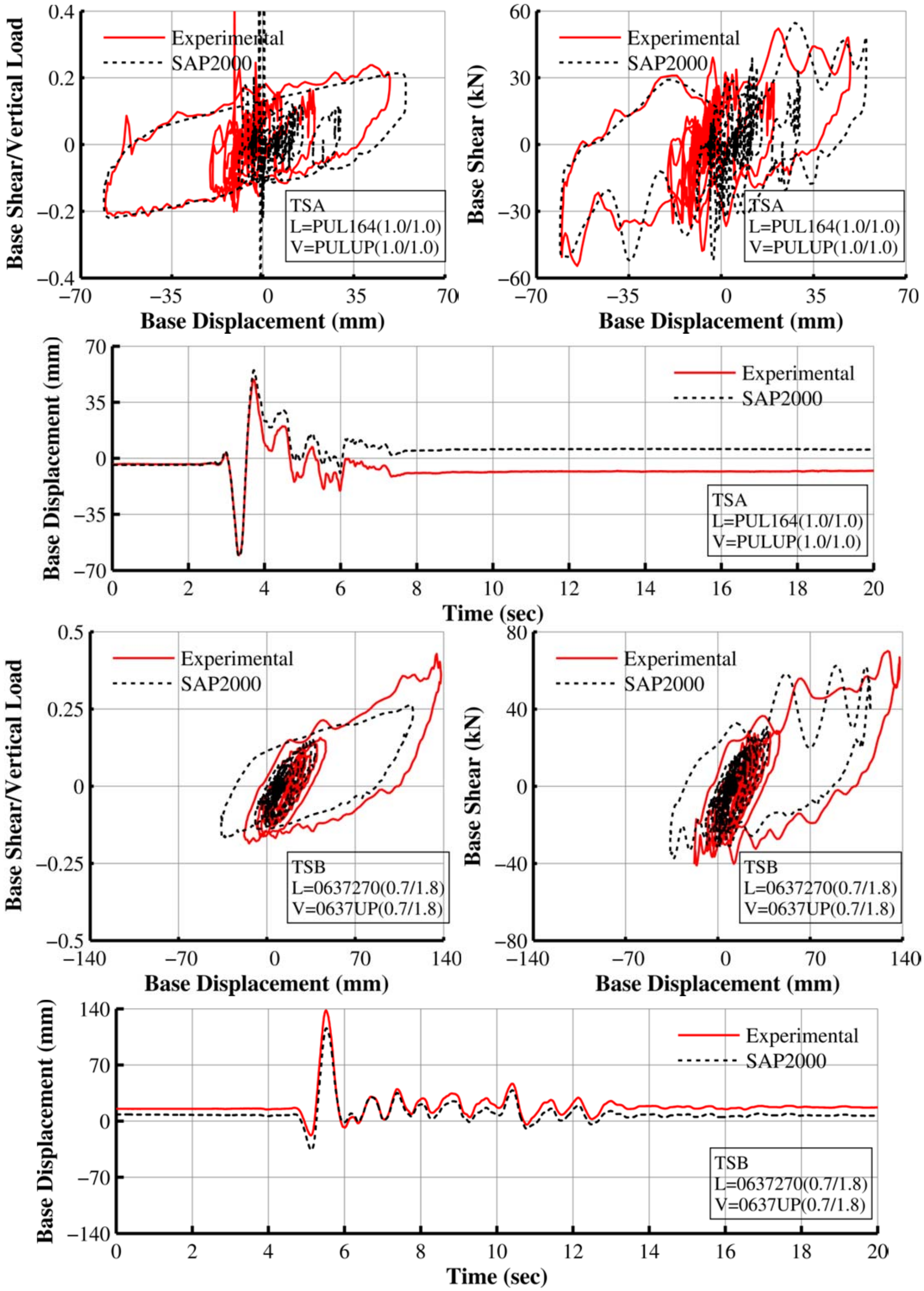

Figure 5-31: Comparison of analytical (program SAP2000) and experimental results for isolated structure in combined horizontal and vertical excitation

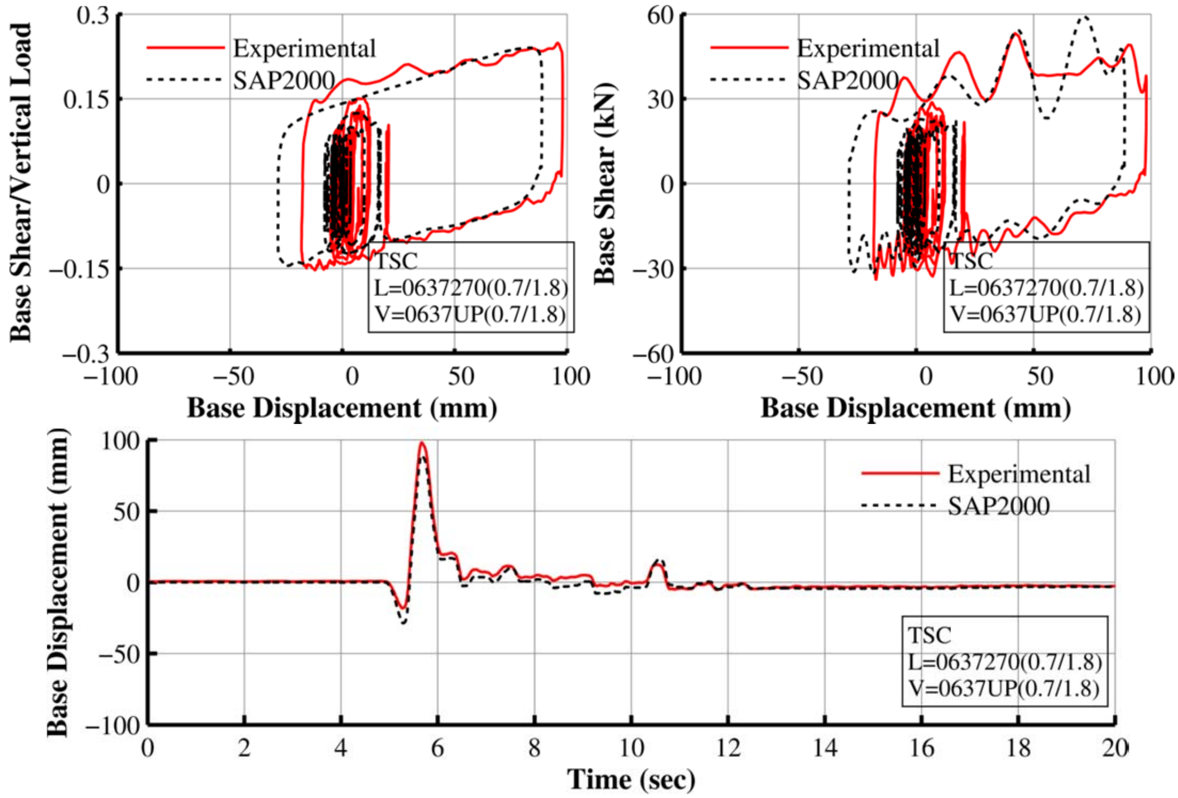

Figure 5-31 (cont'd): Comparison of analytical (program SAP2000) and experimental results for isolated structure in combined horizontal and vertical excitation

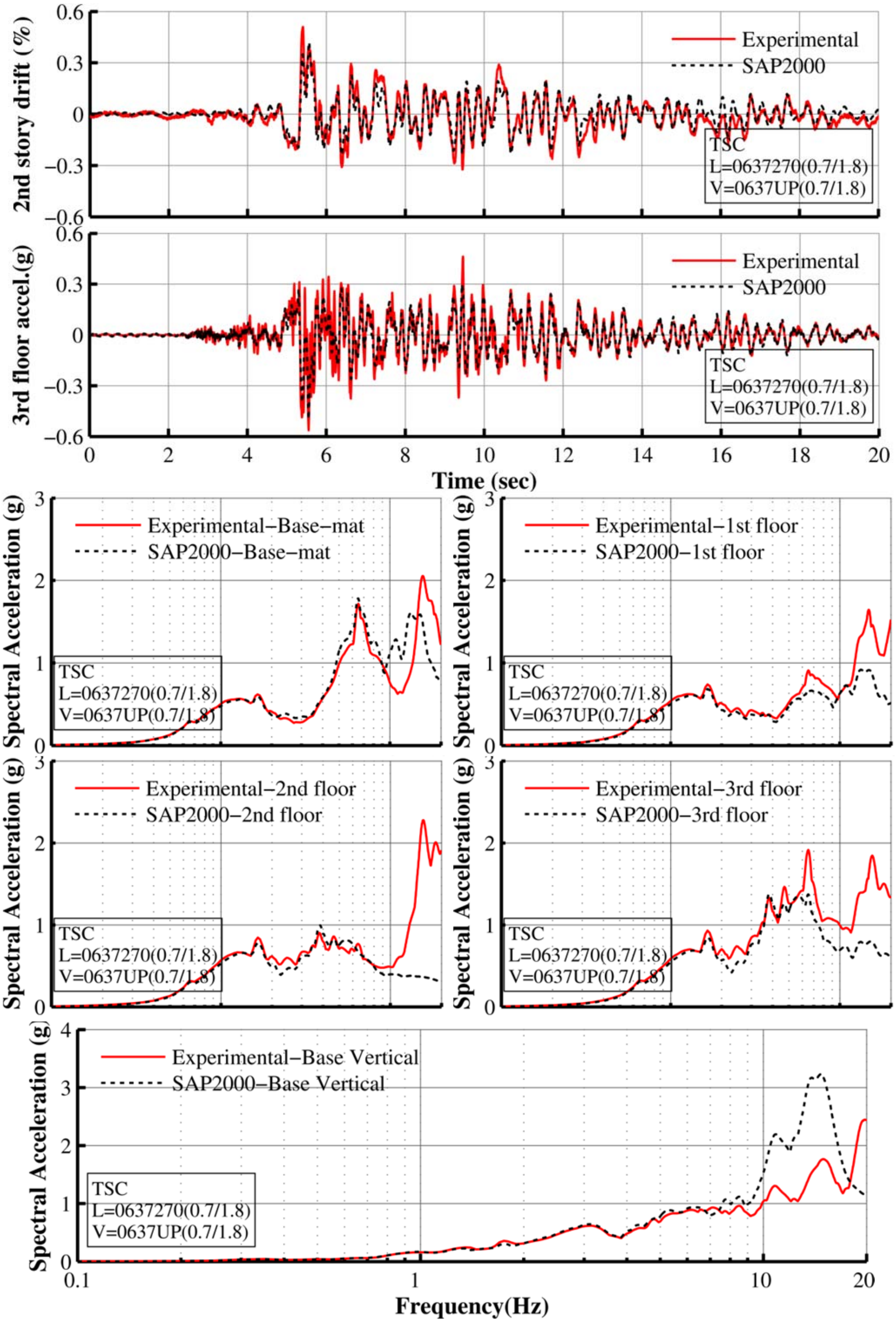

Figure 5-32: Comparison of analytical (program SAP2000) and experimental results of histories of drift and acceleration and 5%-damped floor spectra for isolated structure in combined horizontal and vertical excitation

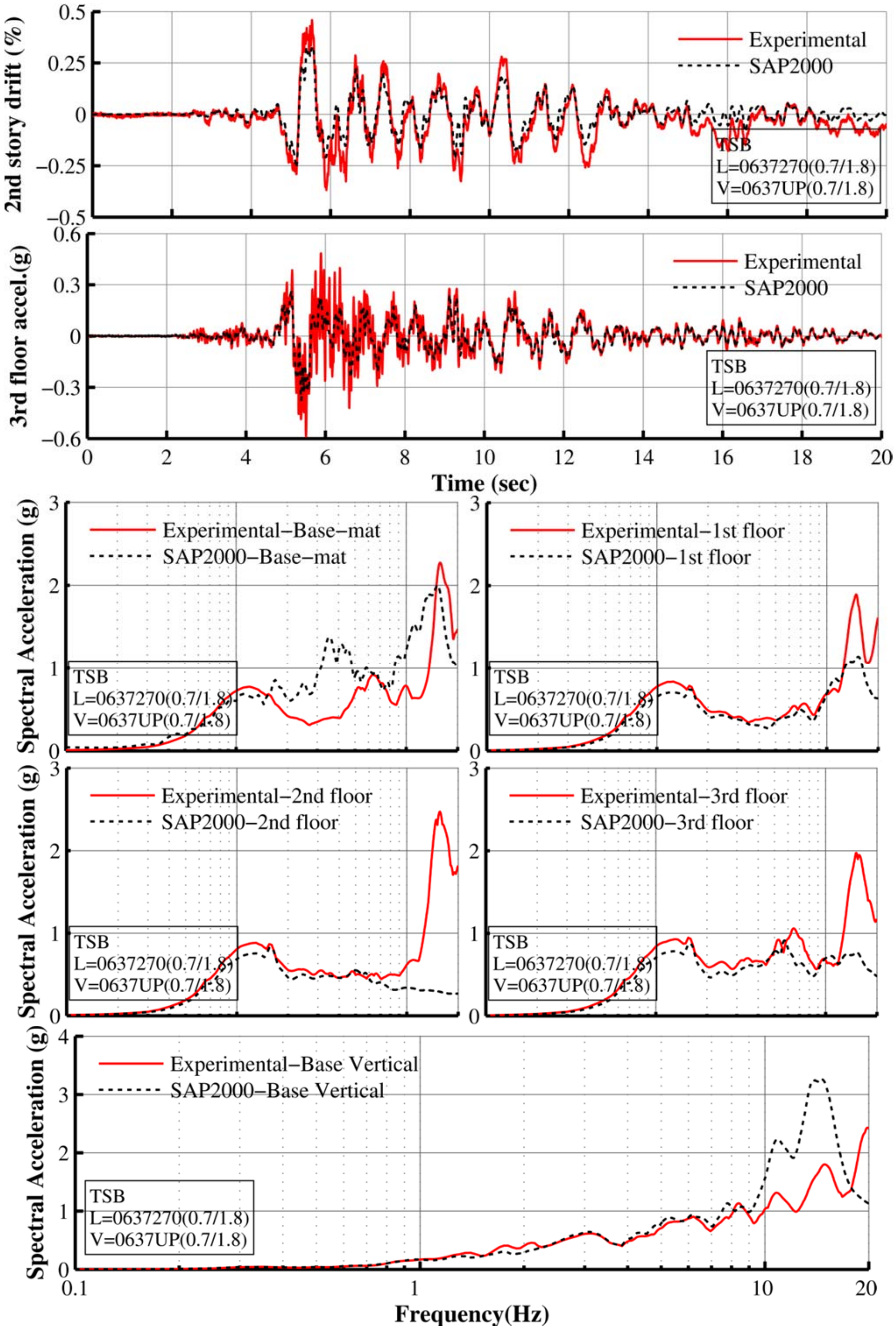

Figure 5-32 (cont'd): Comparison of analytical (program SAP2000) and experimental results of histories of drift and acceleration and 5%-damped floor spectra for isolated structure in combined horizontal and vertical excitation

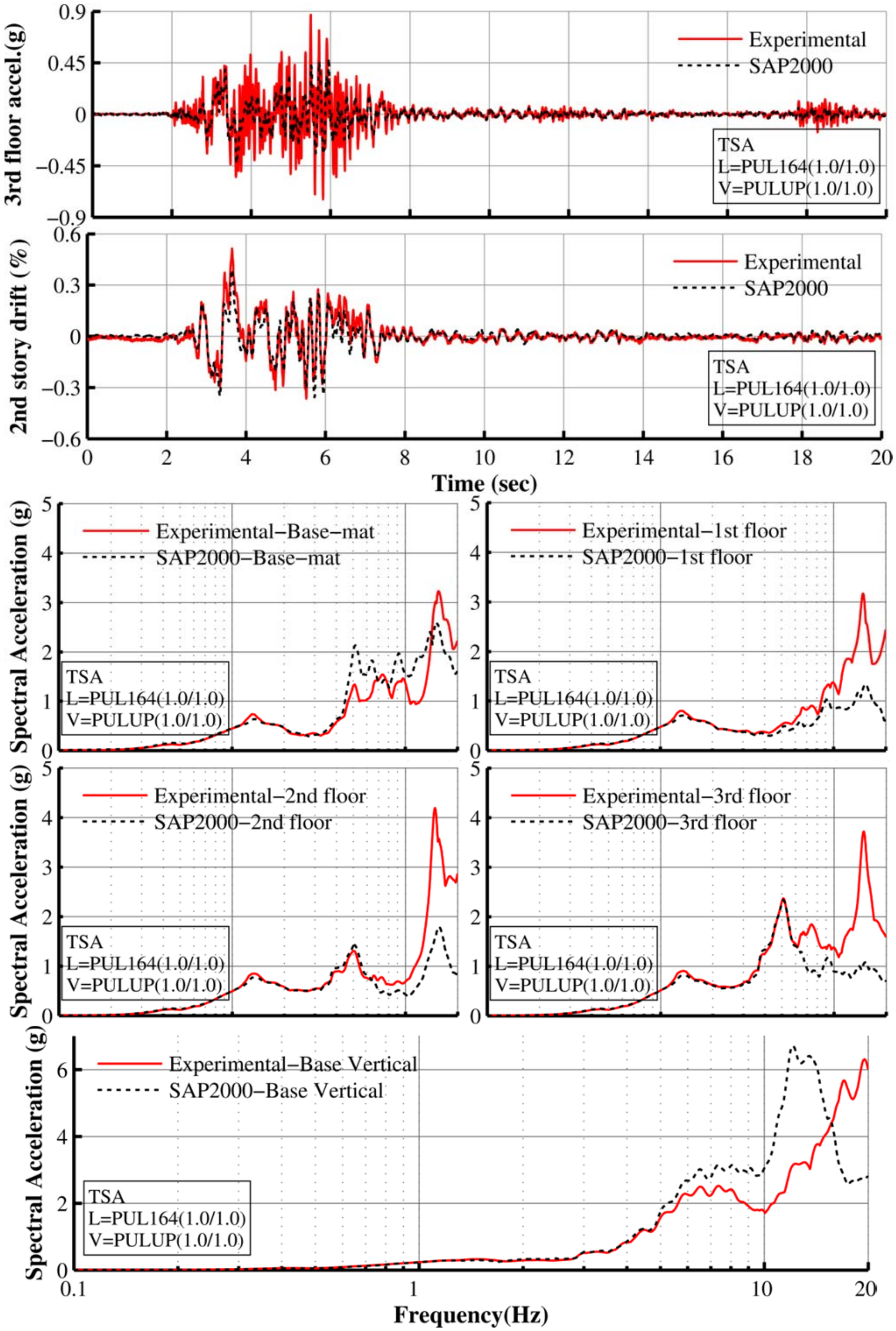

Figure 5-32 (cont'd): Comparison of analytical (program SAP2000) and experimental results of histories of drift and acceleration and 5%-damped floor spectra for isolated structure in combined horizontal and vertical excitation

SECTION 6
CONCLUSIONS

The results of a testing program of an isolated three-story structure supported by Triple FP isolators of three different configurations have been reported. The isolator configurations included two highly adaptive ones that exhibited all five regimes of operation of the isolator. The third configuration lacked adaptability and resembled in behavior the single FP. Testing consisted of horizontal excitation and combined horizontal and vertical excitation in a variety of time and acceleration scales so that the isolators operated in all five regimes of operation, and in some tests experienced uplift and impact on their restrainer rings. In general, the conditions of testing may be characterized as extreme.

Also, the response of the tested structure was predicted by numerical simulation in the commercial program SAP2000 and in the newly developed more advanced program 3pleANI and compared to the experimental results. It was concluded that:

1. The isolators exhibited stable behavior under the extreme conditions of testing. Certain aspects of the measured response were, however, unrealistic due to the very high stiffness and strength of the restrainer rings of the model isolators by comparison to those of full size isolators.
2. The vertical component of excitation had no or insignificant effect on the isolator displacement demand, had some minor effect on structural drifts and had an important effect on the floor accelerations. The effect of the vertical acceleration was enhanced in the testing by large parasitic rocking motion of the shake table.
3. The response of the structure could be predicted accurately in terms of isolator displacement, base shear, drift and acceleration histories, although the peak values (particularly of acceleration) were occasionally under-predicted or over-predicted. It is believed that this was primarily due to incomplete modeling of the superstructure.
4. Programs 3pleANI and SAP2000 provided comparable prediction of response but program 3pleANI has slightly better predictions due to better description of the velocity dependence of friction at each sliding interface, and more accurate consideration of the non-zero initial conditions.
5. Prediction of the response under combined horizontal and vertical excitation was less accurate that when only horizontal excitation was considered. The difference is likely the result of inaccurate modeling of the vertical stiffness of the isolators that may result in numerical errors and affect the prediction of the history of the vertical load on the isolator, and may predict incorrectly or prematurely isolator uplift.

SECTION 7
REFERENCES

1. Becker, T.C, and Mahin, S.A. (2011), "Experimental and analytical study of the bidirectional behavior of the triple friction pendulum isolator," Earthquake Engineering and Structural Dynamics, 41(3), 355-373.

2. Bracci, J.M., Reinhorn, A.M. and Mander, J.B. (1992), “ Seismic Resistance of Reinforced Concrete Frame Structures Designed Only for Gravity Loads: Part I- Design and Properties of a One- Third Scale Model Structure,” Technical Report NCEER-92-0027, National Center for Earthquake Engineering Research, State University of New York at Buffalo, Buffalo, NY.

3. Computers and Structures Inc. (2007), “SAP2000: Integrated Finite Element Analysis and Design of Structures,” Version 11.0.8, Berkeley, CA.

4. Constantinou, M.C., Mokha, A. and Reinhorn, A.M. (1990), “Teflon Bearings in Base Isolation. II: Modeling,” ASCE Journal of Structural Engineering, 116(2), 455-474.

5. Dao, N. D., Ryan, K. L., Sato, E., and Sasaki, T. (2013), "Predicting the Displacement of Triple Pendulum™ Bearings in a Full-Scale Shaking Experiment Using a Three-Dimensional Element," Earthquake Engineering and Structural Dynamics, Vol. 42, 1677-1695.

6. Fenz, D.M. and Constantinou, M.C. (2008a),”Mechanical Behavior of Multi-Spherical Sliding Bearings,” Report No. MCEER-08-0007, Multidisciplinary Center for Earthquake Engineering Research, State University of New York at Buffalo, Buffalo, NY.

7. Fenz, D.M. and Constantinou, M.C. (2008b), “Spherical Sliding Isolation Bearings with Adaptive Behavior: Theory,” Earthquake Engineering and Structural Dynamics, Vol. 37, No. 2, 163-183.

8. Fenz, D.M. and Constantinou, M.C. (2008c), “Spherical Sliding Isolation Bearings with Adaptive Behavior: Experimental Verification,” Earthquake Engineering and Structural Dynamics, Vol. 37, No. 2, 185-205.

9. Fenz, D.M. and Constantinou, M.C., (2008d), “Modeling Triple Friction Pendulum Bearings for Response-History Analysis,” Earthquake Spectra, Vol. 24, No. 4, 1011-1028.

10. Fenz, D.M. and Constantinou, M.C. (2008e), ”Development, Implementation and Verification of Dynamic Analysis Models for Multi-Spherical Sliding,” Report No. MCEER-

08-0018, Multidisciplinary Center for Earthquake Engineering Research, State University of New York at Buffalo, Buffalo, NY.

11. Kasalanati, A. and Constantinou, M.C. (1999), "Experimental Study of Bridge Elastomeric and Other Isolation and Energy Dissipation Systems with Emphasis on Uplift Prevention and High Velocity Near Source Seismic Excitation," Technical Report MCEER-99-0004, Multidisciplinary Center for Earthquake Engineering Research, State University of New York at Buffalo, Buffalo, NY.

12. Mokha, A.S., Constantinou, M.C. and Reinhorn, A.M. (1990), " Experimental Study and Analytical Prediction of Earthquake Response of a Sliding Isolation System with Spherical Surface," Technical Report NCEER-90-0020, National Center for Earthquake Engineering Research, State University of New York at Buffalo, Buffalo, NY.

13. Morgan, T. A. (2007), "The Use of Innovative Base Isolation Systems to Achieve Complex Seismic Performance Objectives," Ph.D. Dissertation, Department of Civil and Environmental Engineering, University of California, Berkeley.

14. Morgan T.A. and Mahin S.A. (2010), "Achieving Reliable Seismic Performance Enhancement Using Multistage Friction Pendulum Isolators," Earthquake Engineering and Structural Dynamics, 39(13), 1443–1461.

15. Ray, T., Sarlis, A. A., Reinhorn, A. M., and Constantinou, M. C. (2013), "Hysteretic Models for Sliding Bearings with Varying Frictional Force", Earthquake Engineering and Structural Dynamics, to appear, published on line on September 30, 2013.

16. Reinhorn, A.M., Soong, T.T., Lin, R.C., Yang, Y.P., Fukao, Y., Abe, H. and Nakai, M. (1989), "1:4 Scale Model Studies of Active Tendon Systems and Active Mass Dampers for Aseismic Protection," Technical Report NCEER-89-0026, National Center for Earthquake Engineering Research, State University of New York at Buffalo, Buffalo, NY.

17. Sarlis, A.A. and Constantinou, M.C. (2010)," Modeling of Triple Friction Pendulum Isolators in Program SAP2000," supplement to MCEER Report 05-0009. Document distributed to the engineering community together with executable version of program and example files, University at Buffalo.

18. Sarlis, A.A. and Constantinou, M.C. (2013), "Model of Triple Friction Pendulum Bearing for General Geometric and Frictional Parameters and for Uplift Conditions", Technical Report No. MCEER-13-0010, Multidisciplinary Center for Earthquake Engineering Research, State University of New York at Buffalo, Buffalo, NY.

19. Wolff, E.D. and Constantinou, M.C. (2004), "Experimental Study of Seismic Isolation Systems with Emphasis on Secondary System Response and Verification of Accuracy of Dynamic Response History Analysis Methods", Technical Report MCEER-04-0001, Multidisciplinary Center for Earthquake Engineering Research, State University of New York at Buffalo, Buffalo, NY.

MCEER Technical Reports

MCEER publishes technical reports on a variety of subjects written by authors funded through MCEER. These reports are available from both MCEER Publications and the National Technical Information Service (NTIS). Requests for reports should be directed to MCEER Publications, MCEER, University at Buffalo, State University of New York, 133A Ketter Hall, Buffalo, New York 14260. Reports can also be requested through NTIS, P.O. Box 1425, Springfield, Virginia 22151. NTIS accession numbers are shown in parenthesis, if available.

NCEER-87-0001 "First-Year Program in Research, Education and Technology Transfer," 3/5/87, (PB88-134275, A04, MF-A01).

NCEER-87-0002 "Experimental Evaluation of Instantaneous Optimal Algorithms for Structural Control," by R.C. Lin, T.T. Soong and A.M. Reinhorn, 4/20/87, (PB88-134341, A04, MF-A01).

NCEER-87-0003 "Experimentation Using the Earthquake Simulation Facilities at University at Buffalo," by A.M. Reinhorn and R.L. Ketter, not available.

NCEER-87-0004 "The System Characteristics and Performance of a Shaking Table," by J.S. Hwang, K.C. Chang and G.C. Lee, 6/1/87, (PB88-134259, A03, MF-A01). This report is available only through NTIS (see address given above).

NCEER-87-0005 "A Finite Element Formulation for Nonlinear Viscoplastic Material Using a Q Model," by O. Gyebi and G. Dasgupta, 11/2/87, (PB88-213764, A08, MF-A01).

NCEER-87-0006 "Symbolic Manipulation Program (SMP) - Algebraic Codes for Two and Three Dimensional Finite Element Formulations," by X. Lee and G. Dasgupta, 11/9/87, (PB88-218522, A05, MF-A01).

NCEER-87-0007 "Instantaneous Optimal Control Laws for Tall Buildings Under Seismic Excitations," by J.N. Yang, A. Akbarpour and P. Ghaemmaghami, 6/10/87, (PB88-134333, A06, MF-A01). This report is only available through NTIS (see address given above).

NCEER-87-0008 "IDARC: Inelastic Damage Analysis of Reinforced Concrete Frame - Shear-Wall Structures," by Y.J. Park, A.M. Reinhorn and S.K. Kunnath, 7/20/87, (PB88-134325, A09, MF-A01). This report is only available through NTIS (see address given above).

NCEER-87-0009 "Liquefaction Potential for New York State: A Preliminary Report on Sites in Manhattan and Buffalo," by M. Budhu, V. Vijayakumar, R.F. Giese and L. Baumgras, 8/31/87, (PB88-163704, A03, MF-A01). This report is available only through NTIS (see address given above).

NCEER-87-0010 "Vertical and Torsional Vibration of Foundations in Inhomogeneous Media," by A.S. Veletsos and K.W. Dotson, 6/1/87, (PB88-134291, A03, MF-A01). This report is only available through NTIS (see address given above).

NCEER-87-0011 "Seismic Probabilistic Risk Assessment and Seismic Margins Studies for Nuclear Power Plants," by Howard H.M. Hwang, 6/15/87, (PB88-134267, A03, MF-A01). This report is only available through NTIS (see address given above).

NCEER-87-0012 "Parametric Studies of Frequency Response of Secondary Systems Under Ground-Acceleration Excitations," by Y. Yong and Y.K. Lin, 6/10/87, (PB88-134309, A03, MF-A01). This report is only available through NTIS (see address given above).

NCEER-87-0013 "Frequency Response of Secondary Systems Under Seismic Excitation," by J.A. HoLung, J. Cai and Y.K. Lin, 7/31/87, (PB88-134317, A05, MF-A01). This report is only available through NTIS (see address given above).

NCEER-87-0014 "Modelling Earthquake Ground Motions in Seismically Active Regions Using Parametric Time Series Methods," by G.W. Ellis and A.S. Cakmak, 8/25/87, (PB88-134283, A08, MF-A01). This report is only available through NTIS (see address given above).

NCEER-87-0015 "Detection and Assessment of Seismic Structural Damage," by E. DiPasquale and A.S. Cakmak, 8/25/87, (PB88-163712, A05, MF-A01). This report is only available through NTIS (see address given above).

NCEER-87-0016 "Pipeline Experiment at Parkfield, California," by J. Isenberg and E. Richardson, 9/15/87, (PB88-163720, A03, MF-A01). This report is available only through NTIS (see address given above).

NCEER-87-0017 "Digital Simulation of Seismic Ground Motion," by M. Shinozuka, G. Deodatis and T. Harada, 8/31/87, (PB88-155197, A04, MF-A01). This report is available only through NTIS (see address given above).

NCEER-87-0018 "Practical Considerations for Structural Control: System Uncertainty, System Time Delay and Truncation of Small Control Forces," J.N. Yang and A. Akbarpour, 8/10/87, (PB88-163738, A08, MF-A01). This report is only available through NTIS (see address given above).

NCEER-87-0019 "Modal Analysis of Nonclassically Damped Structural Systems Using Canonical Transformation," by J.N. Yang, S. Sarkani and F.X. Long, 9/27/87, (PB88-187851, A04, MF-A01).

NCEER-87-0020 "A Nonstationary Solution in Random Vibration Theory," by J.R. Red-Horse and P.D. Spanos, 11/3/87, (PB88-163746, A03, MF-A01).

NCEER-87-0021 "Horizontal Impedances for Radially Inhomogeneous Viscoelastic Soil Layers," by A.S. Veletsos and K.W. Dotson, 10/15/87, (PB88-150859, A04, MF-A01).

NCEER-87-0022 "Seismic Damage Assessment of Reinforced Concrete Members," by Y.S. Chung, C. Meyer and M. Shinozuka, 10/9/87, (PB88-150867, A05, MF-A01). This report is available only through NTIS (see address given above).

NCEER-87-0023 "Active Structural Control in Civil Engineering," by T.T. Soong, 11/11/87, (PB88-187778, A03, MF-A01).

NCEER-87-0024 "Vertical and Torsional Impedances for Radially Inhomogeneous Viscoelastic Soil Layers," by K.W. Dotson and A.S. Veletsos, 12/87, (PB88-187786, A03, MF-A01).

NCEER-87-0025 "Proceedings from the Symposium on Seismic Hazards, Ground Motions, Soil-Liquefaction and Engineering Practice in Eastern North America," October 20-22, 1987, edited by K.H. Jacob, 12/87, (PB88-188115, A23, MF-A01). This report is available only through NTIS (see address given above).

NCEER-87-0026 "Report on the Whittier-Narrows, California, Earthquake of October 1, 1987," by J. Pantelic and A. Reinhorn, 11/87, (PB88-187752, A03, MF-A01). This report is available only through NTIS (see address given above).

NCEER-87-0027 "Design of a Modular Program for Transient Nonlinear Analysis of Large 3-D Building Structures," by S. Srivastav and J.F. Abel, 12/30/87, (PB88-187950, A05, MF-A01). This report is only available through NTIS (see address given above).

NCEER-87-0028 "Second-Year Program in Research, Education and Technology Transfer," 3/8/88, (PB88-219480, A04, MF-A01).

NCEER-88-0001 "Workshop on Seismic Computer Analysis and Design of Buildings With Interactive Graphics," by W. McGuire, J.F. Abel and C.H. Conley, 1/18/88, (PB88-187760, A03, MF-A01). This report is only available through NTIS (see address given above).

NCEER-88-0002 "Optimal Control of Nonlinear Flexible Structures," by J.N. Yang, F.X. Long and D. Wong, 1/22/88, (PB88-213772, A06, MF-A01).

NCEER-88-0003 "Substructuring Techniques in the Time Domain for Primary-Secondary Structural Systems," by G.D. Manolis and G. Juhn, 2/10/88, (PB88-213780, A04, MF-A01).

NCEER-88-0004 "Iterative Seismic Analysis of Primary-Secondary Systems," by A. Singhal, L.D. Lutes and P.D. Spanos, 2/23/88, (PB88-213798, A04, MF-A01).

NCEER-88-0005 "Stochastic Finite Element Expansion for Random Media," by P.D. Spanos and R. Ghanem, 3/14/88, (PB88-213806, A03, MF-A01).

NCEER-88-0006 "Combining Structural Optimization and Structural Control," by F.Y. Cheng and C.P. Pantelides, 1/10/88, (PB88-213814, A05, MF-A01).

NCEER-88-0007 "Seismic Performance Assessment of Code-Designed Structures," by H.H-M. Hwang, J-W. Jaw and H-J. Shau, 3/20/88, (PB88-219423, A04, MF-A01). This report is only available through NTIS (see address given above).

NCEER-88-0008 "Reliability Analysis of Code-Designed Structures Under Natural Hazards," by H.H-M. Hwang, H. Ushiba and M. Shinozuka, 2/29/88, (PB88-229471, A07, MF-A01). This report is only available through NTIS (see address given above).

NCEER-88-0009 "Seismic Fragility Analysis of Shear Wall Structures," by J-W Jaw and H.H-M. Hwang, 4/30/88, (PB89-102867, A04, MF-A01).

NCEER-88-0010 "Base Isolation of a Multi-Story Building Under a Harmonic Ground Motion - A Comparison of Performances of Various Systems," by F-G Fan, G. Ahmadi and I.G. Tadjbakhsh, 5/18/88, (PB89-122238, A06, MF-A01). This report is only available through NTIS (see address given above).

NCEER-88-0011 "Seismic Floor Response Spectra for a Combined System by Green's Functions," by F.M. Lavelle, L.A. Bergman and P.D. Spanos, 5/1/88, (PB89-102875, A03, MF-A01).

NCEER-88-0012 "A New Solution Technique for Randomly Excited Hysteretic Structures," by G.Q. Cai and Y.K. Lin, 5/16/88, (PB89-102883, A03, MF-A01).

NCEER-88-0013 "A Study of Radiation Damping and Soil-Structure Interaction Effects in the Centrifuge," by K. Weissman, supervised by J.H. Prevost, 5/24/88, (PB89-144703, A06, MF-A01).

NCEER-88-0014 "Parameter Identification and Implementation of a Kinematic Plasticity Model for Frictional Soils," by J.H. Prevost and D.V. Griffiths, not available.

NCEER-88-0015 "Two- and Three- Dimensional Dynamic Finite Element Analyses of the Long Valley Dam," by D.V. Griffiths and J.H. Prevost, 6/17/88, (PB89-144711, A04, MF-A01).

NCEER-88-0016 "Damage Assessment of Reinforced Concrete Structures in Eastern United States," by A.M. Reinhorn, M.J. Seidel, S.K. Kunnath and Y.J. Park, 6/15/88, (PB89-122220, A04, MF-A01). This report is only available through NTIS (see address given above).

NCEER-88-0017 "Dynamic Compliance of Vertically Loaded Strip Foundations in Multilayered Viscoelastic Soils," by S. Ahmad and A.S.M. Israil, 6/17/88, (PB89-102891, A04, MF-A01).

NCEER-88-0018 "An Experimental Study of Seismic Structural Response With Added Viscoelastic Dampers," by R.C. Lin, Z. Liang, T.T. Soong and R.H. Zhang, 6/30/88, (PB89-122212, A05, MF-A01). This report is available only through NTIS (see address given above).

NCEER-88-0019 "Experimental Investigation of Primary - Secondary System Interaction," by G.D. Manolis, G. Juhn and A.M. Reinhorn, 5/27/88, (PB89-122204, A04, MF-A01).

NCEER-88-0020 "A Response Spectrum Approach For Analysis of Nonclassically Damped Structures," by J.N. Yang, S. Sarkani and F.X. Long, 4/22/88, (PB89-102909, A04, MF-A01).

NCEER-88-0021 "Seismic Interaction of Structures and Soils: Stochastic Approach," by A.S. Veletsos and A.M. Prasad, 7/21/88, (PB89-122196, A04, MF-A01). This report is only available through NTIS (see address given above).

NCEER-88-0022 "Identification of the Serviceability Limit State and Detection of Seismic Structural Damage," by E. DiPasquale and A.S. Cakmak, 6/15/88, (PB89-122188, A05, MF-A01). This report is available only through NTIS (see address given above).

NCEER-88-0023 "Multi-Hazard Risk Analysis: Case of a Simple Offshore Structure," by B.K. Bhartia and E.H. Vanmarcke, 7/21/88, (PB89-145213, A05, MF-A01).

NCEER-88-0024 "Automated Seismic Design of Reinforced Concrete Buildings," by Y.S. Chung, C. Meyer and M. Shinozuka, 7/5/88, (PB89-122170, A06, MF-A01). This report is available only through NTIS (see address given above).

NCEER-88-0025 "Experimental Study of Active Control of MDOF Structures Under Seismic Excitations," by L.L. Chung, R.C. Lin, T.T. Soong and A.M. Reinhorn, 7/10/88, (PB89-122600, A04, MF-A01).

NCEER-88-0026 "Earthquake Simulation Tests of a Low-Rise Metal Structure," by J.S. Hwang, K.C. Chang, G.C. Lee and R.L. Ketter, 8/1/88, (PB89-102917, A04, MF-A01).

NCEER-88-0027 "Systems Study of Urban Response and Reconstruction Due to Catastrophic Earthquakes," by F. Kozin and H.K. Zhou, 9/22/88, (PB90-162348, A04, MF-A01).

NCEER-88-0028 "Seismic Fragility Analysis of Plane Frame Structures," by H.H-M. Hwang and Y.K. Low, 7/31/88, (PB89-131445, A06, MF-A01).

NCEER-88-0029 "Response Analysis of Stochastic Structures," by A. Kardara, C. Bucher and M. Shinozuka, 9/22/88, (PB89-174429, A04, MF-A01).

NCEER-88-0030 "Nonnormal Accelerations Due to Yielding in a Primary Structure," by D.C.K. Chen and L.D. Lutes, 9/19/88, (PB89-131437, A04, MF-A01).

NCEER-88-0031 "Design Approaches for Soil-Structure Interaction," by A.S. Veletsos, A.M. Prasad and Y. Tang, 12/30/88, (PB89-174437, A03, MF-A01). This report is available only through NTIS (see address given above).

NCEER-88-0032 "A Re-evaluation of Design Spectra for Seismic Damage Control," by C.J. Turkstra and A.G. Tallin, 11/7/88, (PB89-145221, A05, MF-A01).

NCEER-88-0033 "The Behavior and Design of Noncontact Lap Splices Subjected to Repeated Inelastic Tensile Loading," by V.E. Sagan, P. Gergely and R.N. White, 12/8/88, (PB89-163737, A08, MF-A01).

NCEER-88-0034 "Seismic Response of Pile Foundations," by S.M. Mamoon, P.K. Banerjee and S. Ahmad, 11/1/88, (PB89-145239, A04, MF-A01).

NCEER-88-0035 "Modeling of R/C Building Structures With Flexible Floor Diaphragms (IDARC2)," by A.M. Reinhorn, S.K. Kunnath and N. Panahshahi, 9/7/88, (PB89-207153, A07, MF-A01).

NCEER-88-0036 "Solution of the Dam-Reservoir Interaction Problem Using a Combination of FEM, BEM with Particular Integrals, Modal Analysis, and Substructuring," by C-S. Tsai, G.C. Lee and R.L. Ketter, 12/31/88, (PB89-207146, A04, MF-A01).

NCEER-88-0037 "Optimal Placement of Actuators for Structural Control," by F.Y. Cheng and C.P. Pantelides, 8/15/88, (PB89-162846, A05, MF-A01).

NCEER-88-0038 "Teflon Bearings in Aseismic Base Isolation: Experimental Studies and Mathematical Modeling," by A. Mokha, M.C. Constantinou and A.M. Reinhorn, 12/5/88, (PB89-218457, A10, MF-A01). This report is available only through NTIS (see address given above).

NCEER-88-0039 "Seismic Behavior of Flat Slab High-Rise Buildings in the New York City Area," by P. Weidlinger and M. Ettouney, 10/15/88, (PB90-145681, A04, MF-A01).

NCEER-88-0040 "Evaluation of the Earthquake Resistance of Existing Buildings in New York City," by P. Weidlinger and M. Ettouney, 10/15/88, not available.

NCEER-88-0041 "Small-Scale Modeling Techniques for Reinforced Concrete Structures Subjected to Seismic Loads," by W. Kim, A. El-Attar and R.N. White, 11/22/88, (PB89-189625, A05, MF-A01).

NCEER-88-0042 "Modeling Strong Ground Motion from Multiple Event Earthquakes," by G.W. Ellis and A.S. Cakmak, 10/15/88, (PB89-174445, A03, MF-A01).

NCEER-88-0043 "Nonstationary Models of Seismic Ground Acceleration," by M. Grigoriu, S.E. Ruiz and E. Rosenblueth, 7/15/88, (PB89-189617, A04, MF-A01).

NCEER-88-0044 "SARCF User's Guide: Seismic Analysis of Reinforced Concrete Frames," by Y.S. Chung, C. Meyer and M. Shinozuka, 11/9/88, (PB89-174452, A08, MF-A01).

NCEER-88-0045 "First Expert Panel Meeting on Disaster Research and Planning," edited by J. Pantelic and J. Stoyle, 9/15/88, (PB89-174460, A05, MF-A01).

NCEER-88-0046 "Preliminary Studies of the Effect of Degrading Infill Walls on the Nonlinear Seismic Response of Steel Frames," by C.Z. Chrysostomou, P. Gergely and J.F. Abel, 12/19/88, (PB89-208383, A05, MF-A01).

NCEER-88-0047 "Reinforced Concrete Frame Component Testing Facility - Design, Construction, Instrumentation and Operation," by S.P. Pessiki, C. Conley, T. Bond, P. Gergely and R.N. White, 12/16/88, (PB89-174478, A04, MF-A01).

NCEER-89-0001 "Effects of Protective Cushion and Soil Compliancy on the Response of Equipment Within a Seismically Excited Building," by J.A. HoLung, 2/16/89, (PB89-207179, A04, MF-A01).

NCEER-89-0002 "Statistical Evaluation of Response Modification Factors for Reinforced Concrete Structures," by H.H-M. Hwang and J-W. Jaw, 2/17/89, (PB89-207187, A05, MF-A01).

NCEER-89-0003 "Hysteretic Columns Under Random Excitation," by G-Q. Cai and Y.K. Lin, 1/9/89, (PB89-196513, A03, MF-A01).

NCEER-89-0004 "Experimental Study of `Elephant Foot Bulge' Instability of Thin-Walled Metal Tanks," by Z-H. Jia and R.L. Ketter, 2/22/89, (PB89-207195, A03, MF-A01).

NCEER-89-0005 "Experiment on Performance of Buried Pipelines Across San Andreas Fault," by J. Isenberg, E. Richardson and T.D. O'Rourke, 3/10/89, (PB89-218440, A04, MF-A01). This report is available only through NTIS (see address given above).

NCEER-89-0006 "A Knowledge-Based Approach to Structural Design of Earthquake-Resistant Buildings," by M. Subramani, P. Gergely, C.H. Conley, J.F. Abel and A.H. Zaghw, 1/15/89, (PB89-218465, A06, MF-A01).

NCEER-89-0007 "Liquefaction Hazards and Their Effects on Buried Pipelines," by T.D. O'Rourke and P.A. Lane, 2/1/89, (PB89-218481, A09, MF-A01).

NCEER-89-0008 "Fundamentals of System Identification in Structural Dynamics," by H. Imai, C-B. Yun, O. Maruyama and M. Shinozuka, 1/26/89, (PB89-207211, A04, MF-A01).

NCEER-89-0009 "Effects of the 1985 Michoacan Earthquake on Water Systems and Other Buried Lifelines in Mexico," by A.G. Ayala and M.J. O'Rourke, 3/8/89, (PB89-207229, A06, MF-A01).

NCEER-89-R010 "NCEER Bibliography of Earthquake Education Materials," by K.E.K. Ross, Second Revision, 9/1/89, (PB90-125352, A05, MF-A01). This report is replaced by NCEER-92-0018.

NCEER-89-0011 "Inelastic Three-Dimensional Response Analysis of Reinforced Concrete Building Structures (IDARC-3D), Part I - Modeling," by S.K. Kunnath and A.M. Reinhorn, 4/17/89, (PB90-114612, A07, MF-A01). This report is available only through NTIS (see address given above).

NCEER-89-0012 "Recommended Modifications to ATC-14," by C.D. Poland and J.O. Malley, 4/12/89, (PB90-108648, A15, MF-A01).

NCEER-89-0013 "Repair and Strengthening of Beam-to-Column Connections Subjected to Earthquake Loading," by M. Corazao and A.J. Durrani, 2/28/89, (PB90-109885, A06, MF-A01).

NCEER-89-0014 "Program EXKAL2 for Identification of Structural Dynamic Systems," by O. Maruyama, C-B. Yun, M. Hoshiya and M. Shinozuka, 5/19/89, (PB90-109877, A09, MF-A01).

NCEER-89-0015 "Response of Frames With Bolted Semi-Rigid Connections, Part I - Experimental Study and Analytical Predictions," by P.J. DiCorso, A.M. Reinhorn, J.R. Dickerson, J.B. Radziminski and W.L. Harper, 6/1/89, not available.

NCEER-89-0016 "ARMA Monte Carlo Simulation in Probabilistic Structural Analysis," by P.D. Spanos and M.P. Mignolet, 7/10/89, (PB90-109893, A03, MF-A01).

NCEER-89-P017 "Preliminary Proceedings from the Conference on Disaster Preparedness - The Place of Earthquake Education in Our Schools," Edited by K.E.K. Ross, 6/23/89, (PB90-108606, A03, MF-A01).

NCEER-89-0017 "Proceedings from the Conference on Disaster Preparedness - The Place of Earthquake Education in Our Schools," Edited by K.E.K. Ross, 12/31/89, (PB90-207895, A012, MF-A02). This report is available only through NTIS (see address given above).

NCEER-89-0018 "Multidimensional Models of Hysteretic Material Behavior for Vibration Analysis of Shape Memory Energy Absorbing Devices, by E.J. Graesser and F.A. Cozzarelli, 6/7/89, (PB90-164146, A04, MF-A01).

NCEER-89-0019 "Nonlinear Dynamic Analysis of Three-Dimensional Base Isolated Structures (3D-BASIS)," by S. Nagarajaiah, A.M. Reinhorn and M.C. Constantinou, 8/3/89, (PB90-161936, A06, MF-A01). This report has been replaced by NCEER-93-0011.

NCEER-89-0020 "Structural Control Considering Time-Rate of Control Forces and Control Rate Constraints," by F.Y. Cheng and C.P. Pantelides, 8/3/89, (PB90-120445, A04, MF-A01).

NCEER-89-0021 "Subsurface Conditions of Memphis and Shelby County," by K.W. Ng, T-S. Chang and H-H.M. Hwang, 7/26/89, (PB90-120437, A03, MF-A01).

NCEER-89-0022 "Seismic Wave Propagation Effects on Straight Jointed Buried Pipelines," by K. Elhmadi and M.J. O'Rourke, 8/24/89, (PB90-162322, A10, MF-A02).

NCEER-89-0023 "Workshop on Serviceability Analysis of Water Delivery Systems," edited by M. Grigoriu, 3/6/89, (PB90-127424, A03, MF-A01).

NCEER-89-0024 "Shaking Table Study of a 1/5 Scale Steel Frame Composed of Tapered Members," by K.C. Chang, J.S. Hwang and G.C. Lee, 9/18/89, (PB90-160169, A04, MF-A01).

NCEER-89-0025 "DYNA1D: A Computer Program for Nonlinear Seismic Site Response Analysis - Technical Documentation," by Jean H. Prevost, 9/14/89, (PB90-161944, A07, MF-A01). This report is available only through NTIS (see address given above).

NCEER-89-0026 "1:4 Scale Model Studies of Active Tendon Systems and Active Mass Dampers for Aseismic Protection," by A.M. Reinhorn, T.T. Soong, R.C. Lin, Y.P. Yang, Y. Fukao, H. Abe and M. Nakai, 9/15/89, (PB90-173246, A10, MF-A02). This report is available only through NTIS (see address given above).

NCEER-89-0027 "Scattering of Waves by Inclusions in a Nonhomogeneous Elastic Half Space Solved by Boundary Element Methods," by P.K. Hadley, A. Askar and A.S. Cakmak, 6/15/89, (PB90-145699, A07, MF-A01).

NCEER-89-0028 "Statistical Evaluation of Deflection Amplification Factors for Reinforced Concrete Structures," by H.H.M. Hwang, J-W. Jaw and A.L. Ch'ng, 8/31/89, (PB90-164633, A05, MF-A01).

NCEER-89-0029 "Bedrock Accelerations in Memphis Area Due to Large New Madrid Earthquakes," by H.H.M. Hwang, C.H.S. Chen and G. Yu, 11/7/89, (PB90-162330, A04, MF-A01).

NCEER-89-0030 "Seismic Behavior and Response Sensitivity of Secondary Structural Systems," by Y.Q. Chen and T.T. Soong, 10/23/89, (PB90-164658, A08, MF-A01).

NCEER-89-0031 "Random Vibration and Reliability Analysis of Primary-Secondary Structural Systems," by Y. Ibrahim, M. Grigoriu and T.T. Soong, 11/10/89, (PB90-161951, A04, MF-A01).

NCEER-89-0032 "Proceedings from the Second U.S. - Japan Workshop on Liquefaction, Large Ground Deformation and Their Effects on Lifelines, September 26-29, 1989," Edited by T.D. O'Rourke and M. Hamada, 12/1/89, (PB90-209388, A22, MF-A03).

NCEER-89-0033 "Deterministic Model for Seismic Damage Evaluation of Reinforced Concrete Structures," by J.M. Bracci, A.M. Reinhorn, J.B. Mander and S.K. Kunnath, 9/27/89, (PB91-108803, A06, MF-A01).

NCEER-89-0034 "On the Relation Between Local and Global Damage Indices," by E. DiPasquale and A.S. Cakmak, 8/15/89, (PB90-173865, A05, MF-A01).

NCEER-89-0035 "Cyclic Undrained Behavior of Nonplastic and Low Plasticity Silts," by A.J. Walker and H.E. Stewart, 7/26/89, (PB90-183518, A10, MF-A01).

NCEER-89-0036 "Liquefaction Potential of Surficial Deposits in the City of Buffalo, New York," by M. Budhu, R. Giese and L. Baumgrass, 1/17/89, (PB90-208455, A04, MF-A01).

NCEER-89-0037 "A Deterministic Assessment of Effects of Ground Motion Incoherence," by A.S. Veletsos and Y. Tang, 7/15/89, (PB90-164294, A03, MF-A01).

NCEER-89-0038 "Workshop on Ground Motion Parameters for Seismic Hazard Mapping," July 17-18, 1989, edited by R.V. Whitman, 12/1/89, (PB90-173923, A04, MF-A01).

NCEER-89-0039 "Seismic Effects on Elevated Transit Lines of the New York City Transit Authority," by C.J. Costantino, C.A. Miller and E. Heymsfield, 12/26/89, (PB90-207887, A06, MF-A01).

NCEER-89-0040 "Centrifugal Modeling of Dynamic Soil-Structure Interaction," by K. Weissman, Supervised by J.H. Prevost, 5/10/89, (PB90-207879, A07, MF-A01).

NCEER-89-0041 "Linearized Identification of Buildings With Cores for Seismic Vulnerability Assessment," by I-K. Ho and A.E. Aktan, 11/1/89, (PB90-251943, A07, MF-A01).

NCEER-90-0001 "Geotechnical and Lifeline Aspects of the October 17, 1989 Loma Prieta Earthquake in San Francisco," by T.D. O'Rourke, H.E. Stewart, F.T. Blackburn and T.S. Dickerman, 1/90, (PB90-208596, A05, MF-A01).

NCEER-90-0002 "Nonnormal Secondary Response Due to Yielding in a Primary Structure," by D.C.K. Chen and L.D. Lutes, 2/28/90, (PB90-251976, A07, MF-A01).

NCEER-90-0003 "Earthquake Education Materials for Grades K-12," by K.E.K. Ross, 4/16/90, (PB91-251984, A05, MF-A05). This report has been replaced by NCEER-92-0018.

NCEER-90-0004 "Catalog of Strong Motion Stations in Eastern North America," by R.W. Busby, 4/3/90, (PB90-251984, A05, MF-A01).

NCEER-90-0005 "NCEER Strong-Motion Data Base: A User Manual for the GeoBase Release (Version 1.0 for the Sun3)," by P. Friberg and K. Jacob, 3/31/90 (PB90-258062, A04, MF-A01).

NCEER-90-0006 "Seismic Hazard Along a Crude Oil Pipeline in the Event of an 1811-1812 Type New Madrid Earthquake," by H.H.M. Hwang and C-H.S. Chen, 4/16/90, (PB90-258054, A04, MF-A01).

NCEER-90-0007 "Site-Specific Response Spectra for Memphis Sheahan Pumping Station," by H.H.M. Hwang and C.S. Lee, 5/15/90, (PB91-108811, A05, MF-A01).

NCEER-90-0008 "Pilot Study on Seismic Vulnerability of Crude Oil Transmission Systems," by T. Ariman, R. Dobry, M. Grigoriu, F. Kozin, M. O'Rourke, T. O'Rourke and M. Shinozuka, 5/25/90, (PB91-108837, A06, MF-A01).

NCEER-90-0009 "A Program to Generate Site Dependent Time Histories: EQGEN," by G.W. Ellis, M. Srinivasan and A.S. Cakmak, 1/30/90, (PB91-108829, A04, MF-A01).

NCEER-90-0010 "Active Isolation for Seismic Protection of Operating Rooms," by M.E. Talbott, Supervised by M. Shinozuka, 6/8/9, (PB91-110205, A05, MF-A01).

NCEER-90-0011 "Program LINEARID for Identification of Linear Structural Dynamic Systems," by C-B. Yun and M. Shinozuka, 6/25/90, (PB91-110312, A08, MF-A01).

NCEER-90-0012 "Two-Dimensional Two-Phase Elasto-Plastic Seismic Response of Earth Dams," by A.N. Yiagos, Supervised by J.H. Prevost, 6/20/90, (PB91-110197, A13, MF-A02).

NCEER-90-0013 "Secondary Systems in Base-Isolated Structures: Experimental Investigation, Stochastic Response and Stochastic Sensitivity," by G.D. Manolis, G. Juhn, M.C. Constantinou and A.M. Reinhorn, 7/1/90, (PB91-110320, A08, MF-A01).

NCEER-90-0014 "Seismic Behavior of Lightly-Reinforced Concrete Column and Beam-Column Joint Details," by S.P. Pessiki, C.H. Conley, P. Gergely and R.N. White, 8/22/90, (PB91-108795, A11, MF-A02).

NCEER-90-0015 "Two Hybrid Control Systems for Building Structures Under Strong Earthquakes," by J.N. Yang and A. Danielians, 6/29/90, (PB91-125393, A04, MF-A01).

NCEER-90-0016 "Instantaneous Optimal Control with Acceleration and Velocity Feedback," by J.N. Yang and Z. Li, 6/29/90, (PB91-125401, A03, MF-A01).

NCEER-90-0017 "Reconnaissance Report on the Northern Iran Earthquake of June 21, 1990," by M. Mehrain, 10/4/90, (PB91-125377, A03, MF-A01).

NCEER-90-0018 "Evaluation of Liquefaction Potential in Memphis and Shelby County," by T.S. Chang, P.S. Tang, C.S. Lee and H. Hwang, 8/10/90, (PB91-125427, A09, MF-A01).

NCEER-90-0019 "Experimental and Analytical Study of a Combined Sliding Disc Bearing and Helical Steel Spring Isolation System," by M.C. Constantinou, A.S. Mokha and A.M. Reinhorn, 10/4/90, (PB91-125385, A06, MF-A01). This report is available only through NTIS (see address given above).

NCEER-90-0020 "Experimental Study and Analytical Prediction of Earthquake Response of a Sliding Isolation System with a Spherical Surface," by A.S. Mokha, M.C. Constantinou and A.M. Reinhorn, 10/11/90, (PB91-125419, A05, MF-A01).

NCEER-90-0021 "Dynamic Interaction Factors for Floating Pile Groups," by G. Gazetas, K. Fan, A. Kaynia and E. Kausel, 9/10/90, (PB91-170381, A05, MF-A01).

NCEER-90-0022 "Evaluation of Seismic Damage Indices for Reinforced Concrete Structures," by S. Rodriguez-Gomez and A.S. Cakmak, 9/30/90, PB91-171322, A06, MF-A01).

NCEER-90-0023 "Study of Site Response at a Selected Memphis Site," by H. Desai, S. Ahmad, E.S. Gazetas and M.R. Oh, 10/11/90, (PB91-196857, A03, MF-A01).

NCEER-90-0024 "A User's Guide to Strongmo: Version 1.0 of NCEER's Strong-Motion Data Access Tool for PCs and Terminals," by P.A. Friberg and C.A.T. Susch, 11/15/90, (PB91-171272, A03, MF-A01).

NCEER-90-0025 "A Three-Dimensional Analytical Study of Spatial Variability of Seismic Ground Motions," by L-L. Hong and A.H.-S. Ang, 10/30/90, (PB91-170399, A09, MF-A01).

NCEER-90-0026 "MUMOID User's Guide - A Program for the Identification of Modal Parameters," by S. Rodriguez-Gomez and E. DiPasquale, 9/30/90, (PB91-171298, A04, MF-A01).

NCEER-90-0027 "SARCF-II User's Guide - Seismic Analysis of Reinforced Concrete Frames," by S. Rodriguez-Gomez, Y.S. Chung and C. Meyer, 9/30/90, (PB91-171280, A05, MF-A01).

NCEER-90-0028 "Viscous Dampers: Testing, Modeling and Application in Vibration and Seismic Isolation," by N. Makris and M.C. Constantinou, 12/20/90 (PB91-190561, A06, MF-A01).

NCEER-90-0029 "Soil Effects on Earthquake Ground Motions in the Memphis Area," by H. Hwang, C.S. Lee, K.W. Ng and T.S. Chang, 8/2/90, (PB91-190751, A05, MF-A01).

NCEER-91-0001 "Proceedings from the Third Japan-U.S. Workshop on Earthquake Resistant Design of Lifeline Facilities and Countermeasures for Soil Liquefaction, December 17-19, 1990," edited by T.D. O'Rourke and M. Hamada, 2/1/91, (PB91-179259, A99, MF-A04).

NCEER-91-0002 "Physical Space Solutions of Non-Proportionally Damped Systems," by M. Tong, Z. Liang and G.C. Lee, 1/15/91, (PB91-179242, A04, MF-A01).

NCEER-91-0003 "Seismic Response of Single Piles and Pile Groups," by K. Fan and G. Gazetas, 1/10/91, (PB92-174994, A04, MF-A01).

NCEER-91-0004 "Damping of Structures: Part 1 - Theory of Complex Damping," by Z. Liang and G. Lee, 10/10/91, (PB92-197235, A12, MF-A03).

NCEER-91-0005 "3D-BASIS - Nonlinear Dynamic Analysis of Three Dimensional Base Isolated Structures: Part II," by S. Nagarajaiah, A.M. Reinhorn and M.C. Constantinou, 2/28/91, (PB91-190553, A07, MF-A01). This report has been replaced by NCEER-93-0011.

NCEER-91-0006 "A Multidimensional Hysteretic Model for Plasticity Deforming Metals in Energy Absorbing Devices," by E.J. Graesser and F.A. Cozzarelli, 4/9/91, (PB92-108364, A04, MF-A01).

NCEER-91-0007 "A Framework for Customizable Knowledge-Based Expert Systems with an Application to a KBES for Evaluating the Seismic Resistance of Existing Buildings," by E.G. Ibarra-Anaya and S.J. Fenves, 4/9/91, (PB91-210930, A08, MF-A01).

NCEER-91-0008 "Nonlinear Analysis of Steel Frames with Semi-Rigid Connections Using the Capacity Spectrum Method," by G.G. Deierlein, S-H. Hsieh, Y-J. Shen and J.F. Abel, 7/2/91, (PB92-113828, A05, MF-A01).

NCEER-91-0009 "Earthquake Education Materials for Grades K-12," by K.E.K. Ross, 4/30/91, (PB91-212142, A06, MF-A01). This report has been replaced by NCEER-92-0018.

NCEER-91-0010 "Phase Wave Velocities and Displacement Phase Differences in a Harmonically Oscillating Pile," by N. Makris and G. Gazetas, 7/8/91, (PB92-108356, A04, MF-A01).

NCEER-91-0011 "Dynamic Characteristics of a Full-Size Five-Story Steel Structure and a 2/5 Scale Model," by K.C. Chang, G.C. Yao, G.C. Lee, D.S. Hao and Y.C. Yeh," 7/2/91, (PB93-116648, A06, MF-A02).

NCEER-91-0012 "Seismic Response of a 2/5 Scale Steel Structure with Added Viscoelastic Dampers," by K.C. Chang, T.T. Soong, S-T. Oh and M.L. Lai, 5/17/91, (PB92-110816, A05, MF-A01).

NCEER-91-0013 "Earthquake Response of Retaining Walls; Full-Scale Testing and Computational Modeling," by S. Alampalli and A-W.M. Elgamal, 6/20/91, not available.

NCEER-91-0014 "3D-BASIS-M: Nonlinear Dynamic Analysis of Multiple Building Base Isolated Structures," by P.C. Tsopelas, S. Nagarajaiah, M.C. Constantinou and A.M. Reinhorn, 5/28/91, (PB92-113885, A09, MF-A02).

NCEER-91-0015 "Evaluation of SEAOC Design Requirements for Sliding Isolated Structures," by D. Theodossiou and M.C. Constantinou, 6/10/91, (PB92-114602, A11, MF-A03).

NCEER-91-0016 "Closed-Loop Modal Testing of a 27-Story Reinforced Concrete Flat Plate-Core Building," by H.R. Somaprasad, T. Toksoy, H. Yoshiyuki and A.E. Aktan, 7/15/91, (PB92-129980, A07, MF-A02).

NCEER-91-0017 "Shake Table Test of a 1/6 Scale Two-Story Lightly Reinforced Concrete Building," by A.G. El-Attar, R.N. White and P. Gergely, 2/28/91, (PB92-222447, A06, MF-A02).

NCEER-91-0018 "Shake Table Test of a 1/8 Scale Three-Story Lightly Reinforced Concrete Building," by A.G. El-Attar, R.N. White and P. Gergely, 2/28/91, (PB93-116630, A08, MF-A02).

NCEER-91-0019 "Transfer Functions for Rigid Rectangular Foundations," by A.S. Veletsos, A.M. Prasad and W.H. Wu, 7/31/91, not available.

NCEER-91-0020 "Hybrid Control of Seismic-Excited Nonlinear and Inelastic Structural Systems," by J.N. Yang, Z. Li and A. Danielians, 8/1/91, (PB92-143171, A06, MF-A02).

NCEER-91-0021 "The NCEER-91 Earthquake Catalog: Improved Intensity-Based Magnitudes and Recurrence Relations for U.S. Earthquakes East of New Madrid," by L. Seeber and J.G. Armbruster, 8/28/91, (PB92-176742, A06, MF-A02).

NCEER-91-0022 "Proceedings from the Implementation of Earthquake Planning and Education in Schools: The Need for Change - The Roles of the Changemakers," by K.E.K. Ross and F. Winslow, 7/23/91, (PB92-129998, A12, MF-A03).

NCEER-91-0023 "A Study of Reliability-Based Criteria for Seismic Design of Reinforced Concrete Frame Buildings," by H.H.M. Hwang and H-M. Hsu, 8/10/91, (PB92-140235, A09, MF-A02).

NCEER-91-0024 "Experimental Verification of a Number of Structural System Identification Algorithms," by R.G. Ghanem, H. Gavin and M. Shinozuka, 9/18/91, (PB92-176577, A18, MF-A04).

NCEER-91-0025 "Probabilistic Evaluation of Liquefaction Potential," by H.H.M. Hwang and C.S. Lee," 11/25/91, (PB92-143429, A05, MF-A01).

NCEER-91-0026 "Instantaneous Optimal Control for Linear, Nonlinear and Hysteretic Structures - Stable Controllers," by J.N. Yang and Z. Li, 11/15/91, (PB92-163807, A04, MF-A01).

NCEER-91-0027 "Experimental and Theoretical Study of a Sliding Isolation System for Bridges," by M.C. Constantinou, A. Kartoum, A.M. Reinhorn and P. Bradford, 11/15/91, (PB92-176973, A10, MF-A03).

NCEER-92-0001 "Case Studies of Liquefaction and Lifeline Performance During Past Earthquakes, Volume 1: Japanese Case Studies," Edited by M. Hamada and T. O'Rourke, 2/17/92, (PB92-197243, A18, MF-A04).

NCEER-92-0002 "Case Studies of Liquefaction and Lifeline Performance During Past Earthquakes, Volume 2: United States Case Studies," Edited by T. O'Rourke and M. Hamada, 2/17/92, (PB92-197250, A20, MF-A04).

NCEER-92-0003 "Issues in Earthquake Education," Edited by K. Ross, 2/3/92, (PB92-222389, A07, MF-A02).

NCEER-92-0004 "Proceedings from the First U.S. - Japan Workshop on Earthquake Protective Systems for Bridges," Edited by I.G. Buckle, 2/4/92, (PB94-142239, A99, MF-A06).

NCEER-92-0005 "Seismic Ground Motion from a Haskell-Type Source in a Multiple-Layered Half-Space," A.P. Theoharis, G. Deodatis and M. Shinozuka, 1/2/92, not available.

NCEER-92-0006 "Proceedings from the Site Effects Workshop," Edited by R. Whitman, 2/29/92, (PB92-197201, A04, MF-A01).

NCEER-92-0007 "Engineering Evaluation of Permanent Ground Deformations Due to Seismically-Induced Liquefaction," by M.H. Baziar, R. Dobry and A-W.M. Elgamal, 3/24/92, (PB92-222421, A13, MF-A03).

NCEER-92-0008 "A Procedure for the Seismic Evaluation of Buildings in the Central and Eastern United States," by C.D. Poland and J.O. Malley, 4/2/92, (PB92-222439, A20, MF-A04).

NCEER-92-0009 "Experimental and Analytical Study of a Hybrid Isolation System Using Friction Controllable Sliding Bearings," by M.Q. Feng, S. Fujii and M. Shinozuka, 5/15/92, (PB93-150282, A06, MF-A02).

NCEER-92-0010 "Seismic Resistance of Slab-Column Connections in Existing Non-Ductile Flat-Plate Buildings," by A.J. Durrani and Y. Du, 5/18/92, (PB93-116812, A06, MF-A02).

NCEER-92-0011 "The Hysteretic and Dynamic Behavior of Brick Masonry Walls Upgraded by Ferrocement Coatings Under Cyclic Loading and Strong Simulated Ground Motion," by H. Lee and S.P. Prawel, 5/11/92, not available.

NCEER-92-0012 "Study of Wire Rope Systems for Seismic Protection of Equipment in Buildings," by G.F. Demetriades, M.C. Constantinou and A.M. Reinhorn, 5/20/92, (PB93-116655, A08, MF-A02).

NCEER-92-0013 "Shape Memory Structural Dampers: Material Properties, Design and Seismic Testing," by P.R. Witting and F.A. Cozzarelli, 5/26/92, (PB93-116663, A05, MF-A01).

NCEER-92-0014 "Longitudinal Permanent Ground Deformation Effects on Buried Continuous Pipelines," by M.J. O'Rourke, and C. Nordberg, 6/15/92, (PB93-116671, A08, MF-A02).

NCEER-92-0015 "A Simulation Method for Stationary Gaussian Random Functions Based on the Sampling Theorem," by M. Grigoriu and S. Balopoulou, 6/11/92, (PB93-127496, A05, MF-A01).

NCEER-92-0016 "Gravity-Load-Designed Reinforced Concrete Buildings: Seismic Evaluation of Existing Construction and Detailing Strategies for Improved Seismic Resistance," by G.W. Hoffmann, S.K. Kunnath, A.M. Reinhorn and J.B. Mander, 7/15/92, (PB94-142007, A08, MF-A02).

NCEER-92-0017 "Observations on Water System and Pipeline Performance in the Limón Area of Costa Rica Due to the April 22, 1991 Earthquake," by M. O'Rourke and D. Ballantyne, 6/30/92, (PB93-126811, A06, MF-A02).

NCEER-92-0018 "Fourth Edition of Earthquake Education Materials for Grades K-12," Edited by K.E.K. Ross, 8/10/92, (PB93-114023, A07, MF-A02).

NCEER-92-0019 "Proceedings from the Fourth Japan-U.S. Workshop on Earthquake Resistant Design of Lifeline Facilities and Countermeasures for Soil Liquefaction," Edited by M. Hamada and T.D. O'Rourke, 8/12/92, (PB93-163939, A99, MF-E11).

NCEER-92-0020 "Active Bracing System: A Full Scale Implementation of Active Control," by A.M. Reinhorn, T.T. Soong, R.C. Lin, M.A. Riley, Y.P. Wang, S. Aizawa and M. Higashino, 8/14/92, (PB93-127512, A06, MF-A02).

NCEER-92-0021 "Empirical Analysis of Horizontal Ground Displacement Generated by Liquefaction-Induced Lateral Spreads," by S.F. Bartlett and T.L. Youd, 8/17/92, (PB93-188241, A06, MF-A02).

NCEER-92-0022 "IDARC Version 3.0: Inelastic Damage Analysis of Reinforced Concrete Structures," by S.K. Kunnath, A.M. Reinhorn and R.F. Lobo, 8/31/92, (PB93-227502, A07, MF-A02).

NCEER-92-0023 "A Semi-Empirical Analysis of Strong-Motion Peaks in Terms of Seismic Source, Propagation Path and Local Site Conditions, by M. Kamiyama, M.J. O'Rourke and R. Flores-Berrones, 9/9/92, (PB93-150266, A08, MF-A02).

NCEER-92-0024 "Seismic Behavior of Reinforced Concrete Frame Structures with Nonductile Details, Part I: Summary of Experimental Findings of Full Scale Beam-Column Joint Tests," by A. Beres, R.N. White and P. Gergely, 9/30/92, (PB93-227783, A05, MF-A01).

NCEER-92-0025 "Experimental Results of Repaired and Retrofitted Beam-Column Joint Tests in Lightly Reinforced Concrete Frame Buildings," by A. Beres, S. El-Borgi, R.N. White and P. Gergely, 10/29/92, (PB93-227791, A05, MF-A01).

NCEER-92-0026 "A Generalization of Optimal Control Theory: Linear and Nonlinear Structures," by J.N. Yang, Z. Li and S. Vongchavalitkul, 11/2/92, (PB93-188621, A05, MF-A01).

NCEER-92-0027 "Seismic Resistance of Reinforced Concrete Frame Structures Designed Only for Gravity Loads: Part I - Design and Properties of a One-Third Scale Model Structure," by J.M. Bracci, A.M. Reinhorn and J.B. Mander, 12/1/92, (PB94-104502, A08, MF-A02).

NCEER-92-0028 "Seismic Resistance of Reinforced Concrete Frame Structures Designed Only for Gravity Loads: Part II - Experimental Performance of Subassemblages," by L.E. Aycardi, J.B. Mander and A.M. Reinhorn, 12/1/92, (PB94-104510, A08, MF-A02).

NCEER-92-0029 "Seismic Resistance of Reinforced Concrete Frame Structures Designed Only for Gravity Loads: Part III - Experimental Performance and Analytical Study of a Structural Model," by J.M. Bracci, A.M. Reinhorn and J.B. Mander, 12/1/92, (PB93-227528, A09, MF-A01).

NCEER-92-0030 "Evaluation of Seismic Retrofit of Reinforced Concrete Frame Structures: Part I - Experimental Performance of Retrofitted Subassemblages," by D. Choudhuri, J.B. Mander and A.M. Reinhorn, 12/8/92, (PB93-198307, A07, MF-A02).

NCEER-92-0031 "Evaluation of Seismic Retrofit of Reinforced Concrete Frame Structures: Part II - Experimental Performance and Analytical Study of a Retrofitted Structural Model," by J.M. Bracci, A.M. Reinhorn and J.B. Mander, 12/8/92, (PB93-198315, A09, MF-A03).

NCEER-92-0032 "Experimental and Analytical Investigation of Seismic Response of Structures with Supplemental Fluid Viscous Dampers," by M.C. Constantinou and M.D. Symans, 12/21/92, (PB93-191435, A10, MF-A03). This report is available only through NTIS (see address given above).

NCEER-92-0033 "Reconnaissance Report on the Cairo, Egypt Earthquake of October 12, 1992," by M. Khater, 12/23/92, (PB93-188621, A03, MF-A01).

NCEER-92-0034 "Low-Level Dynamic Characteristics of Four Tall Flat-Plate Buildings in New York City," by H. Gavin, S. Yuan, J. Grossman, E. Pekelis and K. Jacob, 12/28/92, (PB93-188217, A07, MF-A02).

NCEER-93-0001 "An Experimental Study on the Seismic Performance of Brick-Infilled Steel Frames With and Without Retrofit," by J.B. Mander, B. Nair, K. Wojtkowski and J. Ma, 1/29/93, (PB93-227510, A07, MF-A02).

NCEER-93-0002 "Social Accounting for Disaster Preparedness and Recovery Planning," by S. Cole, E. Pantoja and V. Razak, 2/22/93, (PB94-142114, A12, MF-A03).

NCEER-93-0003 "Assessment of 1991 NEHRP Provisions for Nonstructural Components and Recommended Revisions," by T.T. Soong, G. Chen, Z. Wu, R-H. Zhang and M. Grigoriu, 3/1/93, (PB93-188639, A06, MF-A02).

NCEER-93-0004 "Evaluation of Static and Response Spectrum Analysis Procedures of SEAOC/UBC for Seismic Isolated Structures," by C.W. Winters and M.C. Constantinou, 3/23/93, (PB93-198299, A10, MF-A03).

NCEER-93-0005 "Earthquakes in the Northeast - Are We Ignoring the Hazard? A Workshop on Earthquake Science and Safety for Educators," edited by K.E.K. Ross, 4/2/93, (PB94-103066, A09, MF-A02).

NCEER-93-0006 "Inelastic Response of Reinforced Concrete Structures with Viscoelastic Braces," by R.F. Lobo, J.M. Bracci, K.L. Shen, A.M. Reinhorn and T.T. Soong, 4/5/93, (PB93-227486, A05, MF-A02).

NCEER-93-0007 "Seismic Testing of Installation Methods for Computers and Data Processing Equipment," by K. Kosar, T.T. Soong, K.L. Shen, J.A. HoLung and Y.K. Lin, 4/12/93, (PB93-198299, A07, MF-A02).

NCEER-93-0008 "Retrofit of Reinforced Concrete Frames Using Added Dampers," by A. Reinhorn, M. Constantinou and C. Li, not available.

NCEER-93-0009 "Seismic Behavior and Design Guidelines for Steel Frame Structures with Added Viscoelastic Dampers," by K.C. Chang, M.L. Lai, T.T. Soong, D.S. Hao and Y.C. Yeh, 5/1/93, (PB94-141959, A07, MF-A02).

NCEER-93-0010 "Seismic Performance of Shear-Critical Reinforced Concrete Bridge Piers," by J.B. Mander, S.M. Waheed, M.T.A. Chaudhary and S.S. Chen, 5/12/93, (PB93-227494, A08, MF-A02).

NCEER-93-0011 "3D-BASIS-TABS: Computer Program for Nonlinear Dynamic Analysis of Three Dimensional Base Isolated Structures," by S. Nagarajaiah, C. Li, A.M. Reinhorn and M.C. Constantinou, 8/2/93, (PB94-141819, A09, MF-A02).

NCEER-93-0012 "Effects of Hydrocarbon Spills from an Oil Pipeline Break on Ground Water," by O.J. Helweg and H.H.M. Hwang, 8/3/93, (PB94-141942, A06, MF-A02).

NCEER-93-0013 "Simplified Procedures for Seismic Design of Nonstructural Components and Assessment of Current Code Provisions," by M.P. Singh, L.E. Suarez, E.E. Matheu and G.O. Maldonado, 8/4/93, (PB94-141827, A09, MF-A02).

NCEER-93-0014 "An Energy Approach to Seismic Analysis and Design of Secondary Systems," by G. Chen and T.T. Soong, 8/6/93, (PB94-142767, A11, MF-A03).

NCEER-93-0015 "Proceedings from School Sites: Becoming Prepared for Earthquakes - Commemorating the Third Anniversary of the Loma Prieta Earthquake," Edited by F.E. Winslow and K.E.K. Ross, 8/16/93, (PB94-154275, A16, MF-A02).

NCEER-93-0016 "Reconnaissance Report of Damage to Historic Monuments in Cairo, Egypt Following the October 12, 1992 Dahshur Earthquake," by D. Sykora, D. Look, G. Croci, E. Karaesmen and E. Karaesmen, 8/19/93, (PB94-142221, A08, MF-A02).

NCEER-93-0017 "The Island of Guam Earthquake of August 8, 1993," by S.W. Swan and S.K. Harris, 9/30/93, (PB94-141843, A04, MF-A01).

NCEER-93-0018 "Engineering Aspects of the October 12, 1992 Egyptian Earthquake," by A.W. Elgamal, M. Amer, K. Adalier and A. Abul-Fadl, 10/7/93, (PB94-141983, A05, MF-A01).

NCEER-93-0019 "Development of an Earthquake Motion Simulator and its Application in Dynamic Centrifuge Testing," by I. Krstelj, Supervised by J.H. Prevost, 10/23/93, (PB94-181773, A-10, MF-A03).

NCEER-93-0020 "NCEER-Taisei Corporation Research Program on Sliding Seismic Isolation Systems for Bridges: Experimental and Analytical Study of a Friction Pendulum System (FPS)," by M.C. Constantinou, P. Tsopelas, Y-S. Kim and S. Okamoto, 11/1/93, (PB94-142775, A08, MF-A02).

NCEER-93-0021 "Finite Element Modeling of Elastomeric Seismic Isolation Bearings," by L.J. Billings, Supervised by R. Shepherd, 11/8/93, not available.

NCEER-93-0022 "Seismic Vulnerability of Equipment in Critical Facilities: Life-Safety and Operational Consequences," by K. Porter, G.S. Johnson, M.M. Zadeh, C. Scawthorn and S. Eder, 11/24/93, (PB94-181765, A16, MF-A03).

NCEER-93-0023 "Hokkaido Nansei-oki, Japan Earthquake of July 12, 1993, by P.I. Yanev and C.R. Scawthorn, 12/23/93, (PB94-181500, A07, MF-A01).

NCEER-94-0001 "An Evaluation of Seismic Serviceability of Water Supply Networks with Application to the San Francisco Auxiliary Water Supply System," by I. Markov, Supervised by M. Grigoriu and T. O'Rourke, 1/21/94, (PB94-204013, A07, MF-A02).

NCEER-94-0002 "NCEER-Taisei Corporation Research Program on Sliding Seismic Isolation Systems for Bridges: Experimental and Analytical Study of Systems Consisting of Sliding Bearings, Rubber Restoring Force Devices and Fluid Dampers," Volumes I and II, by P. Tsopelas, S. Okamoto, M.C. Constantinou, D. Ozaki and S. Fujii, 2/4/94, (PB94-181740, A09, MF-A02 and PB94-181757, A12, MF-A03).

NCEER-94-0003 "A Markov Model for Local and Global Damage Indices in Seismic Analysis," by S. Rahman and M. Grigoriu, 2/18/94, (PB94-206000, A12, MF-A03).

NCEER-94-0004 "Proceedings from the NCEER Workshop on Seismic Response of Masonry Infills," edited by D.P. Abrams, 3/1/94, (PB94-180783, A07, MF-A02).

NCEER-94-0005 "The Northridge, California Earthquake of January 17, 1994: General Reconnaissance Report," edited by J.D. Goltz, 3/11/94, (PB94-193943, A10, MF-A03).

NCEER-94-0006 "Seismic Energy Based Fatigue Damage Analysis of Bridge Columns: Part I - Evaluation of Seismic Capacity," by G.A. Chang and J.B. Mander, 3/14/94, (PB94-219185, A11, MF-A03).

NCEER-94-0007 "Seismic Isolation of Multi-Story Frame Structures Using Spherical Sliding Isolation Systems," by T.M. Al-Hussaini, V.A. Zayas and M.C. Constantinou, 3/17/94, (PB94-193745, A09, MF-A02).

NCEER-94-0008 "The Northridge, California Earthquake of January 17, 1994: Performance of Highway Bridges," edited by I.G. Buckle, 3/24/94, (PB94-193851, A06, MF-A02).

NCEER-94-0009 "Proceedings of the Third U.S.-Japan Workshop on Earthquake Protective Systems for Bridges," edited by I.G. Buckle and I. Friedland, 3/31/94, (PB94-195815, A99, MF-A06).

NCEER-94-0010 "3D-BASIS-ME: Computer Program for Nonlinear Dynamic Analysis of Seismically Isolated Single and Multiple Structures and Liquid Storage Tanks," by P.C. Tsopelas, M.C. Constantinou and A.M. Reinhorn, 4/12/94, (PB94-204922, A09, MF-A02).

NCEER-94-0011 "The Northridge, California Earthquake of January 17, 1994: Performance of Gas Transmission Pipelines," by T.D. O'Rourke and M.C. Palmer, 5/16/94, (PB94-204989, A05, MF-A01).

NCEER-94-0012 "Feasibility Study of Replacement Procedures and Earthquake Performance Related to Gas Transmission Pipelines," by T.D. O'Rourke and M.C. Palmer, 5/25/94, (PB94-206638, A09, MF-A02).

NCEER-94-0013 "Seismic Energy Based Fatigue Damage Analysis of Bridge Columns: Part II - Evaluation of Seismic Demand," by G.A. Chang and J.B. Mander, 6/1/94, (PB95-18106, A08, MF-A02).

NCEER-94-0014 "NCEER-Taisei Corporation Research Program on Sliding Seismic Isolation Systems for Bridges: Experimental and Analytical Study of a System Consisting of Sliding Bearings and Fluid Restoring Force/Damping Devices," by P. Tsopelas and M.C. Constantinou, 6/13/94, (PB94-219144, A10, MF-A03).

NCEER-94-0015 "Generation of Hazard-Consistent Fragility Curves for Seismic Loss Estimation Studies," by H. Hwang and J-R. Huo, 6/14/94, (PB95-181996, A09, MF-A02).

NCEER-94-0016 "Seismic Study of Building Frames with Added Energy-Absorbing Devices," by W.S. Pong, C.S. Tsai and G.C. Lee, 6/20/94, (PB94-219136, A10, A03).

NCEER-94-0017 "Sliding Mode Control for Seismic-Excited Linear and Nonlinear Civil Engineering Structures," by J. Yang, J. Wu, A. Agrawal and Z. Li, 6/21/94, (PB95-138483, A06, MF-A02).

NCEER-94-0018 "3D-BASIS-TABS Version 2.0: Computer Program for Nonlinear Dynamic Analysis of Three Dimensional Base Isolated Structures," by A.M. Reinhorn, S. Nagarajaiah, M.C. Constantinou, P. Tsopelas and R. Li, 6/22/94, (PB95-182176, A08, MF-A02).

NCEER-94-0019 "Proceedings of the International Workshop on Civil Infrastructure Systems: Application of Intelligent Systems and Advanced Materials on Bridge Systems," Edited by G.C. Lee and K.C. Chang, 7/18/94, (PB95-252474, A20, MF-A04).

NCEER-94-0020 "Study of Seismic Isolation Systems for Computer Floors," by V. Lambrou and M.C. Constantinou, 7/19/94, (PB95-138533, A10, MF-A03).

NCEER-94-0021 "Proceedings of the U.S.-Italian Workshop on Guidelines for Seismic Evaluation and Rehabilitation of Unreinforced Masonry Buildings," Edited by D.P. Abrams and G.M. Calvi, 7/20/94, (PB95-138749, A13, MF-A03).

NCEER-94-0022 "NCEER-Taisei Corporation Research Program on Sliding Seismic Isolation Systems for Bridges: Experimental and Analytical Study of a System Consisting of Lubricated PTFE Sliding Bearings and Mild Steel Dampers," by P. Tsopelas and M.C. Constantinou, 7/22/94, (PB95-182184, A08, MF-A02).

NCEER-94-0023 "Development of Reliability-Based Design Criteria for Buildings Under Seismic Load," by Y.K. Wen, H. Hwang and M. Shinozuka, 8/1/94, (PB95-211934, A08, MF-A02).

NCEER-94-0024 "Experimental Verification of Acceleration Feedback Control Strategies for an Active Tendon System," by S.J. Dyke, B.F. Spencer, Jr., P. Quast, M.K. Sain, D.C. Kaspari, Jr. and T.T. Soong, 8/29/94, (PB95-212320, A05, MF-A01).

NCEER-94-0025 "Seismic Retrofitting Manual for Highway Bridges," Edited by I.G. Buckle and I.F. Friedland, published by the Federal Highway Administration (PB95-212676, A15, MF-A03).

NCEER-94-0026 "Proceedings from the Fifth U.S.-Japan Workshop on Earthquake Resistant Design of Lifeline Facilities and Countermeasures Against Soil Liquefaction," Edited by T.D. O'Rourke and M. Hamada, 11/7/94, (PB95-220802, A99, MF-E08).

NCEER-95-0001 "Experimental and Analytical Investigation of Seismic Retrofit of Structures with Supplemental Damping: Part 1 - Fluid Viscous Damping Devices," by A.M. Reinhorn, C. Li and M.C. Constantinou, 1/3/95, (PB95-266599, A09, MF-A02).

NCEER-95-0002 "Experimental and Analytical Study of Low-Cycle Fatigue Behavior of Semi-Rigid Top-And-Seat Angle Connections," by G. Pekcan, J.B. Mander and S.S. Chen, 1/5/95, (PB95-220042, A07, MF-A02).

NCEER-95-0003 "NCEER-ATC Joint Study on Fragility of Buildings," by T. Anagnos, C. Rojahn and A.S. Kiremidjian, 1/20/95, (PB95-220026, A06, MF-A02).

NCEER-95-0004 "Nonlinear Control Algorithms for Peak Response Reduction," by Z. Wu, T.T. Soong, V. Gattulli and R.C. Lin, 2/16/95, (PB95-220349, A05, MF-A01).

NCEER-95-0005 "Pipeline Replacement Feasibility Study: A Methodology for Minimizing Seismic and Corrosion Risks to Underground Natural Gas Pipelines," by R.T. Eguchi, H.A. Seligson and D.G. Honegger, 3/2/95, (PB95-252326, A06, MF-A02).

NCEER-95-0006 "Evaluation of Seismic Performance of an 11-Story Frame Building During the 1994 Northridge Earthquake," by F. Naeim, R. DiSulio, K. Benuska, A. Reinhorn and C. Li, not available.

NCEER-95-0007 "Prioritization of Bridges for Seismic Retrofitting," by N. Basöz and A.S. Kiremidjian, 4/24/95, (PB95-252300, A08, MF-A02).

NCEER-95-0008 "Method for Developing Motion Damage Relationships for Reinforced Concrete Frames," by A. Singhal and A.S. Kiremidjian, 5/11/95, (PB95-266607, A06, MF-A02).

NCEER-95-0009 "Experimental and Analytical Investigation of Seismic Retrofit of Structures with Supplemental Damping: Part II - Friction Devices," by C. Li and A.M. Reinhorn, 7/6/95, (PB96-128087, A11, MF-A03).

NCEER-95-0010 "Experimental Performance and Analytical Study of a Non-Ductile Reinforced Concrete Frame Structure Retrofitted with Elastomeric Spring Dampers," by G. Pekcan, J.B. Mander and S.S. Chen, 7/14/95, (PB96-137161, A08, MF-A02).

NCEER-95-0011 "Development and Experimental Study of Semi-Active Fluid Damping Devices for Seismic Protection of Structures," by M.D. Symans and M.C. Constantinou, 8/3/95, (PB96-136940, A23, MF-A04).

NCEER-95-0012 "Real-Time Structural Parameter Modification (RSPM): Development of Innervated Structures," by Z. Liang, M. Tong and G.C. Lee, 4/11/95, (PB96-137153, A06, MF-A01).

NCEER-95-0013 "Experimental and Analytical Investigation of Seismic Retrofit of Structures with Supplemental Damping: Part III - Viscous Damping Walls," by A.M. Reinhorn and C. Li, 10/1/95, (PB96-176409, A11, MF-A03).

NCEER-95-0014 "Seismic Fragility Analysis of Equipment and Structures in a Memphis Electric Substation," by J-R. Huo and H.H.M. Hwang, 8/10/95, (PB96-128087, A09, MF-A02).

NCEER-95-0015 "The Hanshin-Awaji Earthquake of January 17, 1995: Performance of Lifelines," Edited by M. Shinozuka, 11/3/95, (PB96-176383, A15, MF-A03).

NCEER-95-0016 "Highway Culvert Performance During Earthquakes," by T.L. Youd and C.J. Beckman, available as NCEER-96-0015.

NCEER-95-0017 "The Hanshin-Awaji Earthquake of January 17, 1995: Performance of Highway Bridges," Edited by I.G. Buckle, 12/1/95, not available.

NCEER-95-0018 "Modeling of Masonry Infill Panels for Structural Analysis," by A.M. Reinhorn, A. Madan, R.E. Valles, Y. Reichmann and J.B. Mander, 12/8/95, (PB97-110886, MF-A01, A06).

NCEER-95-0019 "Optimal Polynomial Control for Linear and Nonlinear Structures," by A.K. Agrawal and J.N. Yang, 12/11/95, (PB96-168737, A07, MF-A02).

NCEER-95-0020 "Retrofit of Non-Ductile Reinforced Concrete Frames Using Friction Dampers," by R.S. Rao, P. Gergely and R.N. White, 12/22/95, (PB97-133508, A10, MF-A02).

NCEER-95-0021 "Parametric Results for Seismic Response of Pile-Supported Bridge Bents," by G. Mylonakis, A. Nikolaou and G. Gazetas, 12/22/95, (PB97-100242, A12, MF-A03).

NCEER-95-0022 "Kinematic Bending Moments in Seismically Stressed Piles," by A. Nikolaou, G. Mylonakis and G. Gazetas, 12/23/95, (PB97-113914, MF-A03, A13).

NCEER-96-0001 "Dynamic Response of Unreinforced Masonry Buildings with Flexible Diaphragms," by A.C. Costley and D.P. Abrams," 10/10/96, (PB97-133573, MF-A03, A15).

NCEER-96-0002 "State of the Art Review: Foundations and Retaining Structures," by I. Po Lam, not available.

NCEER-96-0003 "Ductility of Rectangular Reinforced Concrete Bridge Columns with Moderate Confinement," by N. Wehbe, M. Saiidi, D. Sanders and B. Douglas, 11/7/96, (PB97-133557, A06, MF-A02).

NCEER-96-0004 "Proceedings of the Long-Span Bridge Seismic Research Workshop," edited by I.G. Buckle and I.M. Friedland, not available.

NCEER-96-0005 "Establish Representative Pier Types for Comprehensive Study: Eastern United States," by J. Kulicki and Z. Prucz, 5/28/96, (PB98-119217, A07, MF-A02).

NCEER-96-0006 "Establish Representative Pier Types for Comprehensive Study: Western United States," by R. Imbsen, R.A. Schamber and T.A. Osterkamp, 5/28/96, (PB98-118607, A07, MF-A02).

NCEER-96-0007 "Nonlinear Control Techniques for Dynamical Systems with Uncertain Parameters," by R.G. Ghanem and M.I. Bujakov, 5/27/96, (PB97-100259, A17, MF-A03).

NCEER-96-0008 "Seismic Evaluation of a 30-Year Old Non-Ductile Highway Bridge Pier and Its Retrofit," by J.B. Mander, B. Mahmoodzadegan, S. Bhadra and S.S. Chen, 5/31/96, (PB97-110902, MF-A03, A10).

NCEER-96-0009 "Seismic Performance of a Model Reinforced Concrete Bridge Pier Before and After Retrofit," by J.B. Mander, J.H. Kim and C.A. Ligozio, 5/31/96, (PB97-110910, MF-A02, A10).

NCEER-96-0010 "IDARC2D Version 4.0: A Computer Program for the Inelastic Damage Analysis of Buildings," by R.E. Valles, A.M. Reinhorn, S.K. Kunnath, C. Li and A. Madan, 6/3/96, (PB97-100234, A17, MF-A03).

NCEER-96-0011 "Estimation of the Economic Impact of Multiple Lifeline Disruption: Memphis Light, Gas and Water Division Case Study," by S.E. Chang, H.A. Seligson and R.T. Eguchi, 8/16/96, (PB97-133490, A11, MF-A03).

NCEER-96-0012 "Proceedings from the Sixth Japan-U.S. Workshop on Earthquake Resistant Design of Lifeline Facilities and Countermeasures Against Soil Liquefaction, Edited by M. Hamada and T. O'Rourke, 9/11/96, (PB97-133581, A99, MF-A06).

NCEER-96-0013 "Chemical Hazards, Mitigation and Preparedness in Areas of High Seismic Risk: A Methodology for Estimating the Risk of Post-Earthquake Hazardous Materials Release," by H.A. Seligson, R.T. Eguchi, K.J. Tierney and K. Richmond, 11/7/96, (PB97-133565, MF-A02, A08).

NCEER-96-0014 "Response of Steel Bridge Bearings to Reversed Cyclic Loading," by J.B. Mander, D-K. Kim, S.S. Chen and G.J. Premus, 11/13/96, (PB97-140735, A12, MF-A03).

NCEER-96-0015 "Highway Culvert Performance During Past Earthquakes," by T.L. Youd and C.J. Beckman, 11/25/96, (PB97-133532, A06, MF-A01).

NCEER-97-0001 "Evaluation, Prevention and Mitigation of Pounding Effects in Building Structures," by R.E. Valles and A.M. Reinhorn, 2/20/97, (PB97-159552, A14, MF-A03).

NCEER-97-0002 "Seismic Design Criteria for Bridges and Other Highway Structures," by C. Rojahn, R. Mayes, D.G. Anderson, J. Clark, J.H. Hom, R.V. Nutt and M.J. O'Rourke, 4/30/97, (PB97-194658, A06, MF-A03).

NCEER-97-0003 “Proceedings of the U.S.-Italian Workshop on Seismic Evaluation and Retrofit,” Edited by D.P. Abrams and G.M. Calvi, 3/19/97, (PB97-194666, A13, MF-A03).

NCEER-97-0004 "Investigation of Seismic Response of Buildings with Linear and Nonlinear Fluid Viscous Dampers," by A.A. Seleemah and M.C. Constantinou, 5/21/97, (PB98-109002, A15, MF-A03).

NCEER-97-0005 "Proceedings of the Workshop on Earthquake Engineering Frontiers in Transportation Facilities," edited by G.C. Lee and I.M. Friedland, 8/29/97, (PB98-128911, A25, MR-A04).

NCEER-97-0006 "Cumulative Seismic Damage of Reinforced Concrete Bridge Piers," by S.K. Kunnath, A. El-Bahy, A. Taylor and W. Stone, 9/2/97, (PB98-108814, A11, MF-A03).

NCEER-97-0007 "Structural Details to Accommodate Seismic Movements of Highway Bridges and Retaining Walls," by R.A. Imbsen, R.A. Schamber, E. Thorkildsen, A. Kartoum, B.T. Martin, T.N. Rosser and J.M. Kulicki, 9/3/97, (PB98-108996, A09, MF-A02).

NCEER-97-0008 "A Method for Earthquake Motion-Damage Relationships with Application to Reinforced Concrete Frames," by A. Singhal and A.S. Kiremidjian, 9/10/97, (PB98-108988, A13, MF-A03).

NCEER-97-0009 "Seismic Analysis and Design of Bridge Abutments Considering Sliding and Rotation," by K. Fishman and R. Richards, Jr., 9/15/97, (PB98-108897, A06, MF-A02).

NCEER-97-0010 "Proceedings of the FHWA/NCEER Workshop on the National Representation of Seismic Ground Motion for New and Existing Highway Facilities," edited by I.M. Friedland, M.S. Power and R.L. Mayes, 9/22/97, (PB98-128903, A21, MF-A04).

NCEER-97-0011 "Seismic Analysis for Design or Retrofit of Gravity Bridge Abutments," by K.L. Fishman, R. Richards, Jr. and R.C. Divito, 10/2/97, (PB98-128937, A08, MF-A02).

NCEER-97-0012 "Evaluation of Simplified Methods of Analysis for Yielding Structures," by P. Tsopelas, M.C. Constantinou, C.A. Kircher and A.S. Whittaker, 10/31/97, (PB98-128929, A10, MF-A03).

NCEER-97-0013 "Seismic Design of Bridge Columns Based on Control and Repairability of Damage," by C-T. Cheng and J.B. Mander, 12/8/97, (PB98-144249, A11, MF-A03).

NCEER-97-0014 "Seismic Resistance of Bridge Piers Based on Damage Avoidance Design," by J.B. Mander and C-T. Cheng, 12/10/97, (PB98-144223, A09, MF-A02).

NCEER-97-0015 “Seismic Response of Nominally Symmetric Systems with Strength Uncertainty,” by S. Balopoulou and M. Grigoriu, 12/23/97, (PB98-153422, A11, MF-A03).

NCEER-97-0016 “Evaluation of Seismic Retrofit Methods for Reinforced Concrete Bridge Columns,” by T.J. Wipf, F.W. Klaiber and F.M. Russo, 12/28/97, (PB98-144215, A12, MF-A03).

NCEER-97-0017 “Seismic Fragility of Existing Conventional Reinforced Concrete Highway Bridges,” by C.L. Mullen and A.S. Cakmak, 12/30/97, (PB98-153406, A08, MF-A02).

NCEER-97-0018 “Loss Asssessment of Memphis Buildings,” edited by D.P. Abrams and M. Shinozuka, 12/31/97, (PB98-144231, A13, MF-A03).

NCEER-97-0019 “Seismic Evaluation of Frames with Infill Walls Using Quasi-static Experiments,” by K.M. Mosalam, R.N. White and P. Gergely, 12/31/97, (PB98-153455, A07, MF-A02).

NCEER-97-0020 “Seismic Evaluation of Frames with Infill Walls Using Pseudo-dynamic Experiments,” by K.M. Mosalam, R.N. White and P. Gergely, 12/31/97, (PB98-153430, A07, MF-A02).

NCEER-97-0021 “Computational Strategies for Frames with Infill Walls: Discrete and Smeared Crack Analyses and Seismic Fragility,” by K.M. Mosalam, R.N. White and P. Gergely, 12/31/97, (PB98-153414, A10, MF-A02).

NCEER-97-0022 "Proceedings of the NCEER Workshop on Evaluation of Liquefaction Resistance of Soils," edited by T.L. Youd and I.M. Idriss, 12/31/97, (PB98-155617, A15, MF-A03).

MCEER-98-0001 "Extraction of Nonlinear Hysteretic Properties of Seismically Isolated Bridges from Quick-Release Field Tests," by Q. Chen, B.M. Douglas, E.M. Maragakis and I.G. Buckle, 5/26/98, (PB99-118838, A06, MF-A01).

MCEER-98-0002 "Methodologies for Evaluating the Importance of Highway Bridges," by A. Thomas, S. Eshenaur and J. Kulicki, 5/29/98, (PB99-118846, A10, MF-A02).

MCEER-98-0003 "Capacity Design of Bridge Piers and the Analysis of Overstrength," by J.B. Mander, A. Dutta and P. Goel, 6/1/98, (PB99-118853, A09, MF-A02).

MCEER-98-0004 "Evaluation of Bridge Damage Data from the Loma Prieta and Northridge, California Earthquakes," by N. Basoz and A. Kiremidjian, 6/2/98, (PB99-118861, A15, MF-A03).

MCEER-98-0005 "Screening Guide for Rapid Assessment of Liquefaction Hazard at Highway Bridge Sites," by T. L. Youd, 6/16/98, (PB99-118879, A06, not available on microfiche).

MCEER-98-0006 "Structural Steel and Steel/Concrete Interface Details for Bridges," by P. Ritchie, N. Kauhl and J. Kulicki, 7/13/98, (PB99-118945, A06, MF-A01).

MCEER-98-0007 "Capacity Design and Fatigue Analysis of Confined Concrete Columns," by A. Dutta and J.B. Mander, 7/14/98, (PB99-118960, A14, MF-A03).

MCEER-98-0008 "Proceedings of the Workshop on Performance Criteria for Telecommunication Services Under Earthquake Conditions," edited by A.J. Schiff, 7/15/98, (PB99-118952, A08, MF-A02).

MCEER-98-0009 "Fatigue Analysis of Unconfined Concrete Columns," by J.B. Mander, A. Dutta and J.H. Kim, 9/12/98, (PB99-123655, A10, MF-A02).

MCEER-98-0010 "Centrifuge Modeling of Cyclic Lateral Response of Pile-Cap Systems and Seat-Type Abutments in Dry Sands," by A.D. Gadre and R. Dobry, 10/2/98, (PB99-123606, A13, MF-A03).

MCEER-98-0011 "IDARC-BRIDGE: A Computational Platform for Seismic Damage Assessment of Bridge Structures," by A.M. Reinhorn, V. Simeonov, G. Mylonakis and Y. Reichman, 10/2/98, (PB99-162919, A15, MF-A03).

MCEER-98-0012 "Experimental Investigation of the Dynamic Response of Two Bridges Before and After Retrofitting with Elastomeric Bearings," by D.A. Wendichansky, S.S. Chen and J.B. Mander, 10/2/98, (PB99-162927, A15, MF-A03).

MCEER-98-0013 "Design Procedures for Hinge Restrainers and Hinge Sear Width for Multiple-Frame Bridges," by R. Des Roches and G.L. Fenves, 11/3/98, (PB99-140477, A13, MF-A03).

MCEER-98-0014 "Response Modification Factors for Seismically Isolated Bridges," by M.C. Constantinou and J.K. Quarshie, 11/3/98, (PB99-140485, A14, MF-A03).

MCEER-98-0015 "Proceedings of the U.S.-Italy Workshop on Seismic Protective Systems for Bridges," edited by I.M. Friedland and M.C. Constantinou, 11/3/98, (PB2000-101711, A22, MF-A04).

MCEER-98-0016 "Appropriate Seismic Reliability for Critical Equipment Systems: Recommendations Based on Regional Analysis of Financial and Life Loss," by K. Porter, C. Scawthorn, C. Taylor and N. Blais, 11/10/98, (PB99-157265, A08, MF-A02).

MCEER-98-0017 "Proceedings of the U.S. Japan Joint Seminar on Civil Infrastructure Systems Research," edited by M. Shinozuka and A. Rose, 11/12/98, (PB99-156713, A16, MF-A03).

MCEER-98-0018 "Modeling of Pile Footings and Drilled Shafts for Seismic Design," by I. PoLam, M. Kapuskar and D. Chaudhuri, 12/21/98, (PB99-157257, A09, MF-A02).

MCEER-99-0001 "Seismic Evaluation of a Masonry Infilled Reinforced Concrete Frame by Pseudodynamic Testing," by S.G. Buonopane and R.N. White, 2/16/99, (PB99-162851, A09, MF-A02).

MCEER-99-0002 "Response History Analysis of Structures with Seismic Isolation and Energy Dissipation Systems: Verification Examples for Program SAP2000," by J. Scheller and M.C. Constantinou, 2/22/99, (PB99-162869, A08, MF-A02).

MCEER-99-0003 "Experimental Study on the Seismic Design and Retrofit of Bridge Columns Including Axial Load Effects," by A. Dutta, T. Kokorina and J.B. Mander, 2/22/99, (PB99-162877, A09, MF-A02).

MCEER-99-0004 "Experimental Study of Bridge Elastomeric and Other Isolation and Energy Dissipation Systems with Emphasis on Uplift Prevention and High Velocity Near-source Seismic Excitation," by A. Kasalanati and M. C. Constantinou, 2/26/99, (PB99-162885, A12, MF-A03).

MCEER-99-0005 "Truss Modeling of Reinforced Concrete Shear-flexure Behavior," by J.H. Kim and J.B. Mander, 3/8/99, (PB99-163693, A12, MF-A03).

MCEER-99-0006 "Experimental Investigation and Computational Modeling of Seismic Response of a 1:4 Scale Model Steel Structure with a Load Balancing Supplemental Damping System," by G. Pekcan, J.B. Mander and S.S. Chen, 4/2/99, (PB99-162893, A11, MF-A03).

MCEER-99-0007 "Effect of Vertical Ground Motions on the Structural Response of Highway Bridges," by M.R. Button, C.J. Cronin and R.L. Mayes, 4/10/99, (PB2000-101411, A10, MF-A03).

MCEER-99-0008 "Seismic Reliability Assessment of Critical Facilities: A Handbook, Supporting Documentation, and Model Code Provisions," by G.S. Johnson, R.E. Sheppard, M.D. Quilici, S.J. Eder and C.R. Scawthorn, 4/12/99, (PB2000-101701, A18, MF-A04).

MCEER-99-0009 "Impact Assessment of Selected MCEER Highway Project Research on the Seismic Design of Highway Structures," by C. Rojahn, R. Mayes, D.G. Anderson, J.H. Clark, D'Appolonia Engineering, S. Gloyd and R.V. Nutt, 4/14/99, (PB99-162901, A10, MF-A02).

MCEER-99-0010 "Site Factors and Site Categories in Seismic Codes," by R. Dobry, R. Ramos and M.S. Power, 7/19/99, (PB2000-101705, A08, MF-A02).

MCEER-99-0011 "Restrainer Design Procedures for Multi-Span Simply-Supported Bridges," by M.J. Randall, M. Saiidi, E. Maragakis and T. Isakovic, 7/20/99, (PB2000-101702, A10, MF-A02).

MCEER-99-0012 "Property Modification Factors for Seismic Isolation Bearings," by M.C. Constantinou, P. Tsopelas, A. Kasalanati and E. Wolff, 7/20/99, (PB2000-103387, A11, MF-A03).

MCEER-99-0013 "Critical Seismic Issues for Existing Steel Bridges," by P. Ritchie, N. Kauhl and J. Kulicki, 7/20/99, (PB2000-101697, A09, MF-A02).

MCEER-99-0014 "Nonstructural Damage Database," by A. Kao, T.T. Soong and A. Vender, 7/24/99, (PB2000-101407, A06, MF-A01).

MCEER-99-0015 "Guide to Remedial Measures for Liquefaction Mitigation at Existing Highway Bridge Sites," by H.G. Cooke and J. K. Mitchell, 7/26/99, (PB2000-101703, A11, MF-A03).

MCEER-99-0016 "Proceedings of the MCEER Workshop on Ground Motion Methodologies for the Eastern United States," edited by N. Abrahamson and A. Becker, 8/11/99, (PB2000-103385, A07, MF-A02).

MCEER-99-0017 "Quindío, Colombia Earthquake of January 25, 1999: Reconnaissance Report," by A.P. Asfura and P.J. Flores, 10/4/99, (PB2000-106893, A06, MF-A01).

MCEER-99-0018 "Hysteretic Models for Cyclic Behavior of Deteriorating Inelastic Structures," by M.V. Sivaselvan and A.M. Reinhorn, 11/5/99, (PB2000-103386, A08, MF-A02).

MCEER-99-0019 "Proceedings of the 7th U.S.- Japan Workshop on Earthquake Resistant Design of Lifeline Facilities and Countermeasures Against Soil Liquefaction," edited by T.D. O'Rourke, J.P. Bardet and M. Hamada, 11/19/99, (PB2000-103354, A99, MF-A06).

MCEER-99-0020 "Development of Measurement Capability for Micro-Vibration Evaluations with Application to Chip Fabrication Facilities," by G.C. Lee, Z. Liang, J.W. Song, J.D. Shen and W.C. Liu, 12/1/99, (PB2000-105993, A08, MF-A02).

MCEER-99-0021 "Design and Retrofit Methodology for Building Structures with Supplemental Energy Dissipating Systems," by G. Pekcan, J.B. Mander and S.S. Chen, 12/31/99, (PB2000-105994, A11, MF-A03).

MCEER-00-0001 "The Marmara, Turkey Earthquake of August 17, 1999: Reconnaissance Report," edited by C. Scawthorn; with major contributions by M. Bruneau, R. Eguchi, T. Holzer, G. Johnson, J. Mander, J. Mitchell, W. Mitchell, A. Papageorgiou, C. Scaethorn, and G. Webb, 3/23/00, (PB2000-106200, A11, MF-A03).

MCEER-00-0002 "Proceedings of the MCEER Workshop for Seismic Hazard Mitigation of Health Care Facilities," edited by G.C. Lee, M. Ettouney, M. Grigoriu, J. Hauer and J. Nigg, 3/29/00, (PB2000-106892, A08, MF-A02).

MCEER-00-0003 "The Chi-Chi, Taiwan Earthquake of September 21, 1999: Reconnaissance Report," edited by G.C. Lee and C.H. Loh, with major contributions by G.C. Lee, M. Bruneau, I.G. Buckle, S.E. Chang, P.J. Flores, T.D. O'Rourke, M. Shinozuka, T.T. Soong, C-H. Loh, K-C. Chang, Z-J. Chen, J-S. Hwang, M-L. Lin, G-Y. Liu, K-C. Tsai, G.C. Yao and C-L. Yen, 4/30/00, (PB2001-100980, A10, MF-A02).

MCEER-00-0004 "Seismic Retrofit of End-Sway Frames of Steel Deck-Truss Bridges with a Supplemental Tendon System: Experimental and Analytical Investigation," by G. Pekcan, J.B. Mander and S.S. Chen, 7/1/00, (PB2001-100982, A10, MF-A02).

MCEER-00-0005 "Sliding Fragility of Unrestrained Equipment in Critical Facilities," by W.H. Chong and T.T. Soong, 7/5/00, (PB2001-100983, A08, MF-A02).

MCEER-00-0006 "Seismic Response of Reinforced Concrete Bridge Pier Walls in the Weak Direction," by N. Abo-Shadi, M. Saiidi and D. Sanders, 7/17/00, (PB2001-100981, A17, MF-A03).

MCEER-00-0007 "Low-Cycle Fatigue Behavior of Longitudinal Reinforcement in Reinforced Concrete Bridge Columns," by J. Brown and S.K. Kunnath, 7/23/00, (PB2001-104392, A08, MF-A02).

MCEER-00-0008 "Soil Structure Interaction of Bridges for Seismic Analysis," I. PoLam and H. Law, 9/25/00, (PB2001-105397, A08, MF-A02).

MCEER-00-0009 "Proceedings of the First MCEER Workshop on Mitigation of Earthquake Disaster by Advanced Technologies (MEDAT-1), edited by M. Shinozuka, D.J. Inman and T.D. O'Rourke, 11/10/00, (PB2001-105399, A14, MF-A03).

MCEER-00-0010 "Development and Evaluation of Simplified Procedures for Analysis and Design of Buildings with Passive Energy Dissipation Systems, Revision 01," by O.M. Ramirez, M.C. Constantinou, C.A. Kircher, A.S. Whittaker, M.W. Johnson, J.D. Gomez and C. Chrysostomou, 11/16/01, (PB2001-105523, A23, MF-A04).

MCEER-00-0011 "Dynamic Soil-Foundation-Structure Interaction Analyses of Large Caissons," by C-Y. Chang, C-M. Mok, Z-L. Wang, R. Settgast, F. Waggoner, M.A. Ketchum, H.M. Gonnermann and C-C. Chin, 12/30/00, (PB2001-104373, A07, MF-A02).

MCEER-00-0012 "Experimental Evaluation of Seismic Performance of Bridge Restrainers," by A.G. Vlassis, E.M. Maragakis and M. Saiid Saiidi, 12/30/00, (PB2001-104354, A09, MF-A02).

MCEER-00-0013 "Effect of Spatial Variation of Ground Motion on Highway Structures," by M. Shinozuka, V. Saxena and G. Deodatis, 12/31/00, (PB2001-108755, A13, MF-A03).

MCEER-00-0014 "A Risk-Based Methodology for Assessing the Seismic Performance of Highway Systems," by S.D. Werner, C.E. Taylor, J.E. Moore, II, J.S. Walton and S. Cho, 12/31/00, (PB2001-108756, A14, MF-A03).

MCEER-01-0001 “Experimental Investigation of P-Delta Effects to Collapse During Earthquakes,” by D. Vian and M. Bruneau, 6/25/01, (PB2002-100534, A17, MF-A03).

MCEER-01-0002 “Proceedings of the Second MCEER Workshop on Mitigation of Earthquake Disaster by Advanced Technologies (MEDAT-2),” edited by M. Bruneau and D.J. Inman, 7/23/01, (PB2002-100434, A16, MF-A03).

MCEER-01-0003 “Sensitivity Analysis of Dynamic Systems Subjected to Seismic Loads,” by C. Roth and M. Grigoriu, 9/18/01, (PB2003-100884, A12, MF-A03).

MCEER-01-0004 “Overcoming Obstacles to Implementing Earthquake Hazard Mitigation Policies: Stage 1 Report,” by D.J. Alesch and W.J. Petak, 12/17/01, (PB2002-107949, A07, MF-A02).

MCEER-01-0005 “Updating Real-Time Earthquake Loss Estimates: Methods, Problems and Insights,” by C.E. Taylor, S.E. Chang and R.T. Eguchi, 12/17/01, (PB2002-107948, A05, MF-A01).

MCEER-01-0006 “Experimental Investigation and Retrofit of Steel Pile Foundations and Pile Bents Under Cyclic Lateral Loadings,” by A. Shama, J. Mander, B. Blabac and S. Chen, 12/31/01, (PB2002-107950, A13, MF-A03).

MCEER-02-0001 “Assessment of Performance of Bolu Viaduct in the 1999 Duzce Earthquake in Turkey” by P.C. Roussis, M.C. Constantinou, M. Erdik, E. Durukal and M. Dicleli, 5/8/02, (PB2003-100883, A08, MF-A02).

MCEER-02-0002 “Seismic Behavior of Rail Counterweight Systems of Elevators in Buildings,” by M.P. Singh, Rildova and L.E. Suarez, 5/27/02. (PB2003-100882, A11, MF-A03).

MCEER-02-0003 “Development of Analysis and Design Procedures for Spread Footings,” by G. Mylonakis, G. Gazetas, S. Nikolaou and A. Chauncey, 10/02/02, (PB2004-101636, A13, MF-A03, CD-A13).

MCEER-02-0004 “Bare-Earth Algorithms for Use with SAR and LIDAR Digital Elevation Models,” by C.K. Huyck, R.T. Eguchi and B. Houshmand, 10/16/02, (PB2004-101637, A07, CD-A07).

MCEER-02-0005 “Review of Energy Dissipation of Compression Members in Concentrically Braced Frames,” by K.Lee and M. Bruneau, 10/18/02, (PB2004-101638, A10, CD-A10).

MCEER-03-0001 “Experimental Investigation of Light-Gauge Steel Plate Shear Walls for the Seismic Retrofit of Buildings” by J. Berman and M. Bruneau, 5/2/03, (PB2004-101622, A10, MF-A03, CD-A10).

MCEER-03-0002 “Statistical Analysis of Fragility Curves,” by M. Shinozuka, M.Q. Feng, H. Kim, T. Uzawa and T. Ueda, 6/16/03, (PB2004-101849, A09, CD-A09).

MCEER-03-0003 “Proceedings of the Eighth U.S.-Japan Workshop on Earthquake Resistant Design f Lifeline Facilities and Countermeasures Against Liquefaction,” edited by M. Hamada, J.P. Bardet and T.D. O’Rourke, 6/30/03, (PB2004-104386, A99, CD-A99).

MCEER-03-0004 “Proceedings of the PRC-US Workshop on Seismic Analysis and Design of Special Bridges,” edited by L.C. Fan and G.C. Lee, 7/15/03, (PB2004-104387, A14, CD-A14).

MCEER-03-0005 “Urban Disaster Recovery: A Framework and Simulation Model,” by S.B. Miles and S.E. Chang, 7/25/03, (PB2004-104388, A07, CD-A07).

MCEER-03-0006 “Behavior of Underground Piping Joints Due to Static and Dynamic Loading,” by R.D. Meis, M. Maragakis and R. Siddharthan, 11/17/03, (PB2005-102194, A13, MF-A03, CD-A00).

MCEER-04-0001 “Experimental Study of Seismic Isolation Systems with Emphasis on Secondary System Response and Verification of Accuracy of Dynamic Response History Analysis Methods,” by E. Wolff and M. Constantinou, 1/16/04 (PB2005-102195, A99, MF-E08, CD-A00).

MCEER-04-0002 “Tension, Compression and Cyclic Testing of Engineered Cementitious Composite Materials,” by K. Kesner and S.L. Billington, 3/1/04, (PB2005-102196, A08, CD-A08).

MCEER-04-0003 "Cyclic Testing of Braces Laterally Restrained by Steel Studs to Enhance Performance During Earthquakes," by O.C. Celik, J.W. Berman and M. Bruneau, 3/16/04, (PB2005-102197, A13, MF-A03, CD-A00).

MCEER-04-0004 "Methodologies for Post Earthquake Building Damage Detection Using SAR and Optical Remote Sensing: Application to the August 17, 1999 Marmara, Turkey Earthquake," by C.K. Huyck, B.J. Adams, S. Cho, R.T. Eguchi, B. Mansouri and B. Houshmand, 6/15/04, (PB2005-104888, A10, CD-A00).

MCEER-04-0005 "Nonlinear Structural Analysis Towards Collapse Simulation: A Dynamical Systems Approach," by M.V. Sivaselvan and A.M. Reinhorn, 6/16/04, (PB2005-104889, A11, MF-A03, CD-A00).

MCEER-04-0006 "Proceedings of the Second PRC-US Workshop on Seismic Analysis and Design of Special Bridges," edited by G.C. Lee and L.C. Fan, 6/25/04, (PB2005-104890, A16, CD-A00).

MCEER-04-0007 "Seismic Vulnerability Evaluation of Axially Loaded Steel Built-up Laced Members," by K. Lee and M. Bruneau, 6/30/04, (PB2005-104891, A16, CD-A00).

MCEER-04-0008 "Evaluation of Accuracy of Simplified Methods of Analysis and Design of Buildings with Damping Systems for Near-Fault and for Soft-Soil Seismic Motions," by E.A. Pavlou and M.C. Constantinou, 8/16/04, (PB2005-104892, A08, MF-A02, CD-A00).

MCEER-04-0009 "Assessment of Geotechnical Issues in Acute Care Facilities in California," by M. Lew, T.D. O'Rourke, R. Dobry and M. Koch, 9/15/04, (PB2005-104893, A08, CD-A00).

MCEER-04-0010 "Scissor-Jack-Damper Energy Dissipation System," by A.N. Sigaher-Boyle and M.C. Constantinou, 12/1/04 (PB2005-108221).

MCEER-04-0011 "Seismic Retrofit of Bridge Steel Truss Piers Using a Controlled Rocking Approach," by M. Pollino and M. Bruneau, 12/20/04 (PB2006-105795).

MCEER-05-0001 "Experimental and Analytical Studies of Structures Seismically Isolated with an Uplift-Restraint Isolation System," by P.C. Roussis and M.C. Constantinou, 1/10/05 (PB2005-108222).

MCEER-05-0002 "A Versatile Experimentation Model for Study of Structures Near Collapse Applied to Seismic Evaluation of Irregular Structures," by D. Kusumastuti, A.M. Reinhorn and A. Rutenberg, 3/31/05 (PB2006-101523).

MCEER-05-0003 "Proceedings of the Third PRC-US Workshop on Seismic Analysis and Design of Special Bridges," edited by L.C. Fan and G.C. Lee, 4/20/05, (PB2006-105796).

MCEER-05-0004 "Approaches for the Seismic Retrofit of Braced Steel Bridge Piers and Proof-of-Concept Testing of an Eccentrically Braced Frame with Tubular Link," by J.W. Berman and M. Bruneau, 4/21/05 (PB2006-101524).

MCEER-05-0005 "Simulation of Strong Ground Motions for Seismic Fragility Evaluation of Nonstructural Components in Hospitals," by A. Wanitkorkul and A. Filiatrault, 5/26/05 (PB2006-500027).

MCEER-05-0006 "Seismic Safety in California Hospitals: Assessing an Attempt to Accelerate the Replacement or Seismic Retrofit of Older Hospital Facilities," by D.J. Alesch, L.A. Arendt and W.J. Petak, 6/6/05 (PB2006-105794).

MCEER-05-0007 "Development of Seismic Strengthening and Retrofit Strategies for Critical Facilities Using Engineered Cementitious Composite Materials," by K. Kesner and S.L. Billington, 8/29/05 (PB2006-111701).

MCEER-05-0008 "Experimental and Analytical Studies of Base Isolation Systems for Seismic Protection of Power Transformers," by N. Murota, M.Q. Feng and G-Y. Liu, 9/30/05 (PB2006-111702).

MCEER-05-0009 "3D-BASIS-ME-MB: Computer Program for Nonlinear Dynamic Analysis of Seismically Isolated Structures," by P.C. Tsopelas, P.C. Roussis, M.C. Constantinou, R. Buchanan and A.M. Reinhorn, 10/3/05 (PB2006-111703).

MCEER-05-0010 "Steel Plate Shear Walls for Seismic Design and Retrofit of Building Structures," by D. Vian and M. Bruneau, 12/15/05 (PB2006-111704).

MCEER-05-0011 "The Performance-Based Design Paradigm," by M.J. Astrella and A. Whittaker, 12/15/05 (PB2006-111705).

MCEER-06-0001 "Seismic Fragility of Suspended Ceiling Systems," H. Badillo-Almaraz, A.S. Whittaker, A.M. Reinhorn and G.P. Cimellaro, 2/4/06 (PB2006-111706).

MCEER-06-0002 "Multi-Dimensional Fragility of Structures," by G.P. Cimellaro, A.M. Reinhorn and M. Bruneau, 3/1/06 (PB2007-106974, A09, MF-A02, CD A00).

MCEER-06-0003 "Built-Up Shear Links as Energy Dissipators for Seismic Protection of Bridges," by P. Dusicka, A.M. Itani and I.G. Buckle, 3/15/06 (PB2006-111708).

MCEER-06-0004 "Analytical Investigation of the Structural Fuse Concept," by R.E. Vargas and M. Bruneau, 3/16/06 (PB2006-111709).

MCEER-06-0005 "Experimental Investigation of the Structural Fuse Concept," by R.E. Vargas and M. Bruneau, 3/17/06 (PB2006-111710).

MCEER-06-0006 "Further Development of Tubular Eccentrically Braced Frame Links for the Seismic Retrofit of Braced Steel Truss Bridge Piers," by J.W. Berman and M. Bruneau, 3/27/06 (PB2007-105147).

MCEER-06-0007 "REDARS Validation Report," by S. Cho, C.K. Huyck, S. Ghosh and R.T. Eguchi, 8/8/06 (PB2007-106983).

MCEER-06-0008 "Review of Current NDE Technologies for Post-Earthquake Assessment of Retrofitted Bridge Columns," by J.W. Song, Z. Liang and G.C. Lee, 8/21/06 (PB2007-106984).

MCEER-06-0009 "Liquefaction Remediation in Silty Soils Using Dynamic Compaction and Stone Columns," by S. Thevanayagam, G.R. Martin, R. Nashed, T. Shenthan, T. Kanagalingam and N. Ecemis, 8/28/06 (PB2007-106985).

MCEER-06-0010 "Conceptual Design and Experimental Investigation of Polymer Matrix Composite Infill Panels for Seismic Retrofitting," by W. Jung, M. Chiewanichakorn and A.J. Aref, 9/21/06 (PB2007-106986).

MCEER-06-0011 "A Study of the Coupled Horizontal-Vertical Behavior of Elastomeric and Lead-Rubber Seismic Isolation Bearings," by G.P. Warn and A.S. Whittaker, 9/22/06 (PB2007-108679).

MCEER-06-0012 "Proceedings of the Fourth PRC-US Workshop on Seismic Analysis and Design of Special Bridges: Advancing Bridge Technologies in Research, Design, Construction and Preservation," Edited by L.C. Fan, G.C. Lee and L. Ziang, 10/12/06 (PB2007-109042).

MCEER-06-0013 "Cyclic Response and Low Cycle Fatigue Characteristics of Plate Steels," by P. Dusicka, A.M. Itani and I.G. Buckle, 11/1/06 06 (PB2007-106987).

MCEER-06-0014 "Proceedings of the Second US-Taiwan Bridge Engineering Workshop," edited by W.P. Yen, J. Shen, J-Y. Chen and M. Wang, 11/15/06 (PB2008-500041).

MCEER-06-0015 "User Manual and Technical Documentation for the REDARS^{TM} Import Wizard," by S. Cho, S. Ghosh, C.K. Huyck and S.D. Werner, 11/30/06 (PB2007-114766).

MCEER-06-0016 "Hazard Mitigation Strategy and Monitoring Technologies for Urban and Infrastructure Public Buildings: Proceedings of the China-US Workshops," edited by X.Y. Zhou, A.L. Zhang, G.C. Lee and M. Tong, 12/12/06 (PB2008-500018).

MCEER-07-0001 "Static and Kinetic Coefficients of Friction for Rigid Blocks," by C. Kafali, S. Fathali, M. Grigoriu and A.S. Whittaker, 3/20/07 (PB2007-114767).

MCEER-07-0002 "Hazard Mitigation Investment Decision Making: Organizational Response to Legislative Mandate," by L.A. Arendt, D.J. Alesch and W.J. Petak, 4/9/07 (PB2007-114768).

MCEER-07-0003 "Seismic Behavior of Bidirectional-Resistant Ductile End Diaphragms with Unbonded Braces in Straight or Skewed Steel Bridges," by O. Celik and M. Bruneau, 4/11/07 (PB2008-105141).

MCEER-07-0004 "Modeling Pile Behavior in Large Pile Groups Under Lateral Loading," by A.M. Dodds and G.R. Martin, 4/16/07(PB2008-105142).

MCEER-07-0005 "Experimental Investigation of Blast Performance of Seismically Resistant Concrete-Filled Steel Tube Bridge Piers," by S. Fujikura, M. Bruneau and D. Lopez-Garcia, 4/20/07 (PB2008-105143).

MCEER-07-0006 "Seismic Analysis of Conventional and Isolated Liquefied Natural Gas Tanks Using Mechanical Analogs," by I.P. Christovasilis and A.S. Whittaker, 5/1/07, not available.

MCEER-07-0007 "Experimental Seismic Performance Evaluation of Isolation/Restraint Systems for Mechanical Equipment – Part 1: Heavy Equipment Study," by S. Fathali and A. Filiatrault, 6/6/07 (PB2008-105144).

MCEER-07-0008 "Seismic Vulnerability of Timber Bridges and Timber Substructures," by A.A. Sharma, J.B. Mander, I.M. Friedland and D.R. Allicock, 6/7/07 (PB2008-105145).

MCEER-07-0009 "Experimental and Analytical Study of the XY-Friction Pendulum (XY-FP) Bearing for Bridge Applications," by C.C. Marin-Artieda, A.S. Whittaker and M.C. Constantinou, 6/7/07 (PB2008-105191).

MCEER-07-0010 "Proceedings of the PRC-US Earthquake Engineering Forum for Young Researchers," Edited by G.C. Lee and X.Z. Qi, 6/8/07 (PB2008-500058).

MCEER-07-0011 "Design Recommendations for Perforated Steel Plate Shear Walls," by R. Purba and M. Bruneau, 6/18/07, (PB2008-105192).

MCEER-07-0012 "Performance of Seismic Isolation Hardware Under Service and Seismic Loading," by M.C. Constantinou, A.S. Whittaker, Y. Kalpakidis, D.M. Fenz and G.P. Warn, 8/27/07, (PB2008-105193).

MCEER-07-0013 "Experimental Evaluation of the Seismic Performance of Hospital Piping Subassemblies," by E.R. Goodwin, E. Maragakis and A.M. Itani, 9/4/07, (PB2008-105194).

MCEER-07-0014 "A Simulation Model of Urban Disaster Recovery and Resilience: Implementation for the 1994 Northridge Earthquake," by S. Miles and S.E. Chang, 9/7/07, (PB2008-106426).

MCEER-07-0015 "Statistical and Mechanistic Fragility Analysis of Concrete Bridges," by M. Shinozuka, S. Banerjee and S-H. Kim, 9/10/07, (PB2008-106427).

MCEER-07-0016 "Three-Dimensional Modeling of Inelastic Buckling in Frame Structures," by M. Schachter and AM. Reinhorn, 9/13/07, (PB2008-108125).

MCEER-07-0017 "Modeling of Seismic Wave Scattering on Pile Groups and Caissons," by I. Po Lam, H. Law and C.T. Yang, 9/17/07 (PB2008-108150).

MCEER-07-0018 "Bridge Foundations: Modeling Large Pile Groups and Caissons for Seismic Design," by I. Po Lam, H. Law and G.R. Martin (Coordinating Author), 12/1/07 (PB2008-111190).

MCEER-07-0019 "Principles and Performance of Roller Seismic Isolation Bearings for Highway Bridges," by G.C. Lee, Y.C. Ou, Z. Liang, T.C. Niu and J. Song, 12/10/07 (PB2009-110466).

MCEER-07-0020 "Centrifuge Modeling of Permeability and Pinning Reinforcement Effects on Pile Response to Lateral Spreading," by L.L Gonzalez-Lagos, T. Abdoun and R. Dobry, 12/10/07 (PB2008-111191).

MCEER-07-0021 "Damage to the Highway System from the Pisco, Perú Earthquake of August 15, 2007," by J.S. O'Connor, L. Mesa and M. Nykamp, 12/10/07, (PB2008-108126).

MCEER-07-0022 "Experimental Seismic Performance Evaluation of Isolation/Restraint Systems for Mechanical Equipment – Part 2: Light Equipment Study," by S. Fathali and A. Filiatrault, 12/13/07 (PB2008-111192).

MCEER-07-0023 "Fragility Considerations in Highway Bridge Design," by M. Shinozuka, S. Banerjee and S.H. Kim, 12/14/07 (PB2008-111193).

MCEER-07-0024 "Performance Estimates for Seismically Isolated Bridges," by G.P. Warn and A.S. Whittaker, 12/30/07 (PB2008-112230).

MCEER-08-0001 "Seismic Performance of Steel Girder Bridge Superstructures with Conventional Cross Frames," by L.P. Carden, A.M. Itani and I.G. Buckle, 1/7/08, (PB2008-112231).

MCEER-08-0002 "Seismic Performance of Steel Girder Bridge Superstructures with Ductile End Cross Frames with Seismic Isolators," by L.P. Carden, A.M. Itani and I.G. Buckle, 1/7/08 (PB2008-112232).

MCEER-08-0003 "Analytical and Experimental Investigation of a Controlled Rocking Approach for Seismic Protection of Bridge Steel Truss Piers," by M. Pollino and M. Bruneau, 1/21/08 (PB2008-112233).

MCEER-08-0004 "Linking Lifeline Infrastructure Performance and Community Disaster Resilience: Models and Multi-Stakeholder Processes," by S.E. Chang, C. Pasion, K. Tatebe and R. Ahmad, 3/3/08 (PB2008-112234).

MCEER-08-0005 "Modal Analysis of Generally Damped Linear Structures Subjected to Seismic Excitations," by J. Song, Y-L. Chu, Z. Liang and G.C. Lee, 3/4/08 (PB2009-102311).

MCEER-08-0006 "System Performance Under Multi-Hazard Environments," by C. Kafali and M. Grigoriu, 3/4/08 (PB2008-112235).

MCEER-08-0007 "Mechanical Behavior of Multi-Spherical Sliding Bearings," by D.M. Fenz and M.C. Constantinou, 3/6/08 (PB2008-112236).

MCEER-08-0008 "Post-Earthquake Restoration of the Los Angeles Water Supply System," by T.H.P. Tabucchi and R.A. Davidson, 3/7/08 (PB2008-112237).

MCEER-08-0009 "Fragility Analysis of Water Supply Systems," by A. Jacobson and M. Grigoriu, 3/10/08 (PB2009-105545).

MCEER-08-0010 "Experimental Investigation of Full-Scale Two-Story Steel Plate Shear Walls with Reduced Beam Section Connections," by B. Qu, M. Bruneau, C-H. Lin and K-C. Tsai, 3/17/08 (PB2009-106368).

MCEER-08-0011 "Seismic Evaluation and Rehabilitation of Critical Components of Electrical Power Systems," S. Ersoy, B. Feizi, A. Ashrafi and M. Ala Saadeghvaziri, 3/17/08 (PB2009-105546).

MCEER-08-0012 "Seismic Behavior and Design of Boundary Frame Members of Steel Plate Shear Walls," by B. Qu and M. Bruneau, 4/26/08 . (PB2009-106744).

MCEER-08-0013 "Development and Appraisal of a Numerical Cyclic Loading Protocol for Quantifying Building System Performance," by A. Filiatrault, A. Wanitkorkul and M. Constantinou, 4/27/08 (PB2009-107906).

MCEER-08-0014 "Structural and Nonstructural Earthquake Design: The Challenge of Integrating Specialty Areas in Designing Complex, Critical Facilities," by W.J. Petak and D.J. Alesch, 4/30/08 (PB2009-107907).

MCEER-08-0015 "Seismic Performance Evaluation of Water Systems," by Y. Wang and T.D. O'Rourke, 5/5/08 (PB2009-107908).

MCEER-08-0016 "Seismic Response Modeling of Water Supply Systems," by P. Shi and T.D. O'Rourke, 5/5/08 (PB2009-107910).

MCEER-08-0017 "Numerical and Experimental Studies of Self-Centering Post-Tensioned Steel Frames," by D. Wang and A. Filiatrault, 5/12/08 (PB2009-110479).

MCEER-08-0018 "Development, Implementation and Verification of Dynamic Analysis Models for Multi-Spherical Sliding Bearings," by D.M. Fenz and M.C. Constantinou, 8/15/08 (PB2009-107911).

MCEER-08-0019 "Performance Assessment of Conventional and Base Isolated Nuclear Power Plants for Earthquake Blast Loadings," by Y.N. Huang, A.S. Whittaker and N. Luco, 10/28/08 (PB2009-107912).

MCEER-08-0020 "Remote Sensing for Resilient Multi-Hazard Disaster Response – Volume I: Introduction to Damage Assessment Methodologies," by B.J. Adams and R.T. Eguchi, 11/17/08 (PB2010-102695).

MCEER-08-0021 "Remote Sensing for Resilient Multi-Hazard Disaster Response – Volume II: Counting the Number of Collapsed Buildings Using an Object-Oriented Analysis: Case Study of the 2003 Bam Earthquake," by L. Gusella, C.K. Huyck and B.J. Adams, 11/17/08 (PB2010-100925).

MCEER-08-0022 "Remote Sensing for Resilient Multi-Hazard Disaster Response – Volume III: Multi-Sensor Image Fusion Techniques for Robust Neighborhood-Scale Urban Damage Assessment," by B.J. Adams and A. McMillan, 11/17/08 (PB2010-100926).

MCEER-08-0023 "Remote Sensing for Resilient Multi-Hazard Disaster Response – Volume IV: A Study of Multi-Temporal and Multi-Resolution SAR Imagery for Post-Katrina Flood Monitoring in New Orleans," by A. McMillan, J.G. Morley, B.J. Adams and S. Chesworth, 11/17/08 (PB2010-100927).

MCEER-08-0024 "Remote Sensing for Resilient Multi-Hazard Disaster Response – Volume V: Integration of Remote Sensing Imagery and VIEWS^{TM} Field Data for Post-Hurricane Charley Building Damage Assessment," by J.A. Womble, K. Mehta and B.J. Adams, 11/17/08 (PB2009-115532).

MCEER-08-0025 "Building Inventory Compilation for Disaster Management: Application of Remote Sensing and Statistical Modeling," by P. Sarabandi, A.S. Kiremidjian, R.T. Eguchi and B. J. Adams, 11/20/08 (PB2009-110484).

MCEER-08-0026 "New Experimental Capabilities and Loading Protocols for Seismic Qualification and Fragility Assessment of Nonstructural Systems," by R. Retamales, G. Mosqueda, A. Filiatrault and A. Reinhorn, 11/24/08 (PB2009-110485).

MCEER-08-0027 "Effects of Heating and Load History on the Behavior of Lead-Rubber Bearings," by I.V. Kalpakidis and M.C. Constantinou, 12/1/08 (PB2009-115533).

MCEER-08-0028 "Experimental and Analytical Investigation of Blast Performance of Seismically Resistant Bridge Piers," by S.Fujikura and M. Bruneau, 12/8/08 (PB2009-115534).

MCEER-08-0029 "Evolutionary Methodology for Aseismic Decision Support," by Y. Hu and G. Dargush, 12/15/08.

MCEER-08-0030 "Development of a Steel Plate Shear Wall Bridge Pier System Conceived from a Multi-Hazard Perspective," by D. Keller and M. Bruneau, 12/19/08 (PB2010-102696).

MCEER-09-0001 "Modal Analysis of Arbitrarily Damped Three-Dimensional Linear Structures Subjected to Seismic Excitations," by Y.L. Chu, J. Song and G.C. Lee, 1/31/09 (PB2010-100922).

MCEER-09-0002 "Air-Blast Effects on Structural Shapes," by G. Ballantyne, A.S. Whittaker, A.J. Aref and G.F. Dargush, 2/2/09 (PB2010-102697).

MCEER-09-0003 "Water Supply Performance During Earthquakes and Extreme Events," by A.L. Bonneau and T.D. O'Rourke, 2/16/09 (PB2010-100923).

MCEER-09-0004 "Generalized Linear (Mixed) Models of Post-Earthquake Ignitions," by R.A. Davidson, 7/20/09 (PB2010-102698).

MCEER-09-0005 "Seismic Testing of a Full-Scale Two-Story Light-Frame Wood Building: NEESWood Benchmark Test," by I.P. Christovasilis, A. Filiatrault and A. Wanitkorkul, 7/22/09 (PB2012-102401).

MCEER-09-0006 "IDARC2D Version 7.0: A Program for the Inelastic Damage Analysis of Structures," by A.M. Reinhorn, H. Roh, M. Sivaselvan, S.K. Kunnath, R.E. Valles, A. Madan, C. Li, R. Lobo and Y.J. Park, 7/28/09 (PB2010-103199).

MCEER-09-0007 "Enhancements to Hospital Resiliency: Improving Emergency Planning for and Response to Hurricanes," by D.B. Hess and L.A. Arendt, 7/30/09 (PB2010-100924).

MCEER-09-0008 “Assessment of Base-Isolated Nuclear Structures for Design and Beyond-Design Basis Earthquake Shaking,” by Y.N. Huang, A.S. Whittaker, R.P. Kennedy and R.L. Mayes, 8/20/09 (PB2010-102699).

MCEER-09-0009 “Quantification of Disaster Resilience of Health Care Facilities,” by G.P. Cimellaro, C. Fumo, A.M Reinhorn and M. Bruneau, 9/14/09 (PB2010-105384).

MCEER-09-0010 “Performance-Based Assessment and Design of Squat Reinforced Concrete Shear Walls,” by C.K. Gulec and A.S. Whittaker, 9/15/09 (PB2010-102700).

MCEER-09-0011 “Proceedings of the Fourth US-Taiwan Bridge Engineering Workshop,” edited by W.P. Yen, J.J. Shen, T.M. Lee and R.B. Zheng, 10/27/09 (PB2010-500009).

MCEER-09-0012 “Proceedings of the Special International Workshop on Seismic Connection Details for Segmental Bridge Construction,” edited by W. Phillip Yen and George C. Lee, 12/21/09 (PB2012-102402).

MCEER-10-0001 “Direct Displacement Procedure for Performance-Based Seismic Design of Multistory Woodframe Structures,” by W. Pang and D. Rosowsky, 4/26/10 (PB2012-102403).

MCEER-10-0002 “Simplified Direct Displacement Design of Six-Story NEESWood Capstone Building and Pre-Test Seismic Performance Assessment,” by W. Pang, D. Rosowsky, J. van de Lindt and S. Pei, 5/28/10 (PB2012-102404).

MCEER-10-0003 “Integration of Seismic Protection Systems in Performance-Based Seismic Design of Woodframed Structures,” by J.K. Shinde and M.D. Symans, 6/18/10 (PB2012-102405).

MCEER-10-0004 “Modeling and Seismic Evaluation of Nonstructural Components: Testing Frame for Experimental Evaluation of Suspended Ceiling Systems,” by A.M. Reinhorn, K.P. Ryu and G. Maddaloni, 6/30/10 (PB2012-102406).

MCEER-10-0005 “Analytical Development and Experimental Validation of a Structural-Fuse Bridge Pier Concept,” by S. El-Bahey and M. Bruneau, 10/1/10 (PB2012-102407).

MCEER-10-0006 “A Framework for Defining and Measuring Resilience at the Community Scale: The PEOPLES Resilience Framework,” by C.S. Renschler, A.E. Frazier, L.A. Arendt, G.P. Cimellaro, A.M. Reinhorn and M. Bruneau, 10/8/10 (PB2012-102408).

MCEER-10-0007 “Impact of Horizontal Boundary Elements Design on Seismic Behavior of Steel Plate Shear Walls,” by R. Purba and M. Bruneau, 11/14/10 (PB2012-102409).

MCEER-10-0008 “Seismic Testing of a Full-Scale Mid-Rise Building: The NEESWood Capstone Test,” by S. Pei, J.W. van de Lindt, S.E. Pryor, H. Shimizu, H. Isoda and D.R. Rammer, 12/1/10 (PB2012-102410).

MCEER-10-0009 “Modeling the Effects of Detonations of High Explosives to Inform Blast-Resistant Design,” by P. Sherkar, A.S. Whittaker and A.J. Aref, 12/1/10 (PB2012-102411).

MCEER-10-0010 “L’Aquila Earthquake of April 6, 2009 in Italy: Rebuilding a Resilient City to Withstand Multiple Hazards,” by G.P. Cimellaro, I.P. Christovasilis, A.M. Reinhorn, A. De Stefano and T. Kirova, 12/29/10.

MCEER-11-0001 “Numerical and Experimental Investigation of the Seismic Response of Light-Frame Wood Structures,” by I.P. Christovasilis and A. Filiatrault, 8/8/11 (PB2012-102412).

MCEER-11-0002 “Seismic Design and Analysis of a Precast Segmental Concrete Bridge Model,” by M. Anagnostopoulou, A. Filiatrault and A. Aref, 9/15/11.

MCEER-11-0003 ‘Proceedings of the Workshop on Improving Earthquake Response of Substation Equipment,” Edited by A.M. Reinhorn, 9/19/11 (PB2012-102413).

MCEER-11-0004 “LRFD-Based Analysis and Design Procedures for Bridge Bearings and Seismic Isolators,” by M.C. Constantinou, I. Kalpakidis, A. Filiatrault and R.A. Ecker Lay, 9/26/11.

MCEER-11-0005 "Experimental Seismic Evaluation, Model Parameterization, and Effects of Cold-Formed Steel-Framed Gypsum Partition Walls on the Seismic Performance of an Essential Facility," by R. Davies, R. Retamales, G. Mosqueda and A. Filiatrault, 10/12/11.

MCEER-11-0006 "Modeling and Seismic Performance Evaluation of High Voltage Transformers and Bushings," by A.M. Reinhorn, K. Oikonomou, H. Roh, A. Schiff and L. Kempner, Jr., 10/3/11.

MCEER-11-0007 "Extreme Load Combinations: A Survey of State Bridge Engineers," by G.C. Lee, Z. Liang, J.J. Shen and J.S. O'Connor, 10/14/11.

MCEER-12-0001 "Simplified Analysis Procedures in Support of Performance Based Seismic Design," by Y.N. Huang and A.S. Whittaker.

MCEER-12-0002 "Seismic Protection of Electrical Transformer Bushing Systems by Stiffening Techniques," by M. Koliou, A. Filiatrault, A.M. Reinhorn and N. Oliveto, 6/1/12.

MCEER-12-0003 "Post-Earthquake Bridge Inspection Guidelines," by J.S. O'Connor and S. Alampalli, 6/8/12.

MCEER-12-0004 "Integrated Design Methodology for Isolated Floor Systems in Single-Degree-of-Freedom Structural Fuse Systems," by S. Cui, M. Bruneau and M.C. Constantinou, 6/13/12.

MCEER-12-0005 "Characterizing the Rotational Components of Earthquake Ground Motion," by D. Basu, A.S. Whittaker and M.C. Constantinou, 6/15/12.

MCEER-12-0006 "Bayesian Fragility for Nonstructural Systems," by C.H. Lee and M.D. Grigoriu, 9/12/12.

MCEER-12-0007 "A Numerical Model for Capturing the In-Plane Seismic Response of Interior Metal Stud Partition Walls," by R.L. Wood and T.C. Hutchinson, 9/12/12.

MCEER-12-0008 "Assessment of Floor Accelerations in Yielding Buildings," by J.D. Wieser, G. Pekcan, A.E. Zaghi, A.M. Itani and E. Maragakis, 10/5/12.

MCEER-13-0001 "Experimental Seismic Study of Pressurized Fire Sprinkler Piping Systems," by Y. Tian, A. Filiatrault and G. Mosqueda, 4/8/13.

MCEER-13-0002 "Enhancing Resource Coordination for Multi-Modal Evacuation Planning," by D.B. Hess, B.W. Conley and C.M. Farrell, 2/8/13.

MCEER-13-0003 "Seismic Response of Base Isolated Buildings Considering Pounding to Moat Walls," by A. Masroor and G. Mosqueda, 2/26/13.

MCEER-13-0004 "Seismic Response Control of Structures Using a Novel Adaptive Passive Negative Stiffness Device," by D.T.R. Pasala, A.A. Sarlis, S. Nagarajaiah, A.M. Reinhorn, M.C. Constantinou and D.P. Taylor, 6/10/13.

MCEER-13-0005 "Negative Stiffness Device for Seismic Protection of Structures," by A.A. Sarlis, D.T.R. Pasala, M.C. Constantinou, A.M. Reinhorn, S. Nagarajaiah and D.P. Taylor, 6/12/13.

MCEER-13-0006 "Emilia Earthquake of May 20, 2012 in Northern Italy: Rebuilding a Resilient Community to Withstand Multiple Hazards," by G.P. Cimellaro, M. Chiriatti, A.M. Reinhorn and L. Tirca, June 30, 2013.

MCEER-13-0007 "Precast Concrete Segmental Components and Systems for Accelerated Bridge Construction in Seismic Regions," by A.J. Aref, G.C. Lee, Y.C. Ou and P. Sideris, with contributions from K.C. Chang, S. Chen, A. Filiatrault and Y. Zhou, June 13, 2013.

MCEER-13-0008 "A Study of U.S. Bridge Failures (1980-2012)," by G.C. Lee, S.B. Mohan, C. Huang and B.N. Fard, June 15, 2013.

MCEER-13-0009 "Database Development for Damaged Bridge Modeling," by G.C. Lee, J.C. Qi and C. Huang, June 16, 2013.

MCEER-13-0010 “Model of Triple Friction Pendulum Bearing for General Geometric and Frictional Parameters and for Uplift Conditions,” by A.A. Sarlis and M.C. Constantinou, July 1, 2013.

MCEER-13-0011 “Shake Table Testing of Triple Friction Pendulum Isolators under Extreme Conditions,” by A.A. Sarlis, M.C. Constantinou and A.M. Reinhorn, July 2, 2013.

Appendix A

Experimental Data

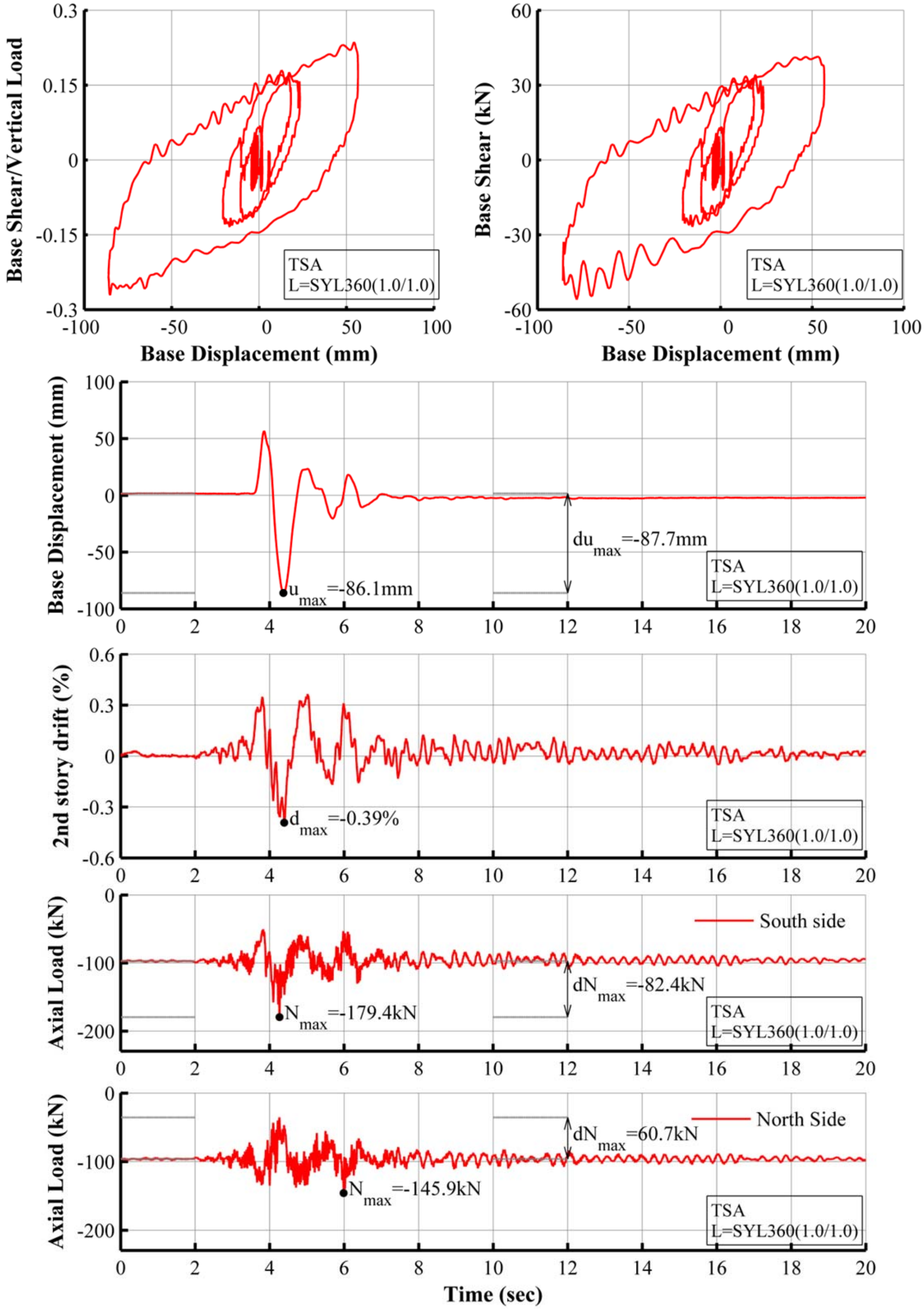

Base Shear/Vertical Load
Base Displacement (mm)
TSA
L=SYL360(1.0/1.0)
Base Shear (kN)
Base Displacement (mm)
TSA
L=SYL360(1.0/1.0)
Base Displacement (mm)
du_{max}=-87.7mm
u_{max}=-86.1mm
TSA
L=SYL360(1.0/1.0)
2nd story drift (%)
d_{max}=-0.39%
TSA
L=SYL360(1.0/1.0)
Axial Load (kN)
South side
dN_{max}=-82.4kN
N_{max}=-179.4kN
TSA
L=SYL360(1.0/1.0)
Axial Load (kN)
North Side
dN_{max}=60.7kN
N_{max}=-145.9kN
TSA
L=SYL360(1.0/1.0)
Time (sec)

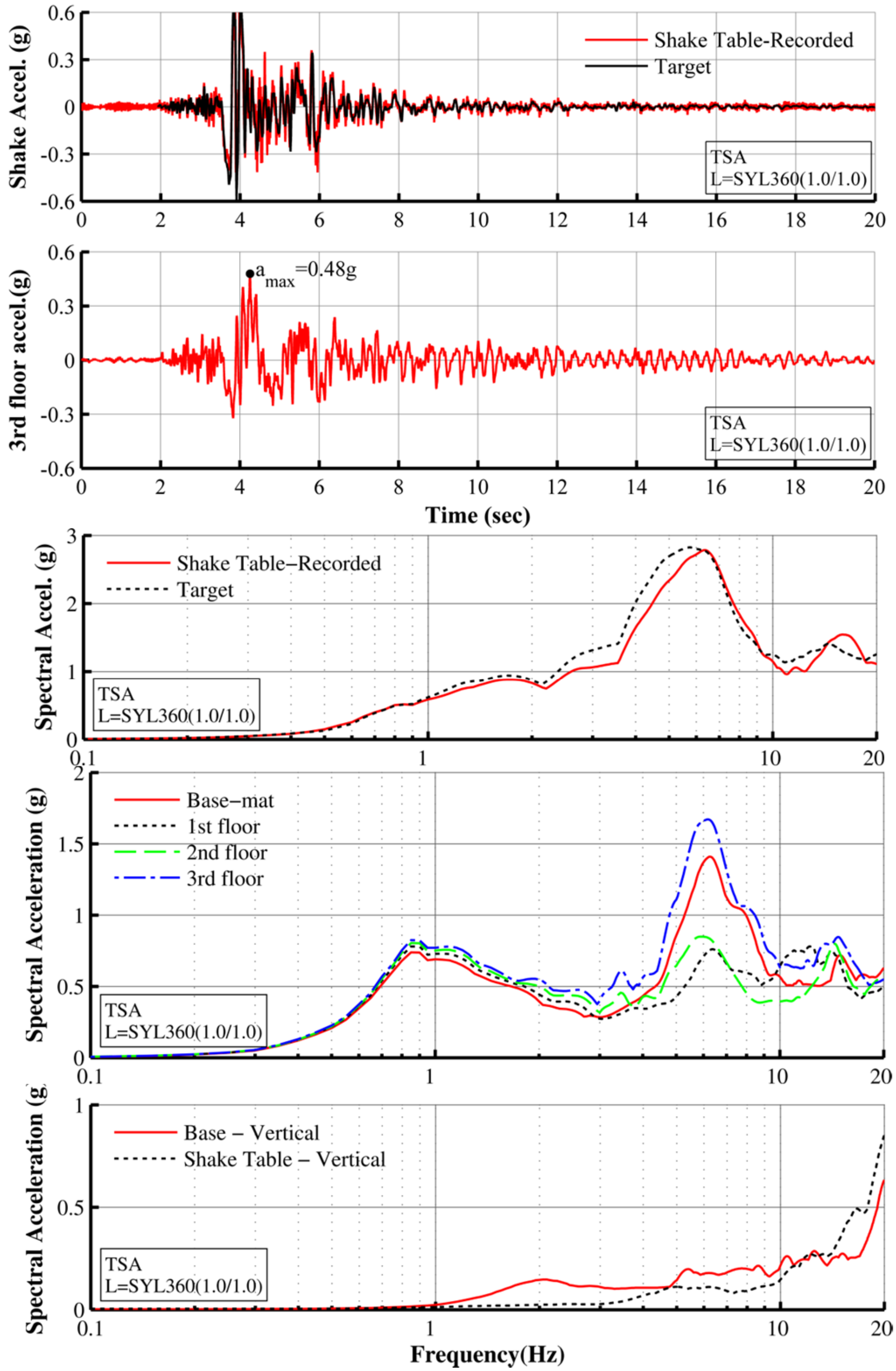

Shake Accel. (g)
Shake Table-Recorded
Target
TSA
L=SYL360(1.0/1.0)
3rd floor accel.(g)
a_{max}=0.48g
TSA
L=SYL360(1.0/1.0)
Time (sec)
Spectral Accel. (g)
Shake Table−Recorded
Target
TSA
L=SYL360(1.0/1.0)
Spectral Acceleration (g)
Base−mat
1st floor
2nd floor
3rd floor
TSA
L=SYL360(1.0/1.0)
Spectral Acceleration (g)
Base − Vertical
Shake Table − Vertical
TSA
L=SYL360(1.0/1.0)
Frequency(Hz)

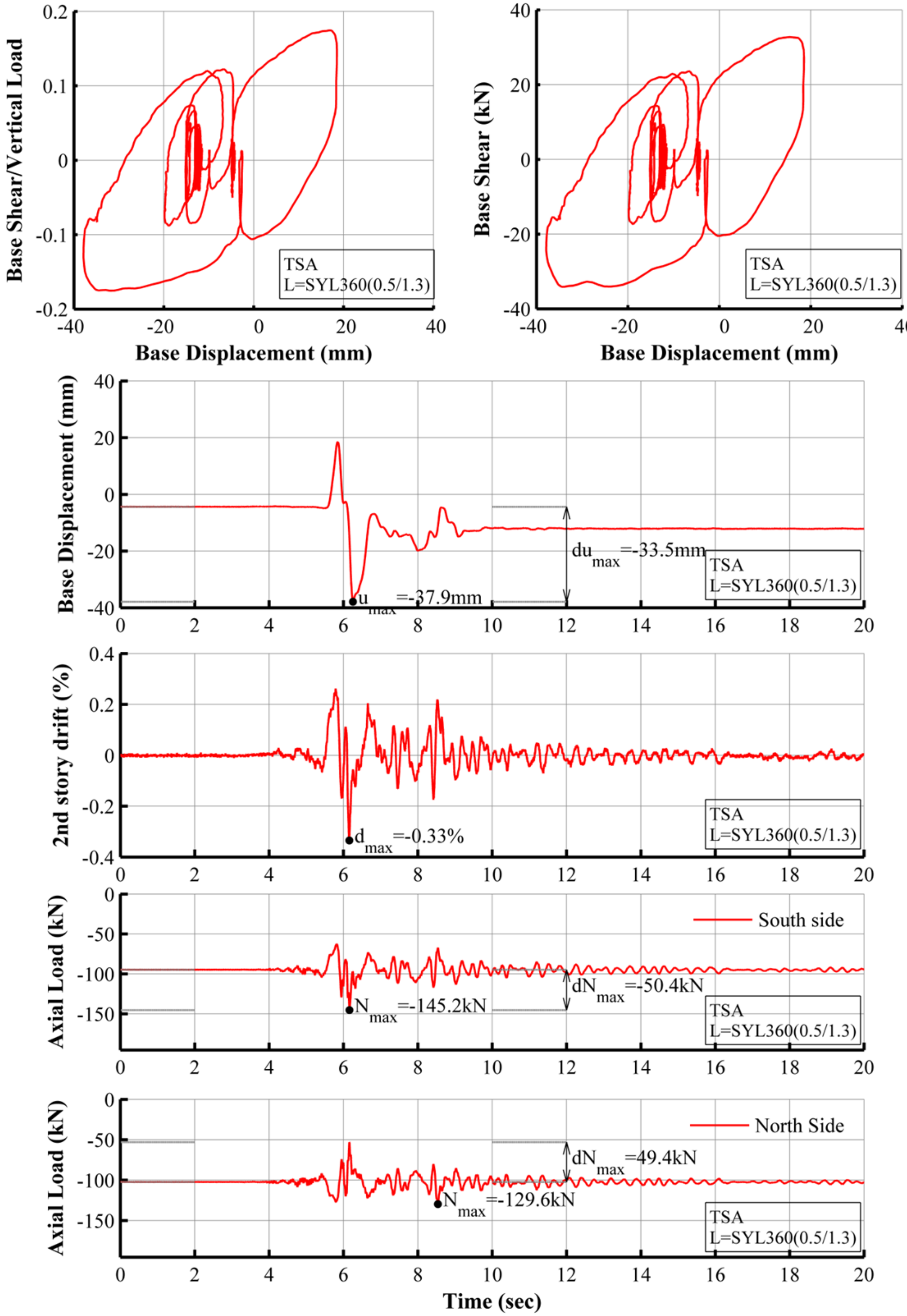
Base Shear/Vertical Load
Base Displacement (mm)
TSA
L=SYL360(0.5/1.3)
Base Shear (kN)
Base Displacement (mm)
TSA
L=SYL360(0.5/1.3)
Base Displacement (mm)
du max =-33.5mm
u max =-37.9mm
TSA
L=SYL360(0.5/1.3)
2nd story drift (%)
d max =-0.33%
TSA
L=SYL360(0.5/1.3)
Axial Load (kN)
South side
dN max =-50.4kN
N max =-145.2kN
TSA
L=SYL360(0.5/1.3)
Axial Load (kN)
North Side
dN max =49.4kN
N max =-129.6kN
TSA
L=SYL360(0.5/1.3)
Time (sec)

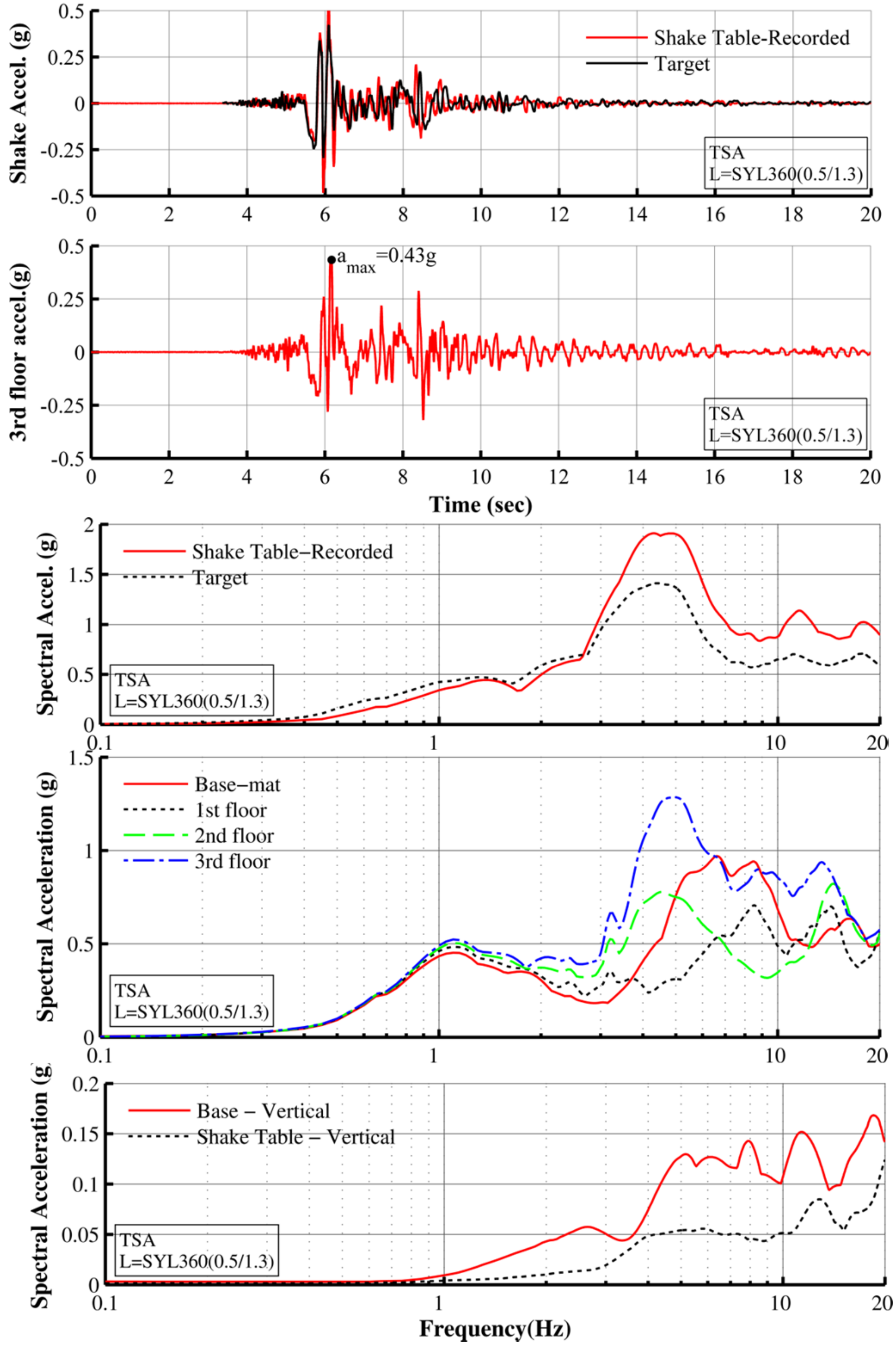

Shake Accel. (g)
Shake Table-Recorded
Target
TSA
L=SYL360(0.5/1.3)
3rd floor accel.(g)
a max =0.43g
TSA
L=SYL360(0.5/1.3)
Time (sec)
Spectral Accel. (g)
Shake Table−Recorded
Target
TSA
L=SYL360(0.5/1.3)
Spectral Acceleration (g)
Base−mat
1st floor
2nd floor
3rd floor
TSA
L=SYL360(0.5/1.3)
Spectral Acceleration (g)
Base − Vertical
Shake Table − Vertical
TSA
L=SYL360(0.5/1.3)
Frequency(Hz)

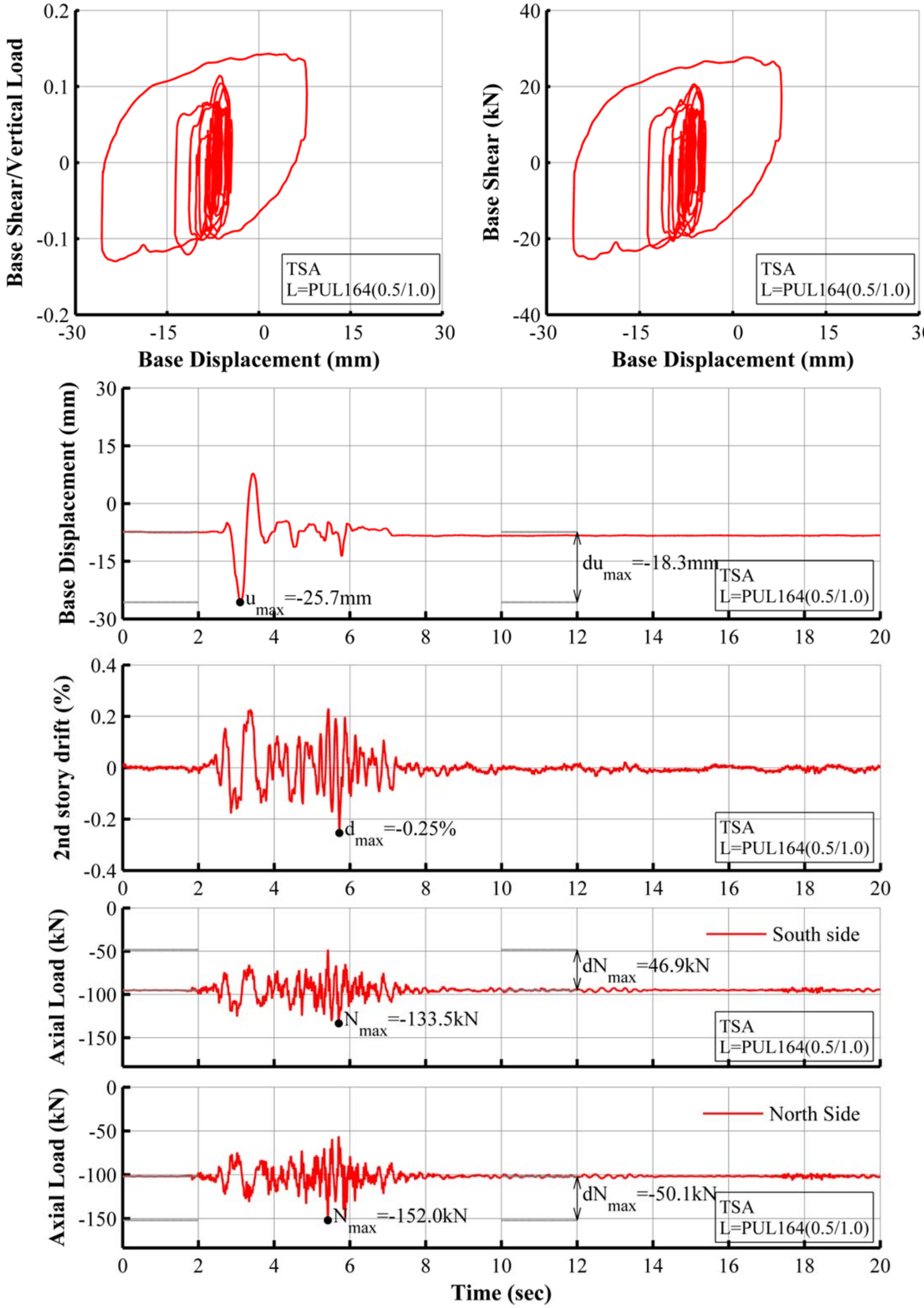
Base Shear/Vertical Load
Base Displacement (mm)
TSA
L=PUL164(0.5/1.0)
Base Shear (kN)
Base Displacement (mm)
TSA
L=PUL164(0.5/1.0)
Base Displacement (mm)
du_{max}=-18.3mm
u_{max}=-25.7mm
TSA
L=PUL164(0.5/1.0)
2nd story drift (%)
d_{max}=-0.25%
TSA
L=PUL164(0.5/1.0)
Axial Load (kN)
South side
dN_{max}=46.9kN
N_{max}=-133.5kN
TSA
L=PUL164(0.5/1.0)
Axial Load (kN)
North Side
dN_{max}=-50.1kN
N_{max}=-152.0kN
TSA
L=PUL164(0.5/1.0)
Time (sec)

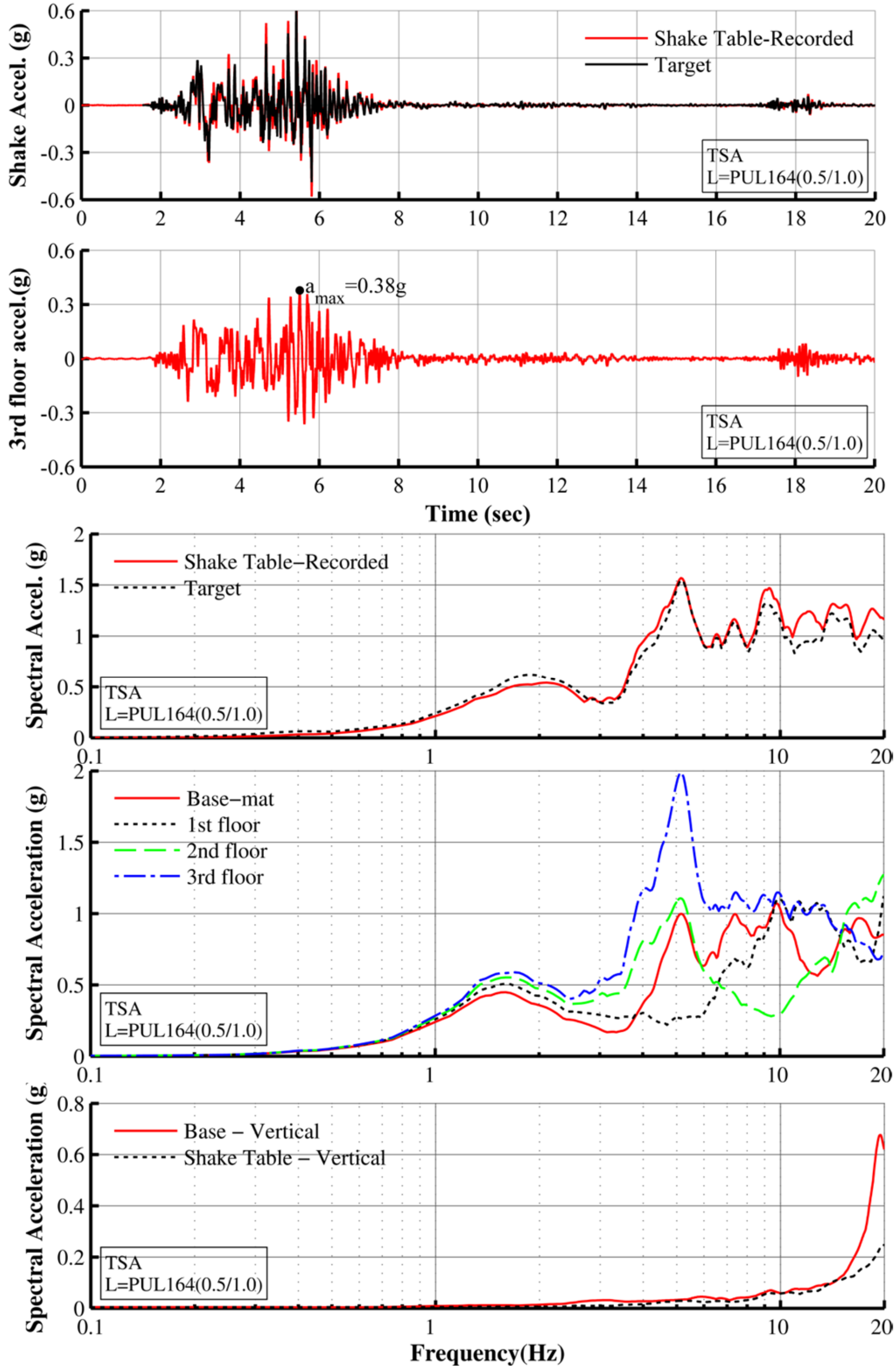

Shake Accel. (g)
Shake Table-Recorded
Target
TSA
L=PUL164(0.5/1.0)
3rd floor accel.(g)
a_{max}=0.38g
TSA
L=PUL164(0.5/1.0)
Time (sec)
Spectral Accel. (g)
Shake Table−Recorded
Target
TSA
L=PUL164(0.5/1.0)
Spectral Acceleration (g)
Base−mat
1st floor
2nd floor
3rd floor
TSA
L=PUL164(0.5/1.0)
Spectral Acceleration (g)
Base − Vertical
Shake Table − Vertical
TSA
L=PUL164(0.5/1.0)
Frequency(Hz)

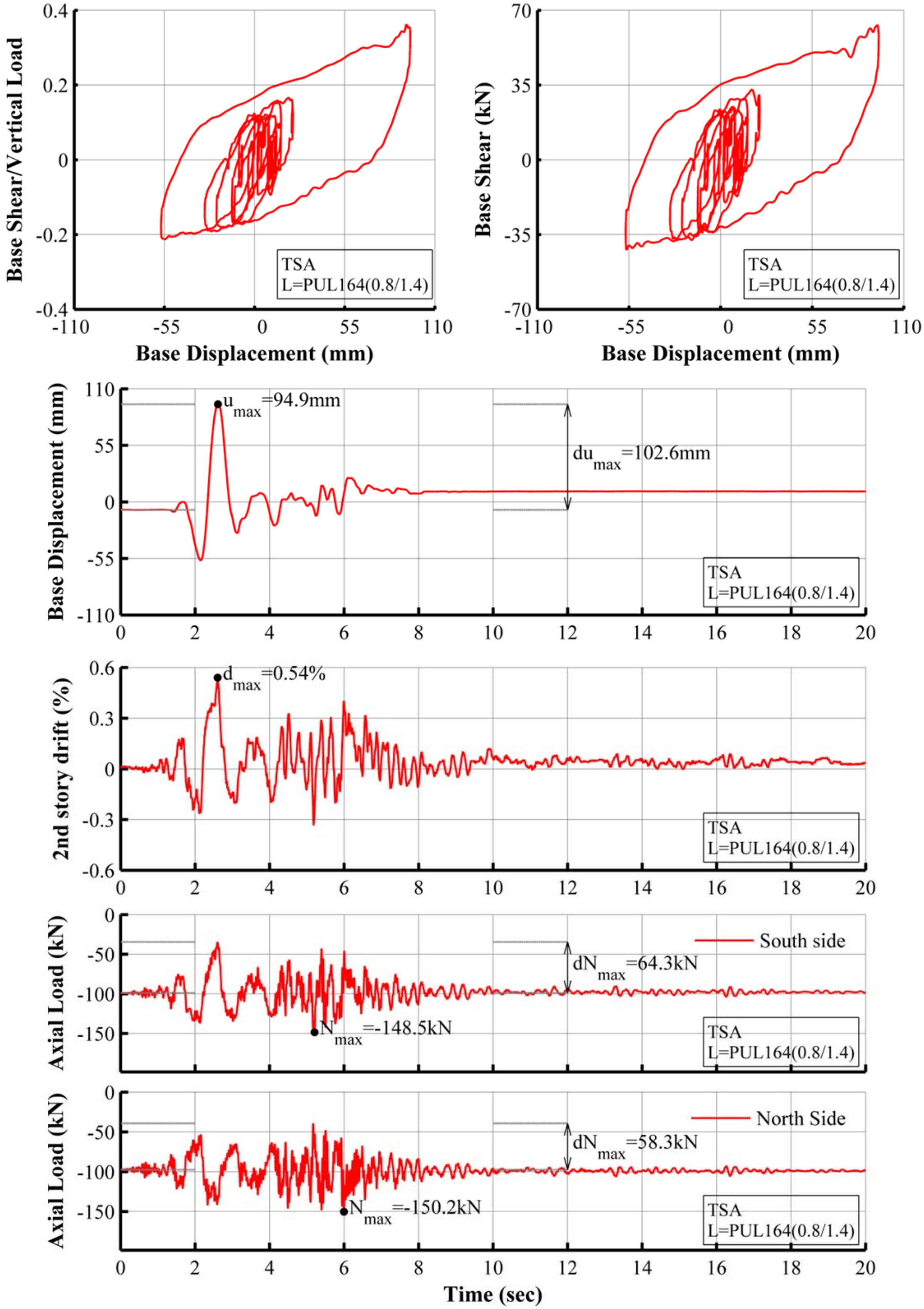
Base Shear/Vertical Load
Base Displacement (mm)
TSA
L=PUL164(0.8/1.4)
Base Shear (kN)
Base Displacement (mm)
TSA
L=PUL164(0.8/1.4)
Base Displacement (mm)
u max =94.9mm
du max =102.6mm
TSA
L=PUL164(0.8/1.4)
2nd story drift (%)
d max =0.54%
TSA
L=PUL164(0.8/1.4)
Axial Load (kN)
South side
dN max =64.3kN
N max =-148.5kN
TSA
L=PUL164(0.8/1.4)
Axial Load (kN)
North Side
dN max =58.3kN
N max =-150.2kN
TSA
L=PUL164(0.8/1.4)
Time (sec)

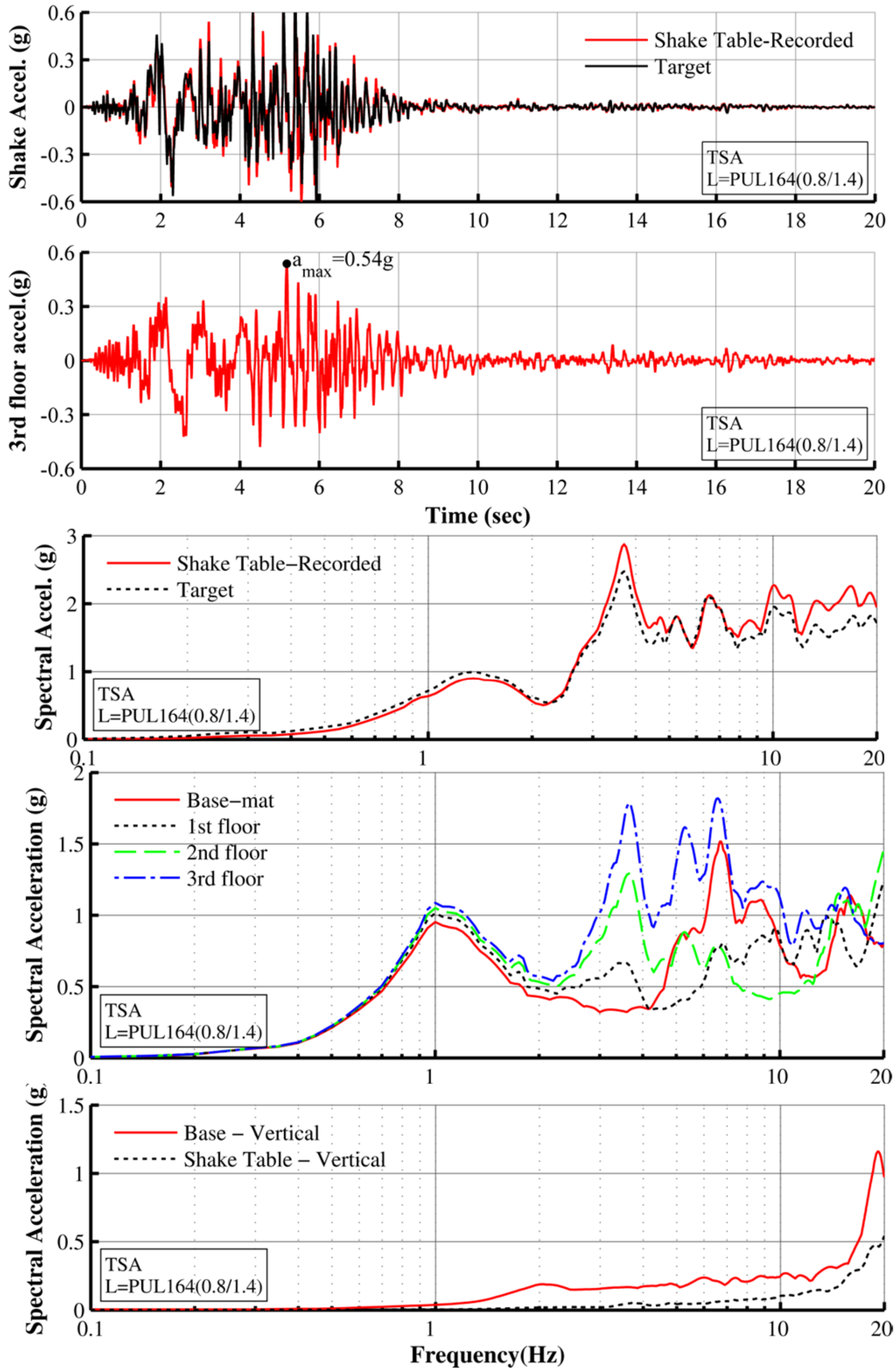
Shake Accel. (g)
Shake Table-Recorded
Target
TSA
L=PUL164(0.8/1.4)
3rd floor accel.(g)
a_{max}=0.54g
TSA
L=PUL164(0.8/1.4)
Time (sec)
Spectral Accel. (g)
Shake Table−Recorded
Target
TSA
L=PUL164(0.8/1.4)
Spectral Acceleration (g)
Base−mat
1st floor
2nd floor
3rd floor
TSA
L=PUL164(0.8/1.4)
Spectral Acceleration (g)
Base − Vertical
Shake Table − Vertical
TSA
L=PUL164(0.8/1.4)
Frequency(Hz)

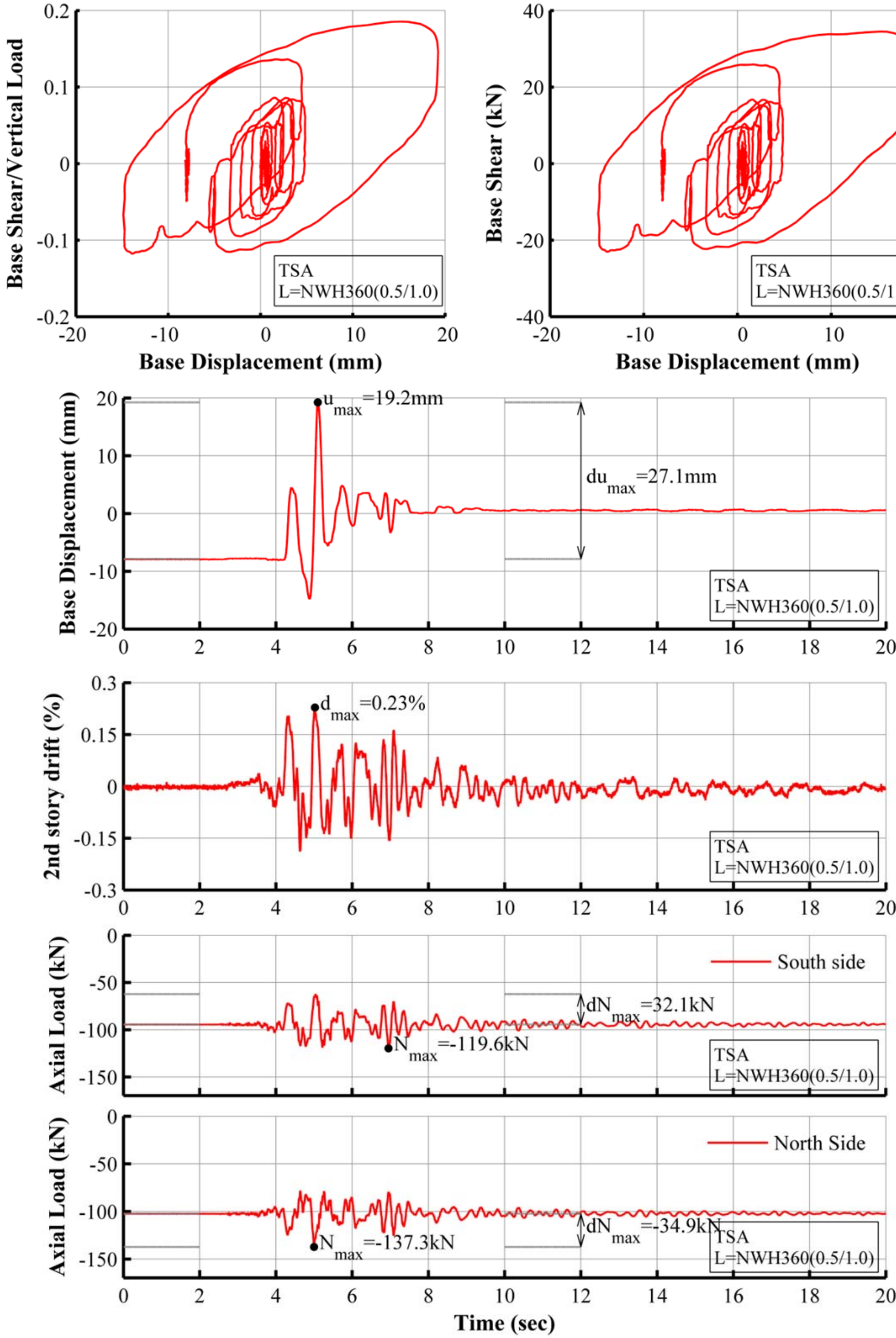

Base Shear/Vertical Load
Base Displacement (mm)
TSA
L=NWH360(0.5/1.0)
Base Shear (kN)
Base Displacement (mm)
TSA
L=NWH360(0.5/1.0)
Base Displacement (mm)
u max =19.2mm
du max =27.1mm
TSA
L=NWH360(0.5/1.0)
2nd story drift (%)
d max =0.23%
TSA
L=NWH360(0.5/1.0)
Axial Load (kN)
South side
dN max =32.1kN
N max =-119.6kN
TSA
L=NWH360(0.5/1.0)
Axial Load (kN)
North Side
dN max =-34.9kN
N max =-137.3kN
TSA
L=NWH360(0.5/1.0)
Time (sec)

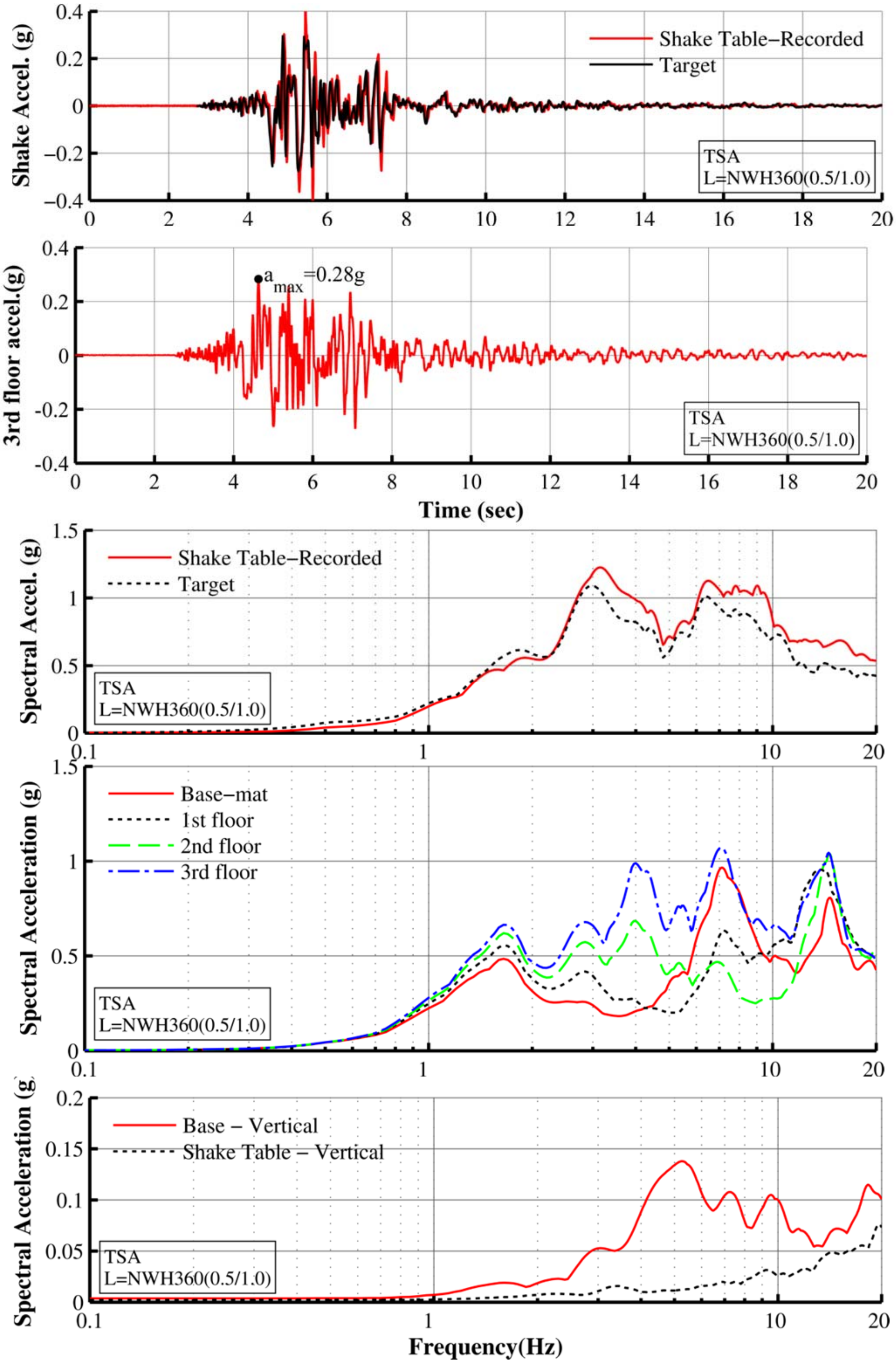
Shake Accel. (g)
Shake Table−Recorded
Target
TSA
L=NWH360(0.5/1.0)
3rd floor accel.(g)
a_{max}=0.28g
TSA
L=NWH360(0.5/1.0)
Time (sec)
Spectral Accel. (g)
Shake Table−Recorded
Target
TSA
L=NWH360(0.5/1.0)
Spectral Acceleration (g)
Base−mat
1st floor
2nd floor
3rd floor
TSA
L=NWH360(0.5/1.0)
Spectral Acceleration (g)
Base − Vertical
Shake Table − Vertical
TSA
L=NWH360(0.5/1.0)
Frequency(Hz)

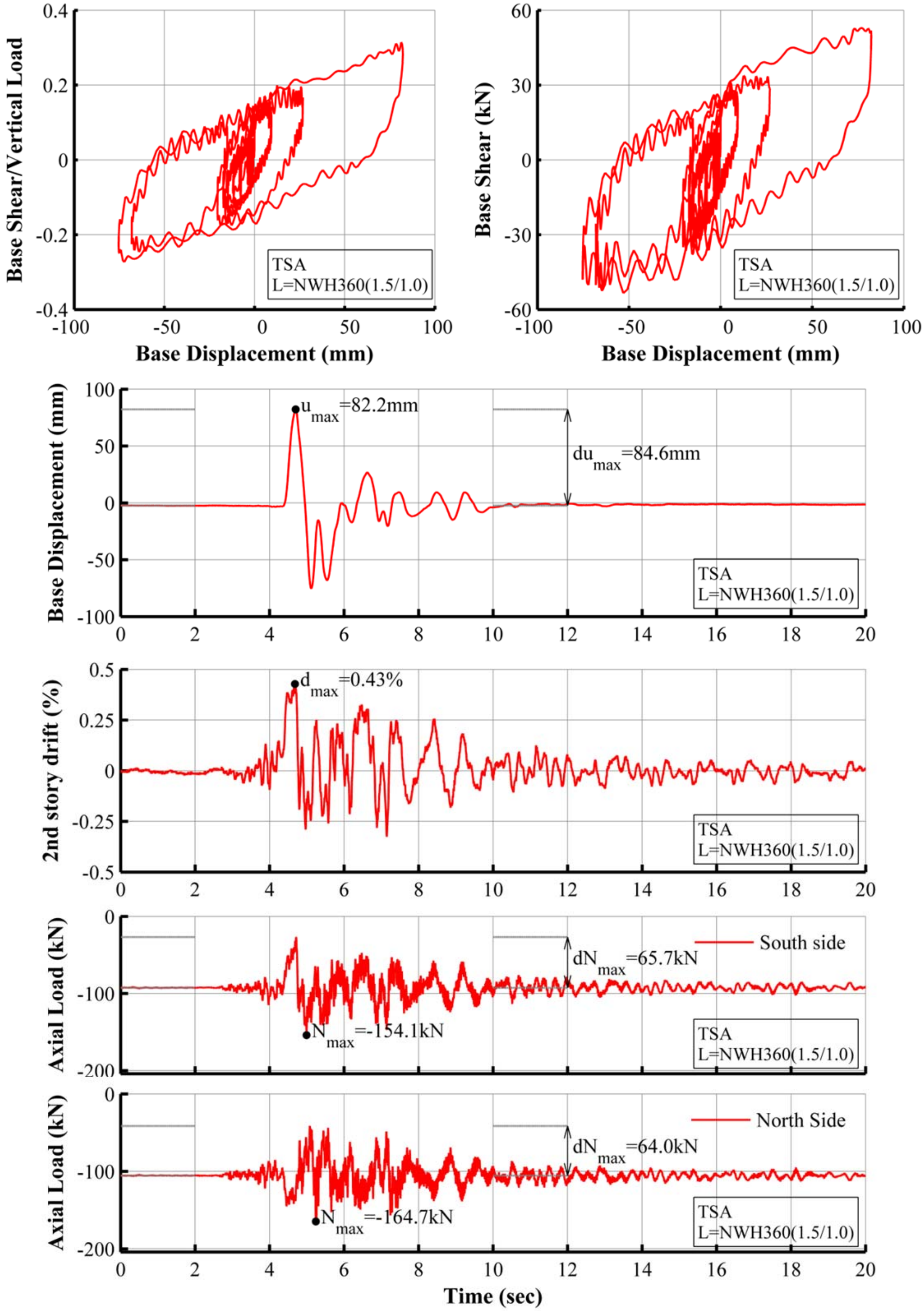

Base Shear/Vertical Load
Base Displacement (mm)
TSA
L=NWH360(1.5/1.0)
Base Shear (kN)
Base Displacement (mm)
TSA
L=NWH360(1.5/1.0)
Base Displacement (mm)
u_{max}=82.2mm
du_{max}=84.6mm
TSA
L=NWH360(1.5/1.0)
2nd story drift (%)
d_{max}=0.43%
TSA
L=NWH360(1.5/1.0)
Axial Load (kN)
South side
dN_{max}=65.7kN
N_{max}=-154.1kN
TSA
L=NWH360(1.5/1.0)
Axial Load (kN)
North Side
dN_{max}=64.0kN
N_{max}=-164.7kN
TSA
L=NWH360(1.5/1.0)
Time (sec)

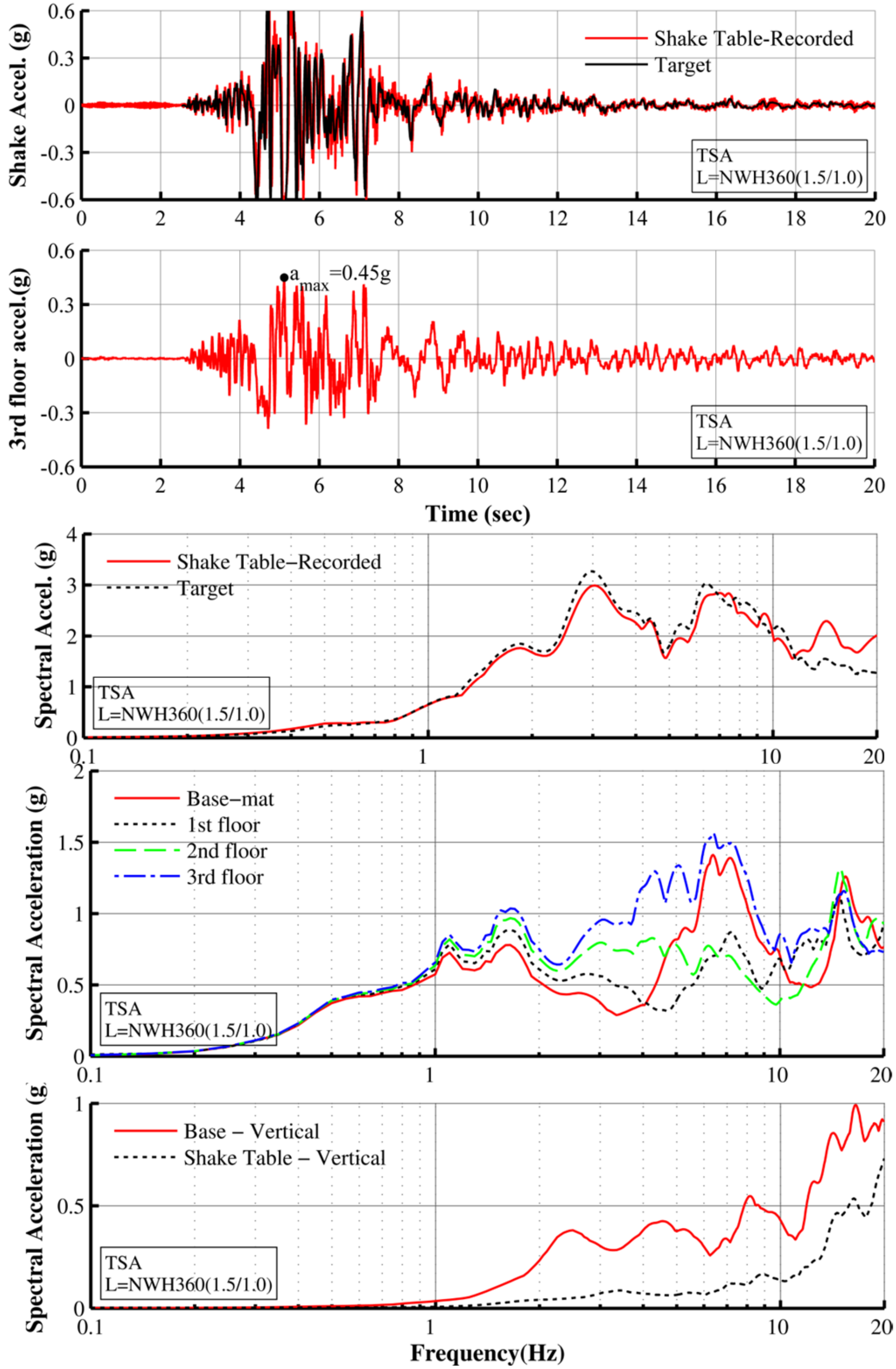
Shake Accel. (g)
Shake Table-Recorded
Target
TSA
L=NWH360(1.5/1.0)
3rd floor accel.(g)
a_{max}=0.45g
TSA
L=NWH360(1.5/1.0)
Time (sec)
Spectral Accel. (g)
Shake Table−Recorded
Target
TSA
L=NWH360(1.5/1.0)
Spectral Acceleration (g)
Base−mat
1st floor
2nd floor
3rd floor
TSA
L=NWH360(1.5/1.0)
Spectral Acceleration (g)
Base − Vertical
Shake Table − Vertical
TSA
L=NWH360(1.5/1.0)
Frequency(Hz)

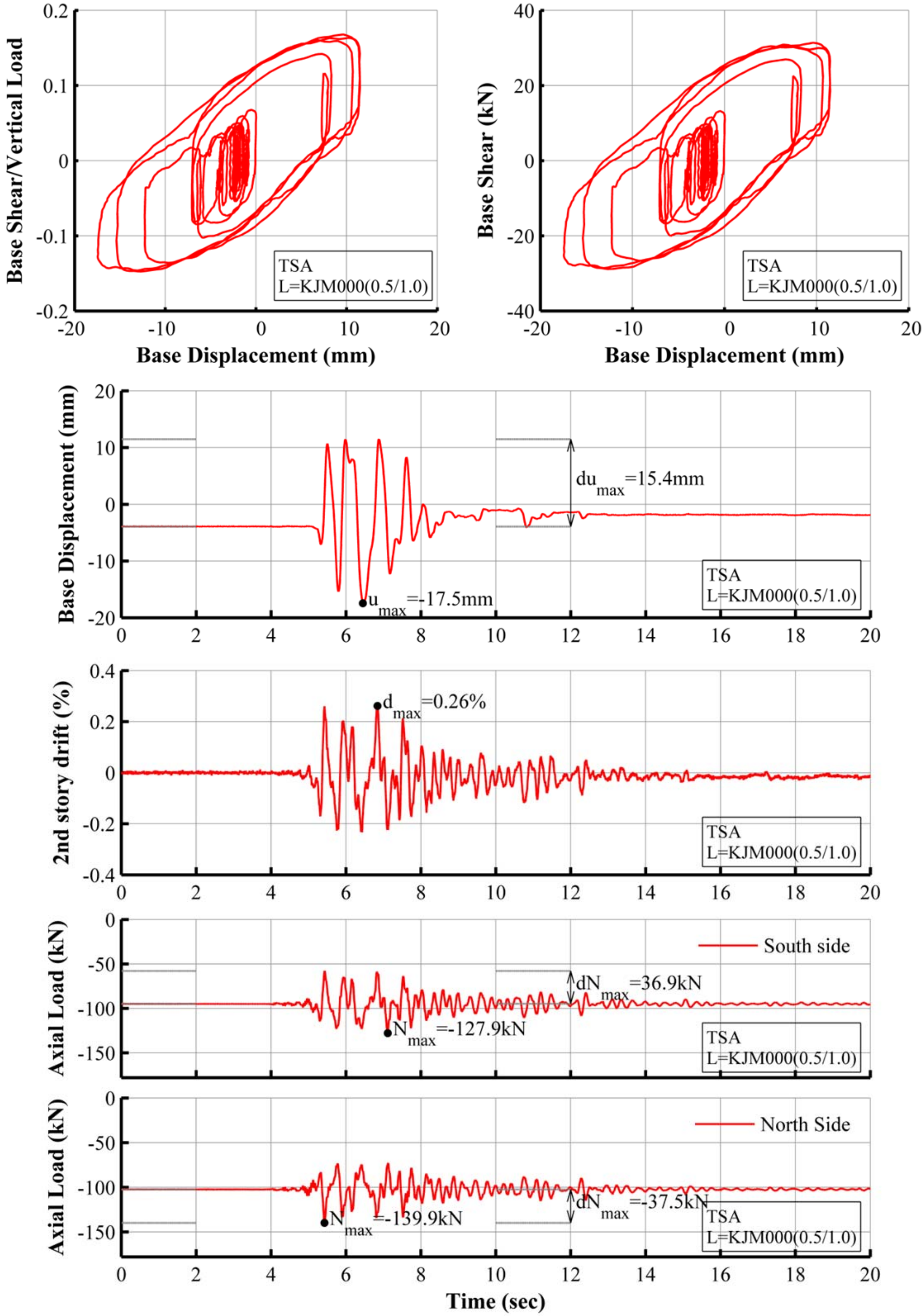
Base Shear/Vertical Load
Base Displacement (mm)
TSA
L=KJM000(0.5/1.0)
Base Shear (kN)
Base Displacement (mm)
TSA
L=KJM000(0.5/1.0)
Base Displacement (mm)
du max =15.4mm
u max =-17.5mm
TSA
L=KJM000(0.5/1.0)
2nd story drift (%)
d max =0.26%
TSA
L=KJM000(0.5/1.0)
Axial Load (kN)
South side
dN max =36.9kN
N max =-127.9kN
TSA
L=KJM000(0.5/1.0)
Axial Load (kN)
North Side
dN max =-37.5kN
N max =-139.9kN
TSA
L=KJM000(0.5/1.0)
Time (sec)

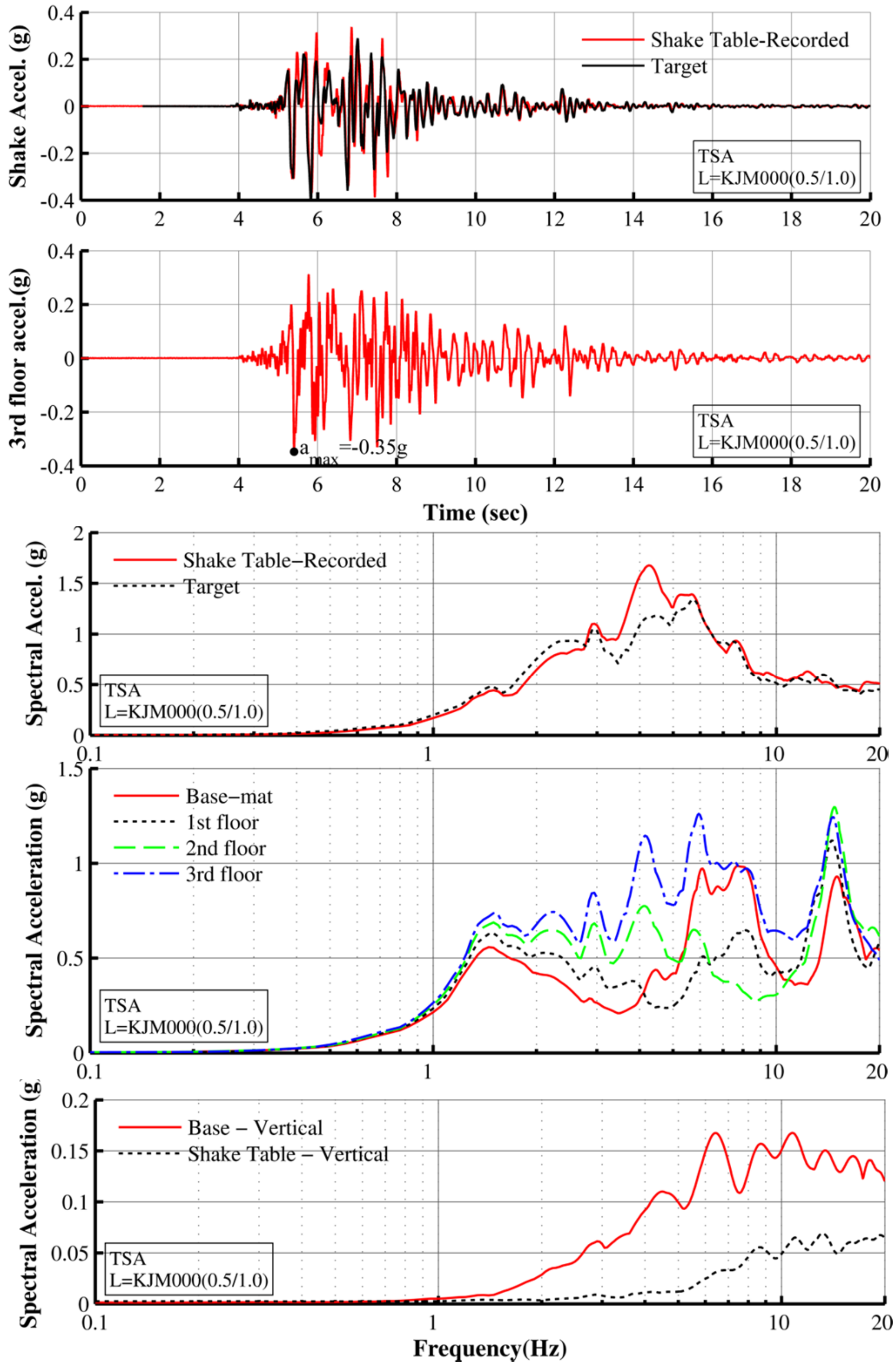
Shake Accel. (g)
Shake Table-Recorded
Target
TSA
L=KJM000(0.5/1.0)
3rd floor accel.(g)
a_{max}=-0.35g
Time (sec)
Spectral Accel. (g)
Shake Table−Recorded
Target
Spectral Acceleration (g)
Base−mat
1st floor
2nd floor
3rd floor
Base − Vertical
Shake Table − Vertical
Frequency(Hz)

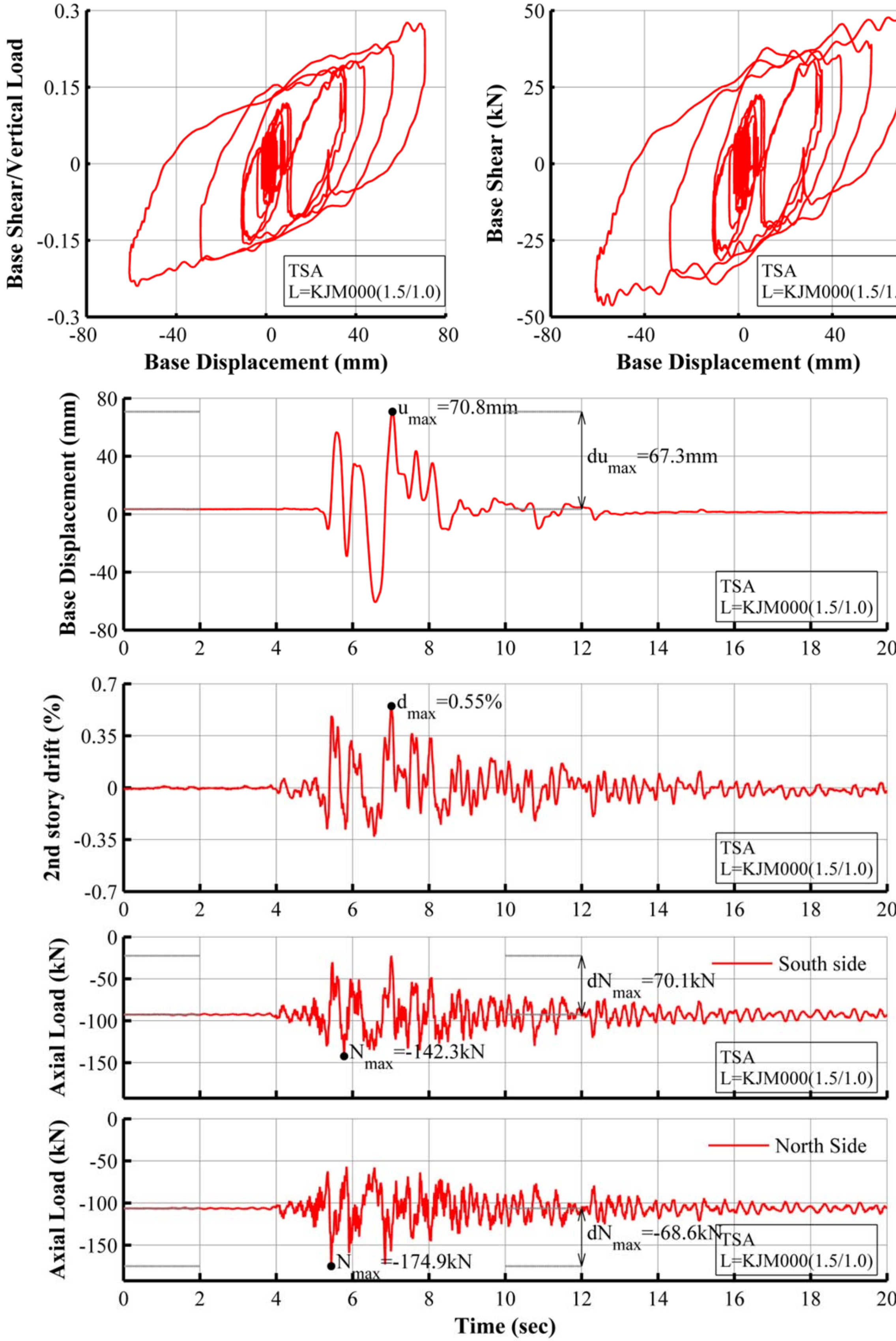

Base Shear/Vertical Load
Base Displacement (mm)
TSA
L=KJM000(1.5/1.0)
Base Shear (kN)
Base Displacement (mm)
TSA
L=KJM000(1.5/1.0)
Base Displacement (mm)
u max =70.8mm
du max =67.3mm
TSA
L=KJM000(1.5/1.0)
2nd story drift (%)
d max =0.55%
TSA
L=KJM000(1.5/1.0)
Axial Load (kN)
South side
dN max =70.1kN
N max =-142.3kN
TSA
L=KJM000(1.5/1.0)
Axial Load (kN)
North Side
dN max =-68.6kN
N max =-174.9kN
TSA
L=KJM000(1.5/1.0)
Time (sec)

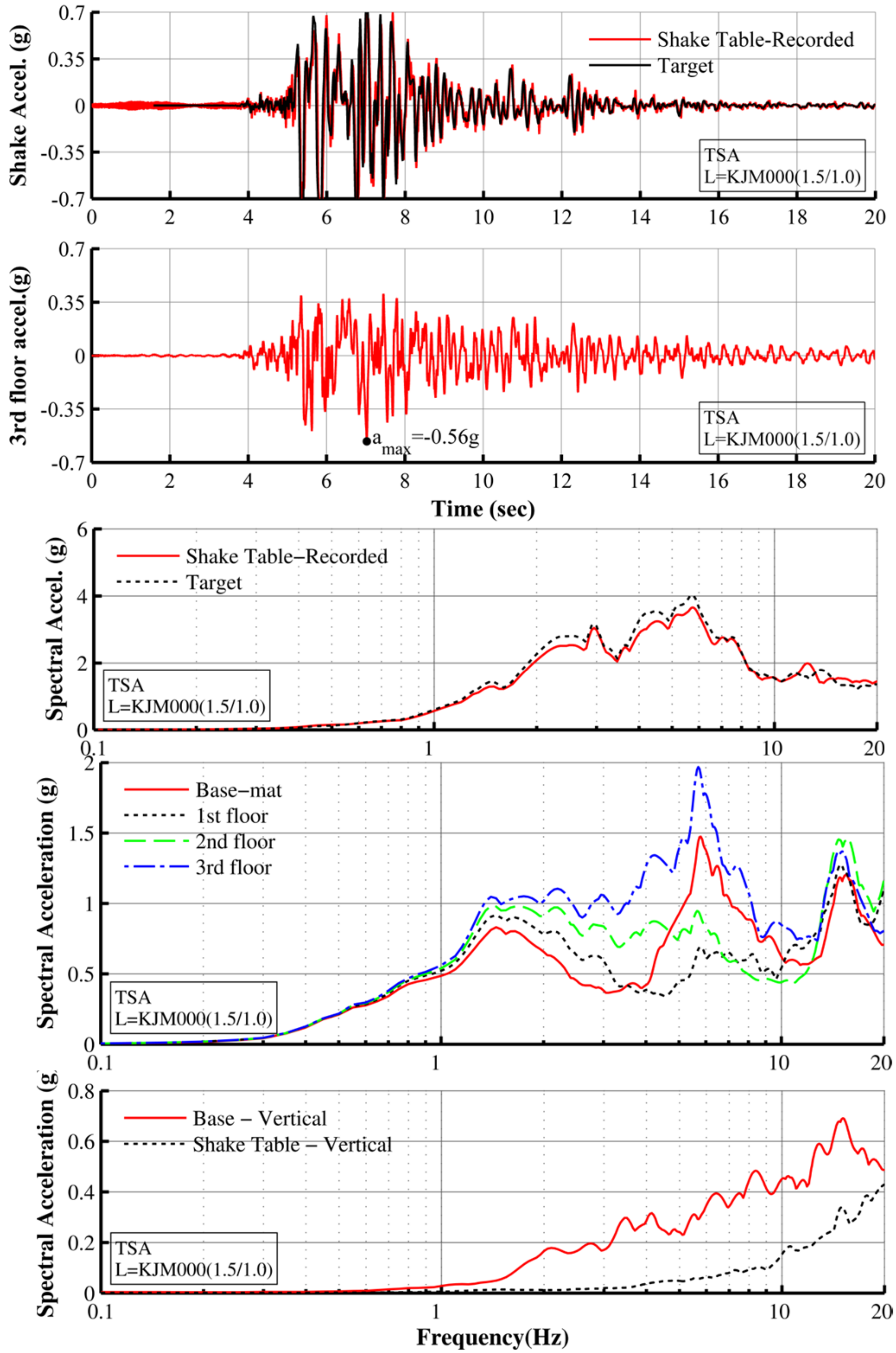

Shake Accel. (g)
Shake Table-Recorded
Target
TSA
L=KJM000(1.5/1.0)
3rd floor accel.(g)
a_{max}=-0.56g
TSA
L=KJM000(1.5/1.0)
Time (sec)
Spectral Accel. (g)
Shake Table−Recorded
Target
TSA
L=KJM000(1.5/1.0)
Spectral Acceleration (g)
Base−mat
1st floor
2nd floor
3rd floor
TSA
L=KJM000(1.5/1.0)
Spectral Acceleration (g)
Base − Vertical
Shake Table − Vertical
TSA
L=KJM000(1.5/1.0)
Frequency(Hz)

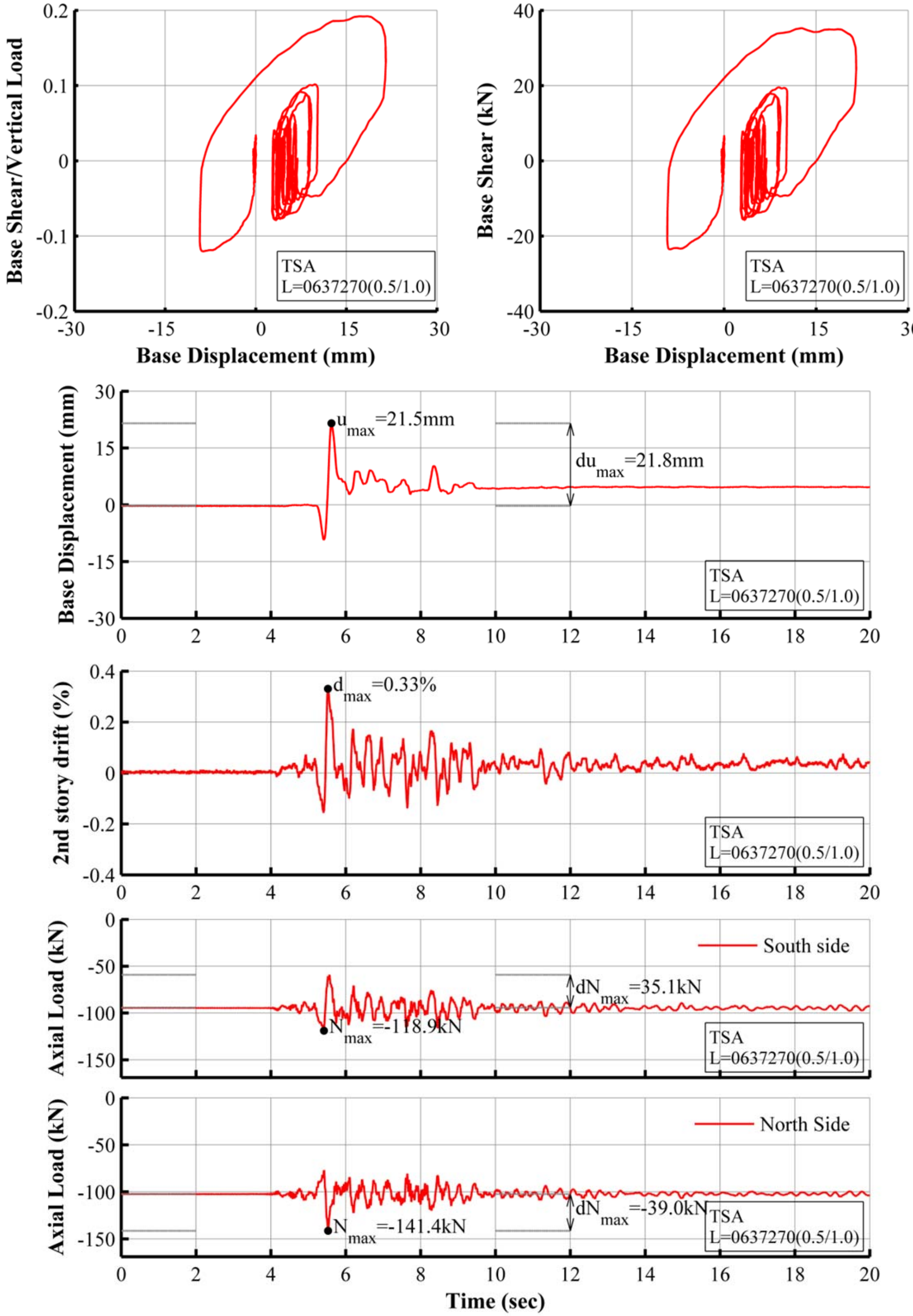

Base Shear/Vertical Load
Base Displacement (mm)
TSA
L=0637270(0.5/1.0)
Base Shear (kN)
Base Displacement (mm)
TSA
L=0637270(0.5/1.0)
Base Displacement (mm)
u max =21.5mm
du max =21.8mm
TSA
L=0637270(0.5/1.0)
2nd story drift (%)
d max =0.33%
TSA
L=0637270(0.5/1.0)
Axial Load (kN)
South side
dN max =35.1kN
N max =-118.9kN
TSA
L=0637270(0.5/1.0)
Axial Load (kN)
North Side
dN max =-39.0kN
N max =-141.4kN
TSA
L=0637270(0.5/1.0)
Time (sec)

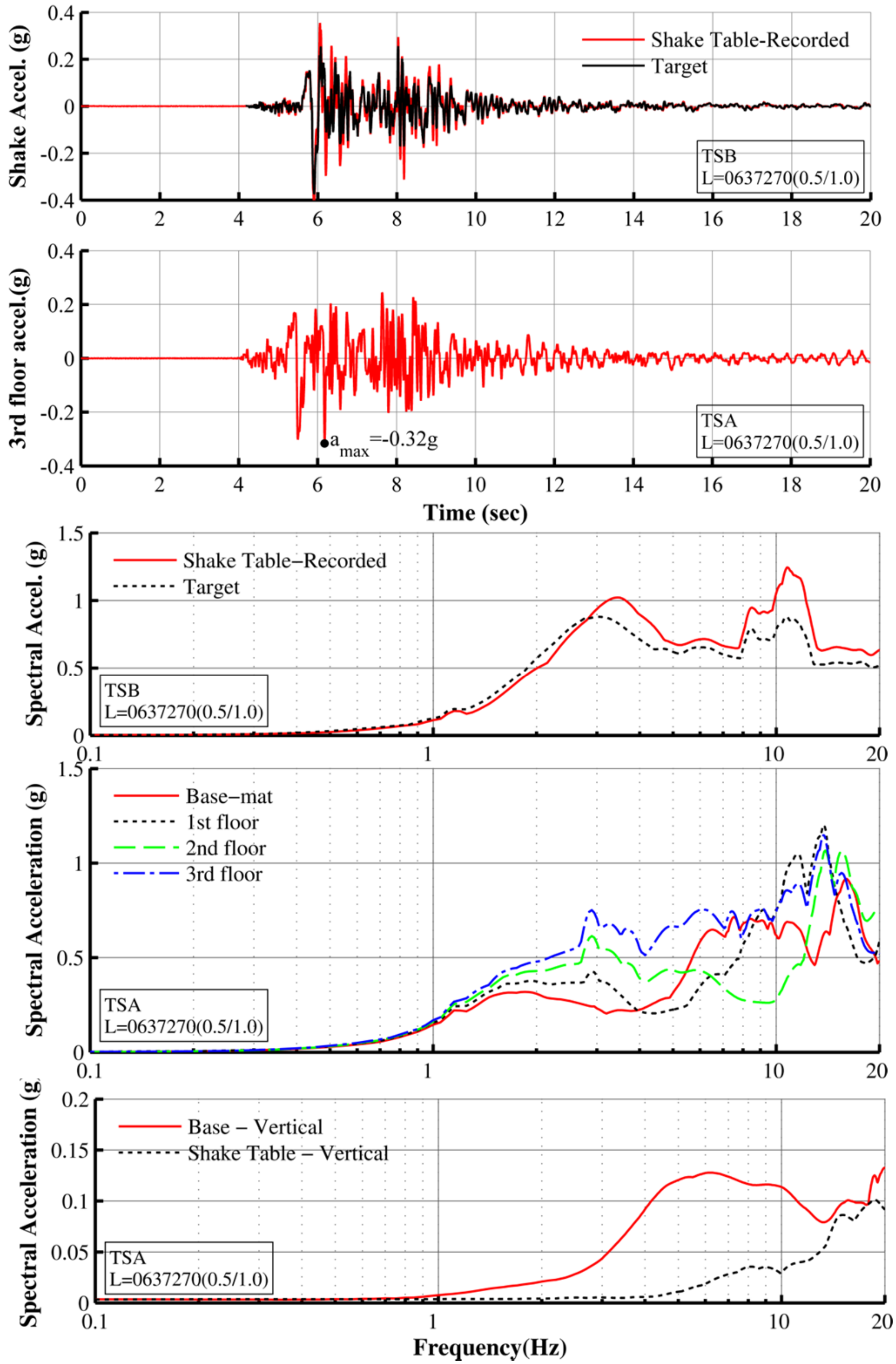

Shake Accel. (g)
Shake Table-Recorded
Target
TSB
L=0637270(0.5/1.0)
3rd floor accel.(g)
a_{max}=-0.32g
TSA
L=0637270(0.5/1.0)
Time (sec)
Spectral Accel. (g)
Shake Table−Recorded
Target
TSB
L=0637270(0.5/1.0)
Spectral Acceleration (g)
Base−mat
1st floor
2nd floor
3rd floor
TSA
L=0637270(0.5/1.0)
Spectral Acceleration (g)
Base − Vertical
Shake Table − Vertical
TSA
L=0637270(0.5/1.0)
Frequency(Hz)

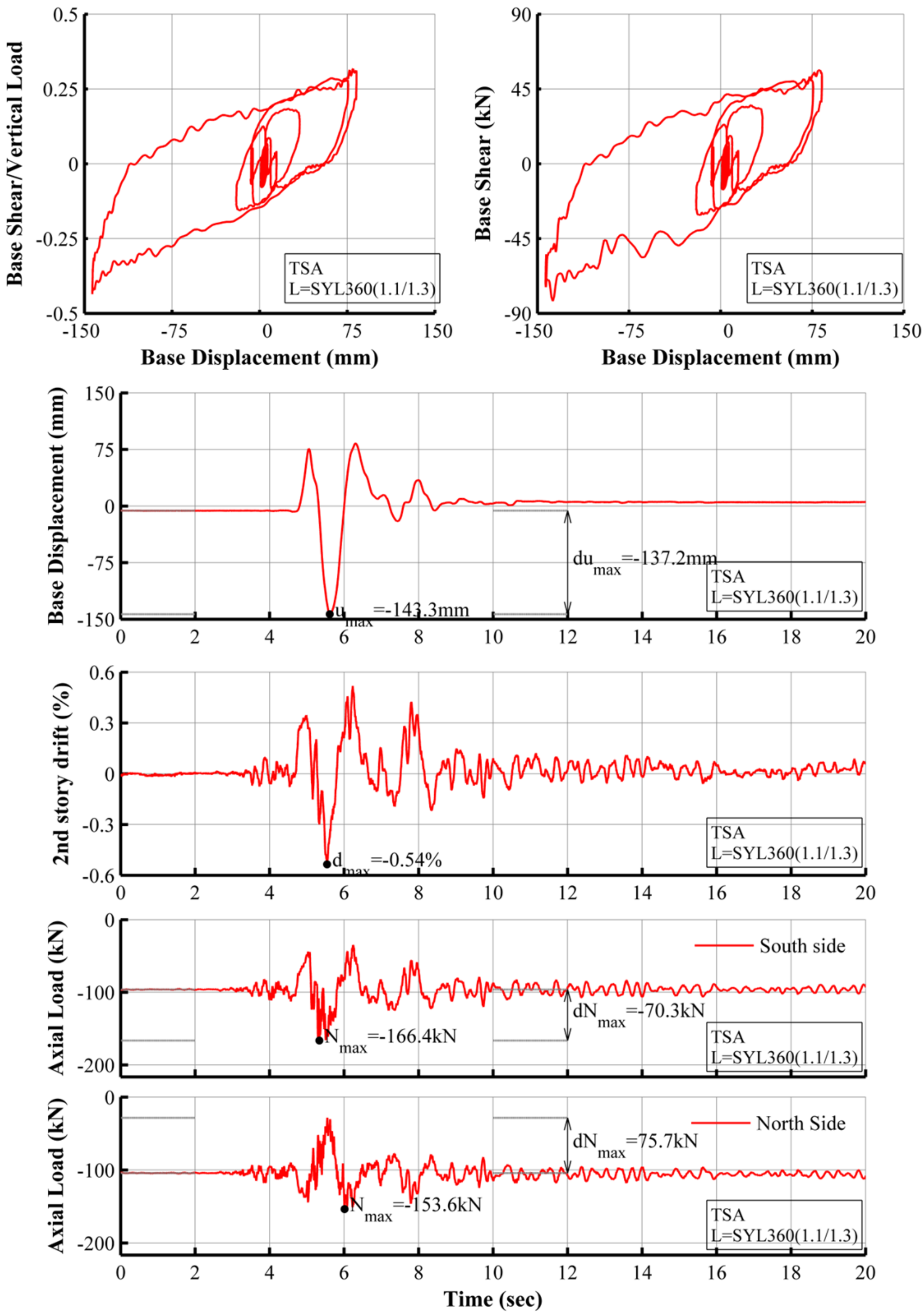
Base Shear/Vertical Load
Base Displacement (mm)
TSA
L=SYL360(1.1/1.3)
Base Shear (kN)
Base Displacement (mm)
TSA
L=SYL360(1.1/1.3)
Base Displacement (mm)
du max =-137.2mm
u max =-143.3mm
TSA
L=SYL360(1.1/1.3)
2nd story drift (%)
d max =-0.54%
TSA
L=SYL360(1.1/1.3)
Axial Load (kN)
South side
dN max =-70.3kN
N max =-166.4kN
TSA
L=SYL360(1.1/1.3)
Axial Load (kN)
North Side
dN max =75.7kN
N max =-153.6kN
TSA
L=SYL360(1.1/1.3)
Time (sec)

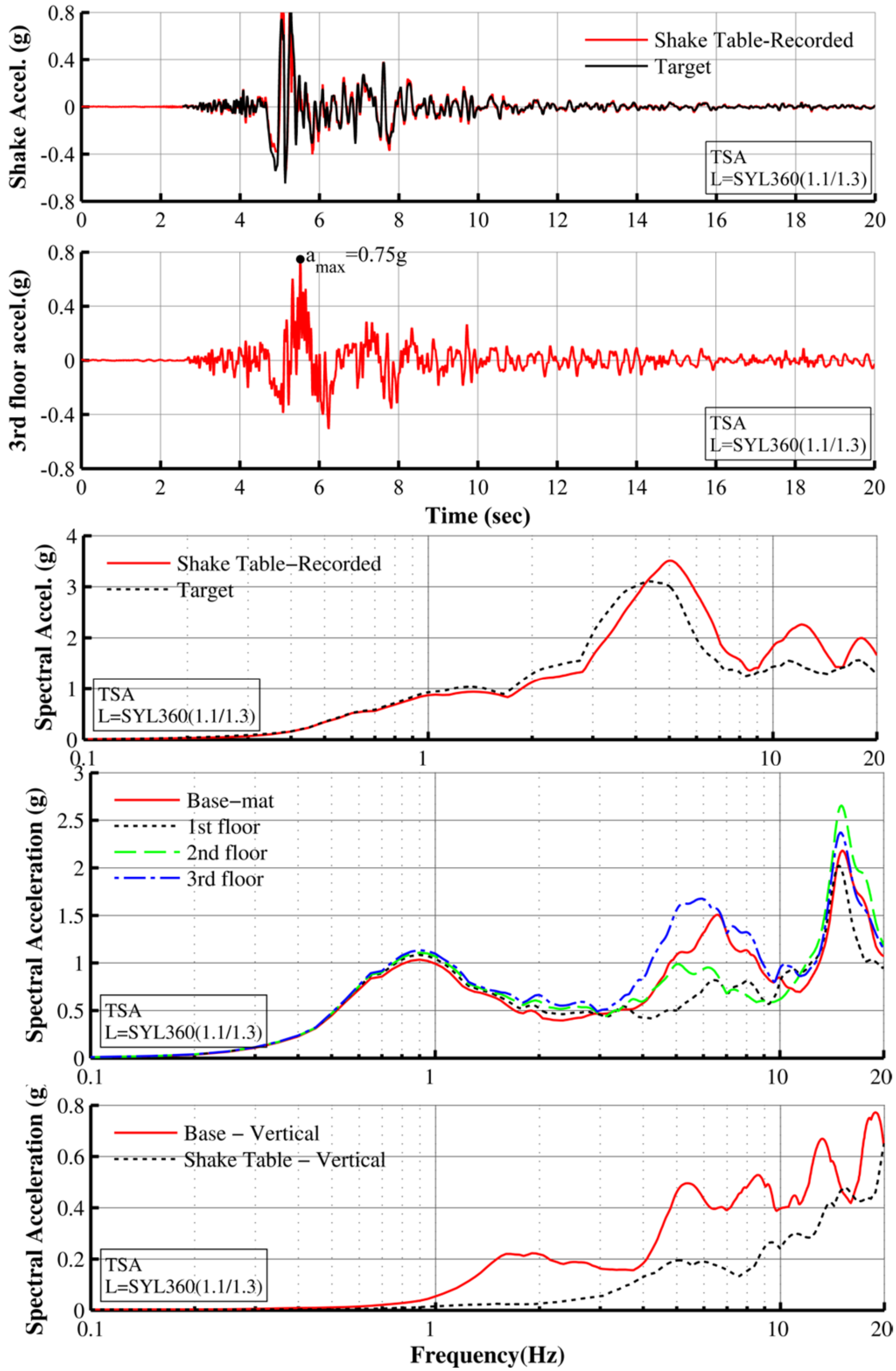
Shake Table-Recorded
Target
TSA
L=SYL360(1.1/1.3)
Shake Accel. (g)
a max =0.75g
TSA
L=SYL360(1.1/1.3)
3rd floor accel.(g)
Time (sec)
Shake Table−Recorded
Target
TSA
L=SYL360(1.1/1.3)
Spectral Accel. (g)
Base−mat
1st floor
2nd floor
3rd floor
TSA
L=SYL360(1.1/1.3)
Spectral Acceleration (g)
Base − Vertical
Shake Table − Vertical
TSA
L=SYL360(1.1/1.3)
Spectral Acceleration (g)
Frequency(Hz)

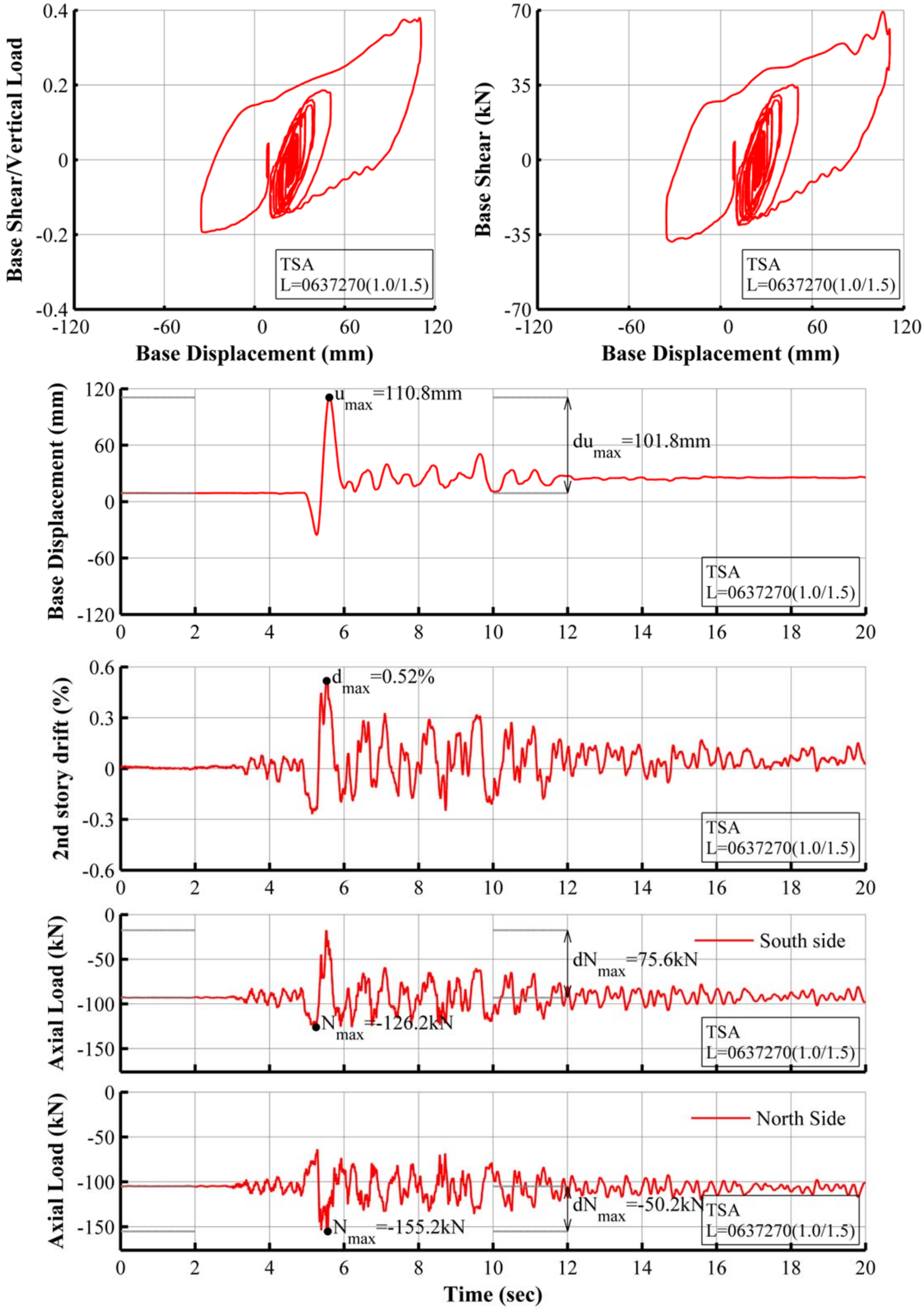
Base Shear/Vertical Load
Base Displacement (mm)
TSA
L=0637270(1.0/1.5)
Base Shear (kN)
Base Displacement (mm)
TSA
L=0637270(1.0/1.5)
Base Displacement (mm)
u_{max}=110.8mm
du_{max}=101.8mm
TSA
L=0637270(1.0/1.5)
2nd story drift (%)
d_{max}=0.52%
TSA
L=0637270(1.0/1.5)
Axial Load (kN)
South side
dN_{max}=75.6kN
N_{max}=-126.2kN
TSA
L=0637270(1.0/1.5)
Axial Load (kN)
North Side
dN_{max}=-50.2kN
N_{max}=-155.2kN
TSA
L=0637270(1.0/1.5)
Time (sec)

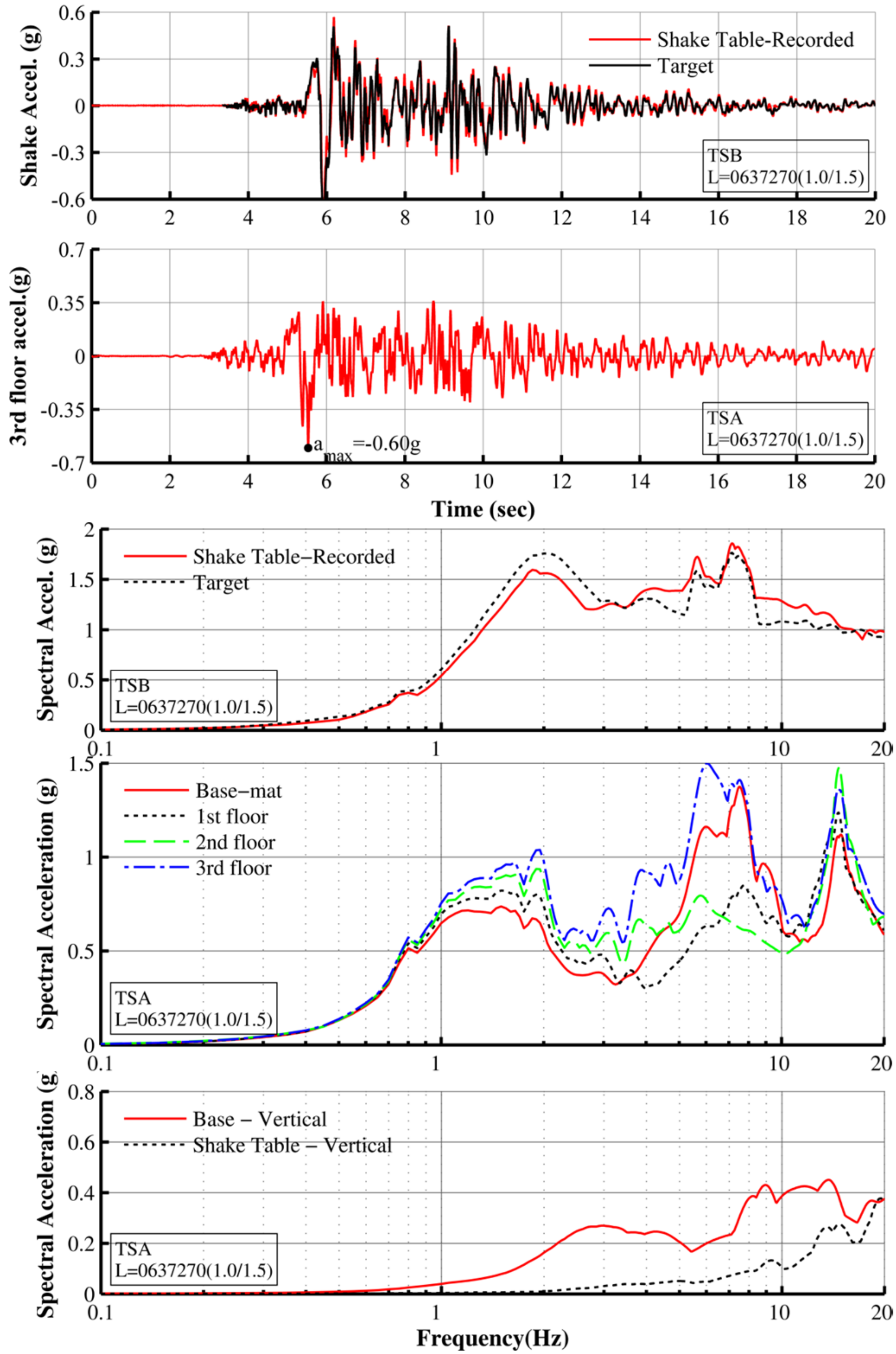
Shake Accel. (g)
Shake Table-Recorded
Target
TSB
L=0637270(1.0/1.5)
3rd floor accel.(g)
TSA
L=0637270(1.0/1.5)
a max =-0.60g
Time (sec)
Spectral Accel. (g)
Shake Table−Recorded
Target
TSB
L=0637270(1.0/1.5)
Spectral Acceleration (g)
Base−mat
1st floor
2nd floor
3rd floor
TSA
L=0637270(1.0/1.5)
Spectral Acceleration (g)
Base − Vertical
Shake Table − Vertical
TSA
L=0637270(1.0/1.5)
Frequency(Hz)

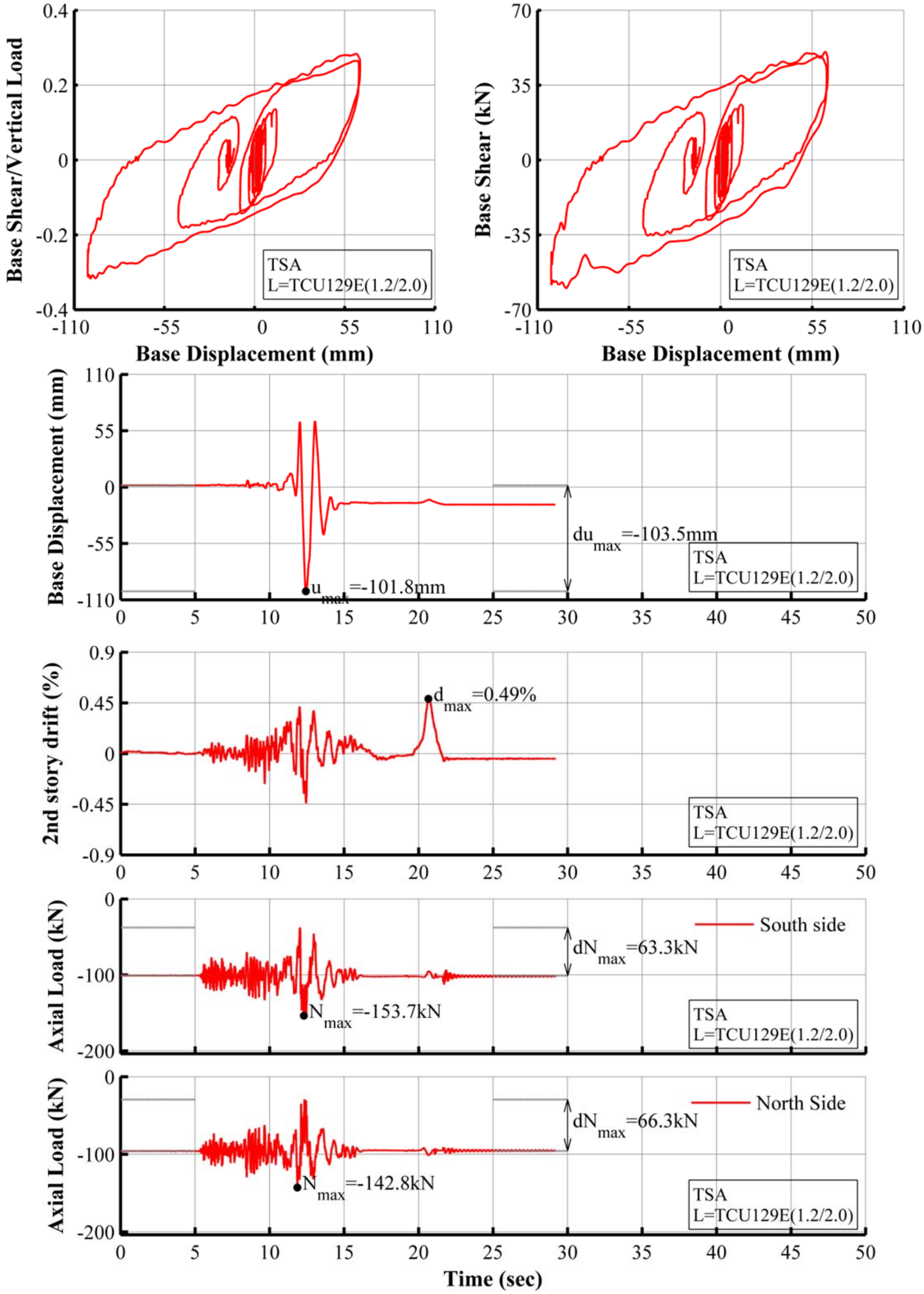
Base Shear/Vertical Load
Base Displacement (mm)
TSA
L=TCU129E(1.2/2.0)
Base Shear (kN)
Base Displacement (mm)
TSA
L=TCU129E(1.2/2.0)
Base Displacement (mm)
du_max=-103.5mm
u_max=-101.8mm
TSA
L=TCU129E(1.2/2.0)
2nd story drift (%)
d_max=0.49%
TSA
L=TCU129E(1.2/2.0)
Axial Load (kN)
South side
dN_max=63.3kN
N_max=-153.7kN
TSA
L=TCU129E(1.2/2.0)
Axial Load (kN)
North Side
dN_max=66.3kN
N_max=-142.8kN
TSA
L=TCU129E(1.2/2.0)
Time (sec)

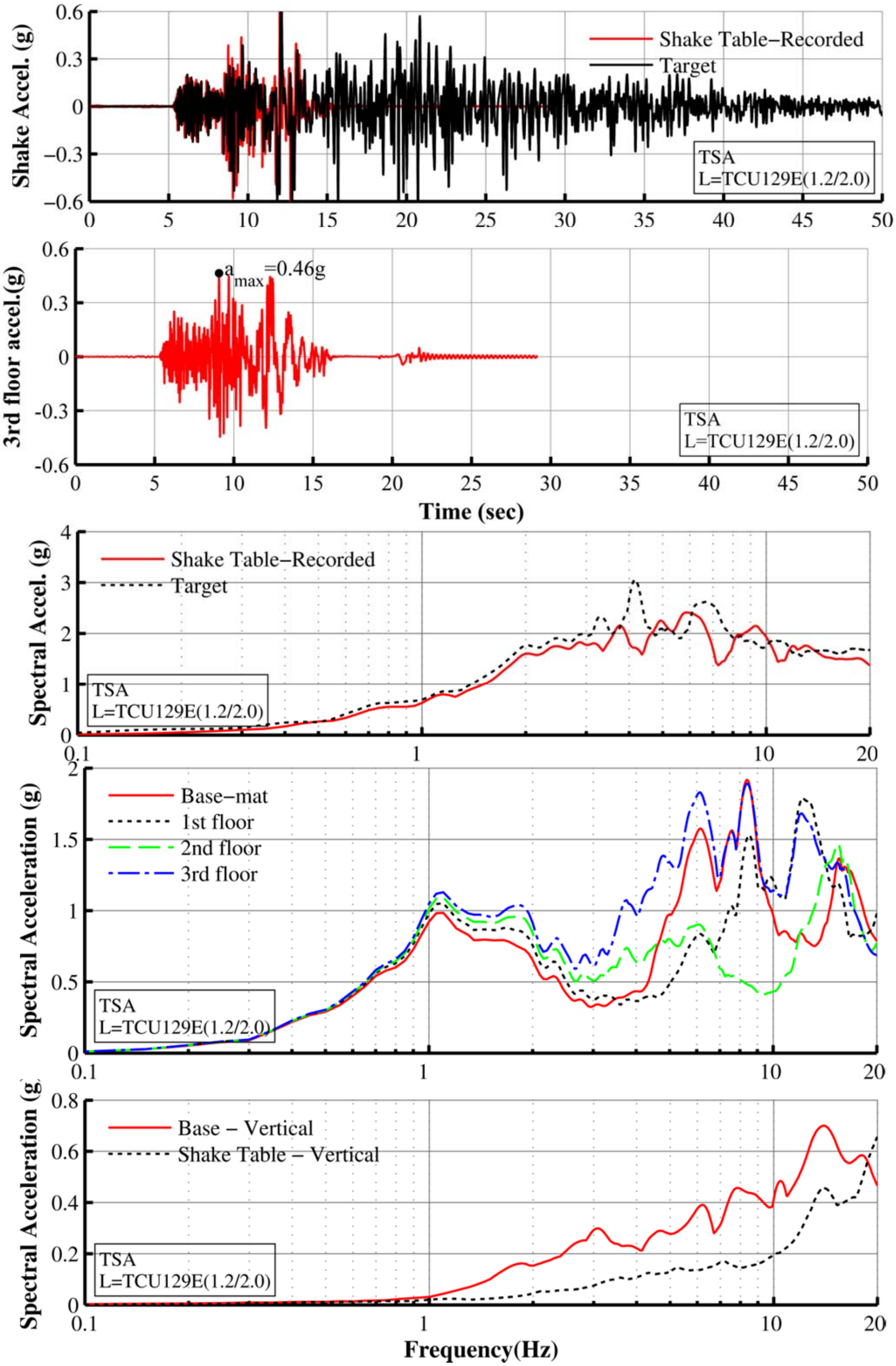
Shake Accel. (g)
Shake Table−Recorded
Target
TSA
L=TCU129E(1.2/2.0)
3rd floor accel.(g)
a_{max}=0.46g
TSA
L=TCU129E(1.2/2.0)
Time (sec)
Spectral Accel. (g)
Shake Table−Recorded
Target
TSA
L=TCU129E(1.2/2.0)
Spectral Acceleration (g)
Base−mat
1st floor
2nd floor
3rd floor
TSA
L=TCU129E(1.2/2.0)
Spectral Acceleration (g)
Base − Vertical
Shake Table − Vertical
TSA
L=TCU129E(1.2/2.0)
Frequency(Hz)

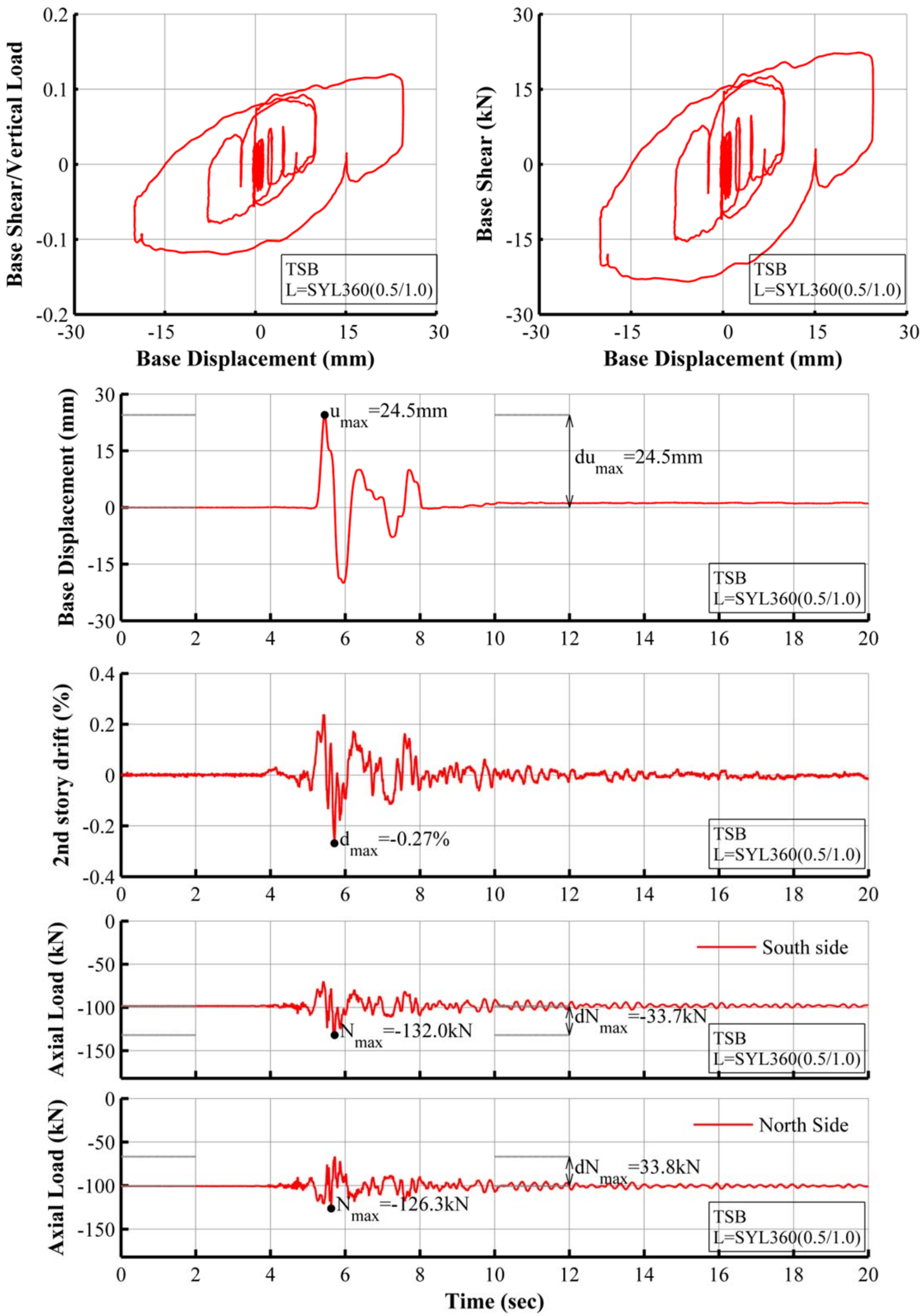
Base Shear/Vertical Load
Base Displacement (mm)
TSB
L=SYL360(0.5/1.0)
Base Shear (kN)
Base Displacement (mm)
TSB
L=SYL360(0.5/1.0)
Base Displacement (mm)
u_{max}=24.5mm
du_{max}=24.5mm
TSB
L=SYL360(0.5/1.0)
2nd story drift (%)
d_{max}=-0.27%
TSB
L=SYL360(0.5/1.0)
Axial Load (kN)
South side
N_{max}=-132.0kN
dN_{max}=-33.7kN
TSB
L=SYL360(0.5/1.0)
Axial Load (kN)
North Side
dN_{max}=33.8kN
N_{max}=-126.3kN
TSB
L=SYL360(0.5/1.0)
Time (sec)

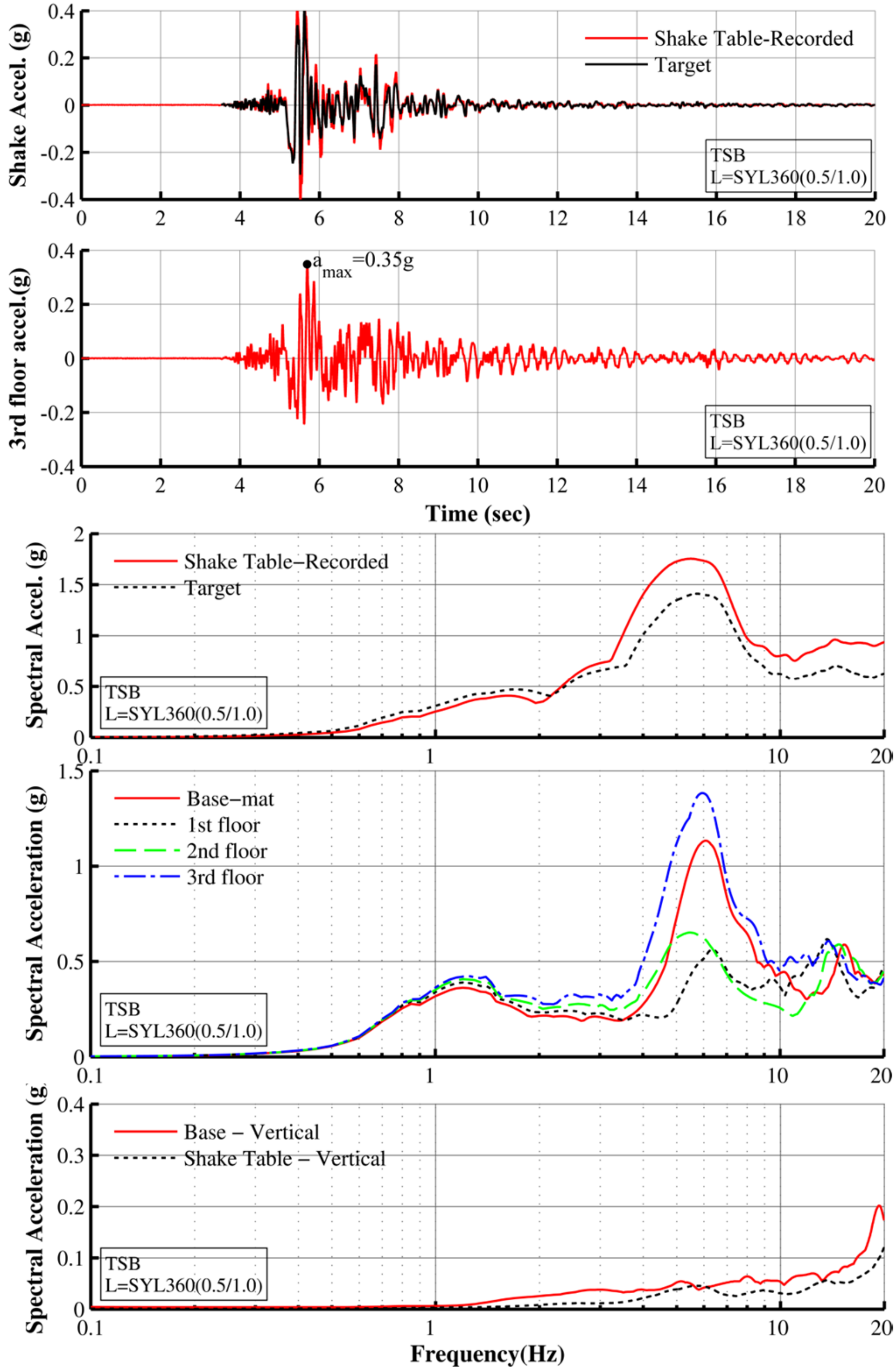
Shake Accel. (g)
Shake Table-Recorded
Target
TSB
L=SYL360(0.5/1.0)
3rd floor accel.(g)
a_{max}=0.35g
TSB
L=SYL360(0.5/1.0)
Time (sec)
Spectral Accel. (g)
Shake Table−Recorded
Target
TSB
L=SYL360(0.5/1.0)
Spectral Acceleration (g)
Base−mat
1st floor
2nd floor
3rd floor
TSB
L=SYL360(0.5/1.0)
Spectral Acceleration (g)
Base − Vertical
Shake Table − Vertical
TSB
L=SYL360(0.5/1.0)
Frequency(Hz)

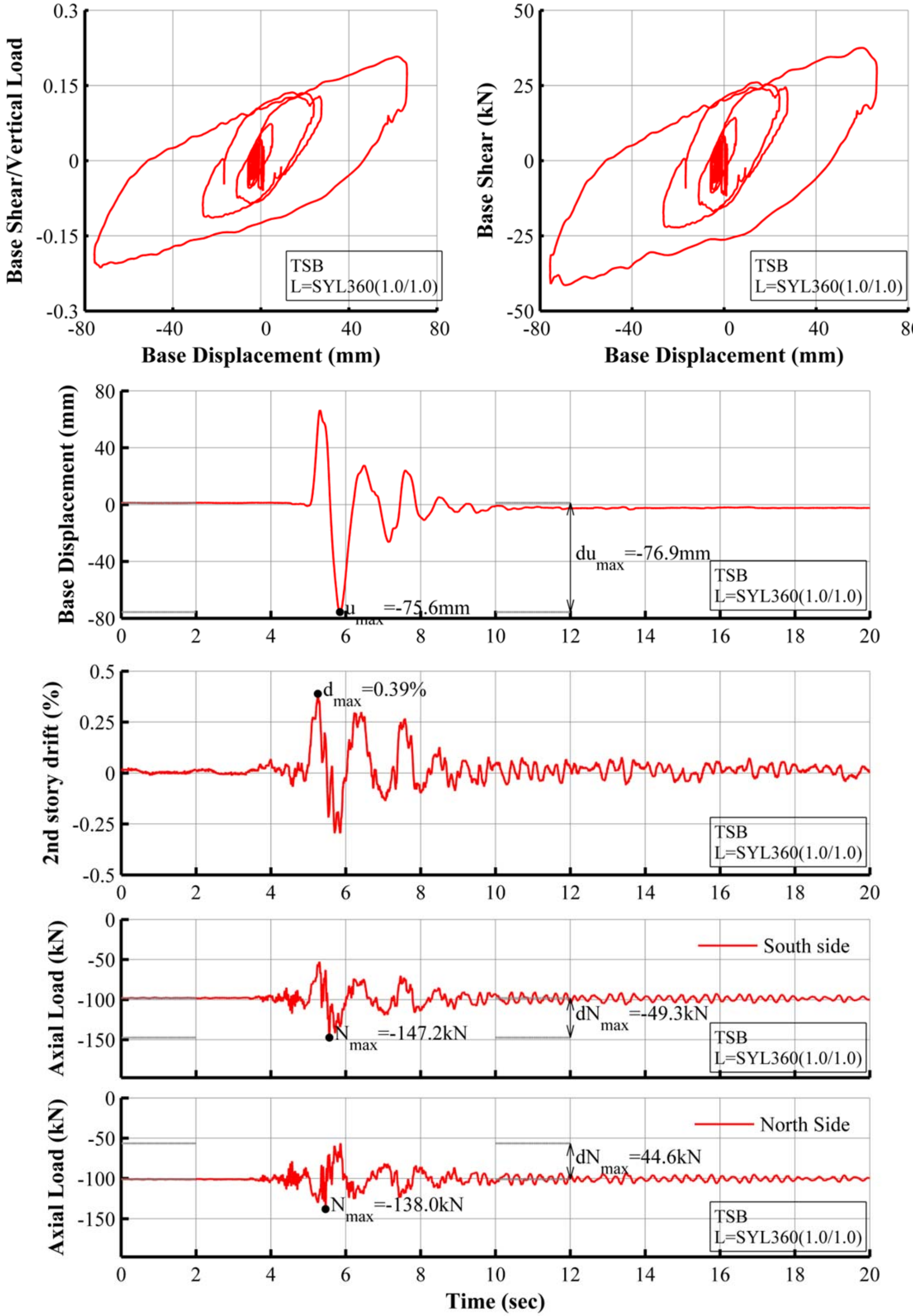
Base Shear/Vertical Load
Base Displacement (mm)
TSB
L=SYL360(1.0/1.0)
Base Shear (kN)
Base Displacement (mm)
TSB
L=SYL360(1.0/1.0)
Base Displacement (mm)
du max =-76.9mm
u max =-75.6mm
TSB
L=SYL360(1.0/1.0)
2nd story drift (%)
d max =0.39%
TSB
L=SYL360(1.0/1.0)
Axial Load (kN)
South side
dN max =-49.3kN
N max =-147.2kN
TSB
L=SYL360(1.0/1.0)
Axial Load (kN)
North Side
dN max =44.6kN
N max =-138.0kN
TSB
L=SYL360(1.0/1.0)
Time (sec)

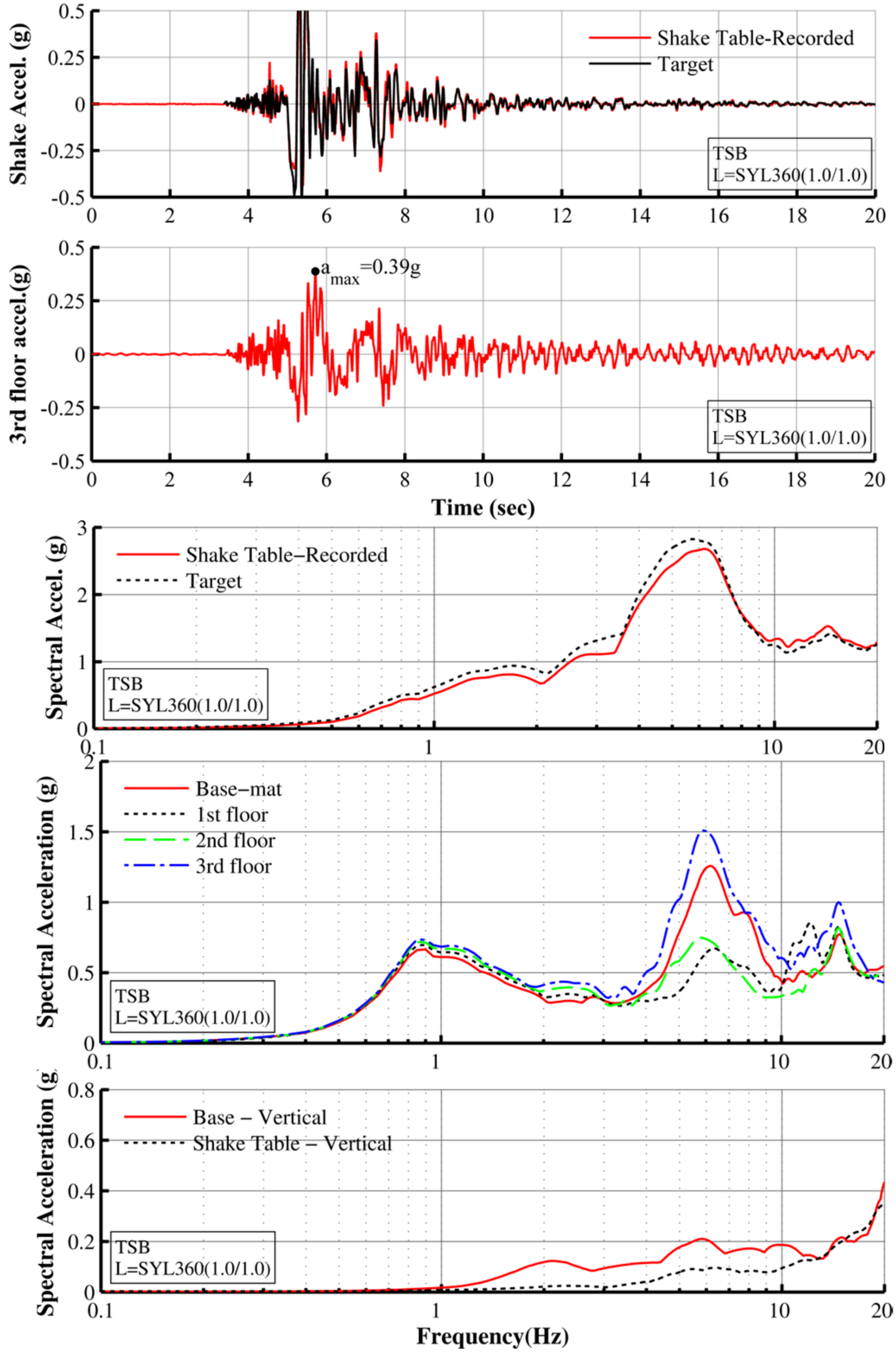

Shake Accel. (g)
Shake Table-Recorded
Target
TSB
L=SYL360(1.0/1.0)
3rd floor accel.(g)
a max =0.39g
TSB
L=SYL360(1.0/1.0)
Time (sec)
Spectral Accel. (g)
Shake Table−Recorded
Target
TSB
L=SYL360(1.0/1.0)
Spectral Acceleration (g)
Base−mat
1st floor
2nd floor
3rd floor
TSB
L=SYL360(1.0/1.0)
Spectral Acceleration (g)
Base − Vertical
Shake Table − Vertical
TSB
L=SYL360(1.0/1.0)
Frequency(Hz)

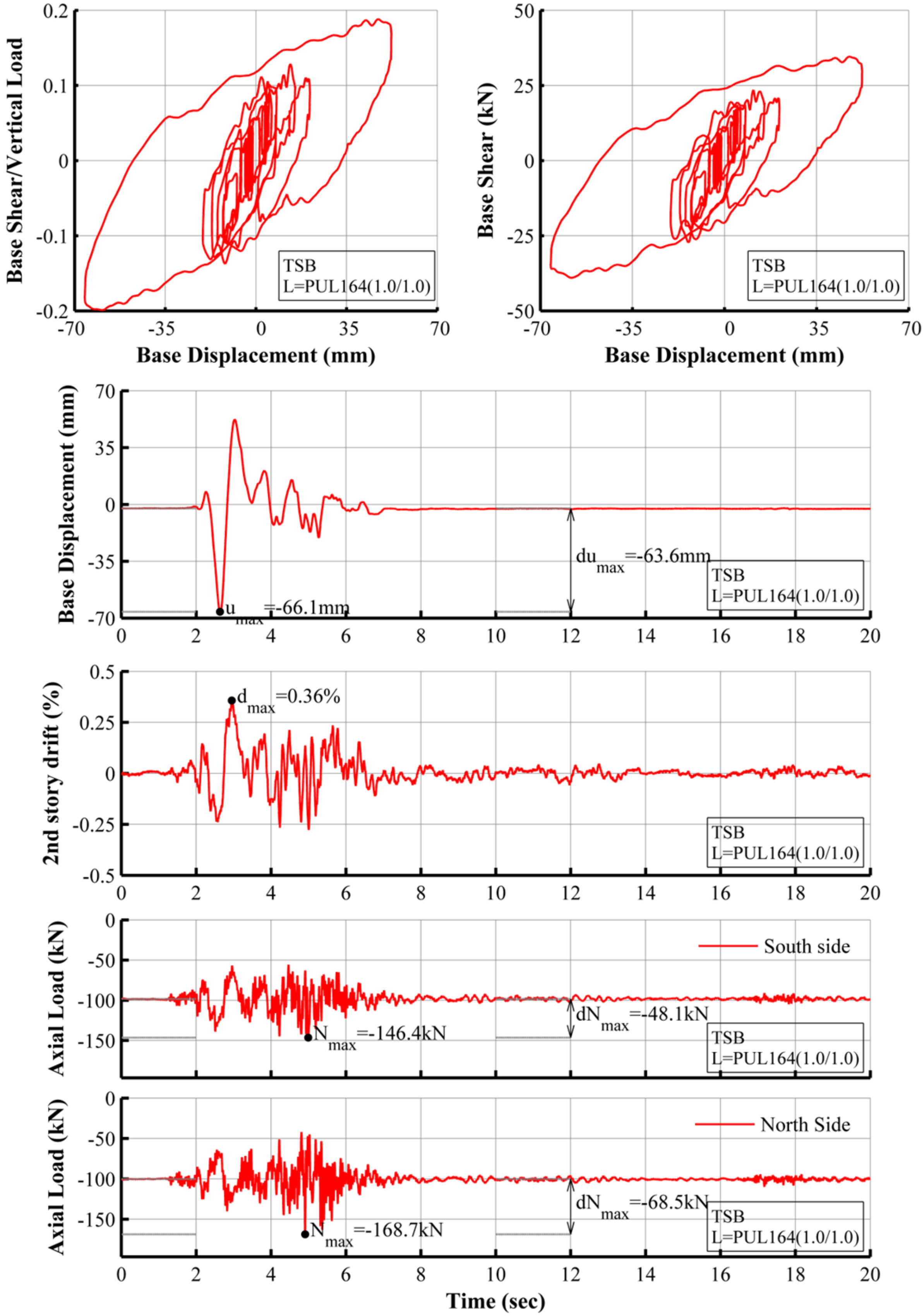

Base Shear/Vertical Load
Base Displacement (mm)
TSB
L=PUL164(1.0/1.0)
Base Shear (kN)
Base Displacement (mm)
TSB
L=PUL164(1.0/1.0)
Base Displacement (mm)
du max =-63.6mm
u max =-66.1mm
TSB
L=PUL164(1.0/1.0)
2nd story drift (%)
d max =0.36%
TSB
L=PUL164(1.0/1.0)
Axial Load (kN)
South side
dN max =-48.1kN
N max =-146.4kN
TSB
L=PUL164(1.0/1.0)
Axial Load (kN)
North Side
dN max =-68.5kN
N max =-168.7kN
TSB
L=PUL164(1.0/1.0)
Time (sec)

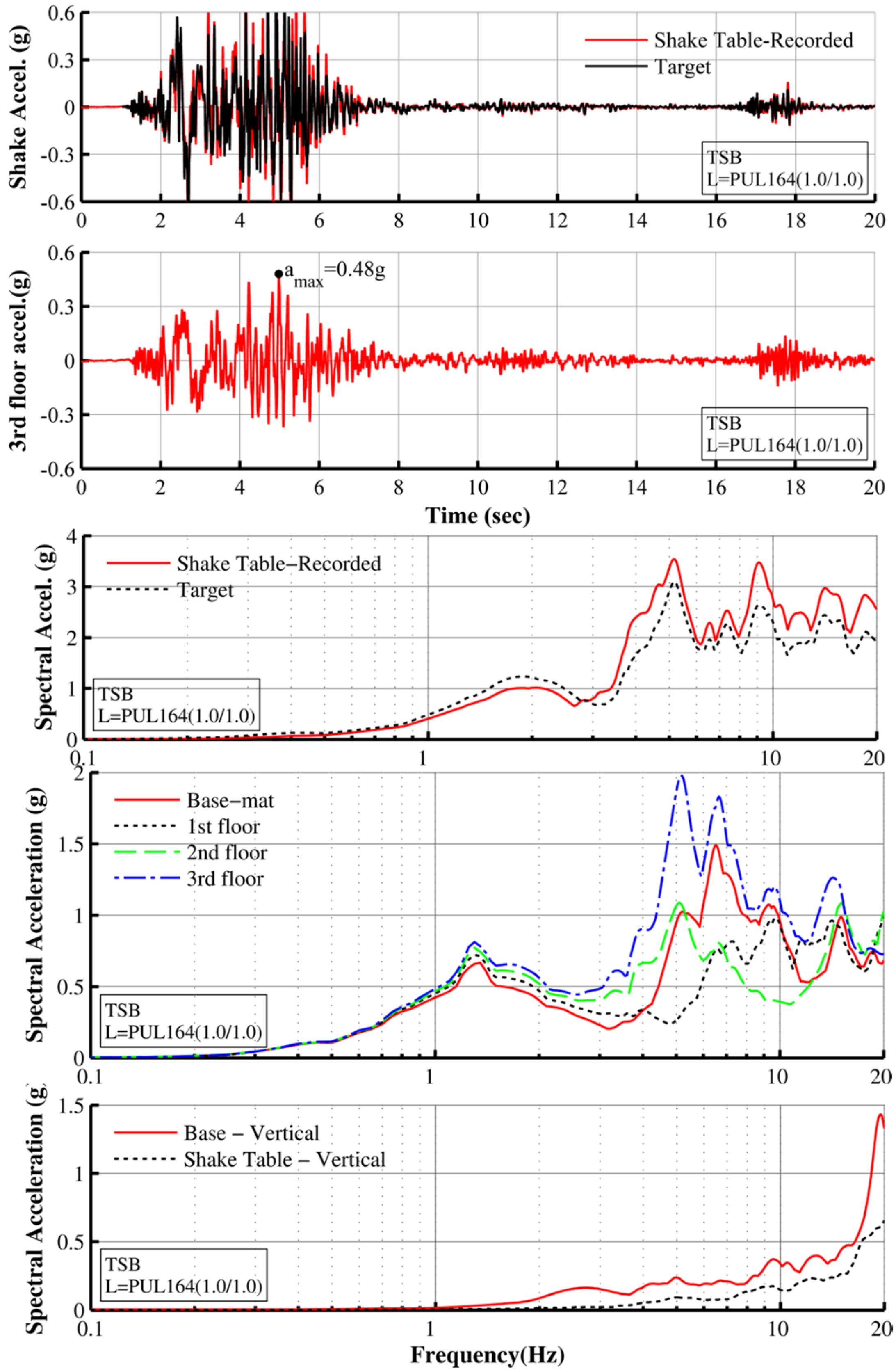
Shake Table-Recorded
Target
TSB
L=PUL164(1.0/1.0)
Shake Accel. (g)
a_{max}=0.48g
3rd floor accel.(g)
Time (sec)
Shake Table−Recorded
Target
Spectral Accel. (g)
Base−mat
1st floor
2nd floor
3rd floor
Spectral Acceleration (g)
Base − Vertical
Shake Table − Vertical
Frequency(Hz)

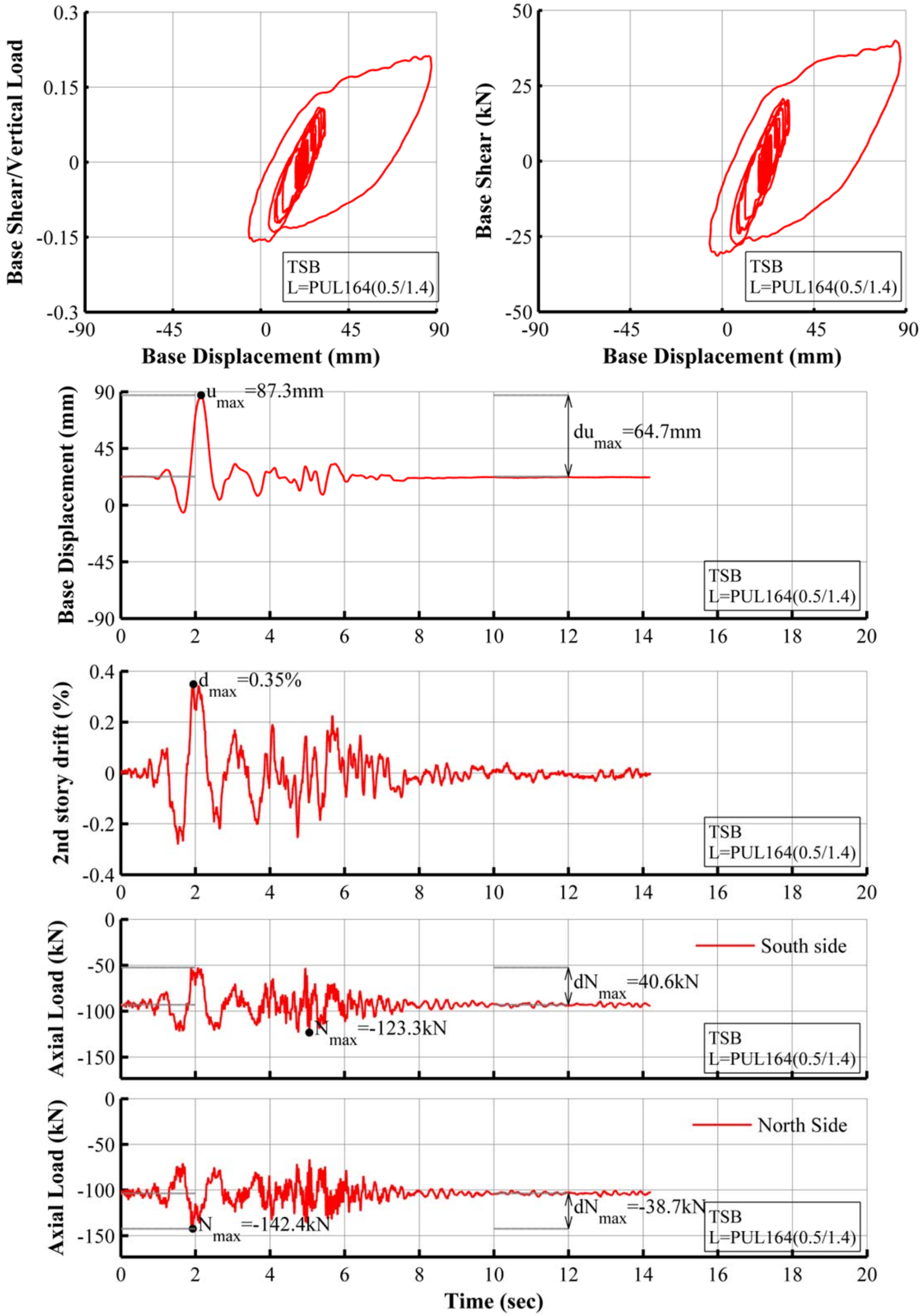
Base Shear/Vertical Load
Base Displacement (mm)
TSB
L=PUL164(0.5/1.4)
Base Shear (kN)
Base Displacement (mm)
TSB
L=PUL164(0.5/1.4)
Base Displacement (mm)
umax=87.3mm
dumax=64.7mm
TSB
L=PUL164(0.5/1.4)
2nd story drift (%)
dmax=0.35%
TSB
L=PUL164(0.5/1.4)
Axial Load (kN)
South side
dNmax=40.6kN
Nmax=-123.3kN
TSB
L=PUL164(0.5/1.4)
Axial Load (kN)
North Side
dNmax=-38.7kN
Nmax=-142.4kN
TSB
L=PUL164(0.5/1.4)
Time (sec)

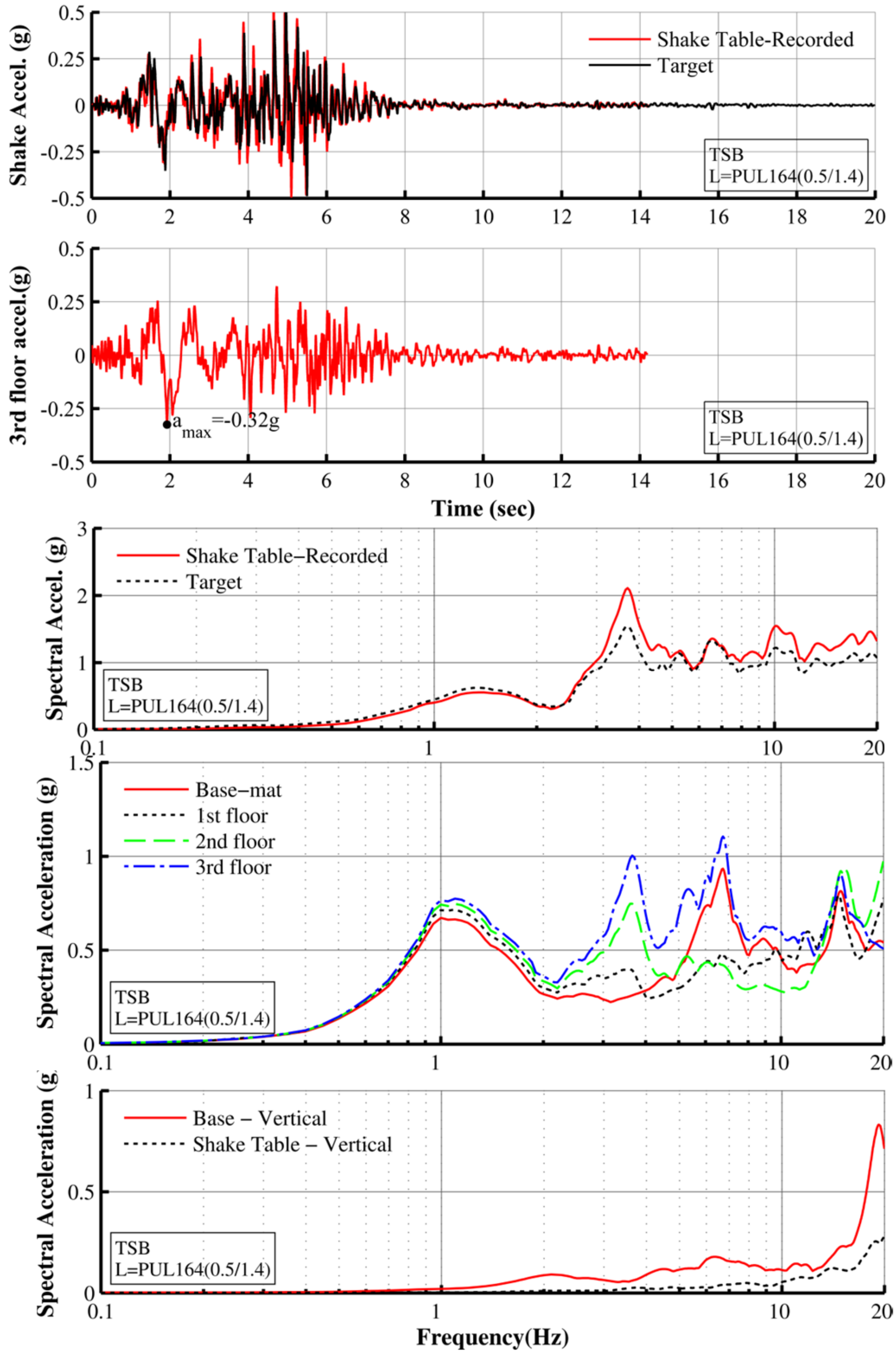
Shake Accel. (g)
Shake Table-Recorded
Target
TSB
L=PUL164(0.5/1.4)
3rd floor accel.(g)
a_{max}=-0.32g
TSB
L=PUL164(0.5/1.4)
Time (sec)
Spectral Accel. (g)
Shake Table−Recorded
Target
TSB
L=PUL164(0.5/1.4)
Spectral Acceleration (g)
Base−mat
1st floor
2nd floor
3rd floor
TSB
L=PUL164(0.5/1.4)
Spectral Acceleration (g)
Base − Vertical
Shake Table − Vertical
TSB
L=PUL164(0.5/1.4)
Frequency(Hz)

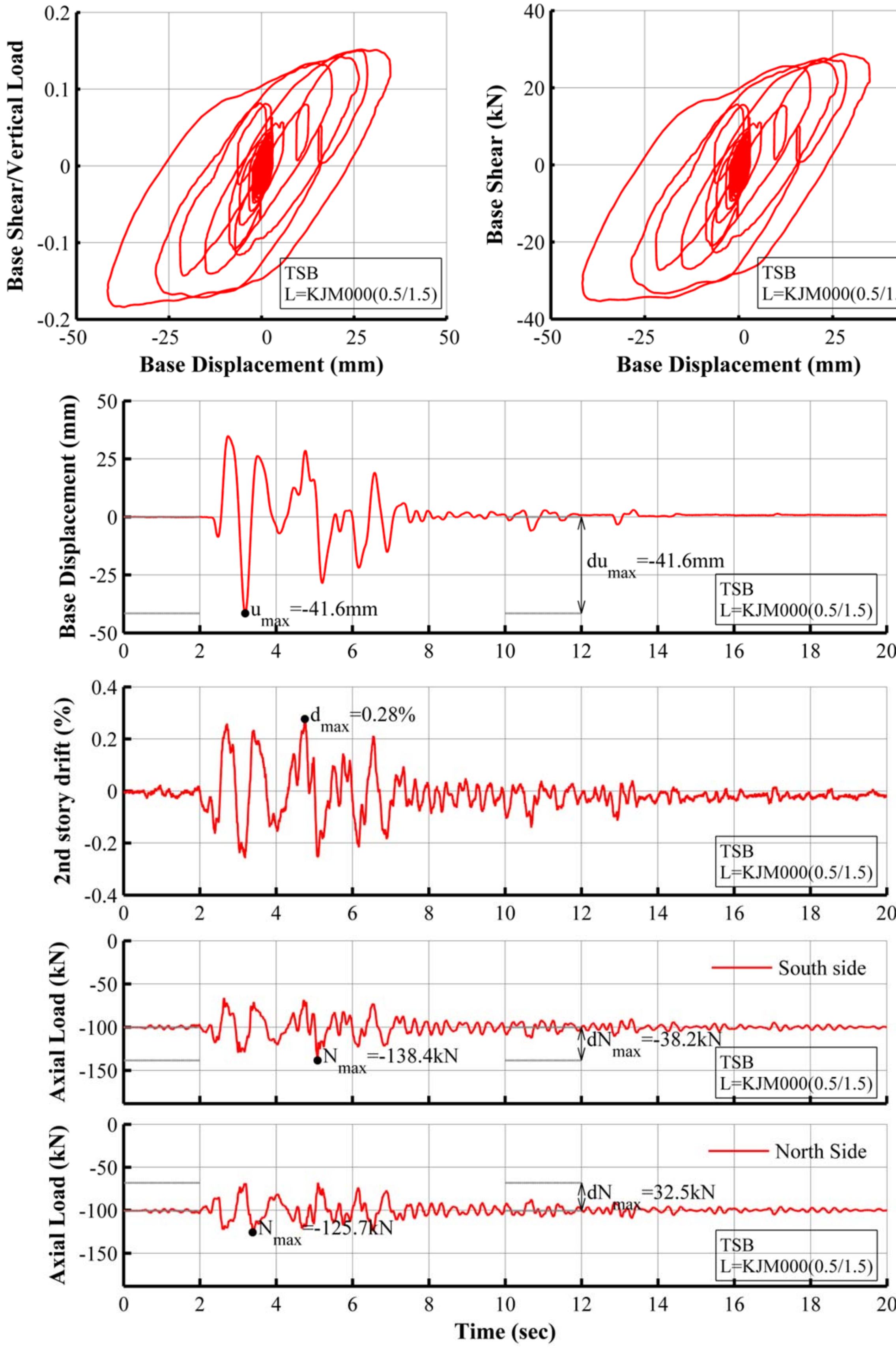

Base Shear/Vertical Load
Base Displacement (mm)
TSB
L=KJM000(0.5/1.5)
Base Shear (kN)
Base Displacement (mm)
TSB
L=KJM000(0.5/1.5)
Base Displacement (mm)
du_{max}=-41.6mm
u_{max}=-41.6mm
TSB
L=KJM000(0.5/1.5)
2nd story drift (%)
d_{max}=0.28%
TSB
L=KJM000(0.5/1.5)
Axial Load (kN)
South side
dN_{max}=-38.2kN
N_{max}=-138.4kN
TSB
L=KJM000(0.5/1.5)
Axial Load (kN)
North Side
dN_{max}=32.5kN
N_{max}=-125.7kN
TSB
L=KJM000(0.5/1.5)
Time (sec)

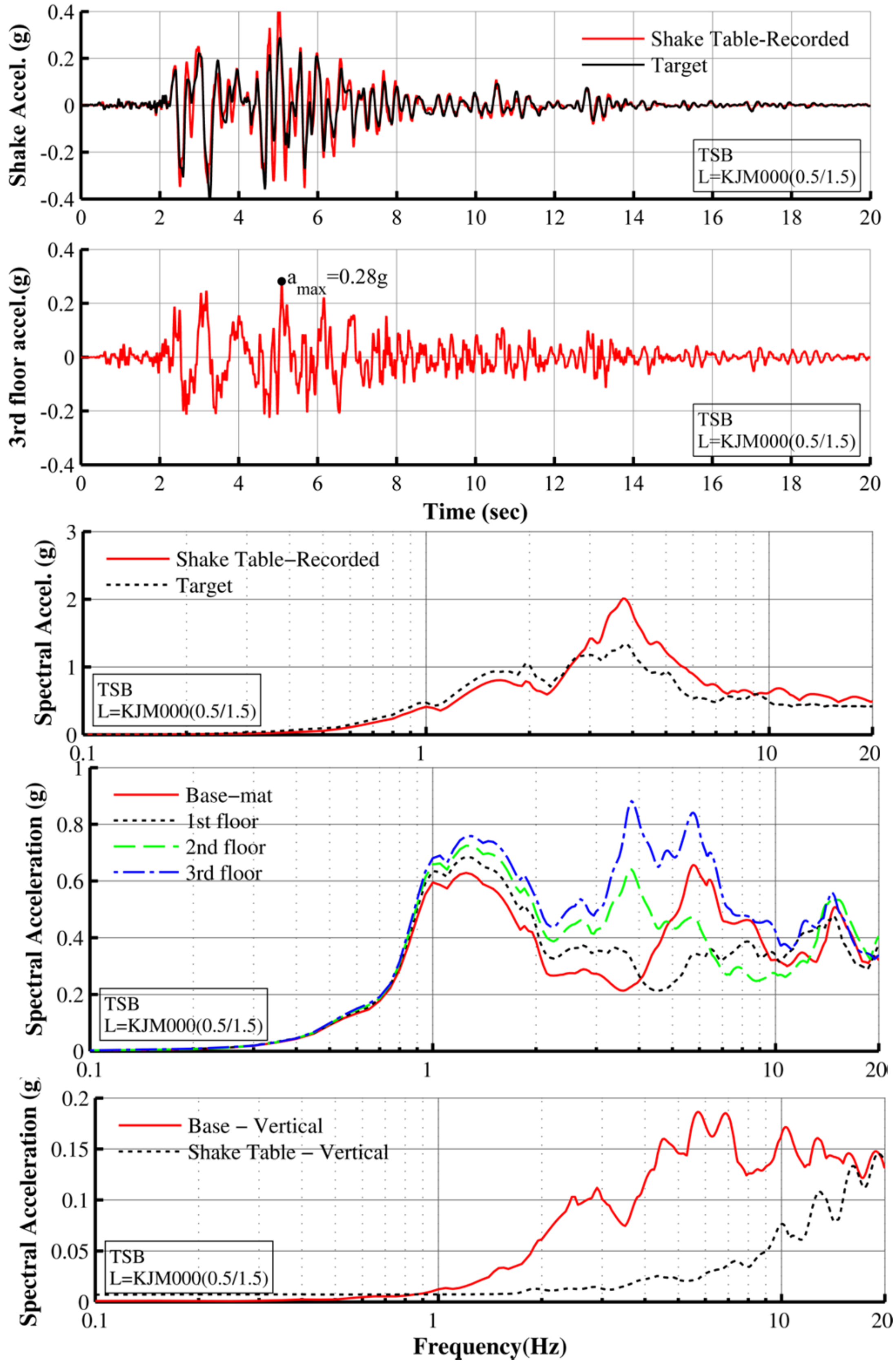

Shake Accel. (g)
Shake Table-Recorded
Target
TSB
L=KJM000(0.5/1.5)
3rd floor accel.(g)
a_{max}=0.28g
TSB
L=KJM000(0.5/1.5)
Time (sec)
Spectral Accel. (g)
Shake Table−Recorded
Target
TSB
L=KJM000(0.5/1.5)
Spectral Acceleration (g)
Base−mat
1st floor
2nd floor
3rd floor
TSB
L=KJM000(0.5/1.5)
Spectral Acceleration (g)
Base − Vertical
Shake Table − Vertical
TSB
L=KJM000(0.5/1.5)
Frequency(Hz)

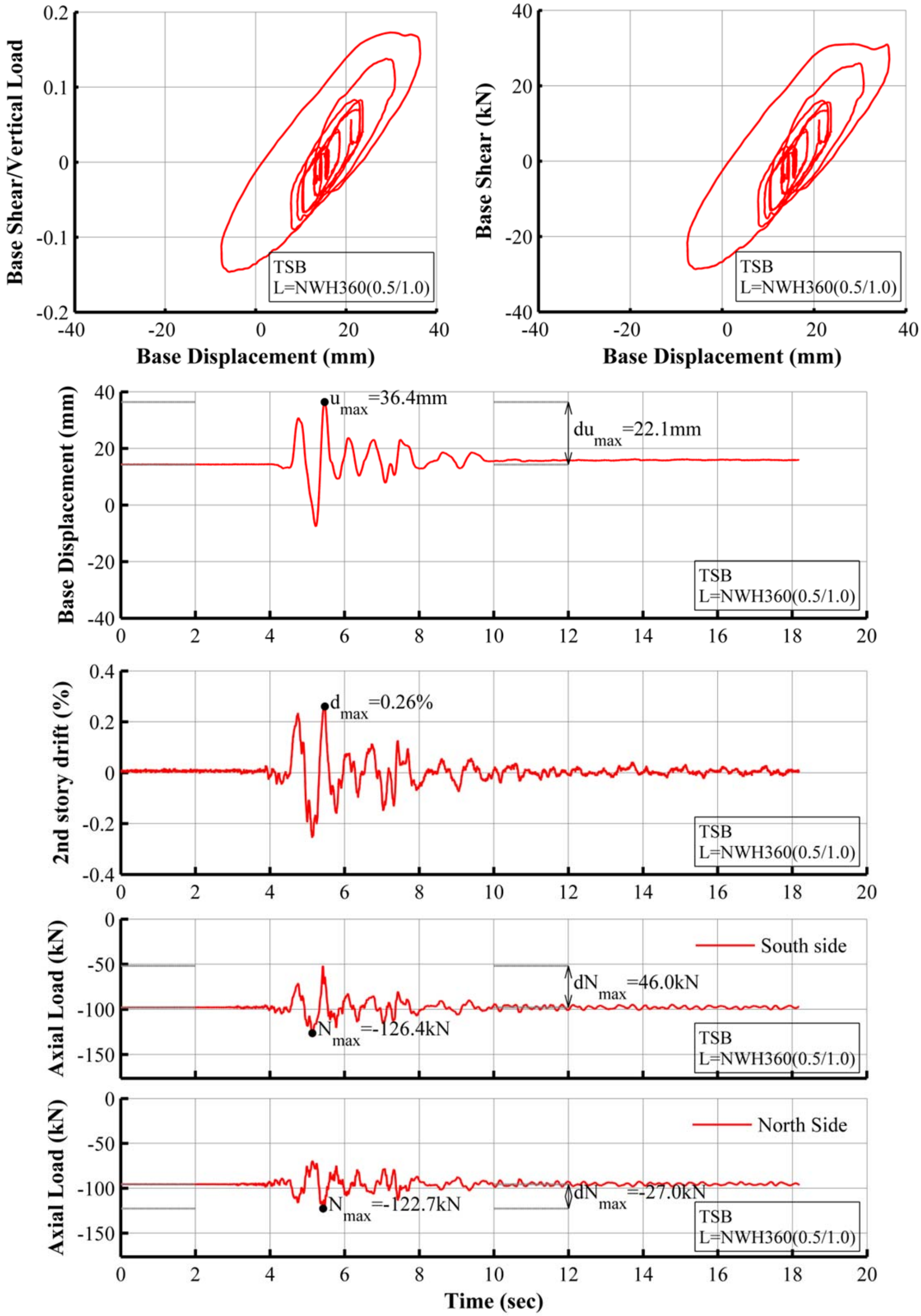
Base Shear/Vertical Load
Base Displacement (mm)
TSB
L=NWH360(0.5/1.0)
Base Shear (kN)
Base Displacement (mm)
TSB
L=NWH360(0.5/1.0)
Base Displacement (mm)
u max =36.4mm
du max =22.1mm
TSB
L=NWH360(0.5/1.0)
2nd story drift (%)
d max =0.26%
TSB
L=NWH360(0.5/1.0)
Axial Load (kN)
South side
dN max =46.0kN
N max =-126.4kN
TSB
L=NWH360(0.5/1.0)
Axial Load (kN)
North Side
N max =-122.7kN
dN max =-27.0kN
TSB
L=NWH360(0.5/1.0)
Time (sec)

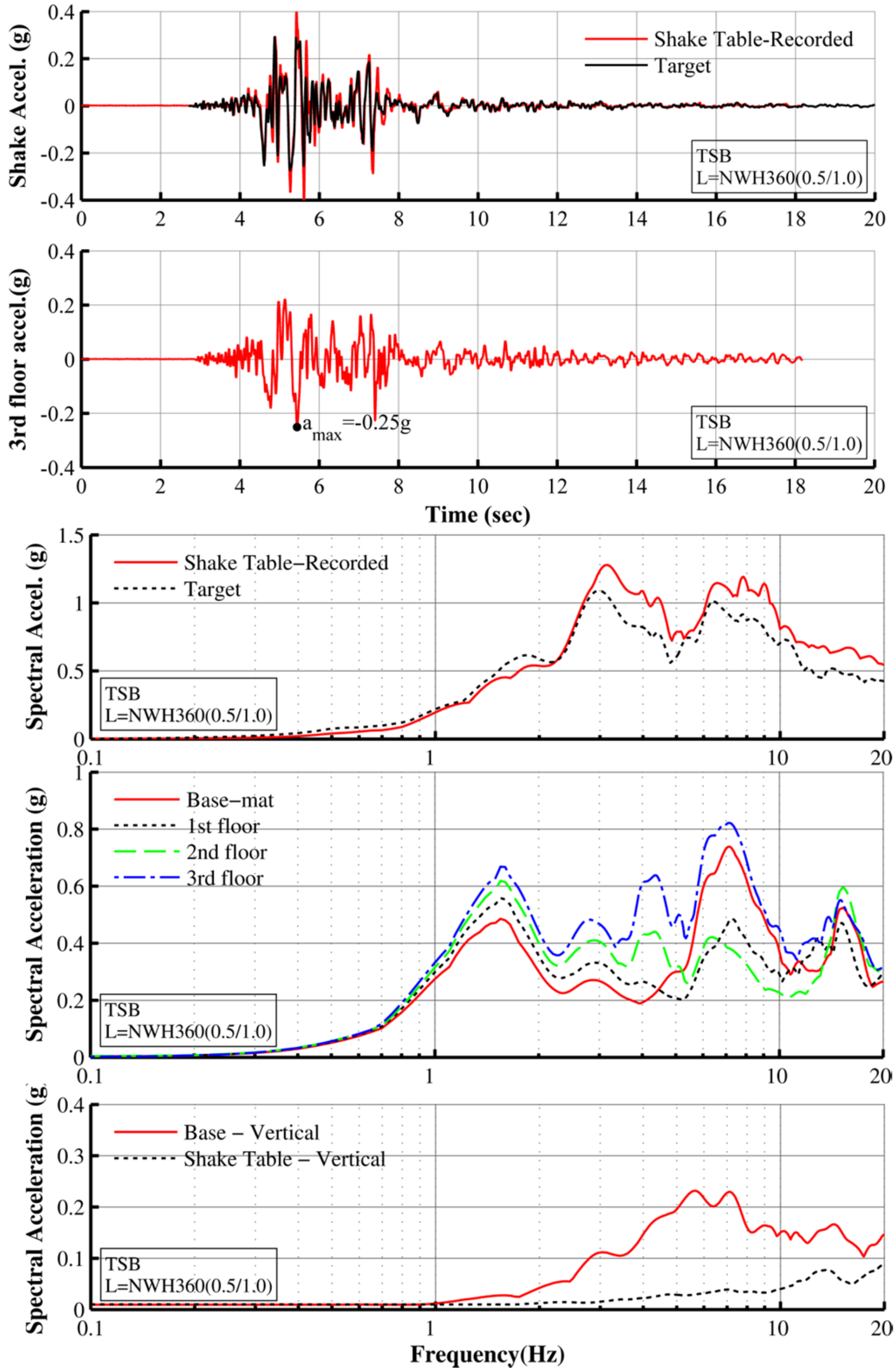
Shake Accel. (g)
Shake Table-Recorded
Target
TSB
L=NWH360(0.5/1.0)
3rd floor accel.(g)
a max =-0.25g
TSB
L=NWH360(0.5/1.0)
Time (sec)
Spectral Accel. (g)
Shake Table−Recorded
Target
TSB
L=NWH360(0.5/1.0)
Spectral Acceleration (g)
Base−mat
1st floor
2nd floor
3rd floor
TSB
L=NWH360(0.5/1.0)
Spectral Acceleration (g)
Base − Vertical
Shake Table − Vertical
TSB
L=NWH360(0.5/1.0)
Frequency(Hz)

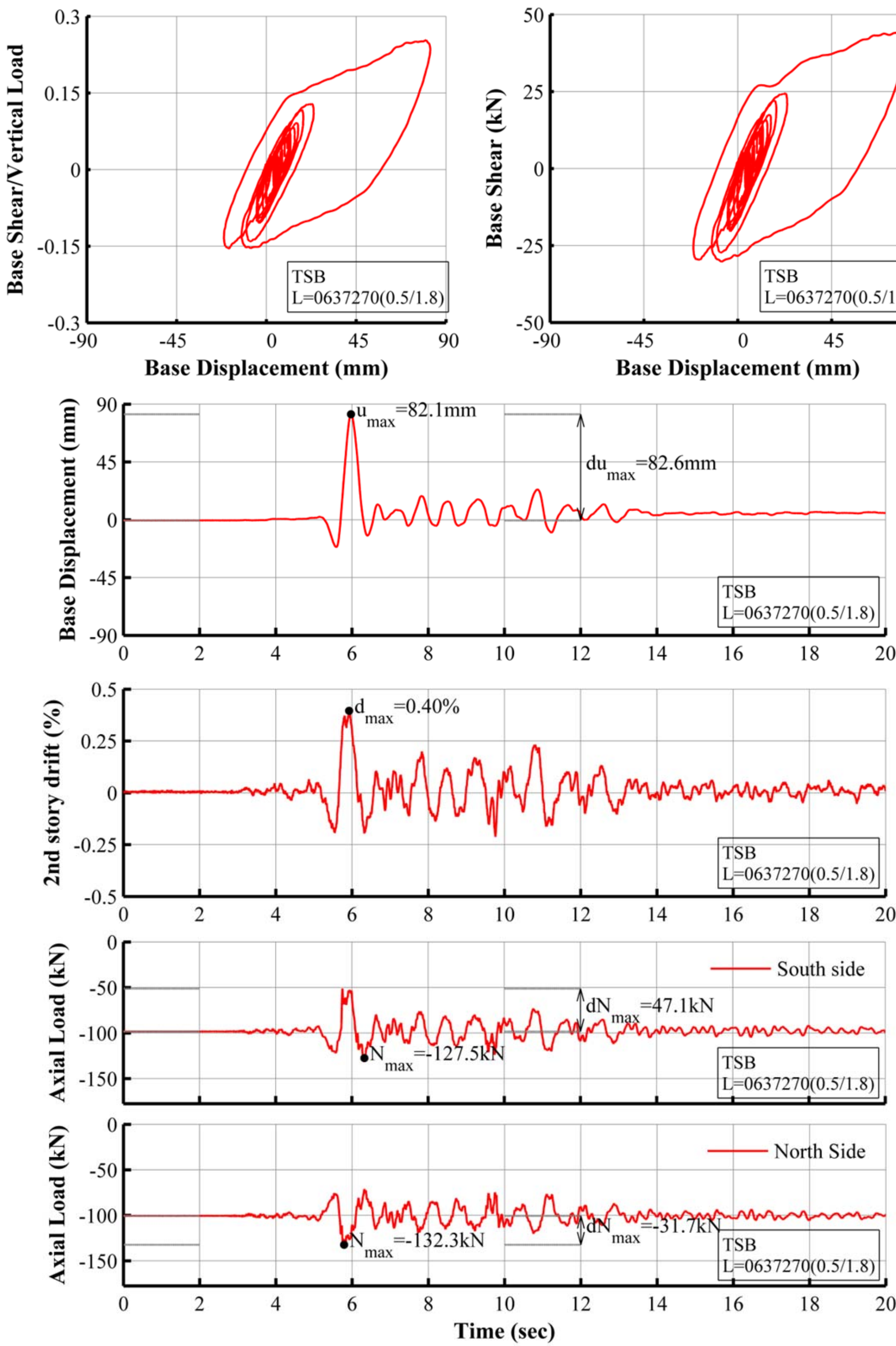
Base Shear/Vertical Load
Base Displacement (mm)
TSB
L=0637270(0.5/1.8)
Base Shear (kN)
Base Displacement (mm)
TSB
L=0637270(0.5/1.8)
Base Displacement (mm)
u max =82.1mm
du max =82.6mm
TSB
L=0637270(0.5/1.8)
2nd story drift (%)
d max =0.40%
TSB
L=0637270(0.5/1.8)
Axial Load (kN)
South side
dN max =47.1kN
N max =-127.5kN
TSB
L=0637270(0.5/1.8)
Axial Load (kN)
North Side
dN max =-31.7kN
N max =-132.3kN
TSB
L=0637270(0.5/1.8)
Time (sec)

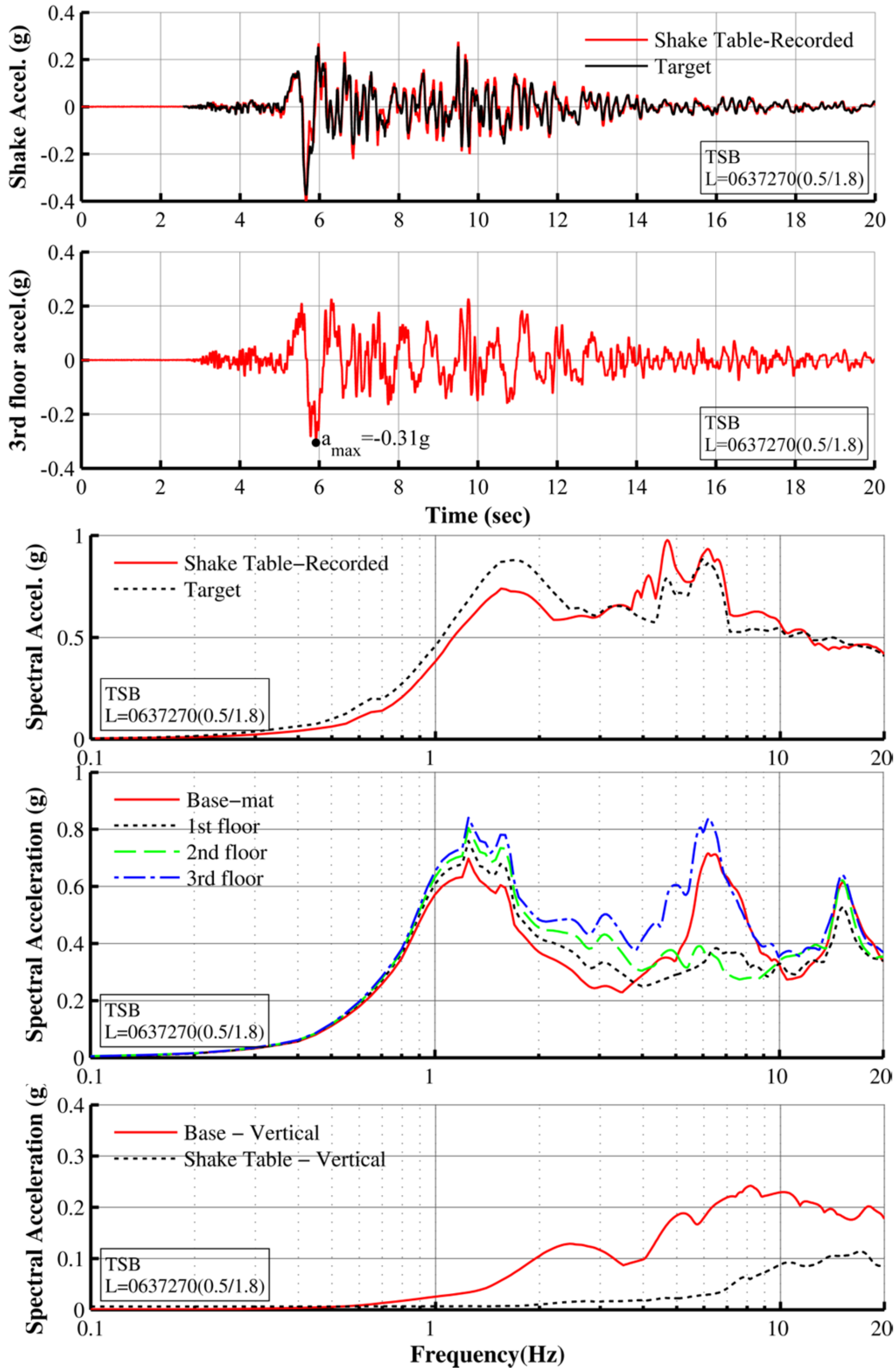
Shake Accel. (g)
Shake Table-Recorded
Target
TSB
L=0637270(0.5/1.8)
3rd floor accel.(g)
a max =-0.31g
TSB
L=0637270(0.5/1.8)
Time (sec)
Spectral Accel. (g)
Shake Table−Recorded
Target
TSB
L=0637270(0.5/1.8)
Spectral Acceleration (g)
Base−mat
1st floor
2nd floor
3rd floor
TSB
L=0637270(0.5/1.8)
Spectral Acceleration (g)
Base − Vertical
Shake Table − Vertical
TSB
L=0637270(0.5/1.8)
Frequency(Hz)

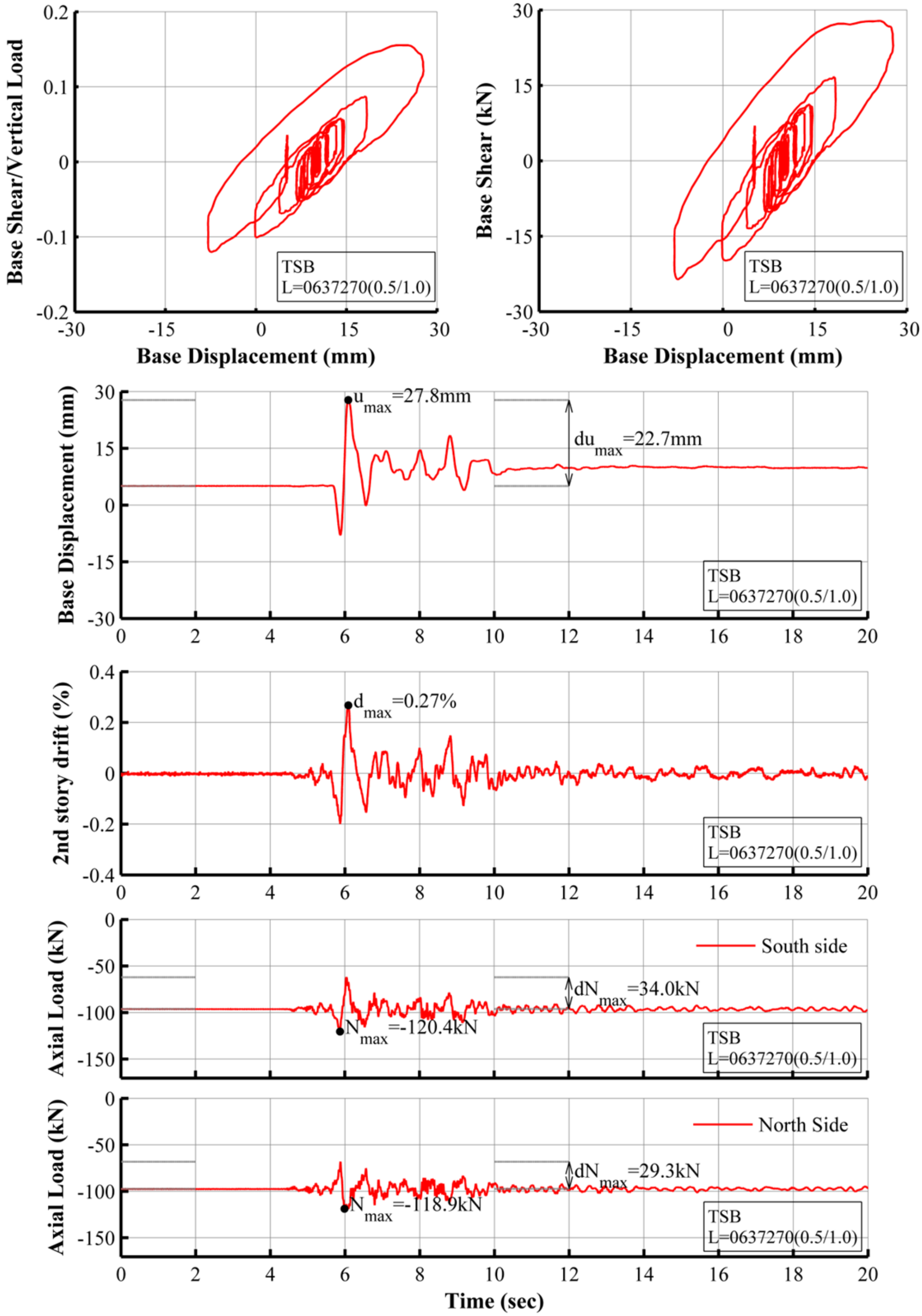
Base Shear/Vertical Load
Base Displacement (mm)
TSB
L=0637270(0.5/1.0)
Base Shear (kN)
Base Displacement (mm)
TSB
L=0637270(0.5/1.0)
Base Displacement (mm)
u max =27.8mm
du max =22.7mm
TSB
L=0637270(0.5/1.0)
2nd story drift (%)
d max =0.27%
TSB
L=0637270(0.5/1.0)
Axial Load (kN)
South side
dN max =34.0kN
N max =-120.4kN
TSB
L=0637270(0.5/1.0)
Axial Load (kN)
North Side
dN max =29.3kN
N max =-118.9kN
TSB
L=0637270(0.5/1.0)
Time (sec)

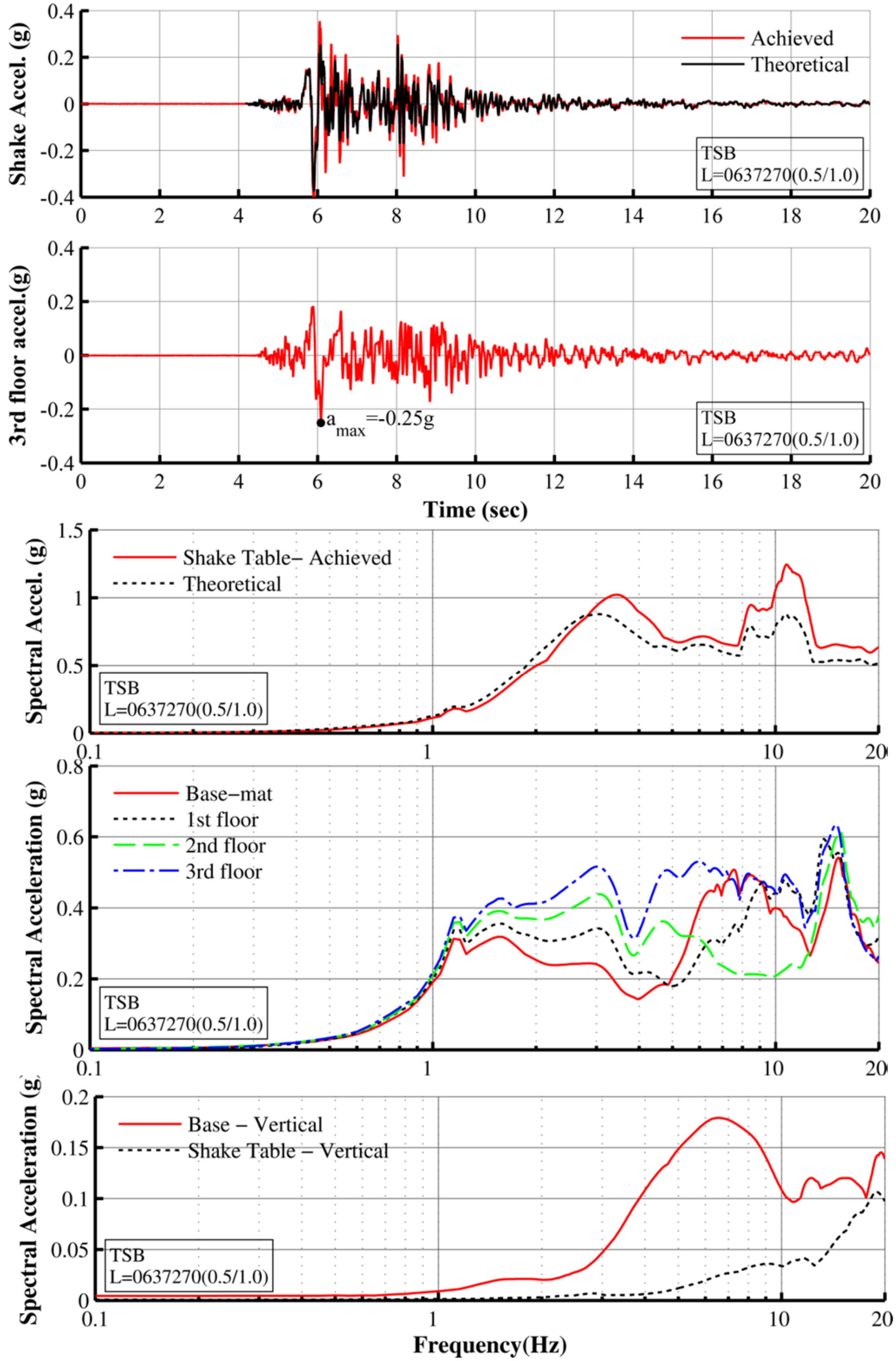
Shake Accel. (g)
Achieved
Theoretical
TSB
L=0637270(0.5/1.0)
3rd floor accel.(g)
a max =-0.25g
TSB
L=0637270(0.5/1.0)
Time (sec)
Spectral Accel. (g)
Shake Table– Achieved
Theoretical
TSB
L=0637270(0.5/1.0)
Spectral Acceleration (g)
Base–mat
1st floor
2nd floor
3rd floor
TSB
L=0637270(0.5/1.0)
Spectral Acceleration (g)
Base – Vertical
Shake Table – Vertical
TSB
L=0637270(0.5/1.0)
Frequency(Hz)

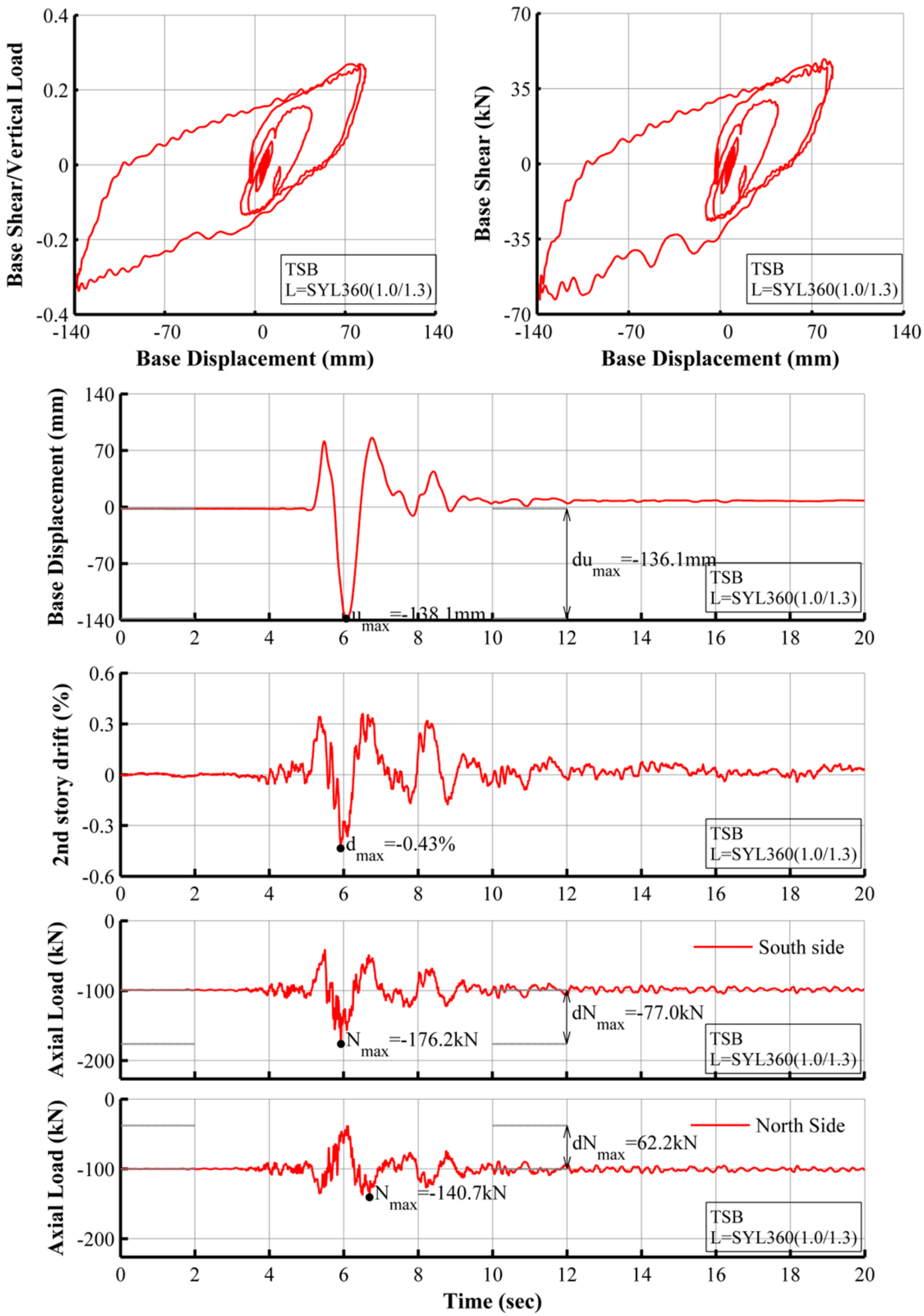
Base Shear/Vertical Load
Base Displacement (mm)
TSB
L=SYL360(1.0/1.3)
Base Shear (kN)
Base Displacement (mm)
TSB
L=SYL360(1.0/1.3)
Base Displacement (mm)
du max =-136.1mm
u max =-138.1mm
TSB
L=SYL360(1.0/1.3)
2nd story drift (%)
d max =-0.43%
TSB
L=SYL360(1.0/1.3)
Axial Load (kN)
South side
dN max =-77.0kN
N max =-176.2kN
TSB
L=SYL360(1.0/1.3)
Axial Load (kN)
North Side
dN max =62.2kN
N max =-140.7kN
TSB
L=SYL360(1.0/1.3)
Time (sec)

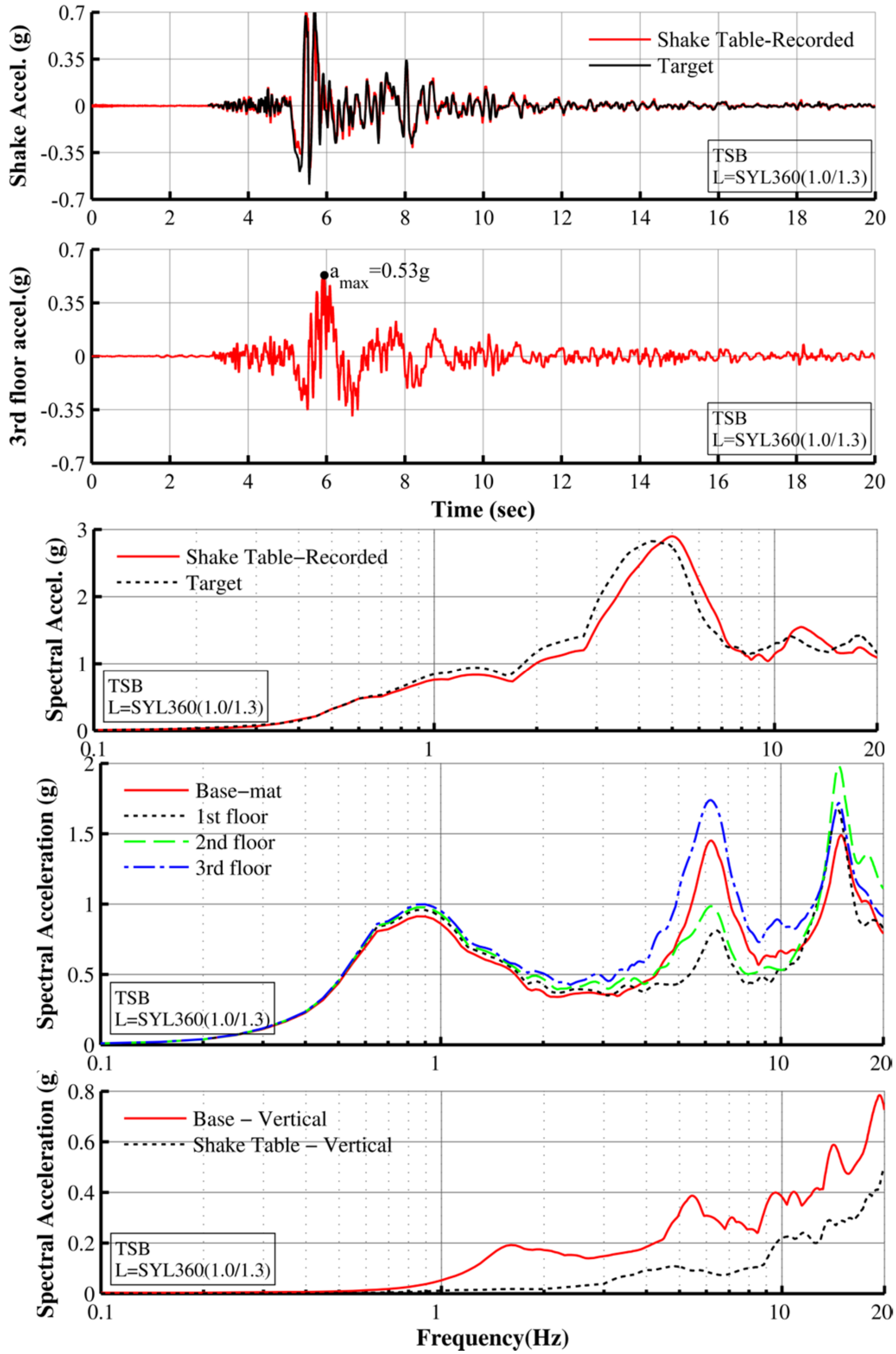
Shake Accel. (g)
Shake Table-Recorded
Target
TSB
L=SYL360(1.0/1.3)
3rd floor accel.(g)
a max =0.53g
TSB
L=SYL360(1.0/1.3)
Time (sec)
Spectral Accel. (g)
Shake Table−Recorded
Target
TSB
L=SYL360(1.0/1.3)
Spectral Acceleration (g)
Base−mat
1st floor
2nd floor
3rd floor
TSB
L=SYL360(1.0/1.3)
Spectral Acceleration (g)
Base − Vertical
Shake Table − Vertical
TSB
L=SYL360(1.0/1.3)
Frequency(Hz)

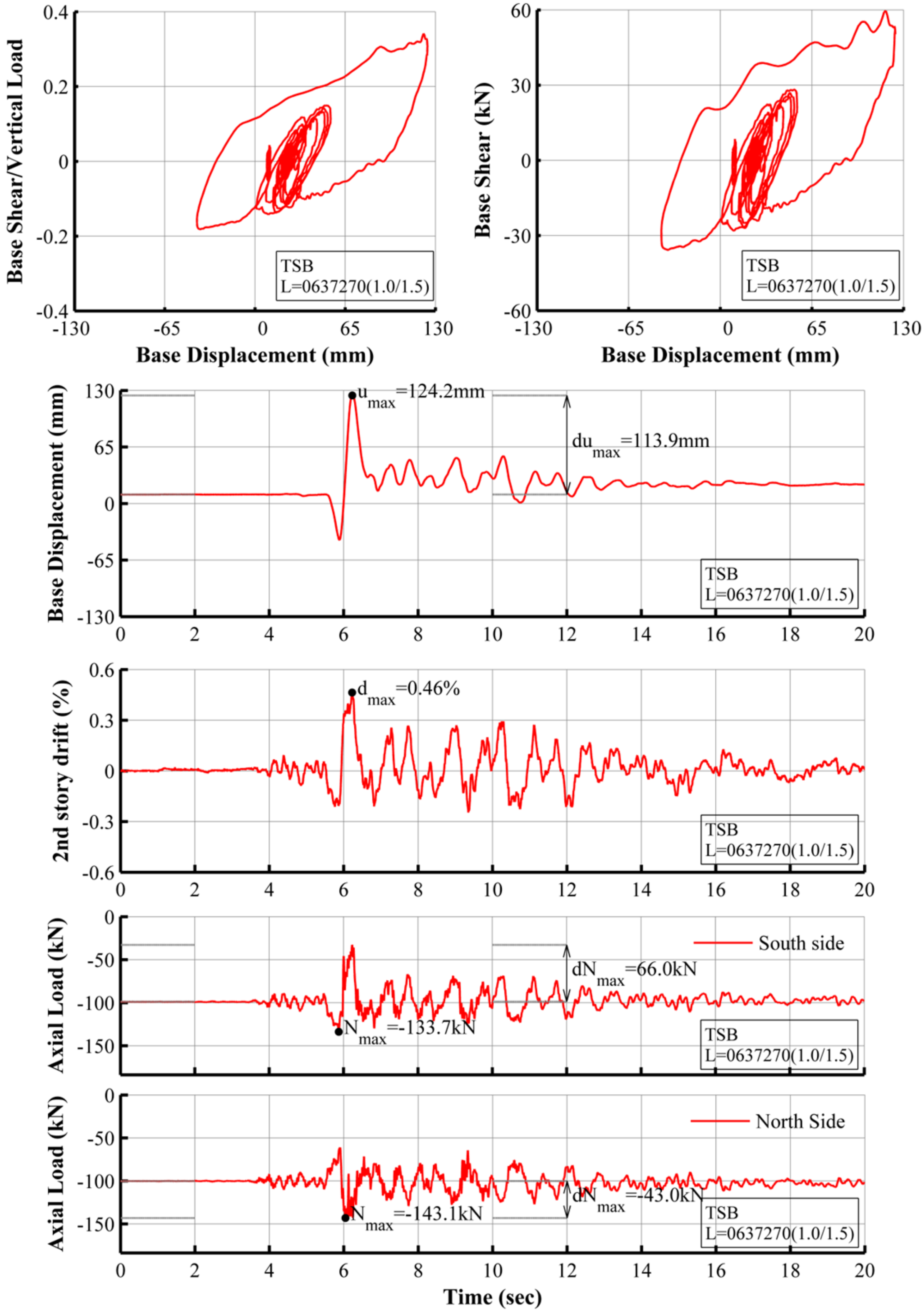

Base Shear/Vertical Load
Base Displacement (mm)
TSB
L=0637270(1.0/1.5)
Base Shear (kN)
Base Displacement (mm)
TSB
L=0637270(1.0/1.5)
Base Displacement (mm)
u max =124.2mm
du max =113.9mm
TSB
L=0637270(1.0/1.5)
2nd story drift (%)
d max =0.46%
TSB
L=0637270(1.0/1.5)
Axial Load (kN)
South side
dN max =66.0kN
N max =-133.7kN
TSB
L=0637270(1.0/1.5)
Axial Load (kN)
North Side
dN max =-43.0kN
N max =-143.1kN
TSB
L=0637270(1.0/1.5)
Time (sec)

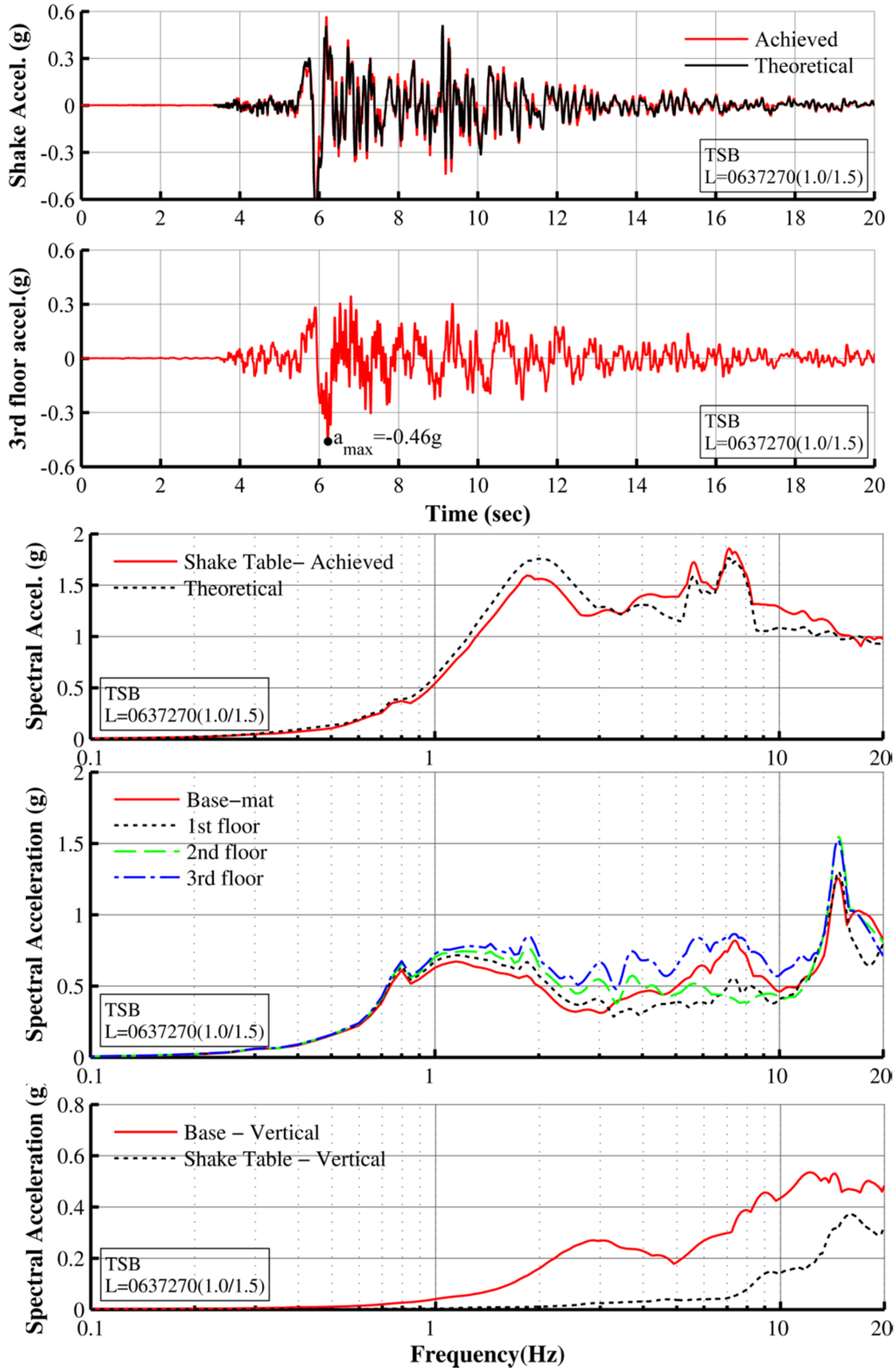

Shake Accel. (g)
Achieved
Theoretical
TSB
L=0637270(1.0/1.5)
3rd floor accel.(g)
a_{max}=-0.46g
TSB
L=0637270(1.0/1.5)
Time (sec)
Spectral Accel. (g)
Shake Table– Achieved
Theoretical
TSB
L=0637270(1.0/1.5)
Spectral Acceleration (g)
Base–mat
1st floor
2nd floor
3rd floor
TSB
L=0637270(1.0/1.5)
Spectral Acceleration (g)
Base – Vertical
Shake Table – Vertical
TSB
L=0637270(1.0/1.5)
Frequency(Hz)

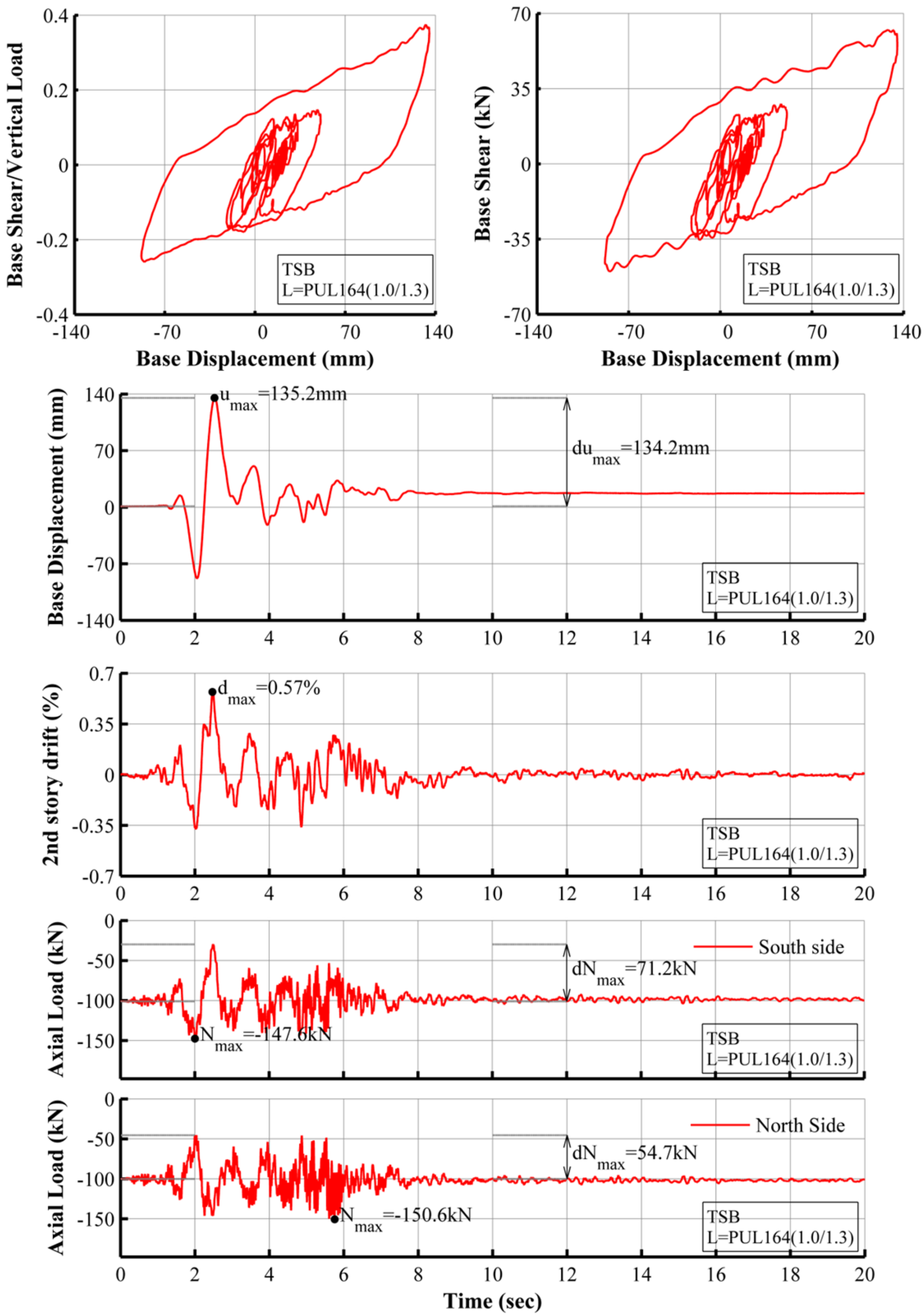

Base Shear/Vertical Load
Base Displacement (mm)
TSB
L=PUL164(1.0/1.3)
Base Shear (kN)
Base Displacement (mm)
TSB
L=PUL164(1.0/1.3)
Base Displacement (mm)
u_{max}=135.2mm
du_{max}=134.2mm
TSB
L=PUL164(1.0/1.3)
2nd story drift (%)
d_{max}=0.57%
TSB
L=PUL164(1.0/1.3)
Axial Load (kN)
South side
dN_{max}=71.2kN
N_{max}=-147.6kN
TSB
L=PUL164(1.0/1.3)
Axial Load (kN)
North Side
dN_{max}=54.7kN
N_{max}=-150.6kN
TSB
L=PUL164(1.0/1.3)
Time (sec)

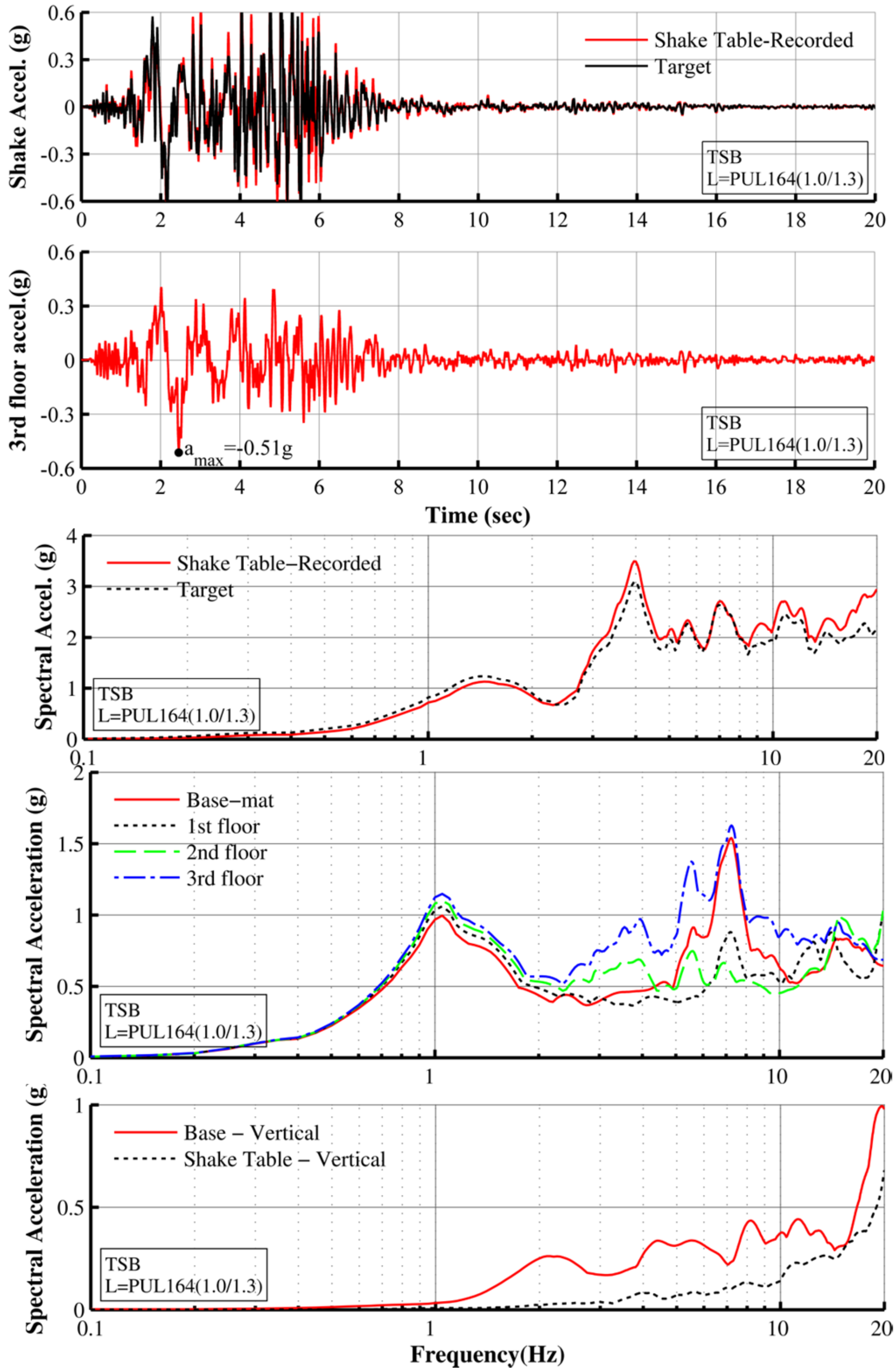
Shake Accel. (g)
Shake Table-Recorded
Target
TSB
L=PUL164(1.0/1.3)
3rd floor accel.(g)
a_{max}=-0.51g
TSB
L=PUL164(1.0/1.3)
Time (sec)
Spectral Accel. (g)
Shake Table−Recorded
Target
TSB
L=PUL164(1.0/1.3)
Spectral Acceleration (g)
Base−mat
1st floor
2nd floor
3rd floor
TSB
L=PUL164(1.0/1.3)
Spectral Acceleration (g)
Base – Vertical
Shake Table – Vertical
TSB
L=PUL164(1.0/1.3)
Frequency(Hz)

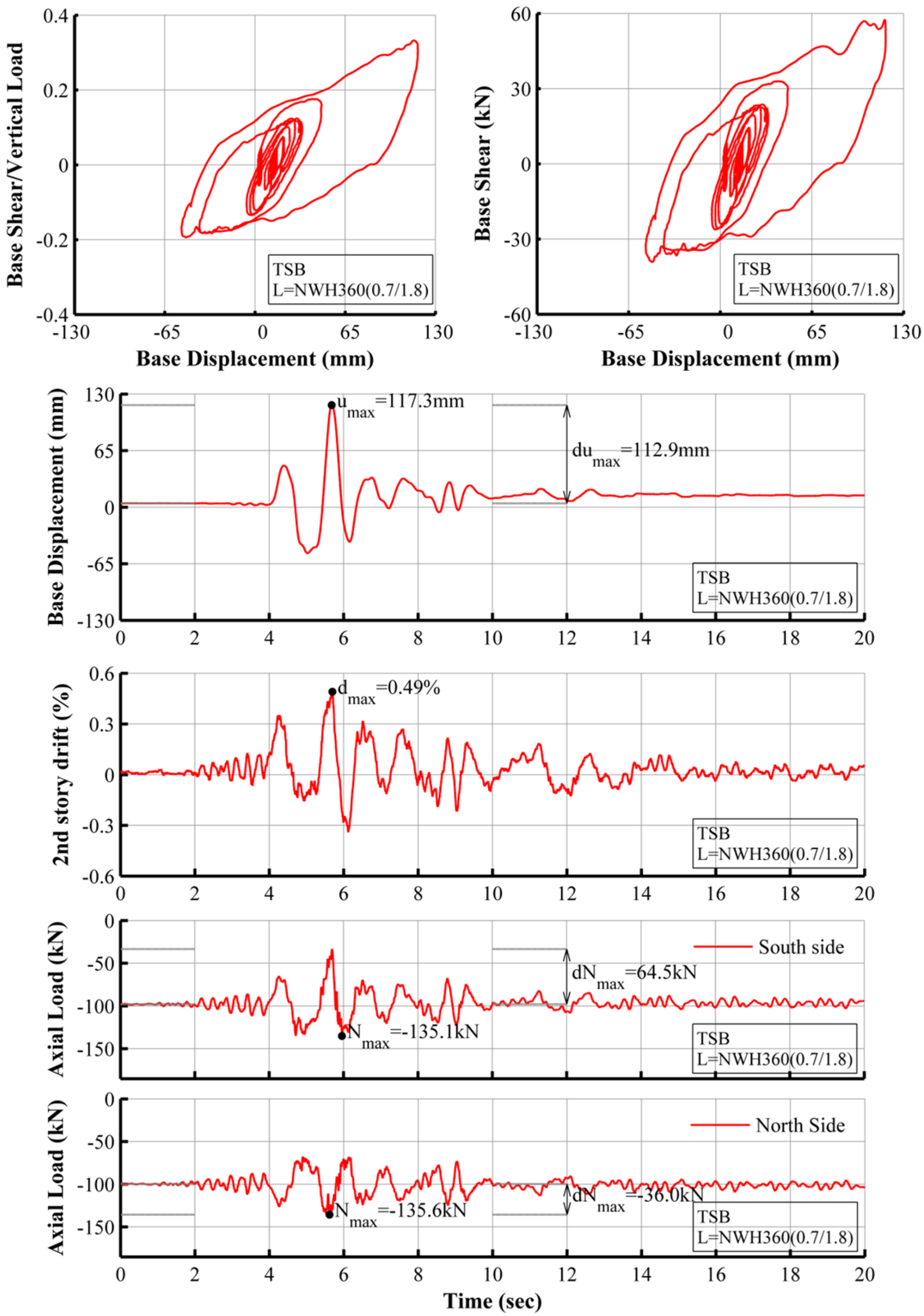

Base Shear/Vertical Load
Base Displacement (mm)
TSB
L=NWH360(0.7/1.8)
Base Shear (kN)
Base Displacement (mm)
TSB
L=NWH360(0.7/1.8)
Base Displacement (mm)
u max =117.3mm
du max =112.9mm
TSB
L=NWH360(0.7/1.8)
2nd story drift (%)
d max =0.49%
TSB
L=NWH360(0.7/1.8)
Axial Load (kN)
South side
dN max =64.5kN
N max =-135.1kN
TSB
L=NWH360(0.7/1.8)
Axial Load (kN)
North Side
dN max =-36.0kN
N max =-135.6kN
TSB
L=NWH360(0.7/1.8)
Time (sec)

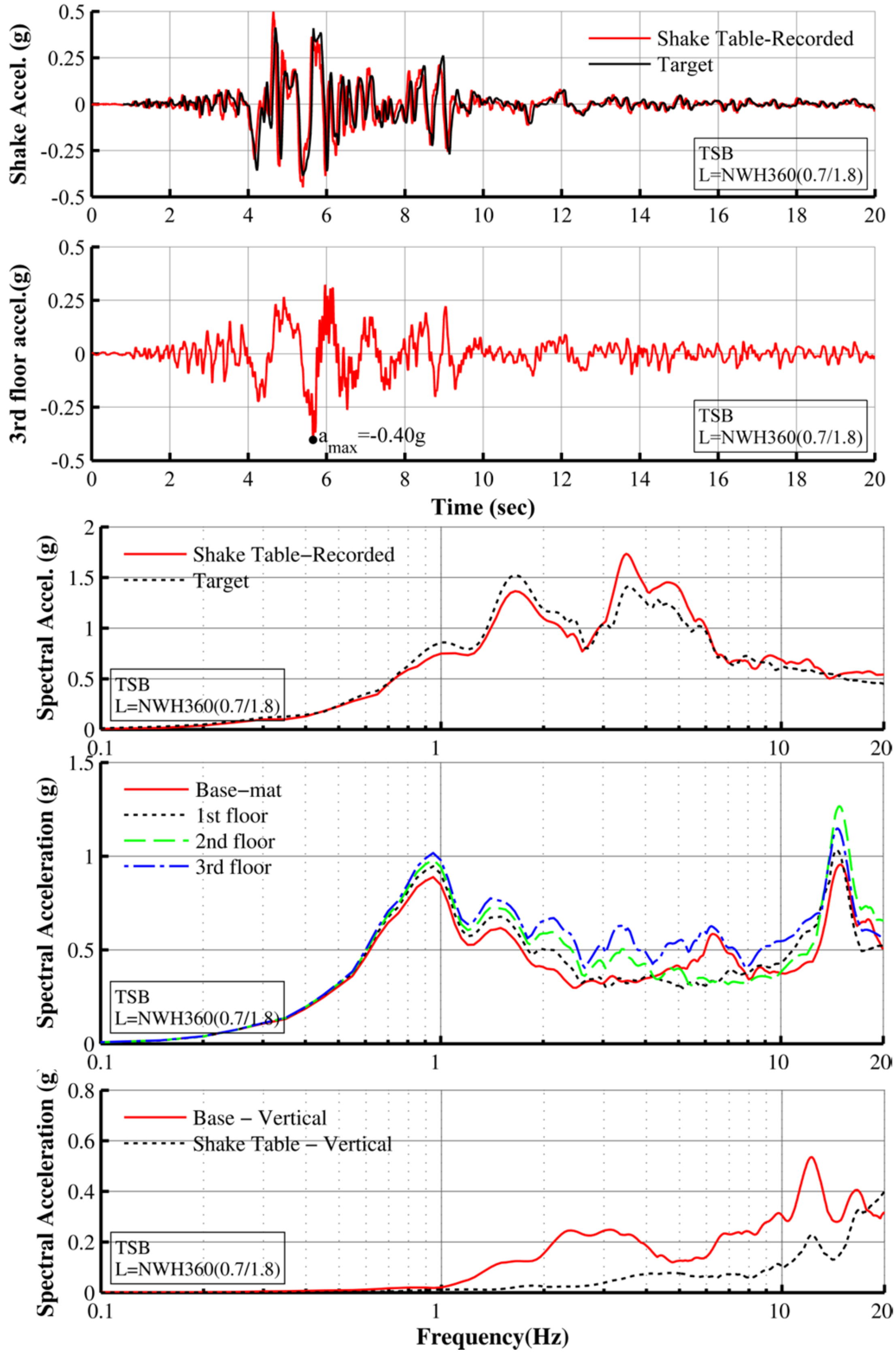

Shake Accel. (g)
Shake Table-Recorded
Target
TSB
L=NWH360(0.7/1.8)
3rd floor accel.(g)
a_{max}=-0.40g
TSB
L=NWH360(0.7/1.8)
Time (sec)
Spectral Accel. (g)
Shake Table−Recorded
Target
TSB
L=NWH360(0.7/1.8)
Spectral Acceleration (g)
Base−mat
1st floor
2nd floor
3rd floor
TSB
L=NWH360(0.7/1.8)
Spectral Acceleration (g)
Base − Vertical
Shake Table − Vertical
TSB
L=NWH360(0.7/1.8)
Frequency(Hz)

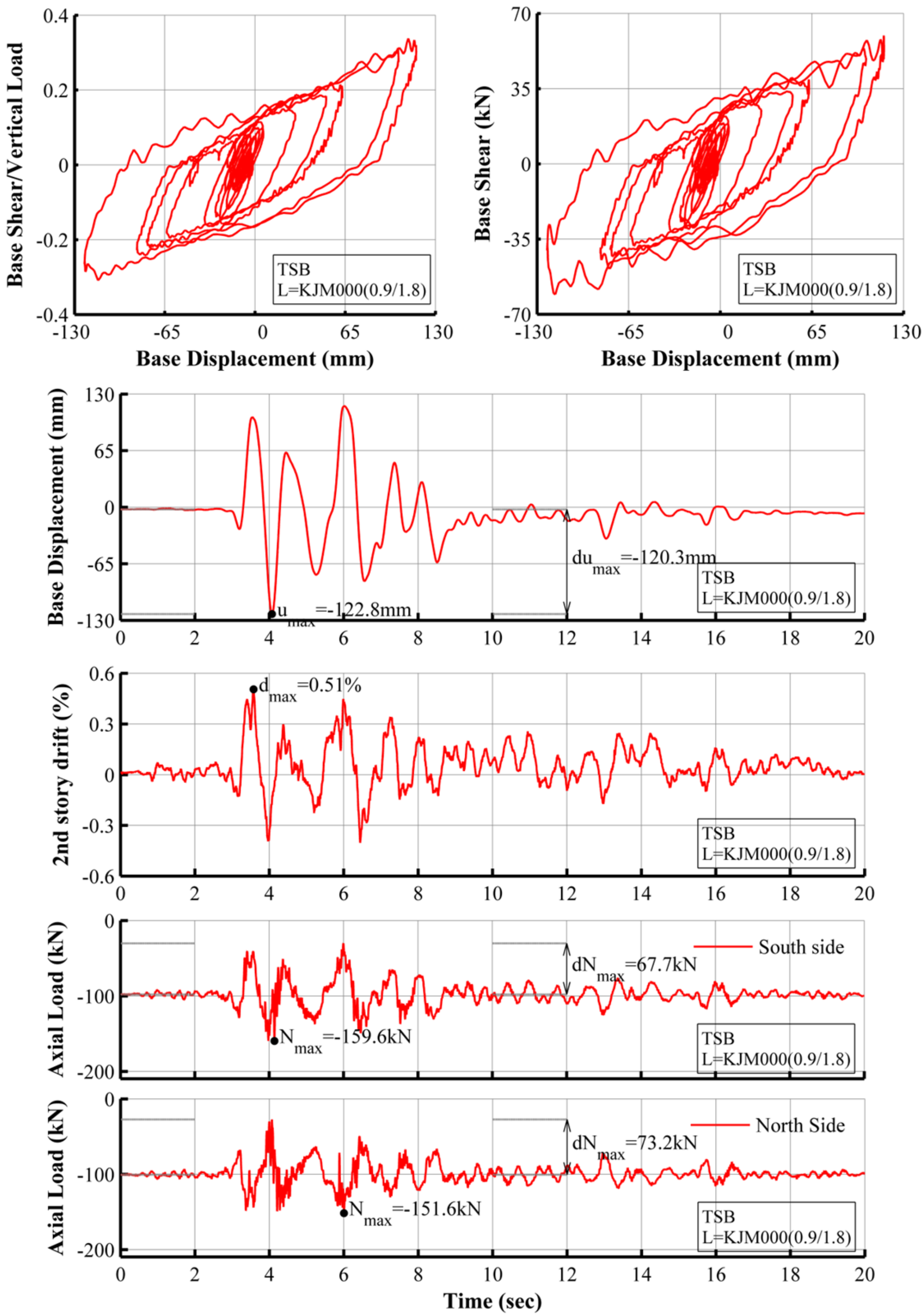
Base Shear/Vertical Load
Base Displacement (mm)
TSB
L=KJM000(0.9/1.8)
Base Shear (kN)
Base Displacement (mm)
TSB
L=KJM000(0.9/1.8)
Base Displacement (mm)
du$_{max}$=-120.3mm
u$_{max}$=-122.8mm
TSB
L=KJM000(0.9/1.8)
2nd story drift (%)
d$_{max}$=0.51%
TSB
L=KJM000(0.9/1.8)
Axial Load (kN)
South side
dN$_{max}$=67.7kN
N$_{max}$=-159.6kN
TSB
L=KJM000(0.9/1.8)
Axial Load (kN)
North Side
dN$_{max}$=73.2kN
N$_{max}$=-151.6kN
TSB
L=KJM000(0.9/1.8)
Time (sec)

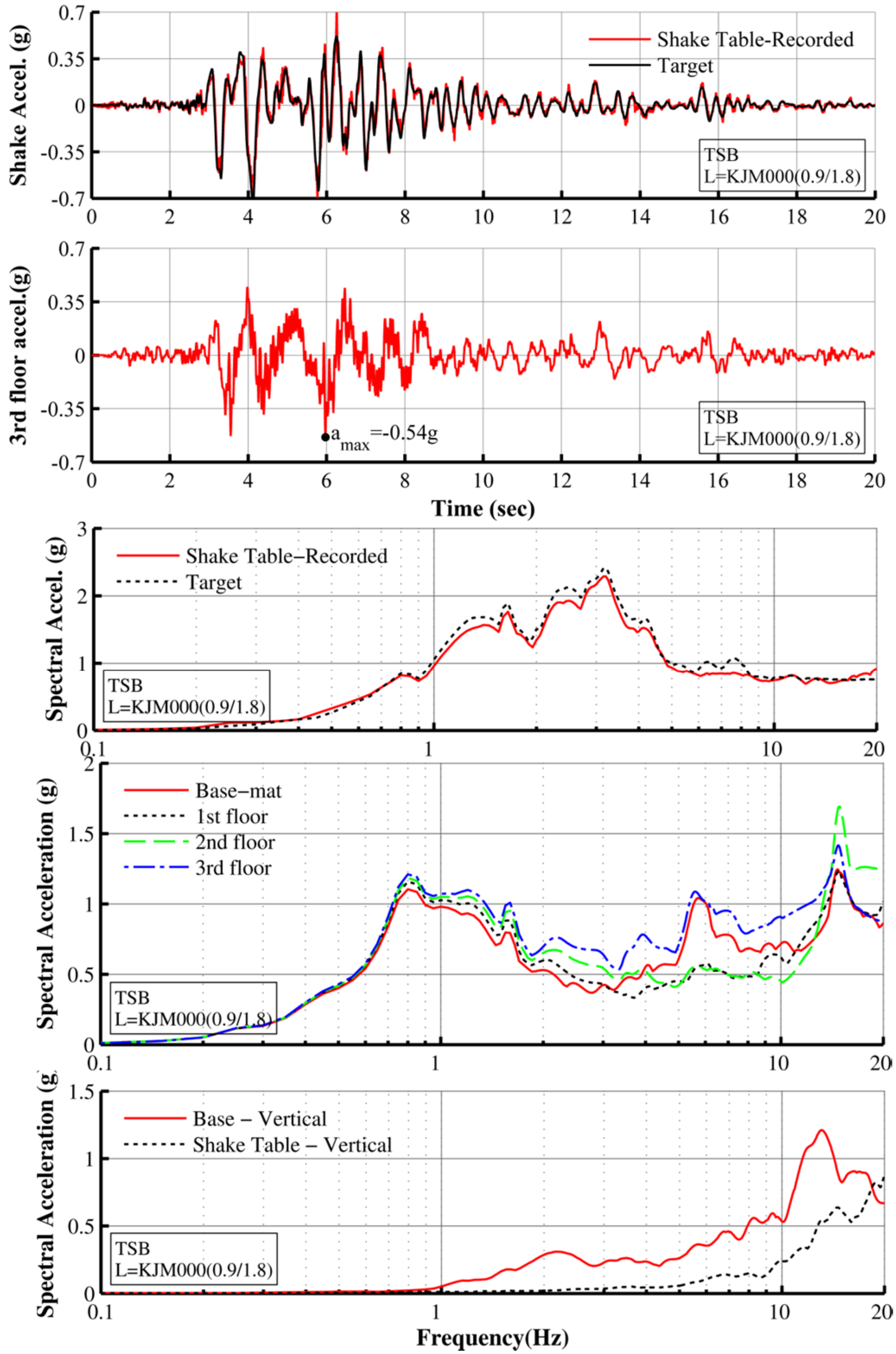
Shake Accel. (g)
Shake Table-Recorded
Target
TSB
L=KJM000(0.9/1.8)
3rd floor accel.(g)
a max =-0.54g
TSB
L=KJM000(0.9/1.8)
Time (sec)
Spectral Accel. (g)
Shake Table−Recorded
Target
TSB
L=KJM000(0.9/1.8)
Spectral Acceleration (g)
Base−mat
1st floor
2nd floor
3rd floor
TSB
L=KJM000(0.9/1.8)
Spectral Acceleration (g)
Base − Vertical
Shake Table − Vertical
TSB
L=KJM000(0.9/1.8)
Frequency(Hz)

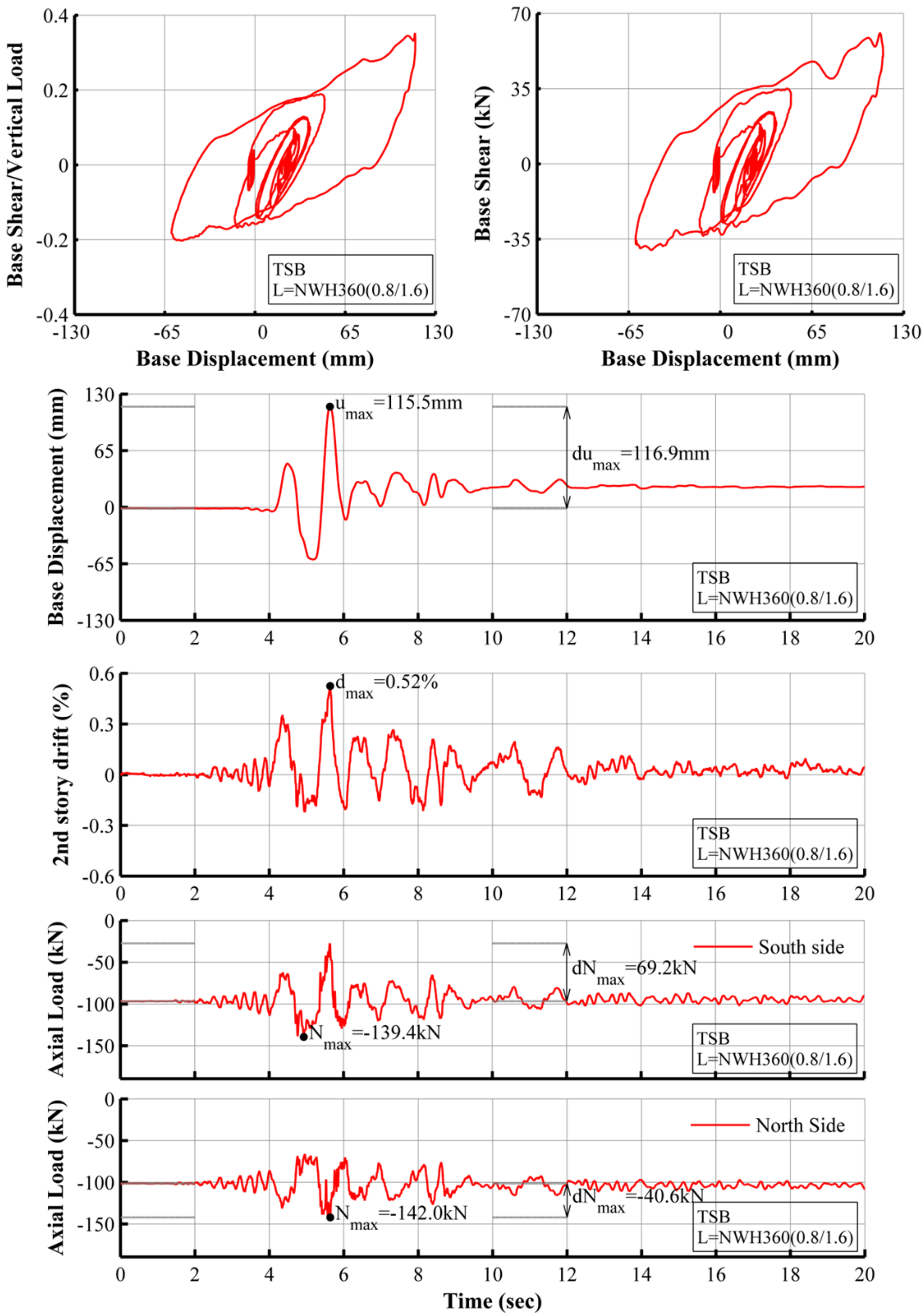

Base Shear/Vertical Load
Base Displacement (mm)
TSB
L=NWH360(0.8/1.6)
Base Shear (kN)
Base Displacement (mm)
TSB
L=NWH360(0.8/1.6)
Base Displacement (mm)
u max =115.5mm
du max =116.9mm
TSB
L=NWH360(0.8/1.6)
2nd story drift (%)
d max =0.52%
TSB
L=NWH360(0.8/1.6)
Axial Load (kN)
South side
dN max =69.2kN
N max =-139.4kN
TSB
L=NWH360(0.8/1.6)
Axial Load (kN)
North Side
dN max =-40.6kN
N max =-142.0kN
TSB
L=NWH360(0.8/1.6)
Time (sec)

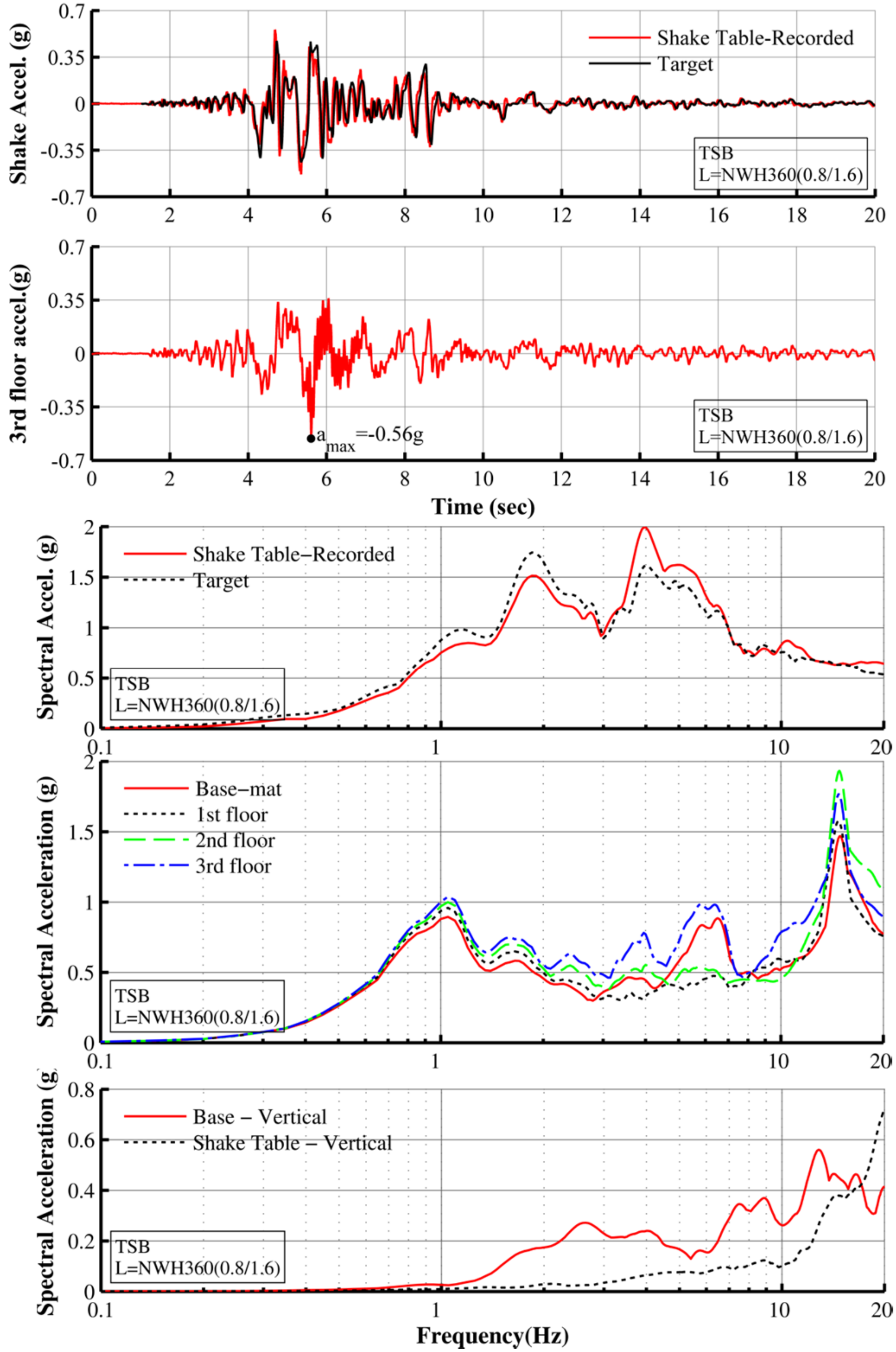
Shake Accel. (g)
Shake Table-Recorded
Target
TSB
L=NWH360(0.8/1.6)
3rd floor accel.(g)
a max =-0.56g
TSB
L=NWH360(0.8/1.6)
Time (sec)
Spectral Accel. (g)
Shake Table−Recorded
Target
TSB
L=NWH360(0.8/1.6)
Spectral Acceleration (g)
Base−mat
1st floor
2nd floor
3rd floor
TSB
L=NWH360(0.8/1.6)
Spectral Acceleration (g)
Base − Vertical
Shake Table − Vertical
TSB
L=NWH360(0.8/1.6)
Frequency(Hz)

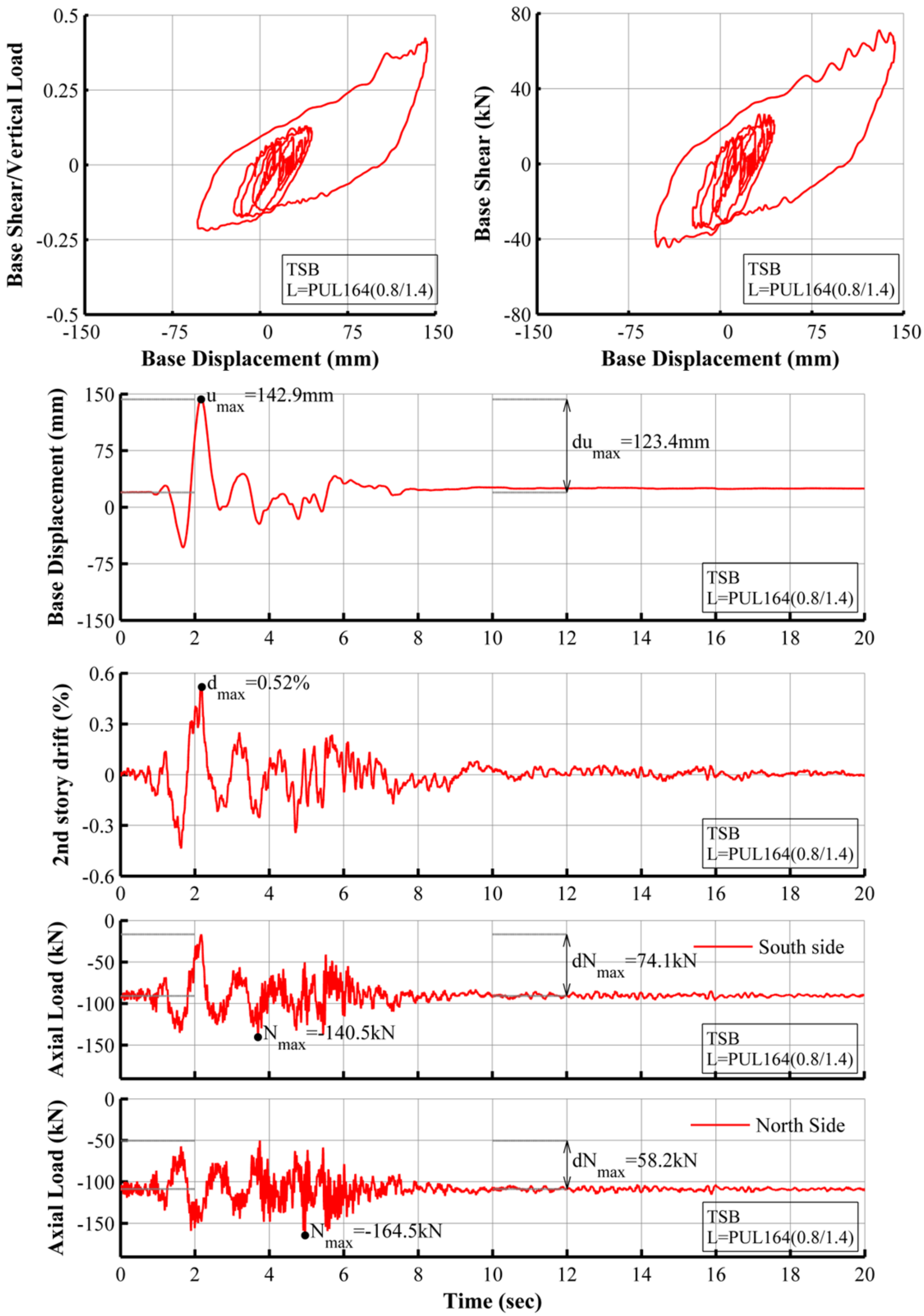
Base Shear/Vertical Load
0.5
0.25
0
-0.25
-0.5
-150
-75
0
75
150
Base Displacement (mm)
TSB
L=PUL164(0.8/1.4)
Base Shear (kN)
80
40
0
-40
-80
Base Displacement (mm)
TSB
L=PUL164(0.8/1.4)
Base Displacement (mm)
150
75
0
-75
-150
u max =142.9mm
du max =123.4mm
TSB
L=PUL164(0.8/1.4)
2nd story drift (%)
0.6
0.3
0
-0.3
-0.6
d max =0.52%
TSB
L=PUL164(0.8/1.4)
Axial Load (kN)
0
-50
-100
-150
South side
dN max =74.1kN
N max =-140.5kN
TSB
L=PUL164(0.8/1.4)
Axial Load (kN)
North Side
dN max =58.2kN
N max =-164.5kN
TSB
L=PUL164(0.8/1.4)
0
2
4
6
8
10
12
14
16
18
20
Time (sec)

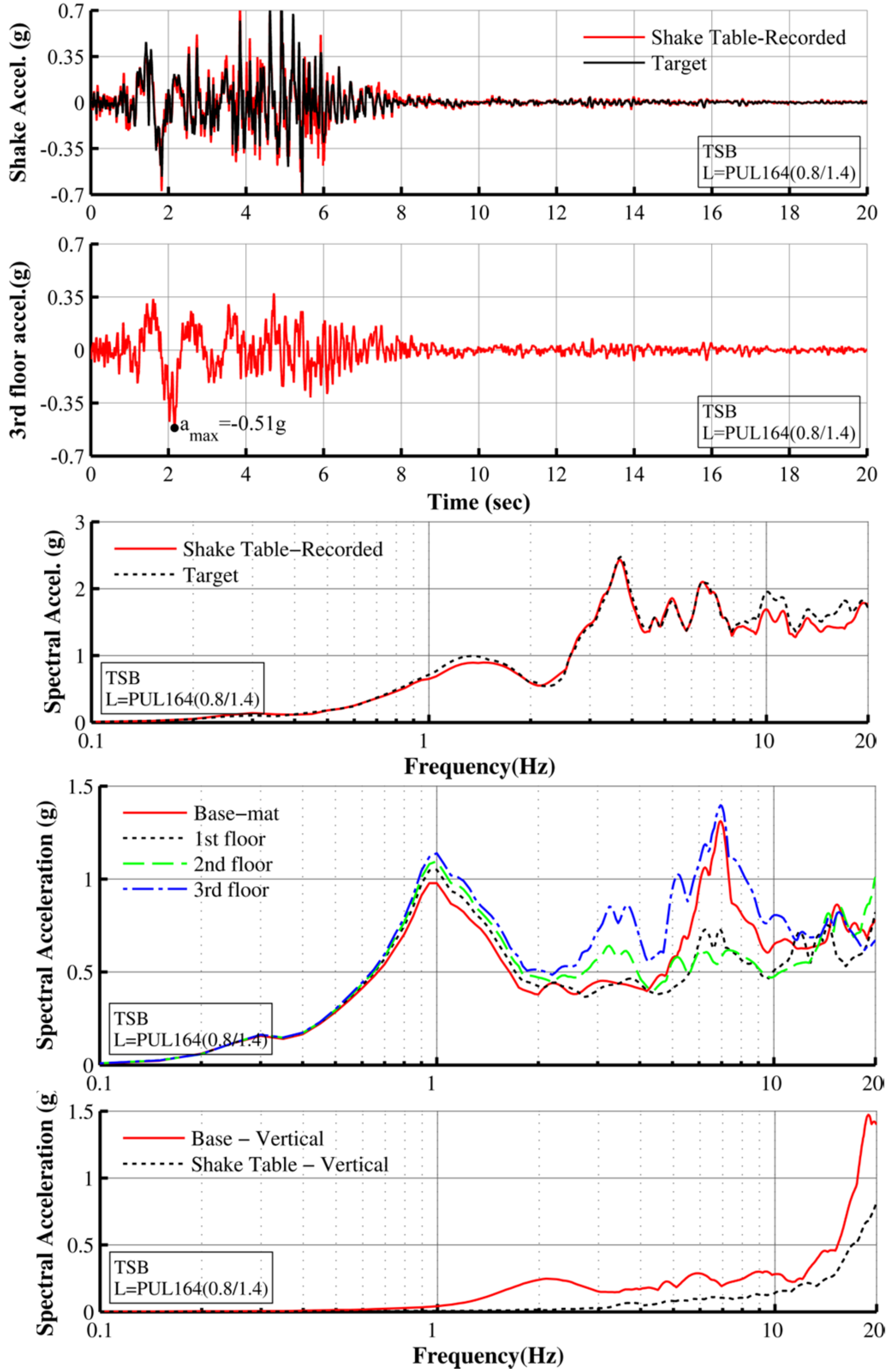
Shake Accel. (g)
Shake Table-Recorded
Target
TSB
L=PUL164(0.8/1.4)
3rd floor accel.(g)
a_{max}=-0.51g
TSB
L=PUL164(0.8/1.4)
Time (sec)
Spectral Accel. (g)
Shake Table−Recorded
Target
TSB
L=PUL164(0.8/1.4)
Frequency(Hz)
Spectral Acceleration (g)
Base−mat
1st floor
2nd floor
3rd floor
TSB
L=PUL164(0.8/1.4)
Spectral Acceleration (g)
Base – Vertical
Shake Table – Vertical
TSB
L=PUL164(0.8/1.4)
Frequency(Hz)

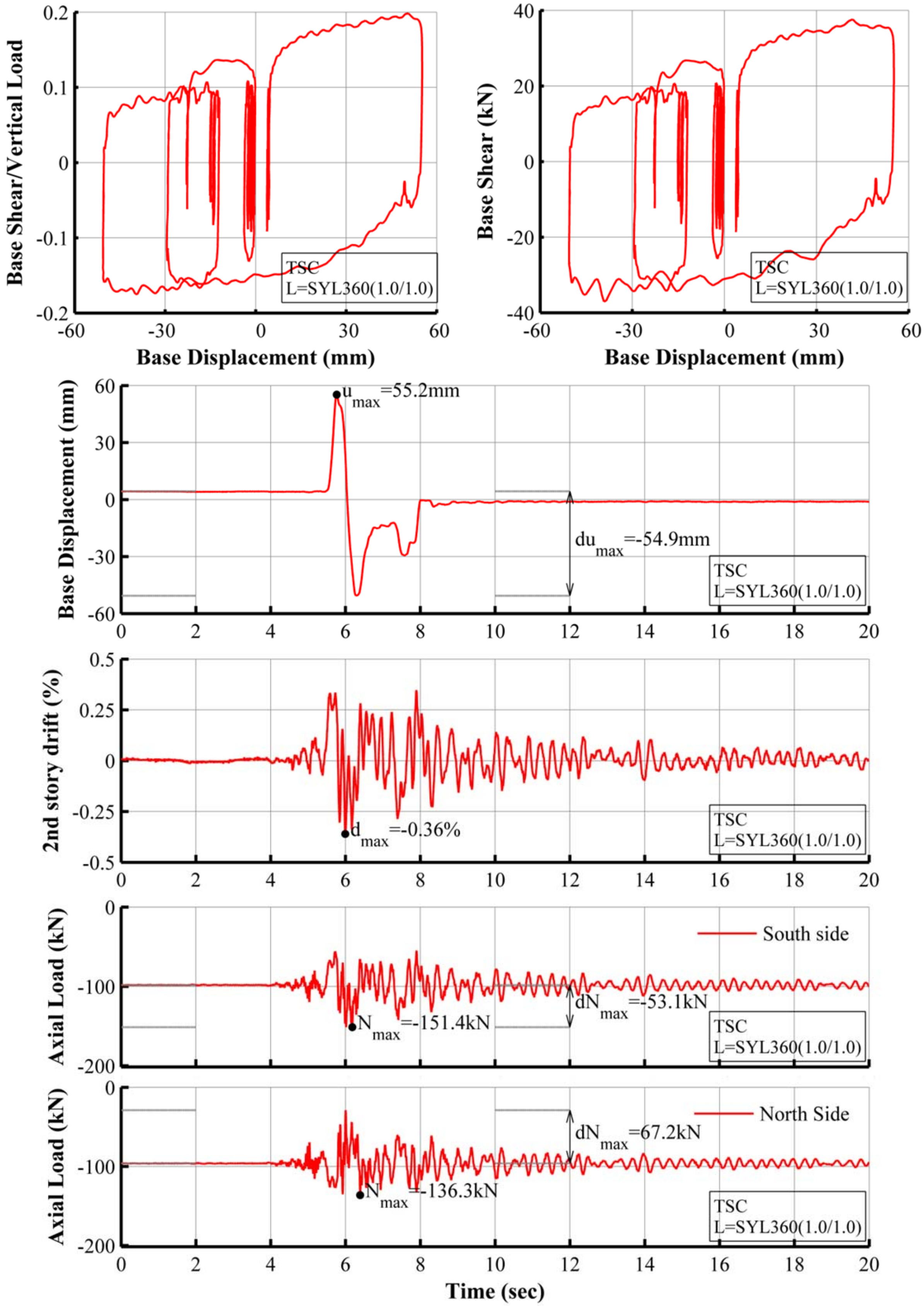

Base Shear/Vertical Load
Base Displacement (mm)
TSC
L=SYL360(1.0/1.0)
Base Shear (kN)
Base Displacement (mm)
TSC
L=SYL360(1.0/1.0)
Base Displacement (mm)
u_{max}=55.2mm
du_{max}=-54.9mm
TSC
L=SYL360(1.0/1.0)
2nd story drift (%)
d_{max}=-0.36%
TSC
L=SYL360(1.0/1.0)
Axial Load (kN)
South side
N_{max}=-151.4kN
dN_{max}=-53.1kN
TSC
L=SYL360(1.0/1.0)
Axial Load (kN)
North Side
dN_{max}=67.2kN
N_{max}=-136.3kN
TSC
L=SYL360(1.0/1.0)
Time (sec)

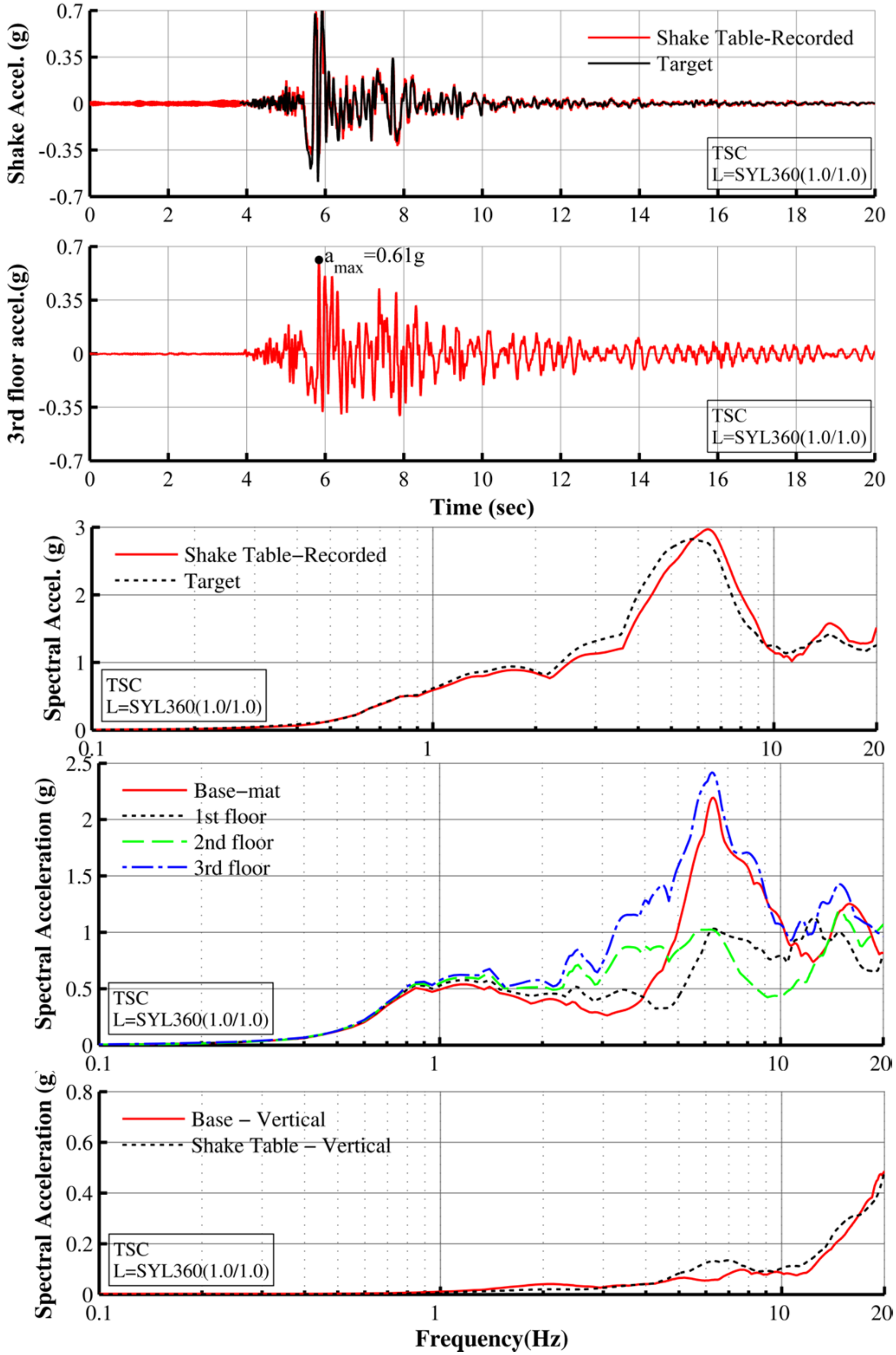
Shake Accel. (g)
Shake Table-Recorded
Target
TSC
L=SYL360(1.0/1.0)
3rd floor accel.(g)
a_{max}=0.61g
TSC
L=SYL360(1.0/1.0)
Time (sec)
Spectral Accel. (g)
Shake Table−Recorded
Target
TSC
L=SYL360(1.0/1.0)
Spectral Acceleration (g)
Base−mat
1st floor
2nd floor
3rd floor
TSC
L=SYL360(1.0/1.0)
Spectral Acceleration (g)
Base − Vertical
Shake Table − Vertical
TSC
L=SYL360(1.0/1.0)
Frequency(Hz)

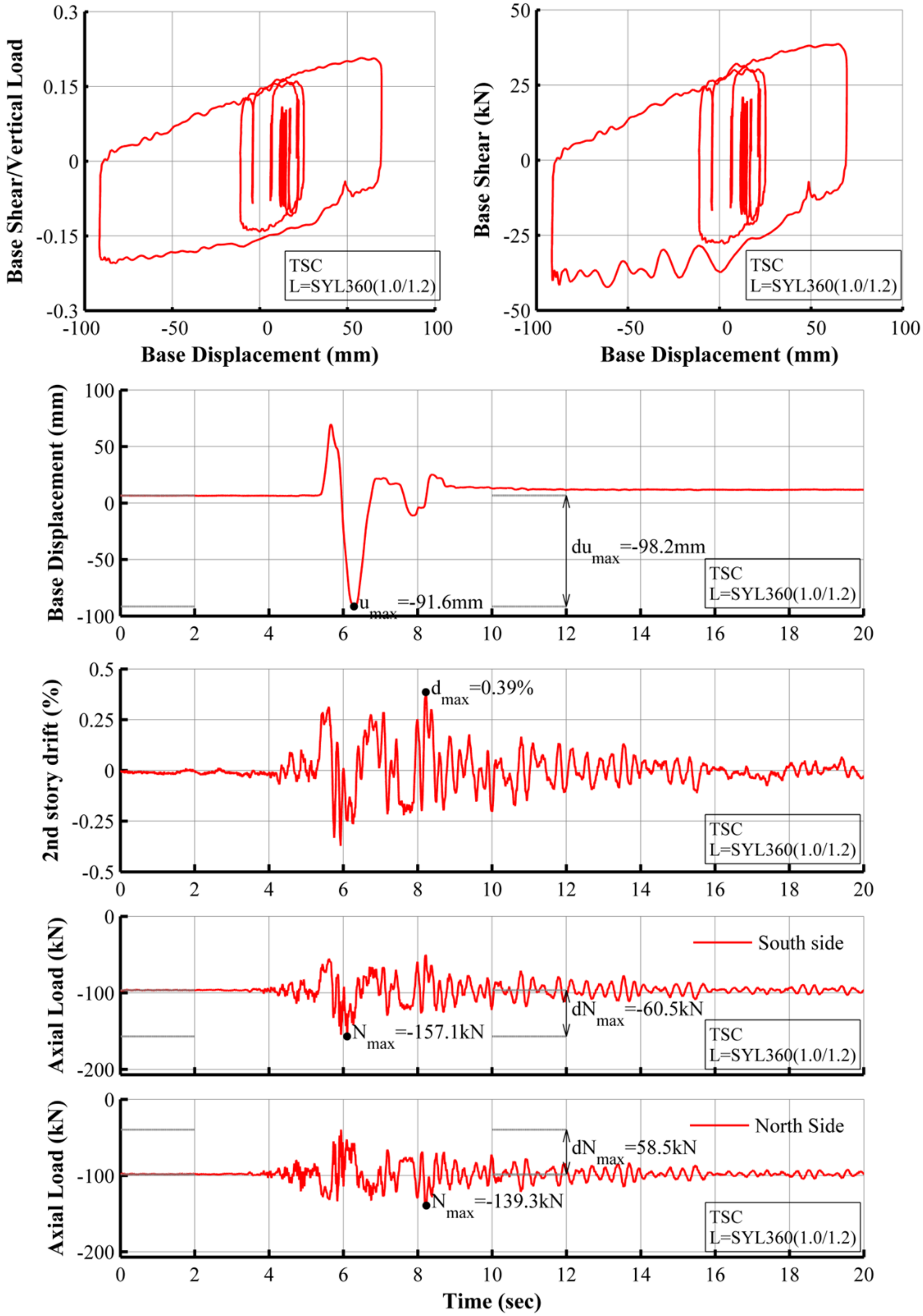

Base Shear/Vertical Load
Base Displacement (mm)
TSC
L=SYL360(1.0/1.2)
Base Shear (kN)
Base Displacement (mm)
TSC
L=SYL360(1.0/1.2)
Base Displacement (mm)
du max =-98.2mm
u max =-91.6mm
TSC
L=SYL360(1.0/1.2)
2nd story drift (%)
d max =0.39%
TSC
L=SYL360(1.0/1.2)
Axial Load (kN)
South side
dN max =-60.5kN
N max =-157.1kN
TSC
L=SYL360(1.0/1.2)
Axial Load (kN)
North Side
dN max =58.5kN
N max =-139.3kN
TSC
L=SYL360(1.0/1.2)
Time (sec)

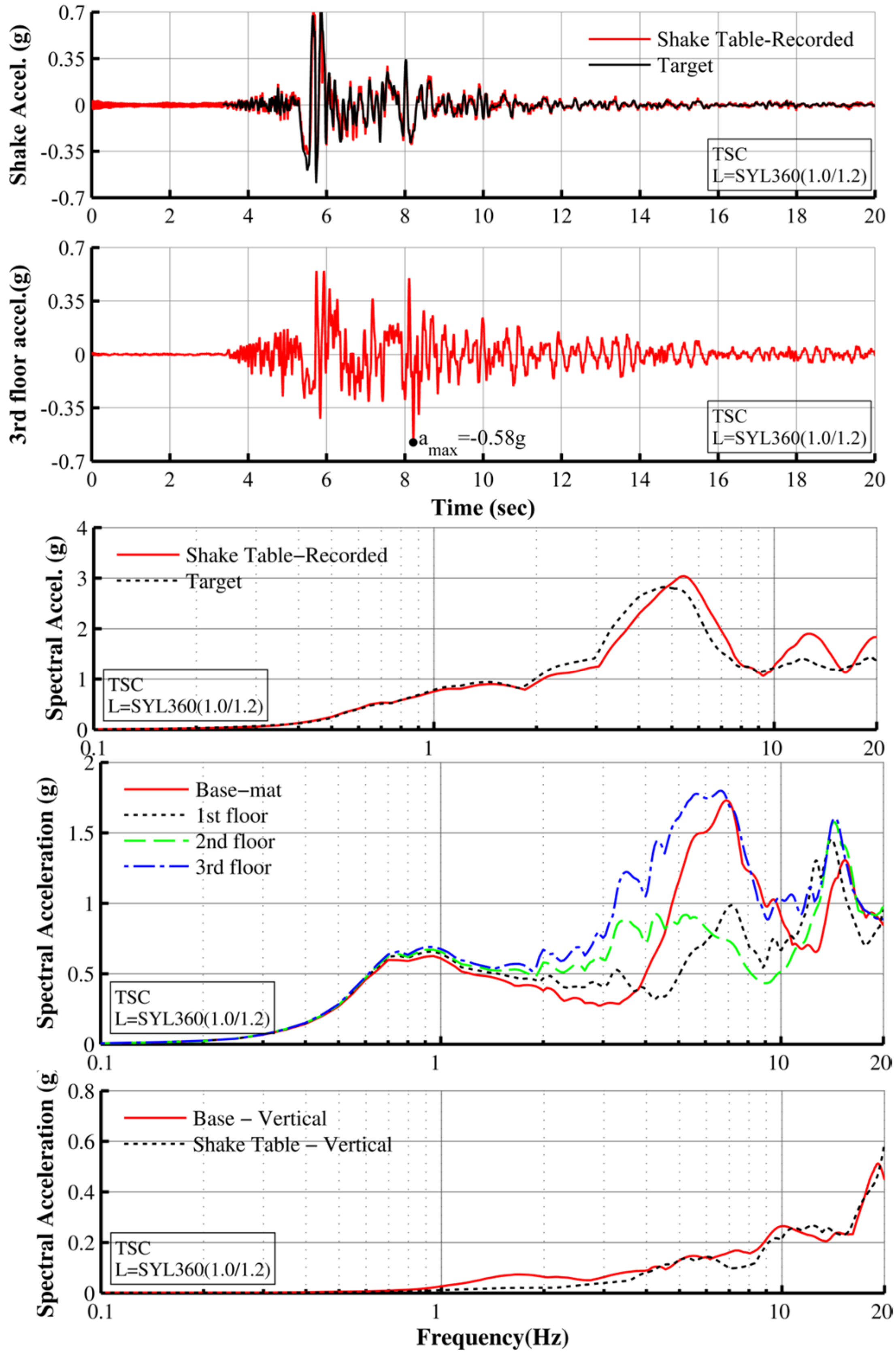
Shake Accel. (g)
Shake Table-Recorded
Target
TSC
L=SYL360(1.0/1.2)
3rd floor accel.(g)
a_{max}=-0.58g
Time (sec)
Spectral Accel. (g)
Shake Table−Recorded
Target
Spectral Acceleration (g)
Base−mat
1st floor
2nd floor
3rd floor
Base − Vertical
Shake Table − Vertical
Frequency(Hz)

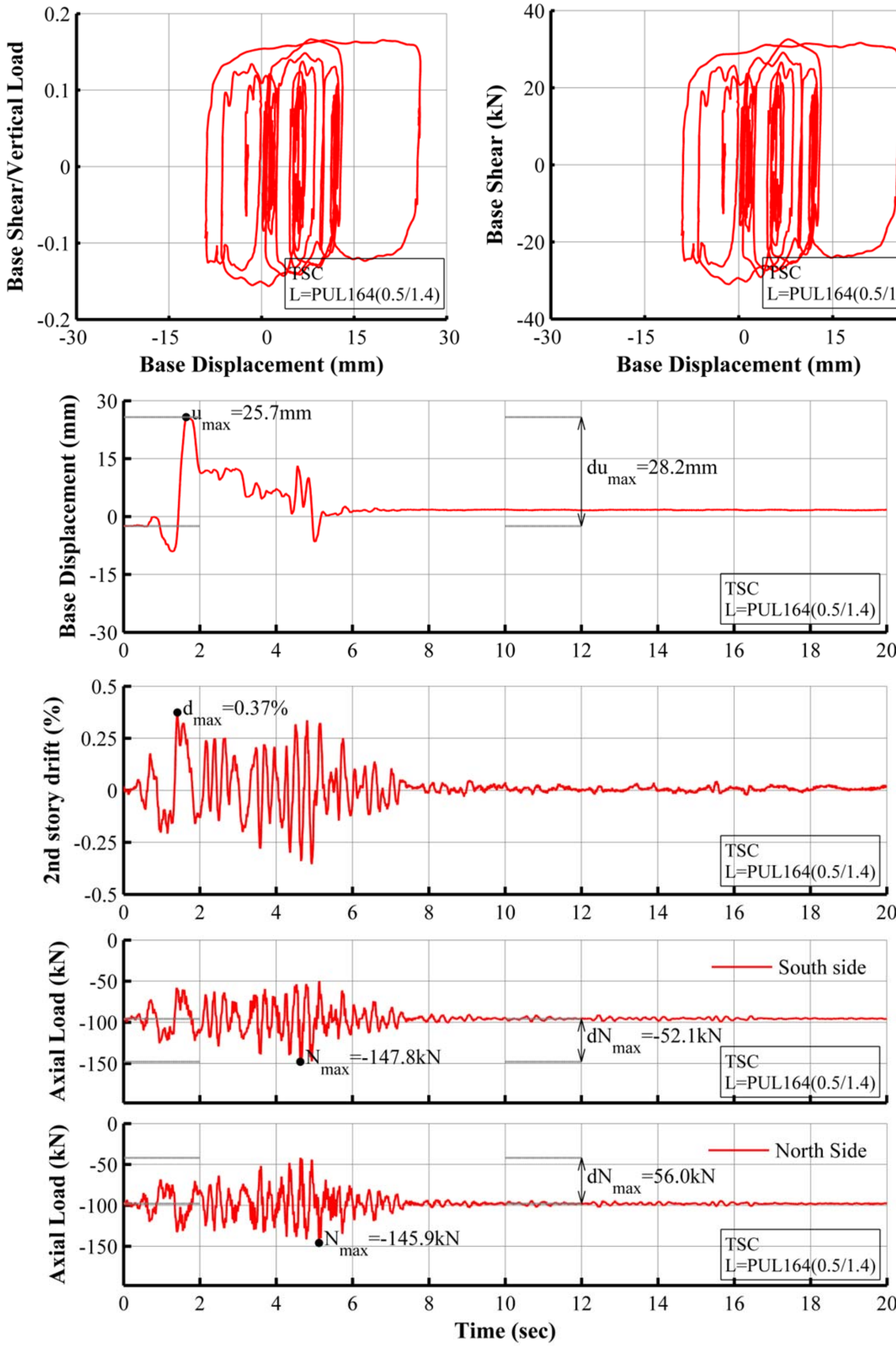

Base Shear/Vertical Load
Base Displacement (mm)
TSC
L=PUL164(0.5/1.4)
Base Shear (kN)
Base Displacement (mm)
TSC
L=PUL164(0.5/1.4)
Base Displacement (mm)
u_{max}=25.7mm
du_{max}=28.2mm
TSC
L=PUL164(0.5/1.4)
2nd story drift (%)
d_{max}=0.37%
TSC
L=PUL164(0.5/1.4)
Axial Load (kN)
South side
dN_{max}=-52.1kN
N_{max}=-147.8kN
TSC
L=PUL164(0.5/1.4)
Axial Load (kN)
North Side
dN_{max}=56.0kN
N_{max}=-145.9kN
TSC
L=PUL164(0.5/1.4)
Time (sec)

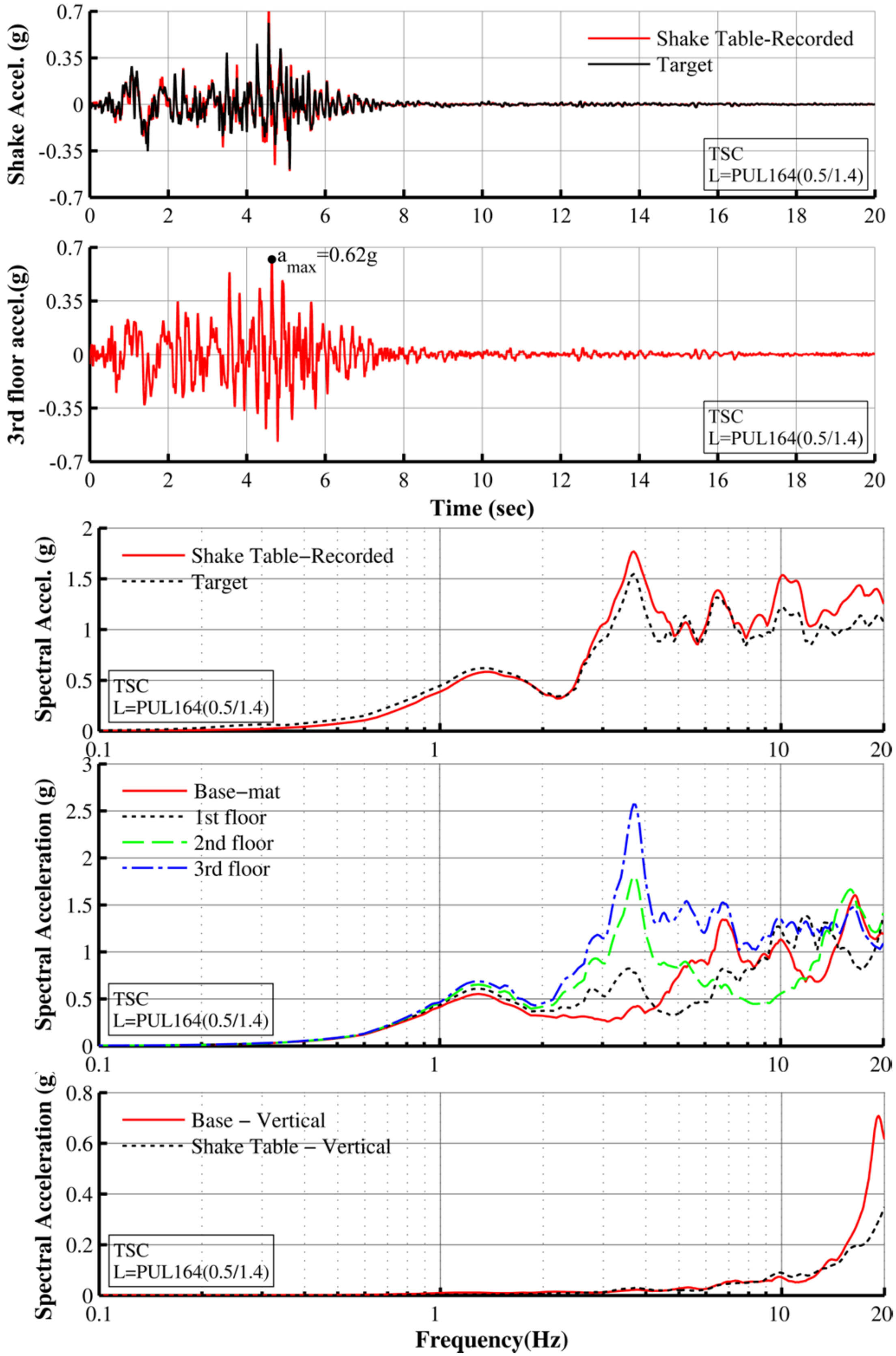

Shake Accel. (g)
Shake Table-Recorded
Target
TSC
L=PUL164(0.5/1.4)
3rd floor accel.(g)
a max =0.62g
TSC
L=PUL164(0.5/1.4)
Time (sec)
Spectral Accel. (g)
Shake Table−Recorded
Target
TSC
L=PUL164(0.5/1.4)
Spectral Acceleration (g)
Base−mat
1st floor
2nd floor
3rd floor
TSC
L=PUL164(0.5/1.4)
Spectral Acceleration (g)
Base − Vertical
Shake Table − Vertical
TSC
L=PUL164(0.5/1.4)
Frequency(Hz)

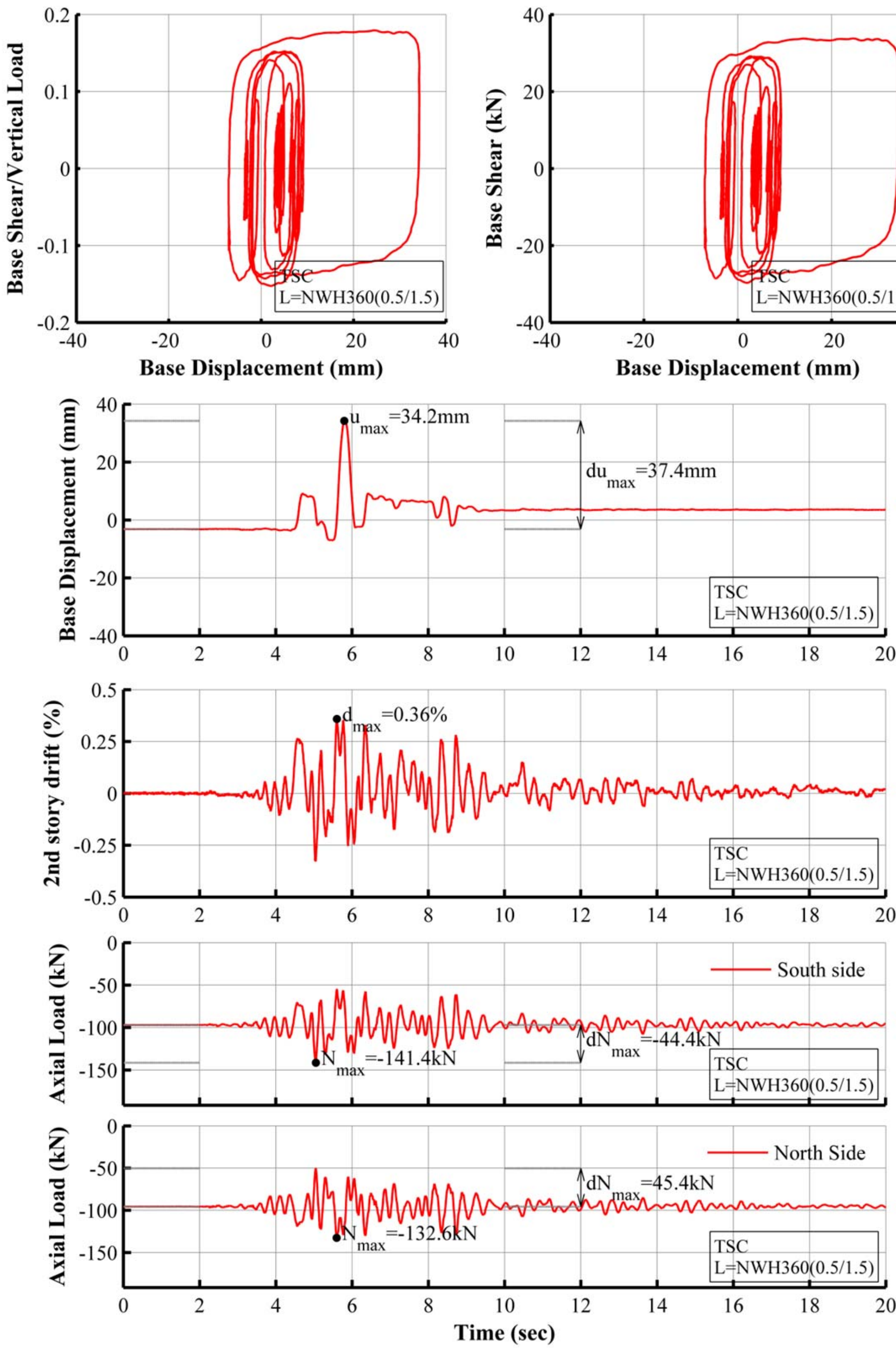

Base Shear/Vertical Load
Base Displacement (mm)
TSC
L=NWH360(0.5/1.5)
Base Shear (kN)
Base Displacement (mm)
TSC
L=NWH360(0.5/1.5)
Base Displacement (mm)
u_{max}=34.2mm
du_{max}=37.4mm
TSC
L=NWH360(0.5/1.5)
2nd story drift (%)
d_{max}=0.36%
TSC
L=NWH360(0.5/1.5)
Axial Load (kN)
South side
dN_{max}=-44.4kN
N_{max}=-141.4kN
TSC
L=NWH360(0.5/1.5)
Axial Load (kN)
North Side
dN_{max}=45.4kN
N_{max}=-132.6kN
TSC
L=NWH360(0.5/1.5)
Time (sec)

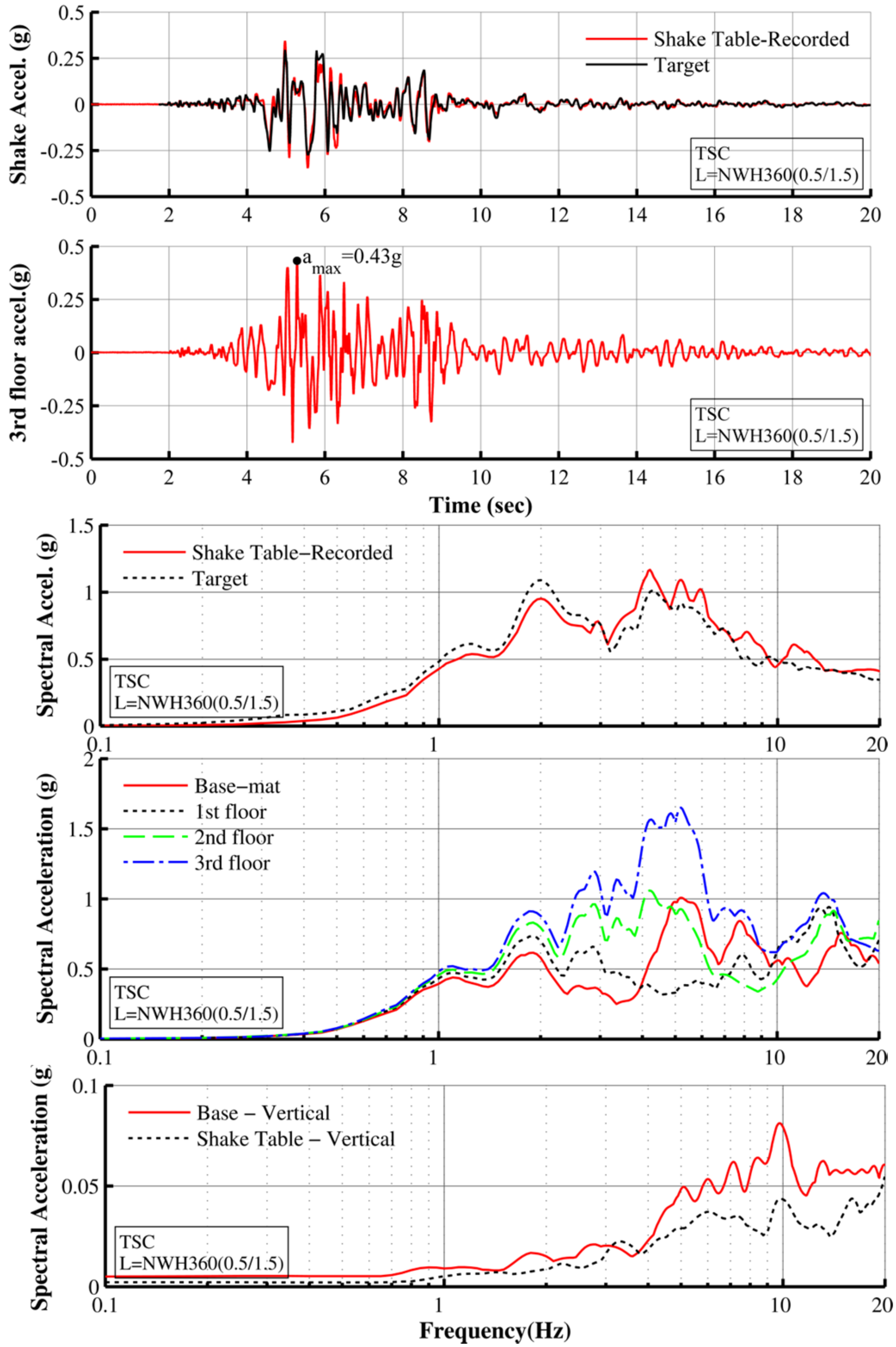
Shake Accel. (g)
Shake Table-Recorded
Target
TSC
L=NWH360(0.5/1.5)
3rd floor accel.(g)
a max =0.43g
TSC
L=NWH360(0.5/1.5)
Time (sec)
Spectral Accel. (g)
Shake Table−Recorded
Target
TSC
L=NWH360(0.5/1.5)
Spectral Acceleration (g)
Base−mat
1st floor
2nd floor
3rd floor
TSC
L=NWH360(0.5/1.5)
Spectral Acceleration (g)
Base − Vertical
Shake Table − Vertical
TSC
L=NWH360(0.5/1.5)
Frequency(Hz)

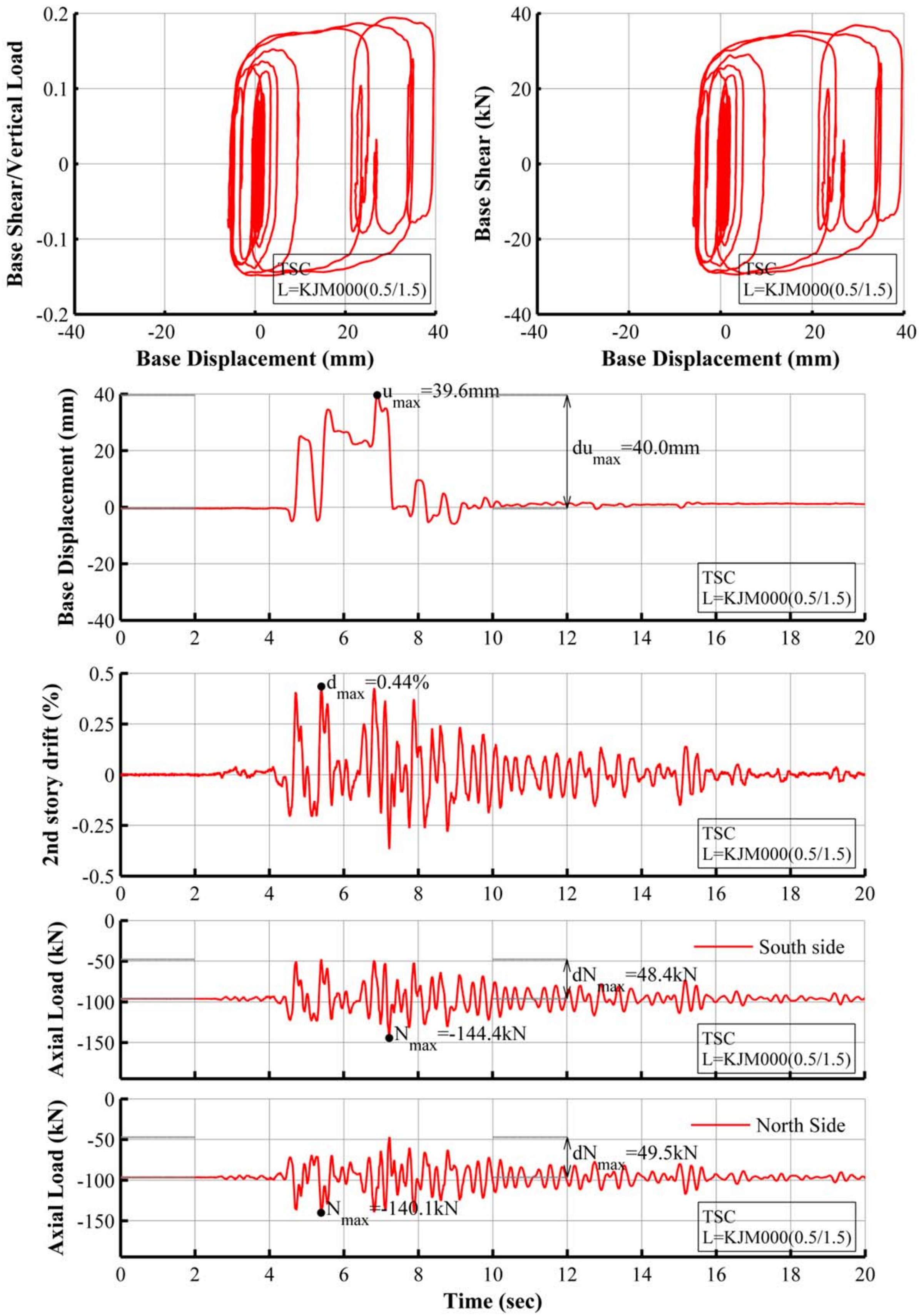
Base Shear/Vertical Load
Base Displacement (mm)
TSC
L=KJM000(0.5/1.5)
Base Shear (kN)
Base Displacement (mm)
TSC
L=KJM000(0.5/1.5)
Base Displacement (mm)
u max =39.6mm
du max =40.0mm
TSC
L=KJM000(0.5/1.5)
2nd story drift (%)
d max =0.44%
TSC
L=KJM000(0.5/1.5)
Axial Load (kN)
South side
dN max =48.4kN
N max =-144.4kN
TSC
L=KJM000(0.5/1.5)
Axial Load (kN)
North Side
dN max =49.5kN
N max =-140.1kN
TSC
L=KJM000(0.5/1.5)
Time (sec)

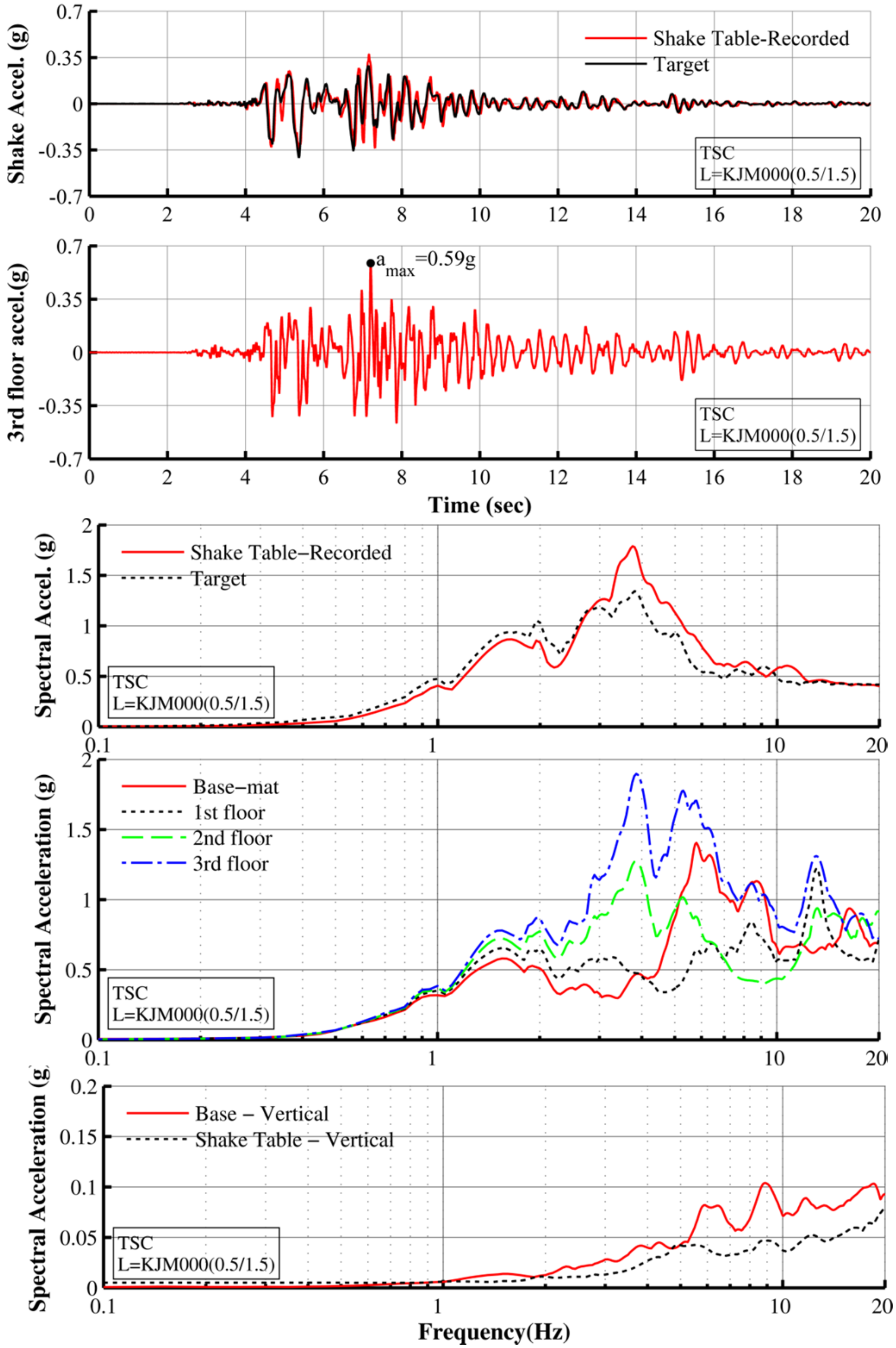

Shake Accel. (g)
Shake Table-Recorded
Target
TSC
L=KJM000(0.5/1.5)
3rd floor accel.(g)
a_{max}=0.59g
TSC
L=KJM000(0.5/1.5)
Time (sec)
Spectral Accel. (g)
Shake Table−Recorded
Target
TSC
L=KJM000(0.5/1.5)
Spectral Acceleration (g)
Base−mat
1st floor
2nd floor
3rd floor
TSC
L=KJM000(0.5/1.5)
Spectral Acceleration (g)
Base − Vertical
Shake Table − Vertical
TSC
L=KJM000(0.5/1.5)
Frequency(Hz)

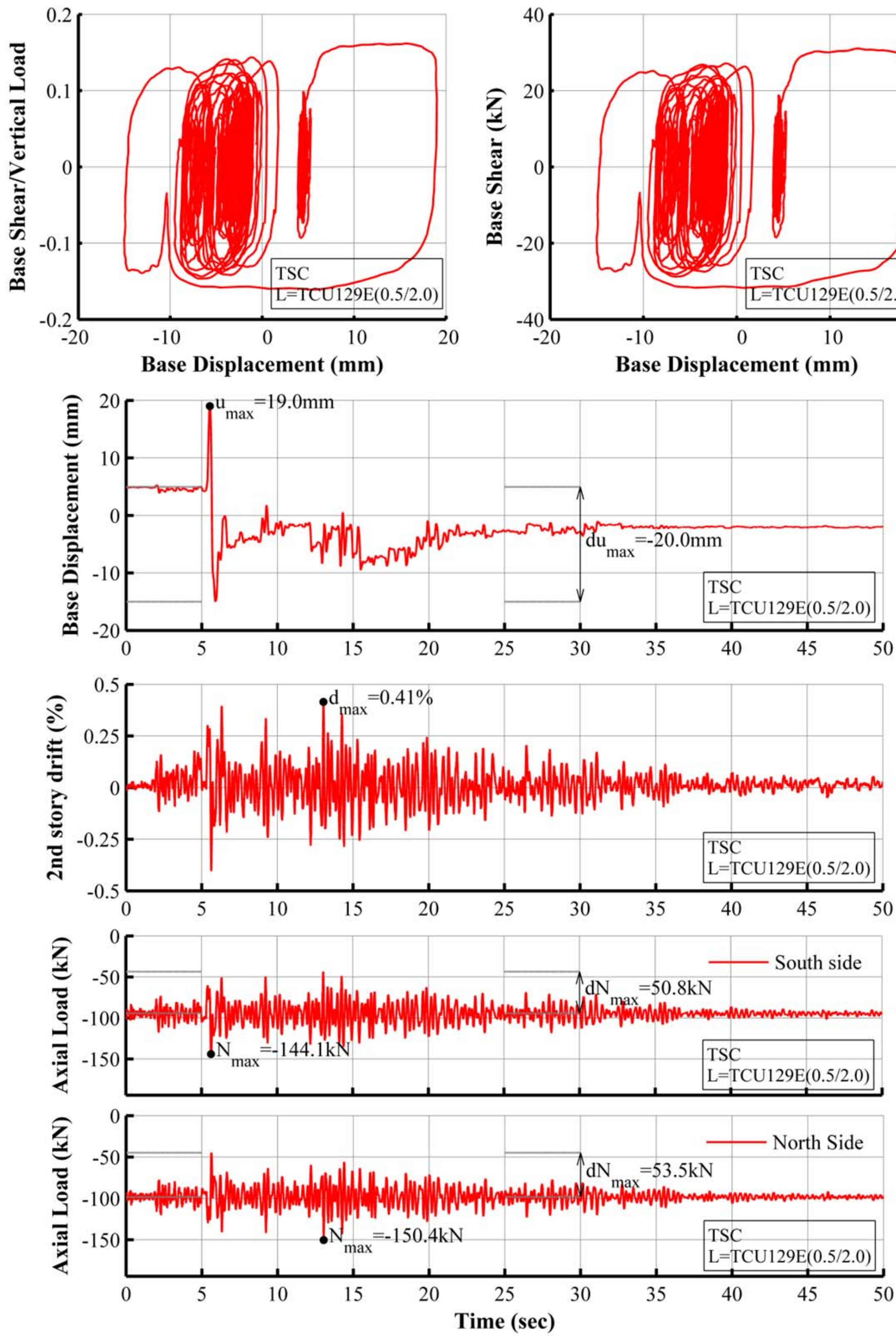
Base Shear/Vertical Load
Base Displacement (mm)
TSC
L=TCU129E(0.5/2.0)
Base Shear (kN)
Base Displacement (mm)
TSC
L=TCU129E(0.5/2.0)
Base Displacement (mm)
u max =19.0mm
du max =-20.0mm
TSC
L=TCU129E(0.5/2.0)
2nd story drift (%)
d max =0.41%
TSC
L=TCU129E(0.5/2.0)
Axial Load (kN)
South side
dN max =50.8kN
N max =-144.1kN
TSC
L=TCU129E(0.5/2.0)
Axial Load (kN)
North Side
dN max =53.5kN
N max =-150.4kN
TSC
L=TCU129E(0.5/2.0)
Time (sec)

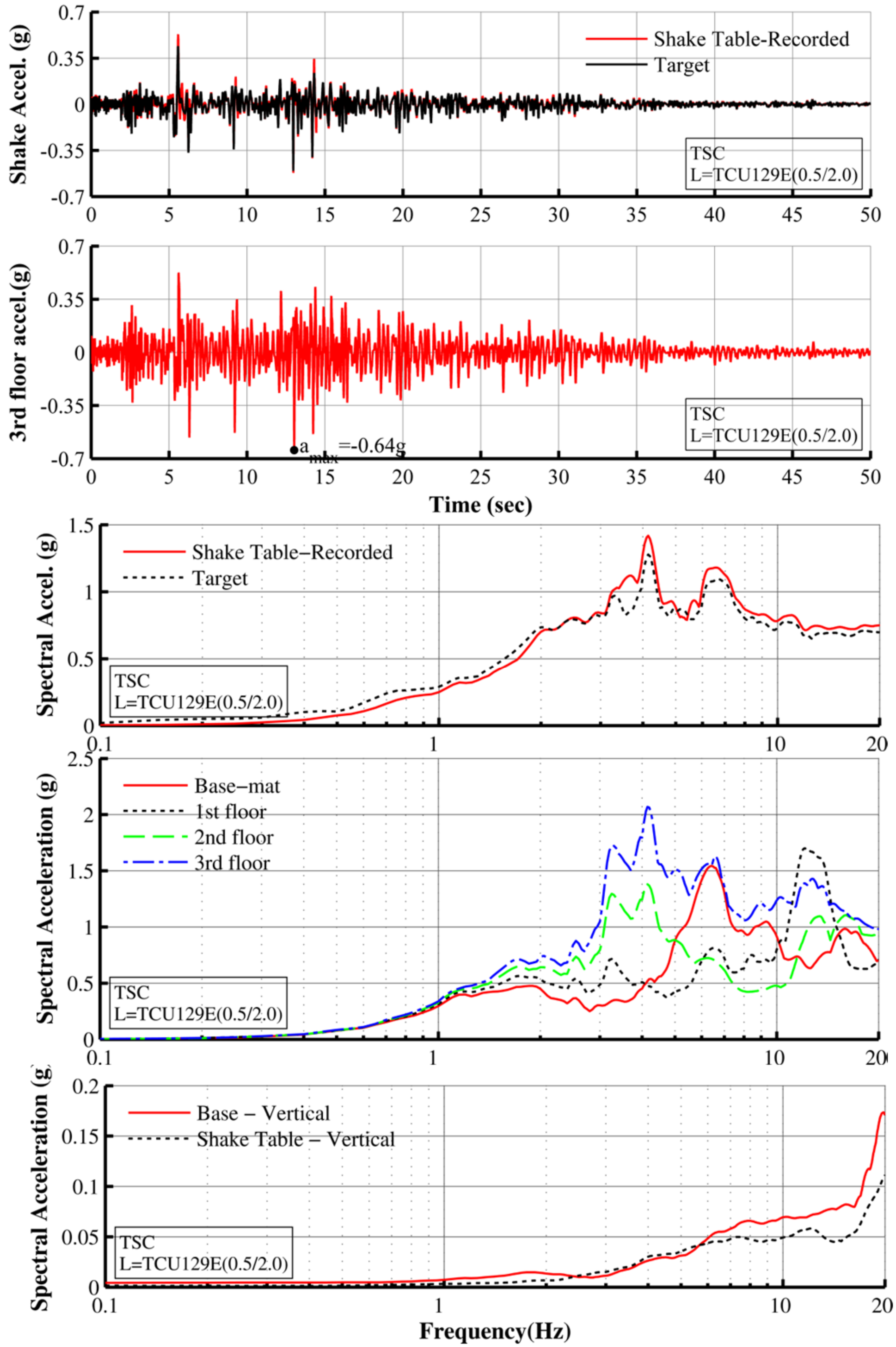
Shake Accel. (g)
Shake Table-Recorded
Target
TSC
L=TCU129E(0.5/2.0)
3rd floor accel.(g)
a max =-0.64g
Time (sec)
Spectral Accel. (g)
Shake Table−Recorded
Target
Spectral Acceleration (g)
Base−mat
1st floor
2nd floor
3rd floor
Base − Vertical
Shake Table − Vertical
Frequency(Hz)

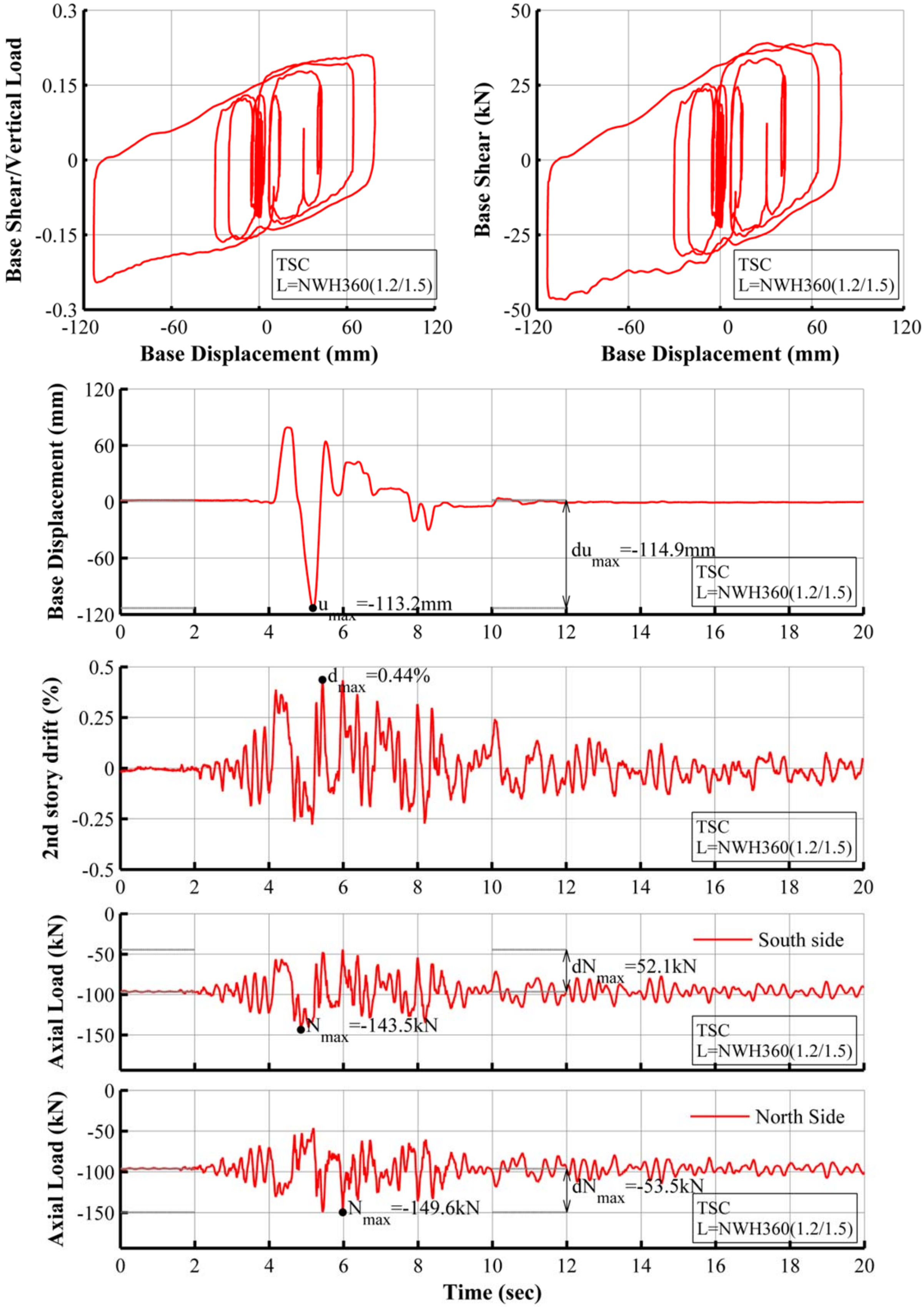
Base Shear/Vertical Load
Base Displacement (mm)
TSC
L=NWH360(1.2/1.5)
Base Shear (kN)
Base Displacement (mm)
TSC
L=NWH360(1.2/1.5)
Base Displacement (mm)
du max =-114.9mm
u max =-113.2mm
TSC
L=NWH360(1.2/1.5)
2nd story drift (%)
d max =0.44%
TSC
L=NWH360(1.2/1.5)
Axial Load (kN)
South side
dN max =52.1kN
N max =-143.5kN
TSC
L=NWH360(1.2/1.5)
Axial Load (kN)
North Side
dN max =-53.5kN
N max =-149.6kN
TSC
L=NWH360(1.2/1.5)
Time (sec)

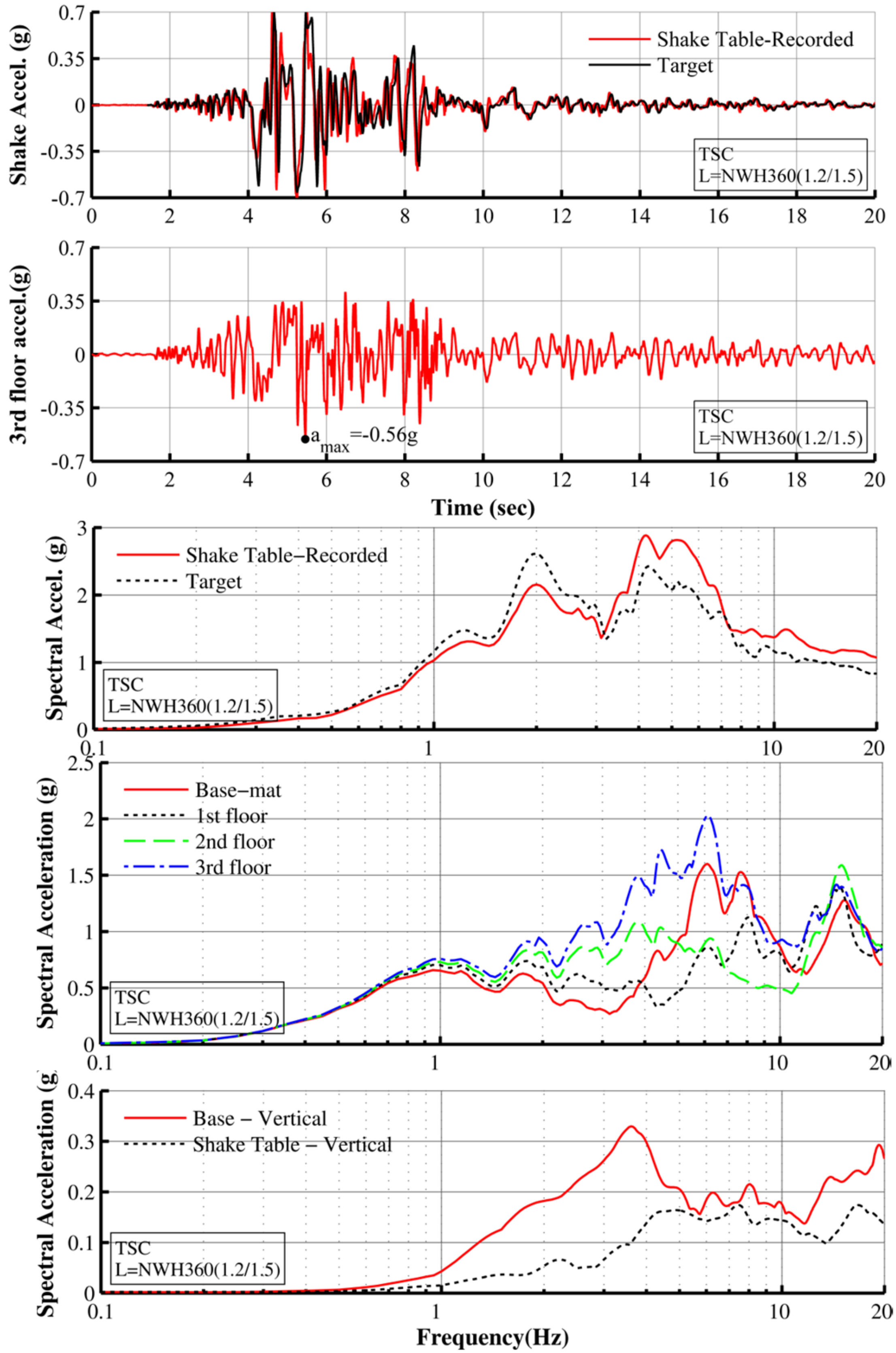

Shake Accel. (g)
Shake Table-Recorded
Target
TSC
L=NWH360(1.2/1.5)
3rd floor accel.(g)
a_{max}=-0.56g
TSC
L=NWH360(1.2/1.5)
Time (sec)
Spectral Accel. (g)
Shake Table−Recorded
Target
TSC
L=NWH360(1.2/1.5)
Spectral Acceleration (g)
Base−mat
1st floor
2nd floor
3rd floor
TSC
L=NWH360(1.2/1.5)
Spectral Acceleration (g)
Base − Vertical
Shake Table − Vertical
TSC
L=NWH360(1.2/1.5)
Frequency(Hz)

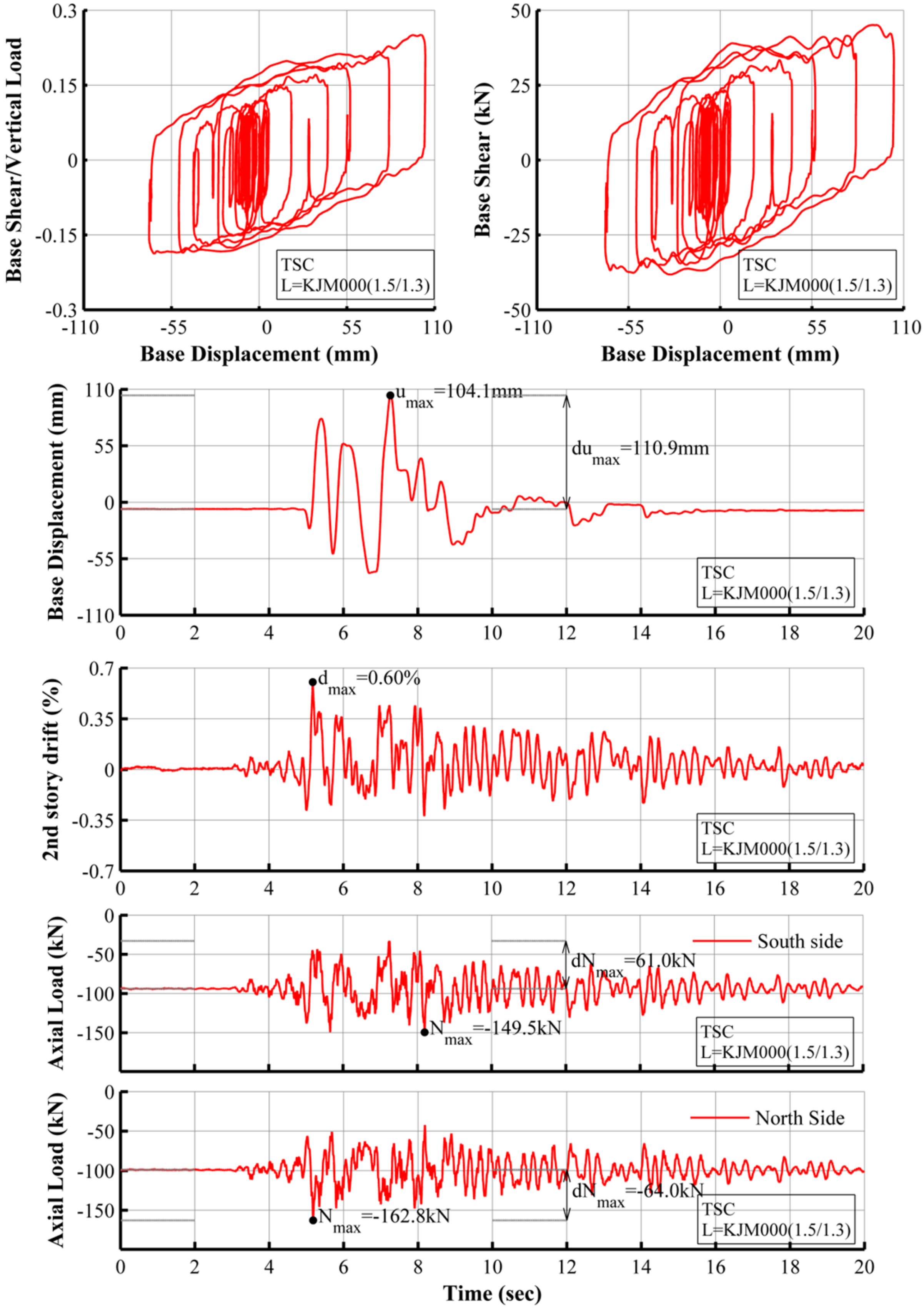
Base Shear/Vertical Load
Base Displacement (mm)
TSC
L=KJM000(1.5/1.3)
Base Shear (kN)
Base Displacement (mm)
TSC
L=KJM000(1.5/1.3)
Base Displacement (mm)
u max =104.1mm
du max =110.9mm
TSC
L=KJM000(1.5/1.3)
2nd story drift (%)
d max =0.60%
TSC
L=KJM000(1.5/1.3)
Axial Load (kN)
South side
dN max =61.0kN
N max =-149.5kN
TSC
L=KJM000(1.5/1.3)
Axial Load (kN)
North Side
dN max =-64.0kN
N max =-162.8kN
TSC
L=KJM000(1.5/1.3)
Time (sec)

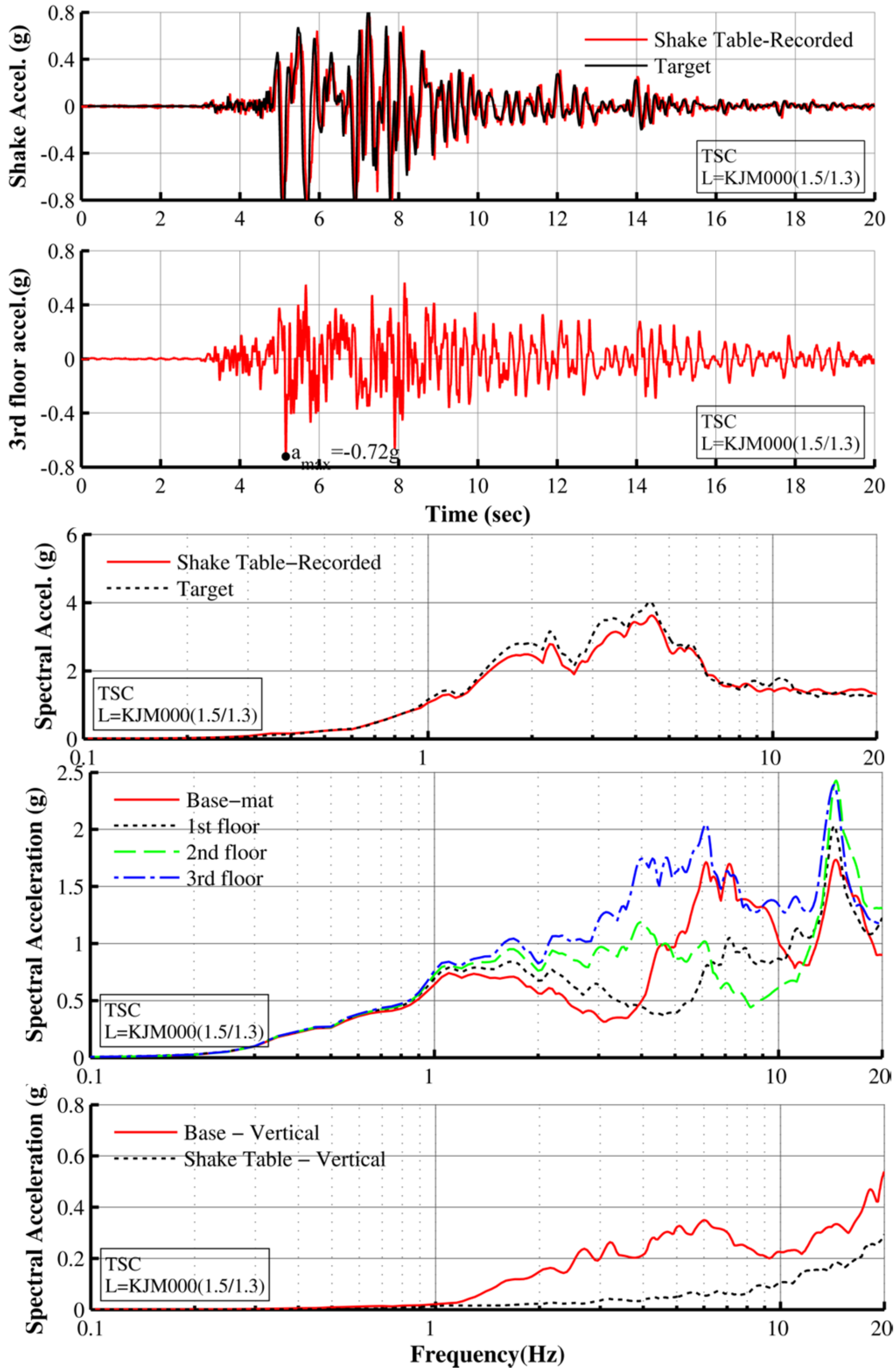
Shake Accel. (g)
Shake Table-Recorded
Target
TSC
L=KJM000(1.5/1.3)
3rd floor accel.(g)
a_{max}=-0.72g
TSC
L=KJM000(1.5/1.3)
Time (sec)
Spectral Accel. (g)
Shake Table−Recorded
Target
TSC
L=KJM000(1.5/1.3)
Spectral Acceleration (g)
Base−mat
1st floor
2nd floor
3rd floor
TSC
L=KJM000(1.5/1.3)
Spectral Acceleration (g)
Base − Vertical
Shake Table − Vertical
TSC
L=KJM000(1.5/1.3)
Frequency(Hz)

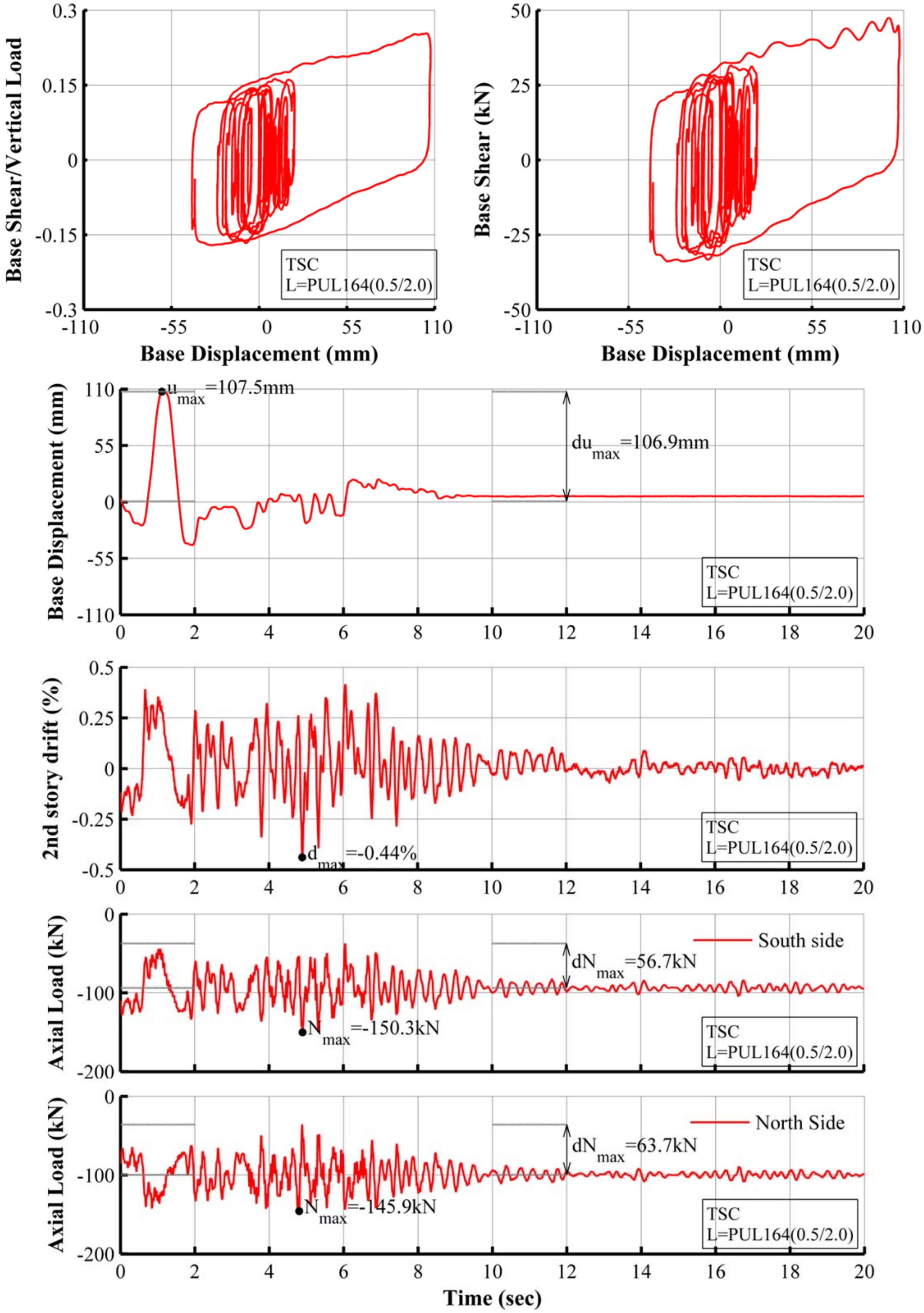
Base Shear/Vertical Load
Base Displacement (mm)
TSC
L=PUL164(0.5/2.0)
Base Shear (kN)
Base Displacement (mm)
TSC
L=PUL164(0.5/2.0)
Base Displacement (mm)
u_{max}=107.5mm
du_{max}=106.9mm
TSC
L=PUL164(0.5/2.0)
2nd story drift (%)
d_{max}=-0.44%
TSC
L=PUL164(0.5/2.0)
Axial Load (kN)
South side
dN_{max}=56.7kN
N_{max}=-150.3kN
TSC
L=PUL164(0.5/2.0)
Axial Load (kN)
North Side
dN_{max}=63.7kN
N_{max}=-145.9kN
TSC
L=PUL164(0.5/2.0)
Time (sec)

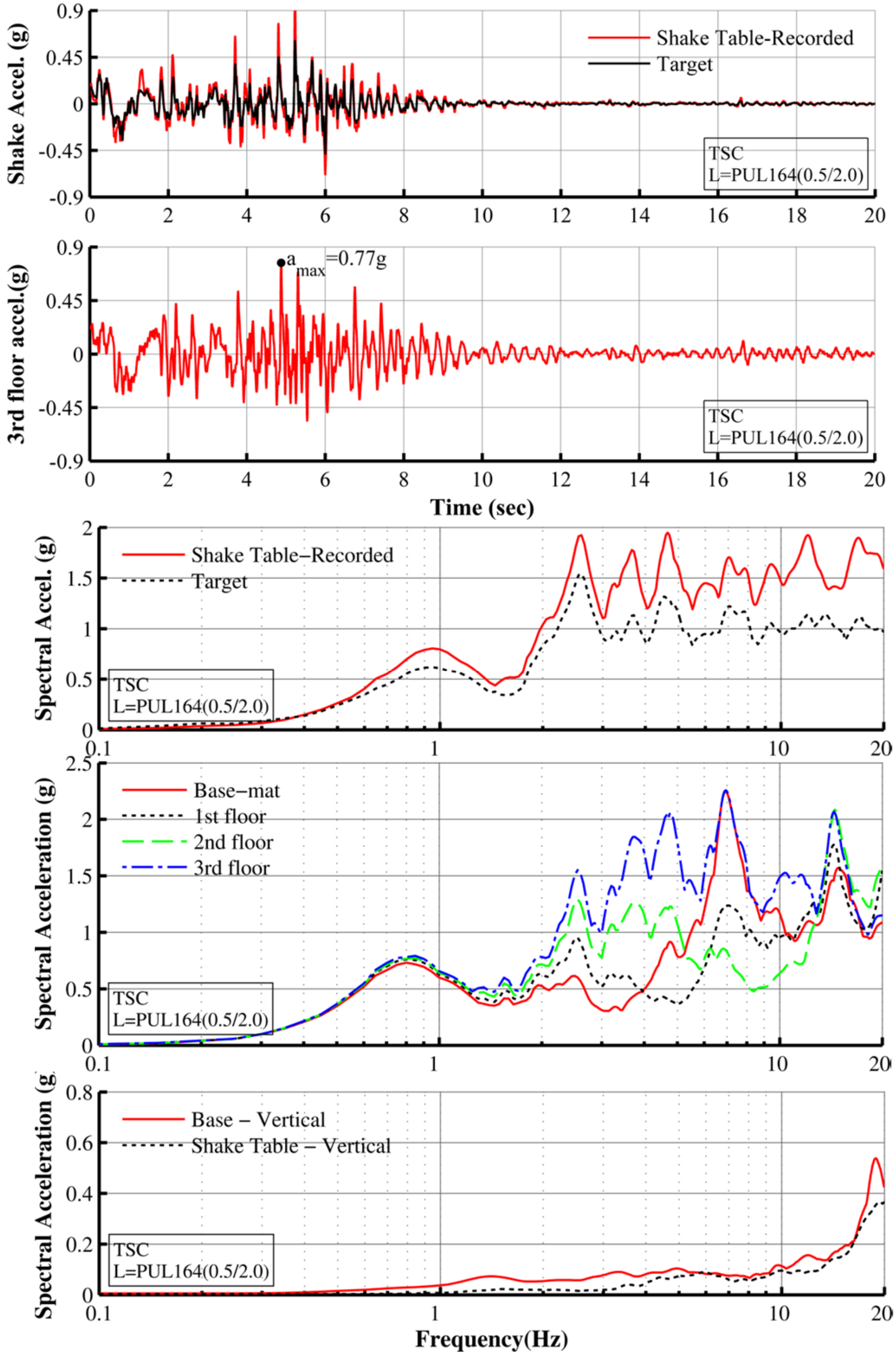
Shake Accel. (g)
Shake Table-Recorded
Target
TSC
L=PUL164(0.5/2.0)
3rd floor accel.(g)
a max =0.77g
TSC
L=PUL164(0.5/2.0)
Time (sec)
Spectral Accel. (g)
Shake Table−Recorded
Target
TSC
L=PUL164(0.5/2.0)
Spectral Acceleration (g)
Base−mat
1st floor
2nd floor
3rd floor
TSC
L=PUL164(0.5/2.0)
Spectral Acceleration (g)
Base − Vertical
Shake Table − Vertical
TSC
L=PUL164(0.5/2.0)
Frequency(Hz)

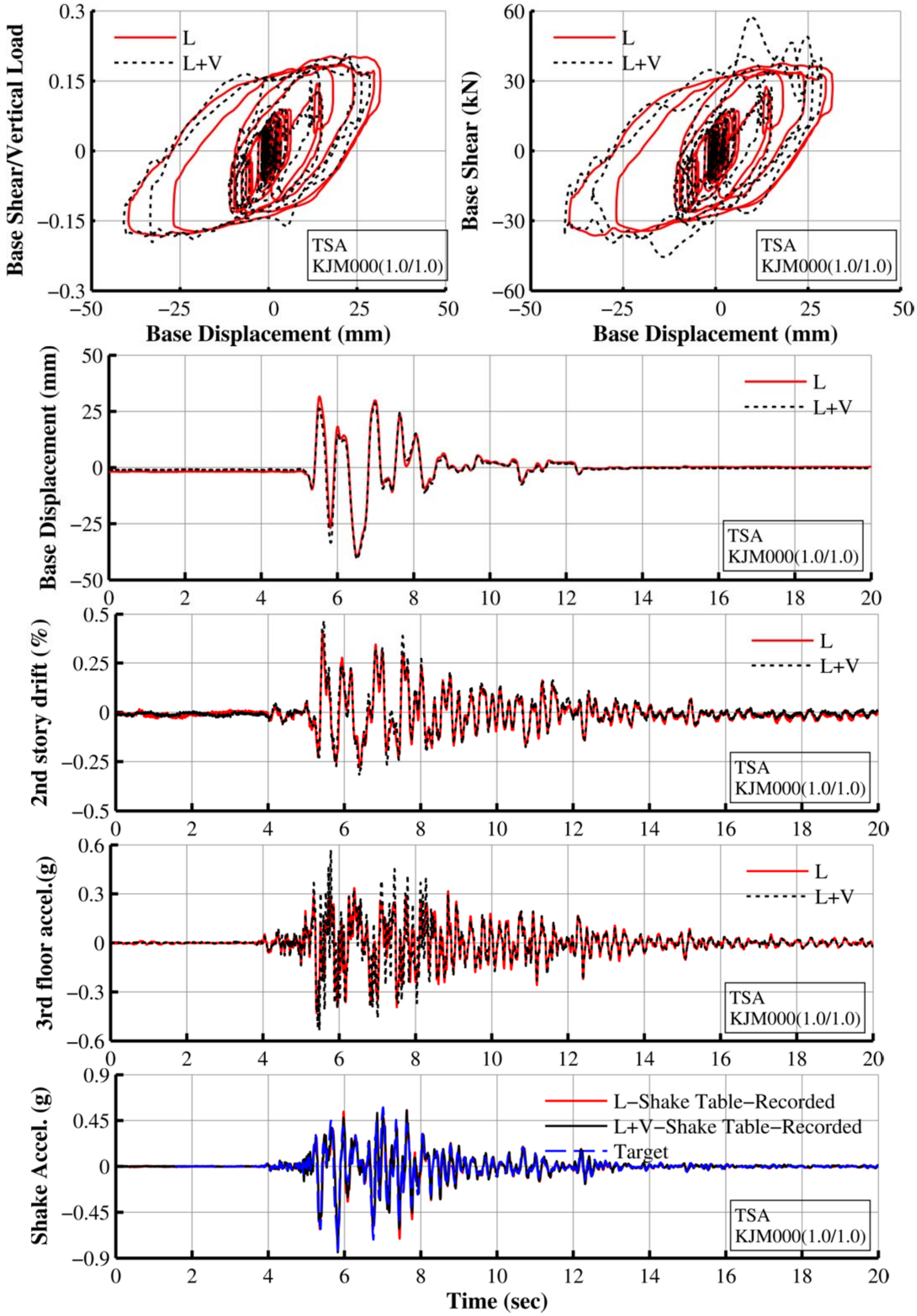
Base Shear/Vertical Load
Base Displacement (mm)
L
L+V
TSA
KJM000(1.0/1.0)
Base Shear (kN)
Base Displacement (mm)
L
L+V
TSA
KJM000(1.0/1.0)
Base Displacement (mm)
L
L+V
TSA
KJM000(1.0/1.0)
2nd story drift (%)
L
L+V
TSA
KJM000(1.0/1.0)
3rd floor accel.(g)
L
L+V
TSA
KJM000(1.0/1.0)
Shake Accel. (g)
L−Shake Table−Recorded
L+V−Shake Table−Recorded
Target
TSA
KJM000(1.0/1.0)
Time (sec)

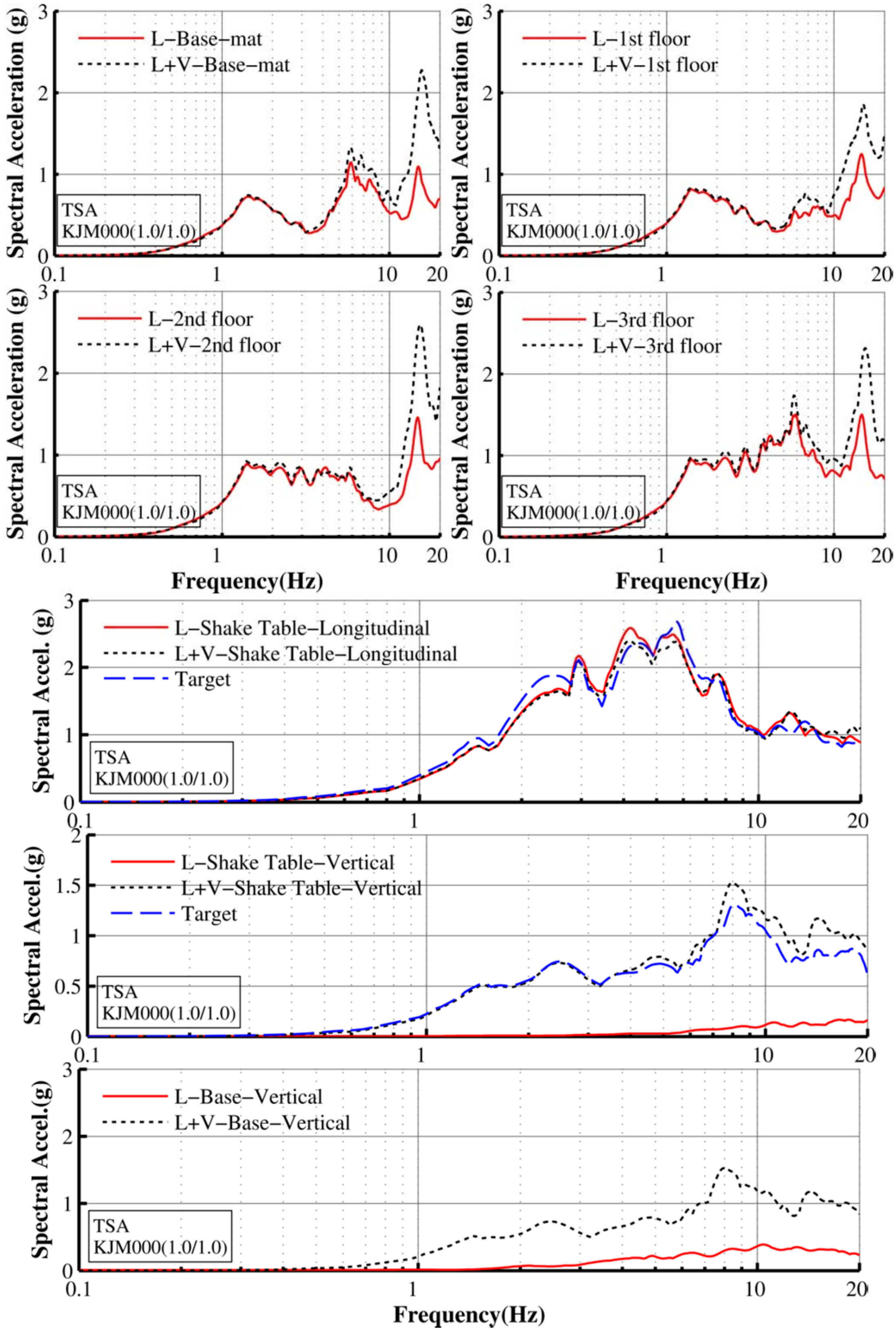

Spectral Acceleration (g)
L−Base−mat
L+V−Base−mat
TSA
KJM000(1.0/1.0)
L−1st floor
L+V−1st floor
L−2nd floor
L+V−2nd floor
L−3rd floor
L+V−3rd floor
Frequency(Hz)
Spectral Accel. (g)
L−Shake Table−Longitudinal
L+V−Shake Table−Longitudinal
Target
L−Shake Table−Vertical
L+V−Shake Table−Vertical
L−Base−Vertical
L+V−Base−Vertical
0.1
1
10
20

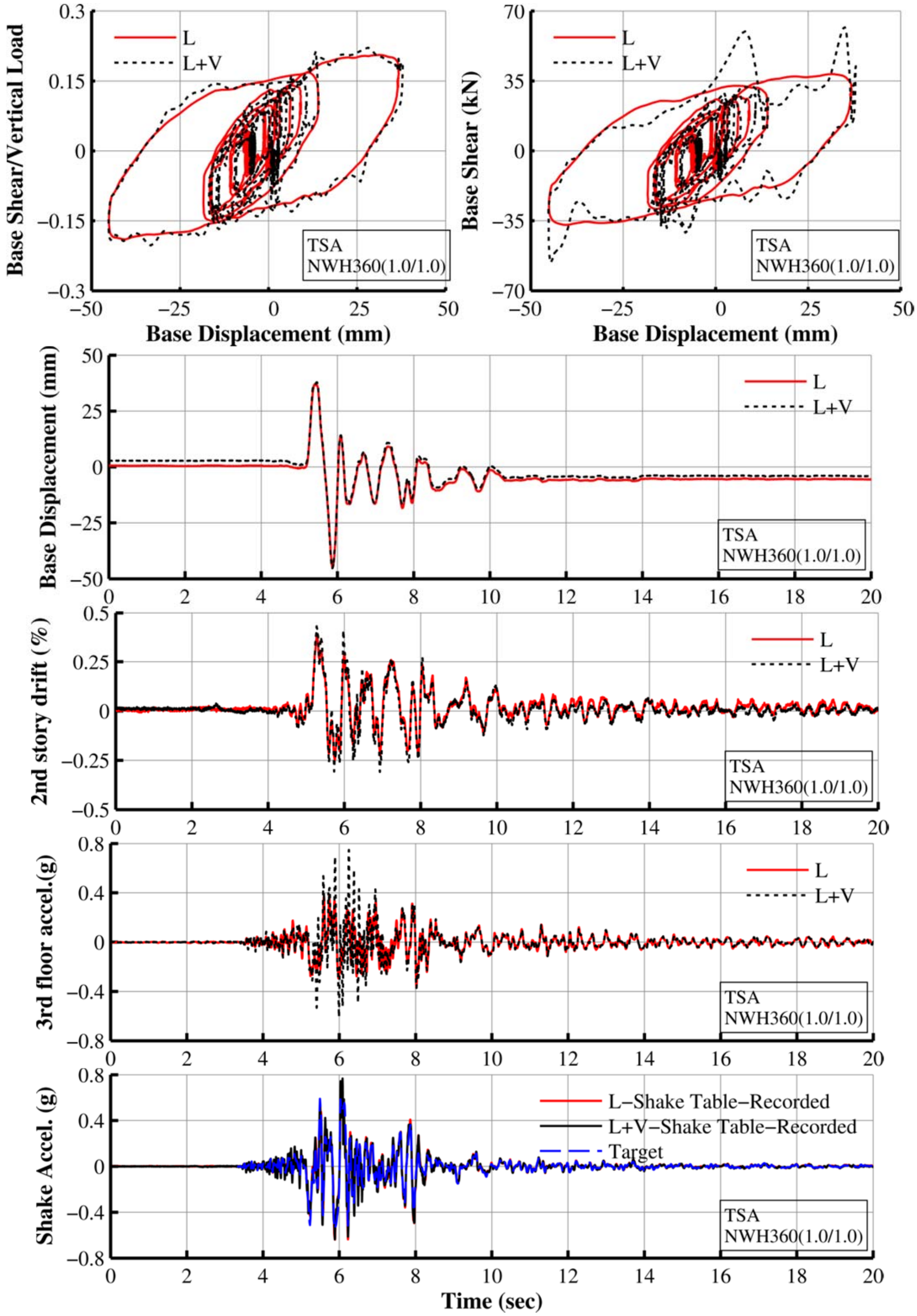
Base Shear/Vertical Load
Base Displacement (mm)
L
L+V
TSA
NWH360(1.0/1.0)
Base Shear (kN)
Base Displacement (mm)
2nd story drift (%)
3rd floor accel.(g)
Shake Accel. (g)
L−Shake Table−Recorded
L+V−Shake Table−Recorded
Target
Time (sec)

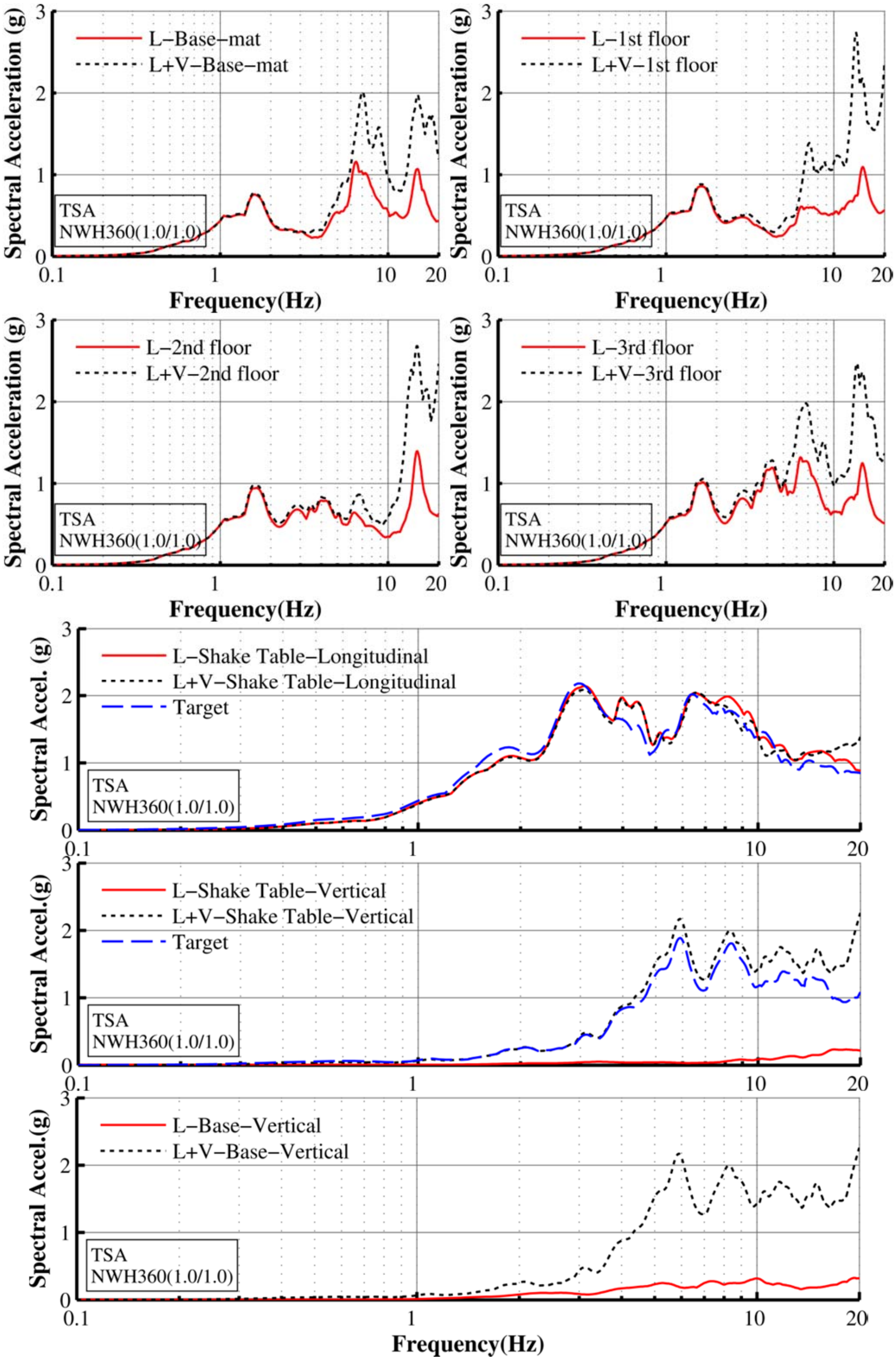
Spectral Acceleration (g)
L−Base−mat
L+V−Base−mat
TSA
NWH360(1.0/1.0)
Frequency(Hz)
L−1st floor
L+V−1st floor
L−2nd floor
L+V−2nd floor
L−3rd floor
L+V−3rd floor
Spectral Accel. (g)
L−Shake Table−Longitudinal
L+V−Shake Table−Longitudinal
Target
L−Shake Table−Vertical
L+V−Shake Table−Vertical
L−Base−Vertical
L+V−Base−Vertical
0.1
1
10
20

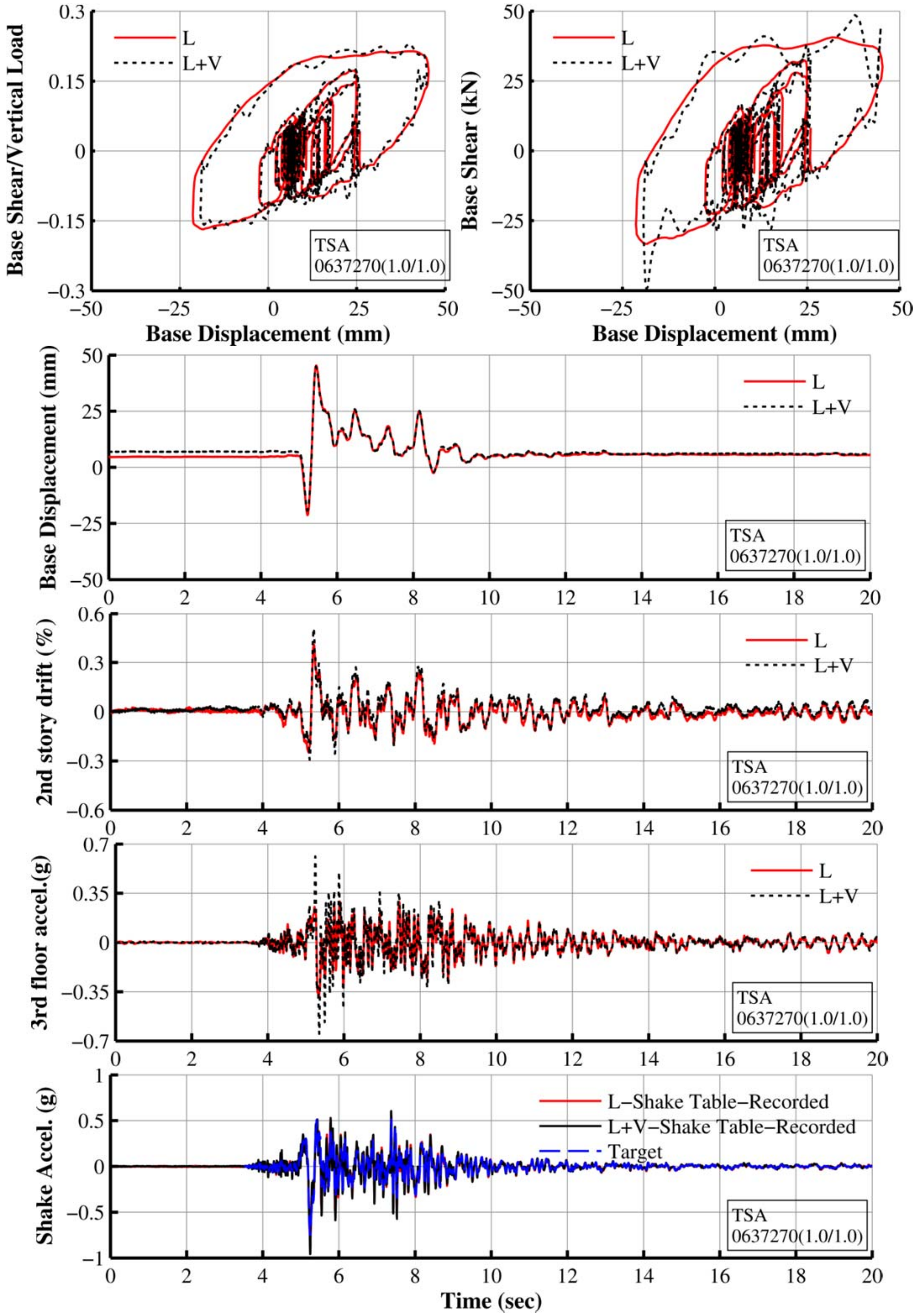
Base Shear/Vertical Load
Base Displacement (mm)
Base Shear (kN)
L
L+V
TSA
0637270(1.0/1.0)
Base Displacement (mm)
2nd story drift (%)
3rd floor accel.(g)
Shake Accel. (g)
L−Shake Table−Recorded
L+V−Shake Table−Recorded
Target
Time (sec)

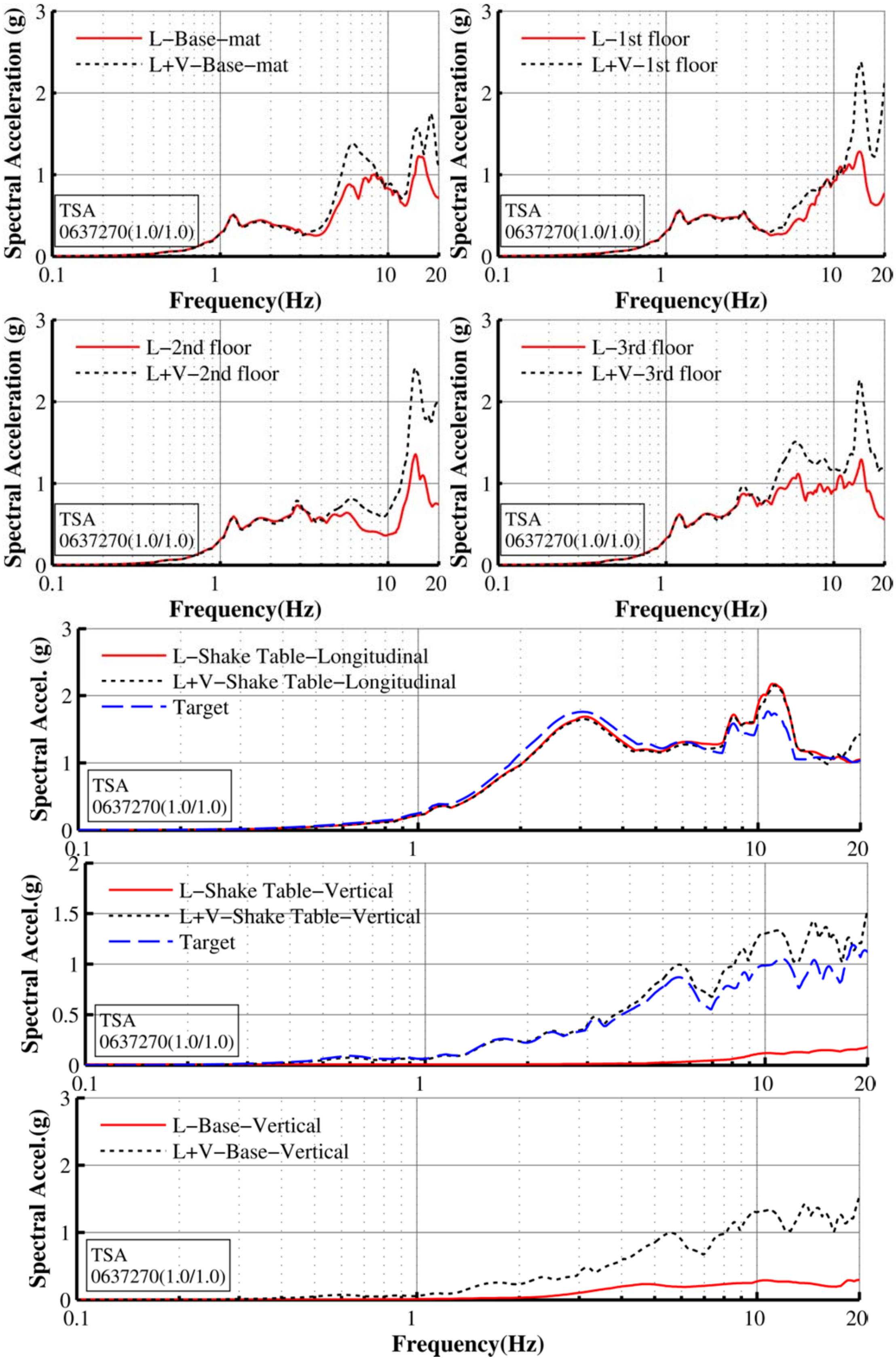
L−Base−mat
L+V−Base−mat
TSA
0637270(1.0/1.0)
Spectral Acceleration (g)
Frequency(Hz)
L−1st floor
L+V−1st floor
TSA
0637270(1.0/1.0)
Spectral Acceleration (g)
Frequency(Hz)
L−2nd floor
L+V−2nd floor
TSA
0637270(1.0/1.0)
Spectral Acceleration (g)
Frequency(Hz)
L−3rd floor
L+V−3rd floor
TSA
0637270(1.0/1.0)
Spectral Acceleration (g)
Frequency(Hz)
L−Shake Table−Longitudinal
L+V−Shake Table−Longitudinal
Target
TSA
0637270(1.0/1.0)
Spectral Accel. (g)
L−Shake Table−Vertical
L+V−Shake Table−Vertical
Target
TSA
0637270(1.0/1.0)
Spectral Accel.(g)
L−Base−Vertical
L+V−Base−Vertical
TSA
0637270(1.0/1.0)
Spectral Accel.(g)
Frequency(Hz)

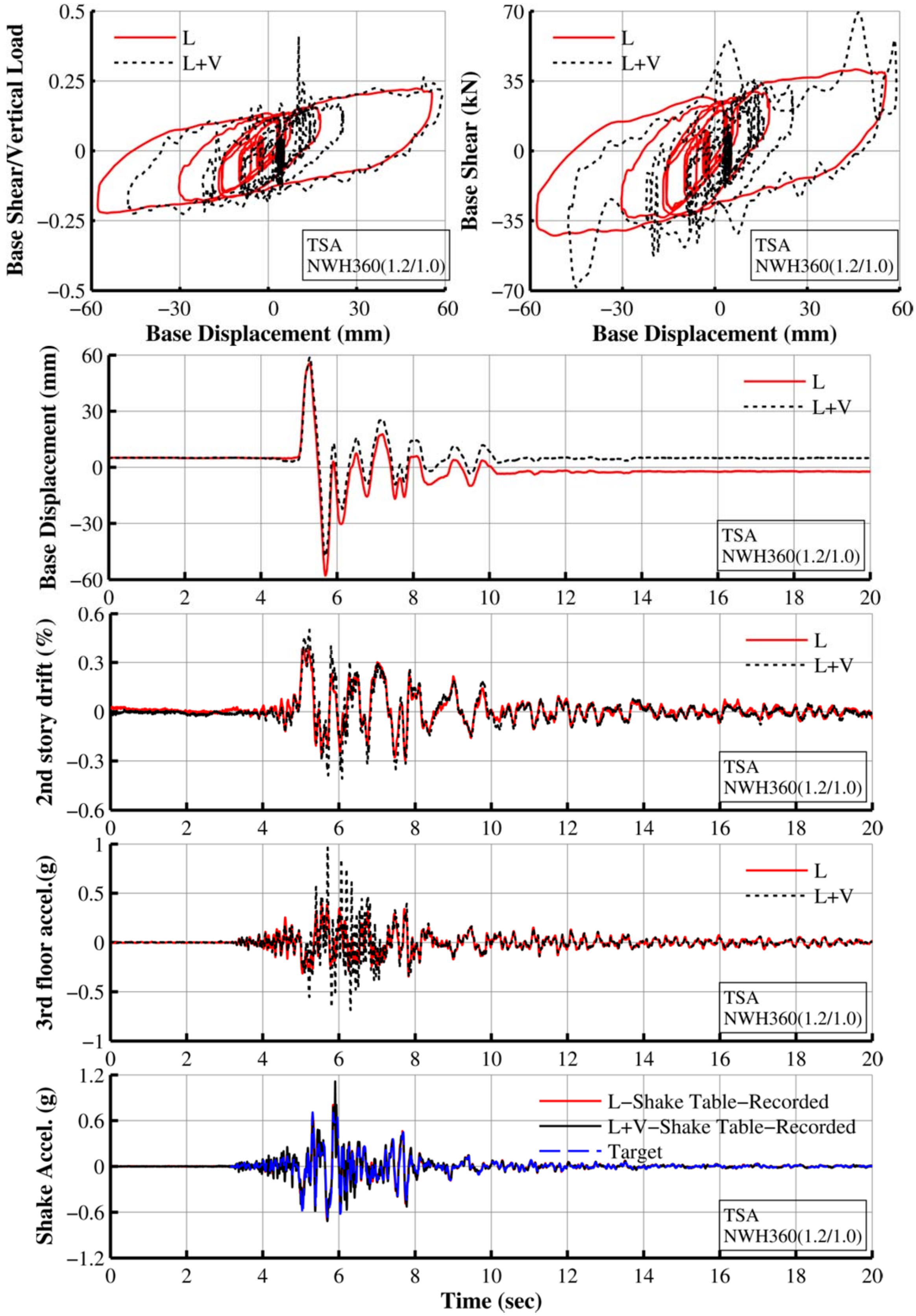

Base Shear/Vertical Load
Base Displacement (mm)
L
L+V
TSA
NWH360(1.2/1.0)
Base Shear (kN)
Base Displacement (mm)
2nd story drift (%)
3rd floor accel.(g)
Shake Accel. (g)
L−Shake Table−Recorded
L+V−Shake Table−Recorded
Target
Time (sec)

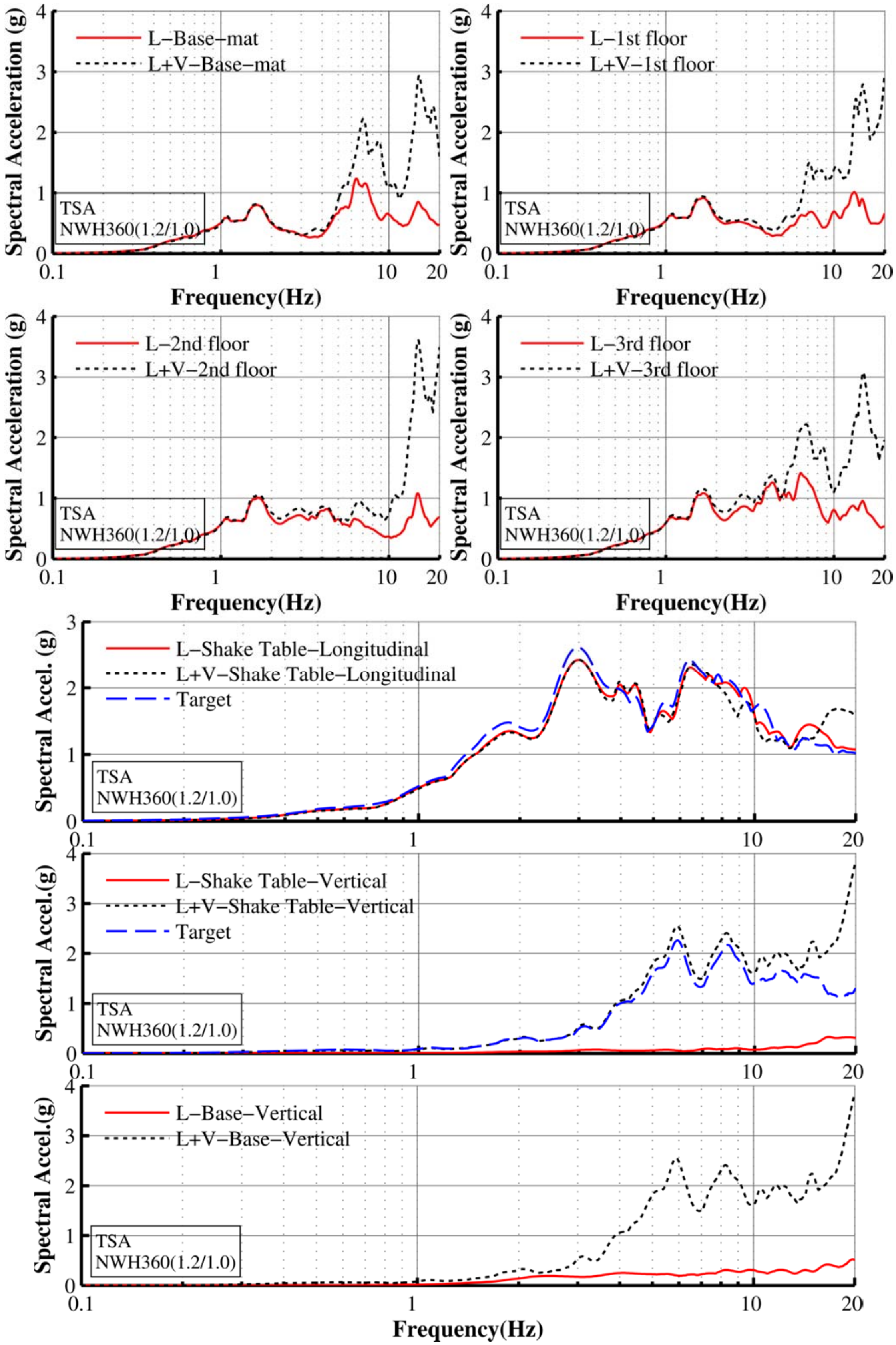

L−Base−mat
L+V−Base−mat
TSA
NWH360(1.2/1.0)
Spectral Acceleration (g)
Frequency(Hz)
L−1st floor
L+V−1st floor
TSA
NWH360(1.2/1.0)
Spectral Acceleration (g)
Frequency(Hz)
L−2nd floor
L+V−2nd floor
TSA
NWH360(1.2/1.0)
Spectral Acceleration (g)
Frequency(Hz)
L−3rd floor
L+V−3rd floor
TSA
NWH360(1.2/1.0)
Spectral Acceleration (g)
Frequency(Hz)
L−Shake Table−Longitudinal
L+V−Shake Table−Longitudinal
Target
TSA
NWH360(1.2/1.0)
Spectral Accel. (g)
L−Shake Table−Vertical
L+V−Shake Table−Vertical
Target
TSA
NWH360(1.2/1.0)
Spectral Accel.(g)
L−Base−Vertical
L+V−Base−Vertical
TSA
NWH360(1.2/1.0)
Spectral Accel.(g)
Frequency(Hz)

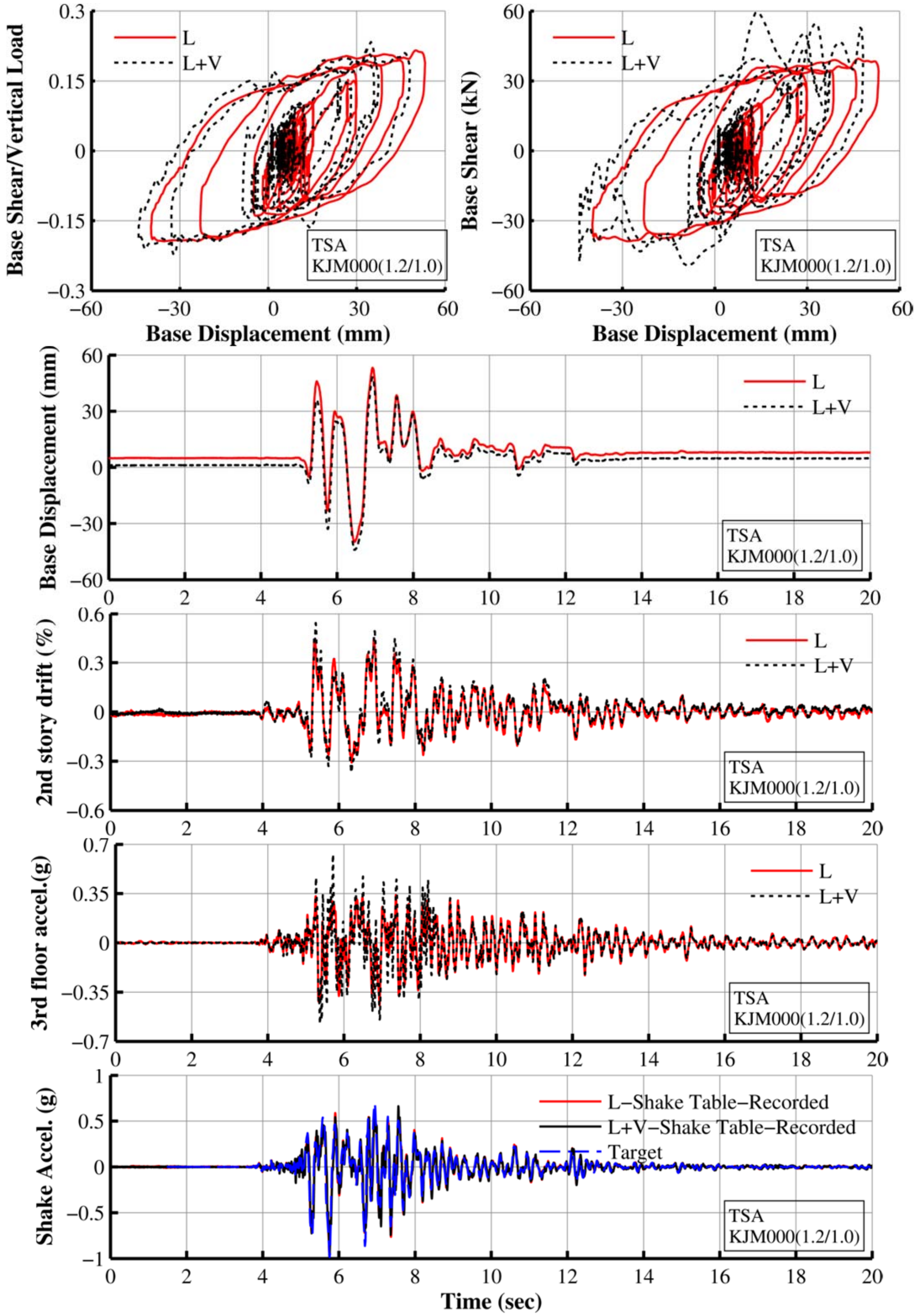
Base Shear/Vertical Load
Base Displacement (mm)
L
L+V
TSA
KJM000(1.2/1.0)
Base Shear (kN)
Base Displacement (mm)
2nd story drift (%)
3rd floor accel.(g)
Shake Accel. (g)
L−Shake Table−Recorded
L+V−Shake Table−Recorded
Target
Time (sec)

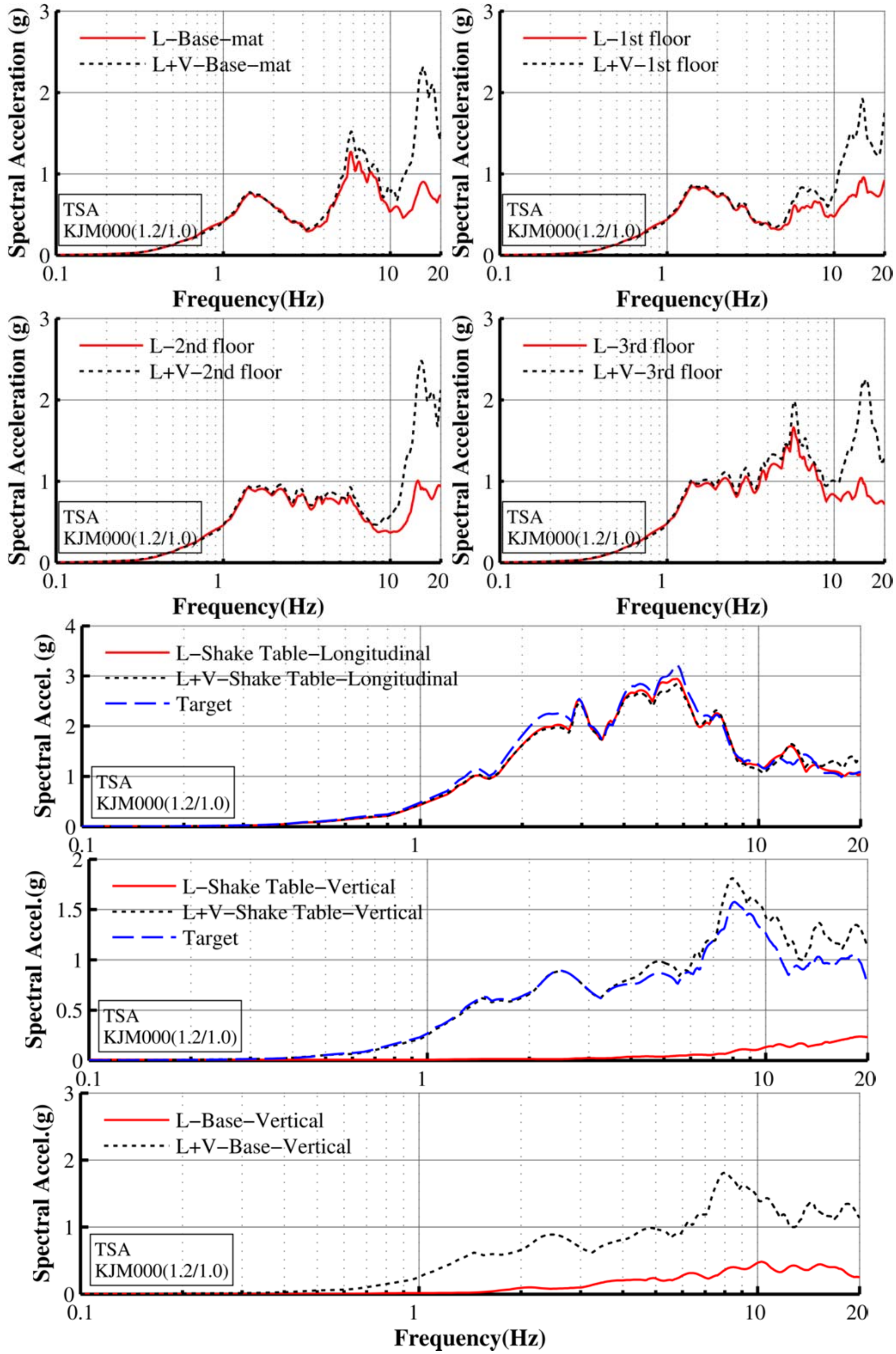

L−Base−mat
L+V−Base−mat
TSA
KJM000(1.2/1.0)
Spectral Acceleration (g)
Frequency(Hz)
L−1st floor
L+V−1st floor
TSA
KJM000(1.2/1.0)
Spectral Acceleration (g)
Frequency(Hz)
L−2nd floor
L+V−2nd floor
TSA
KJM000(1.2/1.0)
Spectral Acceleration (g)
Frequency(Hz)
L−3rd floor
L+V−3rd floor
TSA
KJM000(1.2/1.0)
Spectral Acceleration (g)
Frequency(Hz)
L−Shake Table−Longitudinal
L+V−Shake Table−Longitudinal
Target
TSA
KJM000(1.2/1.0)
Spectral Accel. (g)
L−Shake Table−Vertical
L+V−Shake Table−Vertical
Target
TSA
KJM000(1.2/1.0)
Spectral Accel.(g)
L−Base−Vertical
L+V−Base−Vertical
TSA
KJM000(1.2/1.0)
Spectral Accel.(g)
Frequency(Hz)

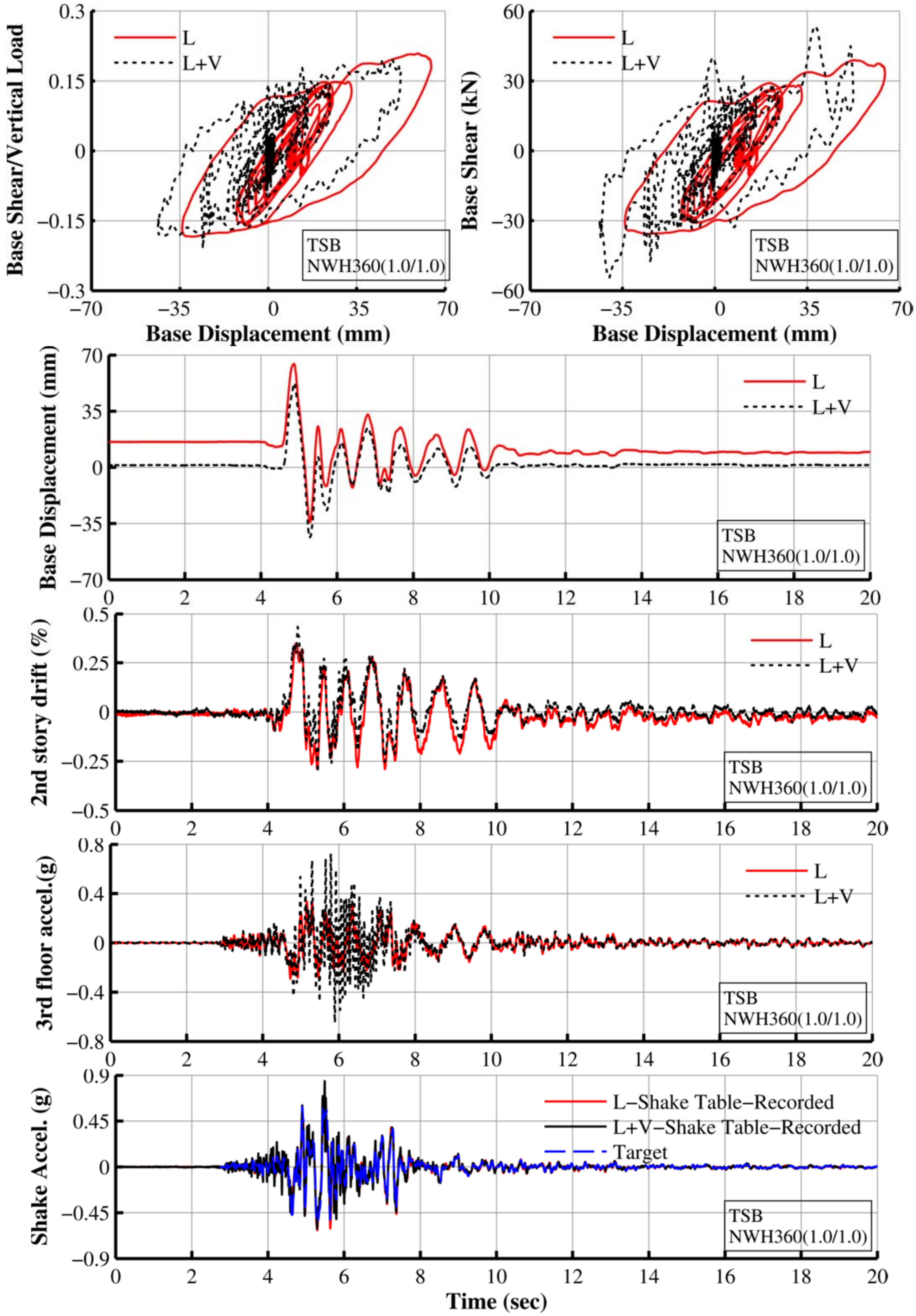

Base Shear/Vertical Load
Base Displacement (mm)
L
L+V
TSB
NWH360(1.0/1.0)
Base Shear (kN)
Base Displacement (mm)
Base Displacement (mm)
2nd story drift (%)
3rd floor accel.(g)
Shake Accel. (g)
L−Shake Table−Recorded
L+V−Shake Table−Recorded
Target
Time (sec)

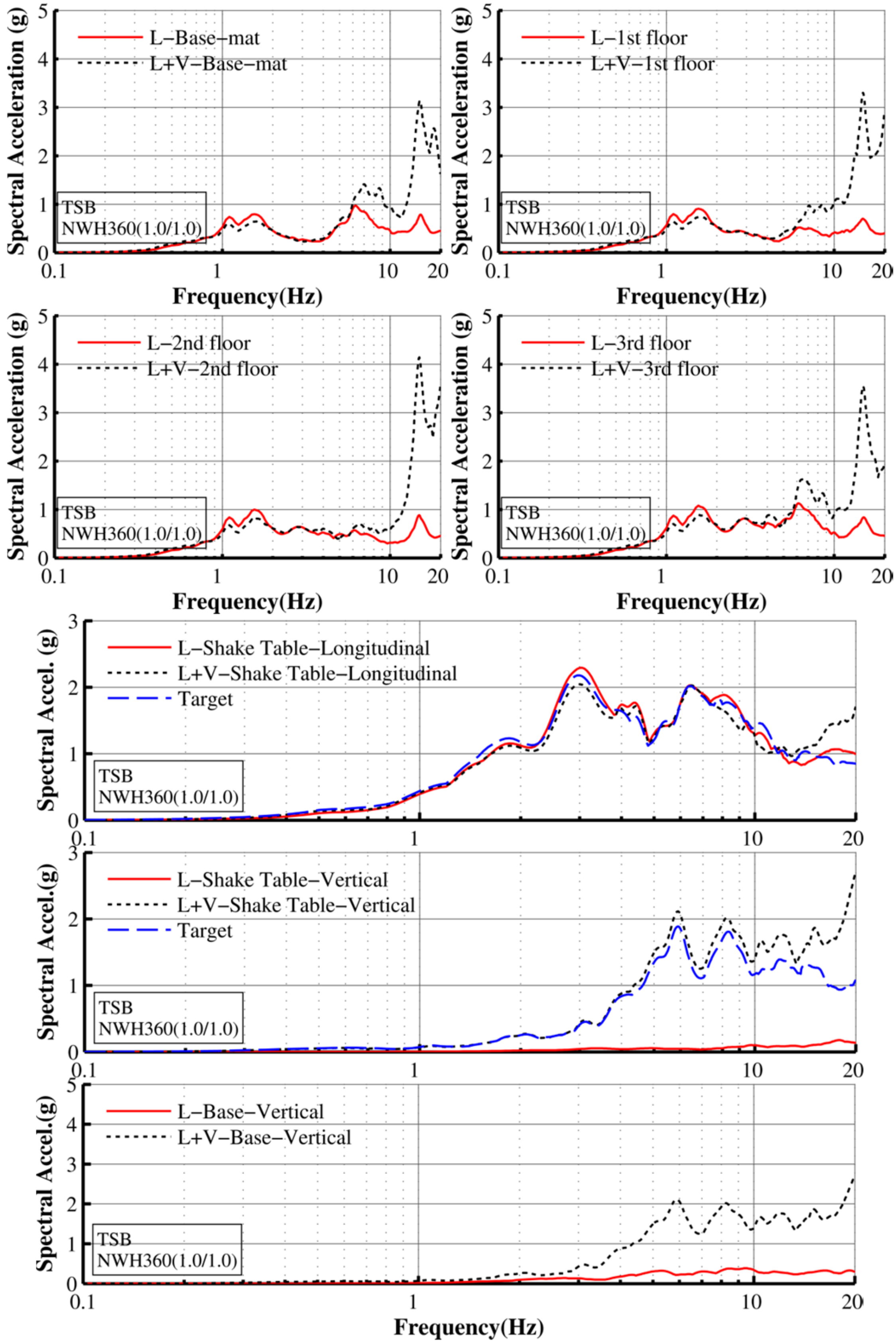

L−Base−mat
L+V−Base−mat
TSB
NWH360(1.0/1.0)
Spectral Acceleration (g)
Frequency(Hz)
L−1st floor
L+V−1st floor
TSB
NWH360(1.0/1.0)
Spectral Acceleration (g)
Frequency(Hz)
L−2nd floor
L+V−2nd floor
TSB
NWH360(1.0/1.0)
Spectral Acceleration (g)
Frequency(Hz)
L−3rd floor
L+V−3rd floor
TSB
NWH360(1.0/1.0)
Spectral Acceleration (g)
Frequency(Hz)
L−Shake Table−Longitudinal
L+V−Shake Table−Longitudinal
Target
TSB
NWH360(1.0/1.0)
Spectral Accel. (g)
L−Shake Table−Vertical
L+V−Shake Table−Vertical
Target
TSB
NWH360(1.0/1.0)
Spectral Accel.(g)
L−Base−Vertical
L+V−Base−Vertical
TSB
NWH360(1.0/1.0)
Spectral Accel.(g)
Frequency(Hz)

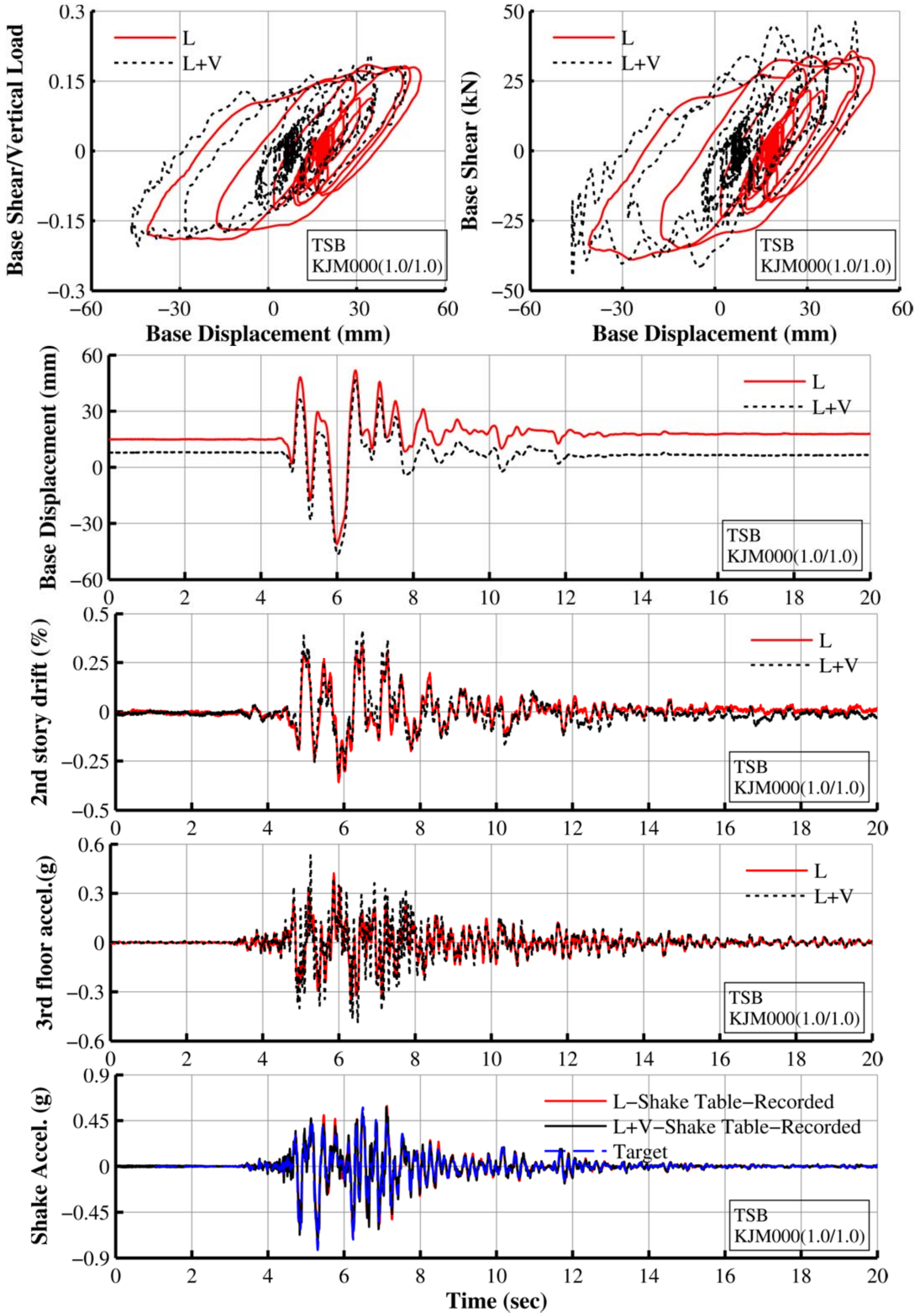
Base Shear/Vertical Load
L
L+V
TSB
KJM000(1.0/1.0)
Base Displacement (mm)
Base Shear (kN)
Base Displacement (mm)
2nd story drift (%)
3rd floor accel.(g)
L−Shake Table−Recorded
L+V−Shake Table−Recorded
Target
Shake Accel. (g)
Time (sec)

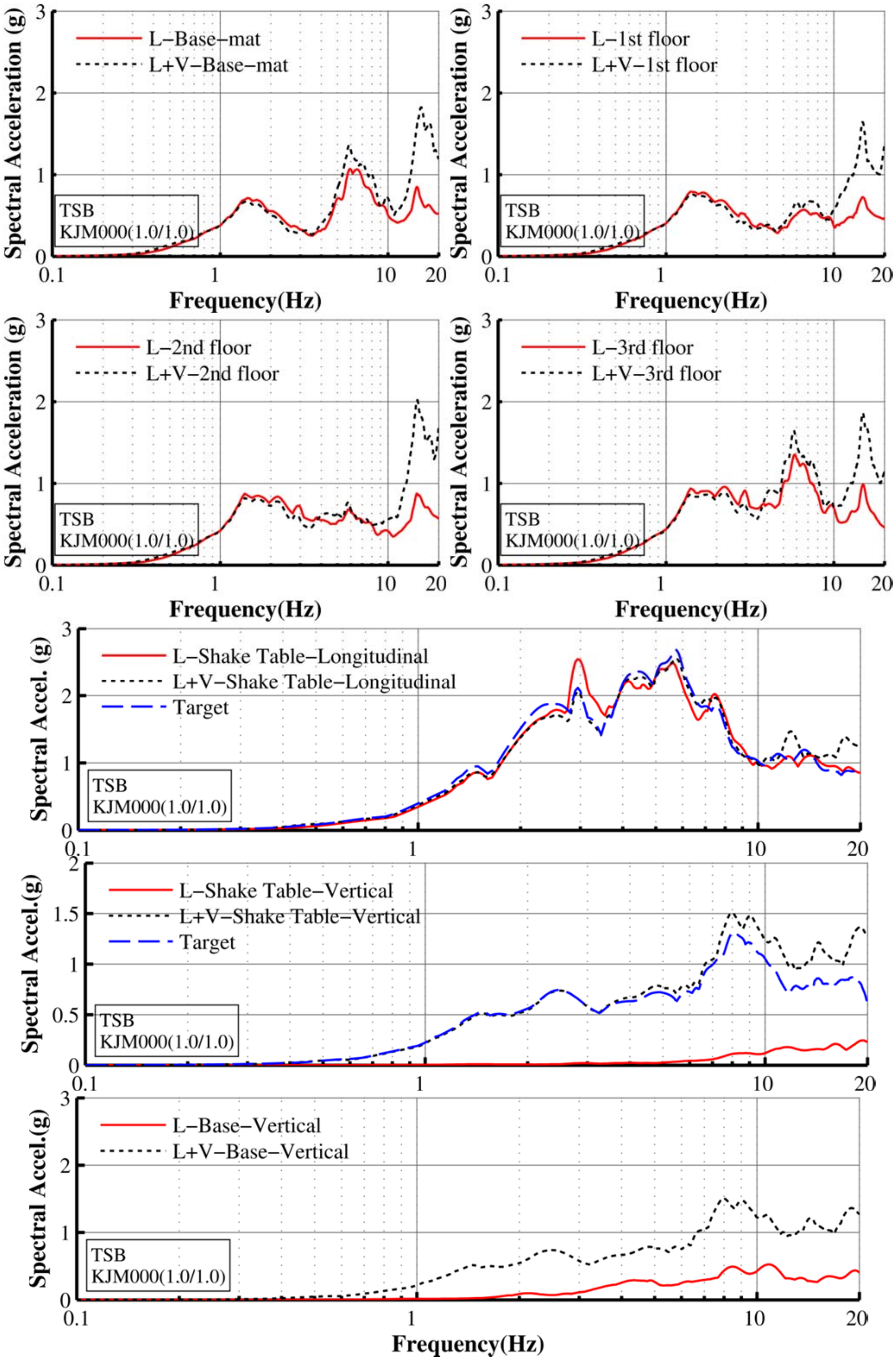

L−Base−mat
L+V−Base−mat
TSB
KJM000(1.0/1.0)
L−1st floor
L+V−1st floor
TSB
KJM000(1.0/1.0)
L−2nd floor
L+V−2nd floor
TSB
KJM000(1.0/1.0)
L−3rd floor
L+V−3rd floor
TSB
KJM000(1.0/1.0)
Spectral Acceleration (g)
Frequency(Hz)
L−Shake Table−Longitudinal
L+V−Shake Table−Longitudinal
Target
TSB
KJM000(1.0/1.0)
Spectral Accel. (g)
L−Shake Table−Vertical
L+V−Shake Table−Vertical
Target
TSB
KJM000(1.0/1.0)
Spectral Accel.(g)
L−Base−Vertical
L+V−Base−Vertical
TSB
KJM000(1.0/1.0)
Spectral Accel.(g)
Frequency(Hz)

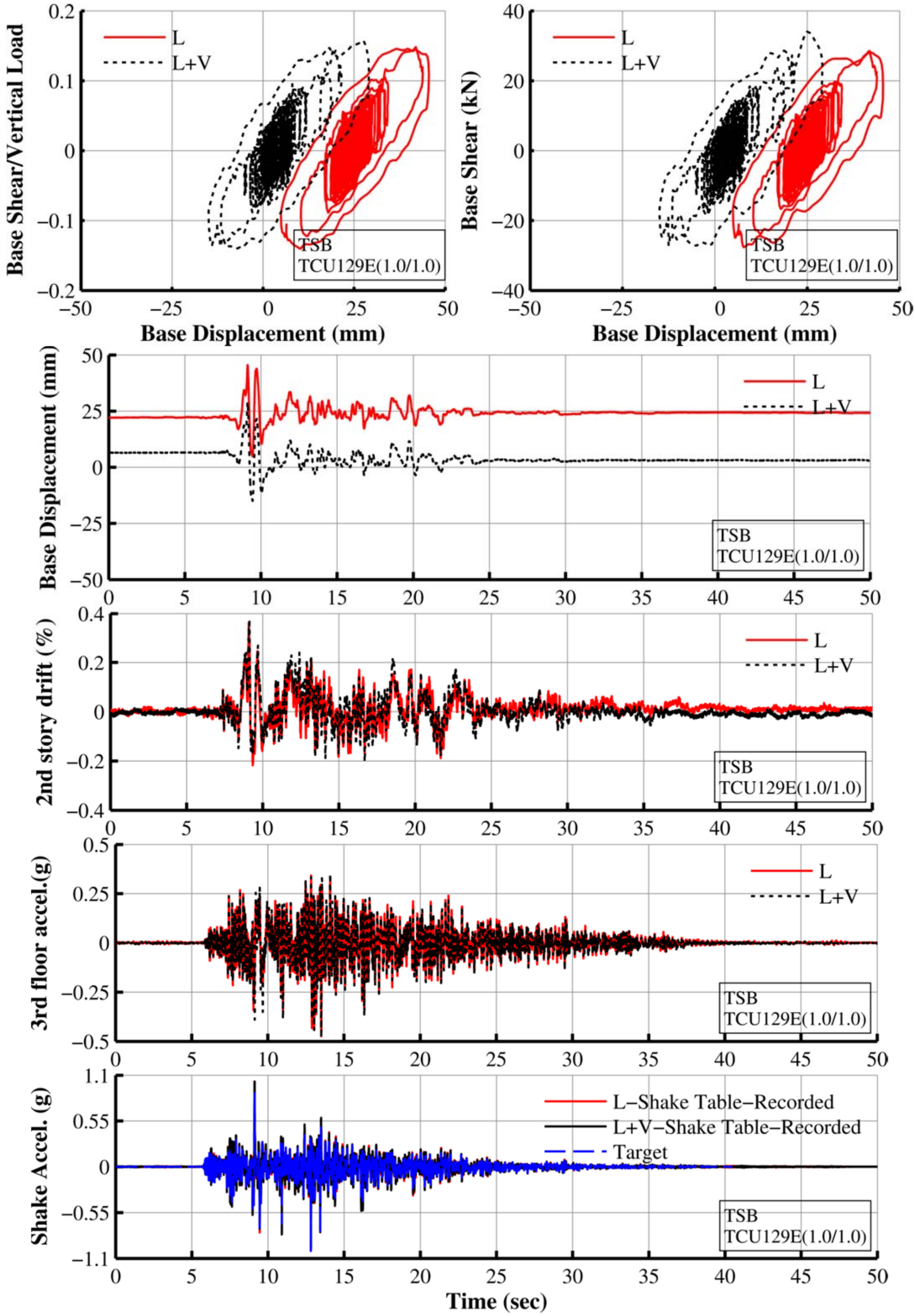
Base Shear/Vertical Load
Base Displacement (mm)
L
L+V
TSB
TCU129E(1.0/1.0)
Base Shear (kN)
Base Displacement (mm)
Base Displacement (mm)
2nd story drift (%)
3rd floor accel.(g)
Shake Accel. (g)
L−Shake Table−Recorded
L+V−Shake Table−Recorded
Target
Time (sec)

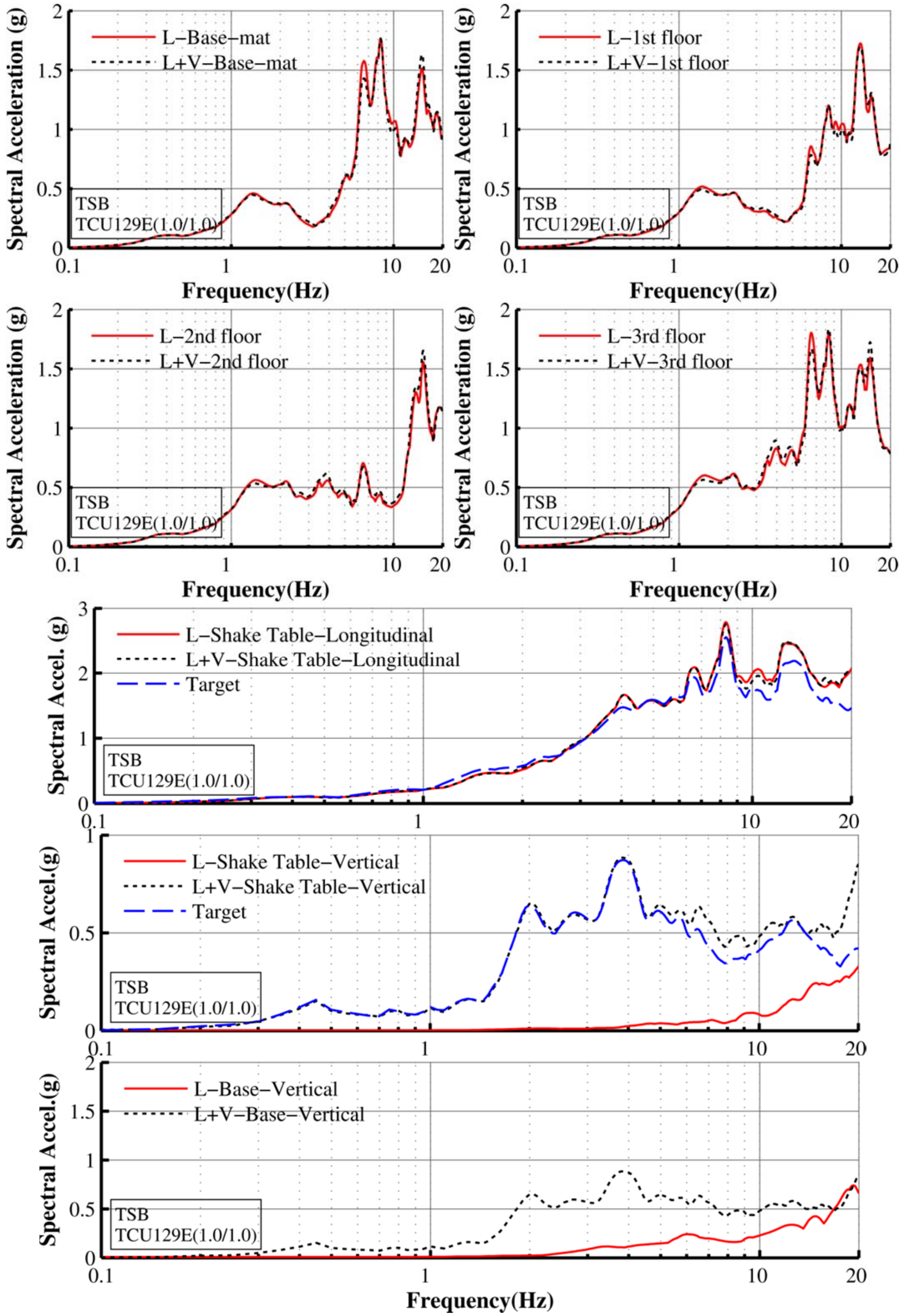

L−Base−mat
L+V−Base−mat
L−1st floor
L+V−1st floor
L−2nd floor
L+V−2nd floor
L−3rd floor
L+V−3rd floor
L−Shake Table−Longitudinal
L+V−Shake Table−Longitudinal
Target
L−Shake Table−Vertical
L+V−Shake Table−Vertical
L−Base−Vertical
L+V−Base−Vertical
TSB
TCU129E(1.0/1.0)
Spectral Acceleration (g)
Spectral Accel. (g)
Spectral Accel.(g)
Frequency(Hz)
0.1
1
10
20
0
0.5
1
1.5
2
3

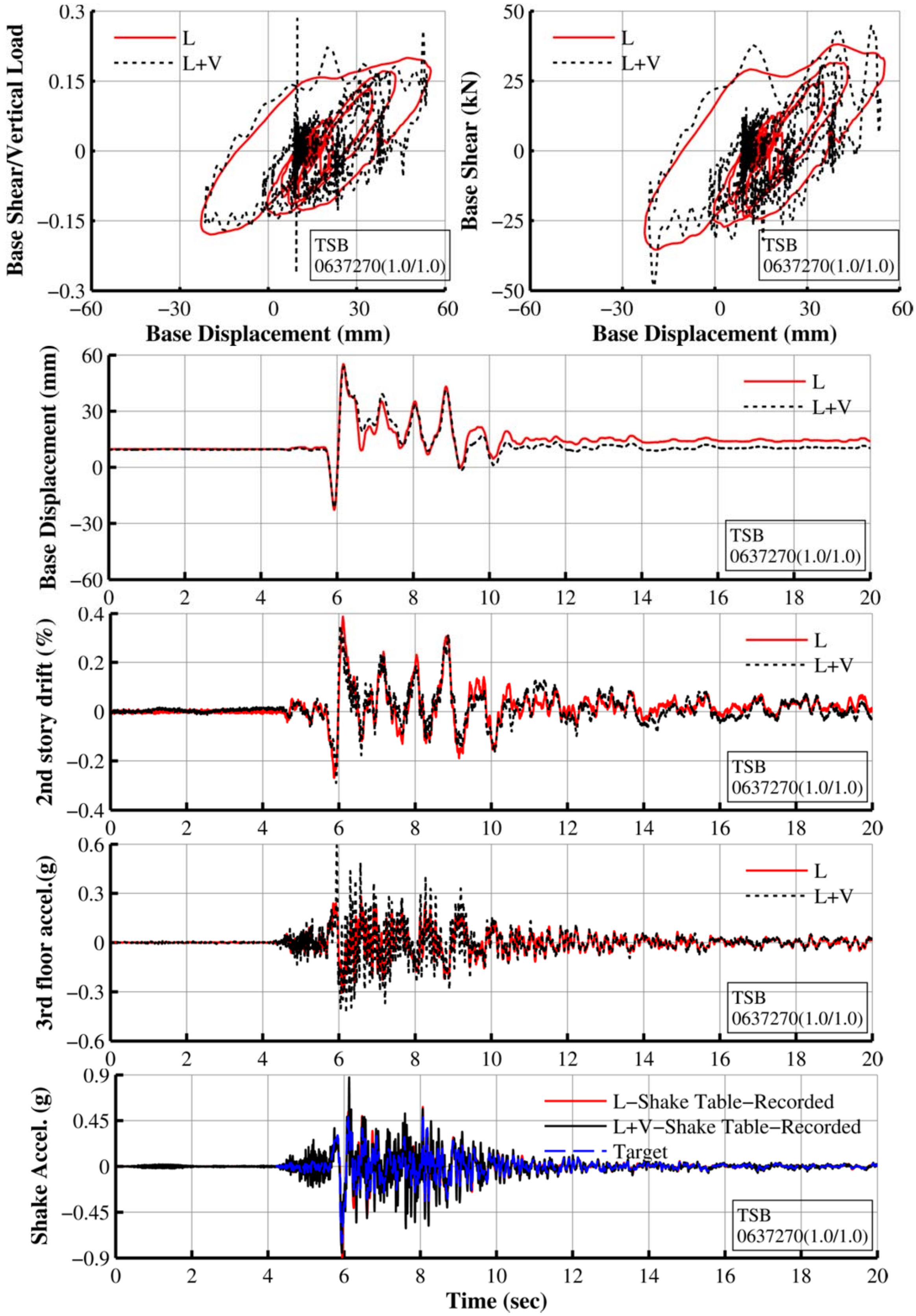
L
L+V
TSB
0637270(1.0/1.0)
Base Shear/Vertical Load
Base Shear (kN)
Base Displacement (mm)
Base Displacement (mm)
2nd story drift (%)
3rd floor accel.(g)
L−Shake Table−Recorded
L+V−Shake Table−Recorded
Target
Shake Accel. (g)
Time (sec)

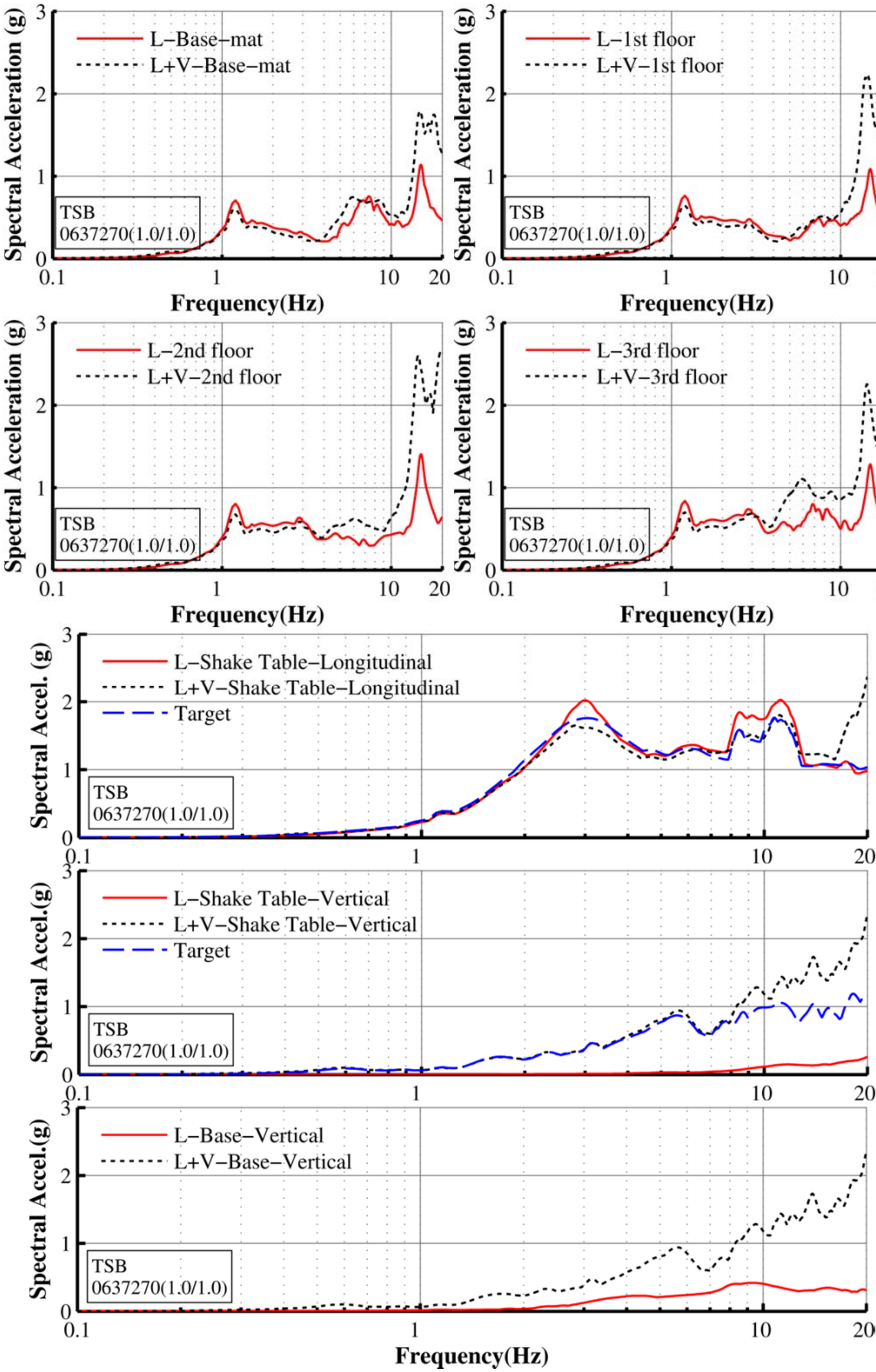
L−Base−mat
L+V−Base−mat
TSB
0637270(1.0/1.0)
L−1st floor
L+V−1st floor
L−2nd floor
L+V−2nd floor
L−3rd floor
L+V−3rd floor
Spectral Acceleration (g)
Frequency(Hz)
L−Shake Table−Longitudinal
L+V−Shake Table−Longitudinal
Target
Spectral Accel. (g)
L−Shake Table−Vertical
L+V−Shake Table−Vertical
L−Base−Vertical
L+V−Base−Vertical
Spectral Accel.(g)

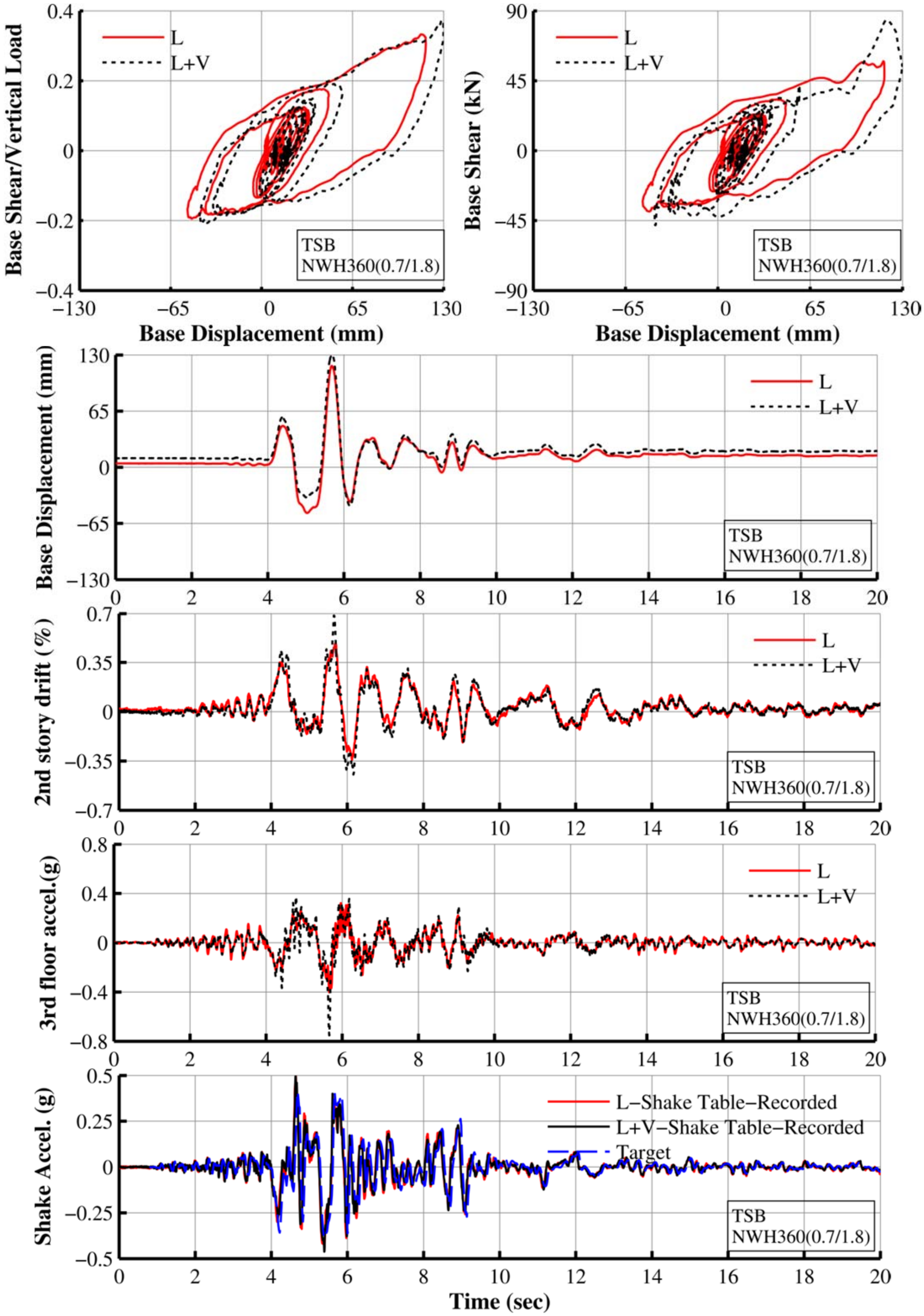

L
L+V
Base Shear/Vertical Load
TSB
NWH360(0.7/1.8)
Base Displacement (mm)
Base Shear (kN)
Base Displacement (mm)
Time (sec)
2nd story drift (%)
3rd floor accel.(g)
Shake Accel. (g)
L−Shake Table−Recorded
L+V−Shake Table−Recorded
Target

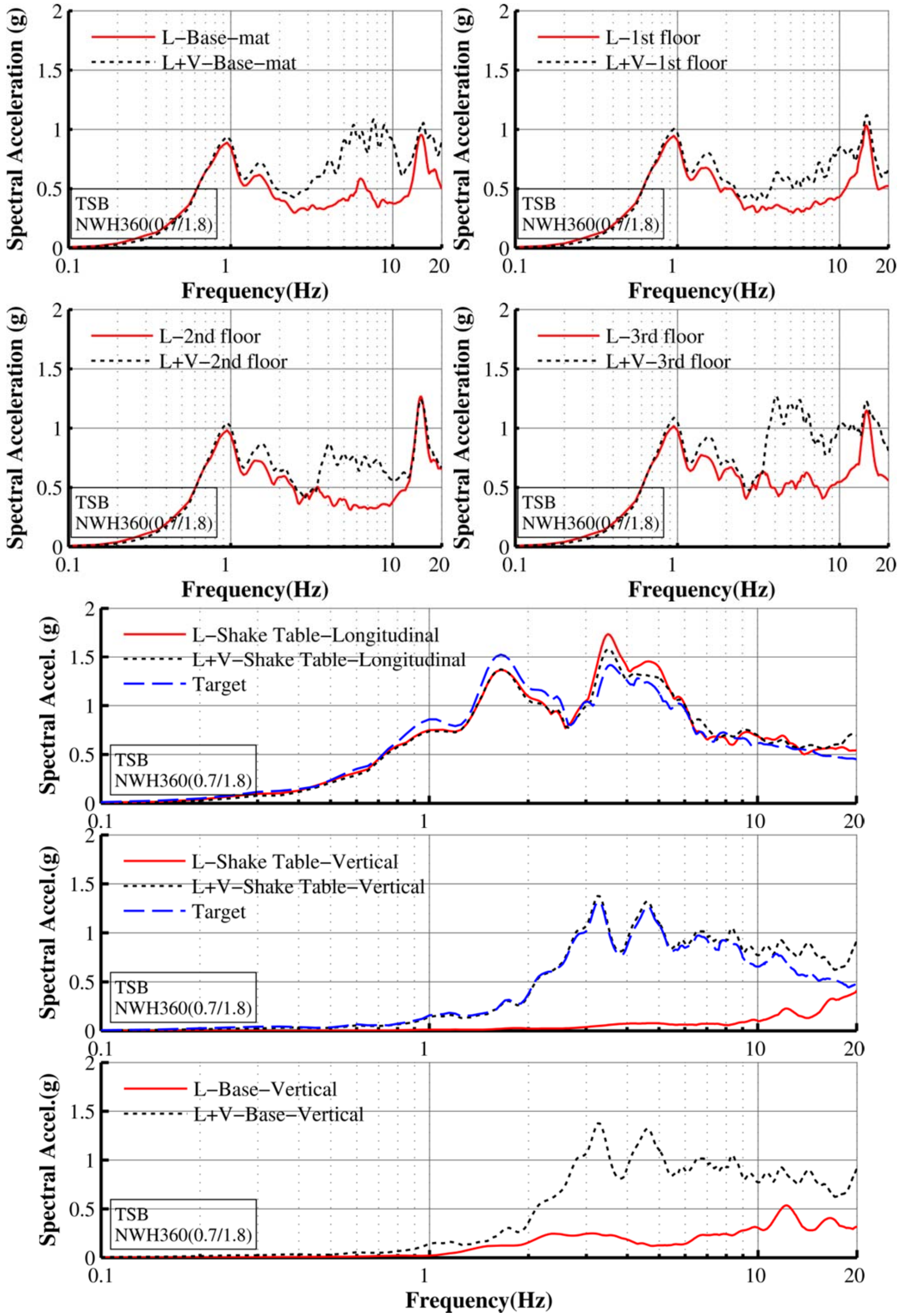
L−Base−mat
L+V−Base−mat
L−1st floor
L+V−1st floor
L−2nd floor
L+V−2nd floor
L−3rd floor
L+V−3rd floor
TSB
NWH360(0.7/1.8)
Spectral Acceleration (g)
Frequency(Hz)
L−Shake Table−Longitudinal
L+V−Shake Table−Longitudinal
Target
Spectral Accel. (g)
L−Shake Table−Vertical
L+V−Shake Table−Vertical
Spectral Accel.(g)
L−Base−Vertical
L+V−Base−Vertical

Appendix B

3pleANI2

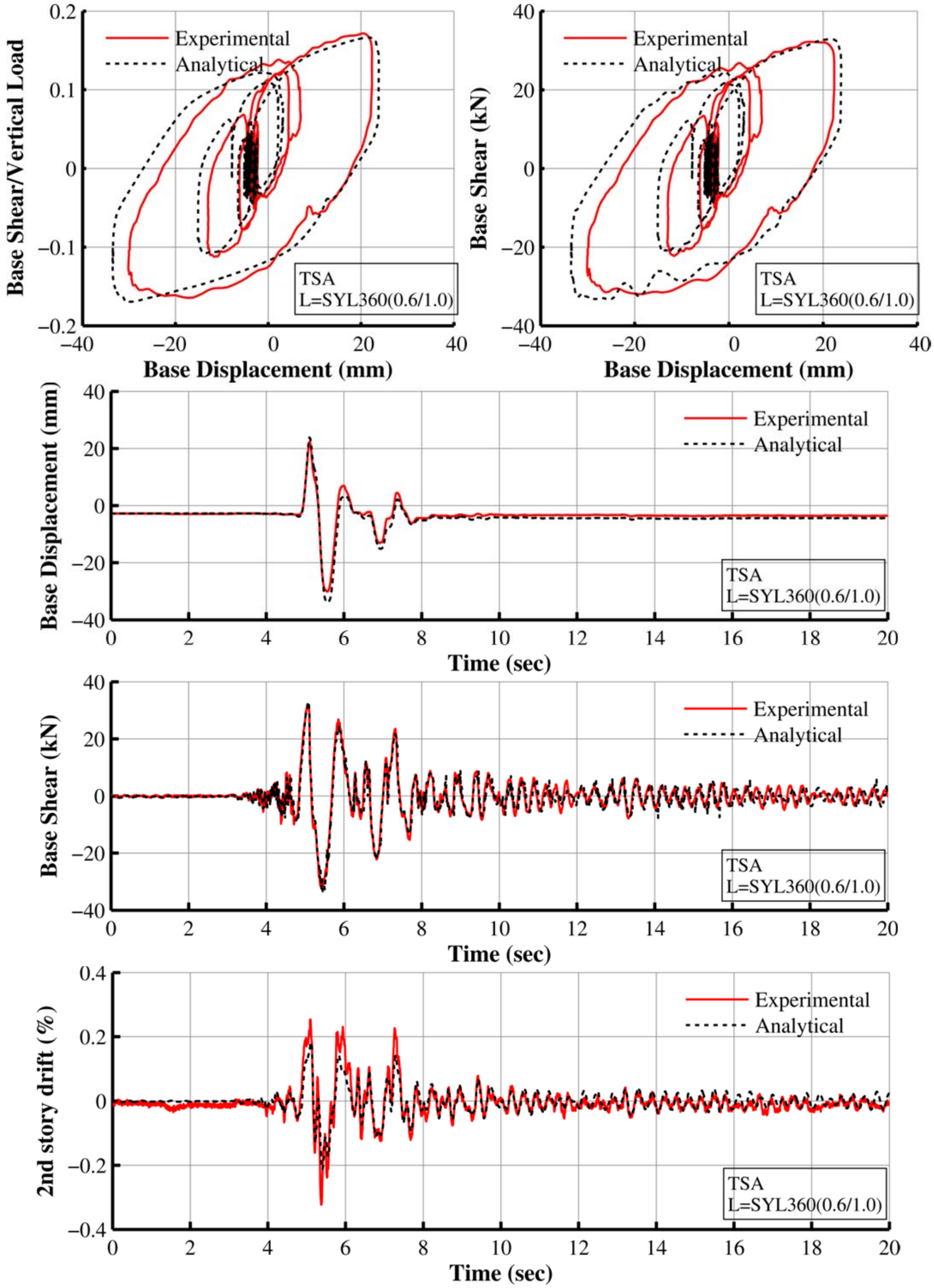

Base Shear/Vertical Load
Base Displacement (mm)
Experimental
Analytical
TSA
L=SYL360(0.6/1.0)
Base Shear (kN)
Base Displacement (mm)
Experimental
Analytical
TSA
L=SYL360(0.6/1.0)
Base Displacement (mm)
Time (sec)
Experimental
Analytical
TSA
L=SYL360(0.6/1.0)
Base Shear (kN)
Time (sec)
Experimental
Analytical
TSA
L=SYL360(0.6/1.0)
2nd story drift (%)
Time (sec)
Experimental
Analytical
TSA
L=SYL360(0.6/1.0)

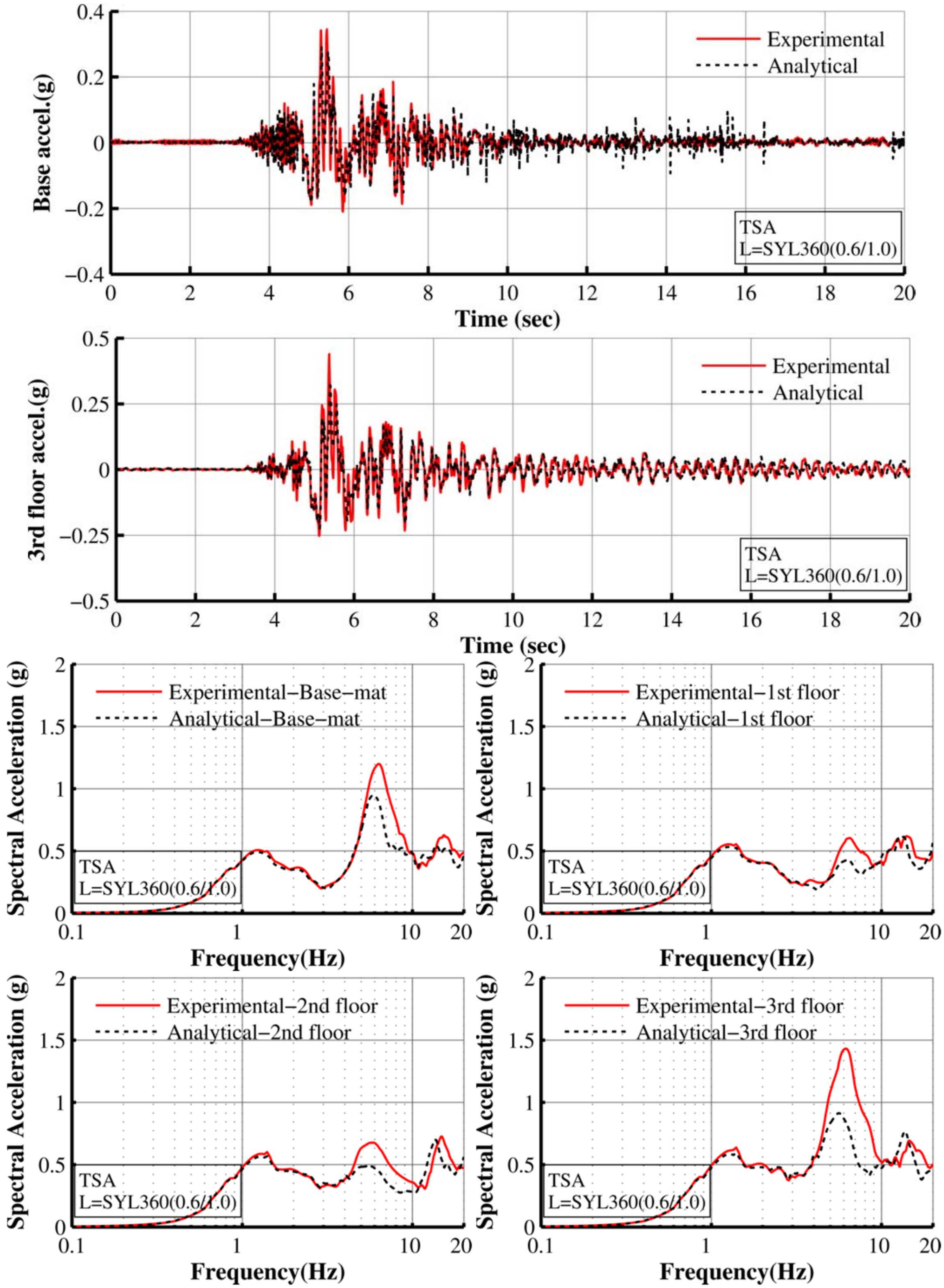
Base accel.(g)
Time (sec)
Experimental
Analytical
TSA
L=SYL360(0.6/1.0)
3rd floor accel.(g)
Time (sec)
Experimental
Analytical
TSA
L=SYL360(0.6/1.0)
Spectral Acceleration (g)
Frequency(Hz)
Experimental−Base−mat
Analytical−Base−mat
TSA
L=SYL360(0.6/1.0)
Spectral Acceleration (g)
Frequency(Hz)
Experimental−1st floor
Analytical−1st floor
TSA
L=SYL360(0.6/1.0)
Spectral Acceleration (g)
Frequency(Hz)
Experimental−2nd floor
Analytical−2nd floor
TSA
L=SYL360(0.6/1.0)
Spectral Acceleration (g)
Frequency(Hz)
Experimental−3rd floor
Analytical−3rd floor
TSA
L=SYL360(0.6/1.0)

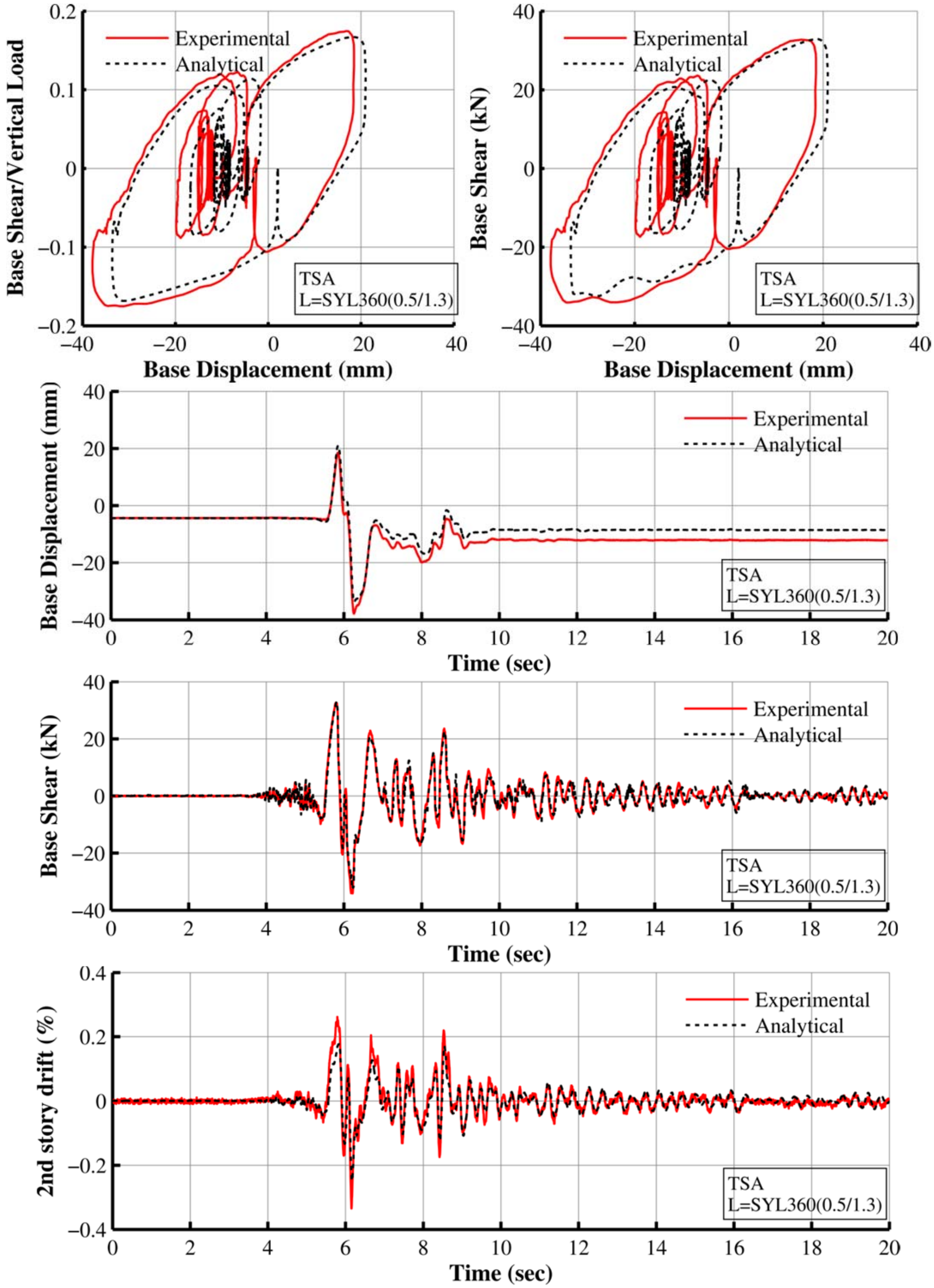
Experimental
Analytical
TSA
L=SYL360(0.5/1.3)
Base Shear/Vertical Load
Base Displacement (mm)
Base Shear (kN)
Base Displacement (mm)
Time (sec)
Base Shear (kN)
Time (sec)
2nd story drift (%)
Time (sec)

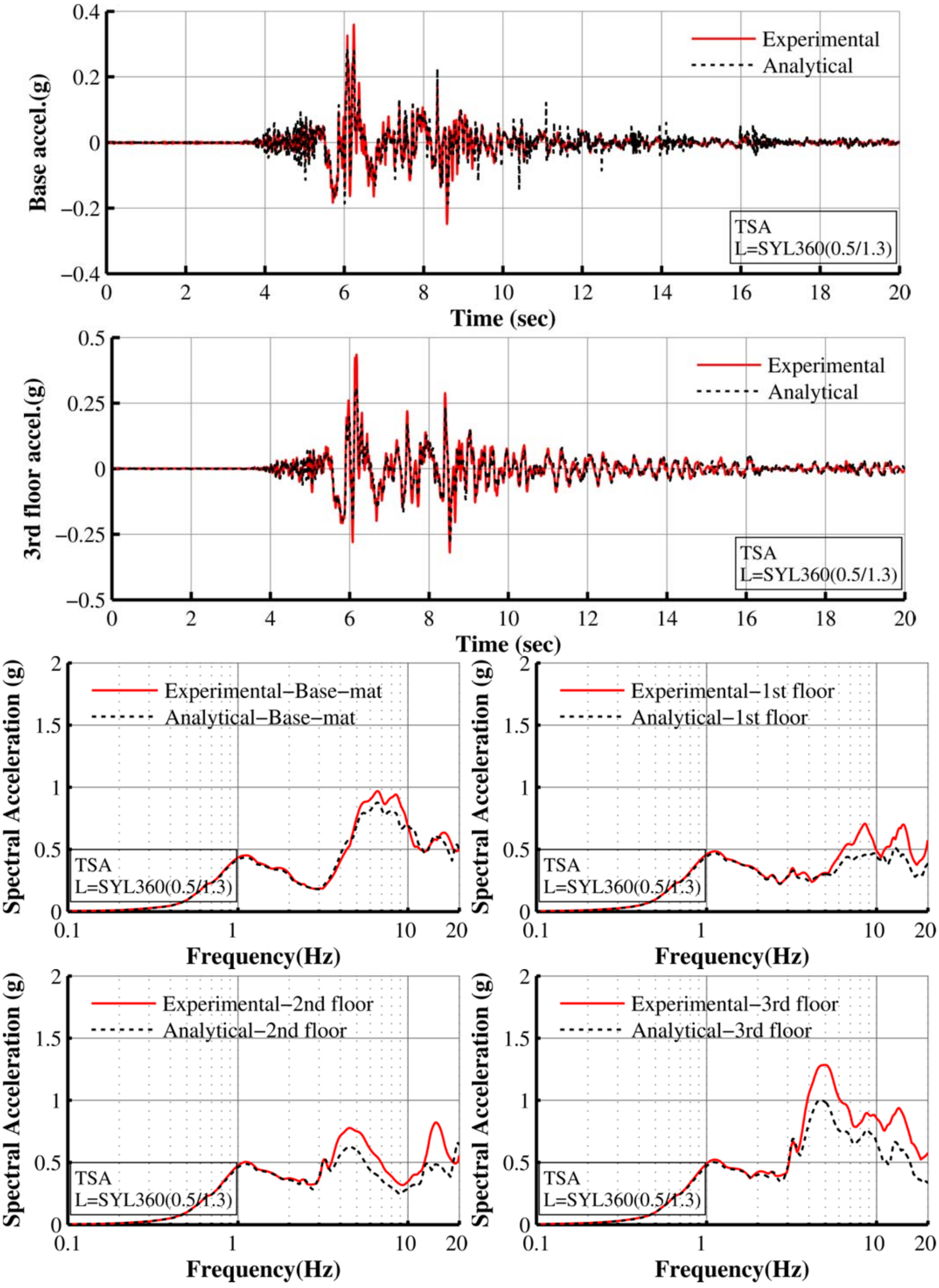
Base accel.(g)
Time (sec)
Experimental
Analytical
TSA
L=SYL360(0.5/1.3)
3rd floor accel.(g)
Time (sec)
Experimental
Analytical
TSA
L=SYL360(0.5/1.3)
Spectral Acceleration (g)
Frequency(Hz)
Experimental−Base−mat
Analytical−Base−mat
TSA
L=SYL360(0.5/1.3)
Spectral Acceleration (g)
Frequency(Hz)
Experimental−1st floor
Analytical−1st floor
TSA
L=SYL360(0.5/1.3)
Spectral Acceleration (g)
Frequency(Hz)
Experimental−2nd floor
Analytical−2nd floor
TSA
L=SYL360(0.5/1.3)
Spectral Acceleration (g)
Frequency(Hz)
Experimental−3rd floor
Analytical−3rd floor
TSA
L=SYL360(0.5/1.3)

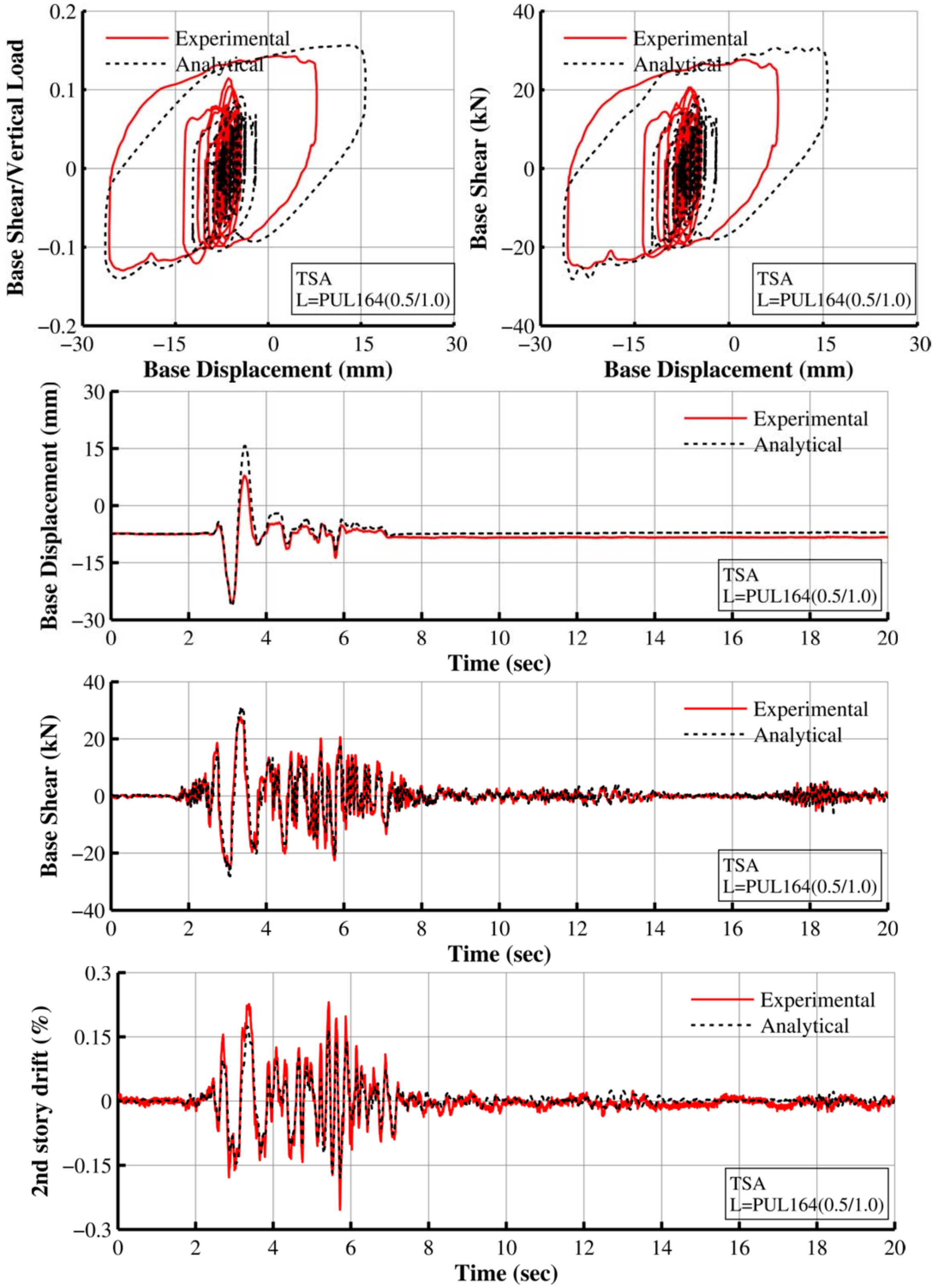
Base Shear/Vertical Load
Base Displacement (mm)
Experimental
Analytical
TSA
L=PUL164(0.5/1.0)
Base Shear (kN)
Base Displacement (mm)
Experimental
Analytical
TSA
L=PUL164(0.5/1.0)
Base Displacement (mm)
Time (sec)
Experimental
Analytical
TSA
L=PUL164(0.5/1.0)
Base Shear (kN)
Time (sec)
Experimental
Analytical
TSA
L=PUL164(0.5/1.0)
2nd story drift (%)
Time (sec)
Experimental
Analytical
TSA
L=PUL164(0.5/1.0)

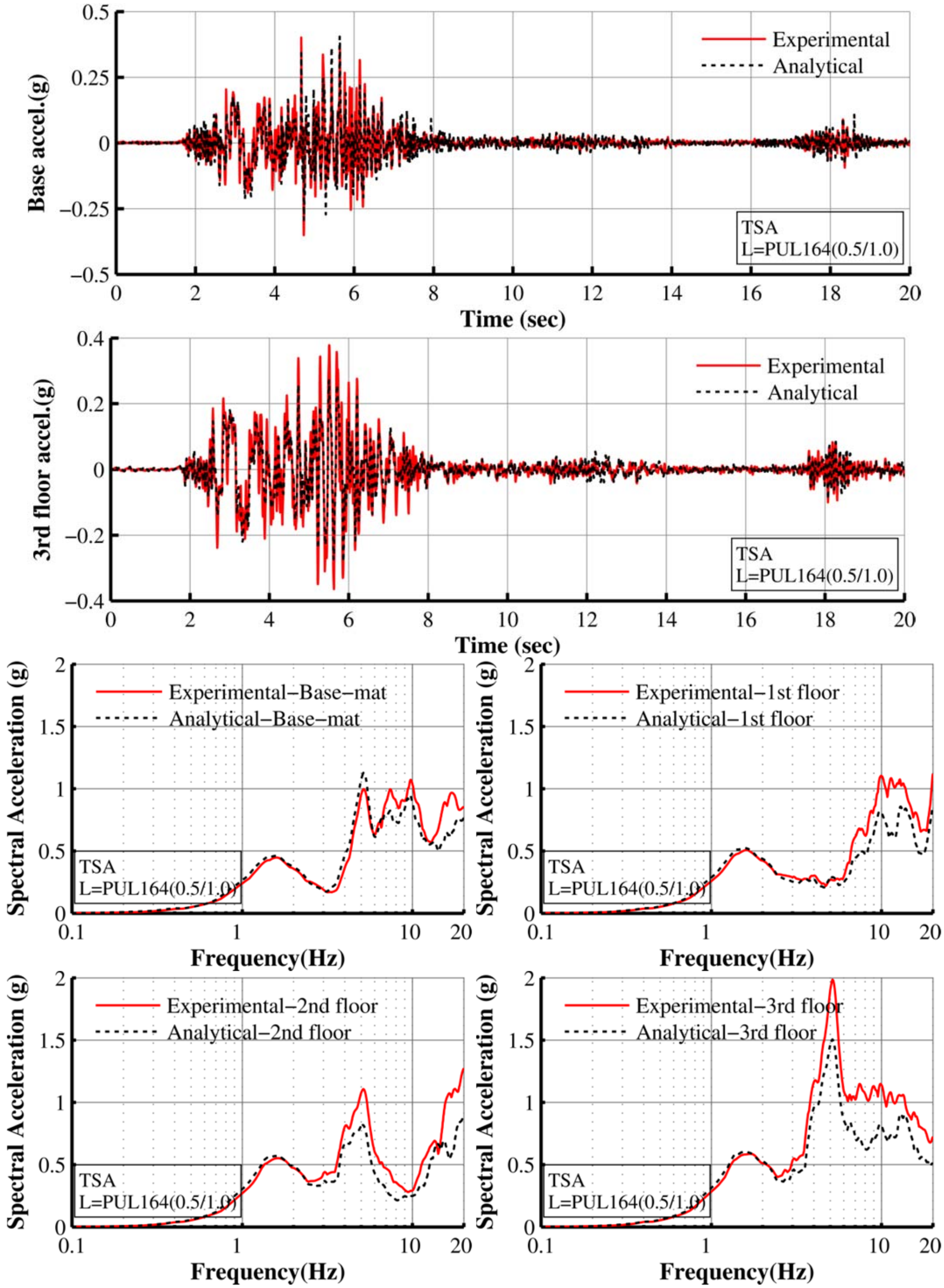
Base accel.(g)
Time (sec)
Experimental
Analytical
TSA
L=PUL164(0.5/1.0)
3rd floor accel.(g)
Time (sec)
Experimental
Analytical
TSA
L=PUL164(0.5/1.0)
Spectral Acceleration (g)
Frequency(Hz)
Experimental−Base−mat
Analytical−Base−mat
TSA
L=PUL164(0.5/1.0)
Spectral Acceleration (g)
Frequency(Hz)
Experimental−1st floor
Analytical−1st floor
TSA
L=PUL164(0.5/1.0)
Spectral Acceleration (g)
Frequency(Hz)
Experimental−2nd floor
Analytical−2nd floor
TSA
L=PUL164(0.5/1.0)
Spectral Acceleration (g)
Frequency(Hz)
Experimental−3rd floor
Analytical−3rd floor
TSA
L=PUL164(0.5/1.0)

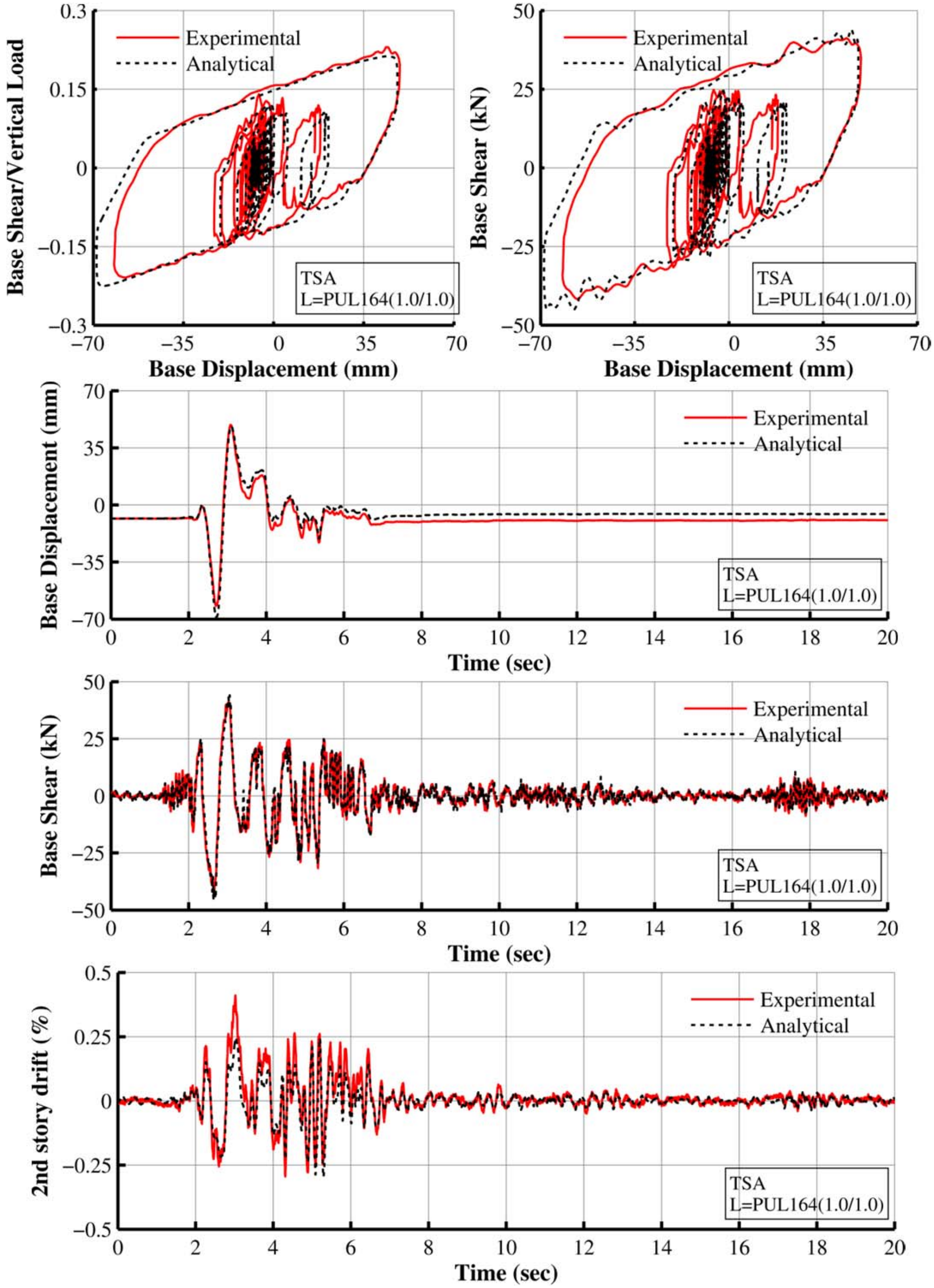
Experimental
Analytical
TSA
L=PUL164(1.0/1.0)
Base Shear/Vertical Load
Base Displacement (mm)
Base Shear (kN)
Base Displacement (mm)
Time (sec)
Base Shear (kN)
Time (sec)
2nd story drift (%)
Time (sec)

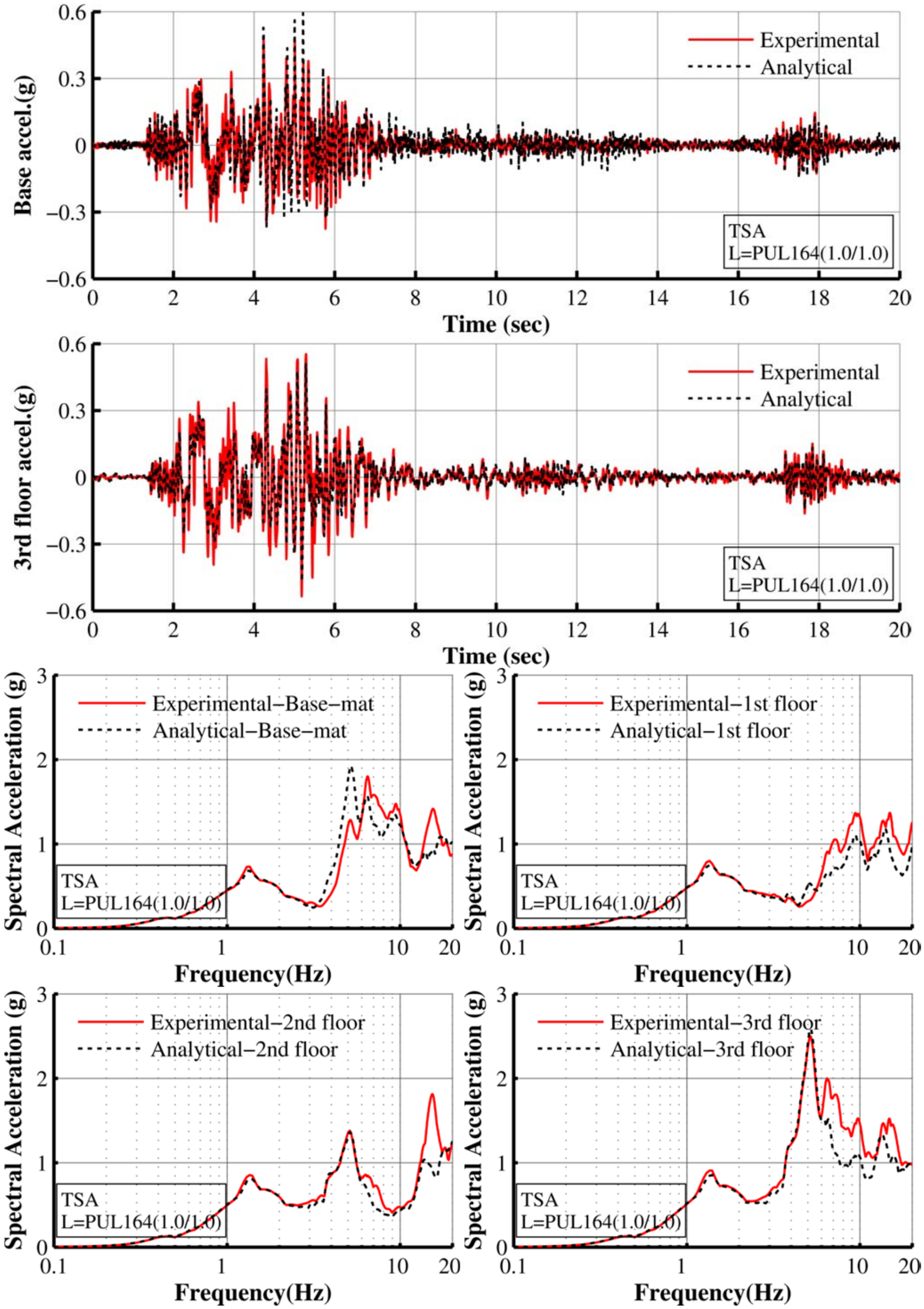
Base accel.(g)
Time (sec)
Experimental
Analytical
TSA
L=PUL164(1.0/1.0)
3rd floor accel.(g)
Time (sec)
Experimental
Analytical
TSA
L=PUL164(1.0/1.0)
Spectral Acceleration (g)
Frequency(Hz)
Experimental−Base−mat
Analytical−Base−mat
TSA
L=PUL164(1.0/1.0)
Spectral Acceleration (g)
Frequency(Hz)
Experimental−1st floor
Analytical−1st floor
TSA
L=PUL164(1.0/1.0)
Spectral Acceleration (g)
Frequency(Hz)
Experimental−2nd floor
Analytical−2nd floor
TSA
L=PUL164(1.0/1.0)
Spectral Acceleration (g)
Frequency(Hz)
Experimental−3rd floor
Analytical−3rd floor
TSA
L=PUL164(1.0/1.0)

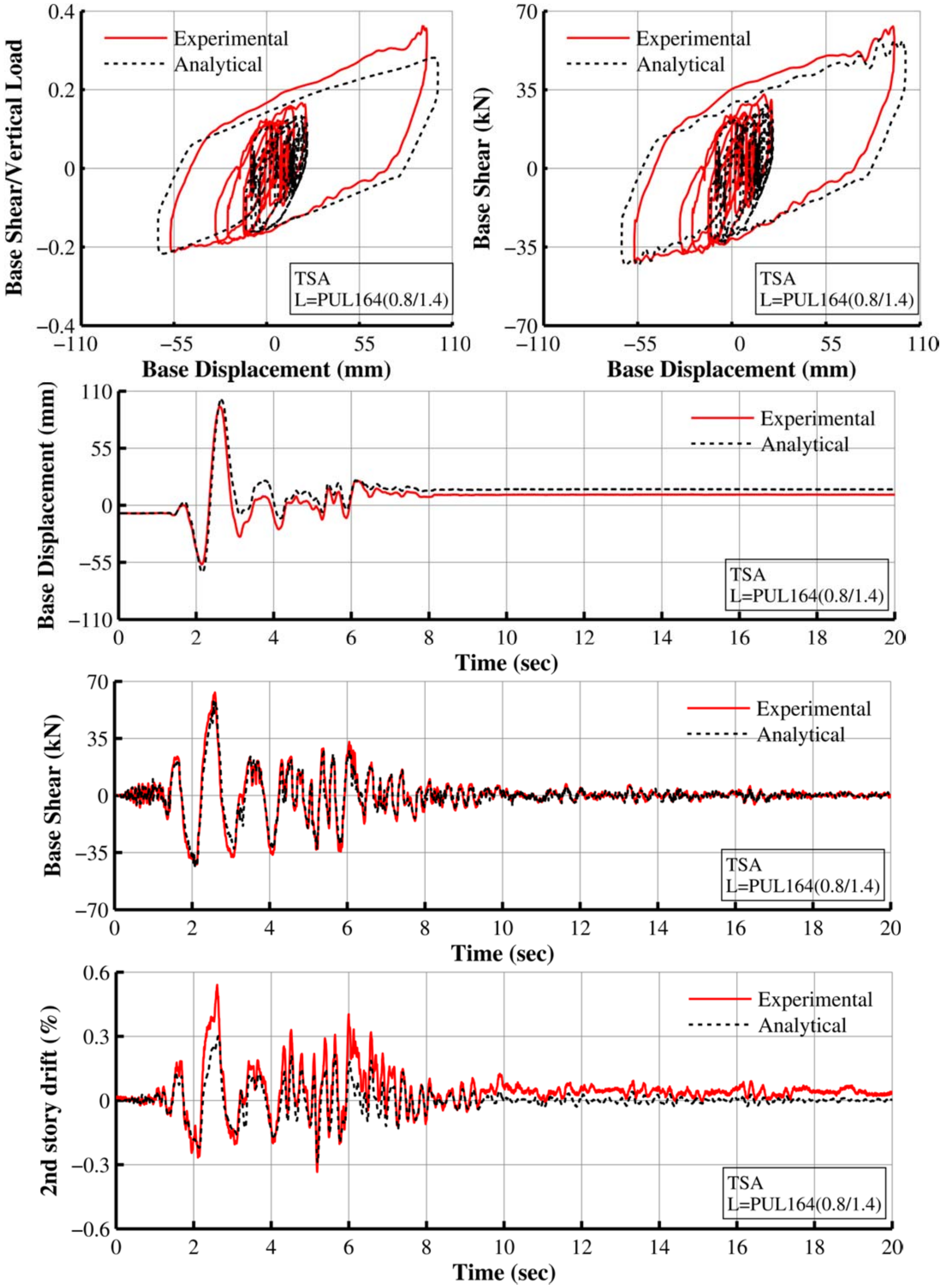
Experimental
Analytical
TSA
L=PUL164(0.8/1.4)
Base Shear/Vertical Load
Base Displacement (mm)
Base Shear (kN)
Base Displacement (mm)
Time (sec)
Base Shear (kN)
Time (sec)
2nd story drift (%)
Time (sec)

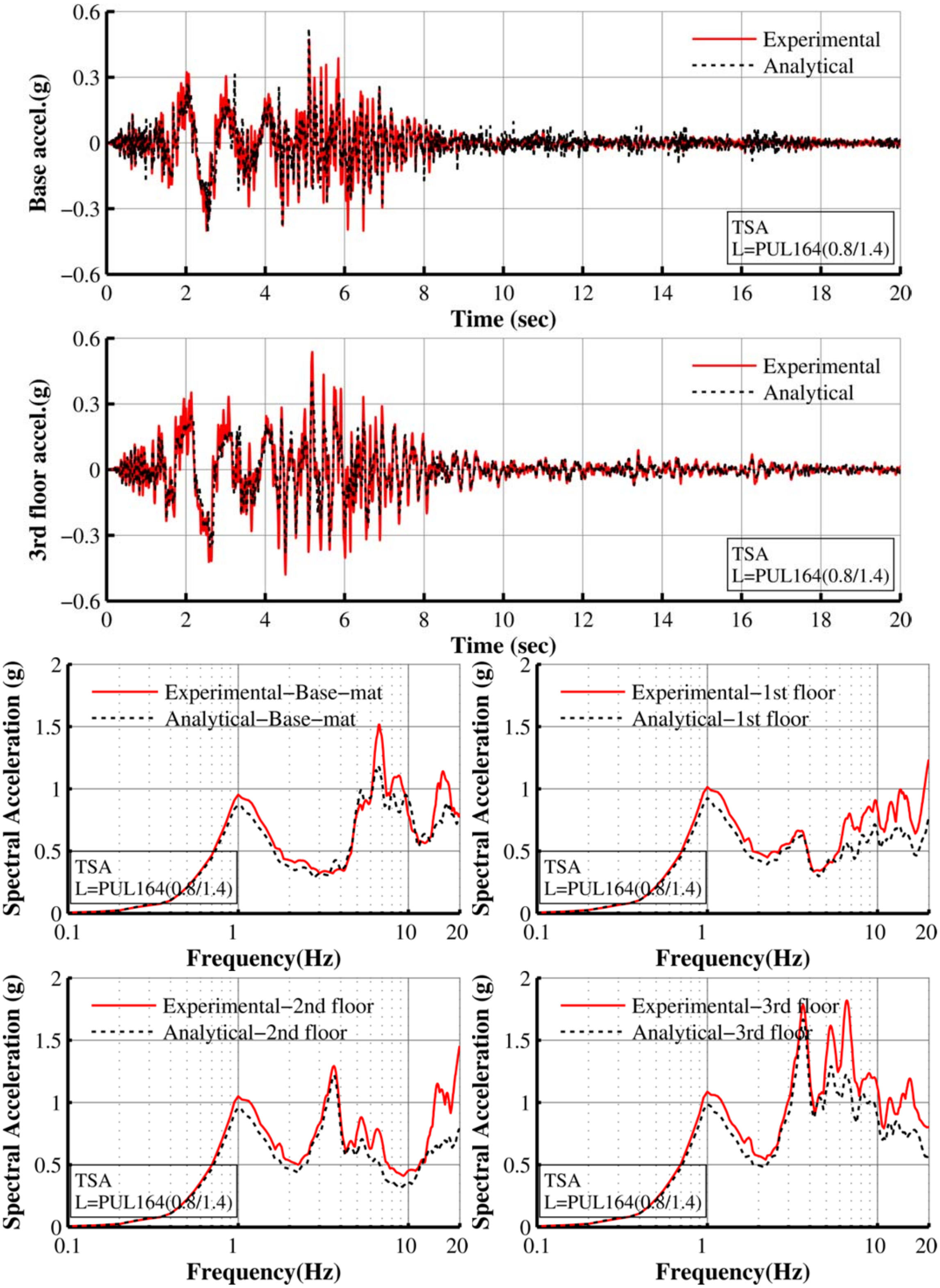

Base accel.(g)
Time (sec)
Experimental
Analytical
TSA
L=PUL164(0.8/1.4)
3rd floor accel.(g)
Time (sec)
Experimental
Analytical
TSA
L=PUL164(0.8/1.4)
Spectral Acceleration (g)
Frequency(Hz)
Experimental−Base−mat
Analytical−Base−mat
TSA
L=PUL164(0.8/1.4)
Spectral Acceleration (g)
Frequency(Hz)
Experimental−1st floor
Analytical−1st floor
TSA
L=PUL164(0.8/1.4)
Spectral Acceleration (g)
Frequency(Hz)
Experimental−2nd floor
Analytical−2nd floor
TSA
L=PUL164(0.8/1.4)
Spectral Acceleration (g)
Frequency(Hz)
Experimental−3rd floor
Analytical−3rd floor
TSA
L=PUL164(0.8/1.4)

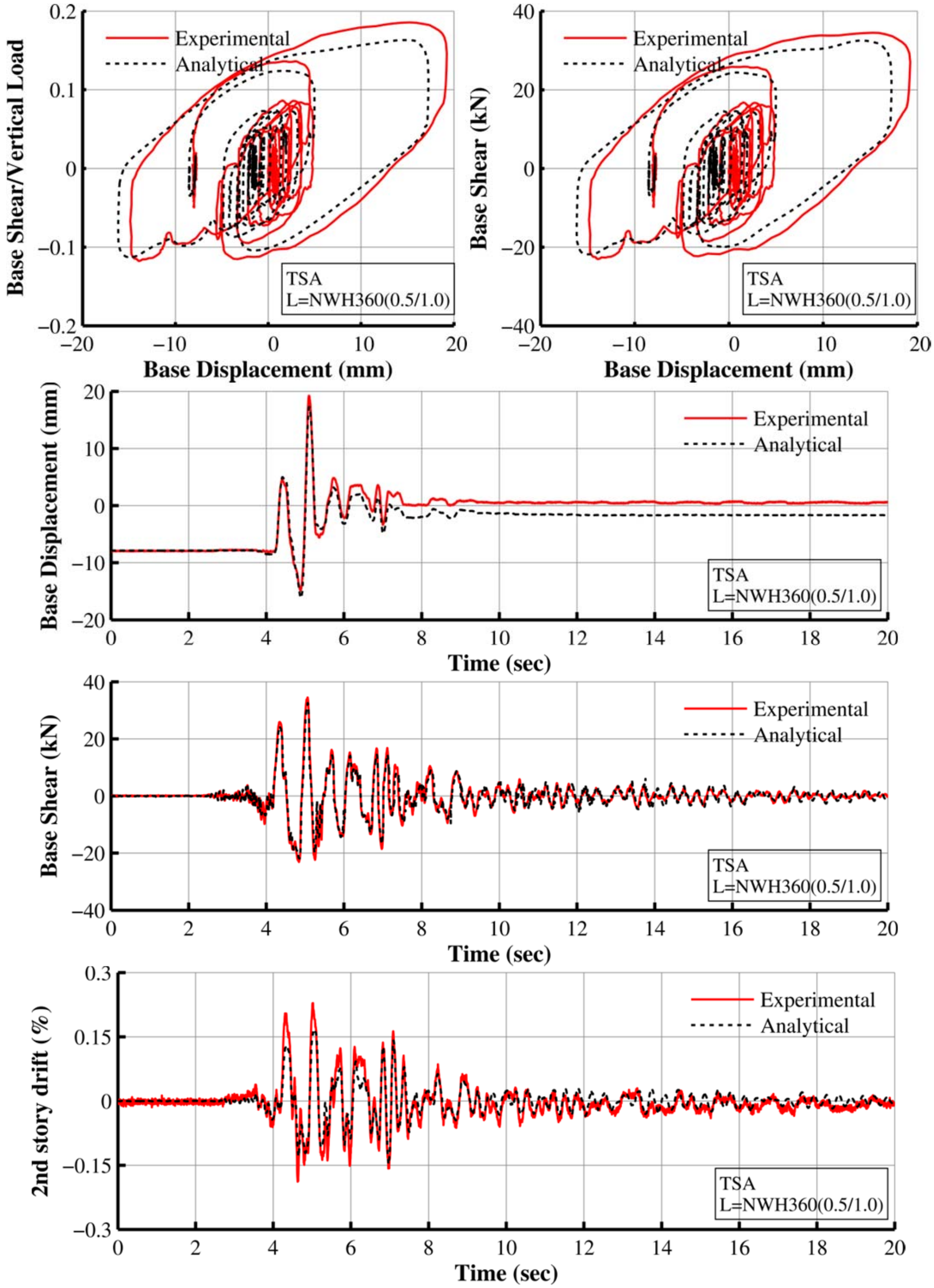
Experimental
Analytical
TSA
L=NWH360(0.5/1.0)
Base Shear/Vertical Load
Base Shear (kN)
Base Displacement (mm)
Time (sec)
Base Shear (kN)
2nd story drift (%)

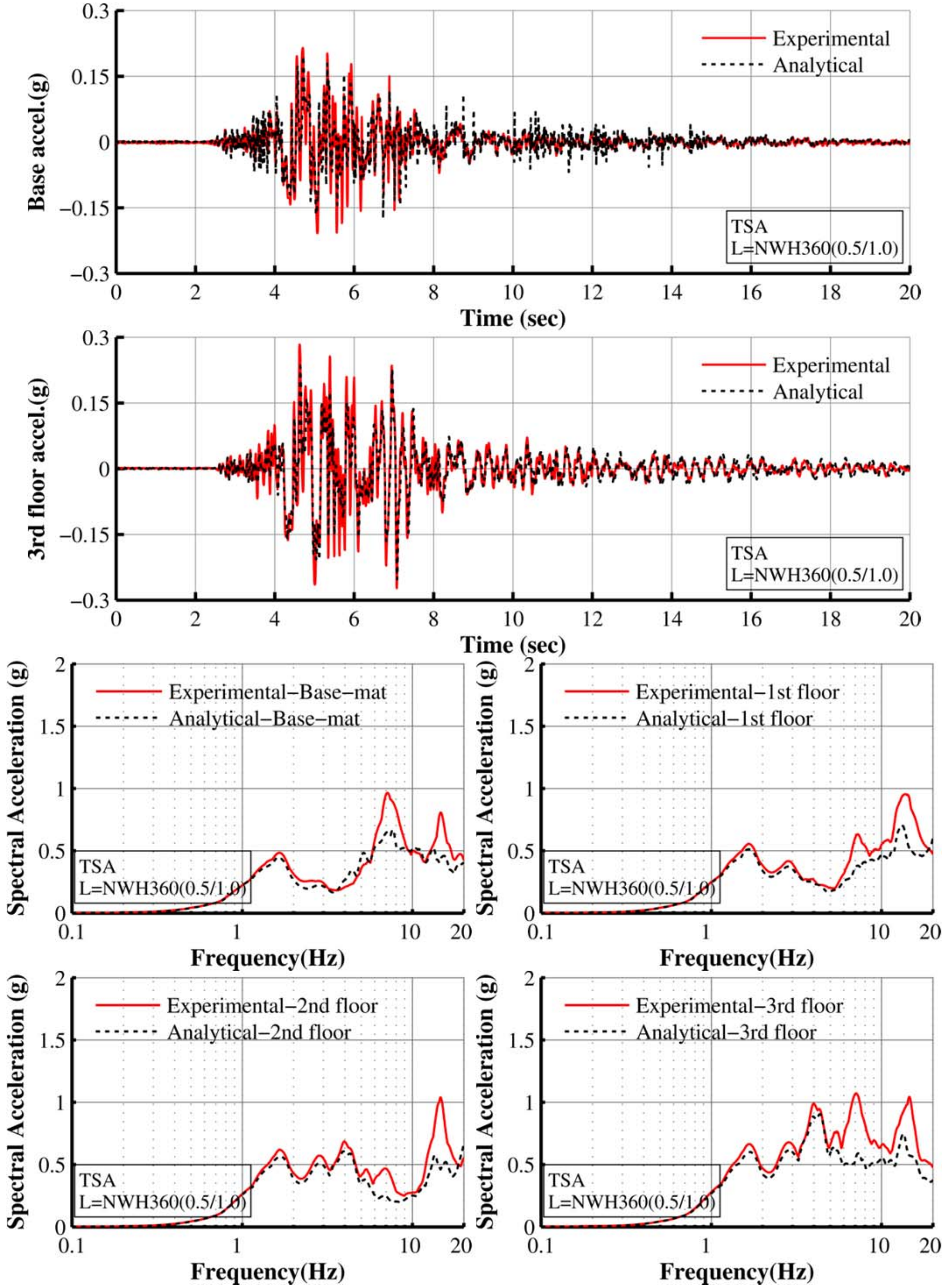
Base accel.(g)
Experimental
Analytical
TSA
L=NWH360(0.5/1.0)
Time (sec)
3rd floor accel.(g)
Experimental
Analytical
TSA
L=NWH360(0.5/1.0)
Time (sec)
Spectral Acceleration (g)
Experimental−Base−mat
Analytical−Base−mat
TSA
L=NWH360(0.5/1.0)
Frequency(Hz)
Spectral Acceleration (g)
Experimental−1st floor
Analytical−1st floor
TSA
L=NWH360(0.5/1.0)
Frequency(Hz)
Spectral Acceleration (g)
Experimental−2nd floor
Analytical−2nd floor
TSA
L=NWH360(0.5/1.0)
Frequency(Hz)
Spectral Acceleration (g)
Experimental−3rd floor
Analytical−3rd floor
TSA
L=NWH360(0.5/1.0)
Frequency(Hz)

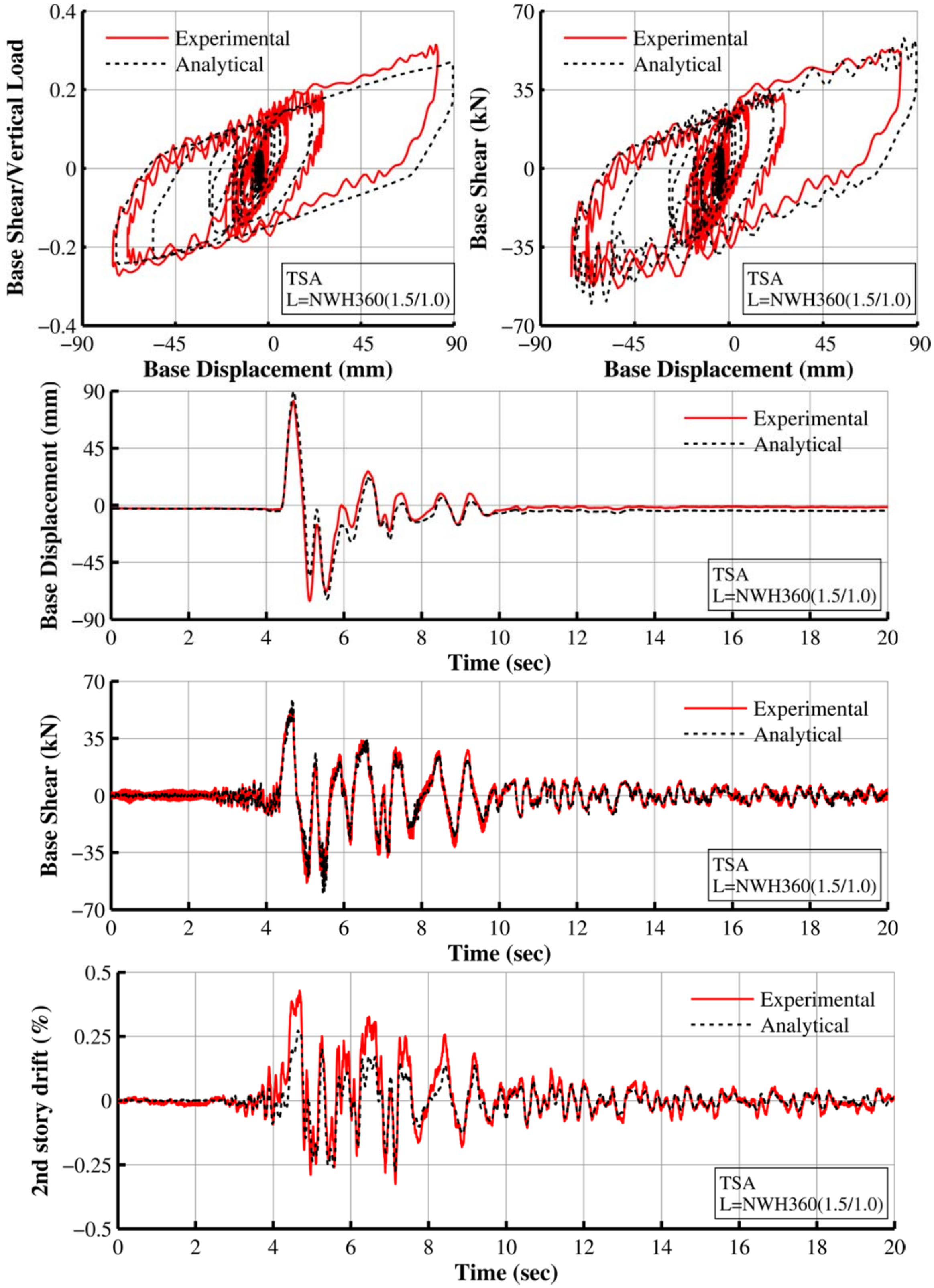
Experimental
Analytical
TSA
L=NWH360(1.5/1.0)
Base Shear/Vertical Load
Base Displacement (mm)
Base Shear (kN)
Base Displacement (mm)
Time (sec)
Base Shear (kN)
2nd story drift (%)

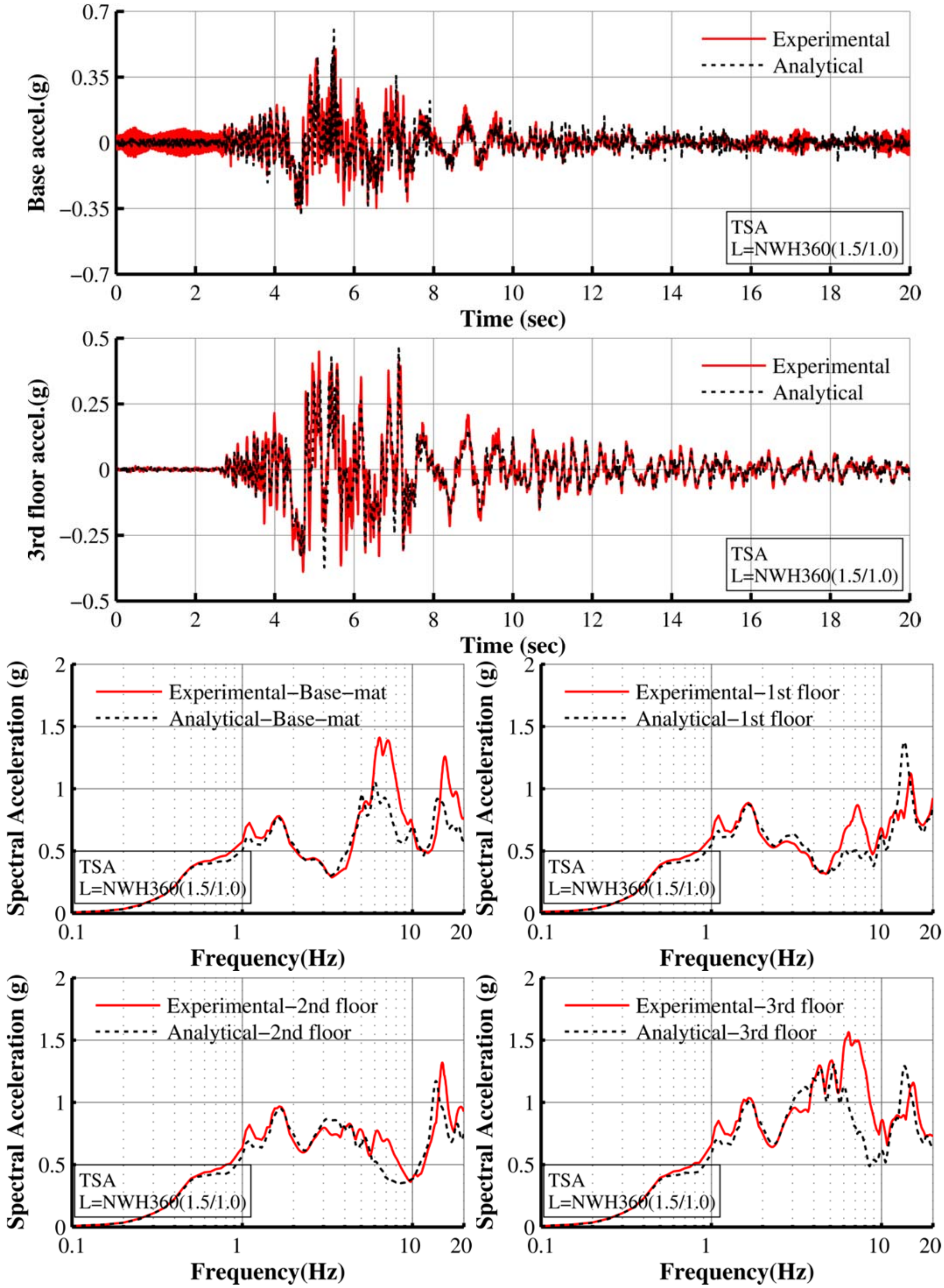

Base accel.(g)
Time (sec)
Experimental
Analytical
TSA
L=NWH360(1.5/1.0)
3rd floor accel.(g)
Time (sec)
Experimental
Analytical
TSA
L=NWH360(1.5/1.0)
Spectral Acceleration (g)
Frequency(Hz)
Experimental−Base−mat
Analytical−Base−mat
TSA
L=NWH360(1.5/1.0)
Spectral Acceleration (g)
Frequency(Hz)
Experimental−1st floor
Analytical−1st floor
TSA
L=NWH360(1.5/1.0)
Spectral Acceleration (g)
Frequency(Hz)
Experimental−2nd floor
Analytical−2nd floor
TSA
L=NWH360(1.5/1.0)
Spectral Acceleration (g)
Frequency(Hz)
Experimental−3rd floor
Analytical−3rd floor
TSA
L=NWH360(1.5/1.0)

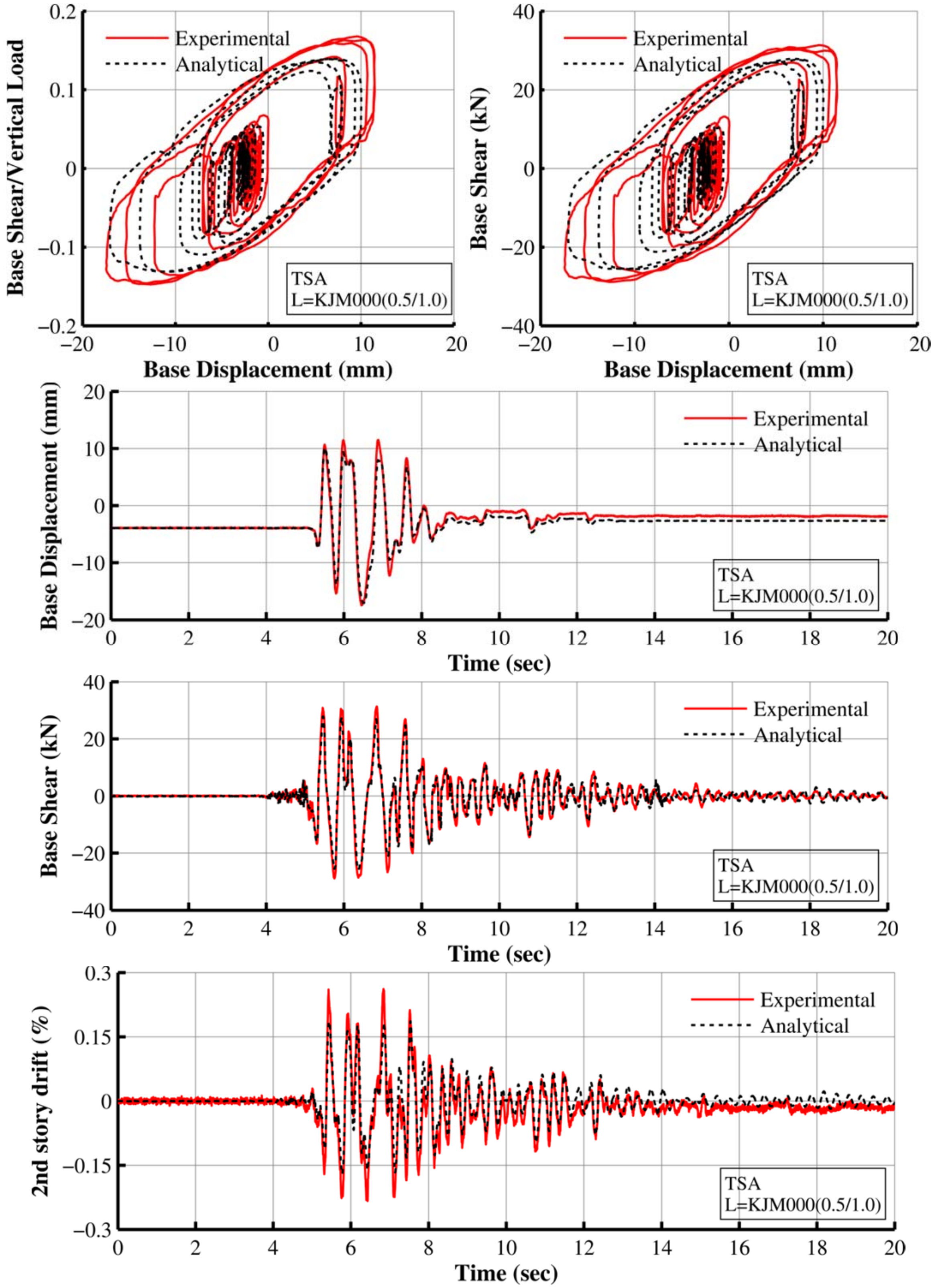
Experimental
Analytical
TSA
L=KJM000(0.5/1.0)
Base Shear/Vertical Load
Base Displacement (mm)
Base Shear (kN)
Base Displacement (mm)
Time (sec)
Base Shear (kN)
2nd story drift (%)

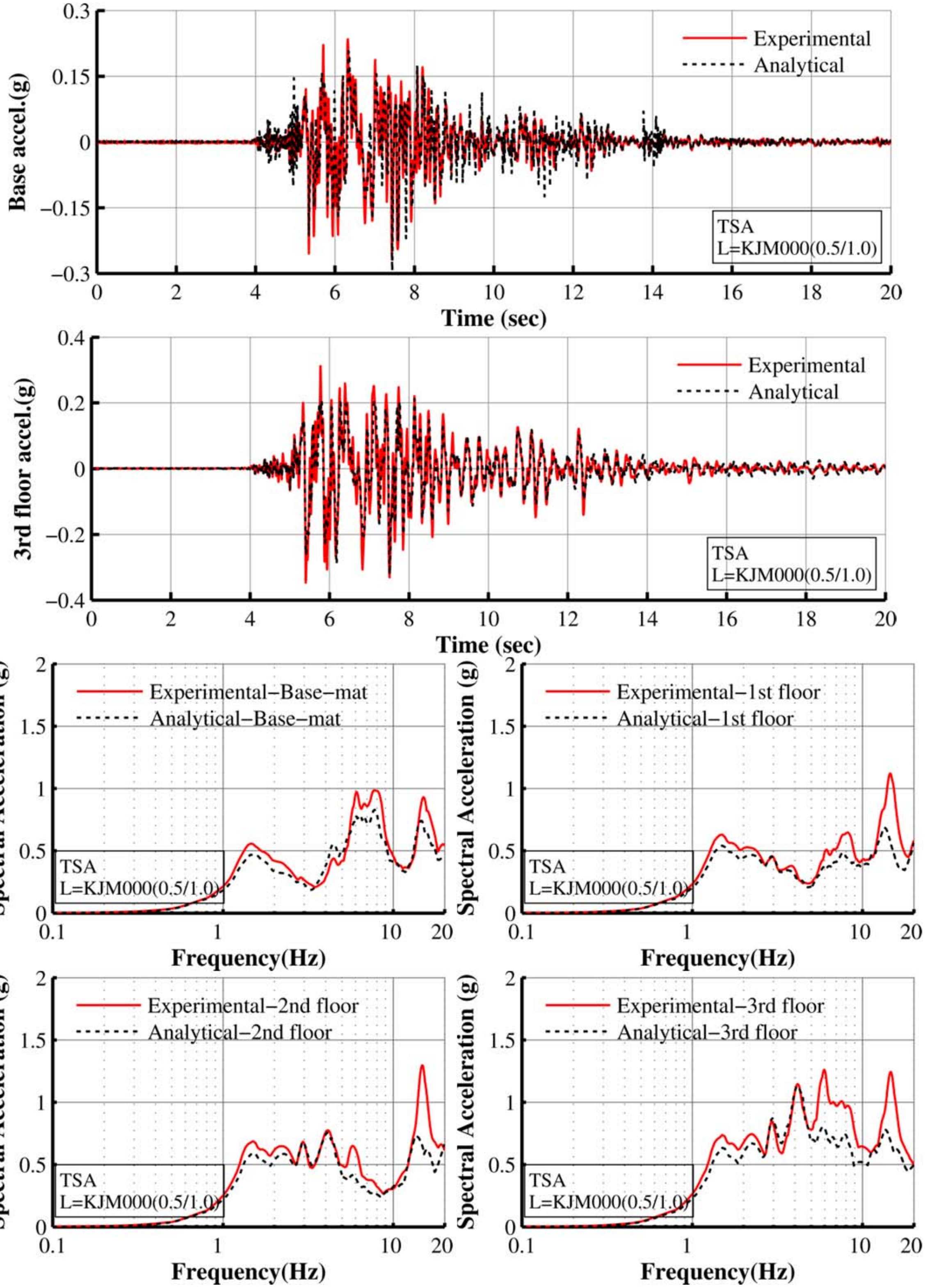
Base accel.(g)
Time (sec)
Experimental
Analytical
TSA
L=KJM000(0.5/1.0)
3rd floor accel.(g)
Time (sec)
Experimental
Analytical
TSA
L=KJM000(0.5/1.0)
Spectral Acceleration (g)
Frequency(Hz)
Experimental−Base−mat
Analytical−Base−mat
TSA
L=KJM000(0.5/1.0)
Spectral Acceleration (g)
Frequency(Hz)
Experimental−1st floor
Analytical−1st floor
TSA
L=KJM000(0.5/1.0)
Spectral Acceleration (g)
Frequency(Hz)
Experimental−2nd floor
Analytical−2nd floor
TSA
L=KJM000(0.5/1.0)
Spectral Acceleration (g)
Frequency(Hz)
Experimental−3rd floor
Analytical−3rd floor
TSA
L=KJM000(0.5/1.0)

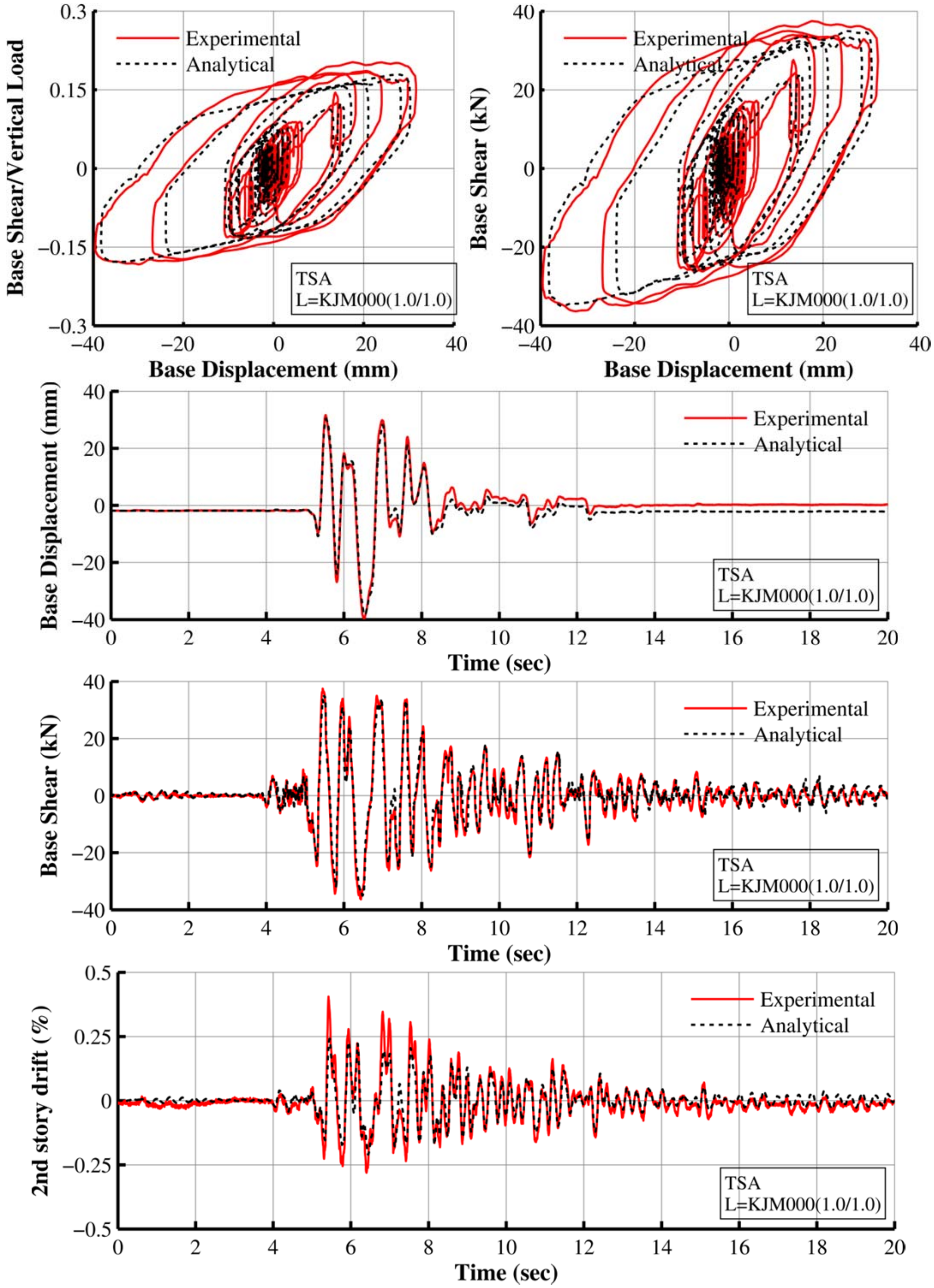
Base Shear/Vertical Load
Base Displacement (mm)
Experimental
Analytical
TSA
L=KJM000(1.0/1.0)
Base Shear (kN)
Base Displacement (mm)
Experimental
Analytical
TSA
L=KJM000(1.0/1.0)
Base Displacement (mm)
Time (sec)
Experimental
Analytical
TSA
L=KJM000(1.0/1.0)
Base Shear (kN)
Time (sec)
Experimental
Analytical
TSA
L=KJM000(1.0/1.0)
2nd story drift (%)
Time (sec)
Experimental
Analytical
TSA
L=KJM000(1.0/1.0)

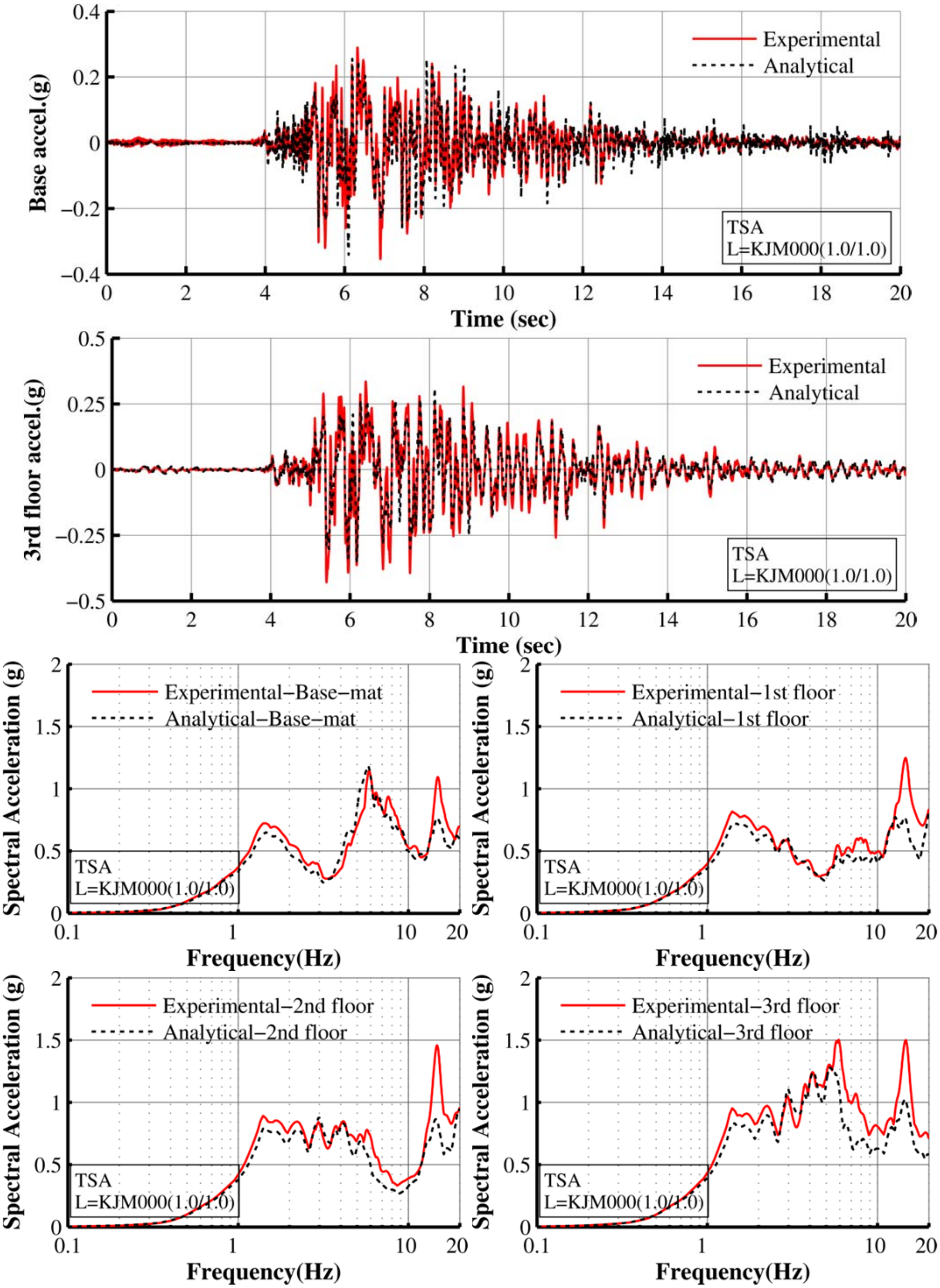
Experimental
Analytical
Base accel.(g)
TSA
L=KJM000(1.0/1.0)
Time (sec)
3rd floor accel.(g)
Experimental−Base−mat
Analytical−Base−mat
Spectral Acceleration (g)
Frequency(Hz)
Experimental−1st floor
Analytical−1st floor
Experimental−2nd floor
Analytical−2nd floor
Experimental−3rd floor
Analytical−3rd floor

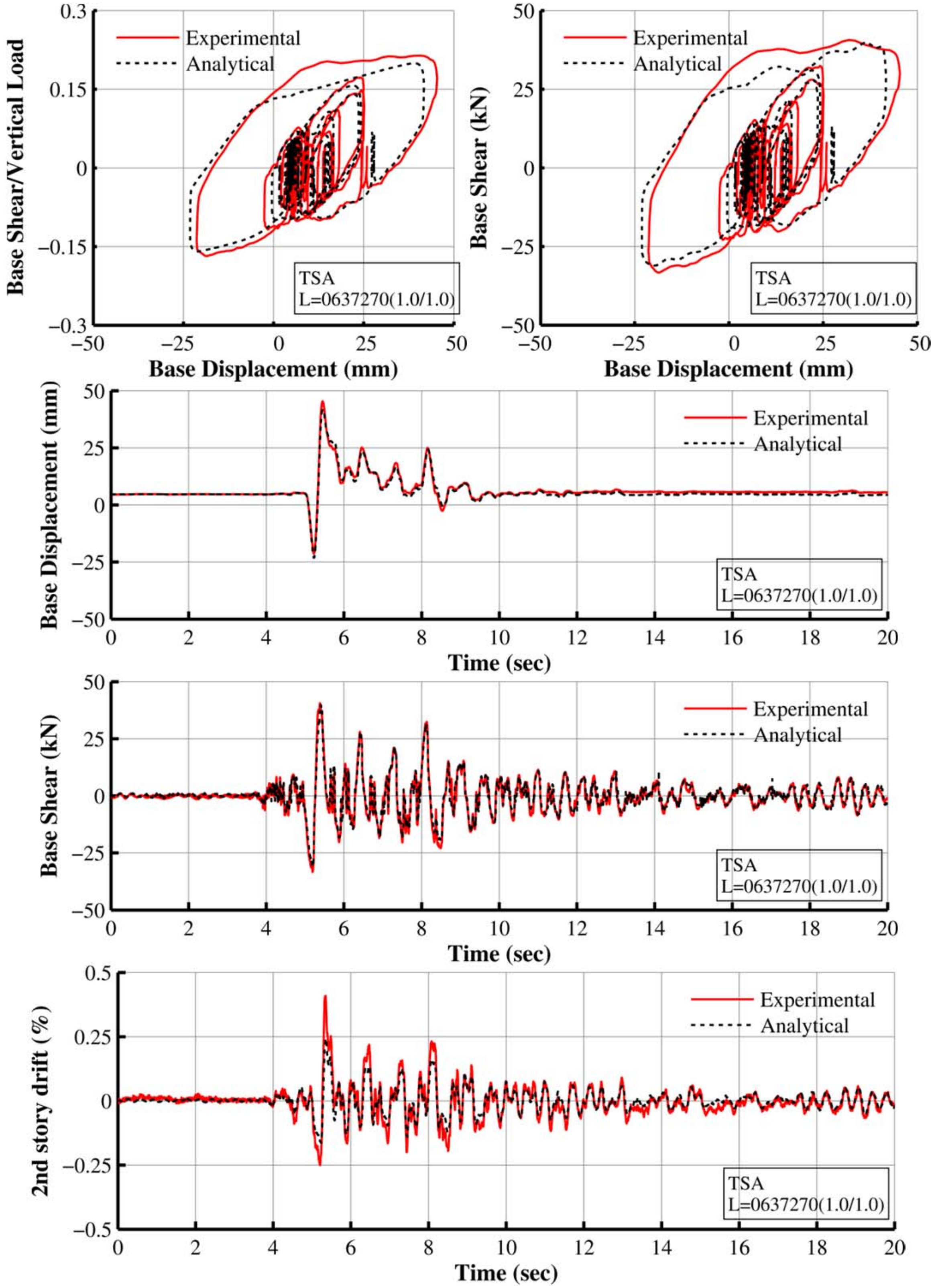
Experimental
Analytical
Base Shear/Vertical Load
Base Shear (kN)
TSA
L=0637270(1.0/1.0)
Base Displacement (mm)
Base Displacement (mm)
Time (sec)
Base Shear (kN)
2nd story drift (%)

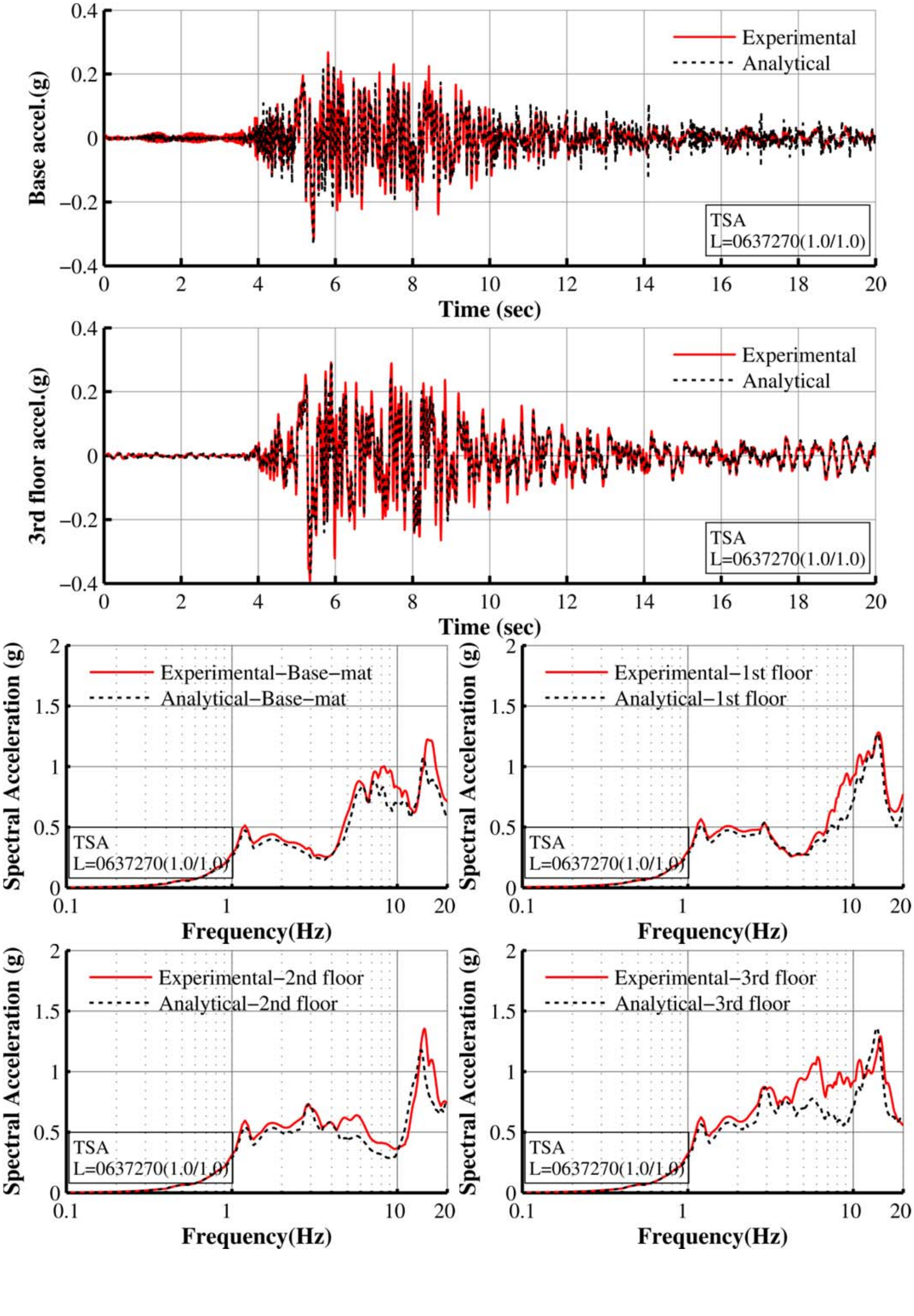
Experimental
Analytical
Base accel.(g)
Time (sec)
TSA
L=0637270(1.0/1.0)
3rd floor accel.(g)
Spectral Acceleration (g)
Frequency(Hz)
Experimental−Base−mat
Analytical−Base−mat
Experimental−1st floor
Analytical−1st floor
Experimental−2nd floor
Analytical−2nd floor
Experimental−3rd floor
Analytical−3rd floor

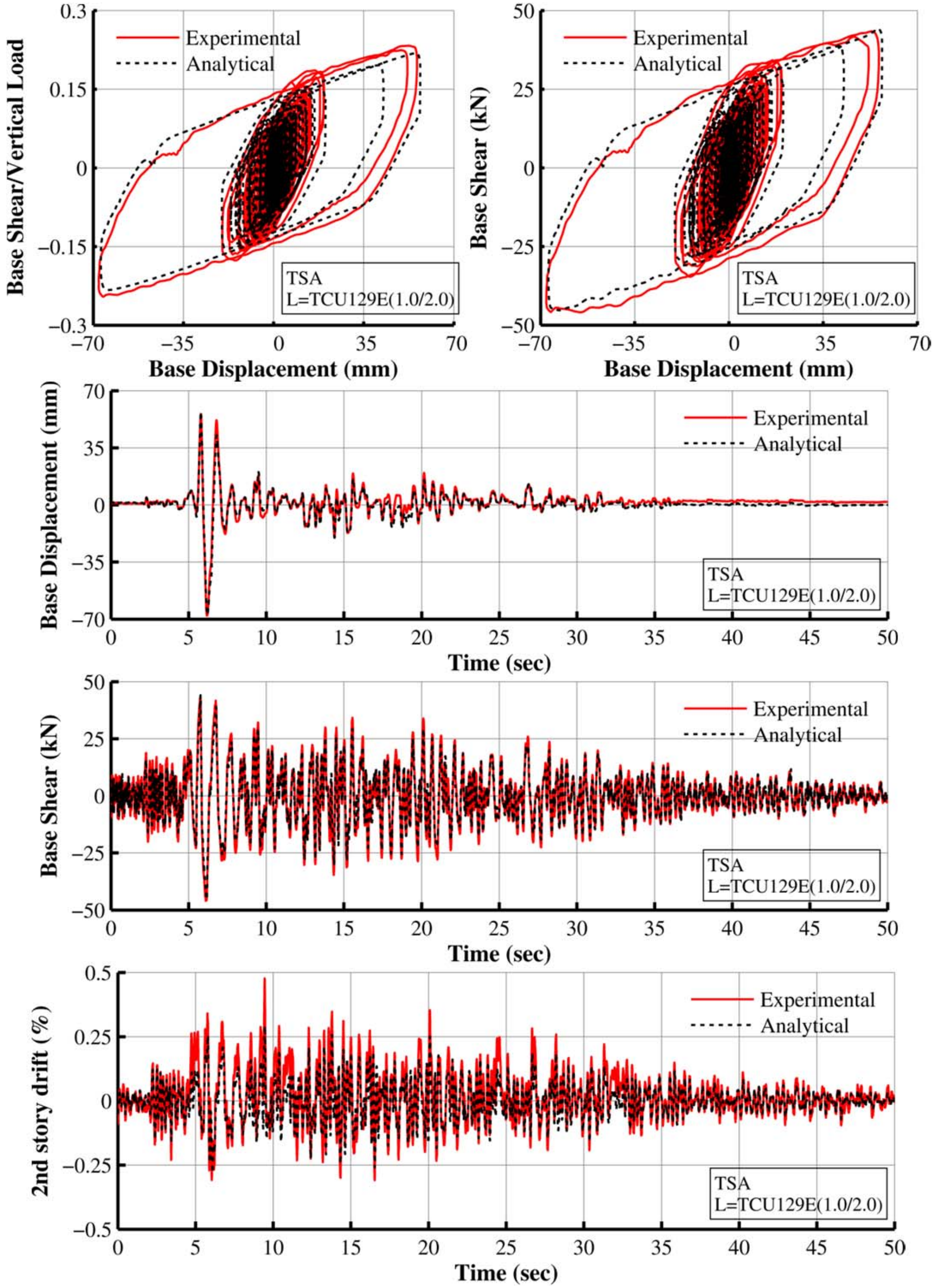
Base Shear/Vertical Load
Base Displacement (mm)
Base Shear (kN)
Base Displacement (mm)
Time (sec)
Base Shear (kN)
Time (sec)
2nd story drift (%)
Time (sec)
Experimental
Analytical
TSA
L=TCU129E(1.0/2.0)

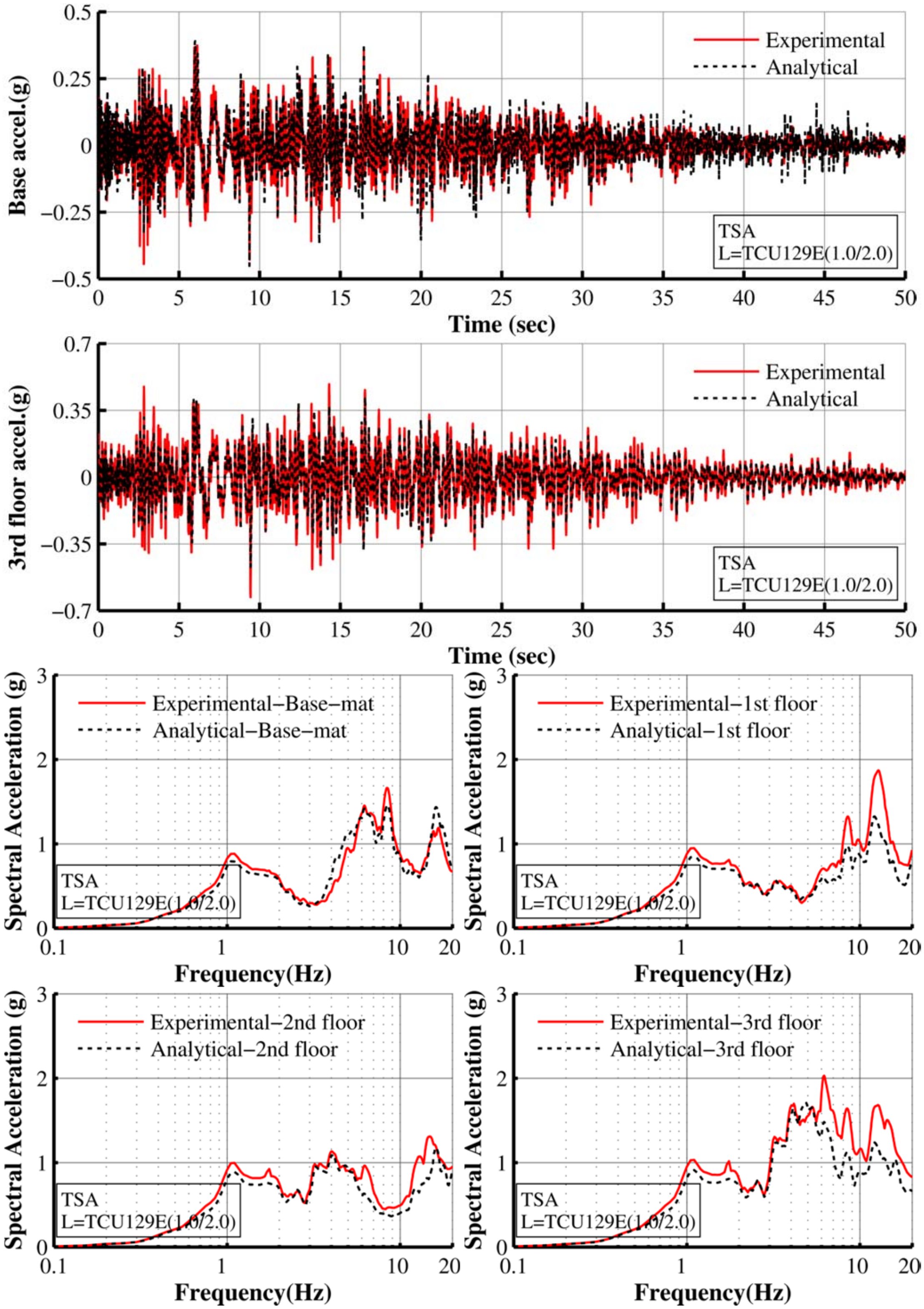

Experimental
Analytical
Base accel.(g)
TSA
L=TCU129E(1.0/2.0)
Time (sec)
Experimental
Analytical
3rd floor accel.(g)
TSA
L=TCU129E(1.0/2.0)
Time (sec)
Experimental−Base−mat
Analytical−Base−mat
Spectral Acceleration (g)
TSA
L=TCU129E(1.0/2.0)
Frequency(Hz)
Experimental−1st floor
Analytical−1st floor
Spectral Acceleration (g)
TSA
L=TCU129E(1.0/2.0)
Frequency(Hz)
Experimental−2nd floor
Analytical−2nd floor
Spectral Acceleration (g)
TSA
L=TCU129E(1.0/2.0)
Frequency(Hz)
Experimental−3rd floor
Analytical−3rd floor
Spectral Acceleration (g)
TSA
L=TCU129E(1.0/2.0)
Frequency(Hz)

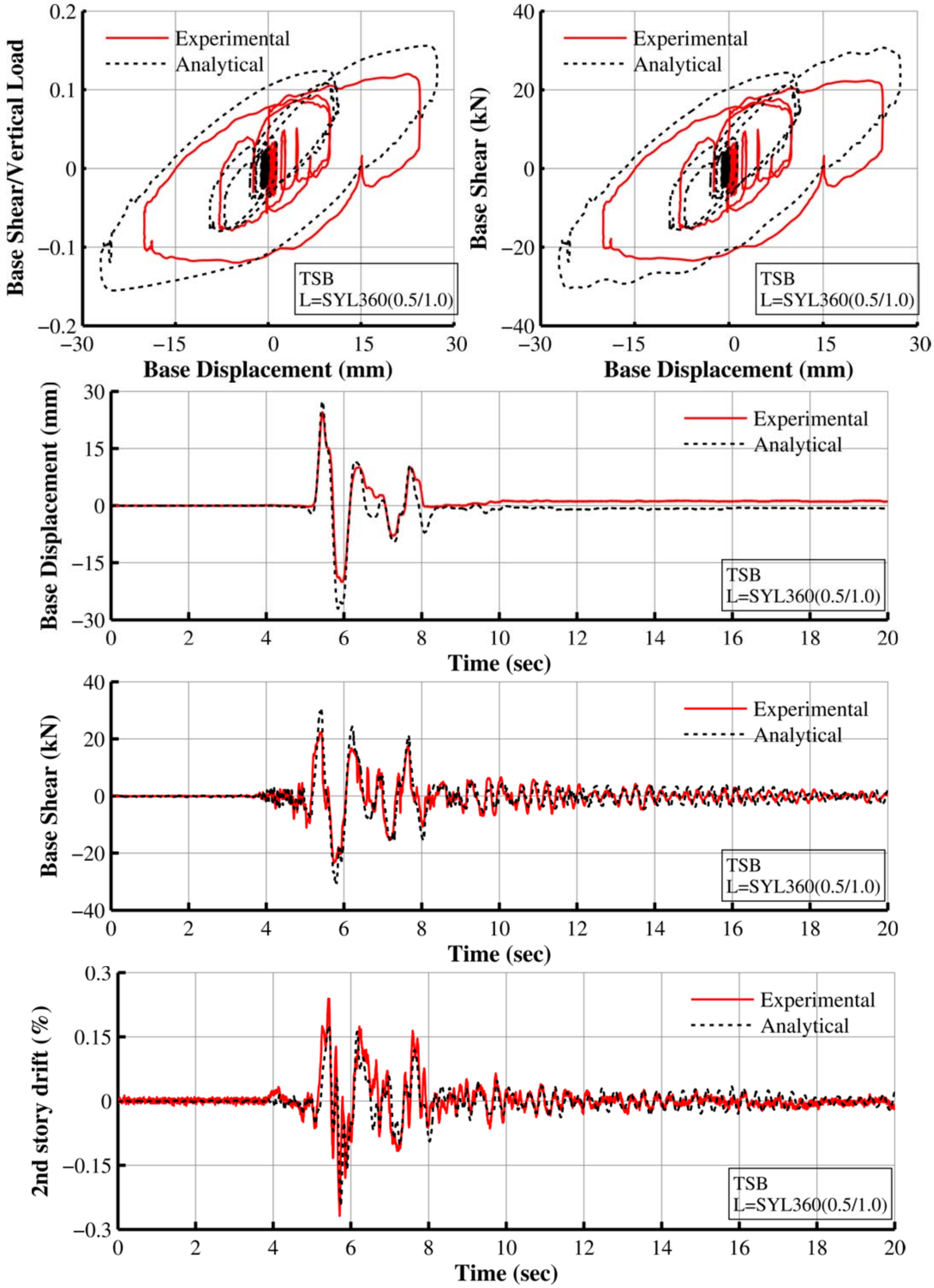
Base Shear/Vertical Load
Base Displacement (mm)
Experimental
Analytical
TSB
L=SYL360(0.5/1.0)
Base Shear (kN)
Base Displacement (mm)
Base Displacement (mm)
Time (sec)
Base Shear (kN)
Time (sec)
2nd story drift (%)
Time (sec)

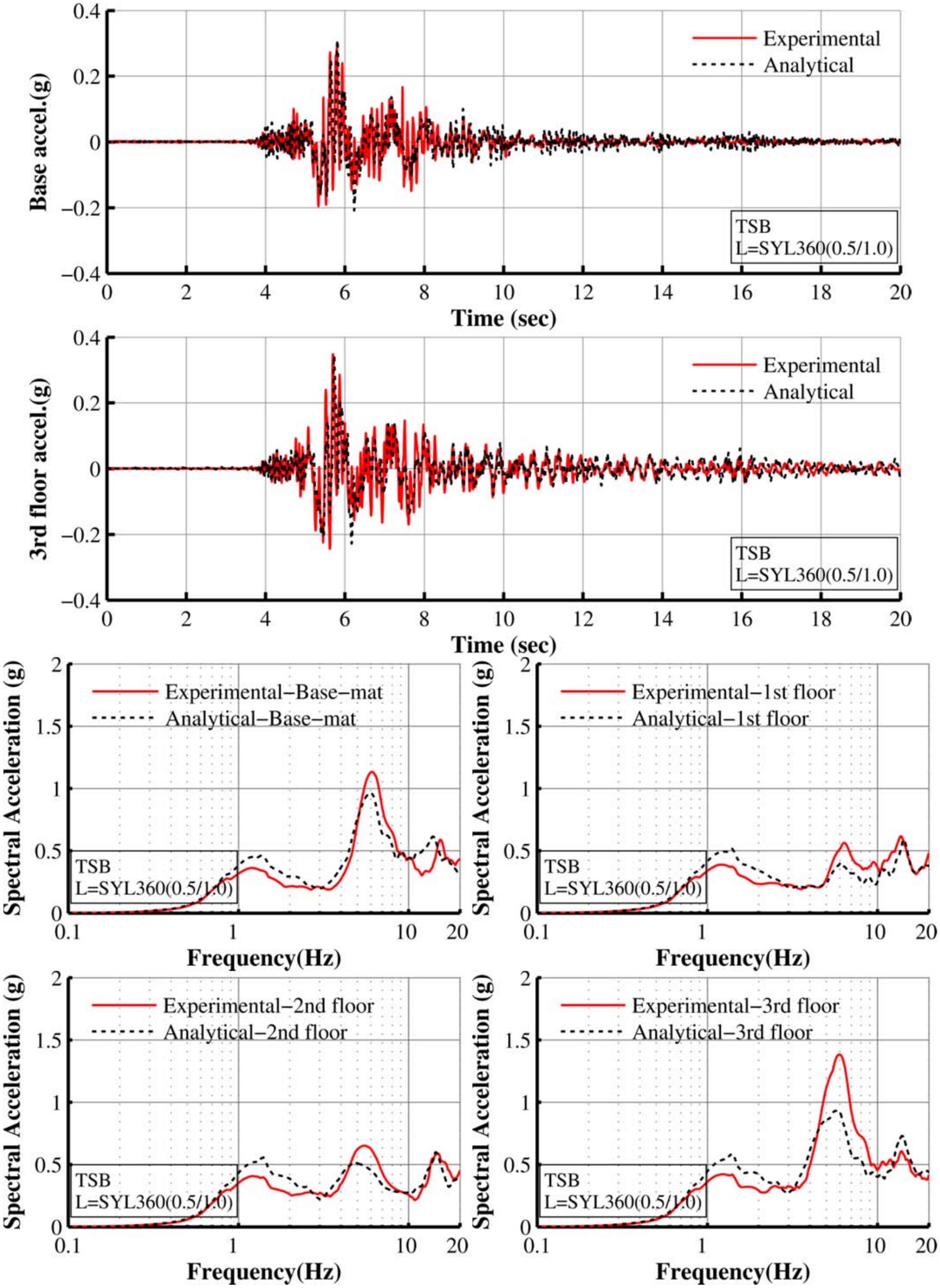

Base accel.(g)
Experimental
Analytical
TSB
L=SYL360(0.5/1.0)
Time (sec)
3rd floor accel.(g)
Experimental
Analytical
TSB
L=SYL360(0.5/1.0)
Time (sec)
Spectral Acceleration (g)
Experimental−Base−mat
Analytical−Base−mat
TSB
L=SYL360(0.5/1.0)
Frequency(Hz)
Spectral Acceleration (g)
Experimental−1st floor
Analytical−1st floor
TSB
L=SYL360(0.5/1.0)
Frequency(Hz)
Spectral Acceleration (g)
Experimental−2nd floor
Analytical−2nd floor
TSB
L=SYL360(0.5/1.0)
Frequency(Hz)
Spectral Acceleration (g)
Experimental−3rd floor
Analytical−3rd floor
TSB
L=SYL360(0.5/1.0)
Frequency(Hz)

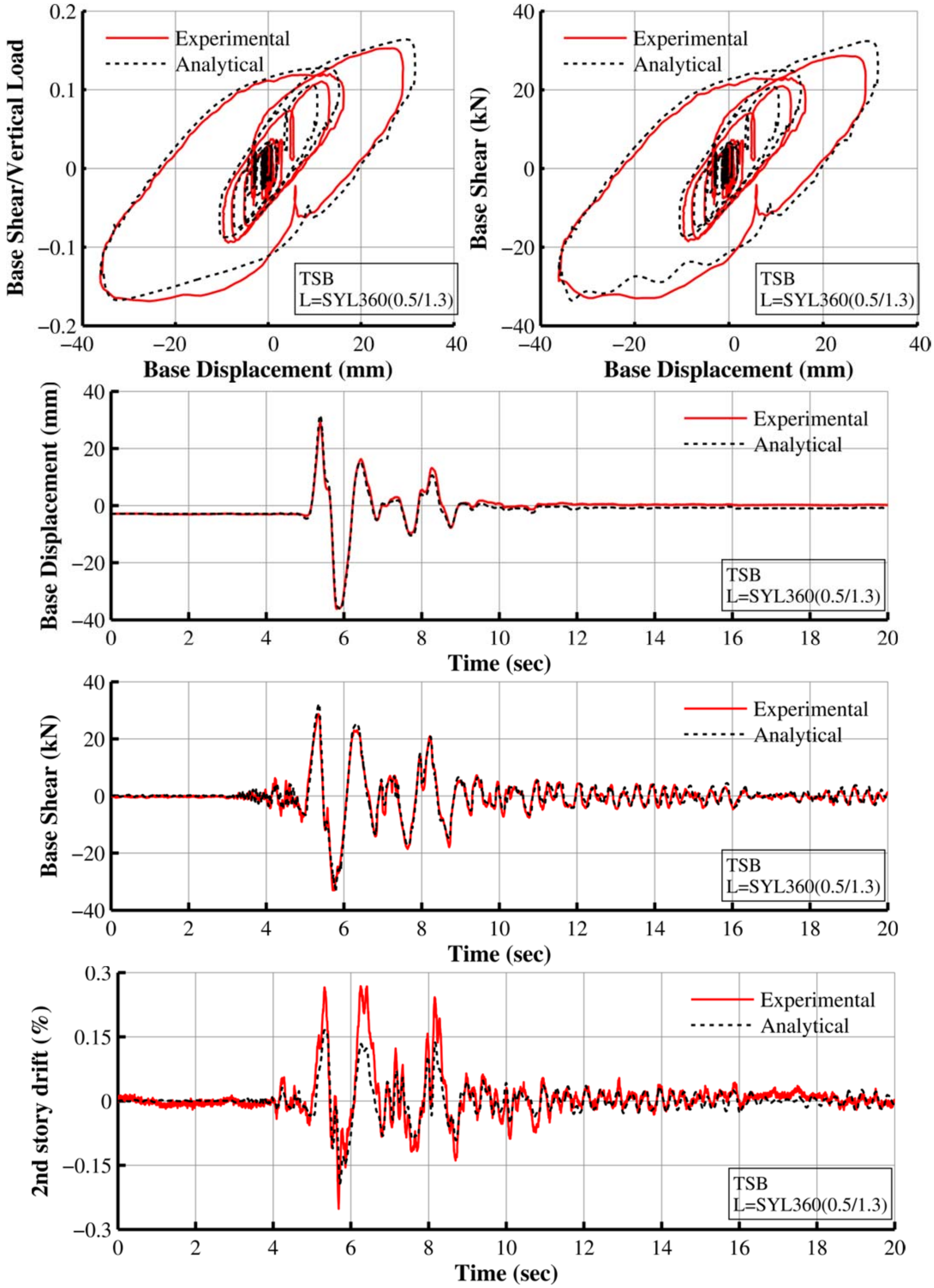
Base Shear/Vertical Load
Experimental
Analytical
TSB
L=SYL360(0.5/1.3)
Base Displacement (mm)
Base Shear (kN)
Experimental
Analytical
TSB
L=SYL360(0.5/1.3)
Base Displacement (mm)
Base Displacement (mm)
Experimental
Analytical
TSB
L=SYL360(0.5/1.3)
Time (sec)
Base Shear (kN)
Experimental
Analytical
TSB
L=SYL360(0.5/1.3)
Time (sec)
2nd story drift (%)
Experimental
Analytical
TSB
L=SYL360(0.5/1.3)
Time (sec)

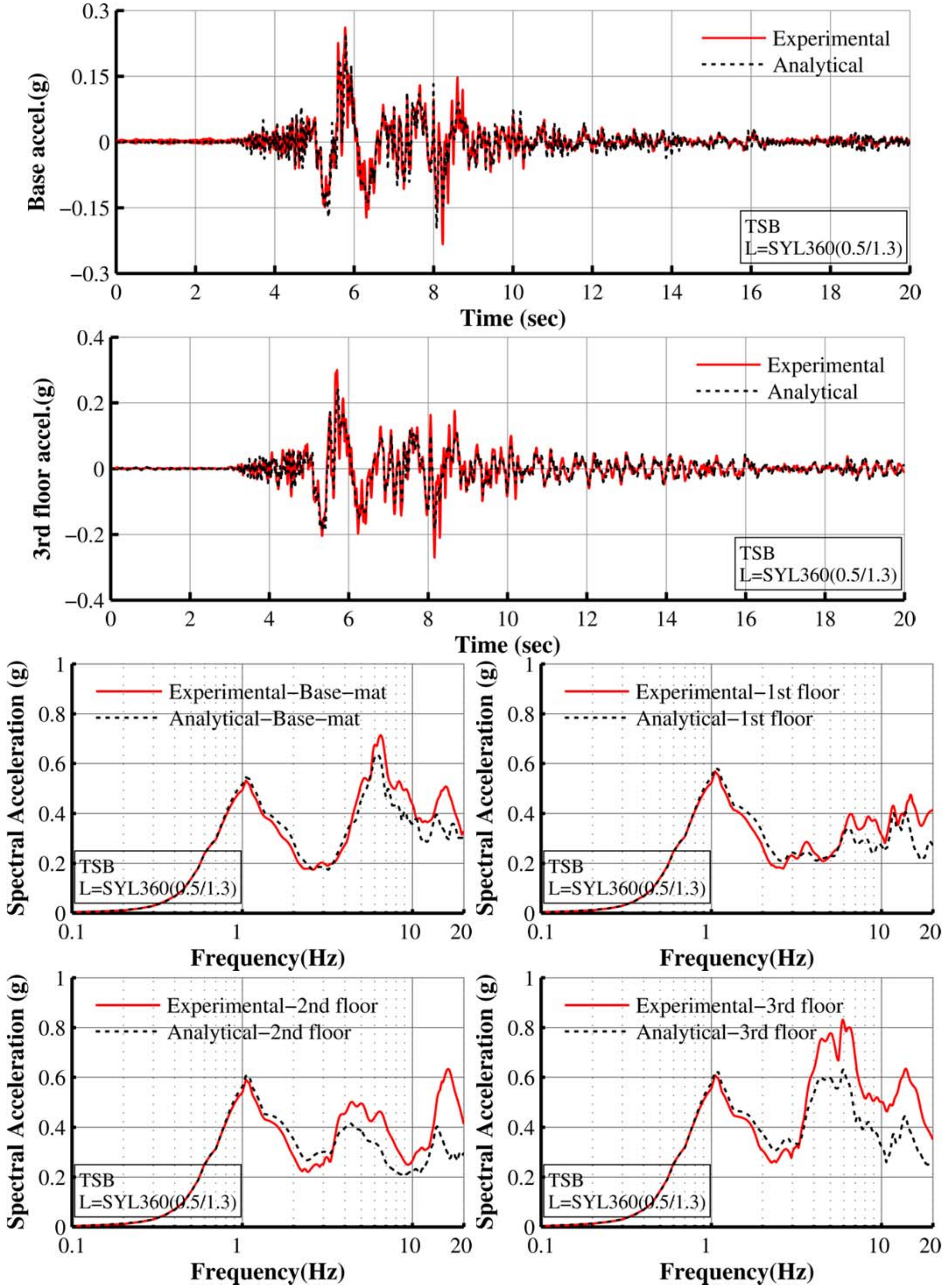
Base accel.(g)
Time (sec)
Experimental
Analytical
TSB
L=SYL360(0.5/1.3)
3rd floor accel.(g)
Time (sec)
Experimental
Analytical
TSB
L=SYL360(0.5/1.3)
Spectral Acceleration (g)
Frequency(Hz)
Experimental−Base−mat
Analytical−Base−mat
TSB
L=SYL360(0.5/1.3)
Spectral Acceleration (g)
Frequency(Hz)
Experimental−1st floor
Analytical−1st floor
TSB
L=SYL360(0.5/1.3)
Spectral Acceleration (g)
Frequency(Hz)
Experimental−2nd floor
Analytical−2nd floor
TSB
L=SYL360(0.5/1.3)
Spectral Acceleration (g)
Frequency(Hz)
Experimental−3rd floor
Analytical−3rd floor
TSB
L=SYL360(0.5/1.3)

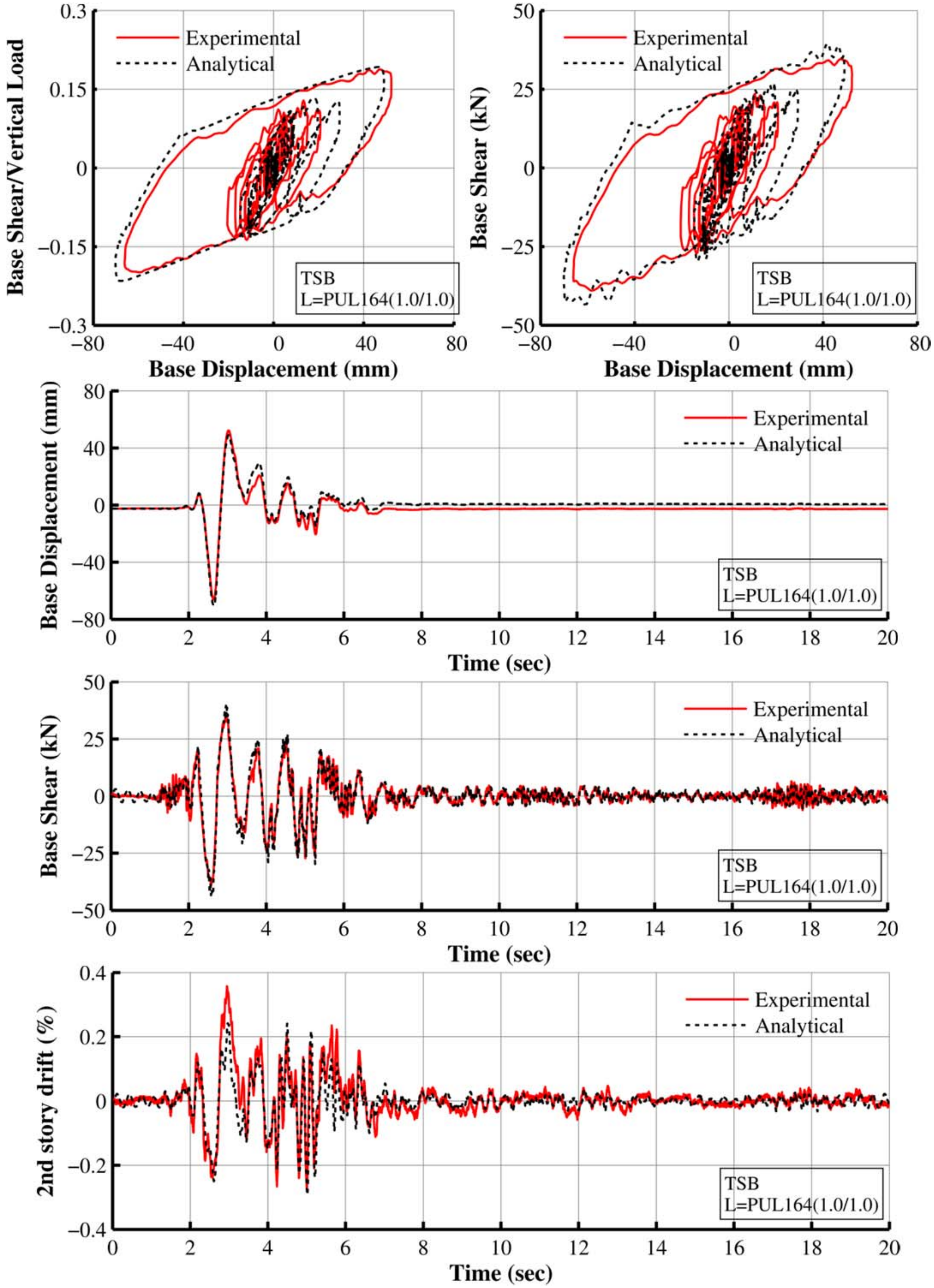
Base Shear/Vertical Load
Base Displacement (mm)
Experimental
Analytical
TSB
L=PUL164(1.0/1.0)
0.3
0.15
0
−0.15
−0.3
−80
−40
0
40
80
Base Shear (kN)
Base Displacement (mm)
Experimental
Analytical
TSB
L=PUL164(1.0/1.0)
50
25
0
−25
−50
Base Displacement (mm)
Time (sec)
Experimental
Analytical
TSB
L=PUL164(1.0/1.0)
Base Shear (kN)
Time (sec)
Experimental
Analytical
TSB
L=PUL164(1.0/1.0)
2nd story drift (%)
Time (sec)
Experimental
Analytical
TSB
L=PUL164(1.0/1.0)
0.4
0.2
−0.2
−0.4
0
2
4
6
8
10
12
14
16
18
20

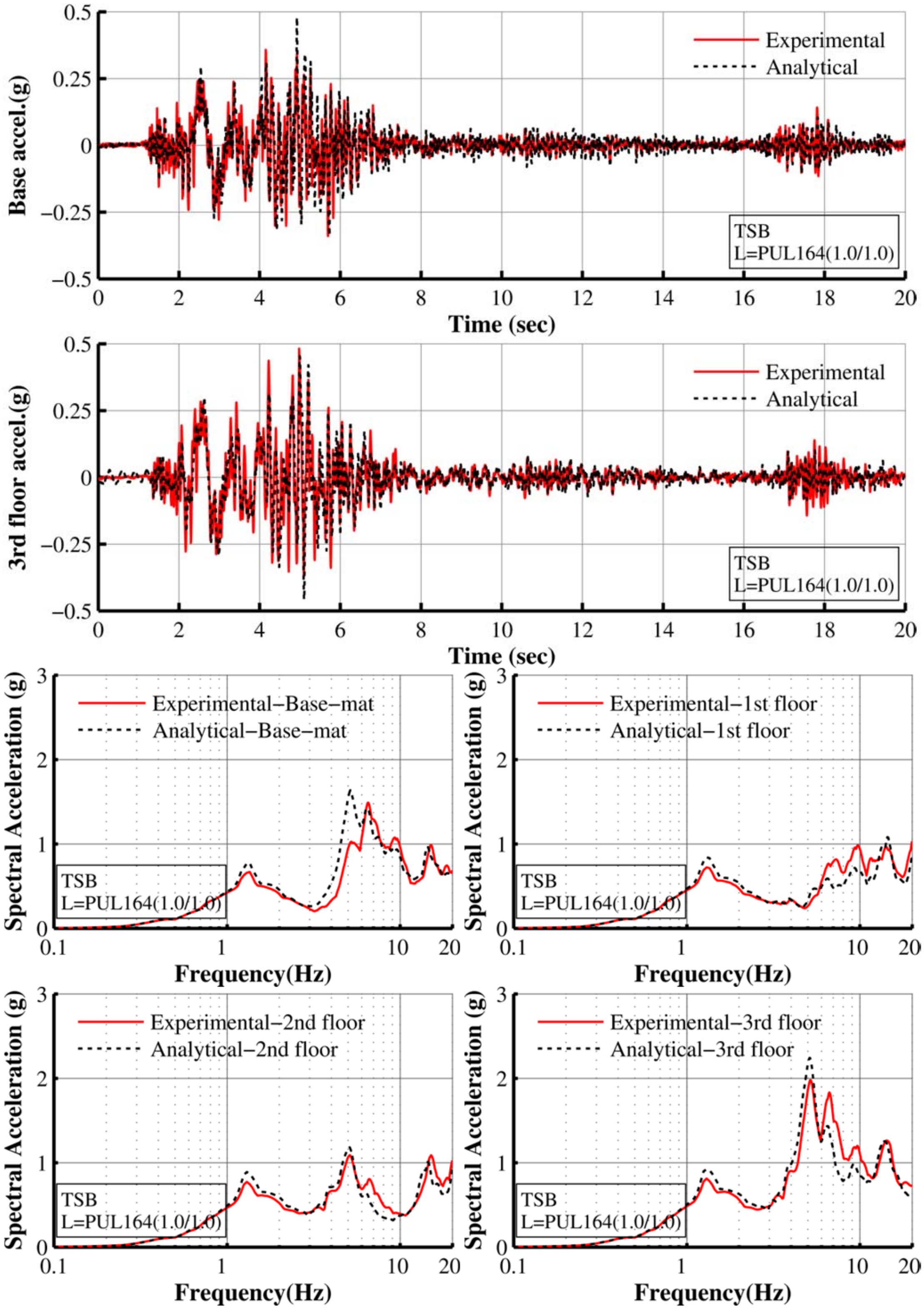

Experimental
Analytical
Base accel.(g)
TSB
L=PUL164(1.0/1.0)
Time (sec)
3rd floor accel.(g)
Experimental−Base−mat
Analytical−Base−mat
Experimental−1st floor
Analytical−1st floor
Experimental−2nd floor
Analytical−2nd floor
Experimental−3rd floor
Analytical−3rd floor
Spectral Acceleration (g)
Frequency(Hz)

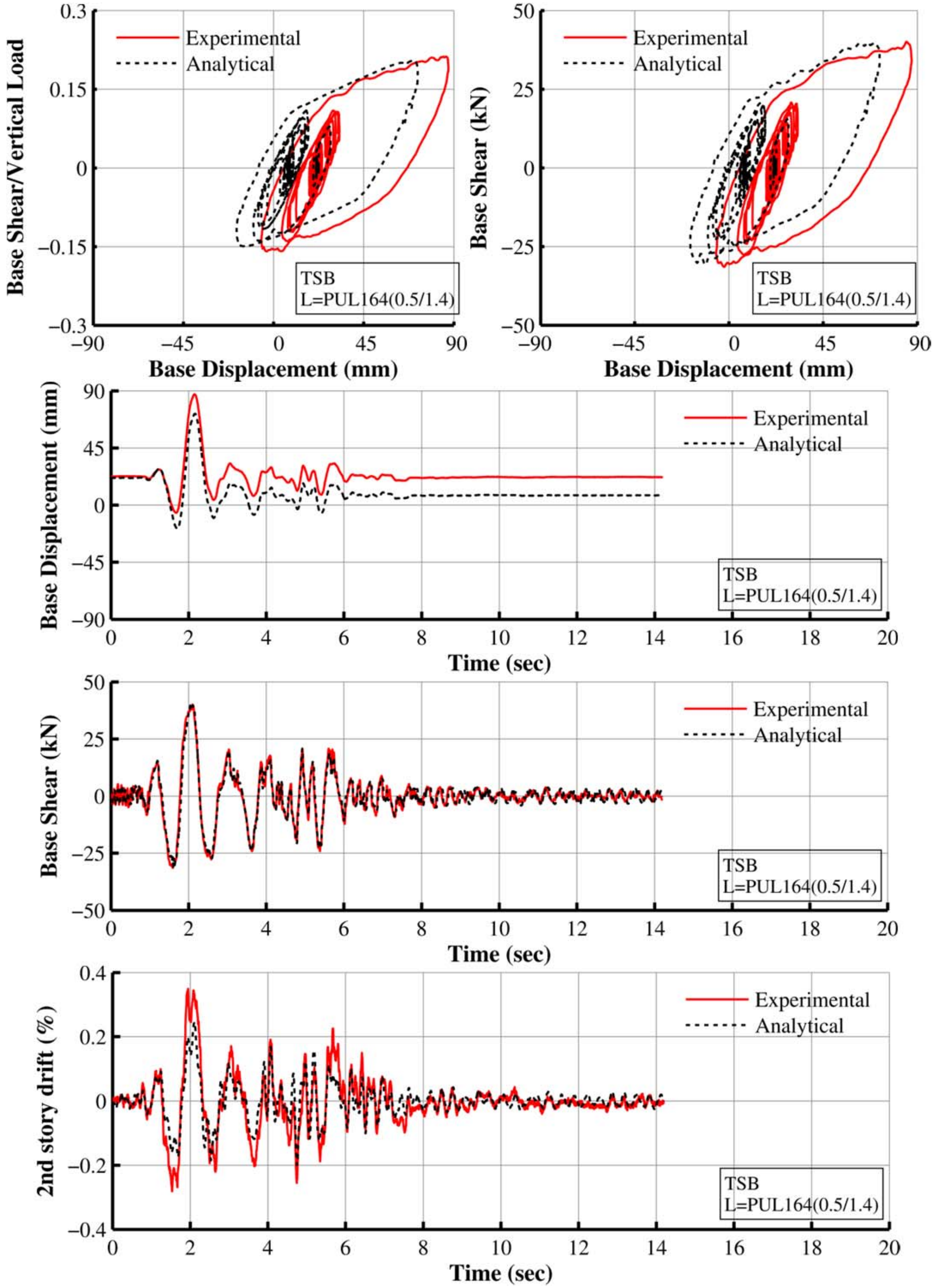
Experimental
Analytical
TSB
L=PUL164(0.5/1.4)
Base Shear/Vertical Load
Base Displacement (mm)
Base Shear (kN)
Base Displacement (mm)
Time (sec)
Base Shear (kN)
2nd story drift (%)

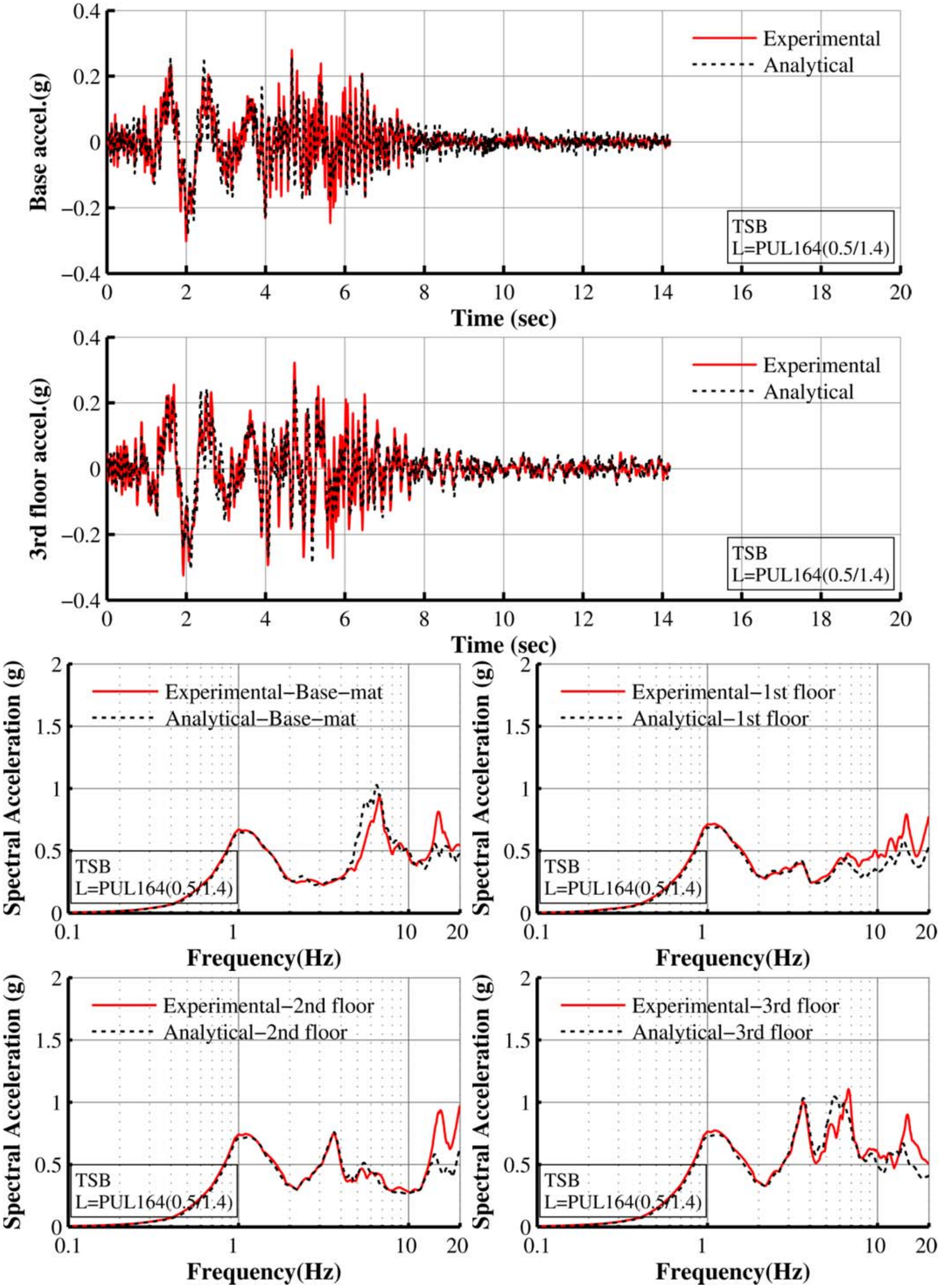

Experimental
Analytical
Base accel.(g)
TSB
L=PUL164(0.5/1.4)
Time (sec)
3rd floor accel.(g)
Experimental−Base−mat
Analytical−Base−mat
Experimental−1st floor
Analytical−1st floor
Experimental−2nd floor
Analytical−2nd floor
Experimental−3rd floor
Analytical−3rd floor
Spectral Acceleration (g)
Frequency(Hz)

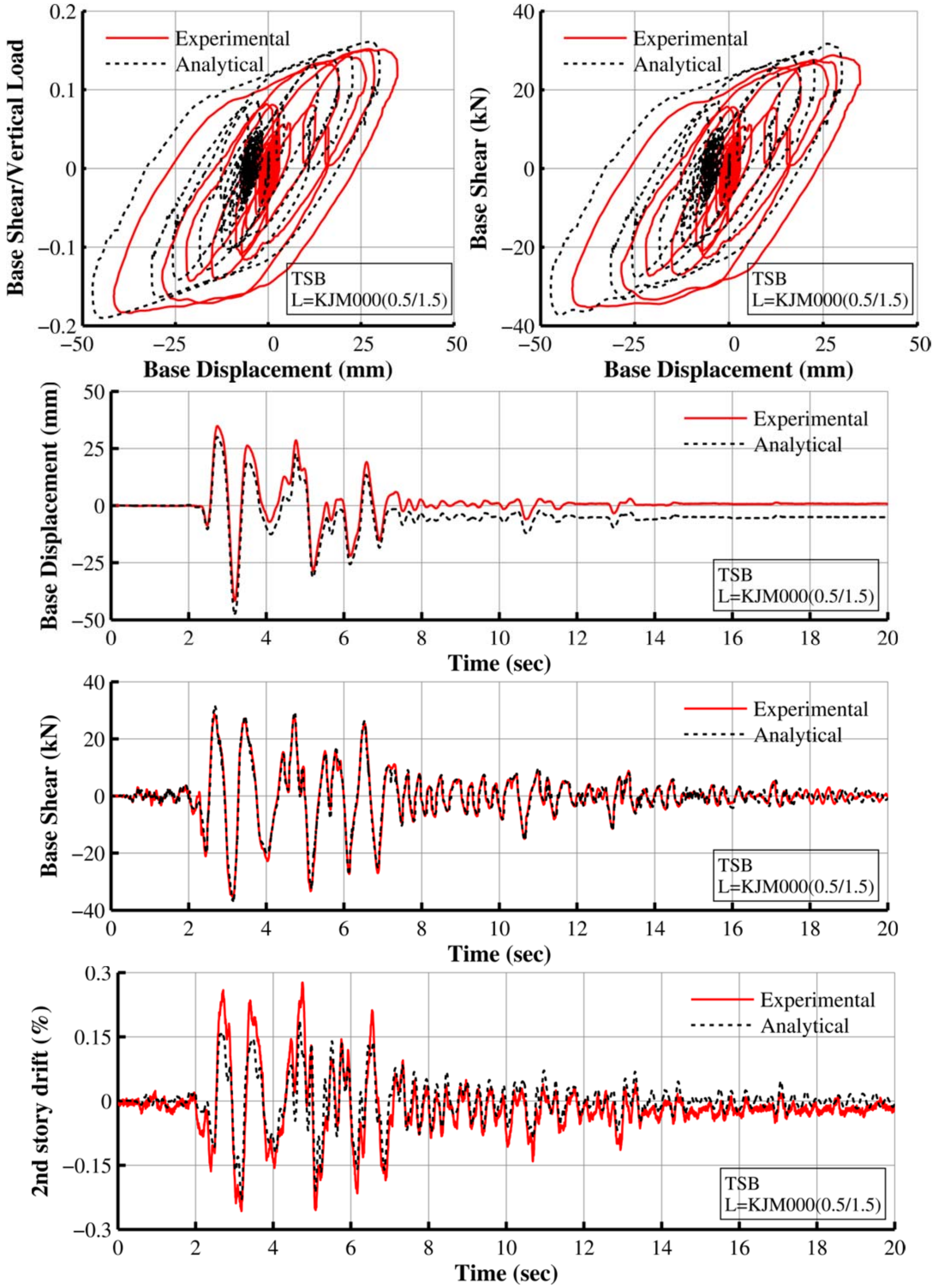
Base Shear/Vertical Load
Base Displacement (mm)
Base Shear (kN)
Base Displacement (mm)
Time (sec)
Base Shear (kN)
2nd story drift (%)
Experimental
Analytical
TSB
L=KJM000(0.5/1.5)

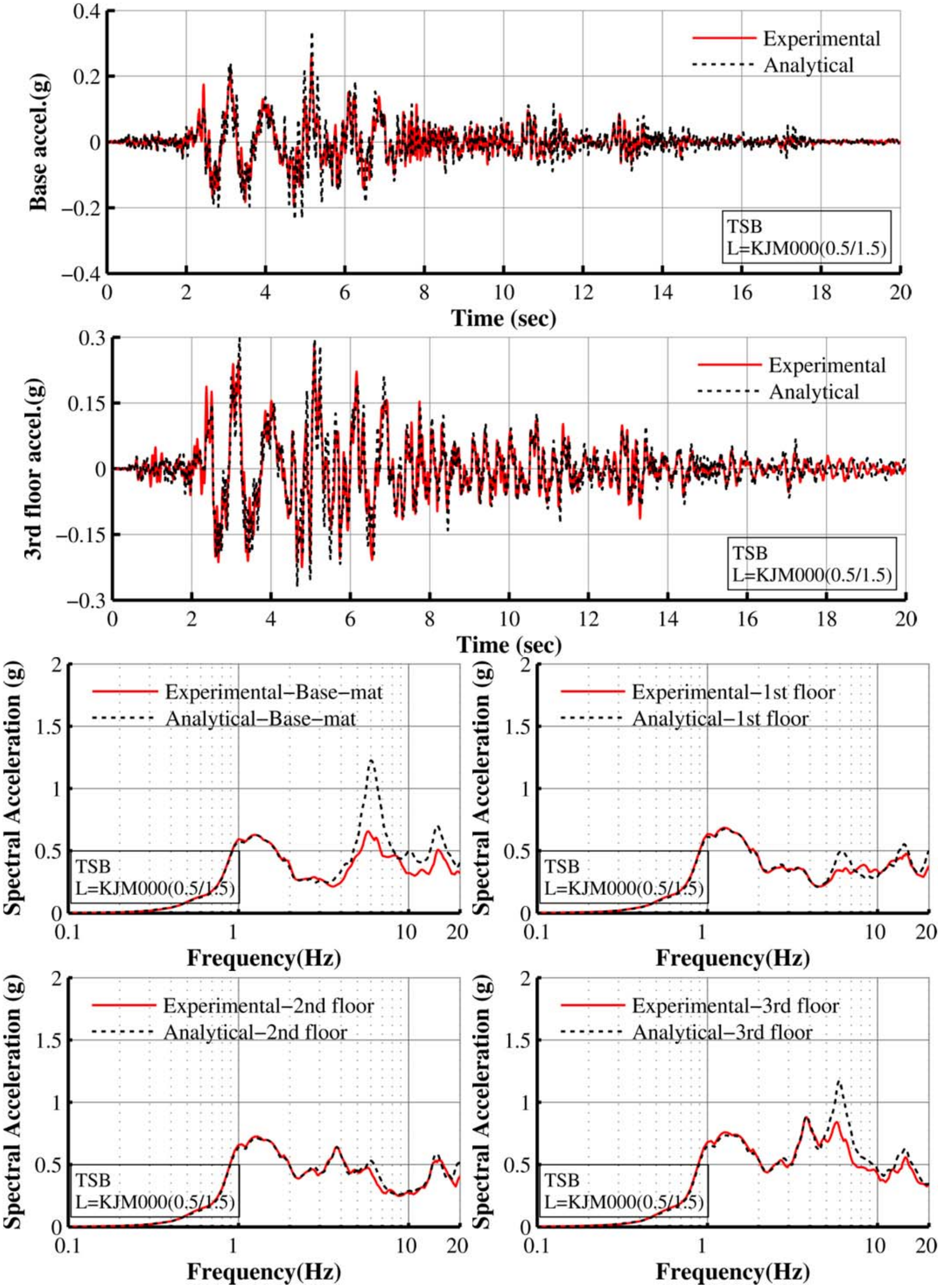
Base accel.(g)
Time (sec)
Experimental
Analytical
TSB
L=KJM000(0.5/1.5)
3rd floor accel.(g)
Time (sec)
Experimental
Analytical
TSB
L=KJM000(0.5/1.5)
Spectral Acceleration (g)
Frequency(Hz)
Experimental−Base−mat
Analytical−Base−mat
TSB
L=KJM000(0.5/1.5)
Spectral Acceleration (g)
Frequency(Hz)
Experimental−1st floor
Analytical−1st floor
TSB
L=KJM000(0.5/1.5)
Spectral Acceleration (g)
Frequency(Hz)
Experimental−2nd floor
Analytical−2nd floor
TSB
L=KJM000(0.5/1.5)
Spectral Acceleration (g)
Frequency(Hz)
Experimental−3rd floor
Analytical−3rd floor
TSB
L=KJM000(0.5/1.5)

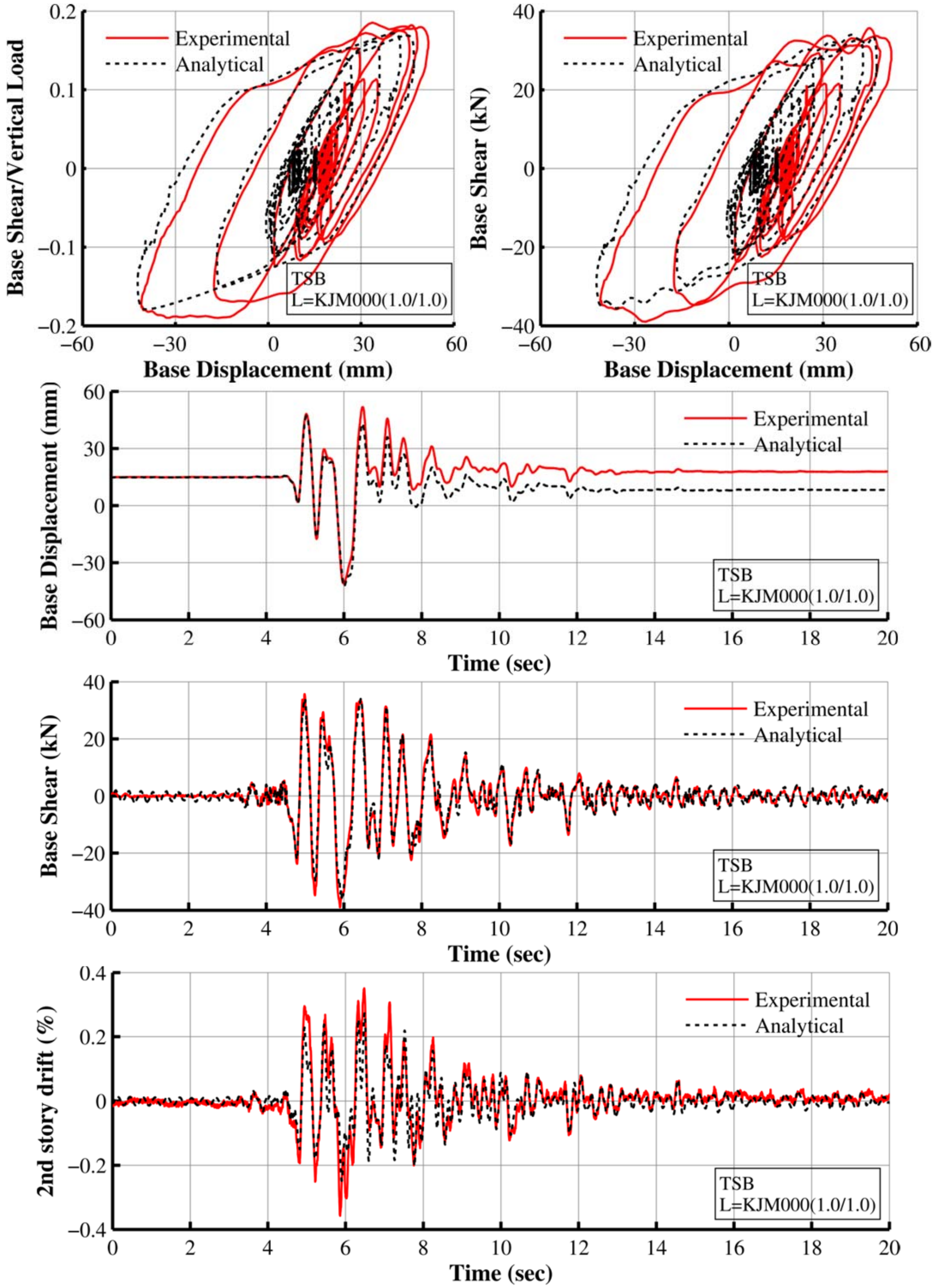
Experimental
Analytical
Base Shear/Vertical Load
Base Displacement (mm)
TSB
L=KJM000(1.0/1.0)
Base Shear (kN)
Base Displacement (mm)
Time (sec)
Base Shear (kN)
2nd story drift (%)

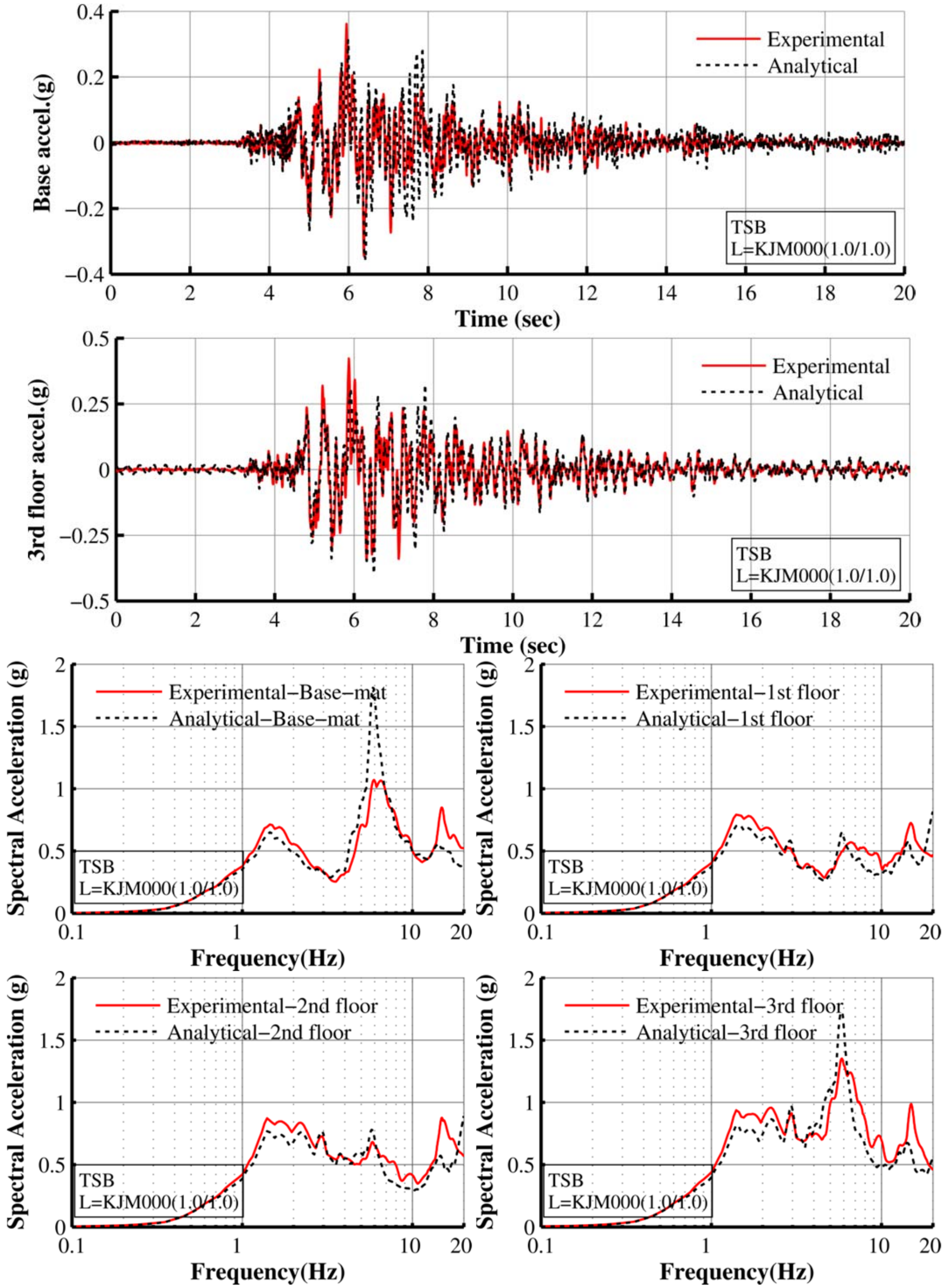

Base accel.(g)
Time (sec)
Experimental
Analytical
TSB
L=KJM000(1.0/1.0)
3rd floor accel.(g)
Time (sec)
Experimental
Analytical
TSB
L=KJM000(1.0/1.0)
Spectral Acceleration (g)
Frequency(Hz)
Experimental−Base−mat
Analytical−Base−mat
TSB
L=KJM000(1.0/1.0)
Spectral Acceleration (g)
Frequency(Hz)
Experimental−1st floor
Analytical−1st floor
TSB
L=KJM000(1.0/1.0)
Spectral Acceleration (g)
Frequency(Hz)
Experimental−2nd floor
Analytical−2nd floor
TSB
L=KJM000(1.0/1.0)
Spectral Acceleration (g)
Frequency(Hz)
Experimental−3rd floor
Analytical−3rd floor
TSB
L=KJM000(1.0/1.0)

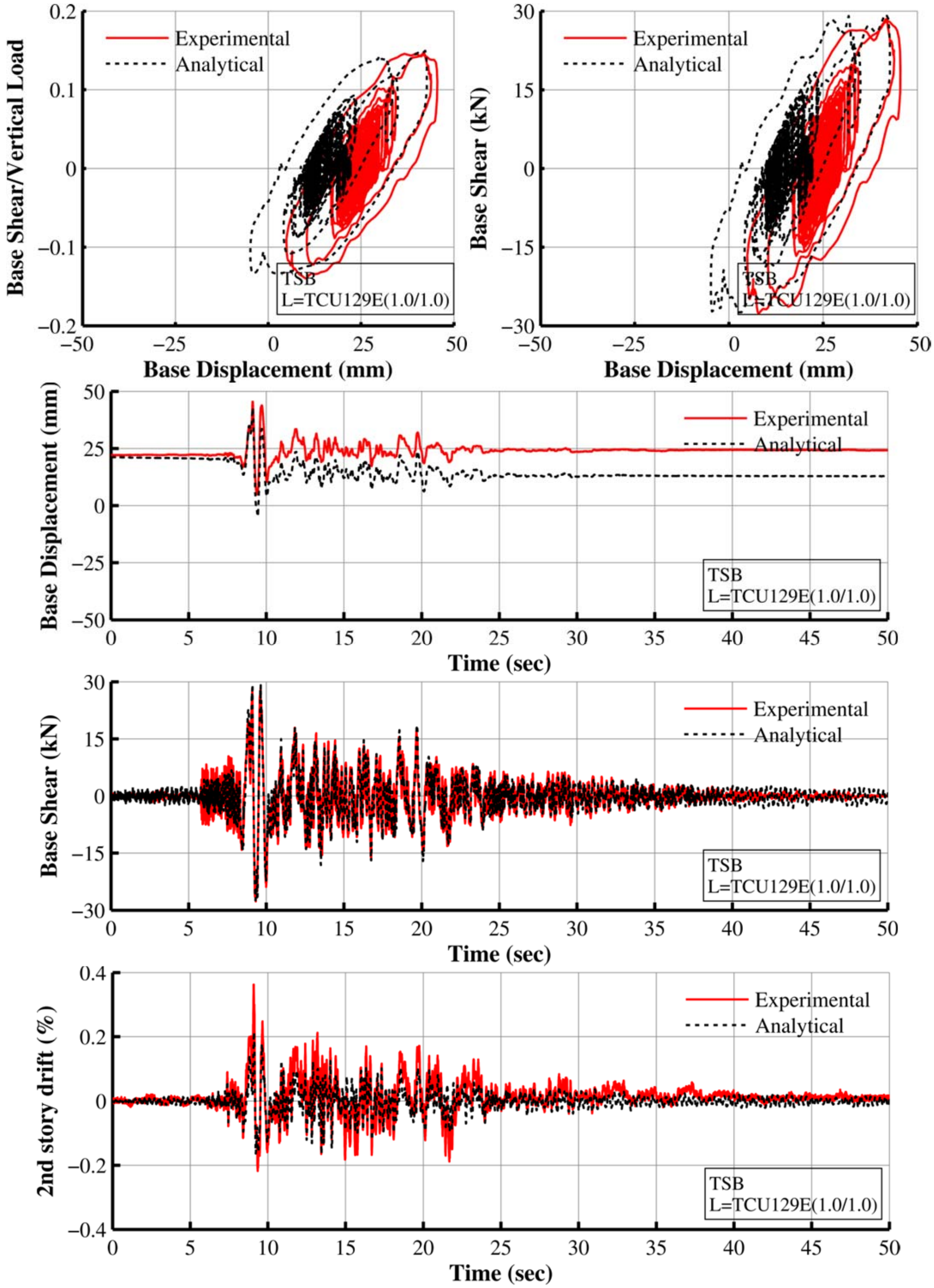

Experimental
Analytical
TSB
L=TCU129E(1.0/1.0)
Base Shear/Vertical Load
Base Displacement (mm)
Base Shear (kN)
Base Displacement (mm)
Time (sec)
Base Shear (kN)
2nd story drift (%)

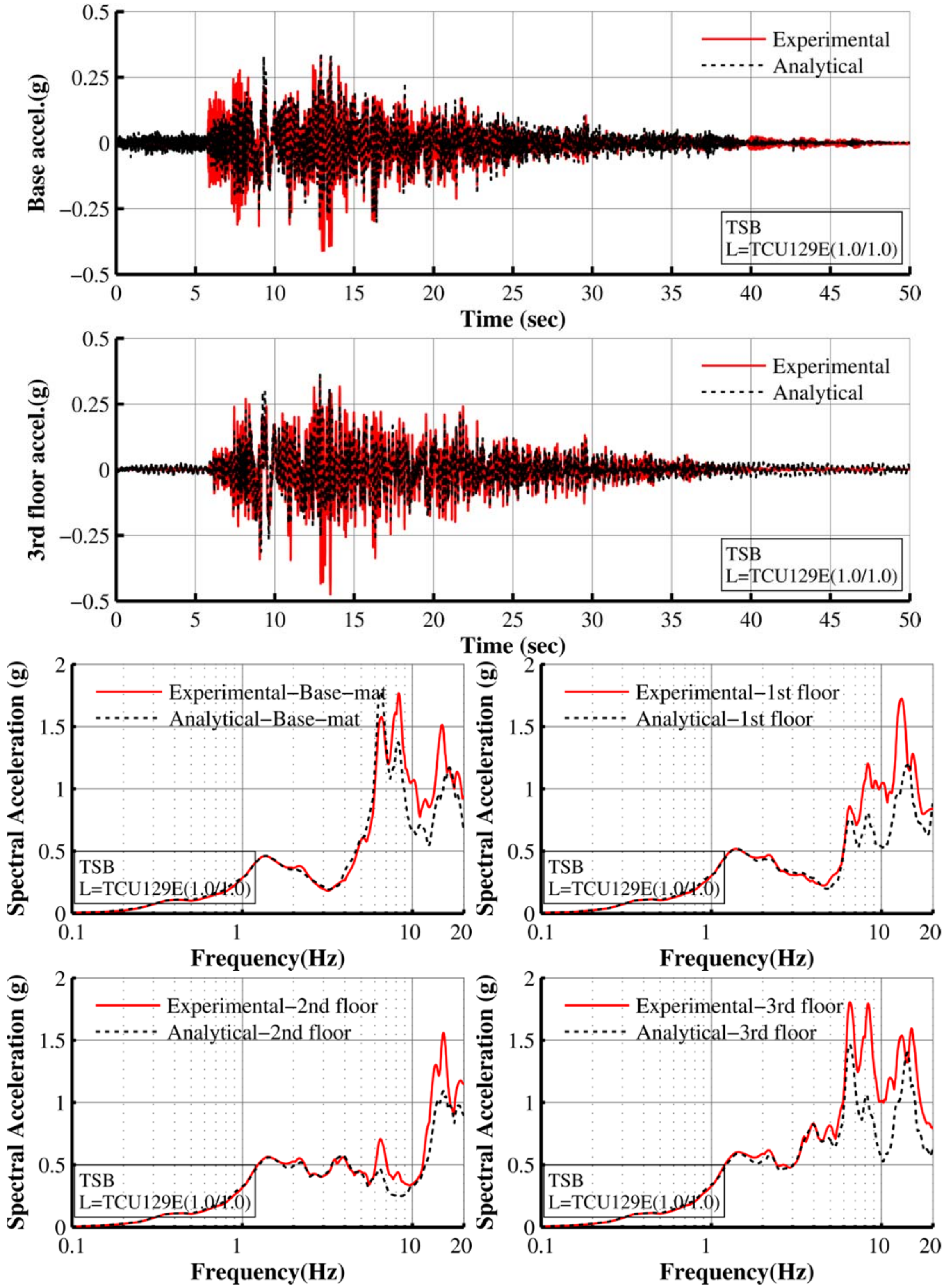
Base accel.(g)
Time (sec)
Experimental
Analytical
TSB
L=TCU129E(1.0/1.0)
3rd floor accel.(g)
Spectral Acceleration (g)
Frequency(Hz)
Experimental−Base−mat
Analytical−Base−mat
Experimental−1st floor
Analytical−1st floor
Experimental−2nd floor
Analytical−2nd floor
Experimental−3rd floor
Analytical−3rd floor

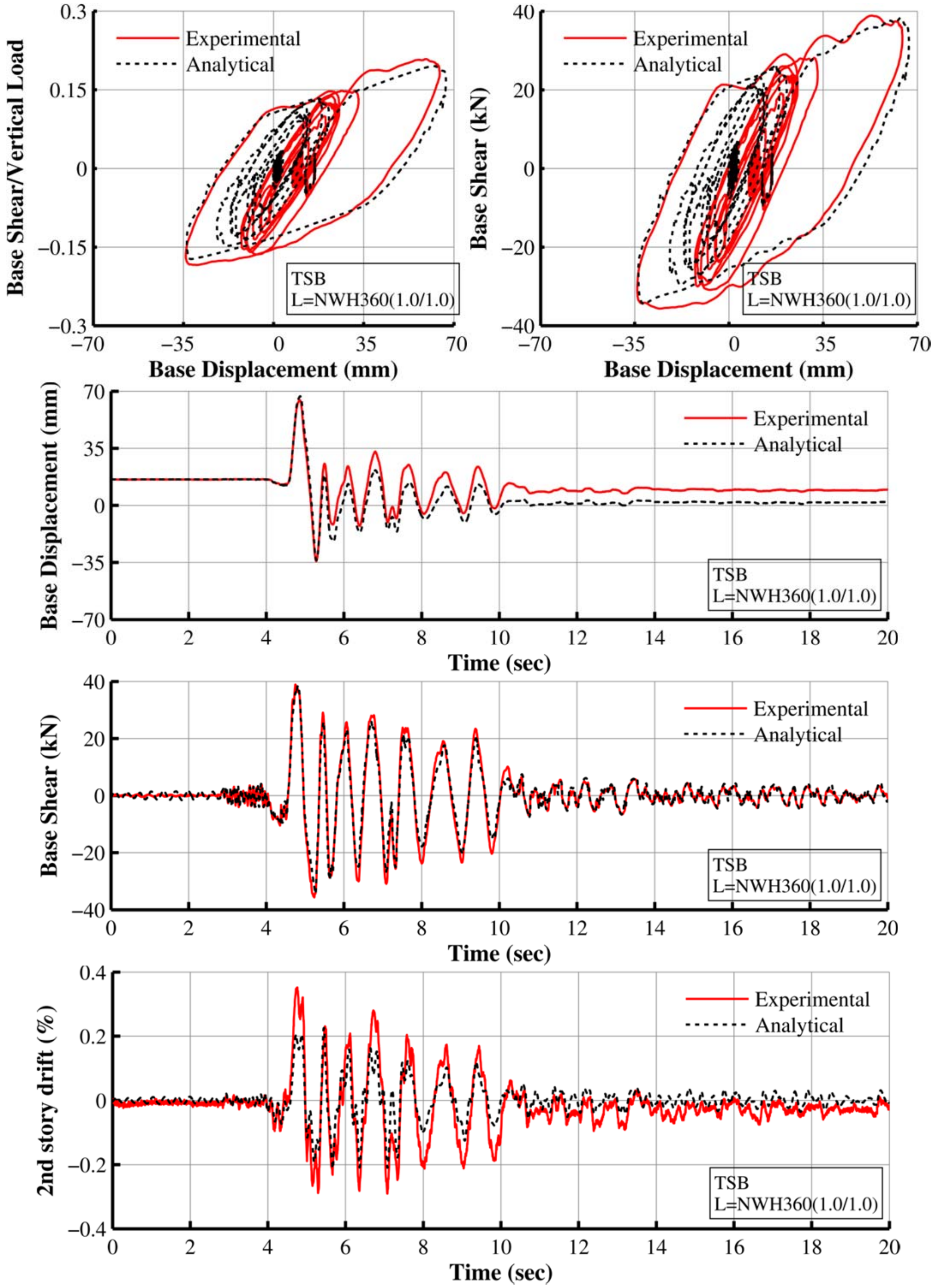

Base Shear/Vertical Load
Base Displacement (mm)
Experimental
Analytical
TSB
L=NWH360(1.0/1.0)
Base Shear (kN)
Base Displacement (mm)
Base Displacement (mm)
Time (sec)
Base Shear (kN)
Time (sec)
2nd story drift (%)
Time (sec)

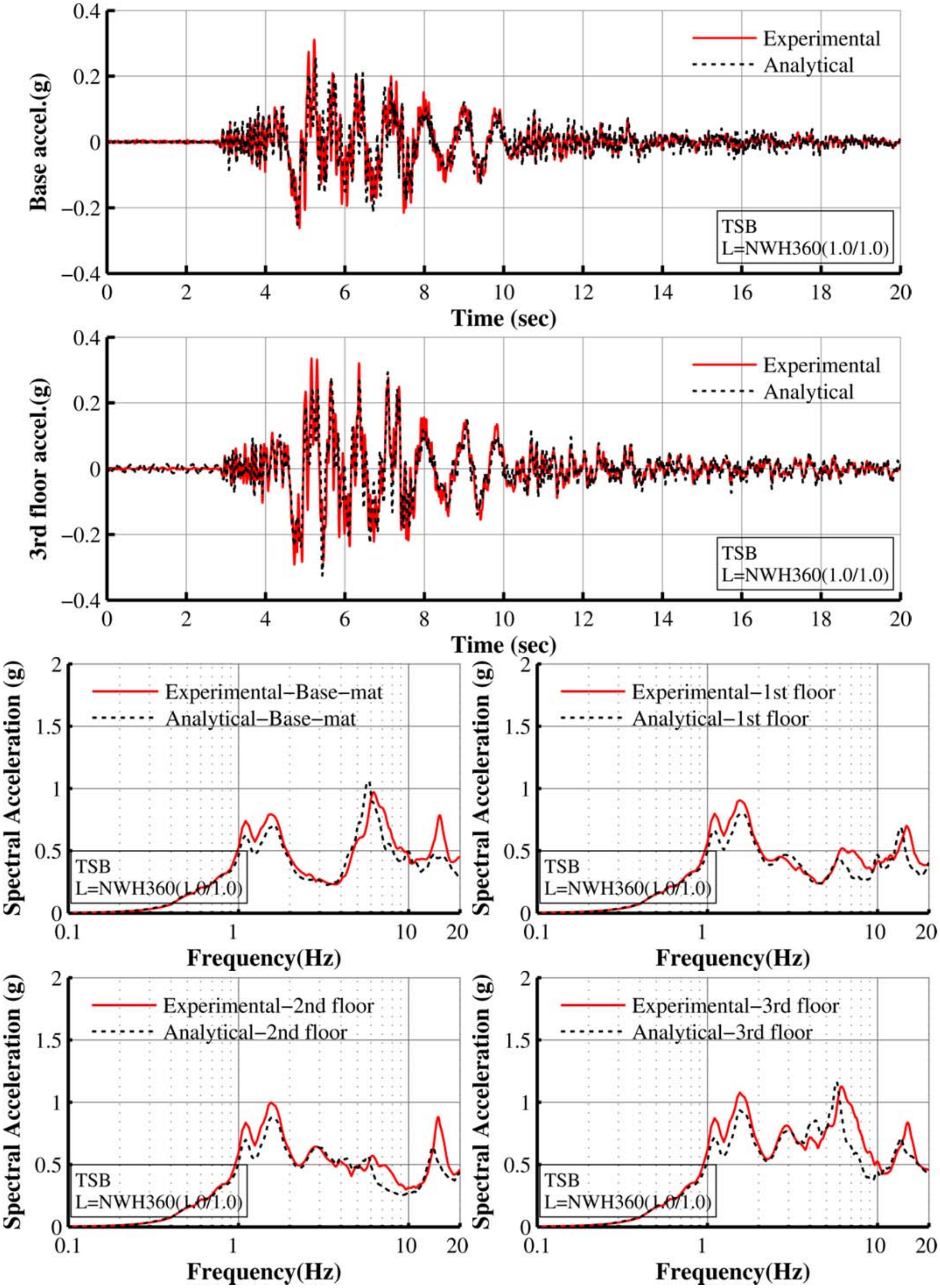
Base accel.(g)
Time (sec)
Experimental
Analytical
TSB
L=NWH360(1.0/1.0)
3rd floor accel.(g)
Time (sec)
Experimental
Analytical
TSB
L=NWH360(1.0/1.0)
Spectral Acceleration (g)
Frequency(Hz)
Experimental−Base−mat
Analytical−Base−mat
TSB
L=NWH360(1.0/1.0)
Spectral Acceleration (g)
Frequency(Hz)
Experimental−1st floor
Analytical−1st floor
TSB
L=NWH360(1.0/1.0)
Spectral Acceleration (g)
Frequency(Hz)
Experimental−2nd floor
Analytical−2nd floor
TSB
L=NWH360(1.0/1.0)
Spectral Acceleration (g)
Frequency(Hz)
Experimental−3rd floor
Analytical−3rd floor
TSB
L=NWH360(1.0/1.0)

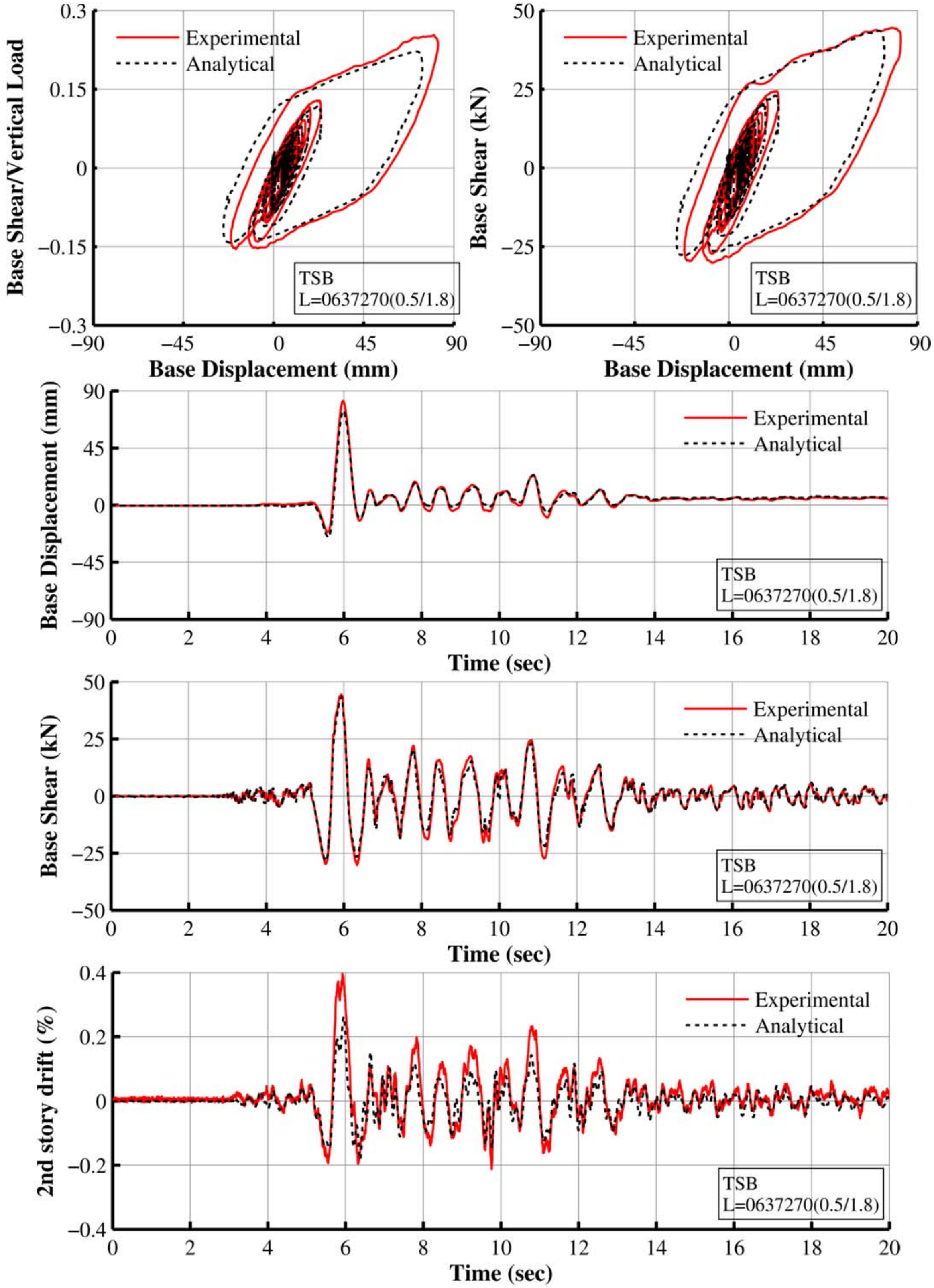
Experimental
Analytical
Base Shear/Vertical Load
Base Displacement (mm)
TSB
L=0637270(0.5/1.8)
Base Shear (kN)
Base Displacement (mm)
Time (sec)
Base Shear (kN)
2nd story drift (%)

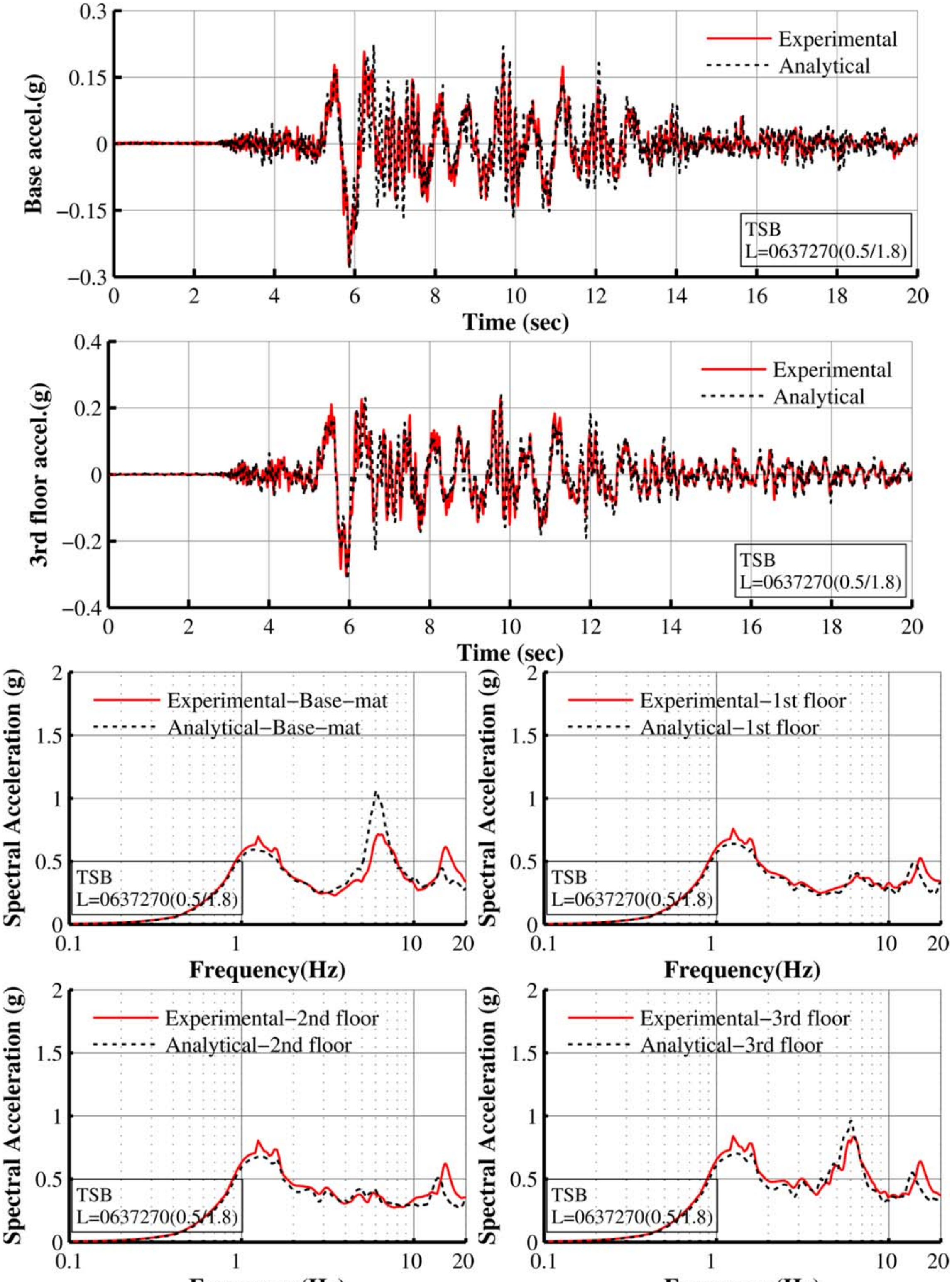

Experimental
Analytical
Base accel.(g)
Time (sec)
TSB
L=0637270(0.5/1.8)
3rd floor accel.(g)
Spectral Acceleration (g)
Frequency(Hz)
Experimental−Base−mat
Analytical−Base−mat
Experimental−1st floor
Analytical−1st floor
Experimental−2nd floor
Analytical−2nd floor
Experimental−3rd floor
Analytical−3rd floor

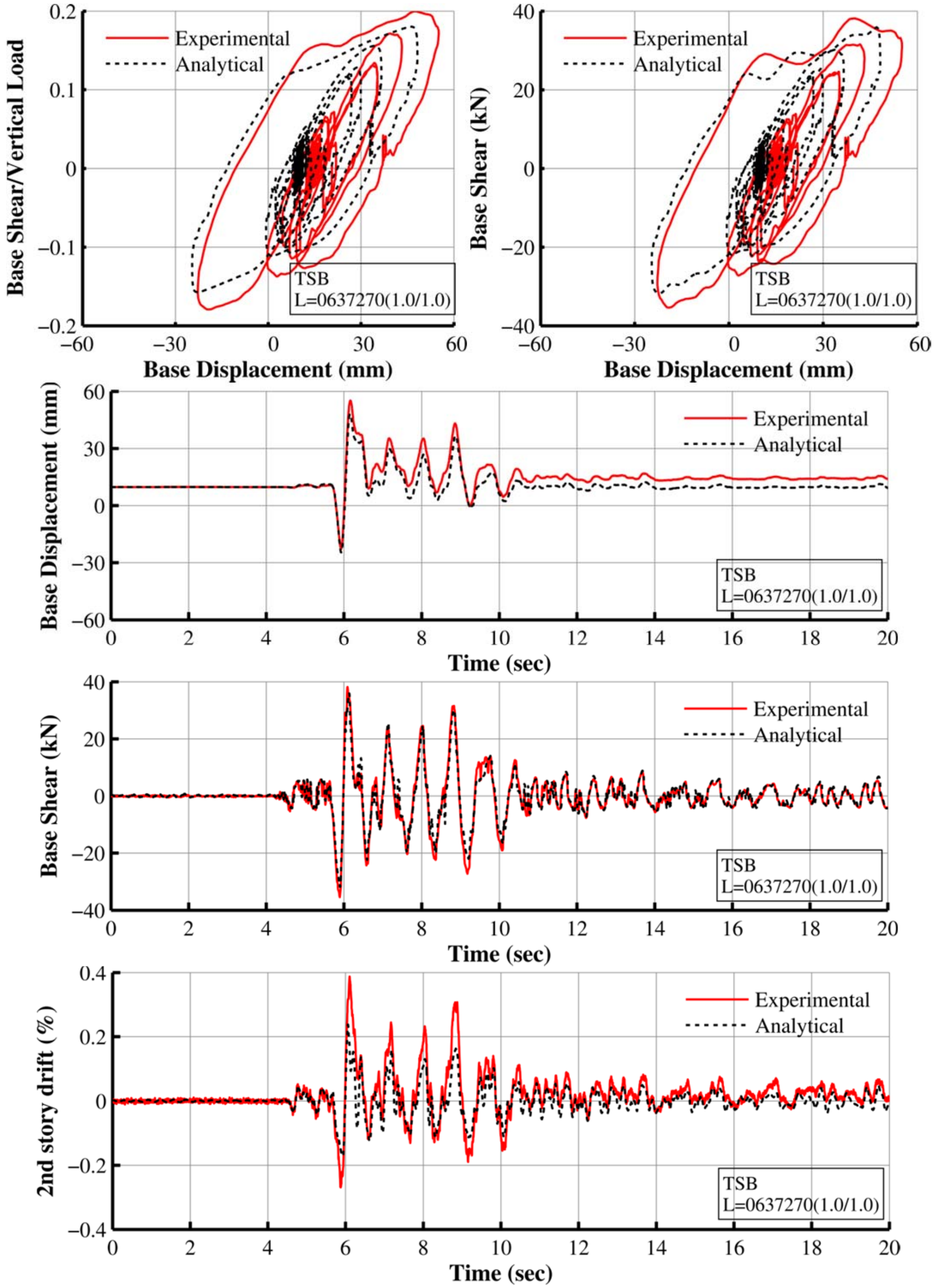
Experimental
Analytical
TSB
L=0637270(1.0/1.0)
Base Shear/Vertical Load
Base Displacement (mm)
Base Shear (kN)
Base Displacement (mm)
Time (sec)
Base Shear (kN)
2nd story drift (%)

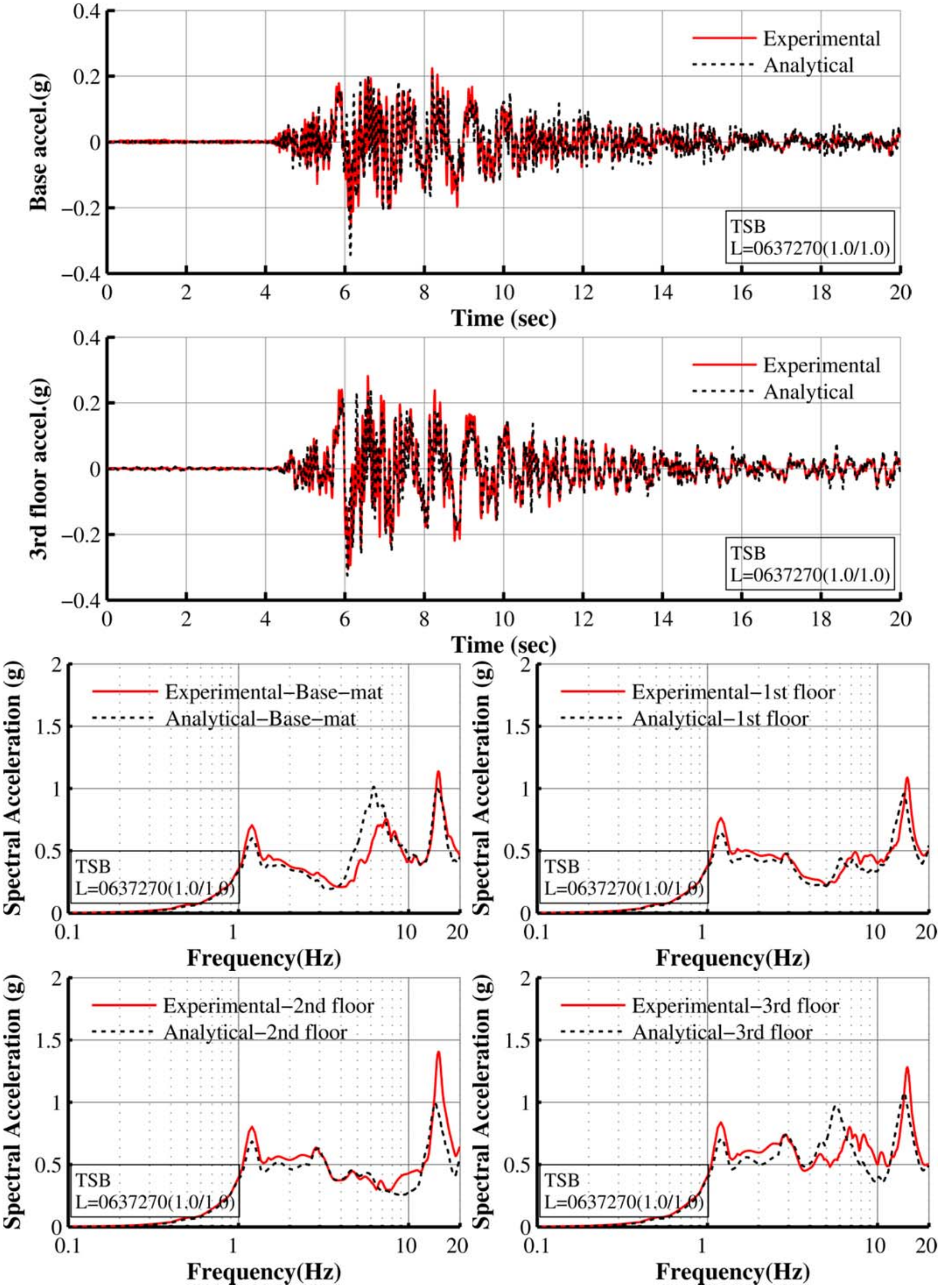

Base accel.(g)
Time (sec)
Experimental
Analytical
TSB
L=0637270(1.0/1.0)
3rd floor accel.(g)
Time (sec)
Experimental
Analytical
TSB
L=0637270(1.0/1.0)
Spectral Acceleration (g)
Frequency(Hz)
Experimental−Base−mat
Analytical−Base−mat
TSB
L=0637270(1.0/1.0)
Experimental−1st floor
Analytical−1st floor
Experimental−2nd floor
Analytical−2nd floor
Experimental−3rd floor
Analytical−3rd floor

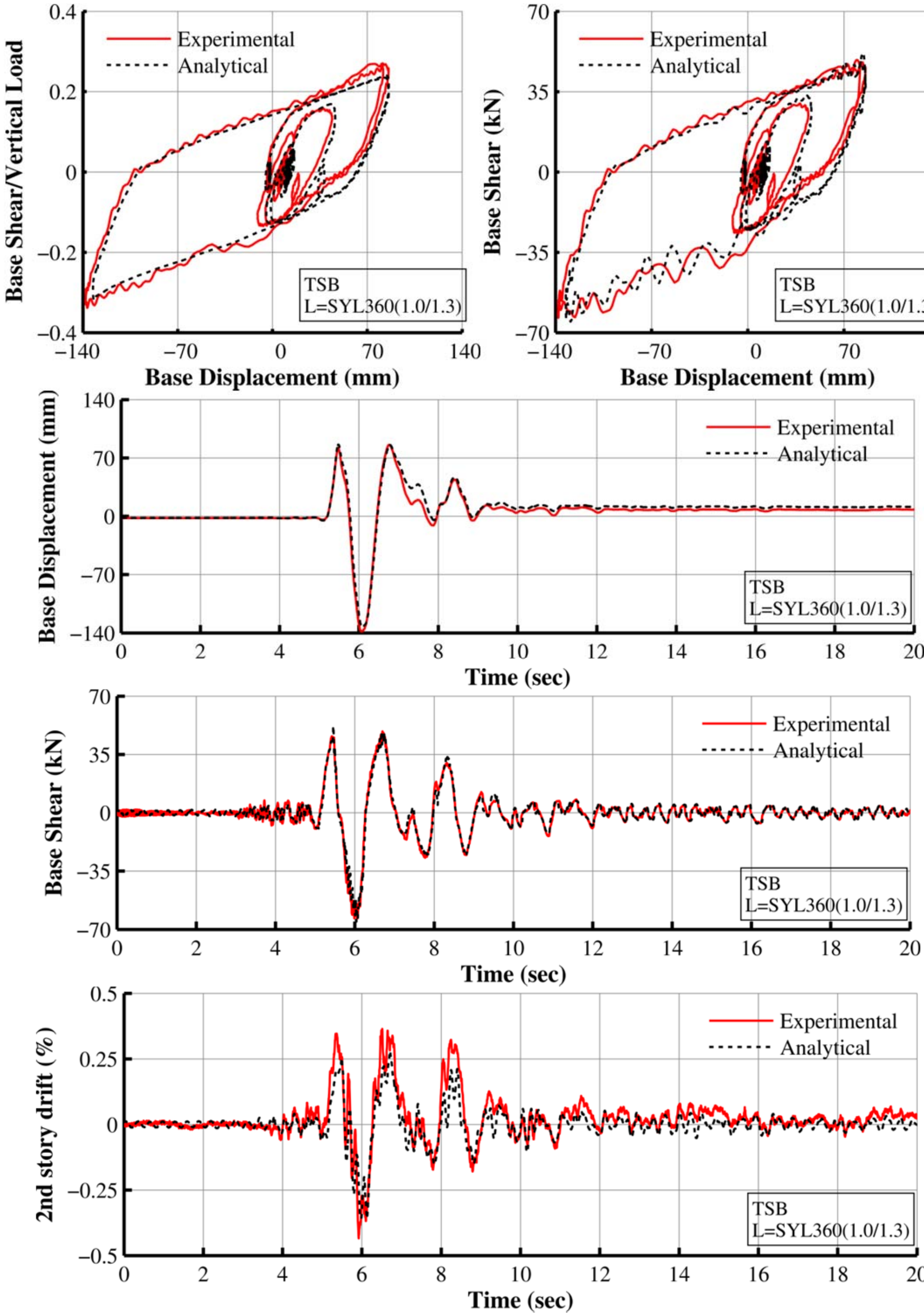

Experimental
Analytical
TSB
L=SYL360(1.0/1.3)
Base Shear/Vertical Load
Base Displacement (mm)
Base Shear (kN)
Base Displacement (mm)
Time (sec)
Base Shear (kN)
2nd story drift (%)

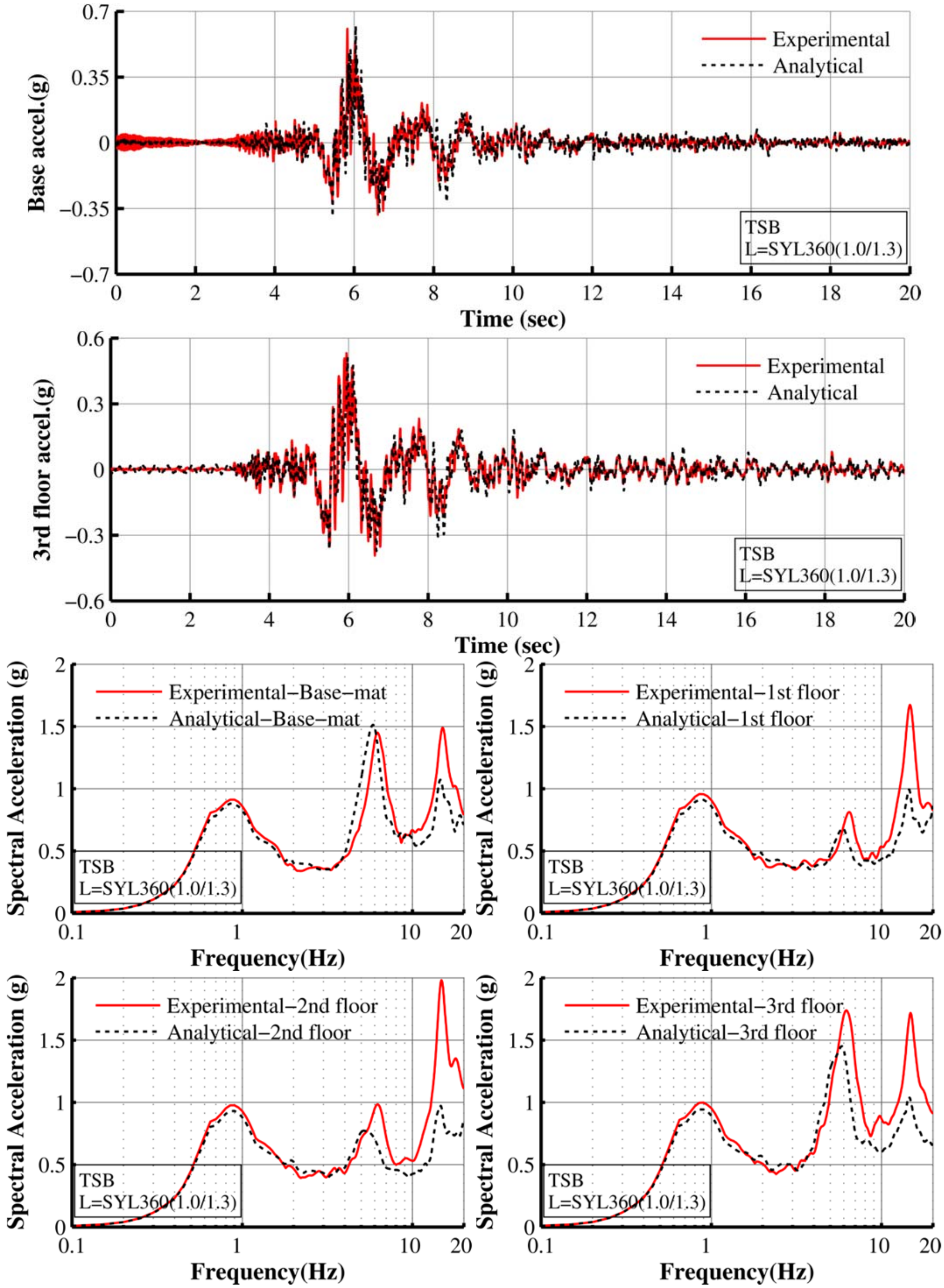

Base accel.(g)
Time (sec)
Experimental
Analytical
TSB
L=SYL360(1.0/1.3)
0.7
0.35
0
−0.35
−0.7
0
2
4
6
8
10
12
14
16
18
20
3rd floor accel.(g)
Time (sec)
Experimental
Analytical
TSB
L=SYL360(1.0/1.3)
0.6
0.3
0
−0.3
−0.6
Spectral Acceleration (g)
Frequency(Hz)
Experimental−Base−mat
Analytical−Base−mat
Experimental−1st floor
Analytical−1st floor
Experimental−2nd floor
Analytical−2nd floor
Experimental−3rd floor
Analytical−3rd floor
TSB
L=SYL360(1.0/1.3)
2
1.5
1
0.5
0
0.1
1
10
20

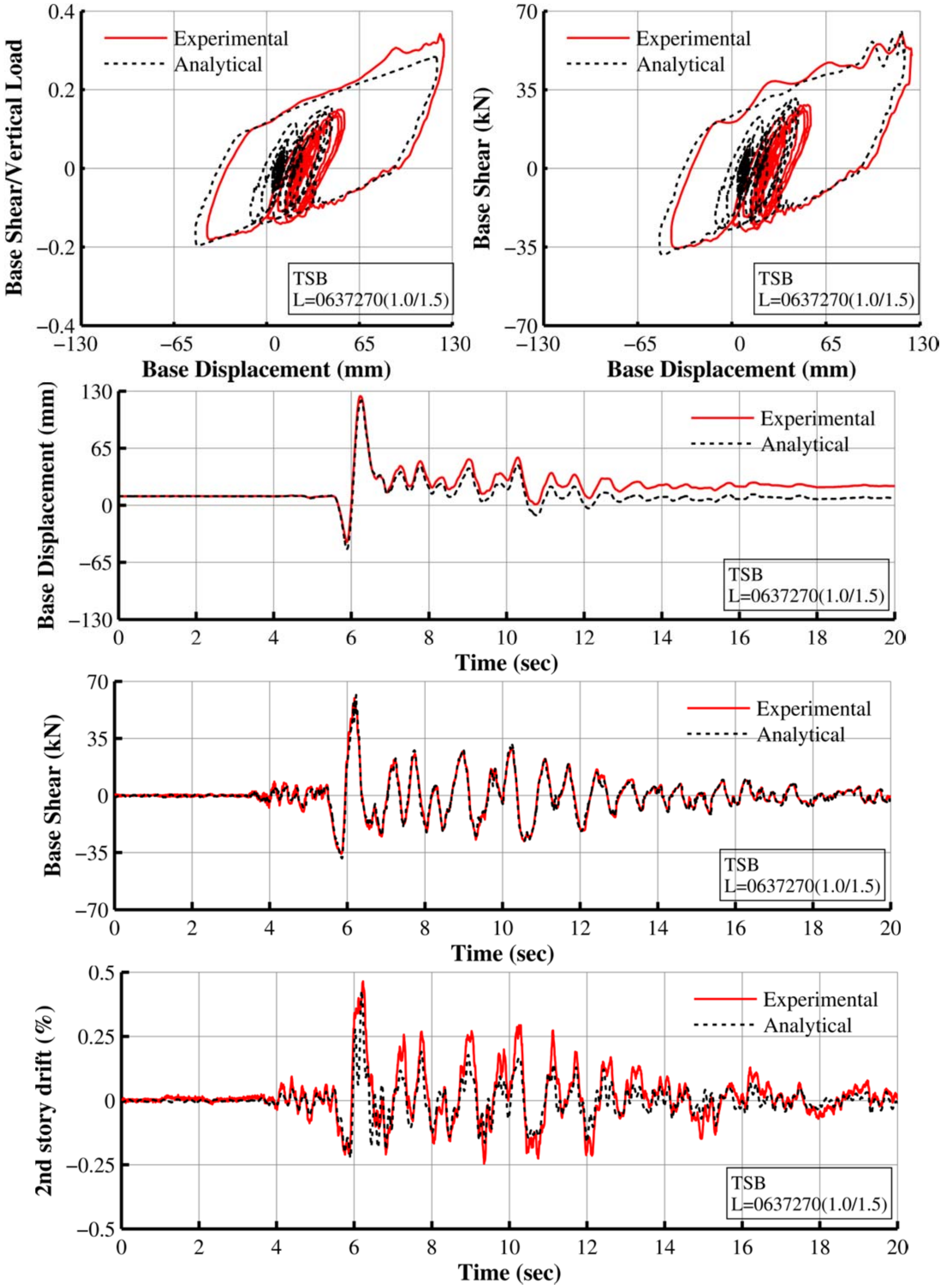
Experimental
Analytical
Base Shear/Vertical Load
Base Displacement (mm)
Base Shear (kN)
Base Displacement (mm)
TSB
L=0637270(1.0/1.5)
Time (sec)
2nd story drift (%)

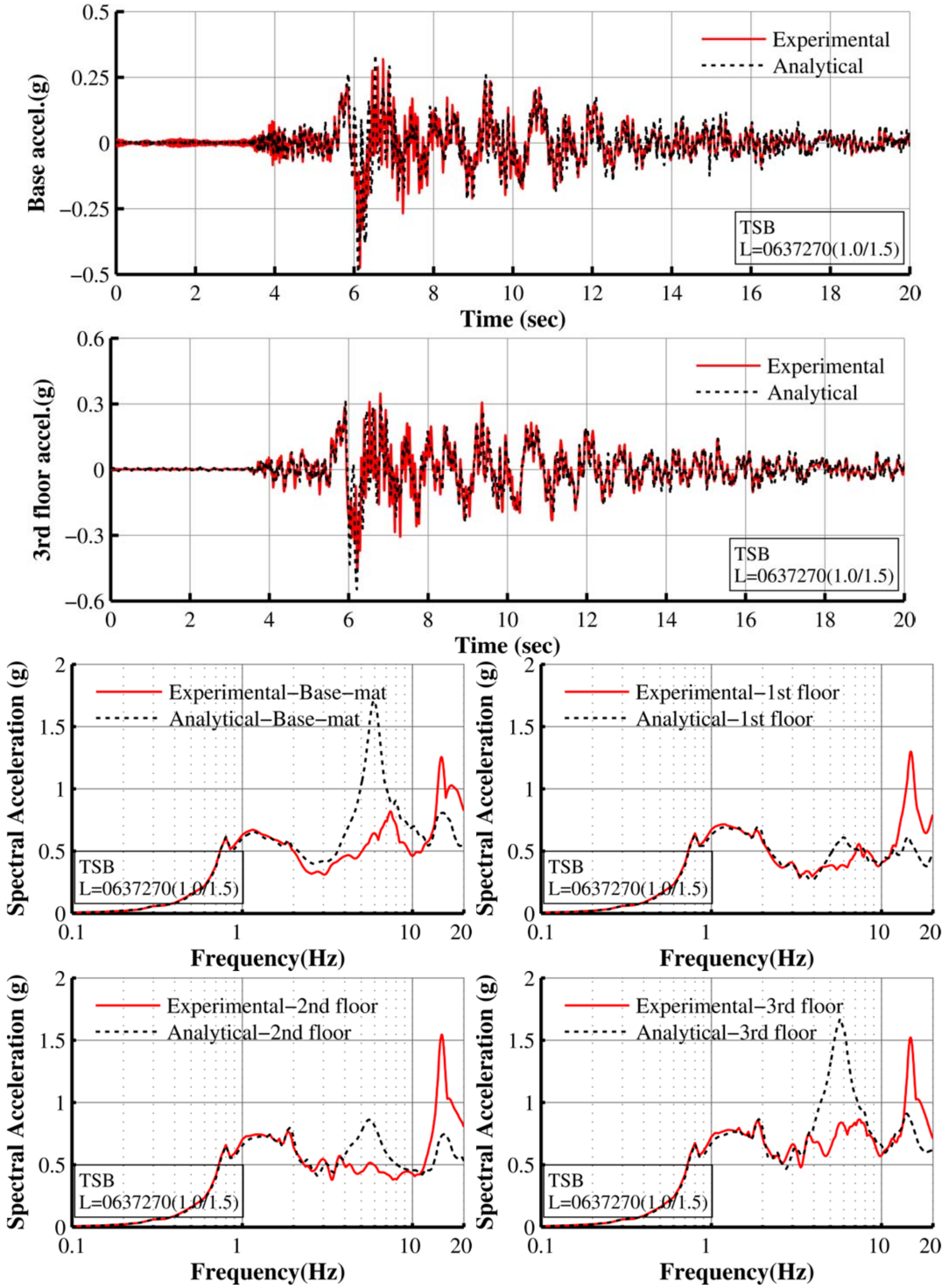

Base accel.(g)
Time (sec)
Experimental
Analytical
TSB
L=0637270(1.0/1.5)
3rd floor accel.(g)
Time (sec)
Experimental
Analytical
TSB
L=0637270(1.0/1.5)
Spectral Acceleration (g)
Frequency(Hz)
Experimental−Base−mat
Analytical−Base−mat
TSB
L=0637270(1.0/1.5)
Spectral Acceleration (g)
Frequency(Hz)
Experimental−1st floor
Analytical−1st floor
TSB
L=0637270(1.0/1.5)
Spectral Acceleration (g)
Frequency(Hz)
Experimental−2nd floor
Analytical−2nd floor
TSB
L=0637270(1.0/1.5)
Spectral Acceleration (g)
Frequency(Hz)
Experimental−3rd floor
Analytical−3rd floor
TSB
L=0637270(1.0/1.5)

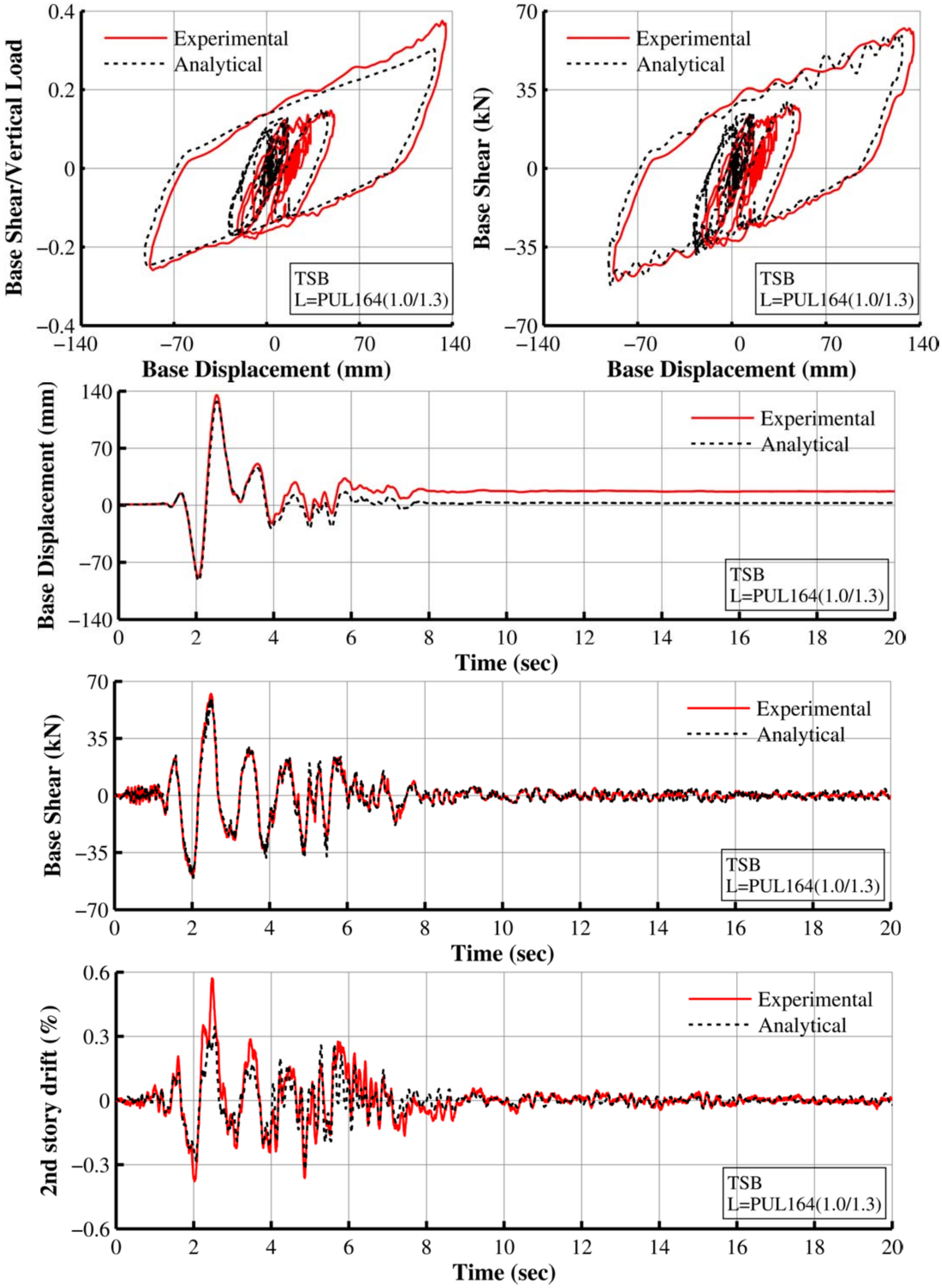
Experimental
Analytical
TSB
L=PUL164(1.0/1.3)
Base Shear/Vertical Load
Base Shear (kN)
Base Displacement (mm)
Time (sec)
Base Shear (kN)
2nd story drift (%)

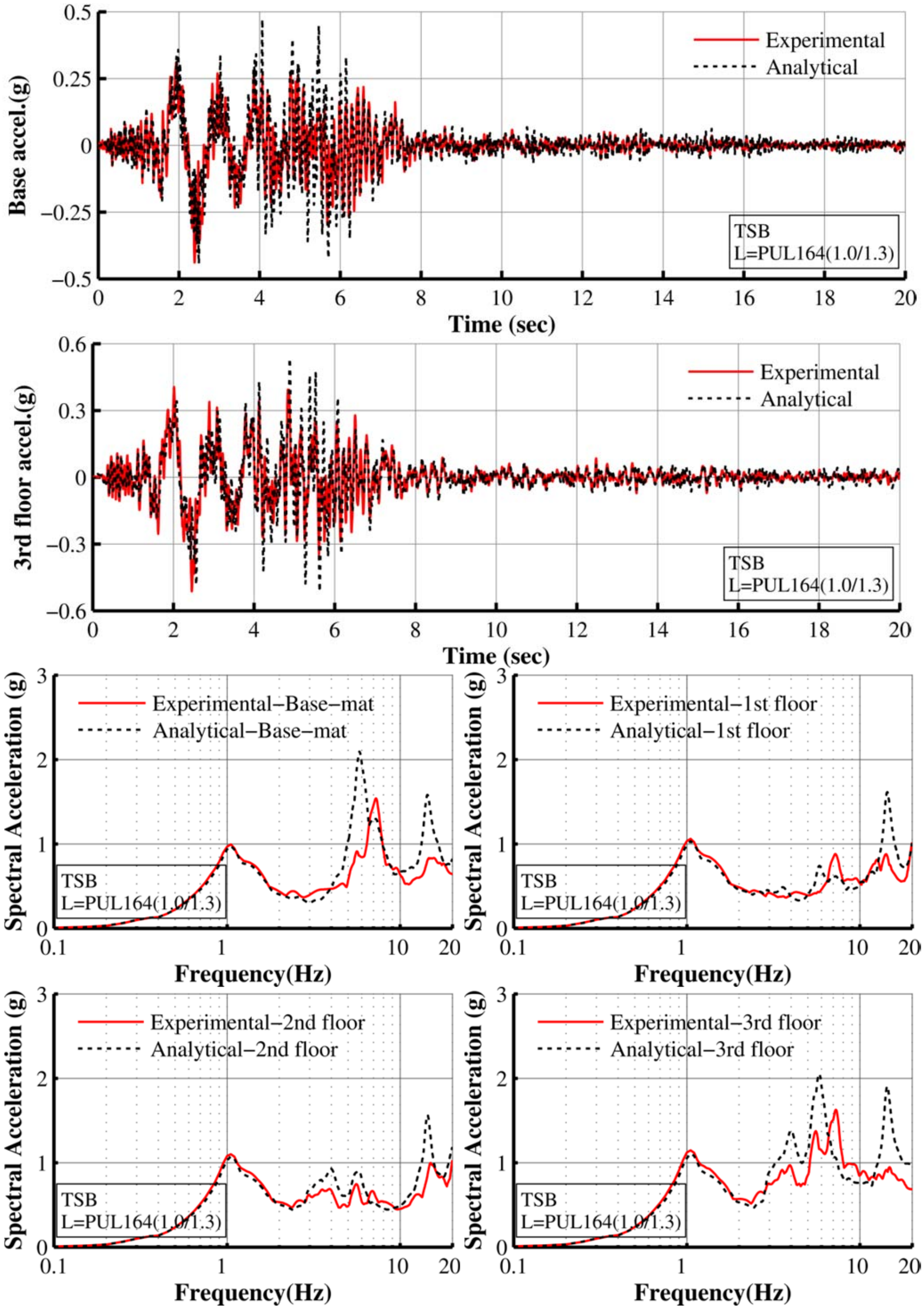
Base accel.(g)
0.5
0.25
0
−0.25
−0.5
Experimental
Analytical
TSB
L=PUL164(1.0/1.3)
0 2 4 6 8 10 12 14 16 18 20
Time (sec)
3rd floor accel.(g)
0.6
0.3
0
−0.3
−0.6
Experimental
Analytical
TSB
L=PUL164(1.0/1.3)
0 2 4 6 8 10 12 14 16 18 20
Time (sec)
Spectral Acceleration (g)
Experimental−Base−mat
Analytical−Base−mat
TSB
L=PUL164(1.0/1.3)
0.1 1 10 20
Frequency(Hz)
Spectral Acceleration (g)
Experimental−1st floor
Analytical−1st floor
TSB
L=PUL164(1.0/1.3)
0.1 1 10 20
Frequency(Hz)
Spectral Acceleration (g)
Experimental−2nd floor
Analytical−2nd floor
TSB
L=PUL164(1.0/1.3)
0.1 1 10 20
Frequency(Hz)
Spectral Acceleration (g)
Experimental−3rd floor
Analytical−3rd floor
TSB
L=PUL164(1.0/1.3)
0.1 1 10 20
Frequency(Hz)

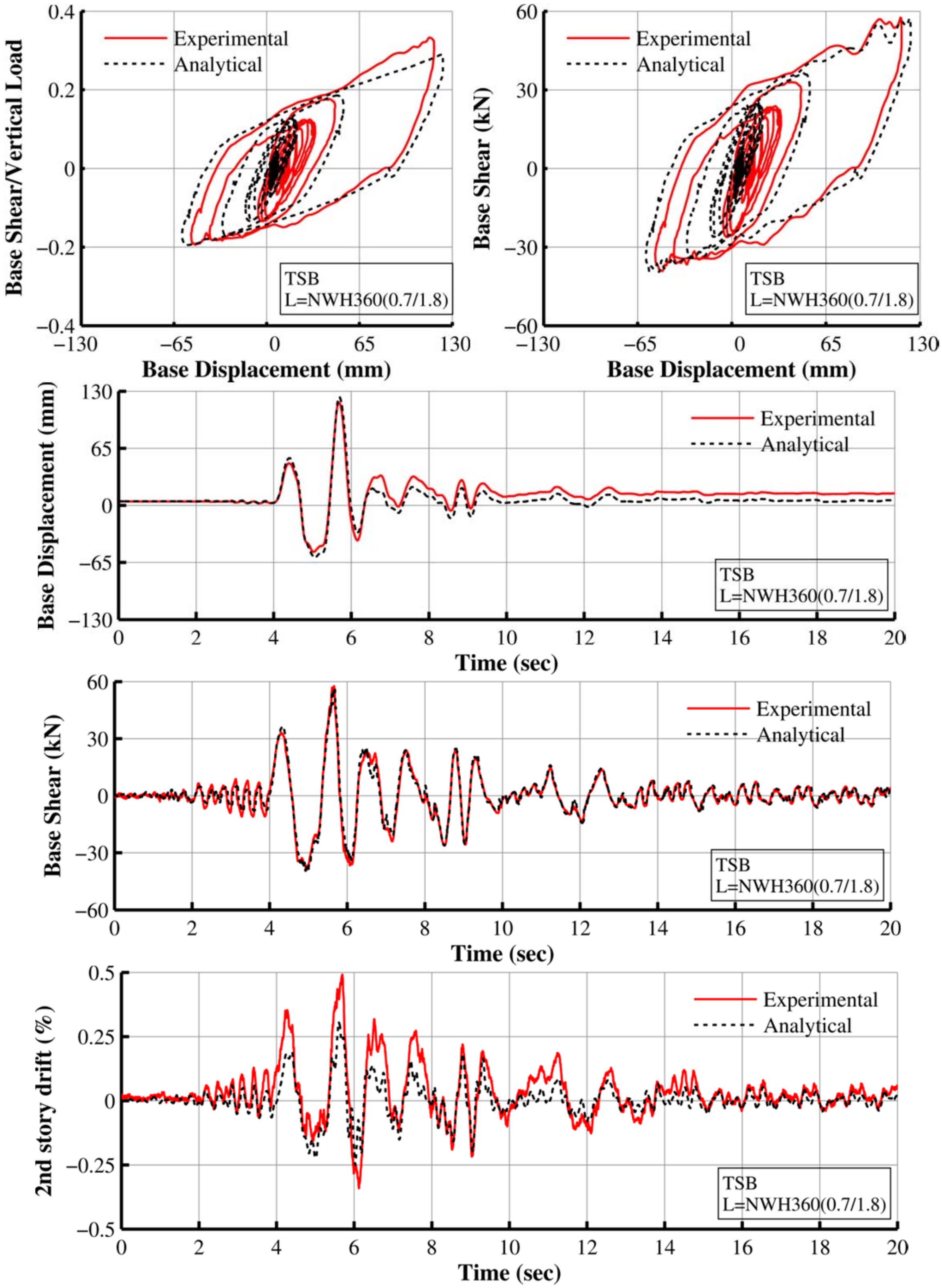

Experimental
Analytical
TSB
L=NWH360(0.7/1.8)
Base Shear/Vertical Load
Base Displacement (mm)
Base Shear (kN)
Base Displacement (mm)
Time (sec)
Base Shear (kN)
Time (sec)
2nd story drift (%)
Time (sec)

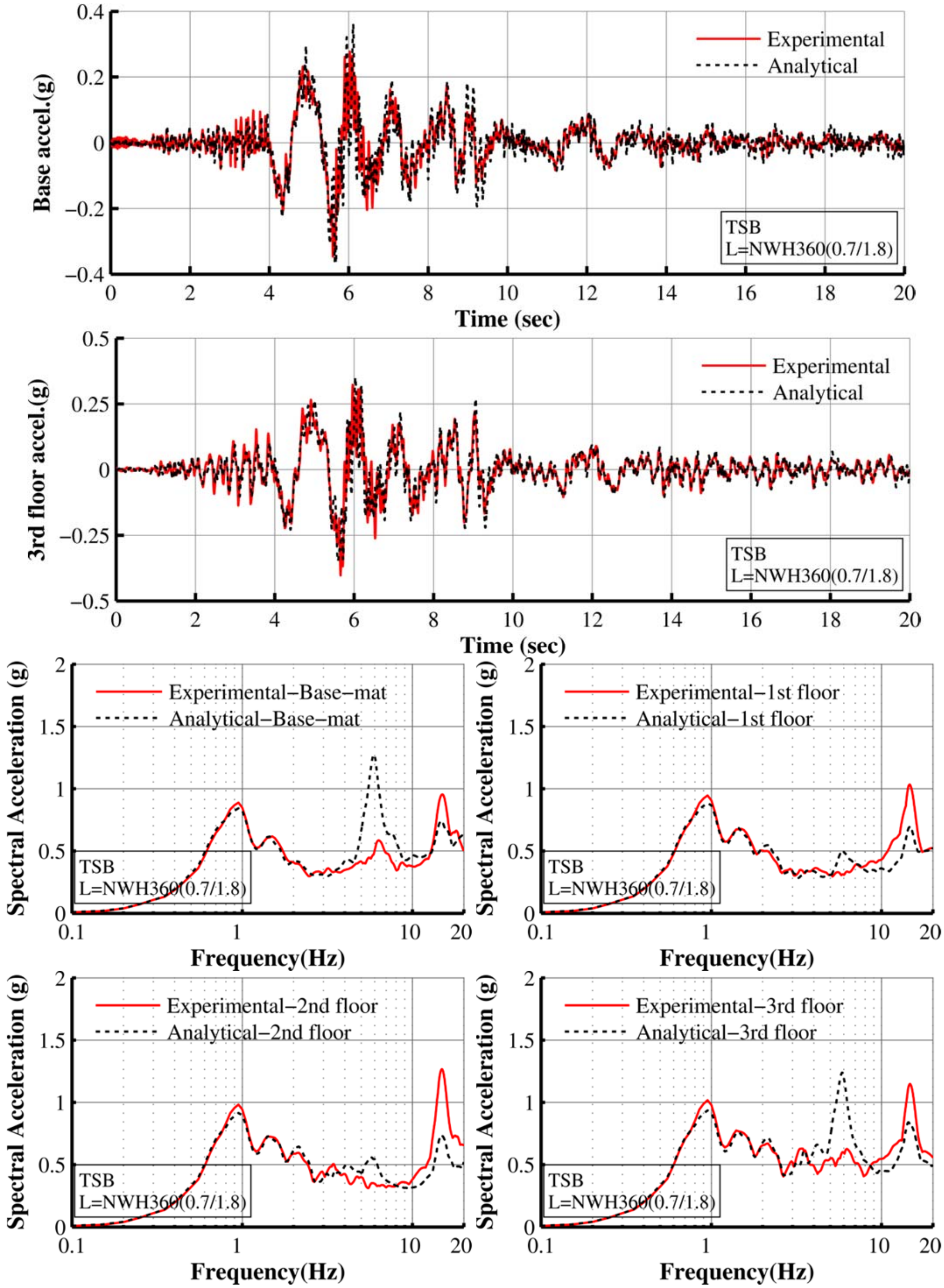
Base accel.(g)
Time (sec)
Experimental
Analytical
TSB
L=NWH360(0.7/1.8)
3rd floor accel.(g)
Time (sec)
Experimental
Analytical
TSB
L=NWH360(0.7/1.8)
Spectral Acceleration (g)
Frequency(Hz)
Experimental−Base−mat
Analytical−Base−mat
TSB
L=NWH360(0.7/1.8)
Spectral Acceleration (g)
Frequency(Hz)
Experimental−1st floor
Analytical−1st floor
TSB
L=NWH360(0.7/1.8)
Spectral Acceleration (g)
Frequency(Hz)
Experimental−2nd floor
Analytical−2nd floor
TSB
L=NWH360(0.7/1.8)
Spectral Acceleration (g)
Frequency(Hz)
Experimental−3rd floor
Analytical−3rd floor
TSB
L=NWH360(0.7/1.8)

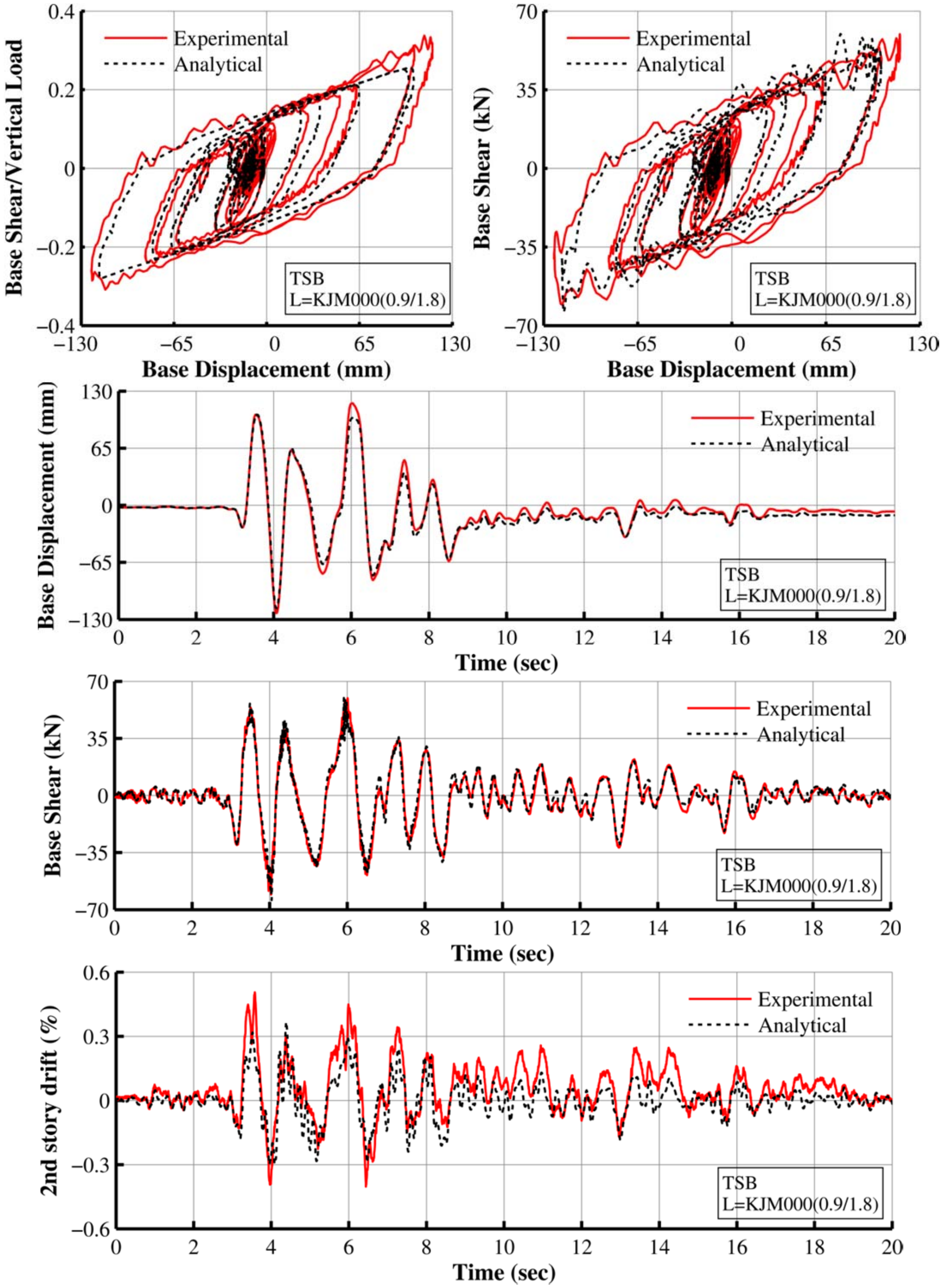
Base Shear/Vertical Load
Base Displacement (mm)
Experimental
Analytical
TSB
L=KJM000(0.9/1.8)
Base Shear (kN)
Base Displacement (mm)
Experimental
Analytical
TSB
L=KJM000(0.9/1.8)
Base Displacement (mm)
Time (sec)
Experimental
Analytical
TSB
L=KJM000(0.9/1.8)
Base Shear (kN)
Time (sec)
Experimental
Analytical
TSB
L=KJM000(0.9/1.8)
2nd story drift (%)
Time (sec)
Experimental
Analytical
TSB
L=KJM000(0.9/1.8)

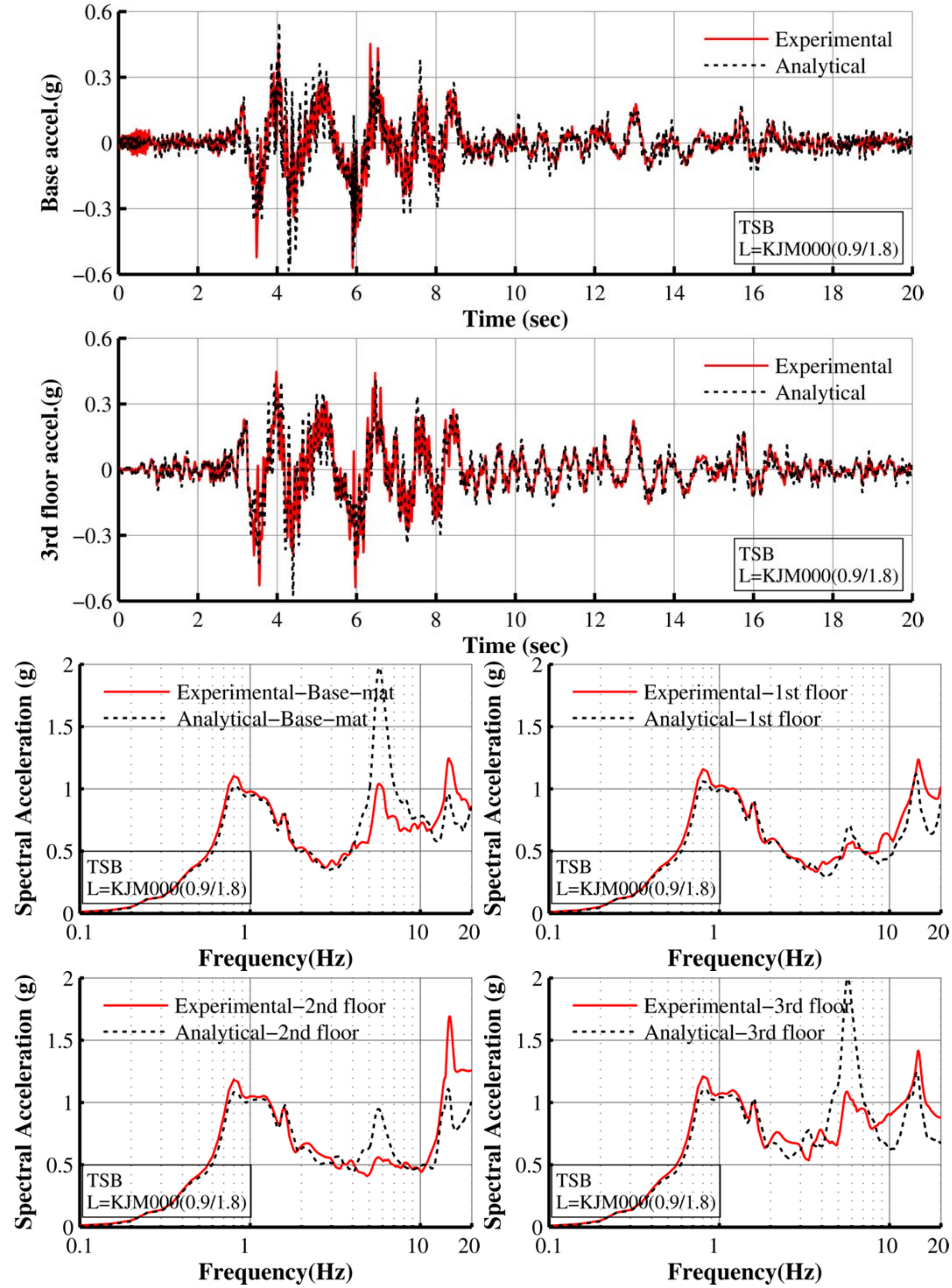
Experimental
Analytical
Base accel.(g)
TSB
L=KJM000(0.9/1.8)
Time (sec)
3rd floor accel.(g)
Experimental−Base−mat
Analytical−Base−mat
Spectral Acceleration (g)
Frequency(Hz)
Experimental−1st floor
Analytical−1st floor
Experimental−2nd floor
Analytical−2nd floor
Experimental−3rd floor
Analytical−3rd floor

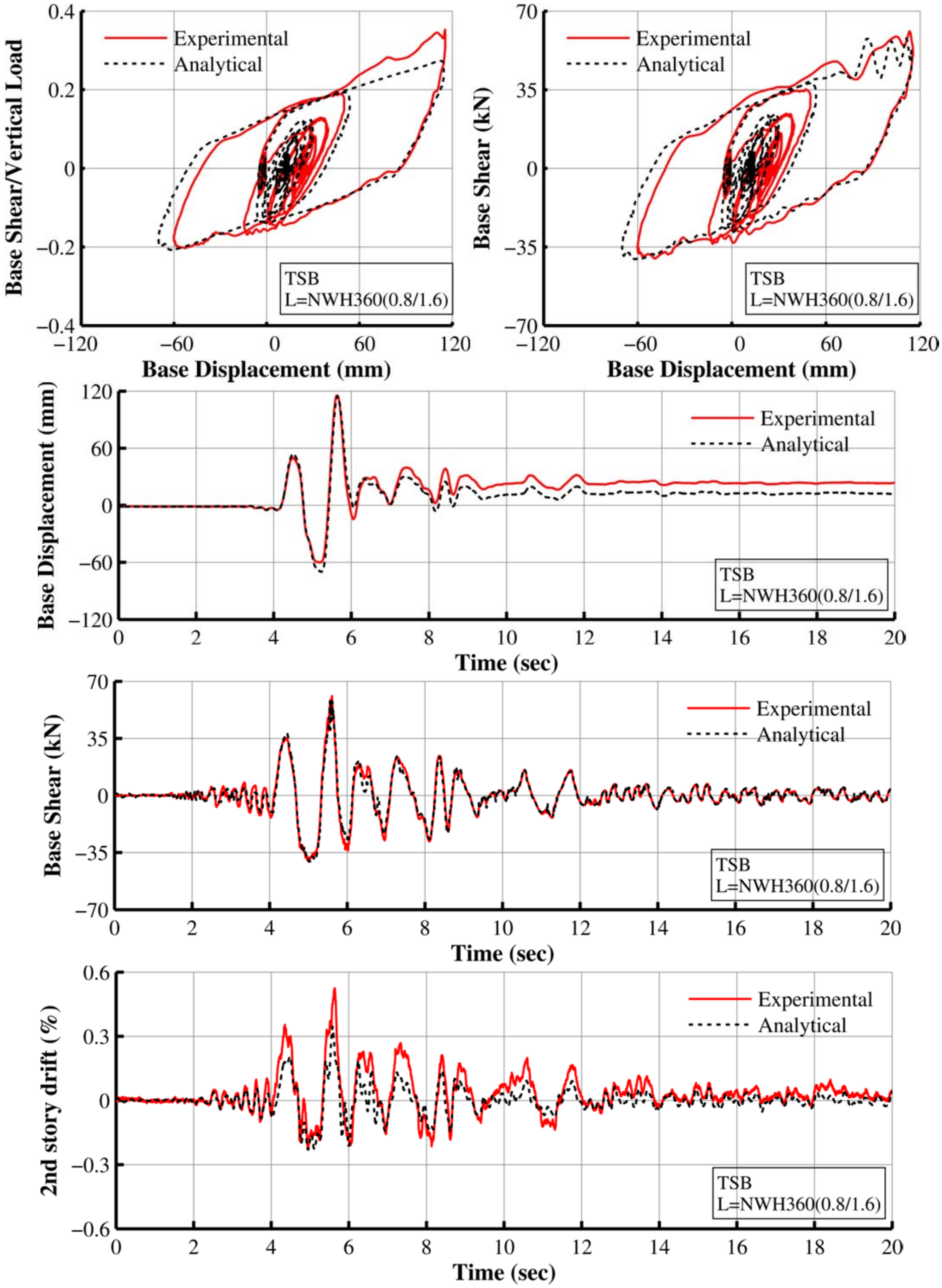
Experimental
Analytical
Base Shear/Vertical Load
Base Displacement (mm)
TSB
L=NWH360(0.8/1.6)
Base Shear (kN)
Base Displacement (mm)
Time (sec)
Base Shear (kN)
2nd story drift (%)

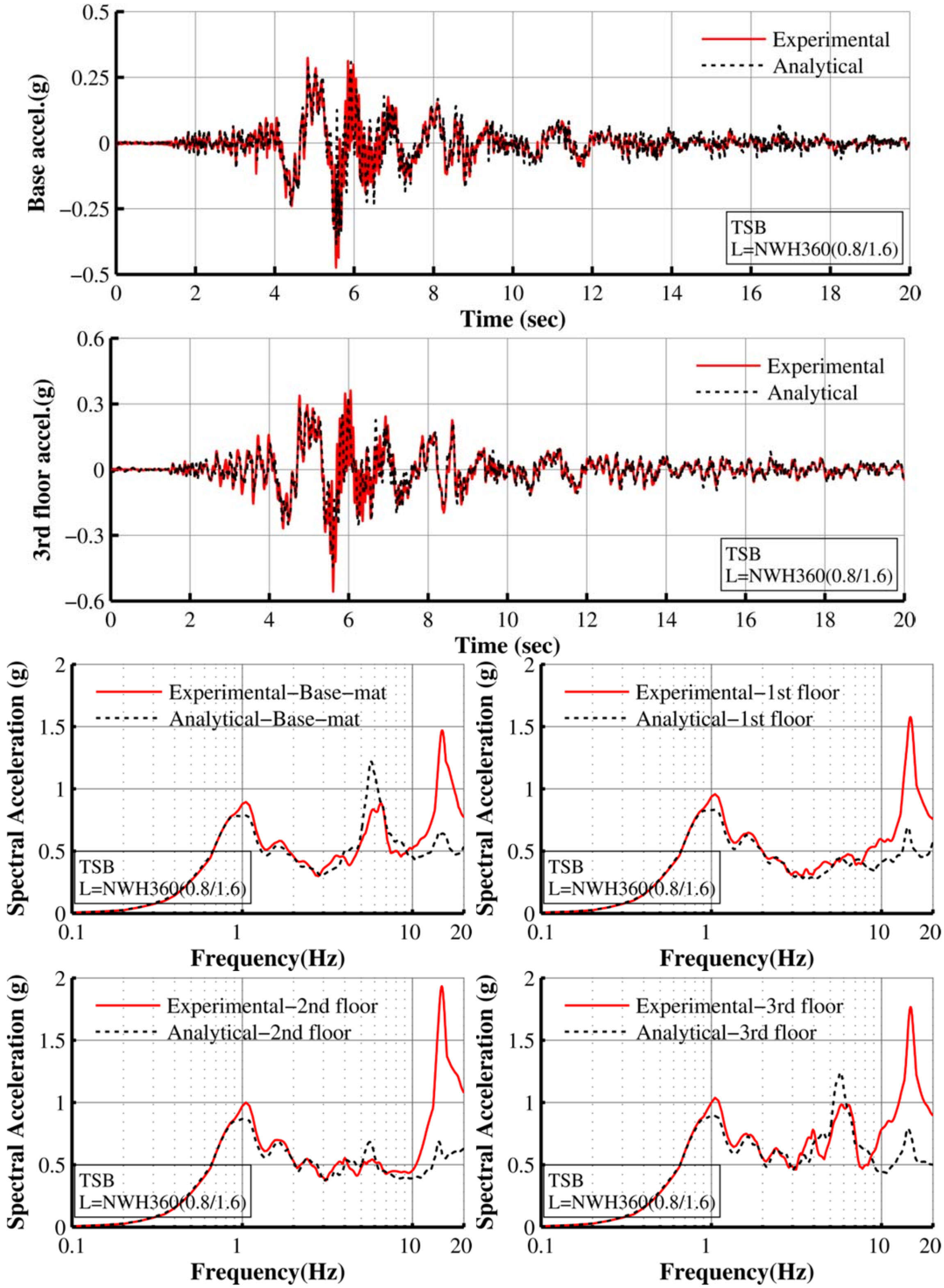

Base accel.(g)
Time (sec)
Experimental
Analytical
TSB
L=NWH360(0.8/1.6)
3rd floor accel.(g)
Time (sec)
Experimental
Analytical
TSB
L=NWH360(0.8/1.6)
Spectral Acceleration (g)
Frequency(Hz)
Experimental−Base−mat
Analytical−Base−mat
Experimental−1st floor
Analytical−1st floor
Experimental−2nd floor
Analytical−2nd floor
Experimental−3rd floor
Analytical−3rd floor

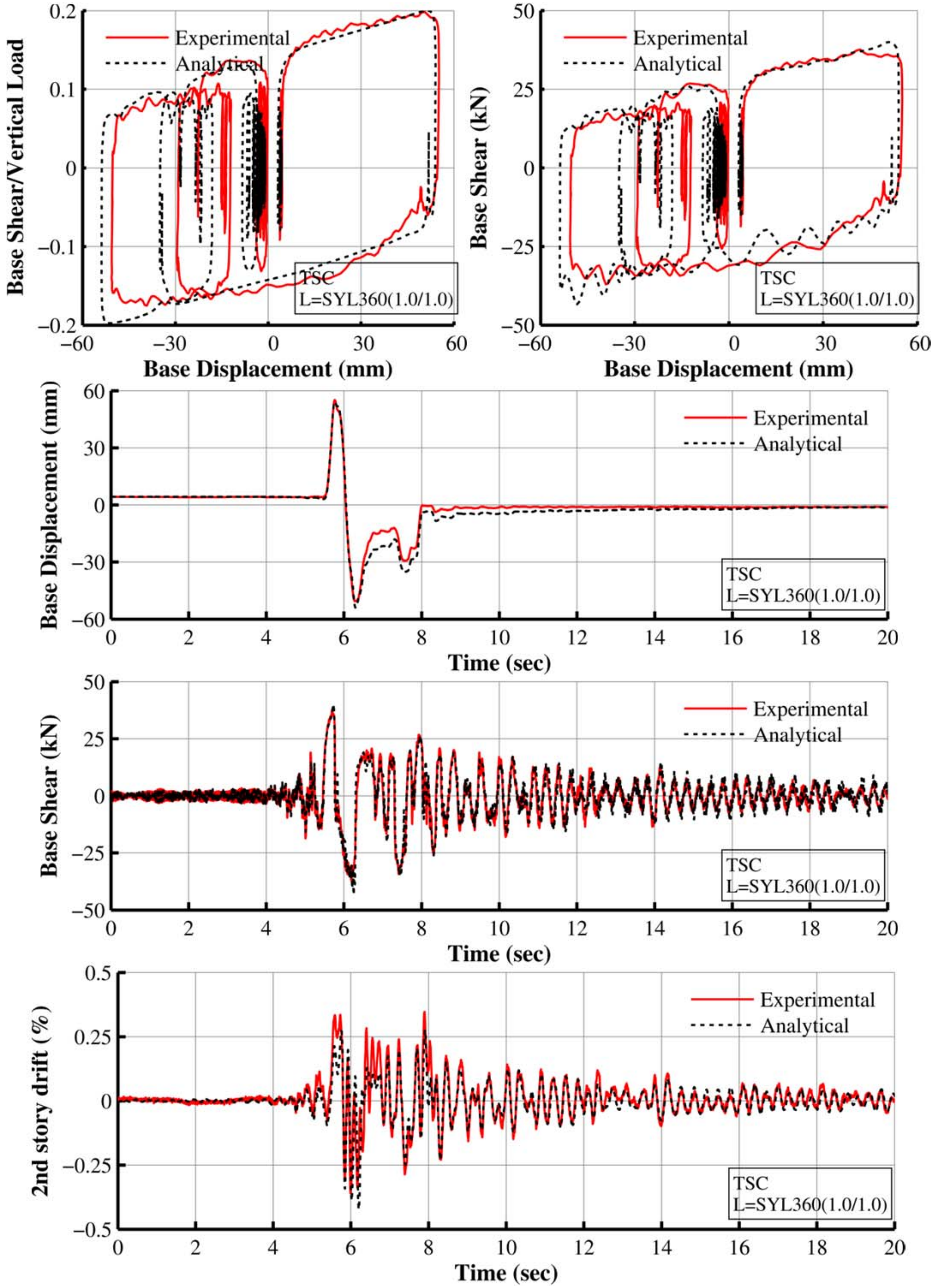

Experimental
Analytical
TSC
L=SYL360(1.0/1.0)
Base Shear/Vertical Load
Base Shear (kN)
Base Displacement (mm)
Time (sec)
2nd story drift (%)

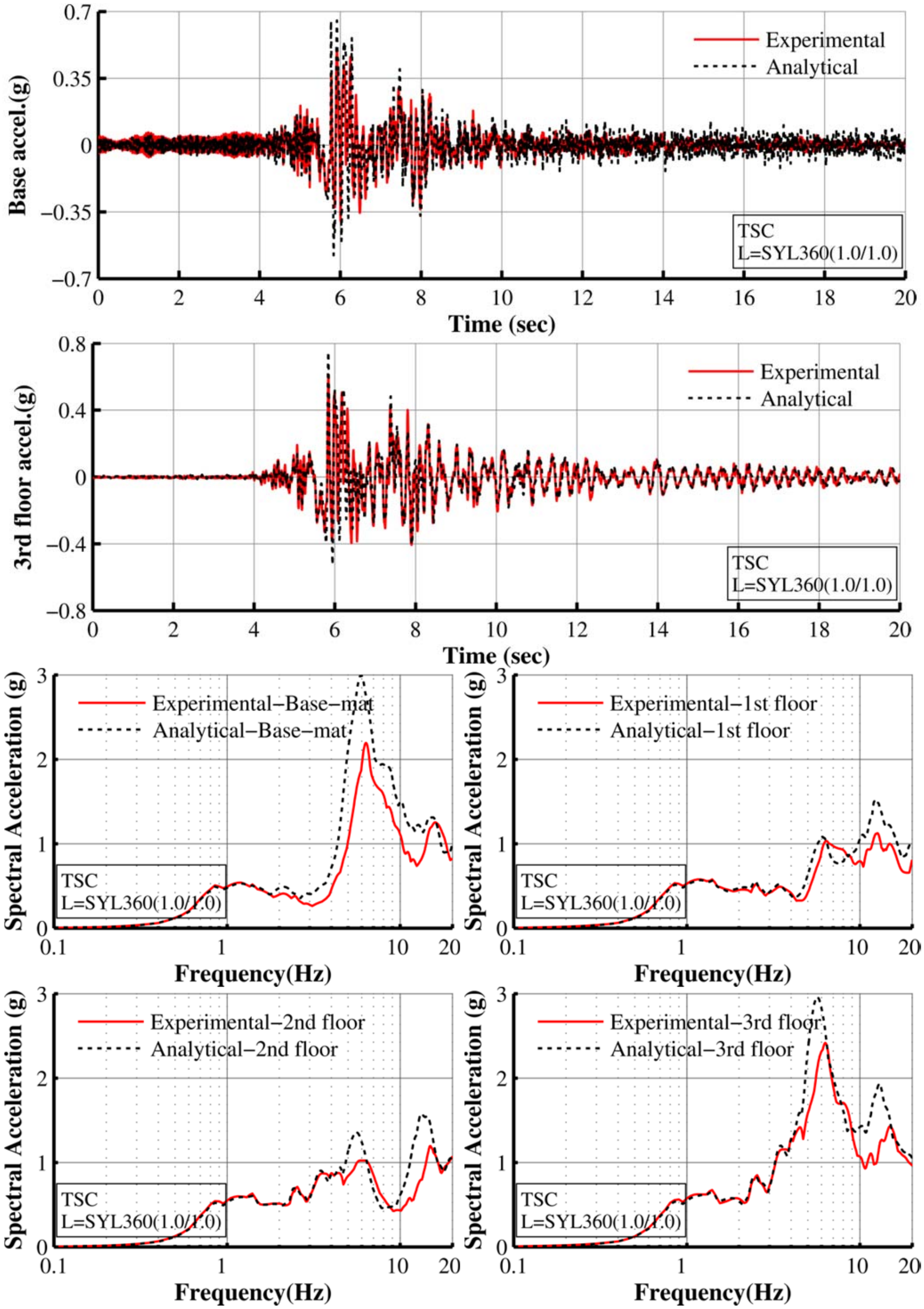

Base accel.(g)
Time (sec)
Experimental
Analytical
TSC
L=SYL360(1.0/1.0)
3rd floor accel.(g)
Time (sec)
Experimental
Analytical
TSC
L=SYL360(1.0/1.0)
Spectral Acceleration (g)
Frequency(Hz)
Experimental−Base−mat
Analytical−Base−mat
TSC
L=SYL360(1.0/1.0)
Spectral Acceleration (g)
Frequency(Hz)
Experimental−1st floor
Analytical−1st floor
TSC
L=SYL360(1.0/1.0)
Spectral Acceleration (g)
Frequency(Hz)
Experimental−2nd floor
Analytical−2nd floor
TSC
L=SYL360(1.0/1.0)
Spectral Acceleration (g)
Frequency(Hz)
Experimental−3rd floor
Analytical−3rd floor
TSC
L=SYL360(1.0/1.0)

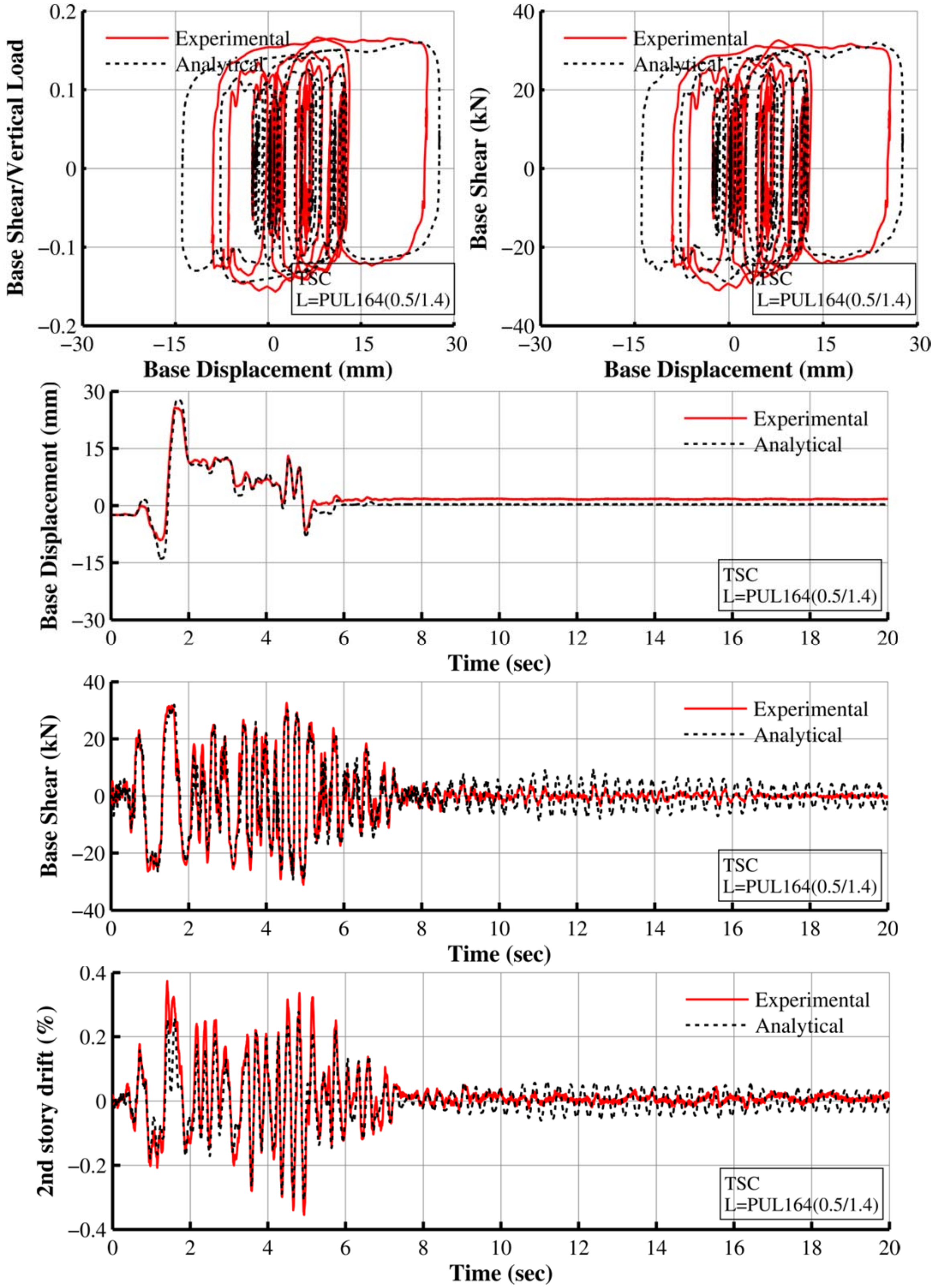
Experimental
Analytical
TSC
L=PUL164(0.5/1.4)
Base Shear/Vertical Load
Base Displacement (mm)
Base Shear (kN)
Base Displacement (mm)
Time (sec)
Base Shear (kN)
Time (sec)
2nd story drift (%)
Time (sec)

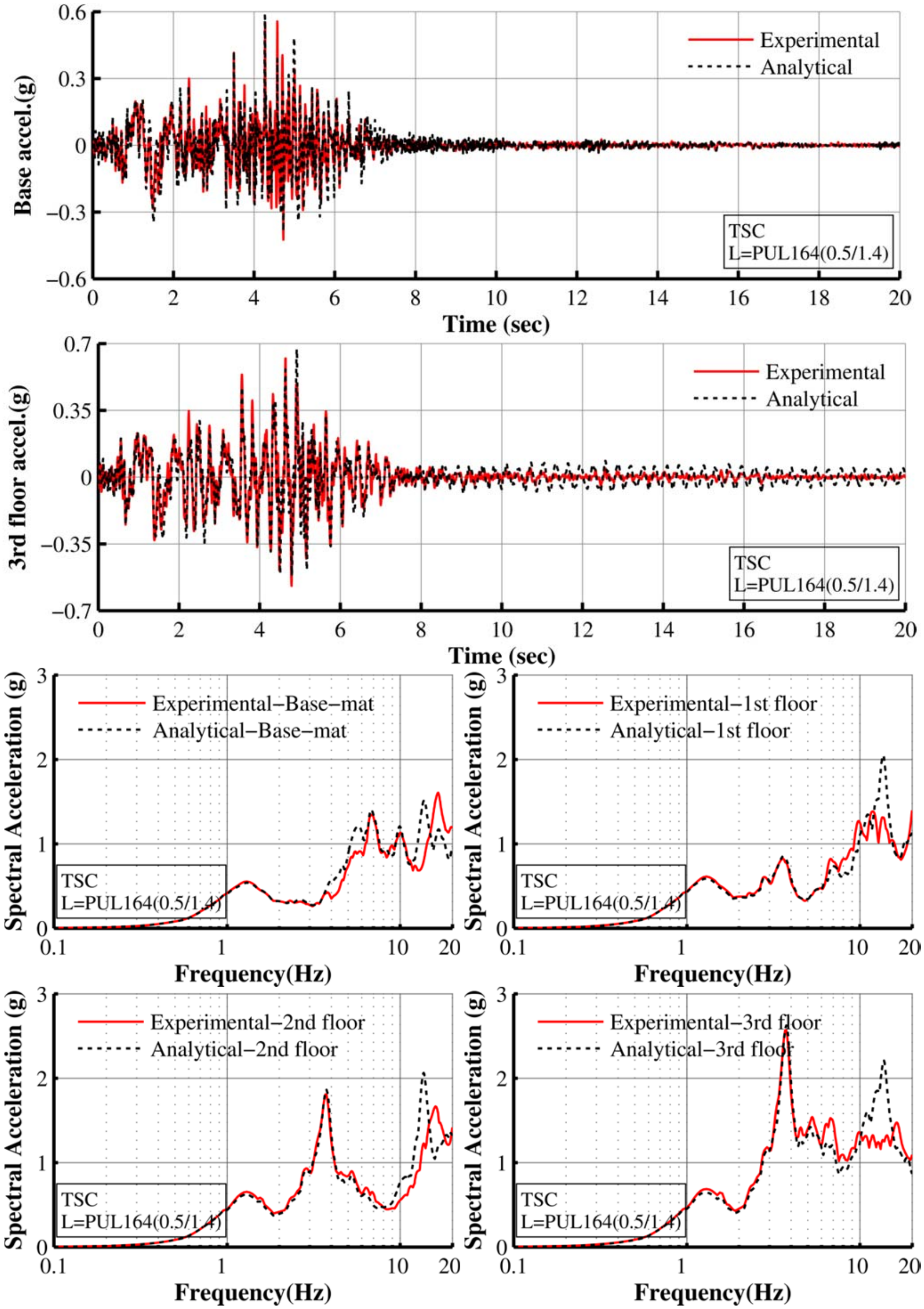
Base accel.(g)
Time (sec)
Experimental
Analytical
TSC
L=PUL164(0.5/1.4)
3rd floor accel.(g)
Time (sec)
Experimental
Analytical
TSC
L=PUL164(0.5/1.4)
Spectral Acceleration (g)
Frequency(Hz)
Experimental−Base−mat
Analytical−Base−mat
Experimental−1st floor
Analytical−1st floor
Experimental−2nd floor
Analytical−2nd floor
Experimental−3rd floor
Analytical−3rd floor

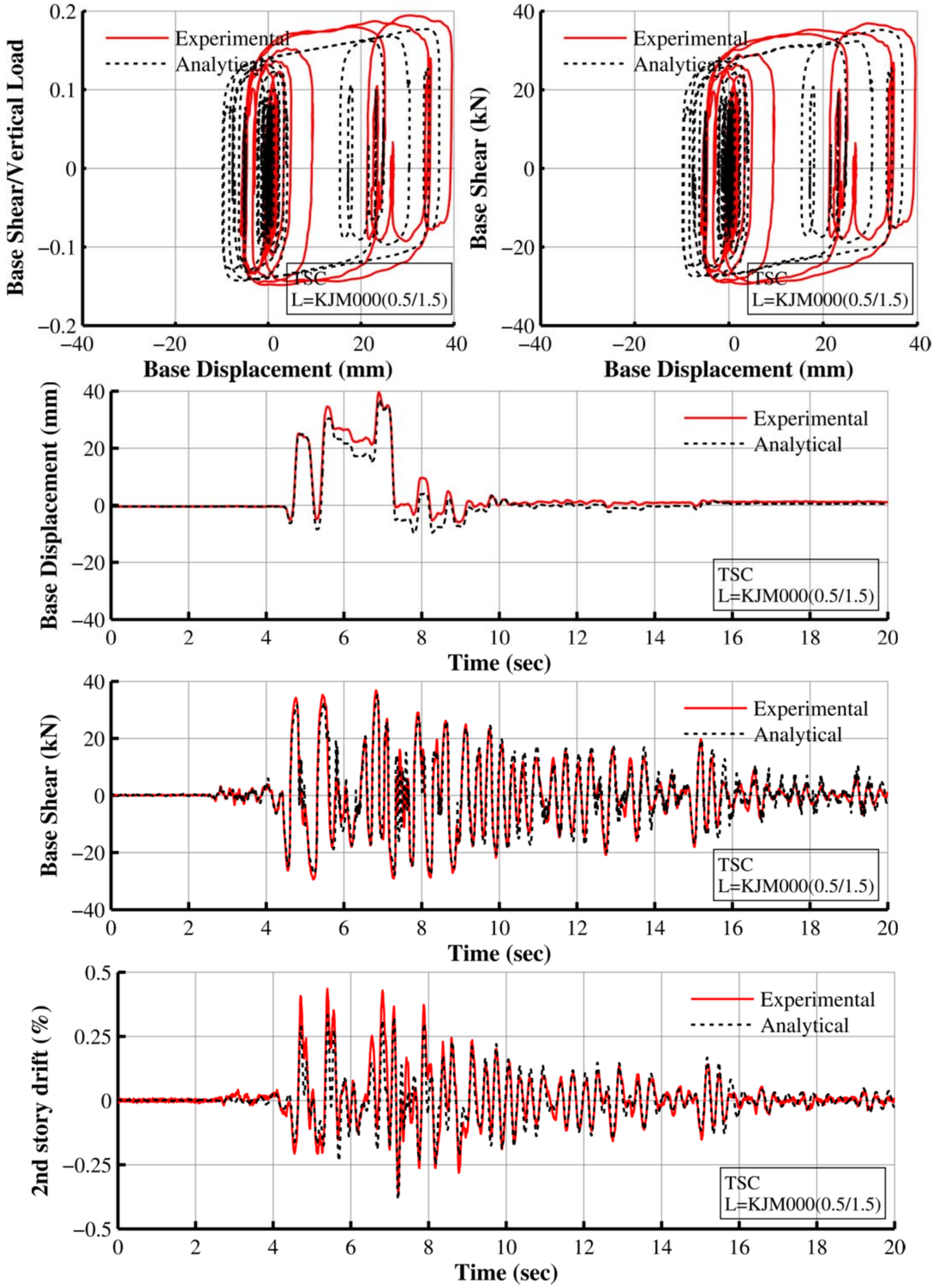
Experimental
Analytical
TSC
L=KJM000(0.5/1.5)
Base Shear/Vertical Load
Base Displacement (mm)
Base Shear (kN)
Base Displacement (mm)
Time (sec)
Base Shear (kN)
Time (sec)
2nd story drift (%)
Time (sec)

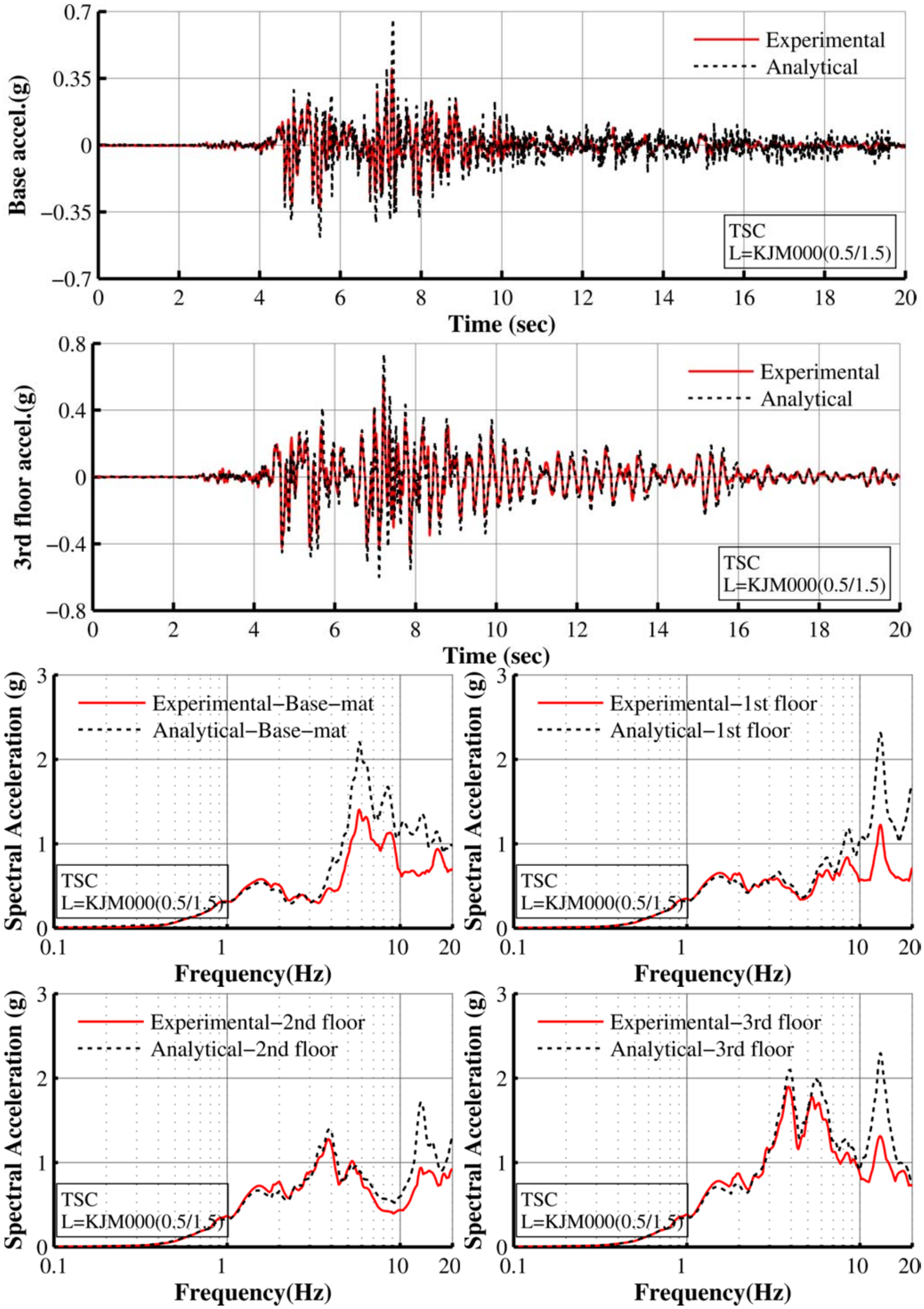
Base accel.(g)
Time (sec)
Experimental
Analytical
TSC
L=KJM000(0.5/1.5)
3rd floor accel.(g)
Time (sec)
Experimental
Analytical
TSC
L=KJM000(0.5/1.5)
Spectral Acceleration (g)
Frequency(Hz)
Experimental−Base−mat
Analytical−Base−mat
TSC
L=KJM000(0.5/1.5)
Spectral Acceleration (g)
Frequency(Hz)
Experimental−1st floor
Analytical−1st floor
TSC
L=KJM000(0.5/1.5)
Spectral Acceleration (g)
Frequency(Hz)
Experimental−2nd floor
Analytical−2nd floor
TSC
L=KJM000(0.5/1.5)
Spectral Acceleration (g)
Frequency(Hz)
Experimental−3rd floor
Analytical−3rd floor
TSC
L=KJM000(0.5/1.5)

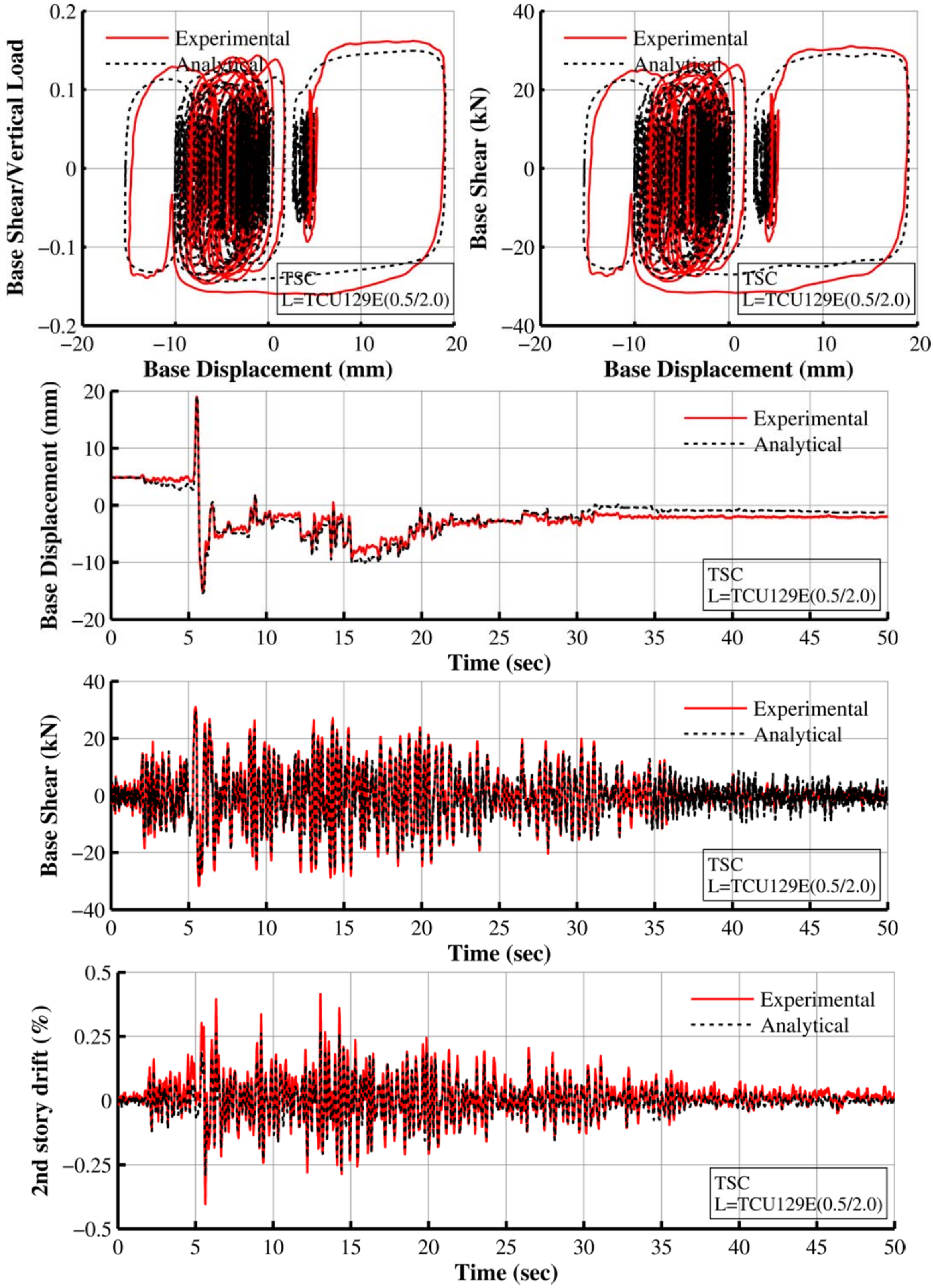
Experimental
Analytical
TSC
L=TCU129E(0.5/2.0)
Base Shear/Vertical Load
Base Displacement (mm)
Base Shear (kN)
Time (sec)
2nd story drift (%)

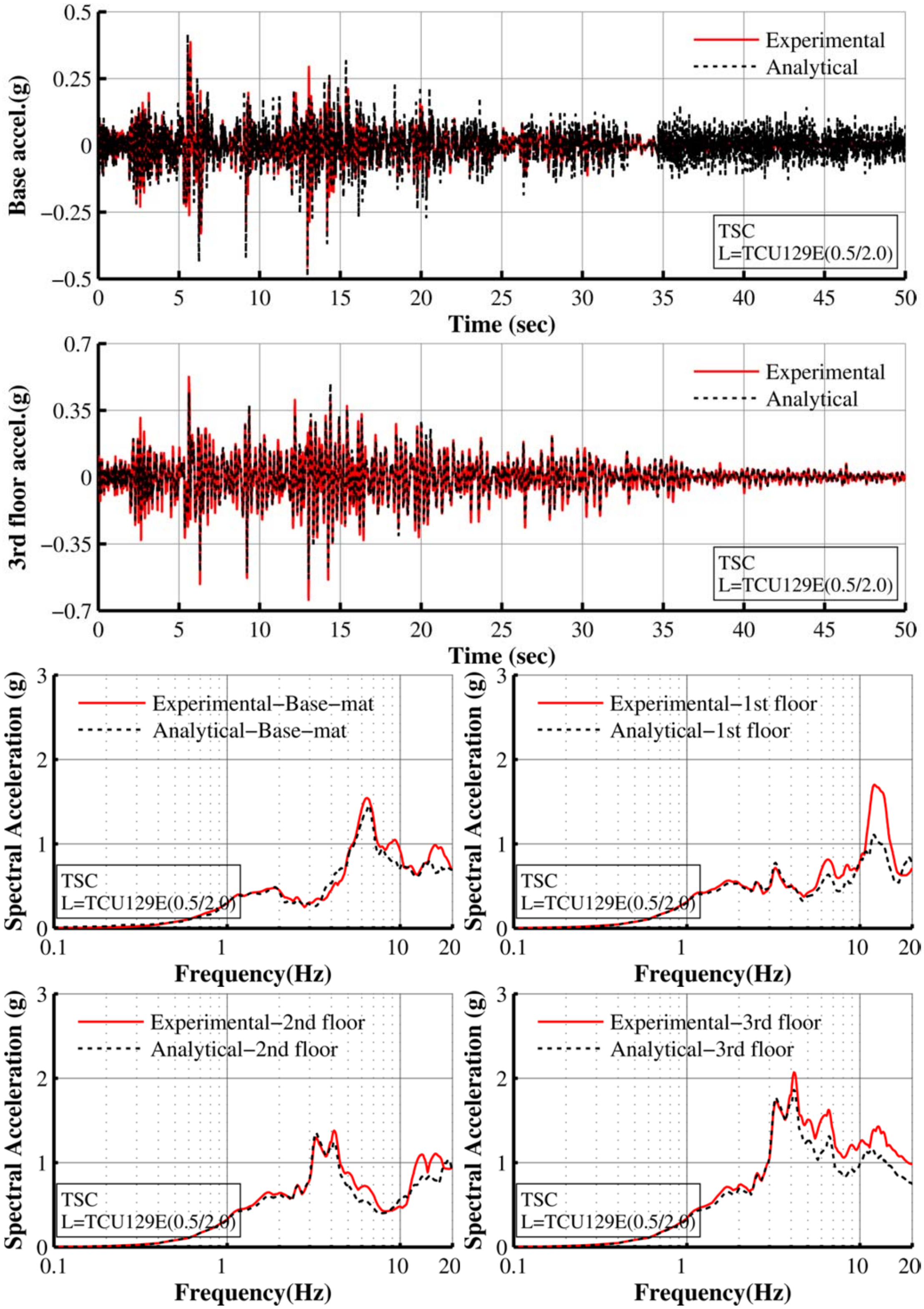
Base accel.(g)
Time (sec)
Experimental
Analytical
TSC
L=TCU129E(0.5/2.0)
3rd floor accel.(g)
Time (sec)
Experimental
Analytical
TSC
L=TCU129E(0.5/2.0)
Spectral Acceleration (g)
Frequency(Hz)
Experimental−Base−mat
Analytical−Base−mat
Experimental−1st floor
Analytical−1st floor
Experimental−2nd floor
Analytical−2nd floor
Experimental−3rd floor
Analytical−3rd floor
TSC
L=TCU129E(0.5/2.0)

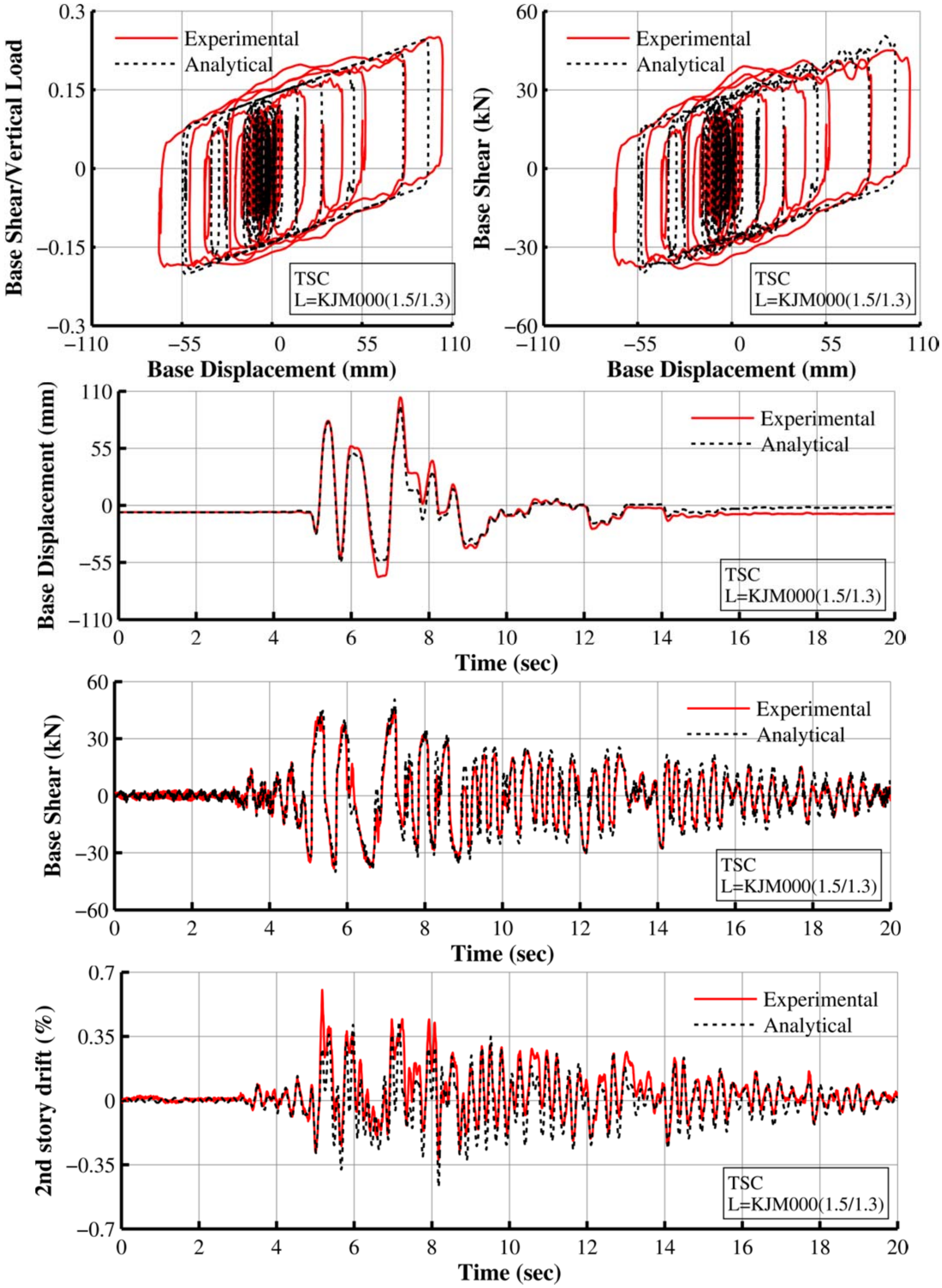
Experimental
Analytical
Base Shear/Vertical Load
Base Displacement (mm)
TSC
L=KJM000(1.5/1.3)
Base Shear (kN)
Base Displacement (mm)
Time (sec)
Base Shear (kN)
Time (sec)
2nd story drift (%)
Time (sec)

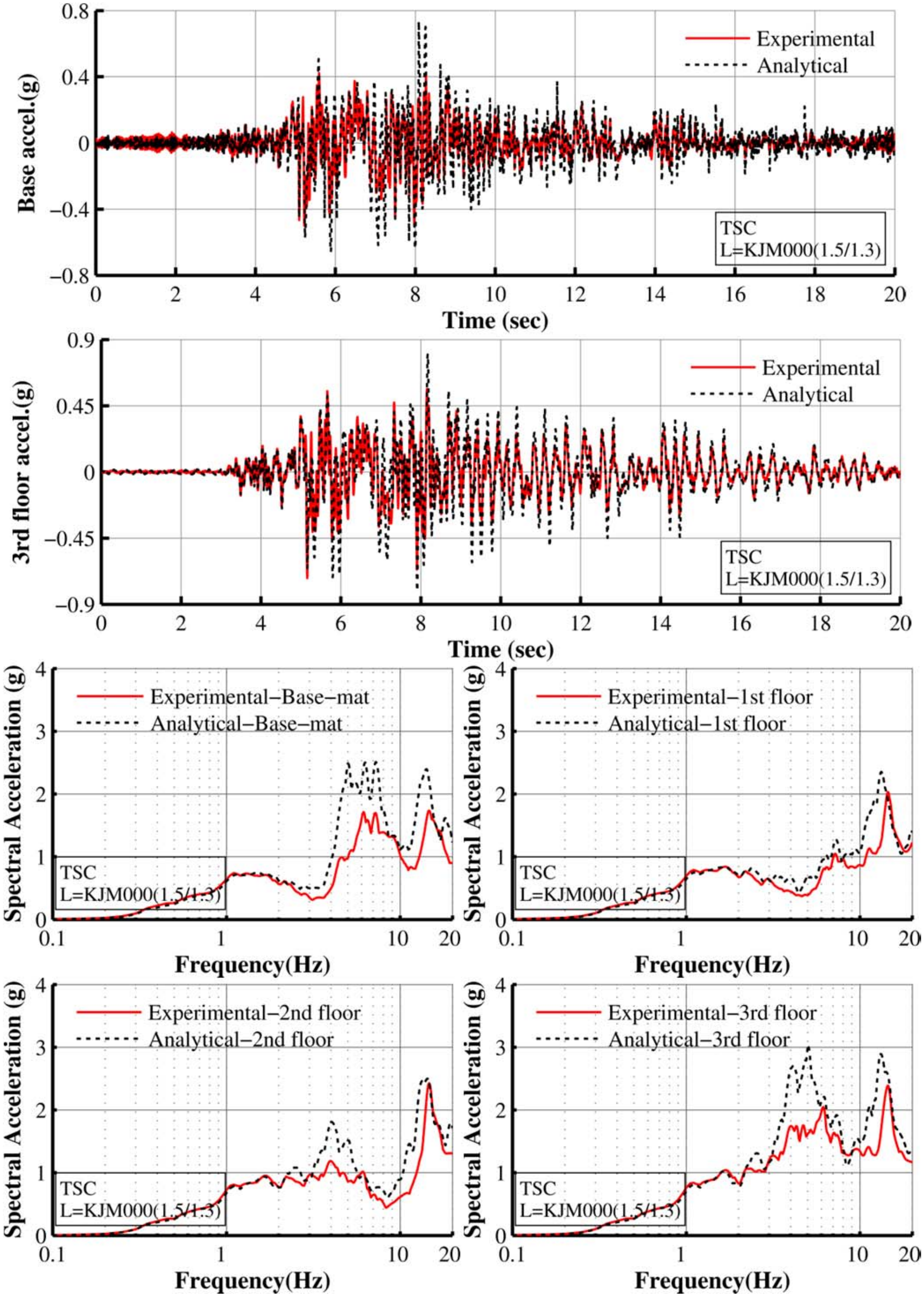
Base accel.(g)
Time (sec)
Experimental
Analytical
TSC
L=KJM000(1.5/1.3)
3rd floor accel.(g)
Time (sec)
Experimental
Analytical
TSC
L=KJM000(1.5/1.3)
Spectral Acceleration (g)
Frequency(Hz)
Experimental−Base−mat
Analytical−Base−mat
TSC
L=KJM000(1.5/1.3)
Spectral Acceleration (g)
Frequency(Hz)
Experimental−1st floor
Analytical−1st floor
TSC
L=KJM000(1.5/1.3)
Spectral Acceleration (g)
Frequency(Hz)
Experimental−2nd floor
Analytical−2nd floor
TSC
L=KJM000(1.5/1.3)
Spectral Acceleration (g)
Frequency(Hz)
Experimental−3rd floor
Analytical−3rd floor
TSC
L=KJM000(1.5/1.3)

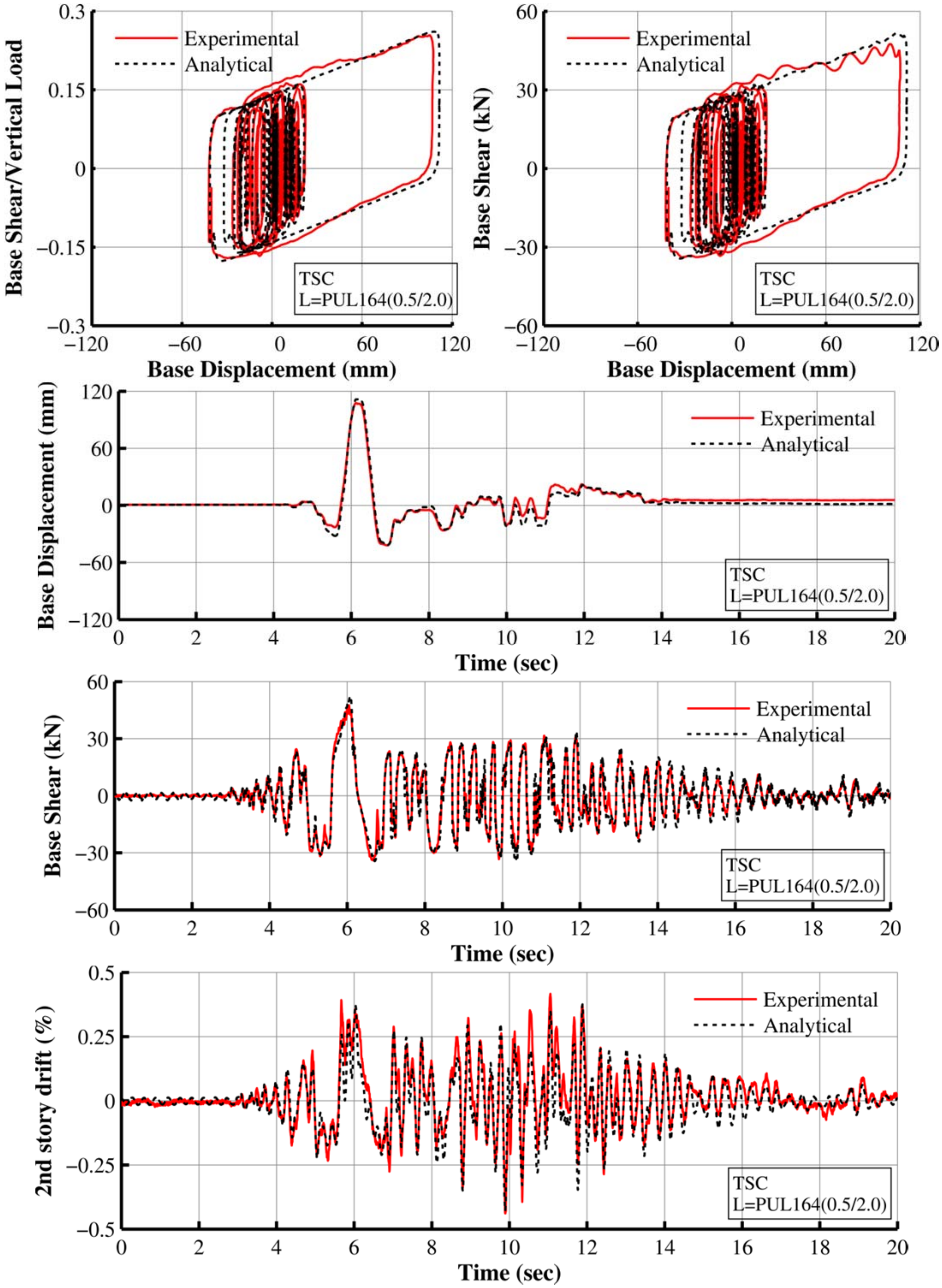
Experimental
Analytical
TSC
L=PUL164(0.5/2.0)
Base Shear/Vertical Load
Base Displacement (mm)
Base Shear (kN)
Base Displacement (mm)
Time (sec)
Base Shear (kN)
Time (sec)
2nd story drift (%)
Time (sec)

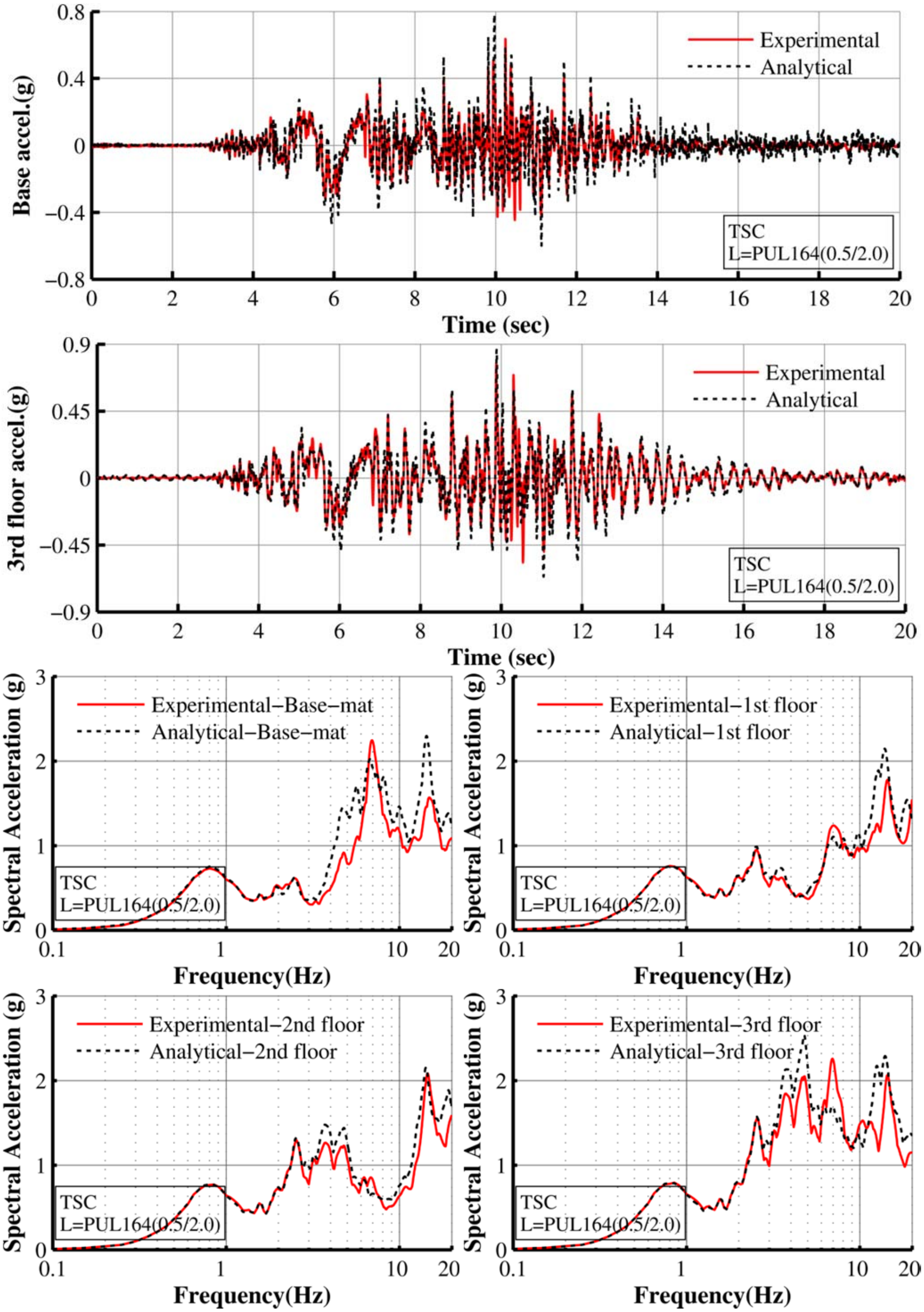
Base accel.(g)
Time (sec)
Experimental
Analytical
TSC
L=PUL164(0.5/2.0)
3rd floor accel.(g)
Time (sec)
Experimental
Analytical
TSC
L=PUL164(0.5/2.0)
Spectral Acceleration (g)
Frequency(Hz)
Experimental−Base−mat
Analytical−Base−mat
TSC
L=PUL164(0.5/2.0)
Spectral Acceleration (g)
Frequency(Hz)
Experimental−1st floor
Analytical−1st floor
TSC
L=PUL164(0.5/2.0)
Spectral Acceleration (g)
Frequency(Hz)
Experimental−2nd floor
Analytical−2nd floor
TSC
L=PUL164(0.5/2.0)
Spectral Acceleration (g)
Frequency(Hz)
Experimental−3rd floor
Analytical−3rd floor
TSC
L=PUL164(0.5/2.0)

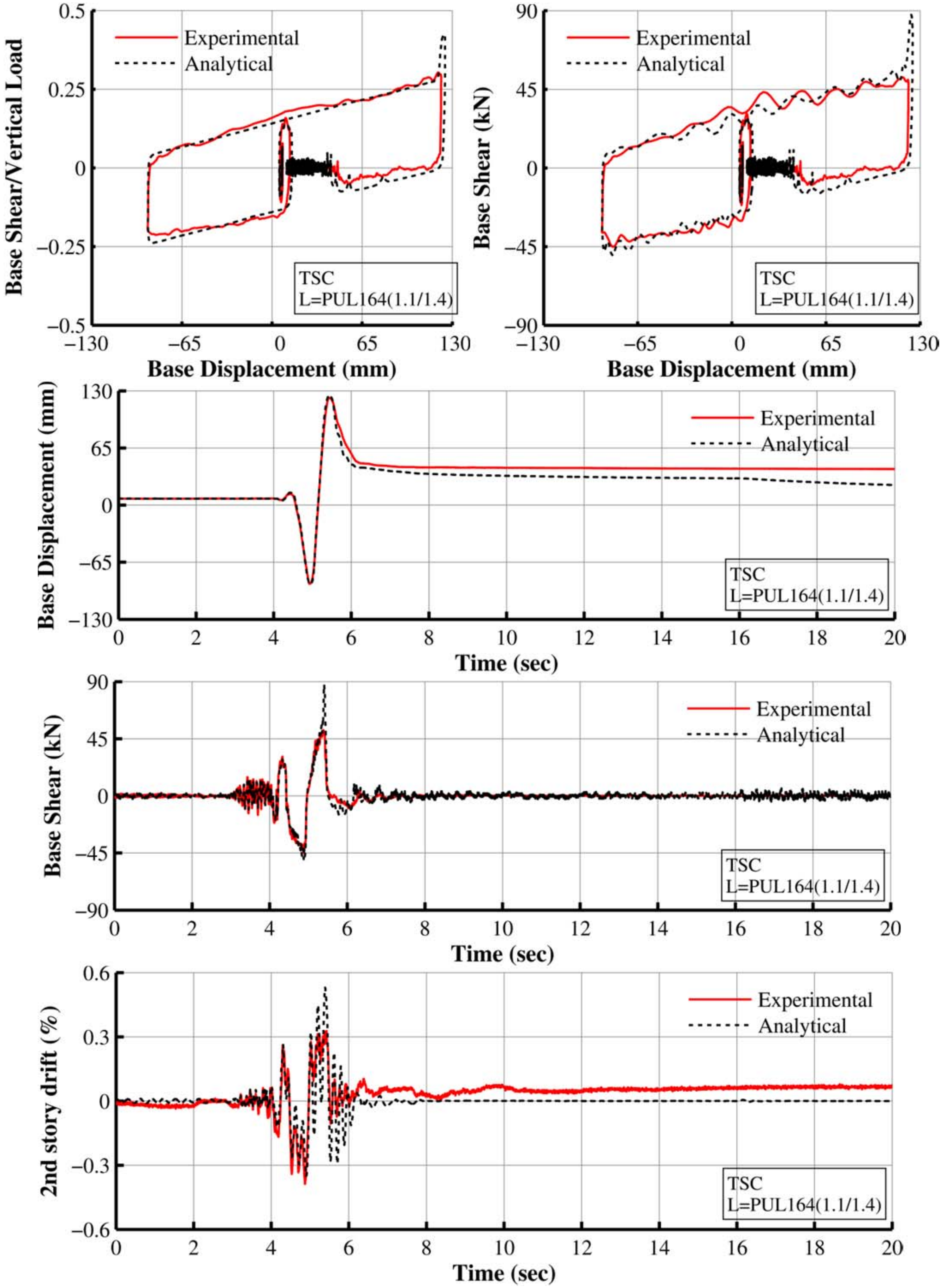
Experimental
Analytical
TSC
L=PUL164(1.1/1.4)
Base Shear/Vertical Load
Base Shear (kN)
Base Displacement (mm)
Time (sec)
Base Shear (kN)
2nd story drift (%)

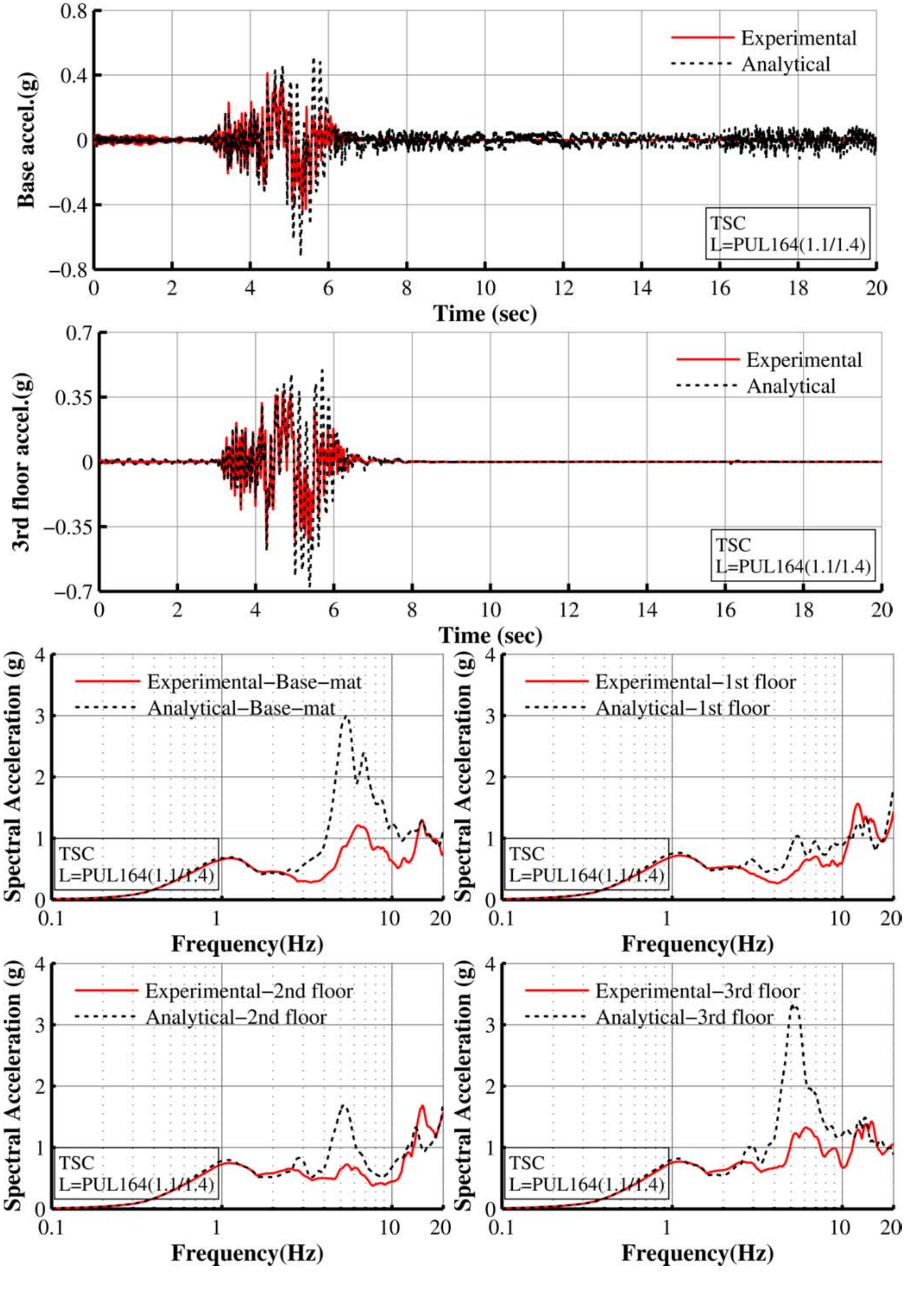
Base accel.(g)
Time (sec)
Experimental
Analytical
TSC
L=PUL164(1.1/1.4)
3rd floor accel.(g)
Time (sec)
Experimental
Analytical
TSC
L=PUL164(1.1/1.4)
Spectral Acceleration (g)
Frequency(Hz)
Experimental−Base−mat
Analytical−Base−mat
TSC
L=PUL164(1.1/1.4)
Spectral Acceleration (g)
Frequency(Hz)
Experimental−1st floor
Analytical−1st floor
TSC
L=PUL164(1.1/1.4)
Spectral Acceleration (g)
Frequency(Hz)
Experimental−2nd floor
Analytical−2nd floor
TSC
L=PUL164(1.1/1.4)
Spectral Acceleration (g)
Frequency(Hz)
Experimental−3rd floor
Analytical−3rd floor
TSC
L=PUL164(1.1/1.4)

Appendix C

SAP 2000

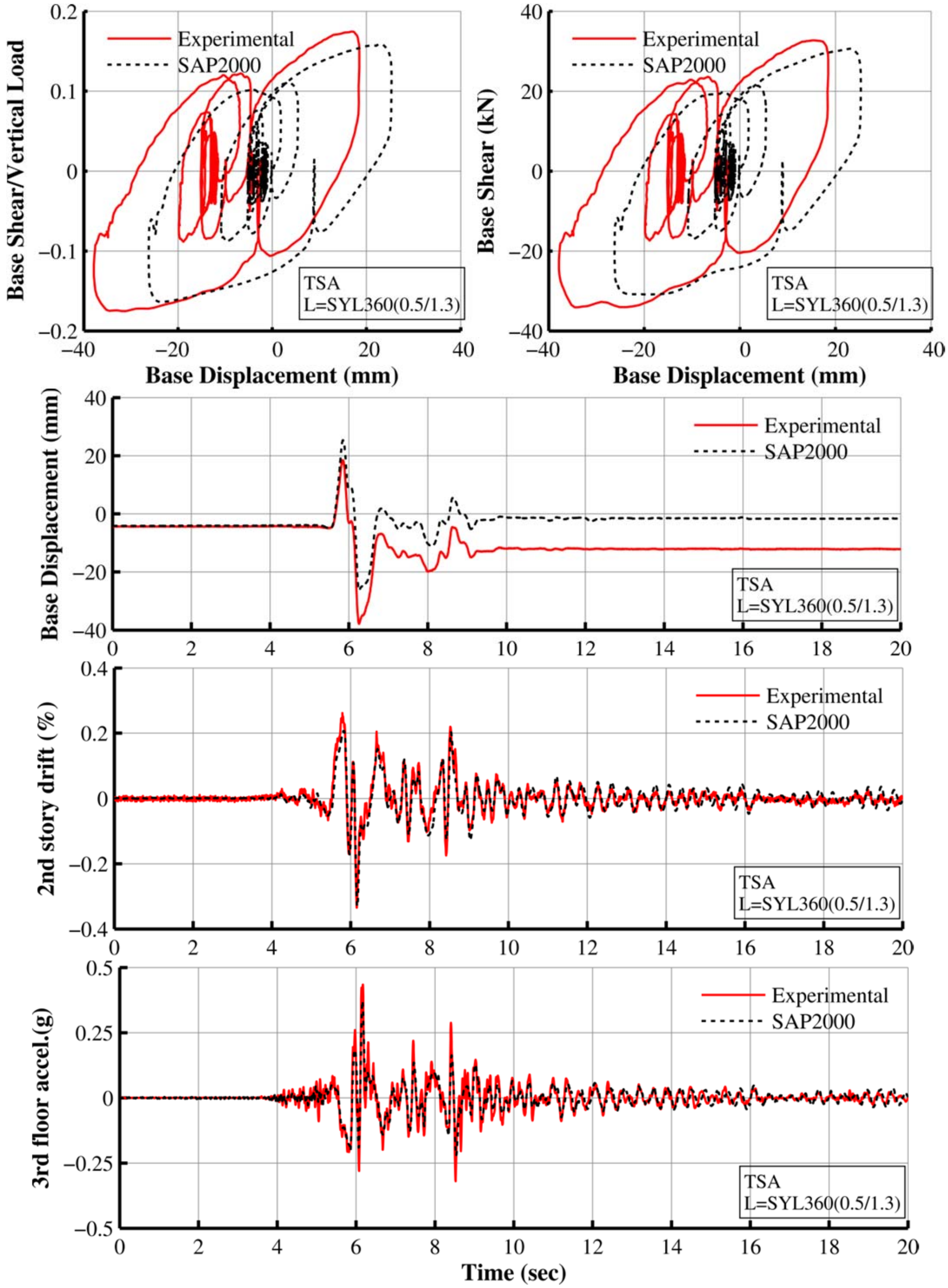
Experimental
SAP2000
TSA
L=SYL360(0.5/1.3)
Base Shear/Vertical Load
Base Shear (kN)
Base Displacement (mm)
2nd story drift (%)
3rd floor accel.(g)
Time (sec)

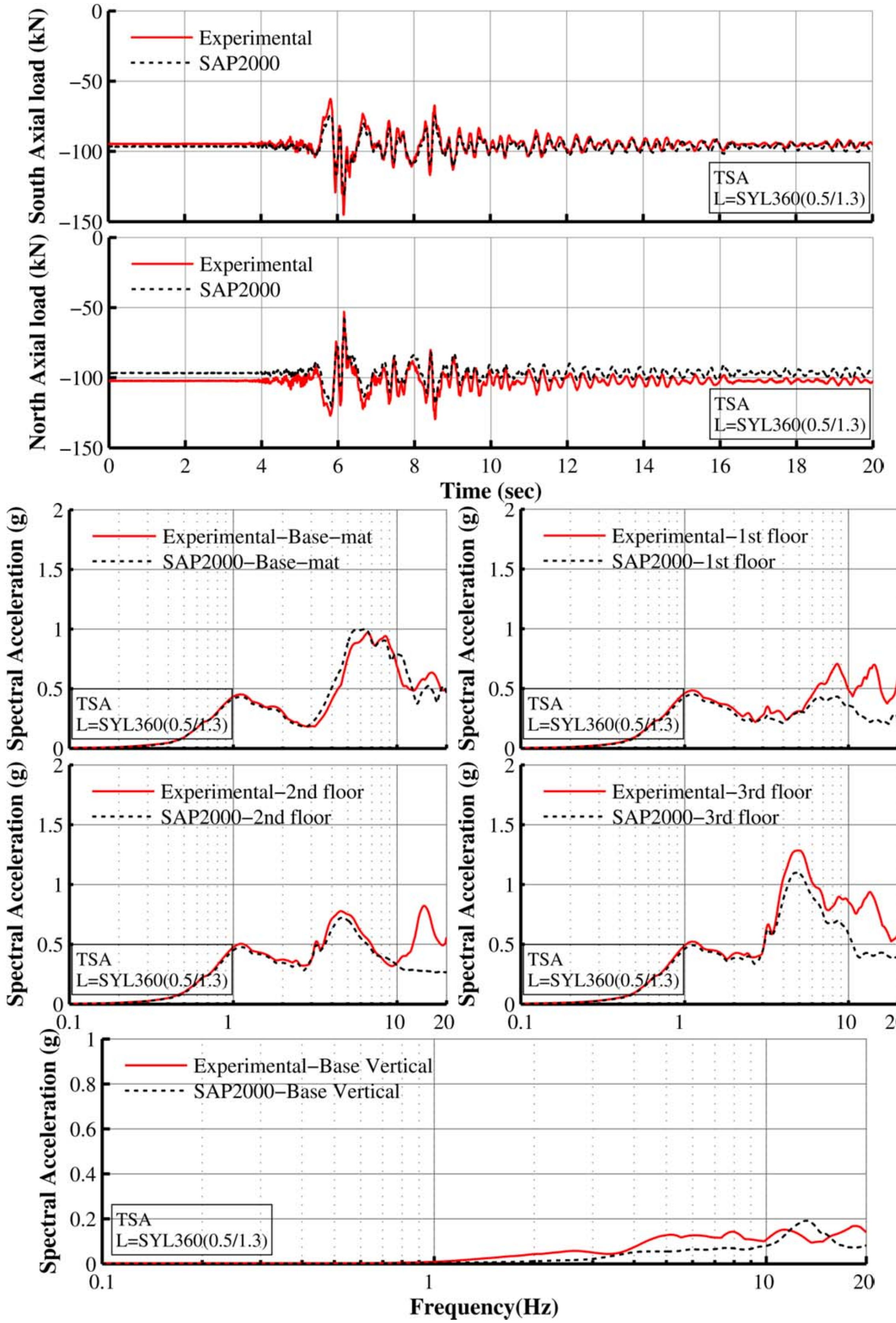

South Axial load (kN)
Experimental
SAP2000
TSA
L=SYL360(0.5/1.3)
North Axial load (kN)
Experimental
SAP2000
TSA
L=SYL360(0.5/1.3)
Time (sec)
Spectral Acceleration (g)
Experimental−Base−mat
SAP2000−Base−mat
Experimental−1st floor
SAP2000−1st floor
Experimental−2nd floor
SAP2000−2nd floor
Experimental−3rd floor
SAP2000−3rd floor
Experimental−Base Vertical
SAP2000−Base Vertical
Frequency(Hz)

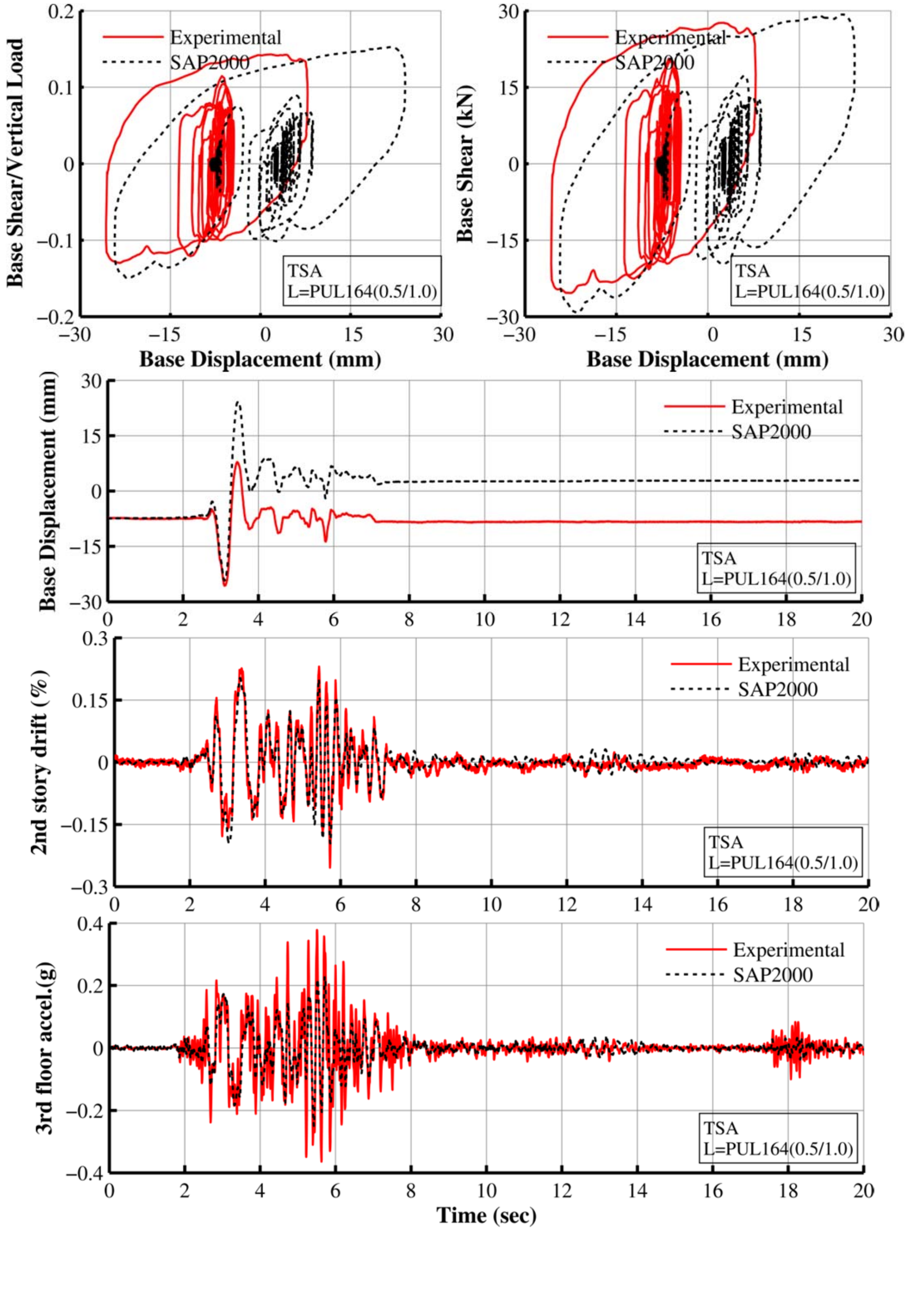

Experimental
SAP2000
TSA
L=PUL164(0.5/1.0)
Base Shear/Vertical Load
Base Displacement (mm)
Base Shear (kN)
Base Displacement (mm)
2nd story drift (%)
3rd floor accel.(g)
Time (sec)

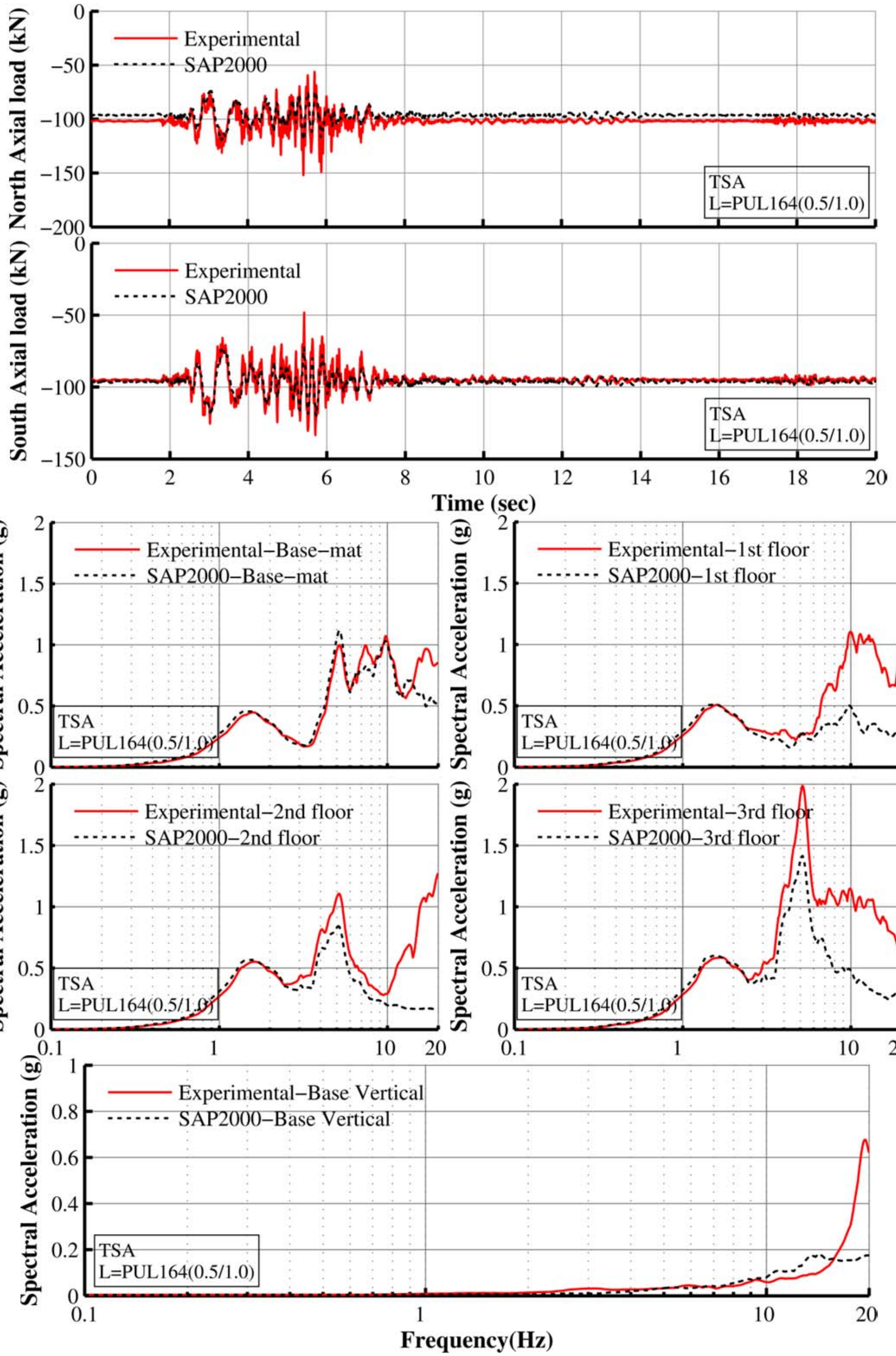

North Axial load (kN)
South Axial load (kN)
Time (sec)
Experimental
SAP2000
TSA
L=PUL164(0.5/1.0)
Spectral Acceleration (g)
Experimental−Base−mat
SAP2000−Base−mat
Experimental−1st floor
SAP2000−1st floor
Experimental−2nd floor
SAP2000−2nd floor
Experimental−3rd floor
SAP2000−3rd floor
Experimental−Base Vertical
SAP2000−Base Vertical
Frequency(Hz)

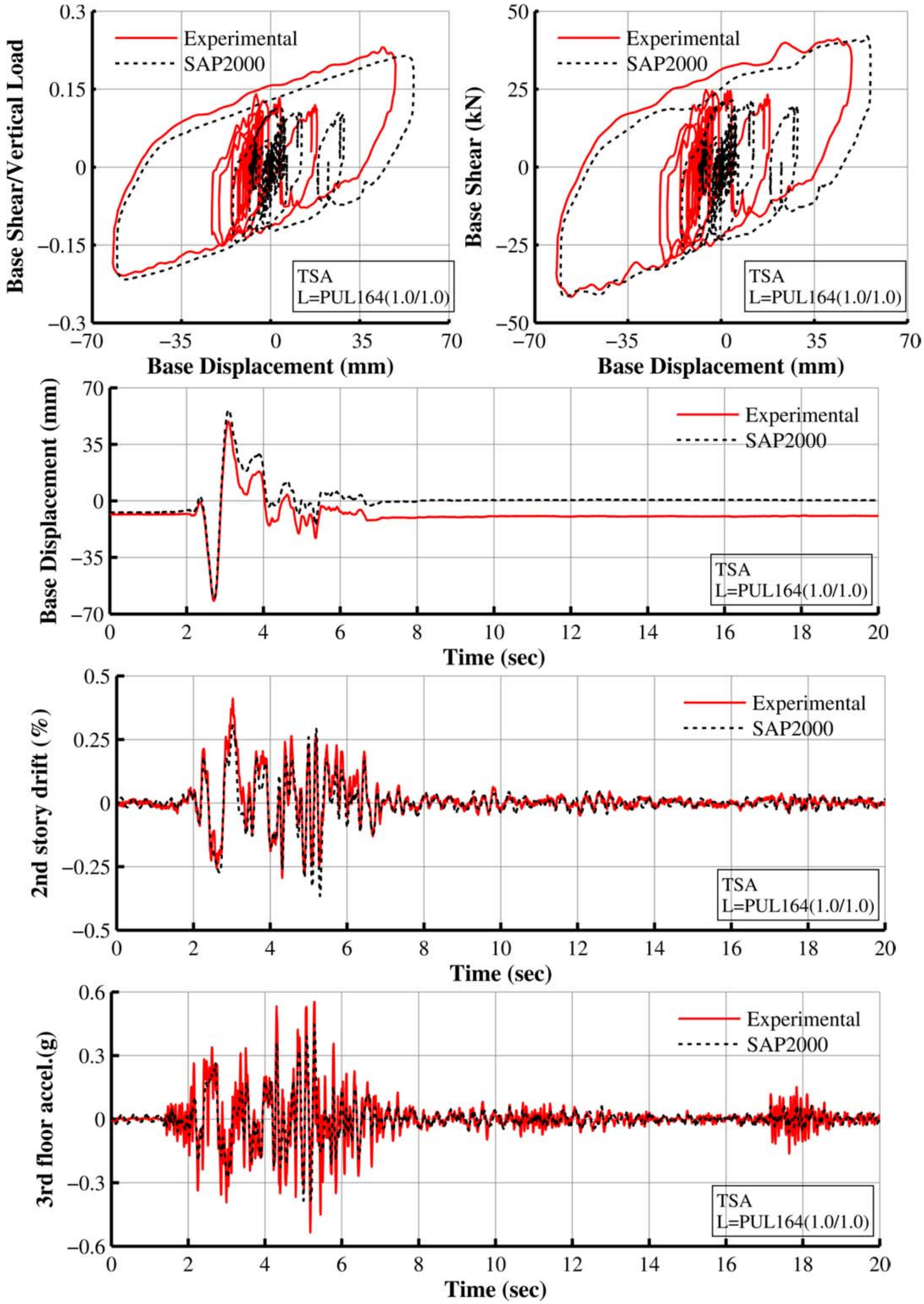
Base Shear/Vertical Load
Base Displacement (mm)
Experimental
SAP2000
TSA
L=PUL164(1.0/1.0)
Base Shear (kN)
Base Displacement (mm)
Experimental
SAP2000
TSA
L=PUL164(1.0/1.0)
Base Displacement (mm)
Time (sec)
Experimental
SAP2000
TSA
L=PUL164(1.0/1.0)
2nd story drift (%)
Time (sec)
Experimental
SAP2000
TSA
L=PUL164(1.0/1.0)
3rd floor accel.(g)
Time (sec)
Experimental
SAP2000
TSA
L=PUL164(1.0/1.0)

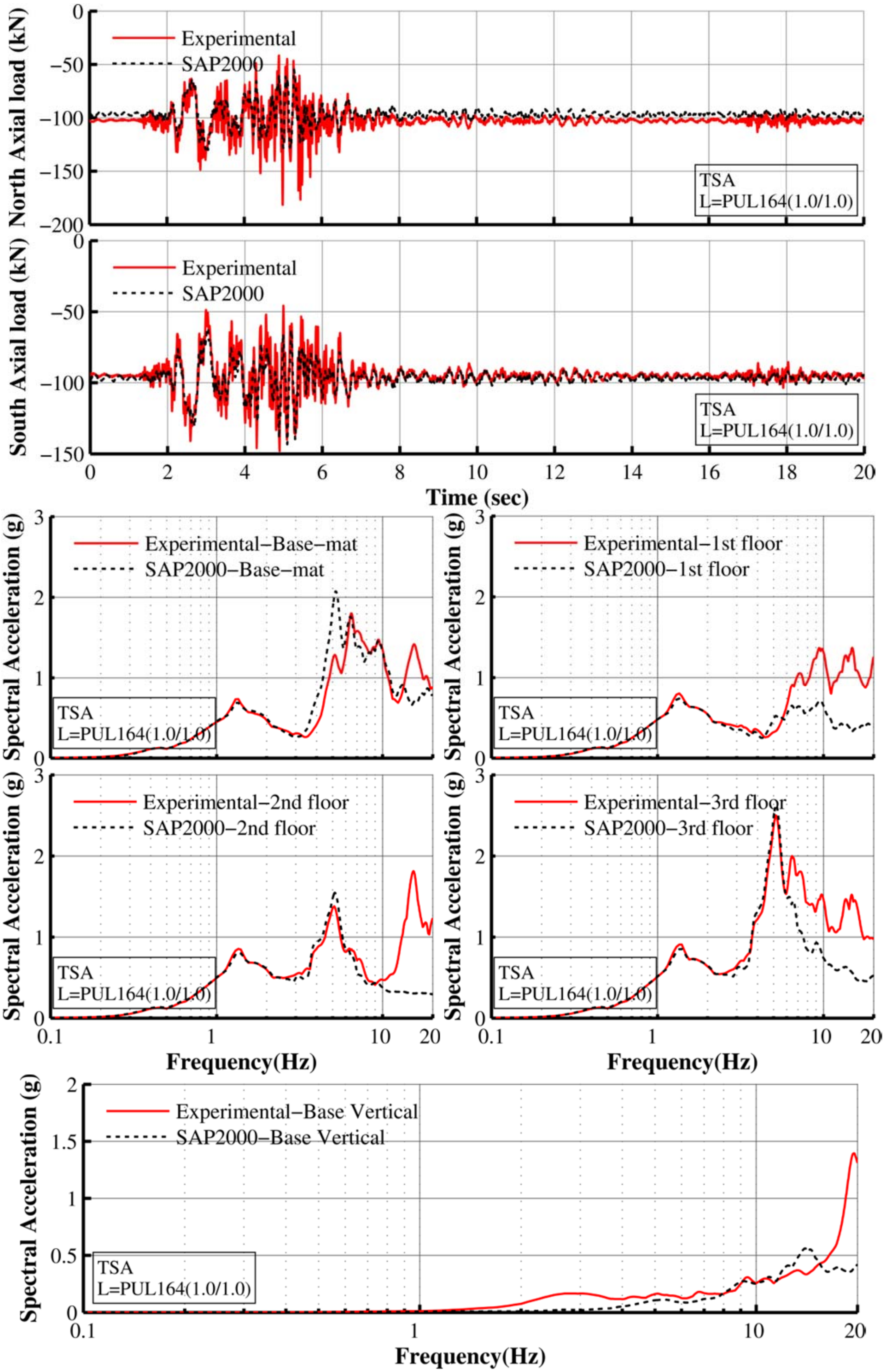
North Axial load (kN)
Experimental
SAP2000
TSA
L=PUL164(1.0/1.0)
South Axial load (kN)
Experimental
SAP2000
TSA
L=PUL164(1.0/1.0)
Time (sec)
Spectral Acceleration (g)
Experimental−Base−mat
SAP2000−Base−mat
Experimental−1st floor
SAP2000−1st floor
Experimental−2nd floor
SAP2000−2nd floor
Experimental−3rd floor
SAP2000−3rd floor
TSA
L=PUL164(1.0/1.0)
Frequency(Hz)
Experimental−Base Vertical
SAP2000−Base Vertical
TSA
L=PUL164(1.0/1.0)
Frequency(Hz)

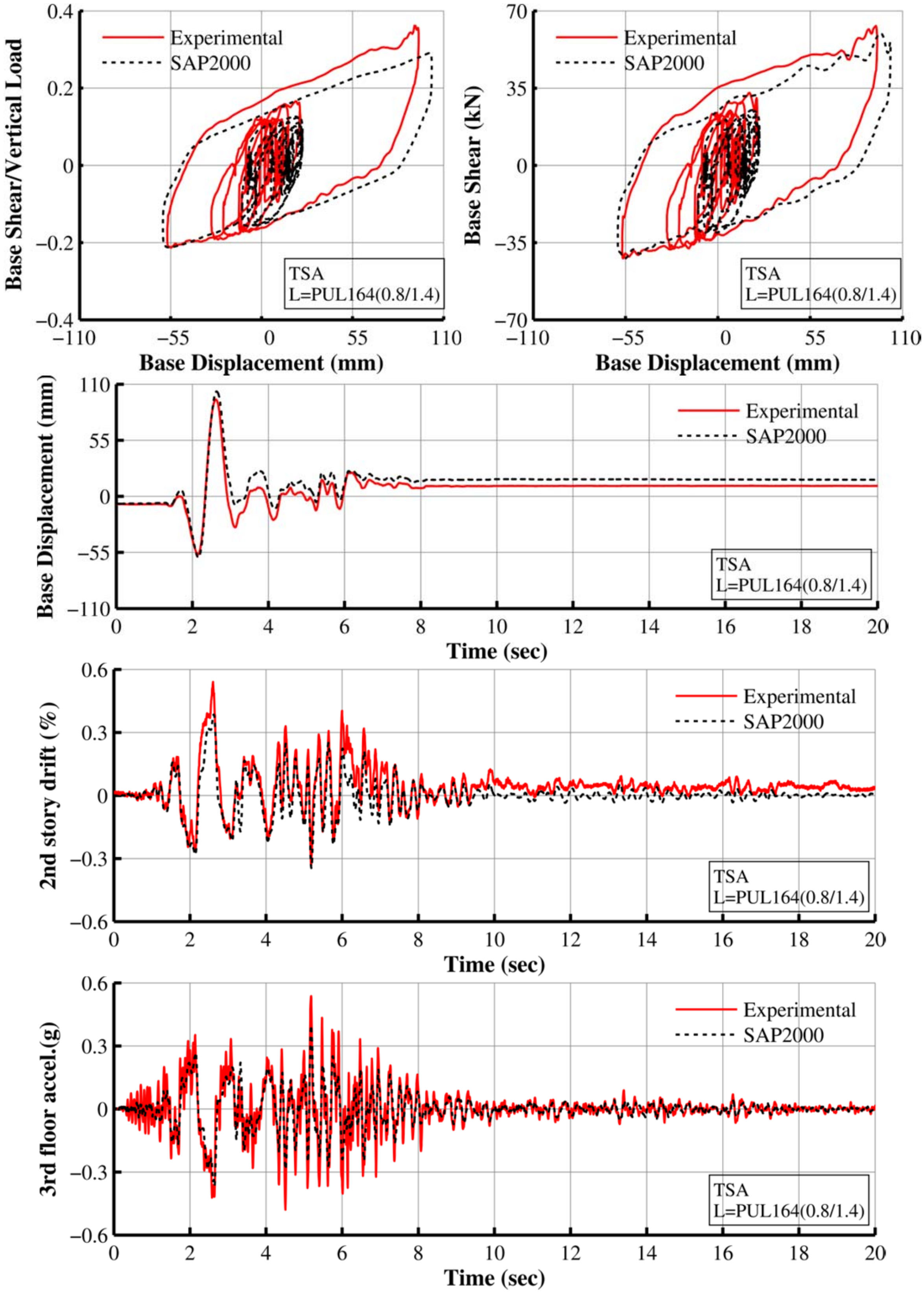
Experimental
SAP2000
TSA
L=PUL164(0.8/1.4)
Base Shear/Vertical Load
Base Displacement (mm)
Base Shear (kN)
Base Displacement (mm)
Time (sec)
2nd story drift (%)
3rd floor accel.(g)

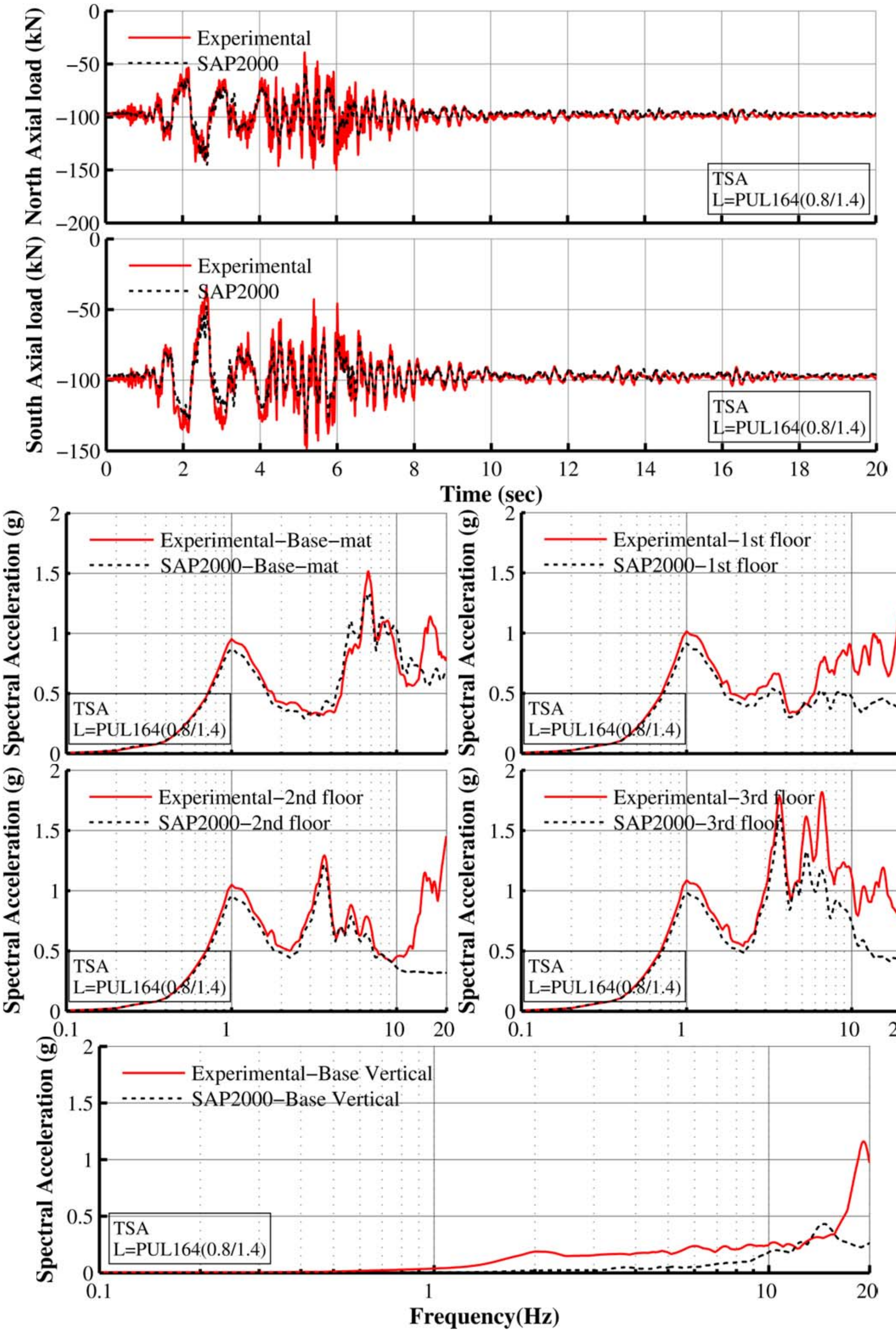
North Axial load (kN)
South Axial load (kN)
Experimental
SAP2000
TSA
L=PUL164(0.8/1.4)
Time (sec)
Spectral Acceleration (g)
Experimental−Base−mat
SAP2000−Base−mat
Experimental−1st floor
SAP2000−1st floor
Experimental−2nd floor
SAP2000−2nd floor
Experimental−3rd floor
SAP2000−3rd floor
Experimental−Base Vertical
SAP2000−Base Vertical
Frequency(Hz)

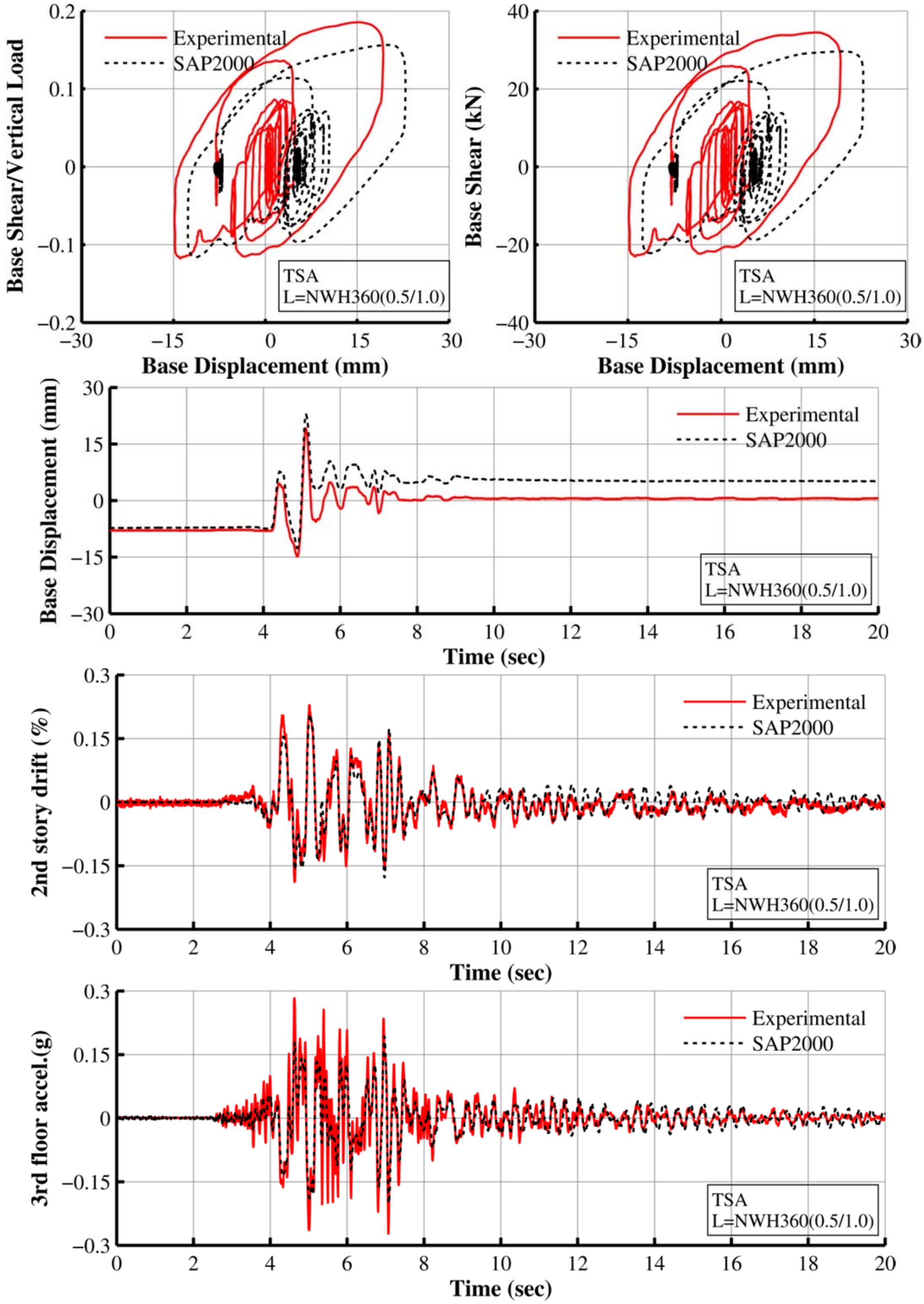
Base Shear/Vertical Load
Base Displacement (mm)
Base Shear (kN)
Experimental
SAP2000
TSA
L=NWH360(0.5/1.0)
Base Displacement (mm)
Time (sec)
2nd story drift (%)
3rd floor accel.(g)

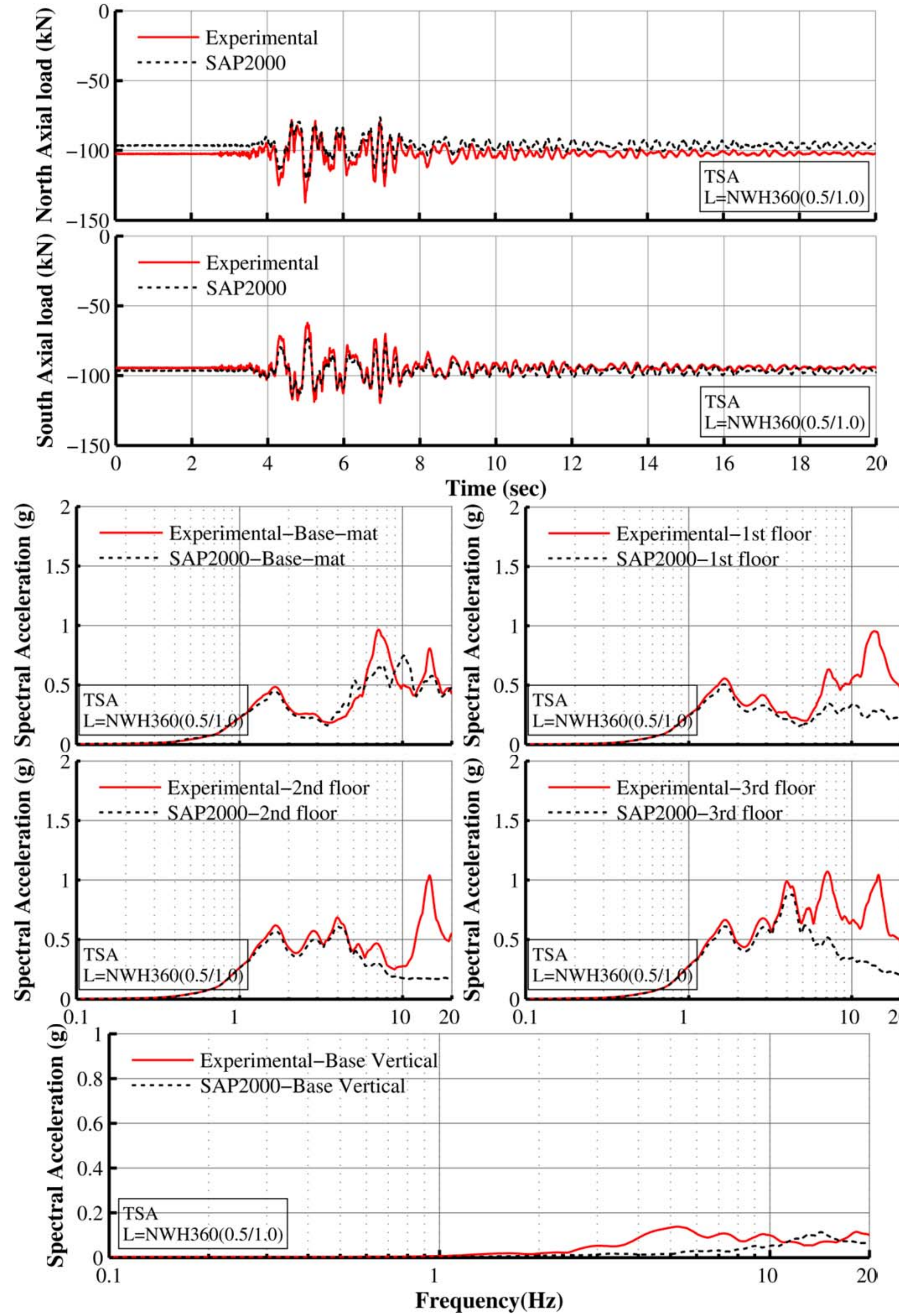
North Axial load (kN)
Experimental
SAP2000
TSA
L=NWH360(0.5/1.0)
South Axial load (kN)
Experimental
SAP2000
TSA
L=NWH360(0.5/1.0)
Time (sec)
Spectral Acceleration (g)
Experimental−Base−mat
SAP2000−Base−mat
TSA
L=NWH360(0.5/1.0)
Experimental−1st floor
SAP2000−1st floor
TSA
L=NWH360(0.5/1.0)
Experimental−2nd floor
SAP2000−2nd floor
TSA
L=NWH360(0.5/1.0)
Experimental−3rd floor
SAP2000−3rd floor
TSA
L=NWH360(0.5/1.0)
Experimental−Base Vertical
SAP2000−Base Vertical
TSA
L=NWH360(0.5/1.0)
Frequency(Hz)

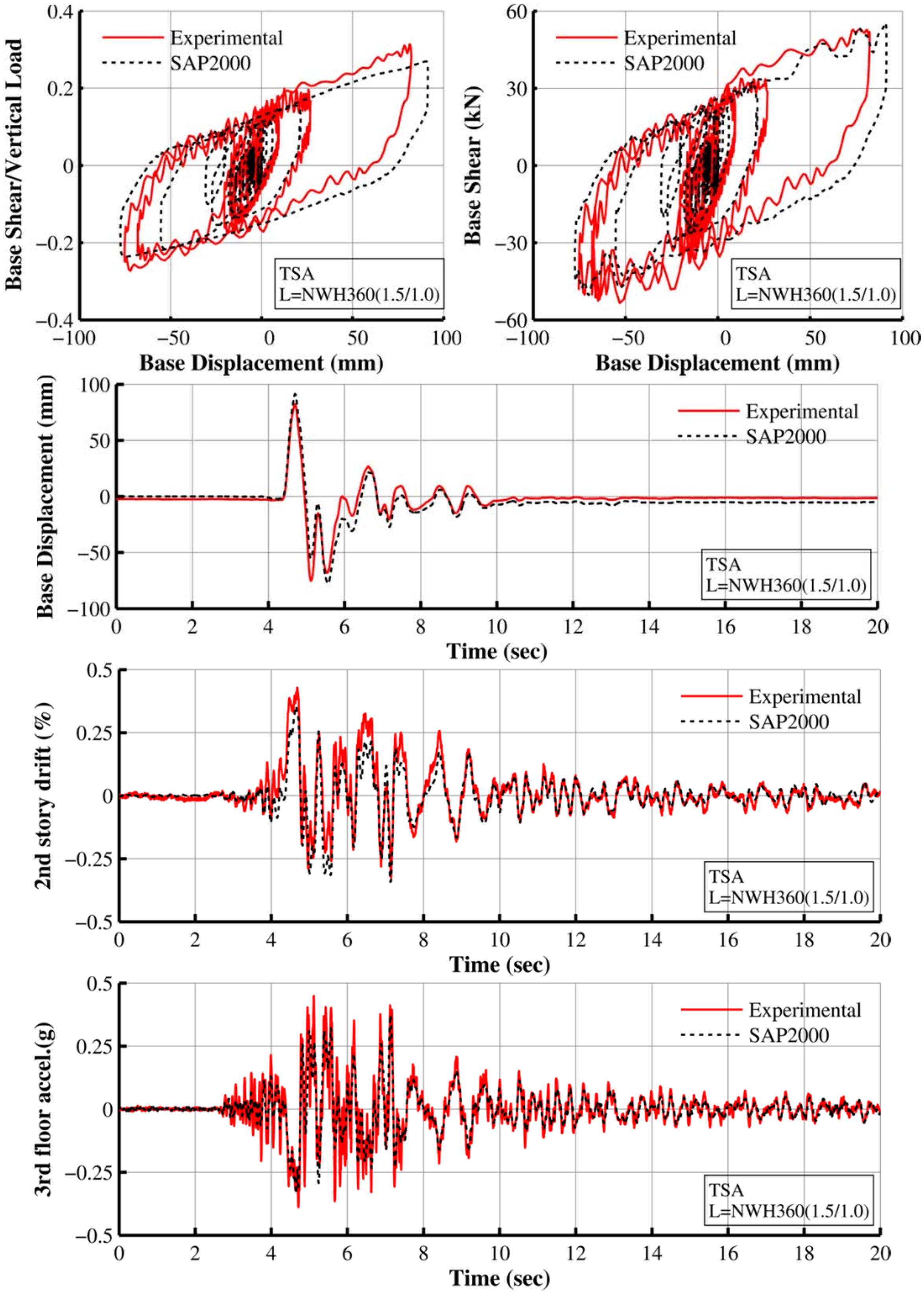
Experimental
SAP2000
TSA
L=NWH360(1.5/1.0)
Base Shear/Vertical Load
Base Displacement (mm)
Base Shear (kN)
Base Displacement (mm)
Time (sec)
2nd story drift (%)
3rd floor accel.(g)

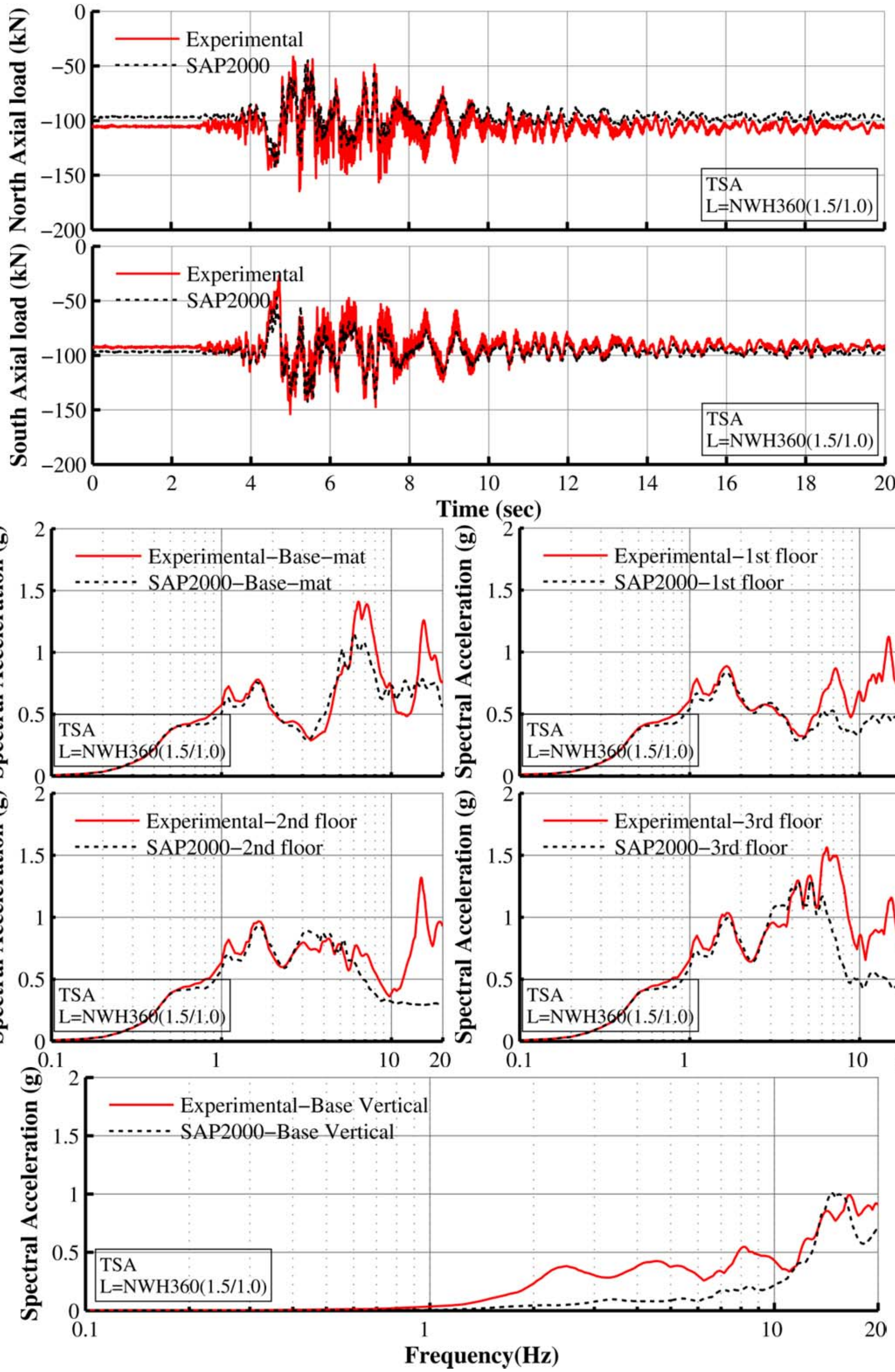
North Axial load (kN)
Experimental
SAP2000
TSA
L=NWH360(1.5/1.0)
South Axial load (kN)
Experimental
SAP2000
TSA
L=NWH360(1.5/1.0)
Time (sec)
Spectral Acceleration (g)
Experimental−Base−mat
SAP2000−Base−mat
TSA
L=NWH360(1.5/1.0)
Spectral Acceleration (g)
Experimental−1st floor
SAP2000−1st floor
TSA
L=NWH360(1.5/1.0)
Spectral Acceleration (g)
Experimental−2nd floor
SAP2000−2nd floor
TSA
L=NWH360(1.5/1.0)
Spectral Acceleration (g)
Experimental−3rd floor
SAP2000−3rd floor
TSA
L=NWH360(1.5/1.0)
Spectral Acceleration (g)
Experimental−Base Vertical
SAP2000−Base Vertical
TSA
L=NWH360(1.5/1.0)
Frequency(Hz)

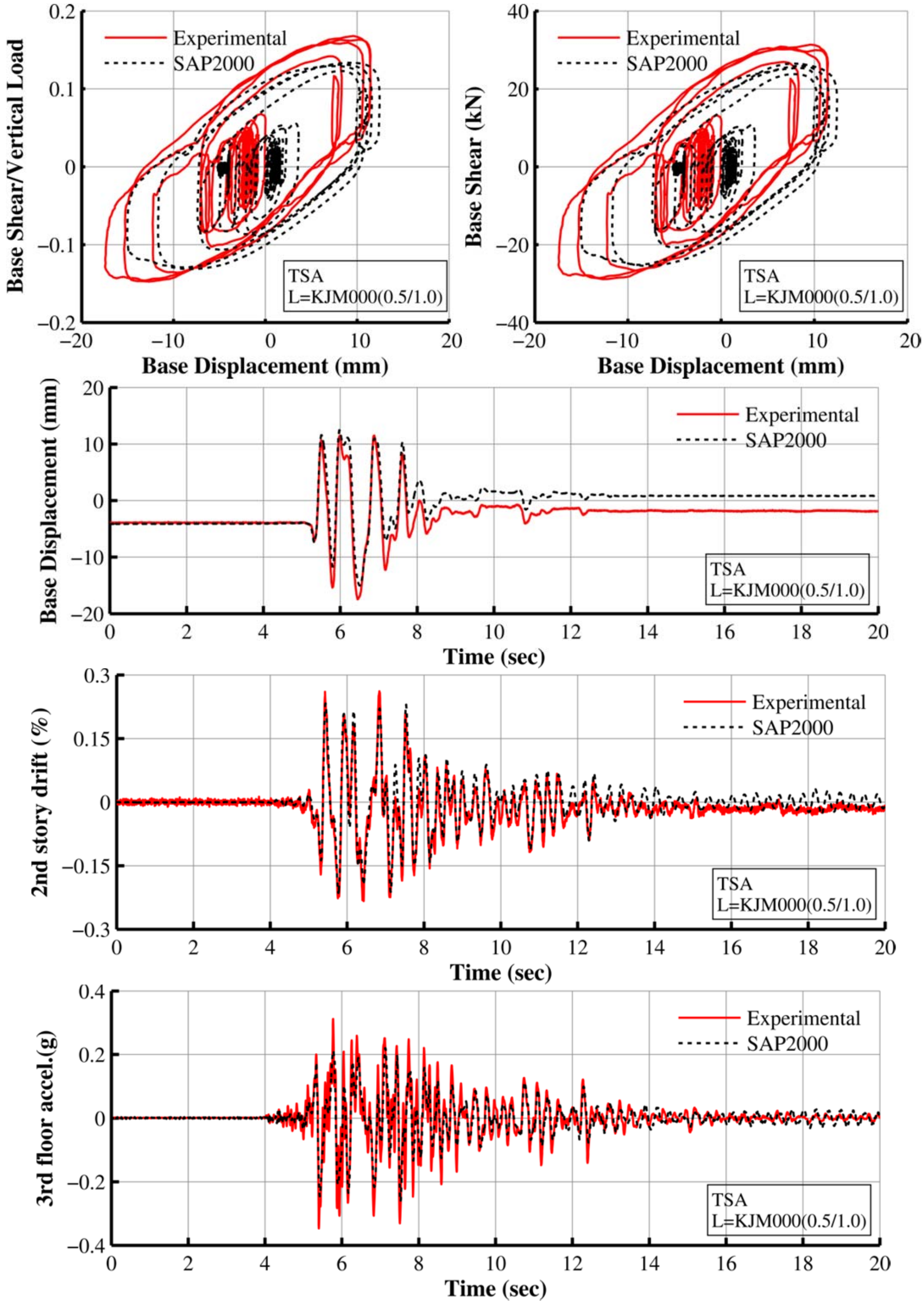

Experimental
SAP2000
TSA
L=KJM000(0.5/1.0)
Base Shear/Vertical Load
Base Shear (kN)
Base Displacement (mm)
Time (sec)
2nd story drift (%)
3rd floor accel.(g)

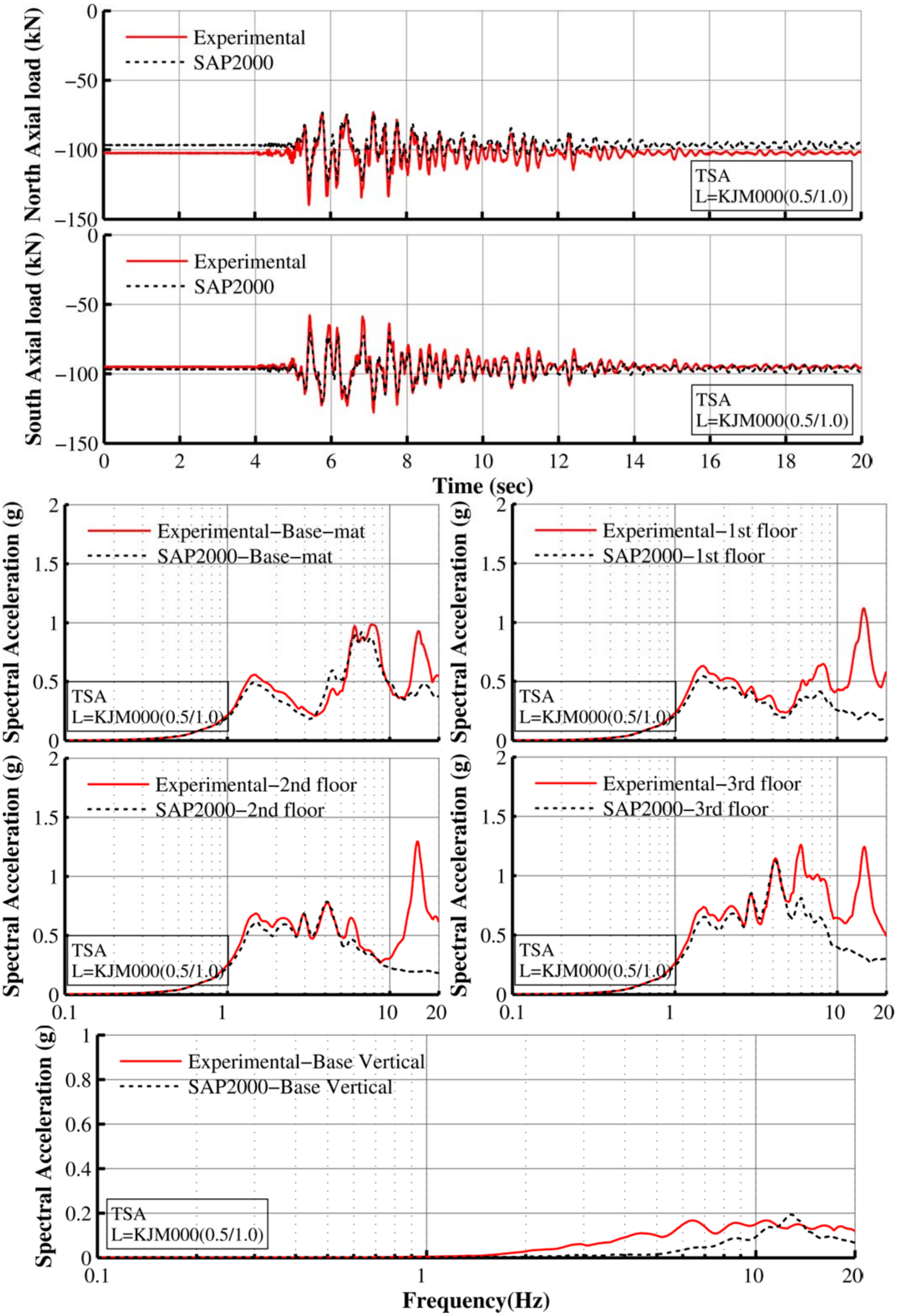
North Axial load (kN)
South Axial load (kN)
Experimental
SAP2000
TSA
L=KJM000(0.5/1.0)
Time (sec)
Spectral Acceleration (g)
Experimental−Base−mat
SAP2000−Base−mat
Experimental−1st floor
SAP2000−1st floor
Experimental−2nd floor
SAP2000−2nd floor
Experimental−3rd floor
SAP2000−3rd floor
Experimental−Base Vertical
SAP2000−Base Vertical
Frequency(Hz)

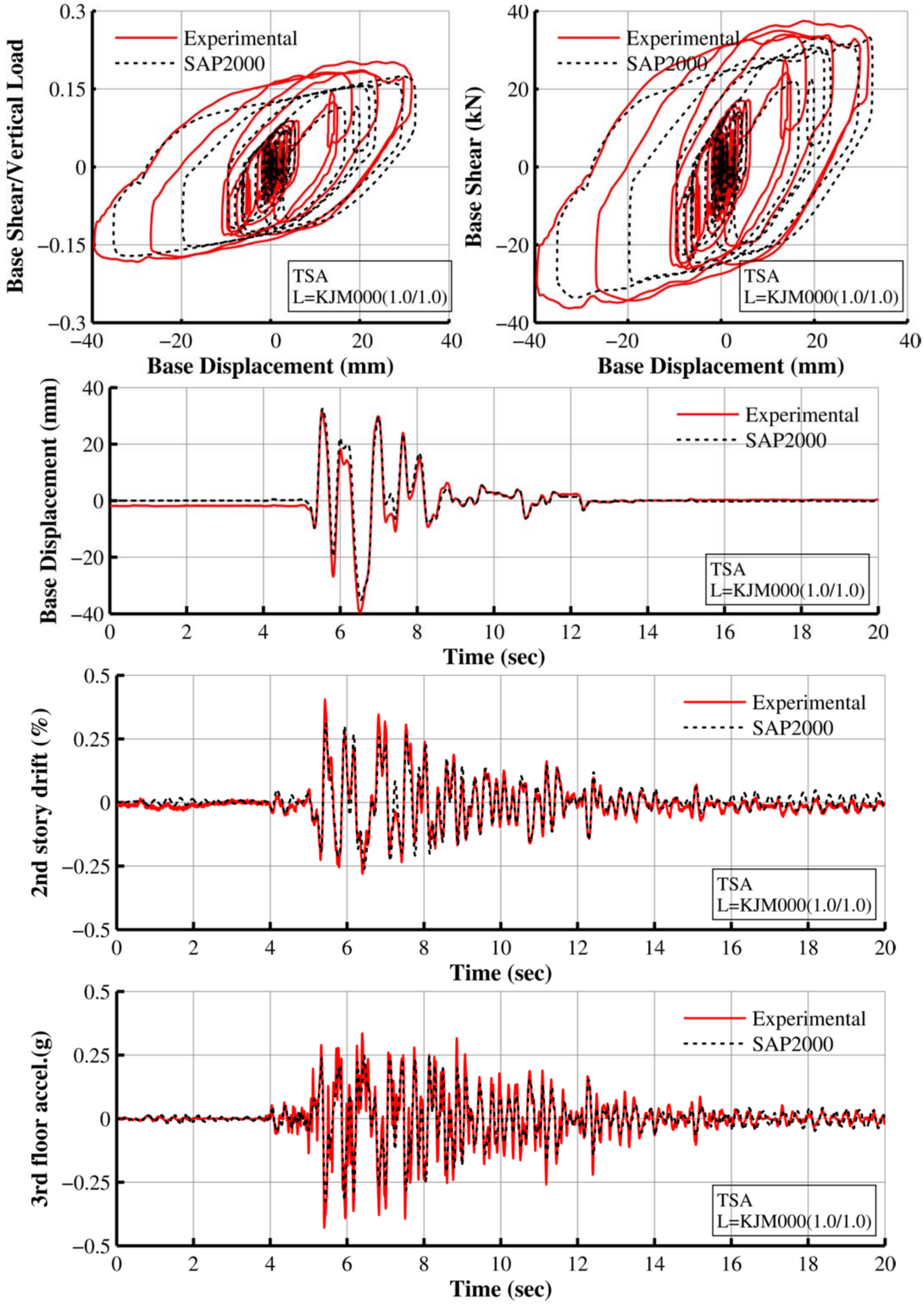
Base Shear/Vertical Load
Base Displacement (mm)
Experimental
SAP2000
TSA
L=KJM000(1.0/1.0)
Base Shear (kN)
Base Displacement (mm)
Experimental
SAP2000
TSA
L=KJM000(1.0/1.0)
Base Displacement (mm)
Time (sec)
Experimental
SAP2000
TSA
L=KJM000(1.0/1.0)
2nd story drift (%)
Time (sec)
Experimental
SAP2000
TSA
L=KJM000(1.0/1.0)
3rd floor accel.(g)
Time (sec)
Experimental
SAP2000
TSA
L=KJM000(1.0/1.0)

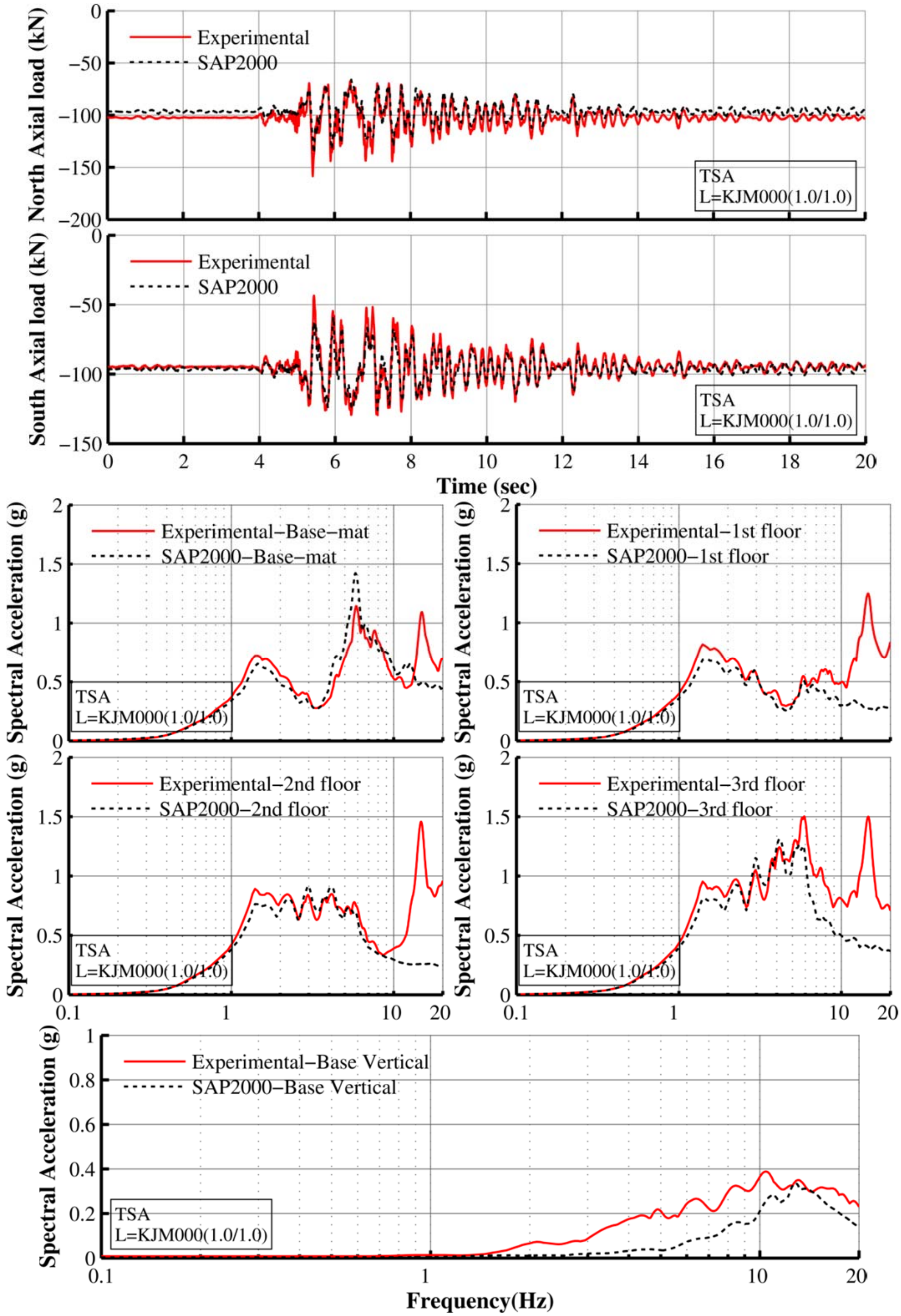
North Axial load (kN)
South Axial load (kN)
Experimental
SAP2000
TSA
L=KJM000(1.0/1.0)
Time (sec)
Spectral Acceleration (g)
Experimental−Base−mat
SAP2000−Base−mat
Experimental−1st floor
SAP2000−1st floor
Experimental−2nd floor
SAP2000−2nd floor
Experimental−3rd floor
SAP2000−3rd floor
Experimental−Base Vertical
SAP2000−Base Vertical
Frequency(Hz)

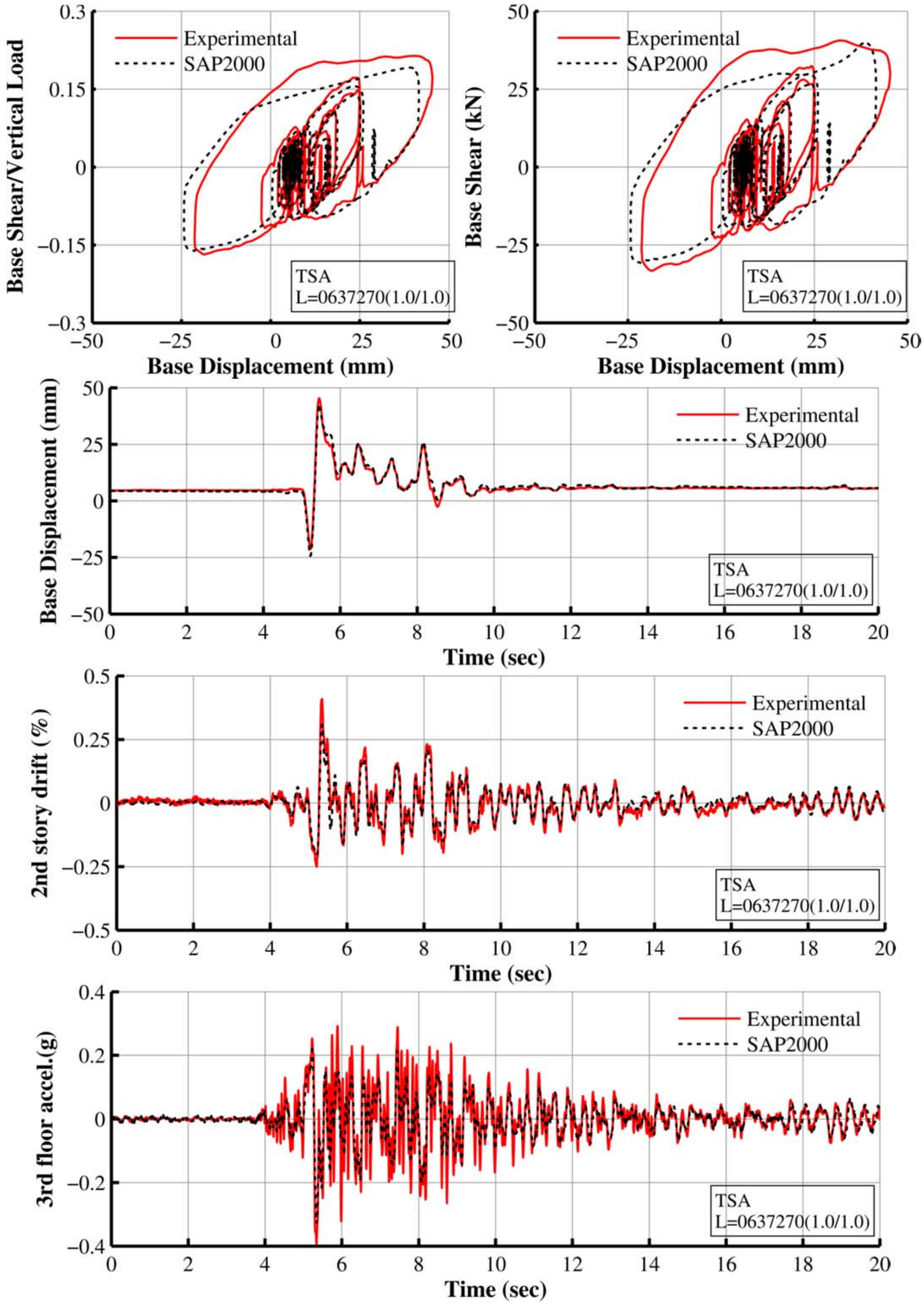
Base Shear/Vertical Load
Base Displacement (mm)
Experimental
SAP2000
TSA
L=0637270(1.0/1.0)
Base Shear (kN)
Base Displacement (mm)
Time (sec)
2nd story drift (%)
3rd floor accel.(g)

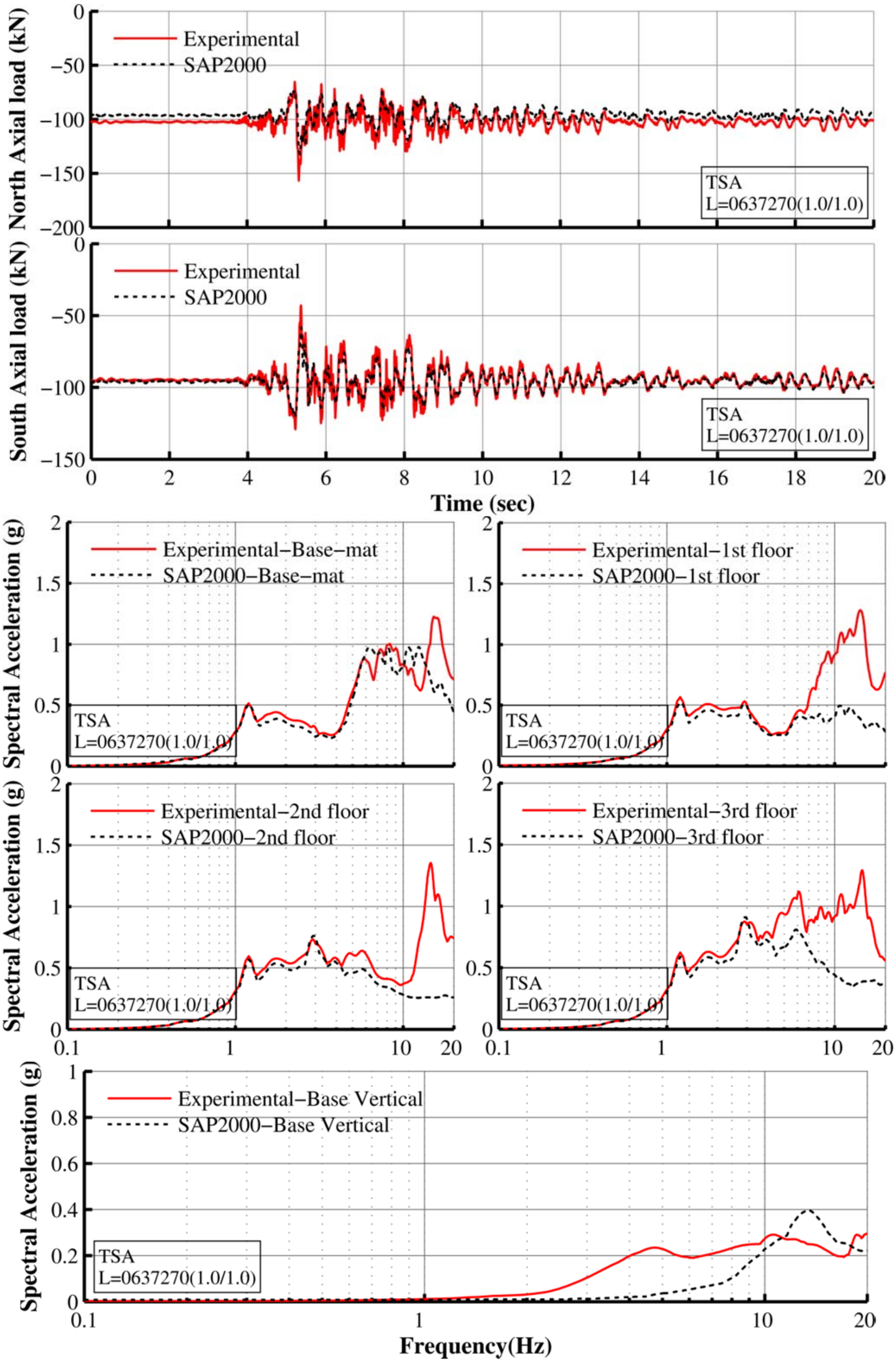
North Axial load (kN)
Experimental
SAP2000
TSA
L=0637270(1.0/1.0)
South Axial load (kN)
Experimental
SAP2000
TSA
L=0637270(1.0/1.0)
Time (sec)
Spectral Acceleration (g)
Experimental−Base−mat
SAP2000−Base−mat
TSA
L=0637270(1.0/1.0)
Experimental−1st floor
SAP2000−1st floor
TSA
L=0637270(1.0/1.0)
Spectral Acceleration (g)
Experimental−2nd floor
SAP2000−2nd floor
TSA
L=0637270(1.0/1.0)
Experimental−3rd floor
SAP2000−3rd floor
TSA
L=0637270(1.0/1.0)
Spectral Acceleration (g)
Experimental−Base Vertical
SAP2000−Base Vertical
TSA
L=0637270(1.0/1.0)
Frequency(Hz)

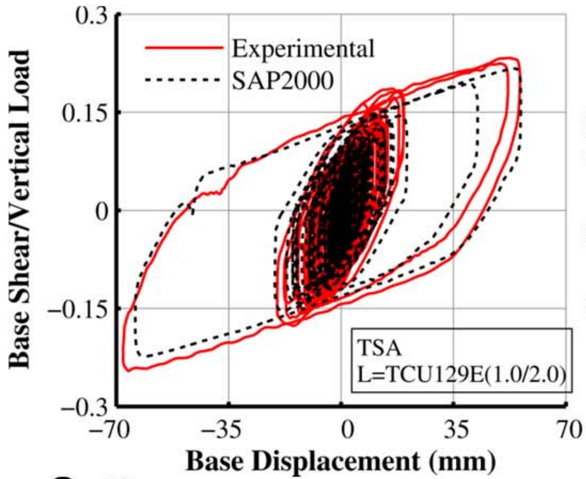
Experimental
SAP2000
Base Shear/Vertical Load
0.3
0.15
0
−0.15
−0.3
−70
−35
0
35
70
Base Displacement (mm)
TSA
L=TCU129E(1.0/2.0)

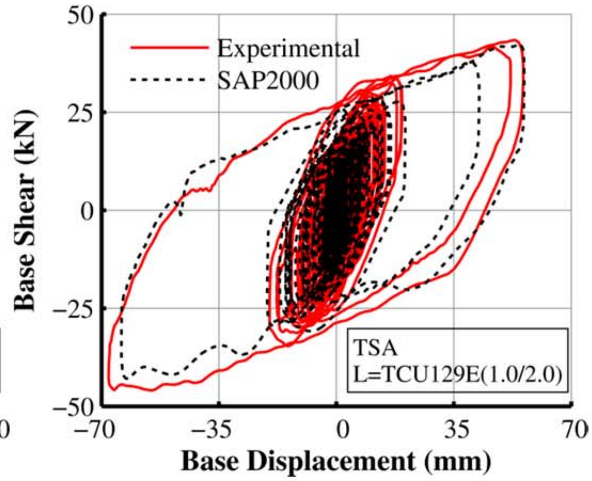
Experimental
SAP2000
Base Shear (kN)
50
25
0
−25
−50
−70
−35
0
35
70
Base Displacement (mm)
TSA
L=TCU129E(1.0/2.0)

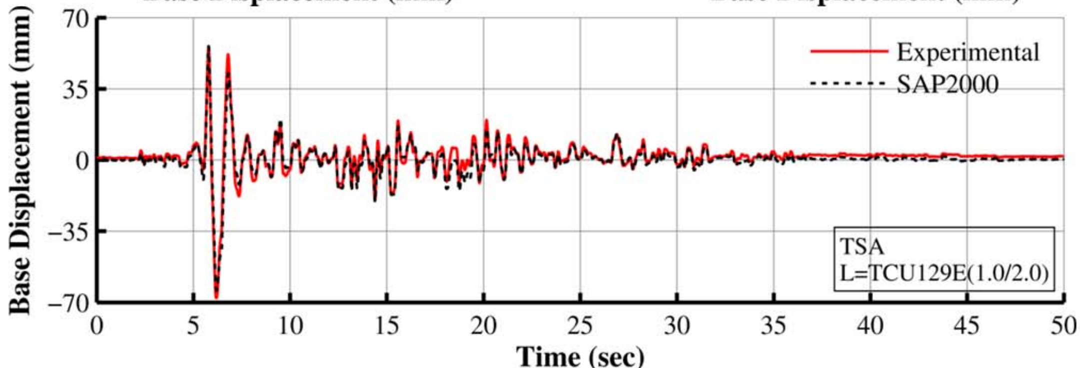
Experimental
SAP2000
Base Displacement (mm)
70
35
0
−35
−70
0
5
10
15
20
25
30
35
40
45
50
Time (sec)
TSA
L=TCU129E(1.0/2.0)

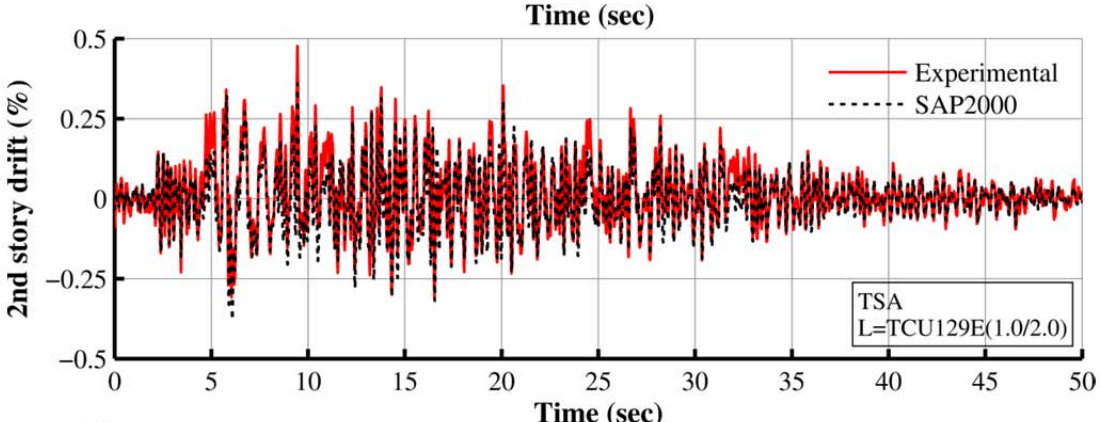
Experimental
SAP2000
2nd story drift (%)
0.5
0.25
0
−0.25
−0.5
0
5
10
15
20
25
30
35
40
45
50
Time (sec)
TSA
L=TCU129E(1.0/2.0)

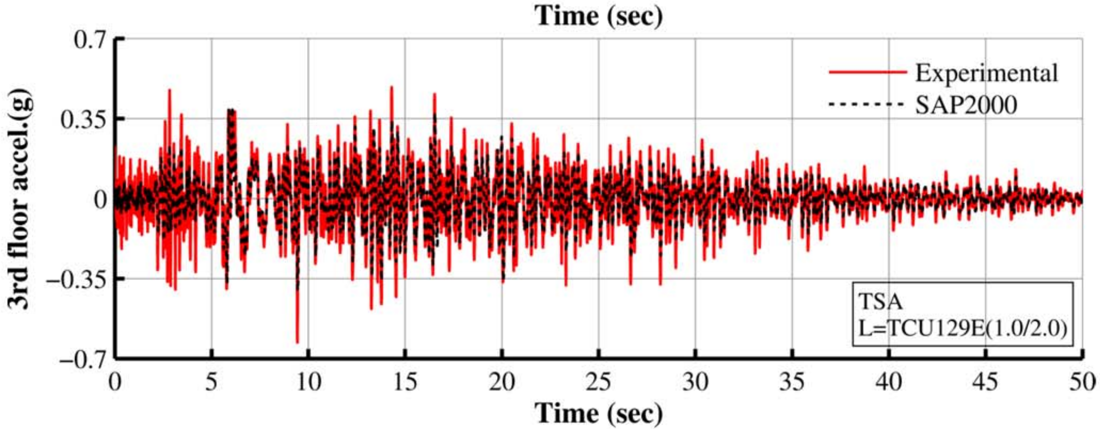
Experimental
SAP2000
3rd floor accel.(g)
0.7
0.35
0
−0.35
−0.7
0
5
10
15
20
25
30
35
40
45
50
Time (sec)
TSA
L=TCU129E(1.0/2.0)

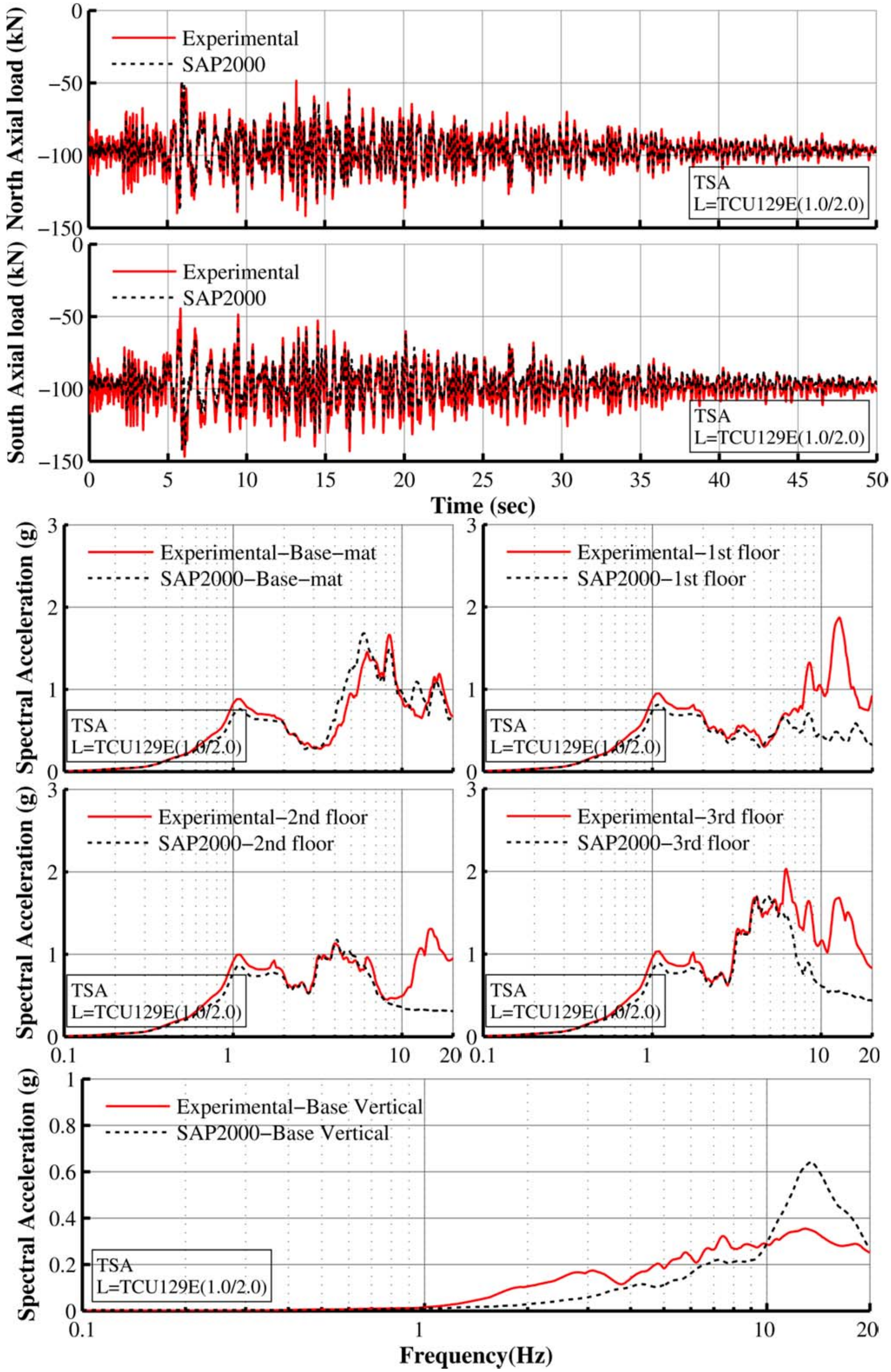

North Axial load (kN)
Experimental
SAP2000
TSA
L=TCU129E(1.0/2.0)
South Axial load (kN)
Time (sec)
Spectral Acceleration (g)
Experimental−Base−mat
SAP2000−Base−mat
Experimental−1st floor
SAP2000−1st floor
Experimental−2nd floor
SAP2000−2nd floor
Experimental−3rd floor
SAP2000−3rd floor
Experimental−Base Vertical
SAP2000−Base Vertical
Frequency(Hz)

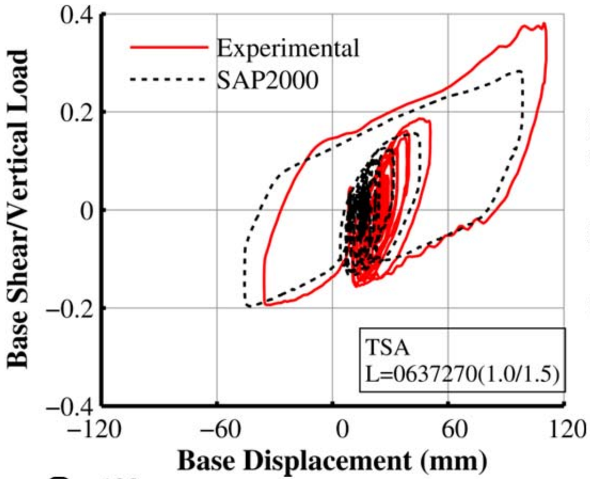
Experimental
SAP2000
TSA
L=0637270(1.0/1.5)
Base Shear/Vertical Load
Base Displacement (mm)
0.4
0.2
0
−0.2
−0.4
−120
−60
0
60
120

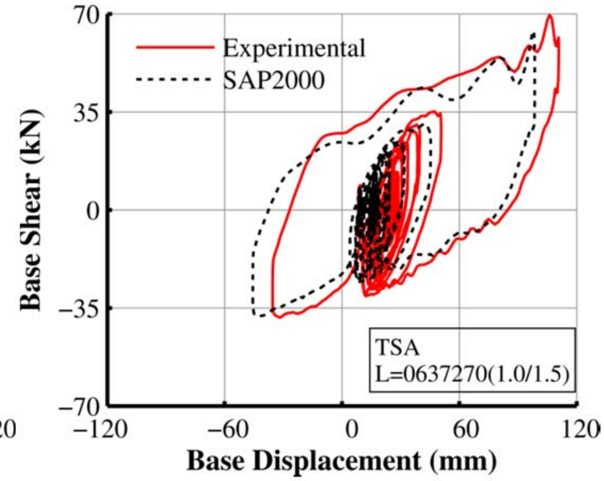
Experimental
SAP2000
TSA
L=0637270(1.0/1.5)
Base Shear (kN)
Base Displacement (mm)
70
35
0
−35
−70
−120
−60
0
60
120

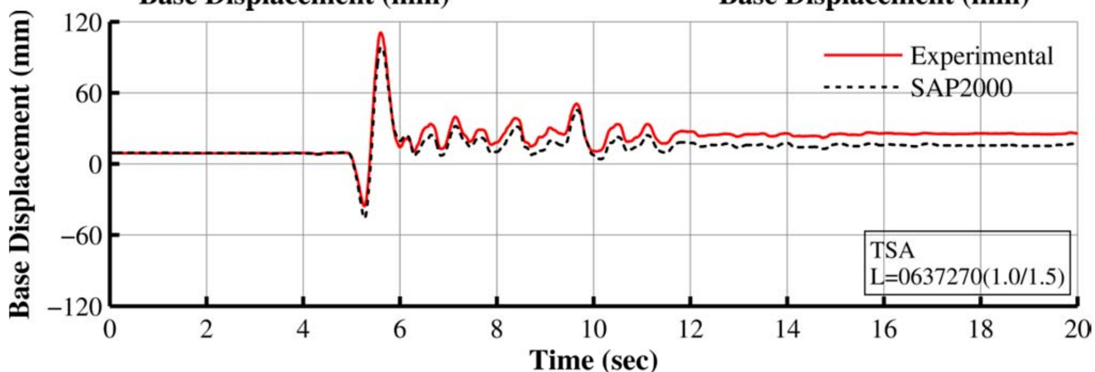
Experimental
SAP2000
TSA
L=0637270(1.0/1.5)
Base Displacement (mm)
Time (sec)
120
60
0
−60
−120
0
2
4
6
8
10
12
14
16
18
20

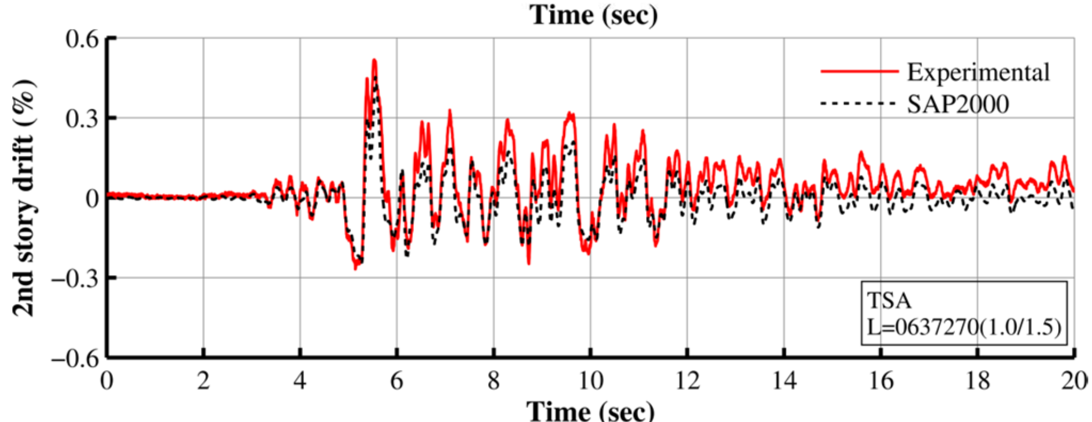
Experimental
SAP2000
TSA
L=0637270(1.0/1.5)
2nd story drift (%)
Time (sec)
0.6
0.3
0
−0.3
−0.6
0
2
4
6
8
10
12
14
16
18
20

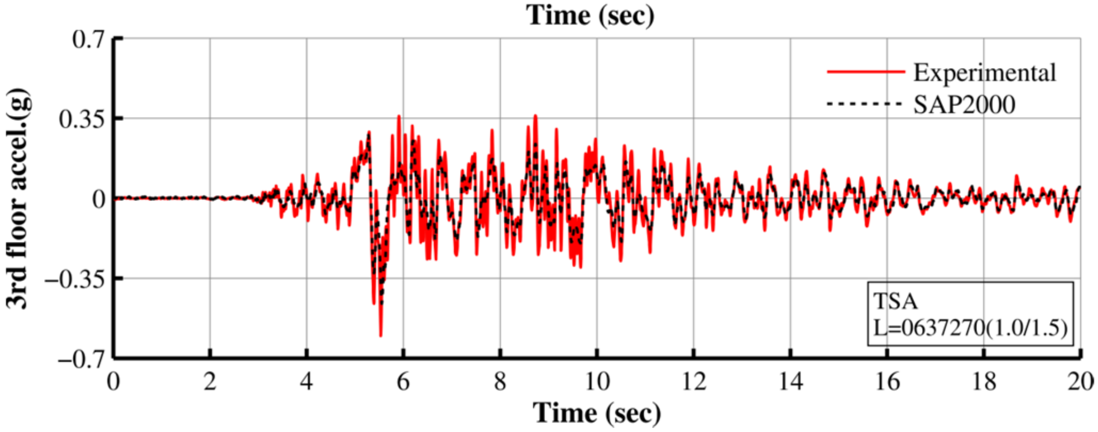
Experimental
SAP2000
TSA
L=0637270(1.0/1.5)
3rd floor accel.(g)
Time (sec)
0.7
0.35
0
−0.35
−0.7
0
2
4
6
8
10
12
14
16
18
20

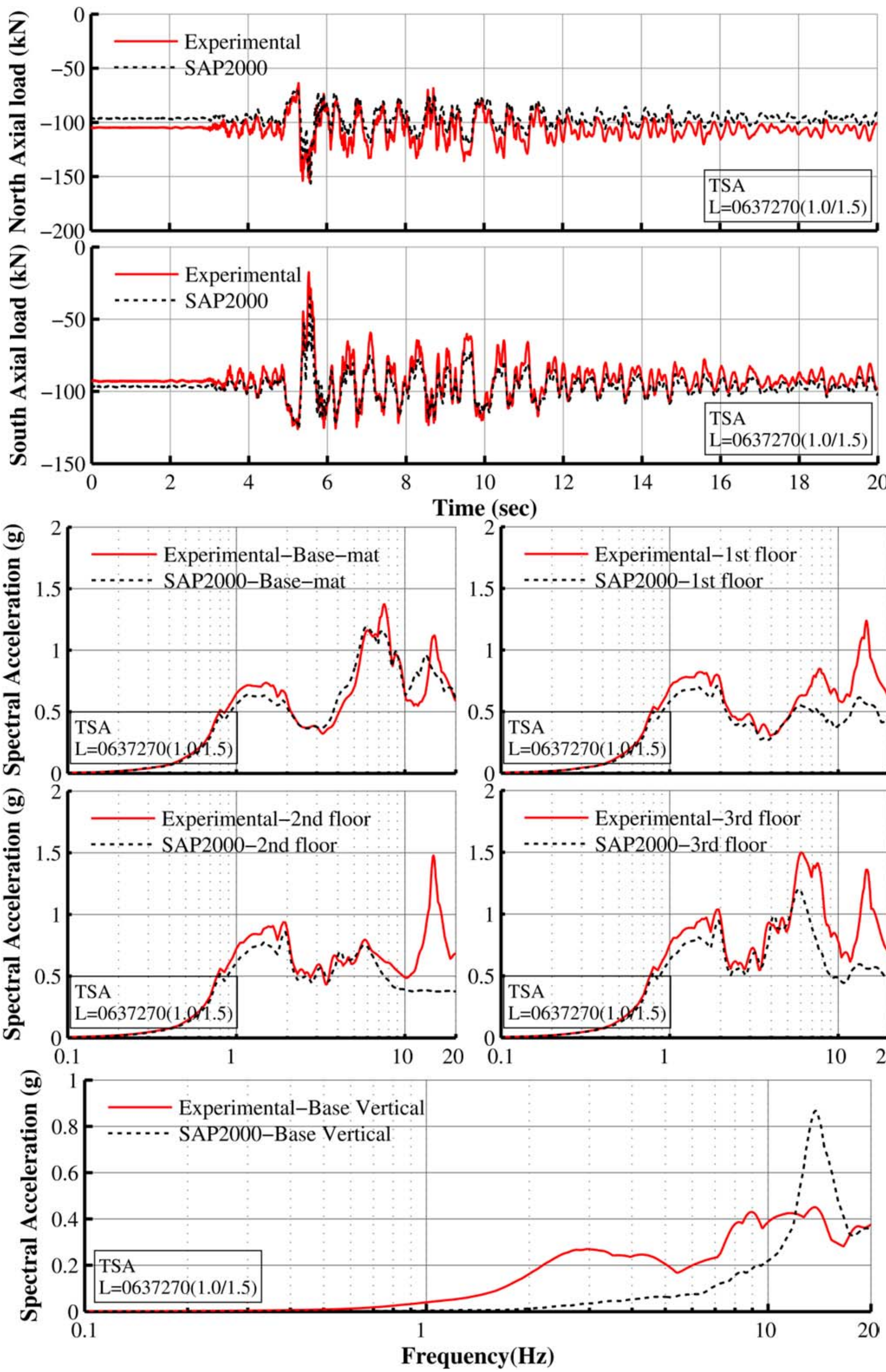
North Axial load (kN)
Experimental
SAP2000
TSA
L=0637270(1.0/1.5)
South Axial load (kN)
Time (sec)
Spectral Acceleration (g)
Experimental−Base−mat
SAP2000−Base−mat
Experimental−1st floor
SAP2000−1st floor
Experimental−2nd floor
SAP2000−2nd floor
Experimental−3rd floor
SAP2000−3rd floor
Experimental−Base Vertical
SAP2000−Base Vertical
Frequency(Hz)

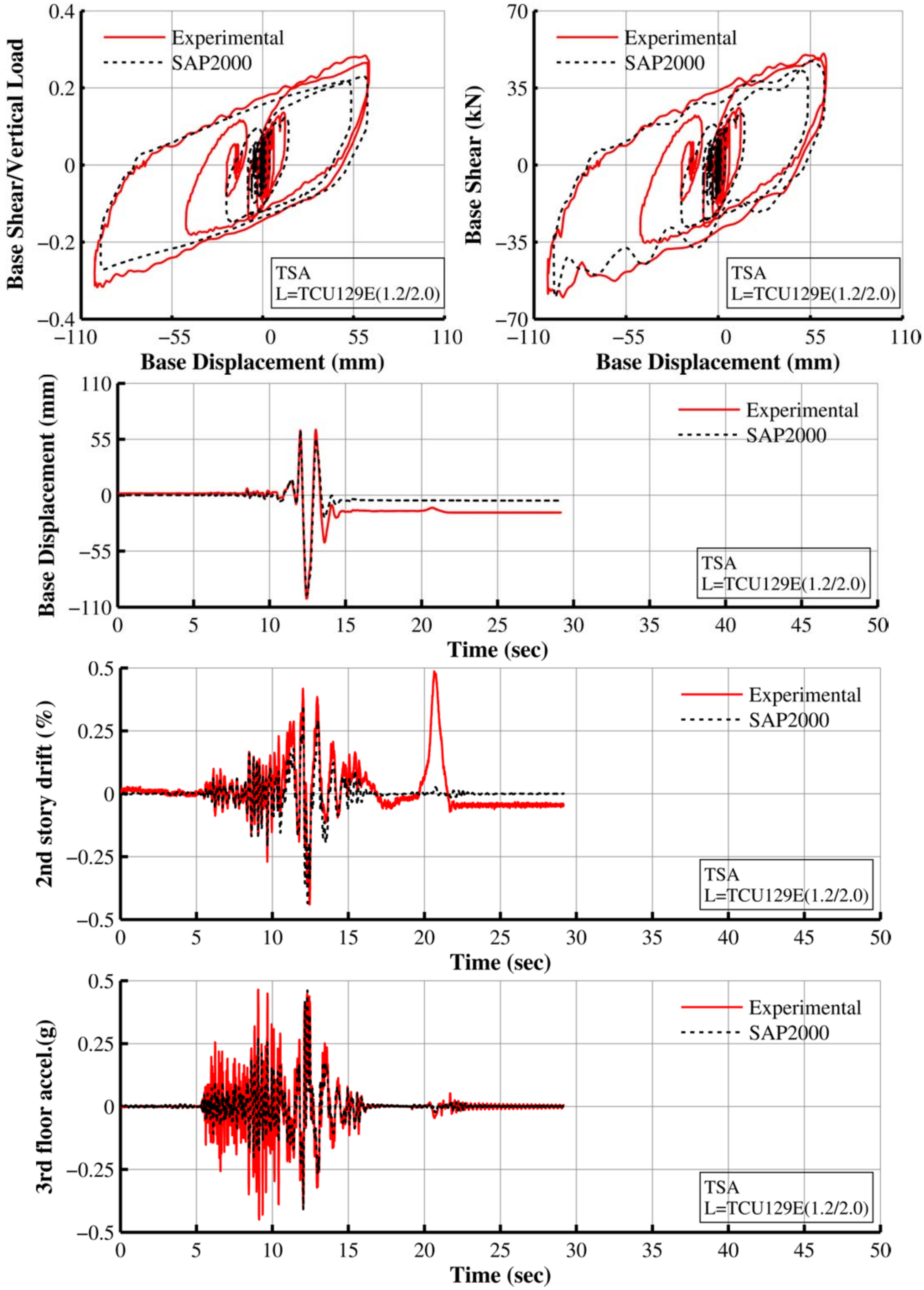
Experimental
SAP2000
Base Shear/Vertical Load
Base Displacement (mm)
TSA
L=TCU129E(1.2/2.0)
Base Shear (kN)
Base Displacement (mm)
Time (sec)
2nd story drift (%)
3rd floor accel.(g)

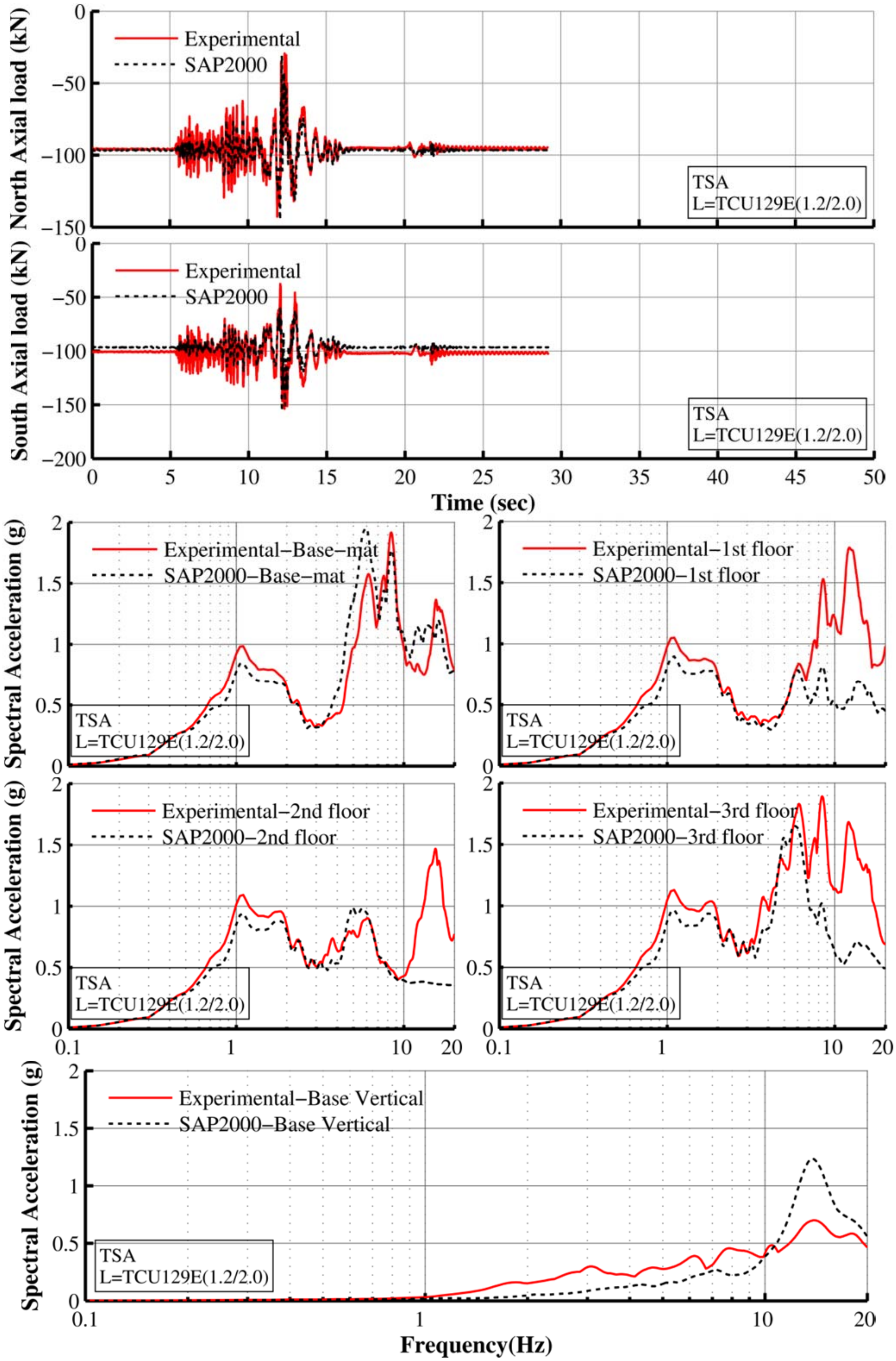
North Axial load (kN)
Experimental
SAP2000
TSA
L=TCU129E(1.2/2.0)
South Axial load (kN)
Experimental
SAP2000
TSA
L=TCU129E(1.2/2.0)
Time (sec)
Spectral Acceleration (g)
Experimental−Base−mat
SAP2000−Base−mat
TSA
L=TCU129E(1.2/2.0)
Experimental−1st floor
SAP2000−1st floor
TSA
L=TCU129E(1.2/2.0)
Spectral Acceleration (g)
Experimental−2nd floor
SAP2000−2nd floor
TSA
L=TCU129E(1.2/2.0)
Experimental−3rd floor
SAP2000−3rd floor
TSA
L=TCU129E(1.2/2.0)
Spectral Acceleration (g)
Experimental−Base Vertical
SAP2000−Base Vertical
TSA
L=TCU129E(1.2/2.0)
Frequency(Hz)

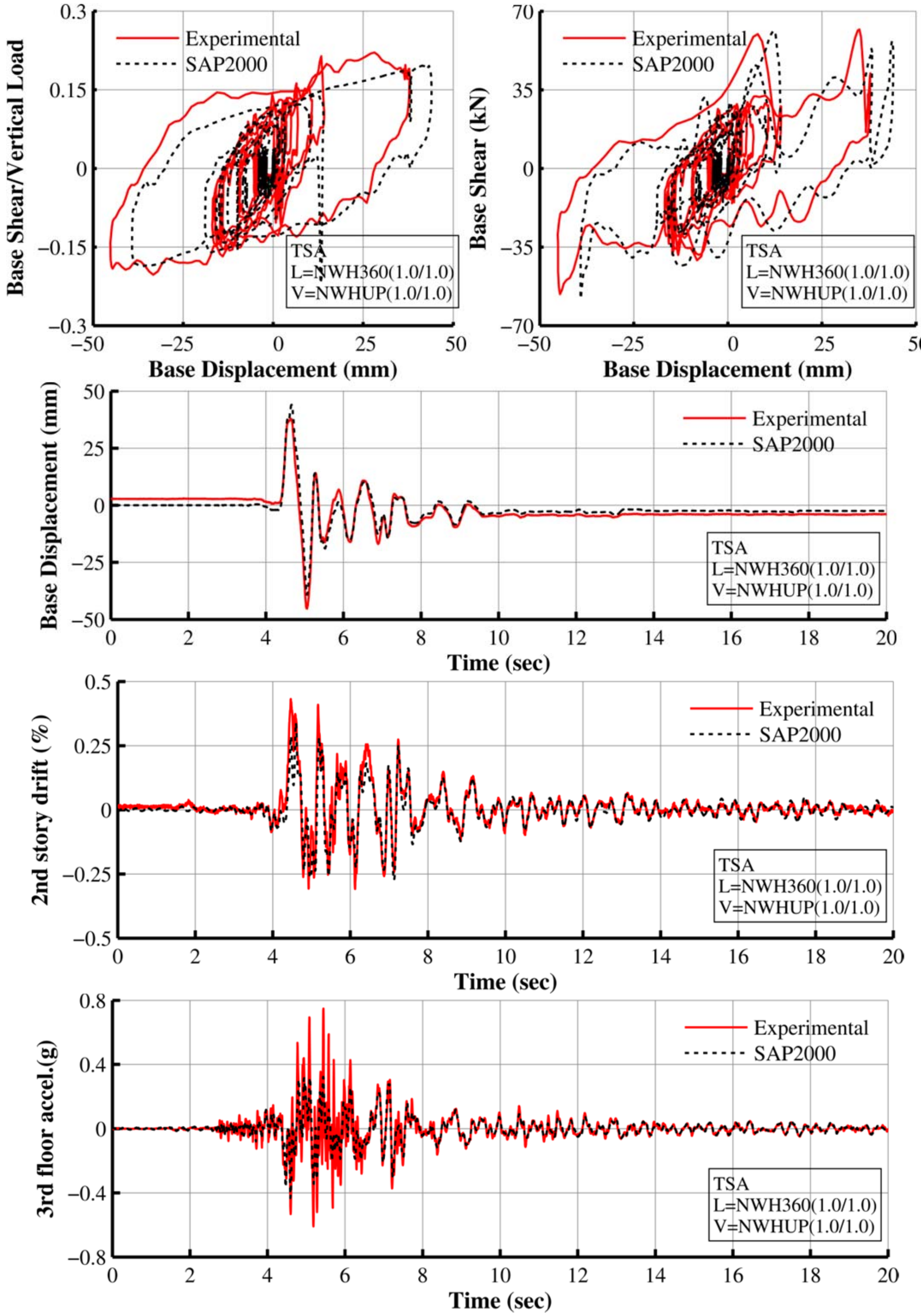
Experimental
SAP2000
TSA
L=NWH360(1.0/1.0)
V=NWHUP(1.0/1.0)
Base Shear/Vertical Load
Base Displacement (mm)
Base Shear (kN)
Base Displacement (mm)
Time (sec)
2nd story drift (%)
3rd floor accel.(g)

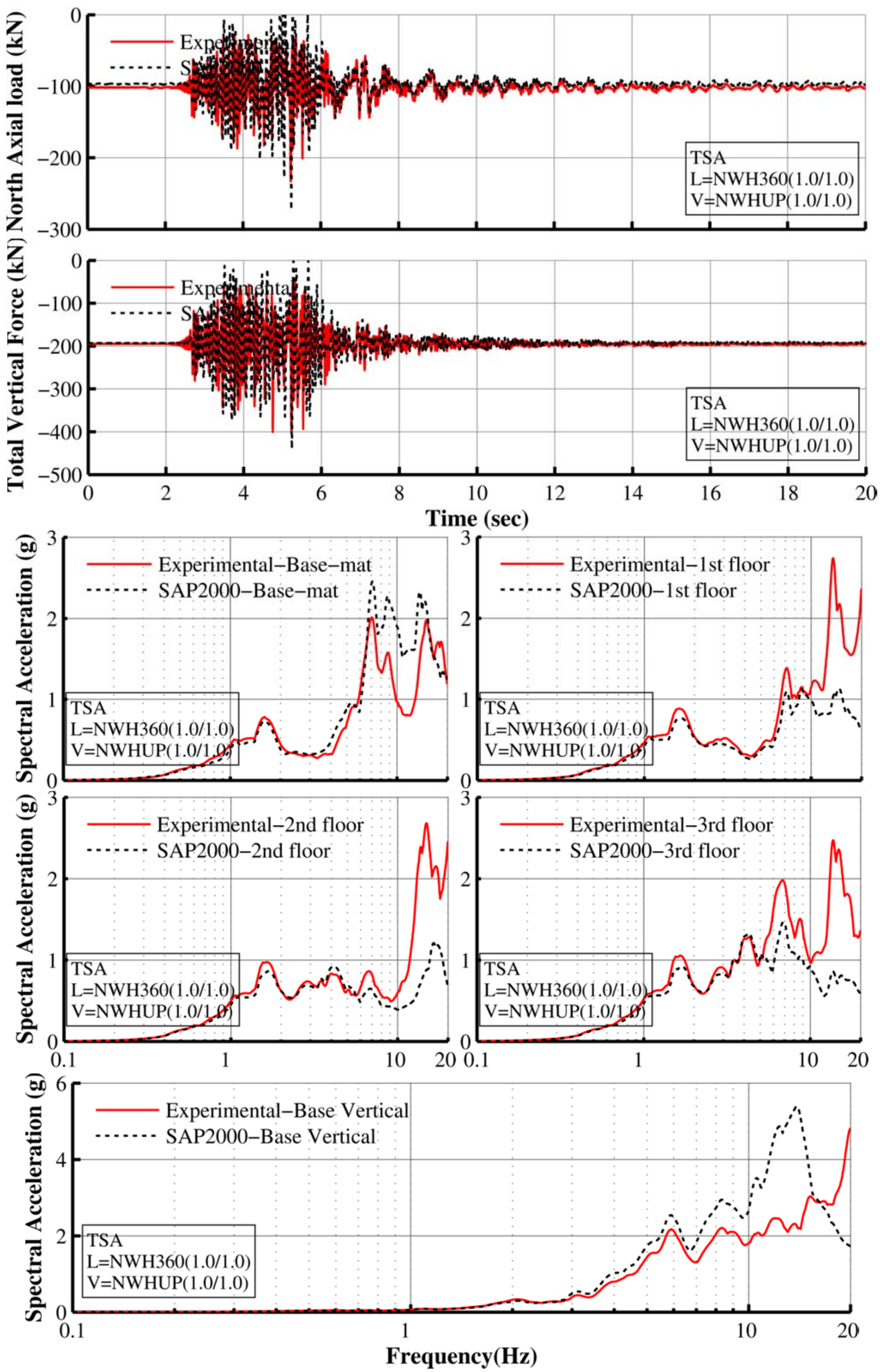

North Axial load (kN)
Experimental
SAP2000
TSA
L=NWH360(1.0/1.0)
V=NWHUP(1.0/1.0)
Total Vertical Force (kN)
Time (sec)
Spectral Acceleration (g)
Experimental−Base−mat
SAP2000−Base−mat
Experimental−1st floor
SAP2000−1st floor
Experimental−2nd floor
SAP2000−2nd floor
Experimental−3rd floor
SAP2000−3rd floor
Experimental−Base Vertical
SAP2000−Base Vertical
Frequency(Hz)

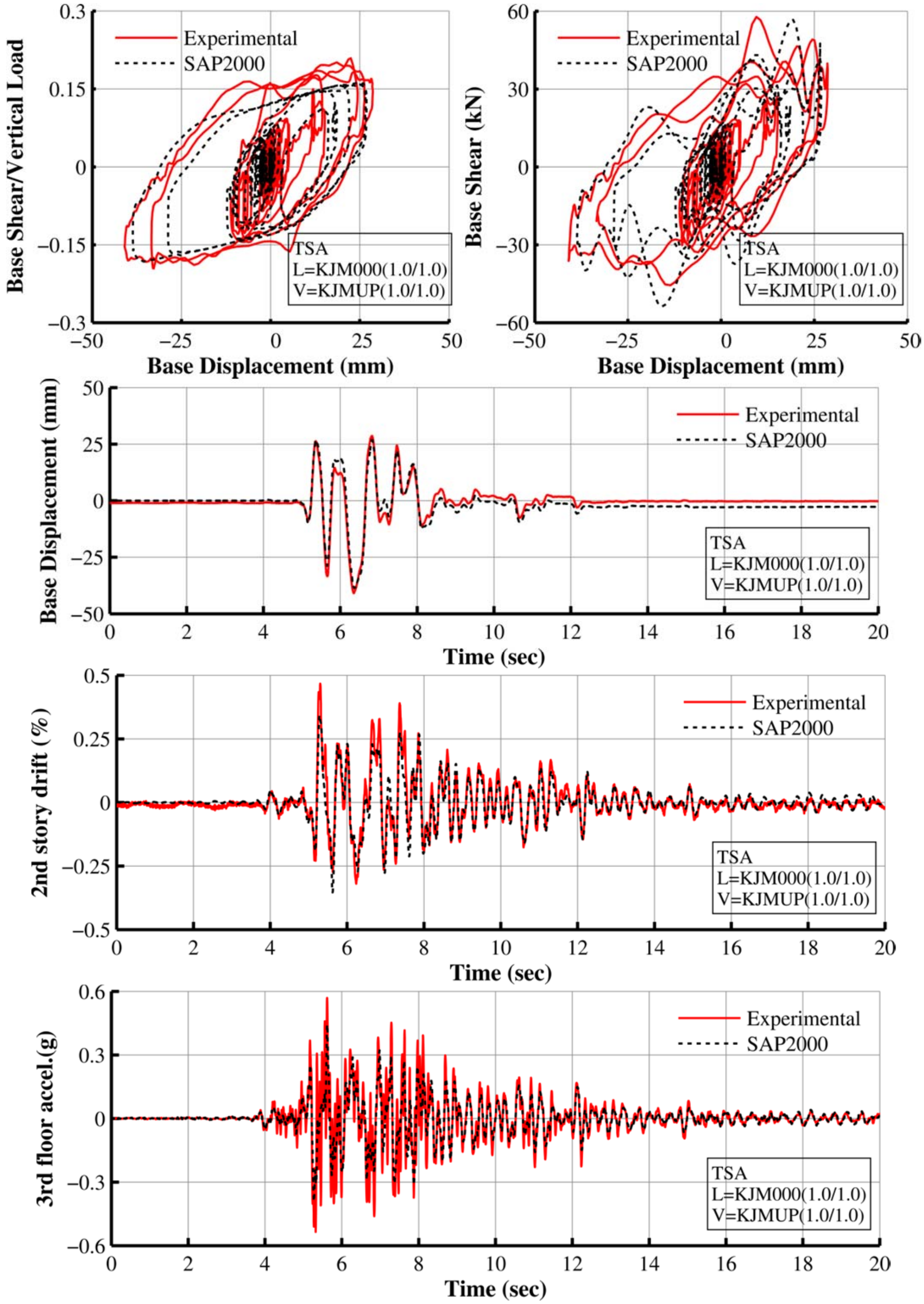
Experimental
SAP2000
TSA
L=KJM000(1.0/1.0)
V=KJMUP(1.0/1.0)
Base Shear/Vertical Load
Base Shear (kN)
Base Displacement (mm)
Time (sec)
2nd story drift (%)
3rd floor accel.(g)

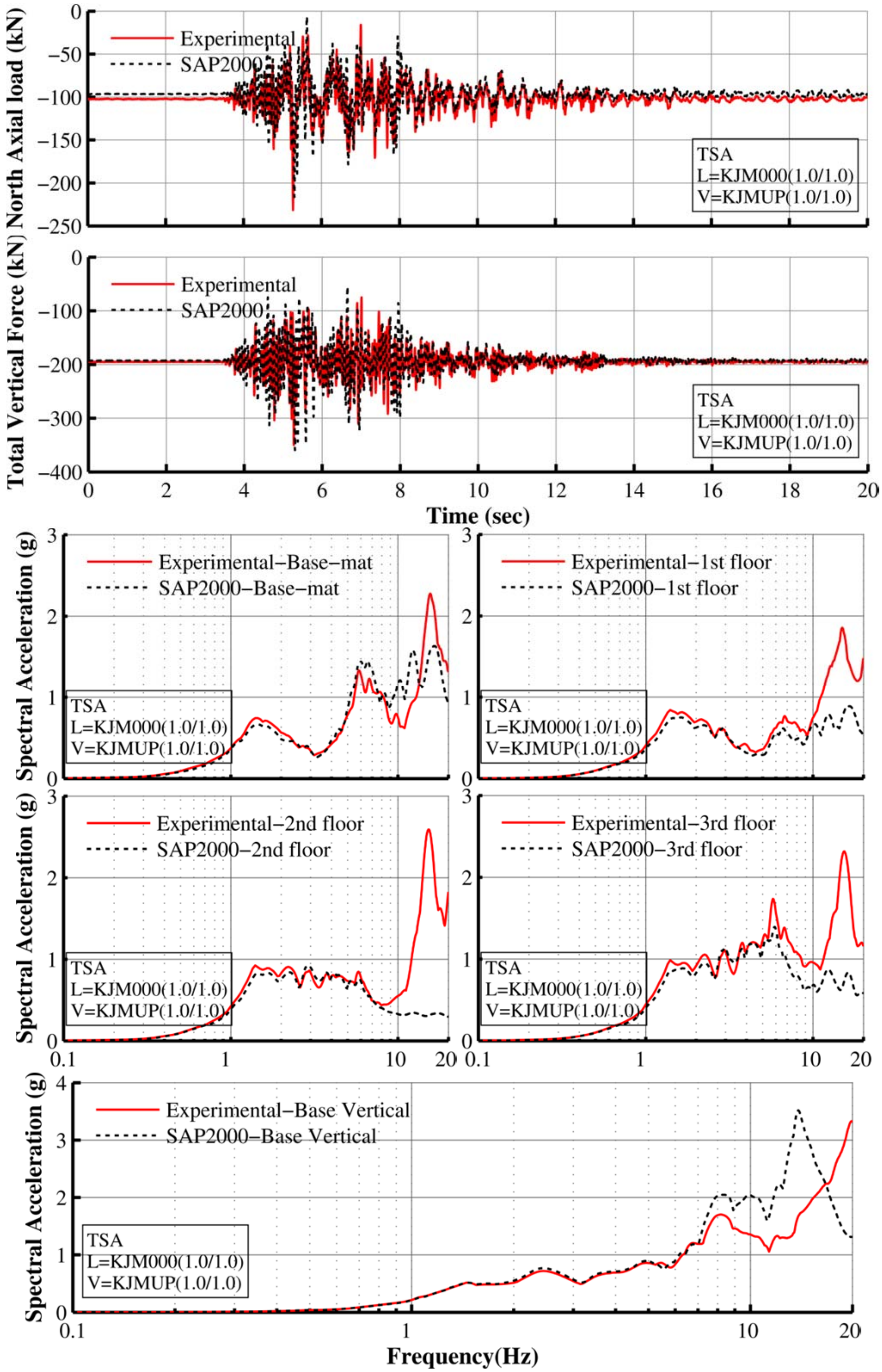
North Axial load (kN)
Experimental
SAP2000
TSA
L=KJM000(1.0/1.0)
V=KJMUP(1.0/1.0)
Total Vertical Force (kN)
Time (sec)
Spectral Acceleration (g)
Experimental−Base−mat
SAP2000−Base−mat
Experimental−1st floor
SAP2000−1st floor
Experimental−2nd floor
SAP2000−2nd floor
Experimental−3rd floor
SAP2000−3rd floor
Experimental−Base Vertical
SAP2000−Base Vertical
Frequency(Hz)

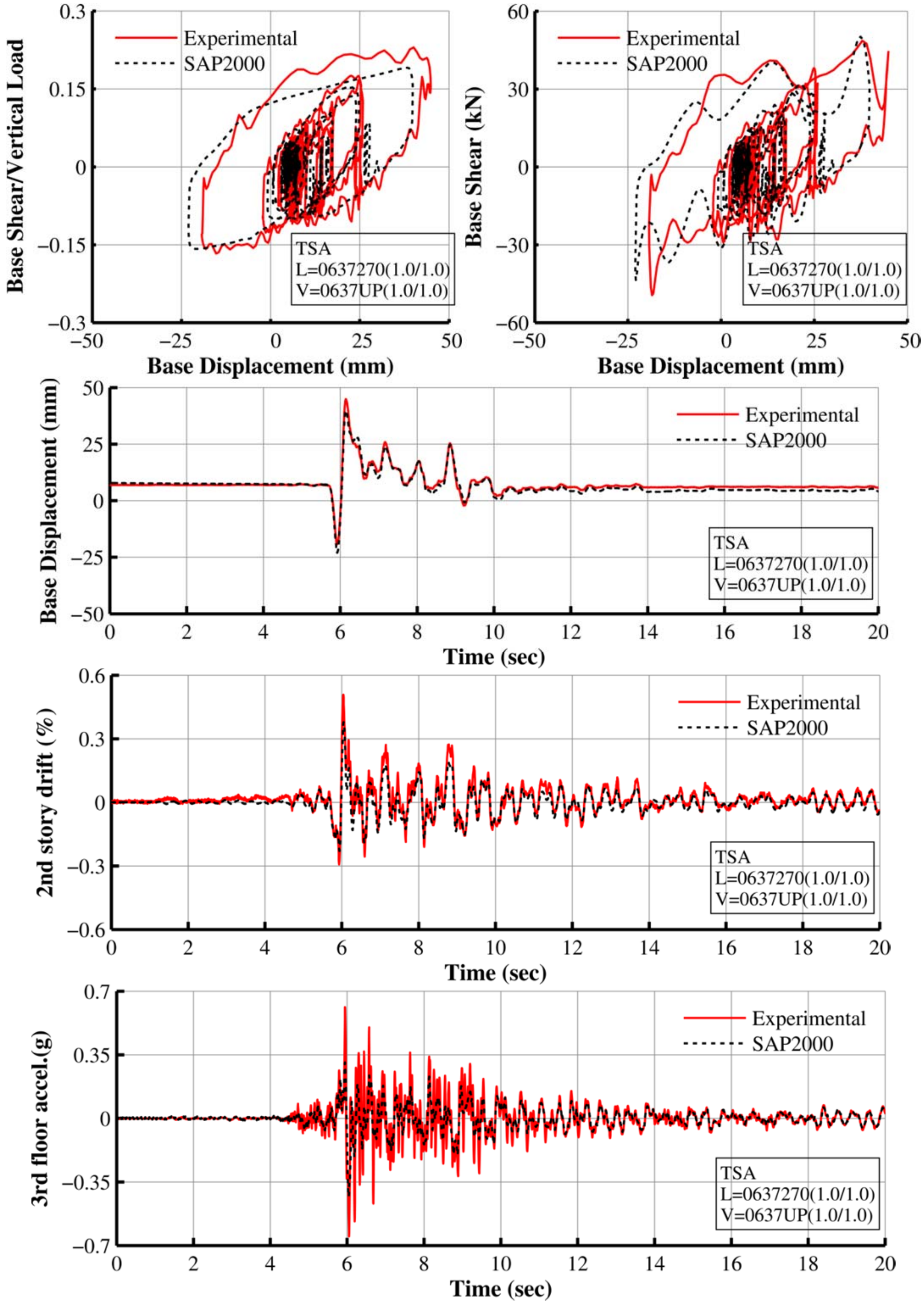
Experimental
SAP2000
TSA
L=0637270(1.0/1.0)
V=0637UP(1.0/1.0)
Base Shear/Vertical Load
Base Shear (kN)
Base Displacement (mm)
Time (sec)
2nd story drift (%)
3rd floor accel.(g)

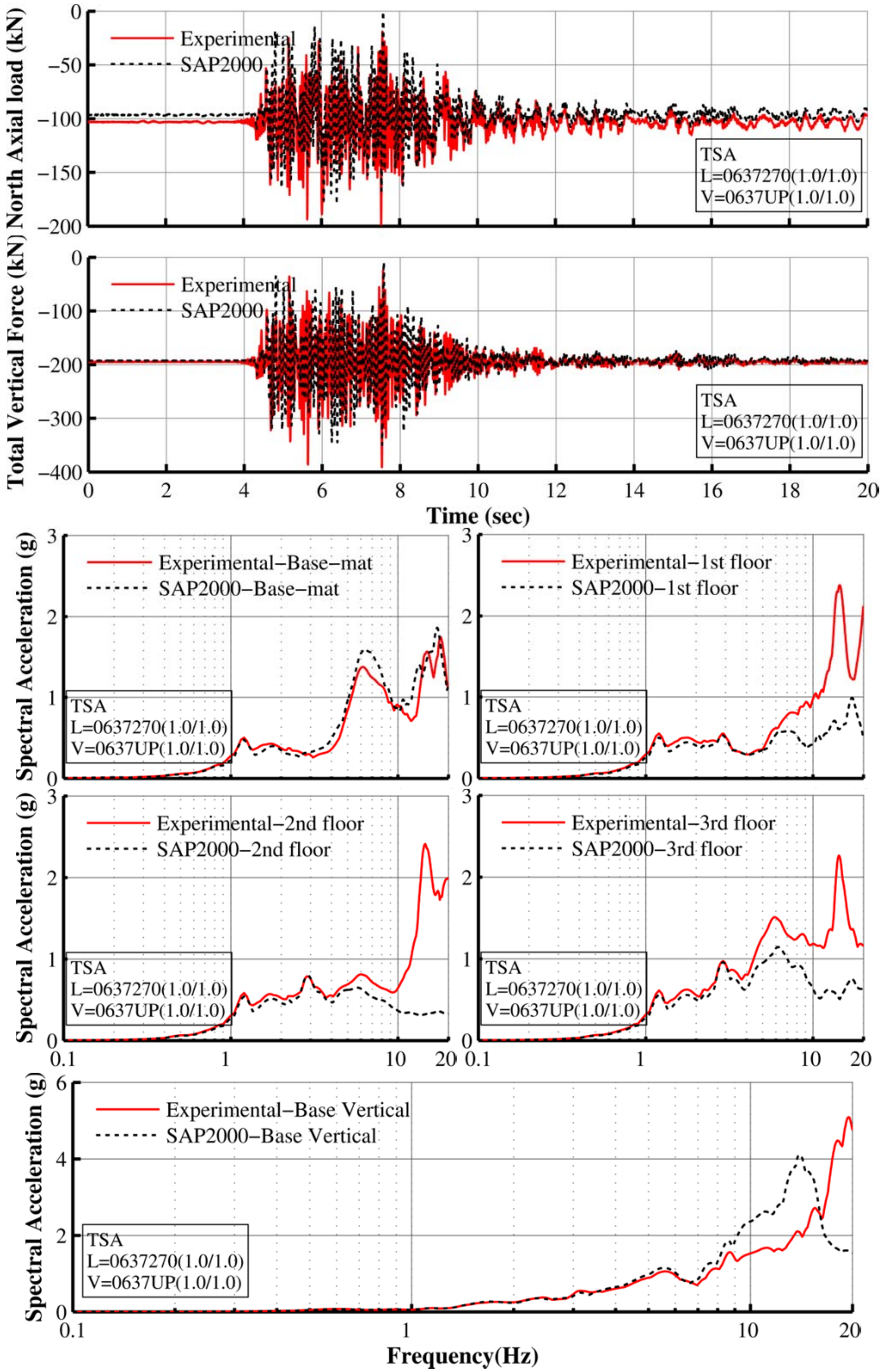

Experimental
SAP2000
TSA
L=0637270(1.0/1.0)
V=0637UP(1.0/1.0)
North Axial load (kN)
Total Vertical Force (kN)
Time (sec)
Experimental−Base−mat
SAP2000−Base−mat
Experimental−1st floor
SAP2000−1st floor
Experimental−2nd floor
SAP2000−2nd floor
Experimental−3rd floor
SAP2000−3rd floor
Spectral Acceleration (g)
Experimental−Base Vertical
SAP2000−Base Vertical
Frequency(Hz)

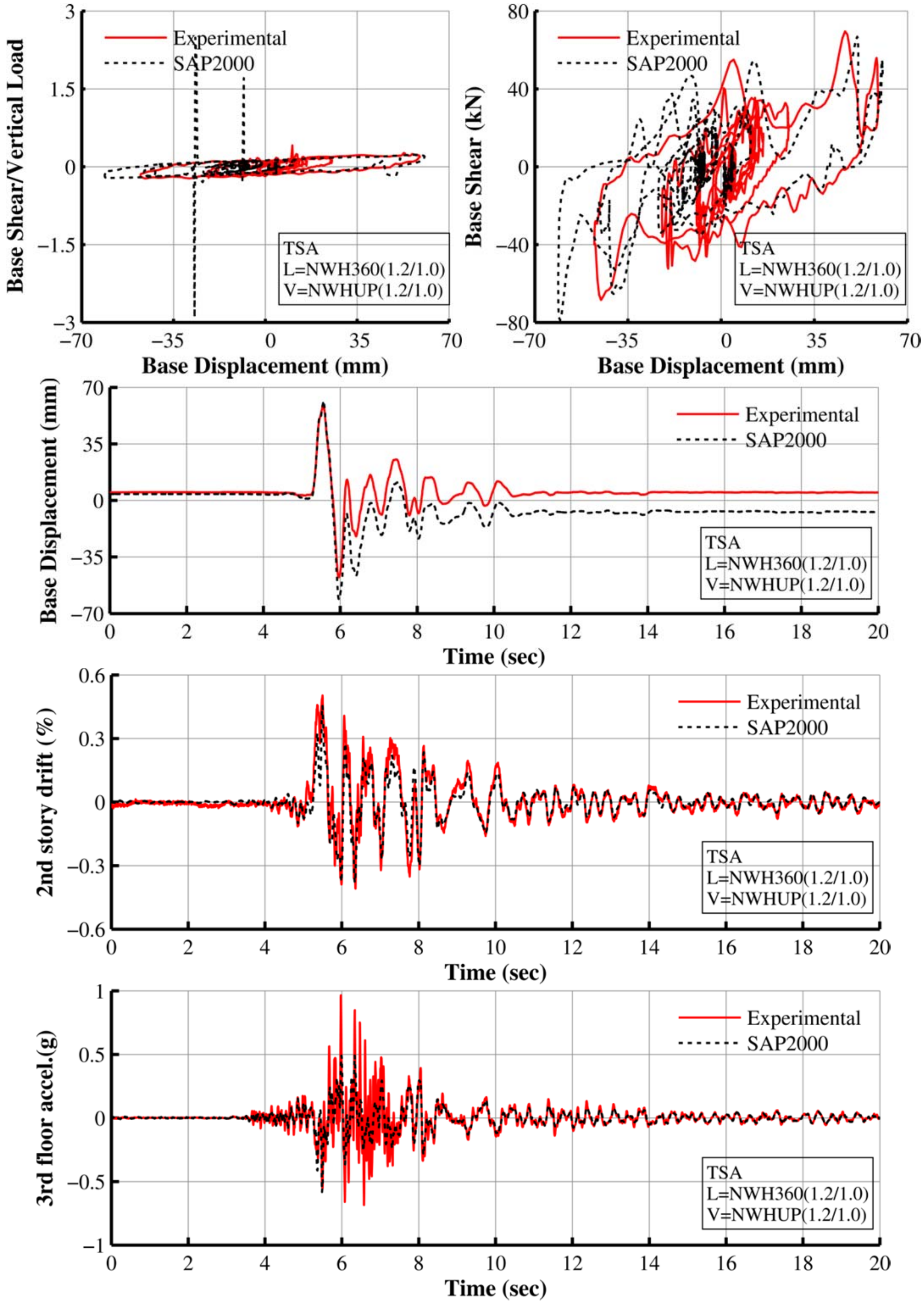
Experimental
SAP2000
TSA
L=NWH360(1.2/1.0)
V=NWHUP(1.2/1.0)
Base Shear/Vertical Load
Base Displacement (mm)
Base Shear (kN)
Base Displacement (mm)
Time (sec)
2nd story drift (%)
3rd floor accel.(g)

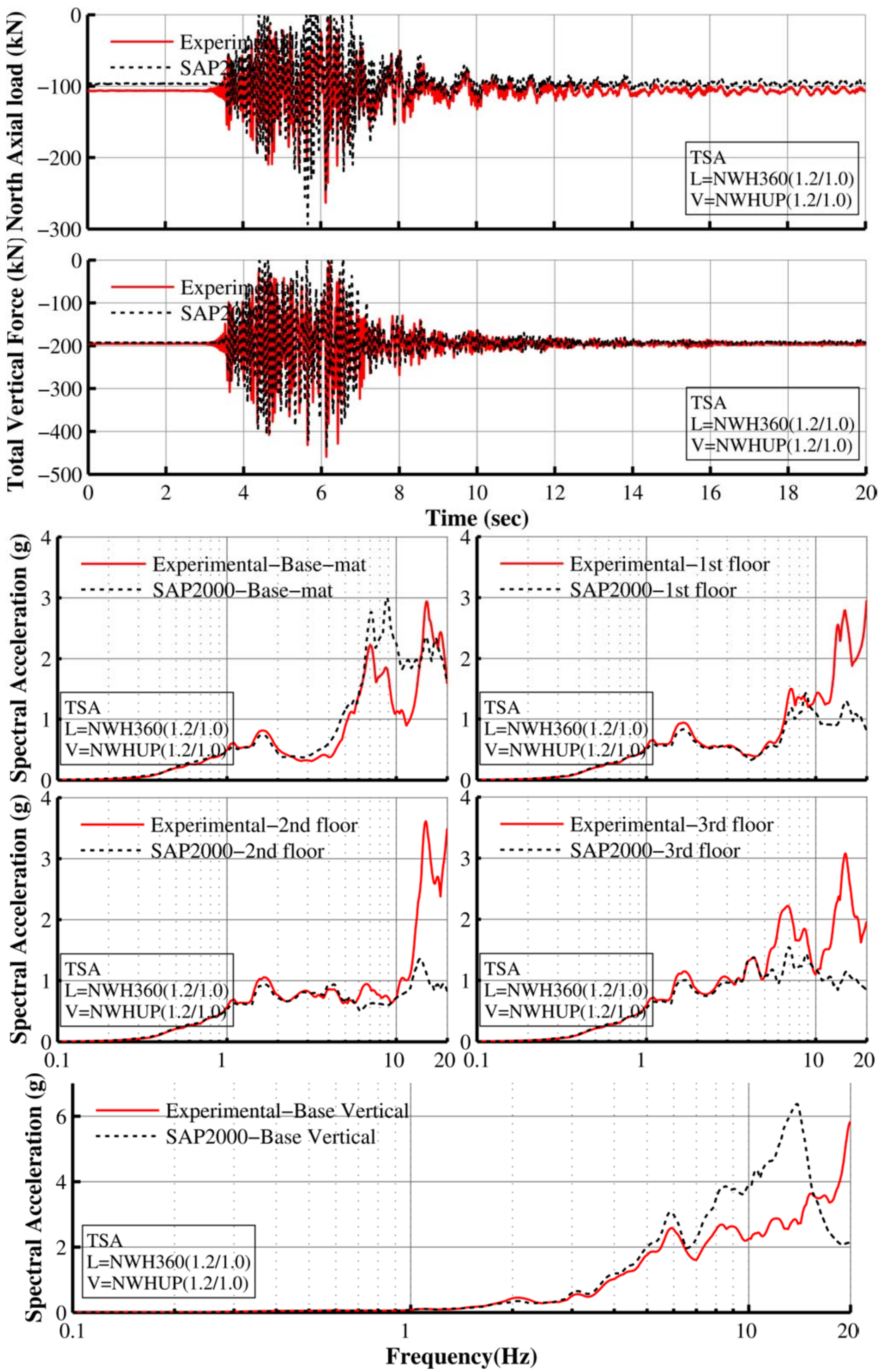

North Axial load (kN)
Experimental
SAP2000
TSA
L=NWH360(1.2/1.0)
V=NWHUP(1.2/1.0)
Total Vertical Force (kN)
Time (sec)
Spectral Acceleration (g)
Experimental−Base−mat
SAP2000−Base−mat
Experimental−1st floor
SAP2000−1st floor
Experimental−2nd floor
SAP2000−2nd floor
Experimental−3rd floor
SAP2000−3rd floor
Experimental−Base Vertical
SAP2000−Base Vertical
Frequency(Hz)

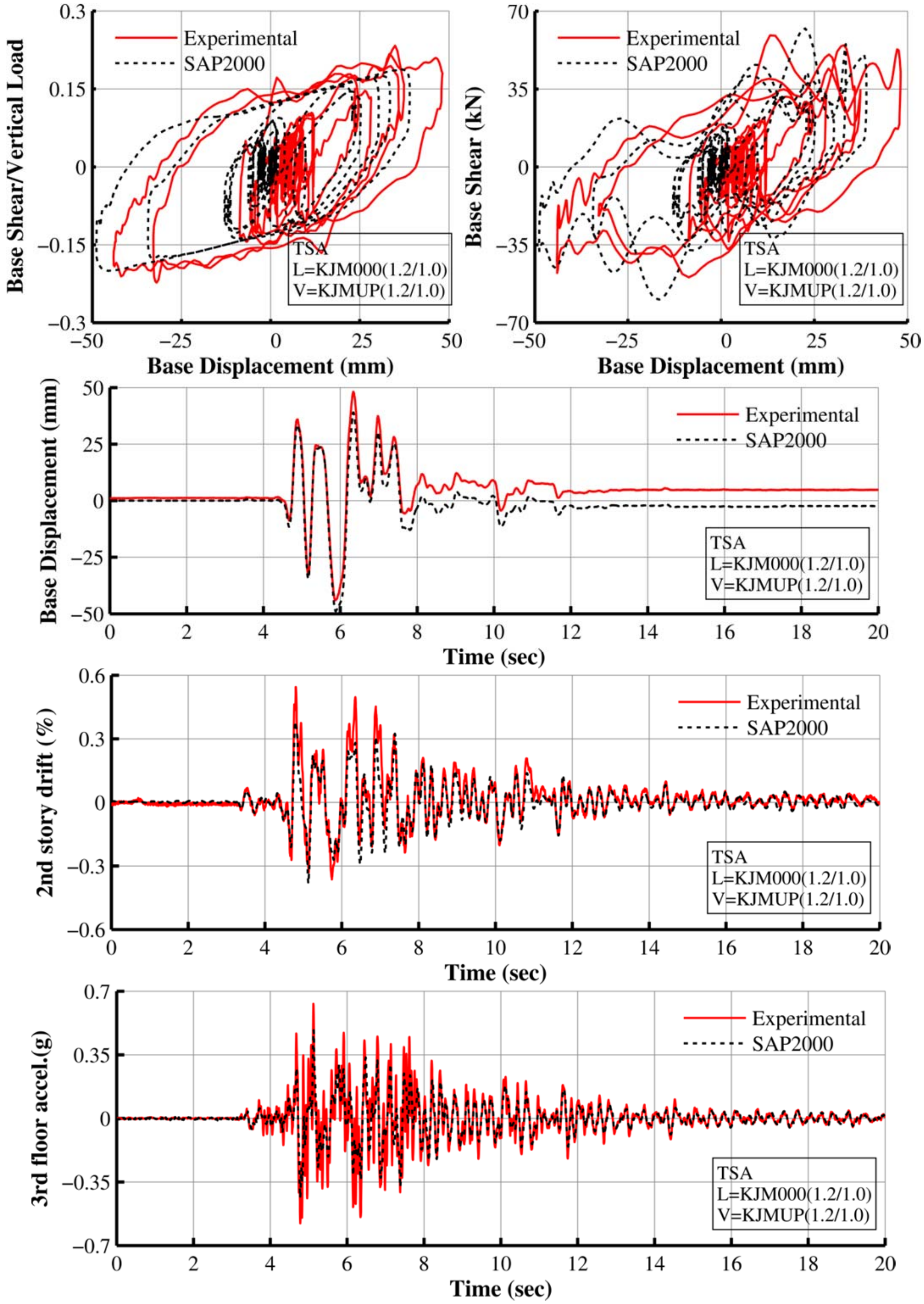
Experimental
SAP2000
TSA
L=KJM000(1.2/1.0)
V=KJMUP(1.2/1.0)
Base Shear/Vertical Load
Base Displacement (mm)
Base Shear (kN)
Base Displacement (mm)
Time (sec)
2nd story drift (%)
3rd floor accel.(g)

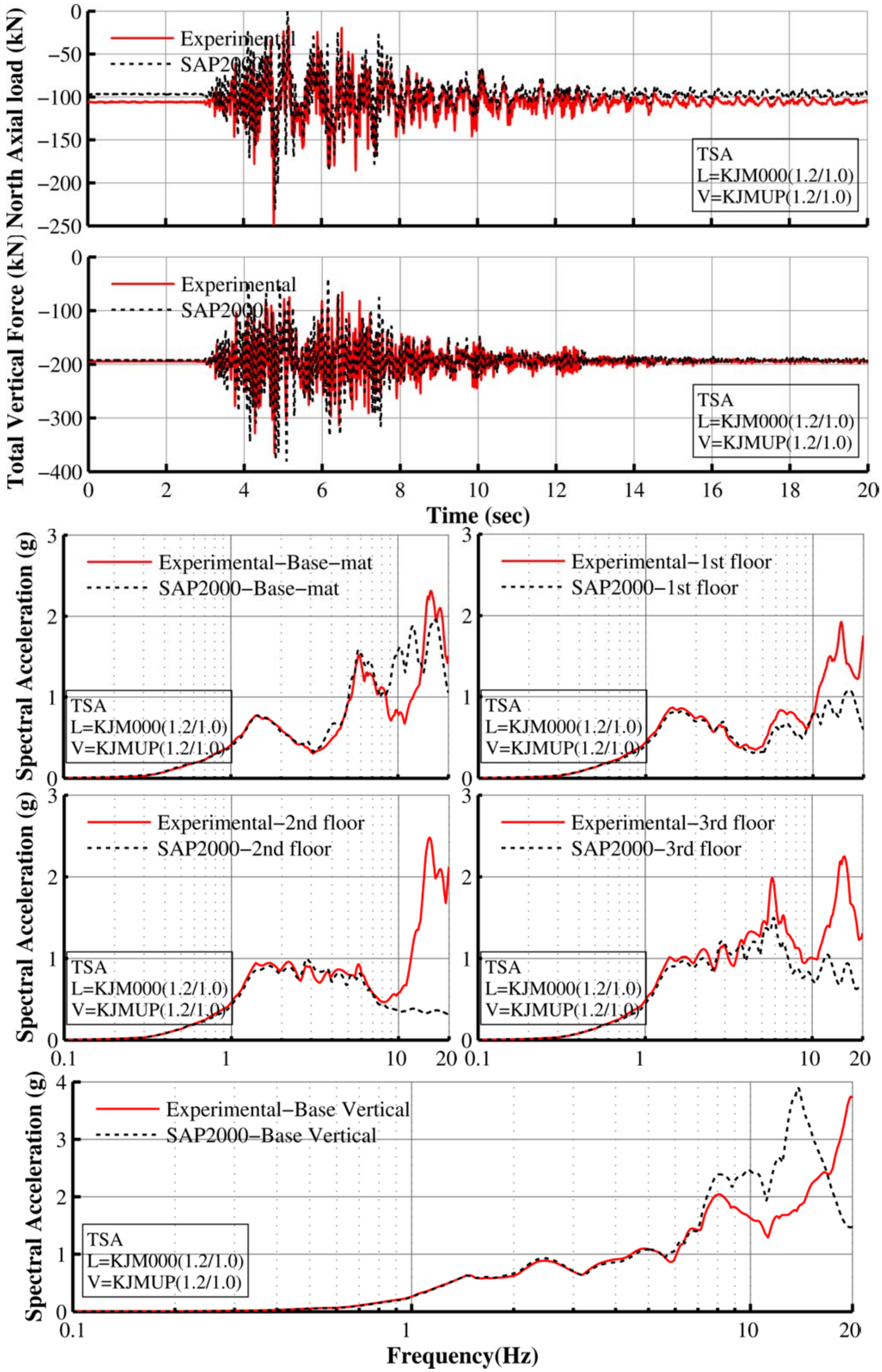
North Axial load (kN)
Experimental
SAP2000
TSA
L=KJM000(1.2/1.0)
V=KJMUP(1.2/1.0)
Total Vertical Force (kN)
Experimental
SAP2000
TSA
L=KJM000(1.2/1.0)
V=KJMUP(1.2/1.0)
Time (sec)
Spectral Acceleration (g)
Experimental−Base−mat
SAP2000−Base−mat
Experimental−1st floor
SAP2000−1st floor
Experimental−2nd floor
SAP2000−2nd floor
Experimental−3rd floor
SAP2000−3rd floor
Experimental−Base Vertical
SAP2000−Base Vertical
TSA
L=KJM000(1.2/1.0)
V=KJMUP(1.2/1.0)
Frequency(Hz)

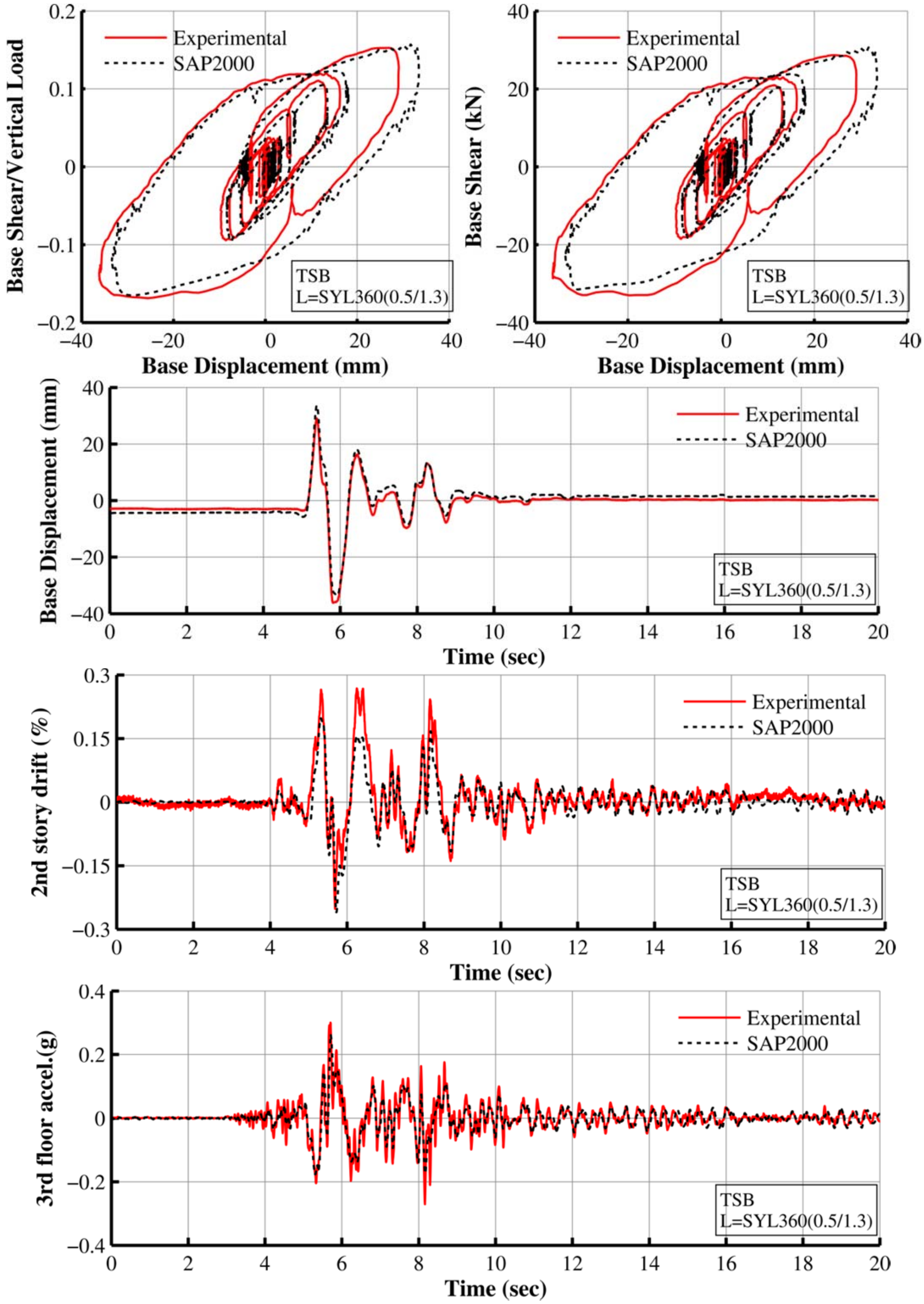
Experimental
SAP2000
TSB
L=SYL360(0.5/1.3)
Base Shear/Vertical Load
Base Displacement (mm)
Base Shear (kN)
Base Displacement (mm)
Time (sec)
2nd story drift (%)
Time (sec)
3rd floor accel.(g)
Time (sec)

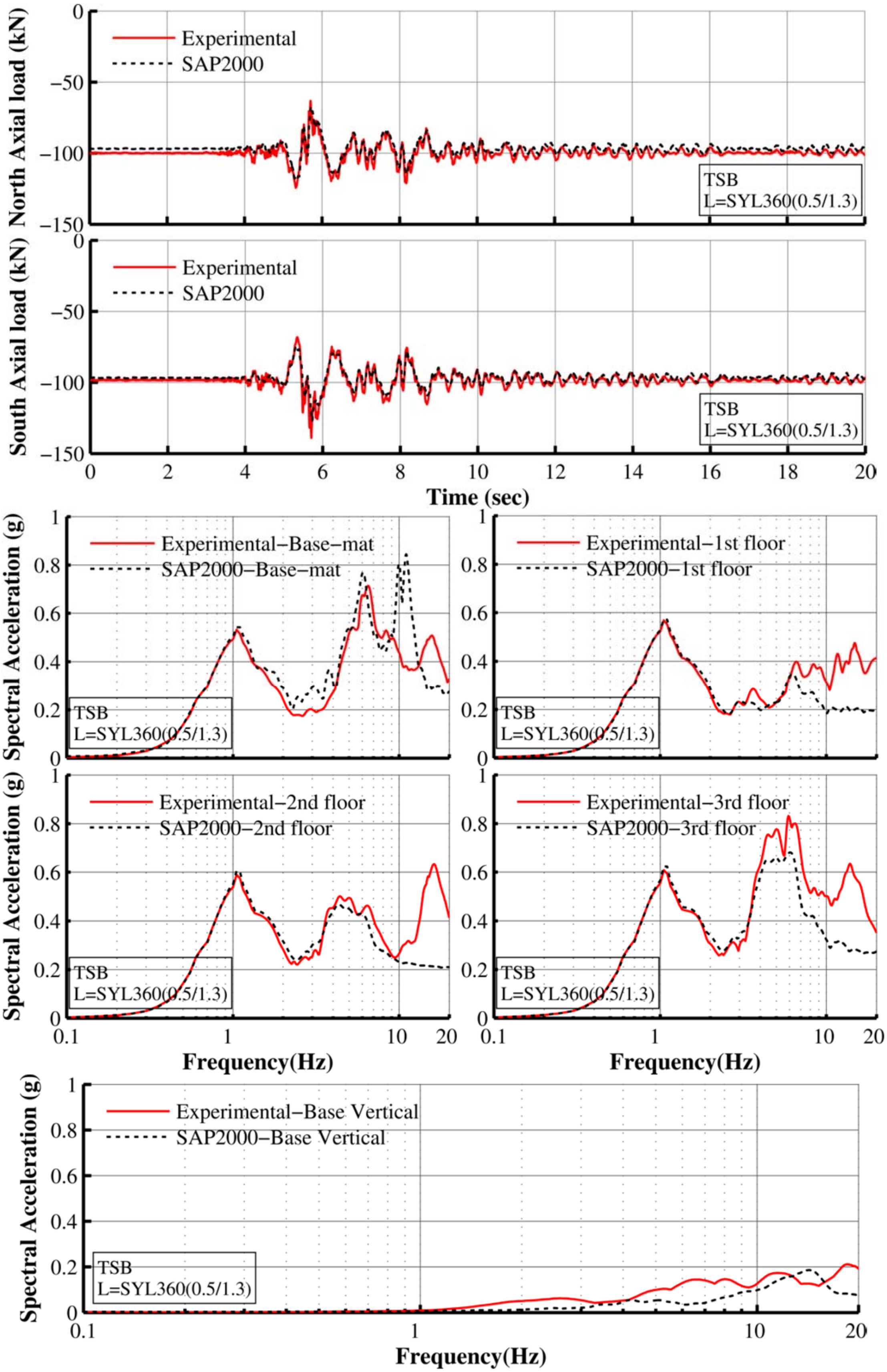
North Axial load (kN)
Experimental
SAP2000
TSB
L=SYL360(0.5/1.3)
South Axial load (kN)
Experimental
SAP2000
TSB
L=SYL360(0.5/1.3)
Time (sec)
Spectral Acceleration (g)
Experimental−Base−mat
SAP2000−Base−mat
Experimental−1st floor
SAP2000−1st floor
Experimental−2nd floor
SAP2000−2nd floor
Experimental−3rd floor
SAP2000−3rd floor
TSB
L=SYL360(0.5/1.3)
Frequency(Hz)
Experimental−Base Vertical
SAP2000−Base Vertical
TSB
L=SYL360(0.5/1.3)
Frequency(Hz)

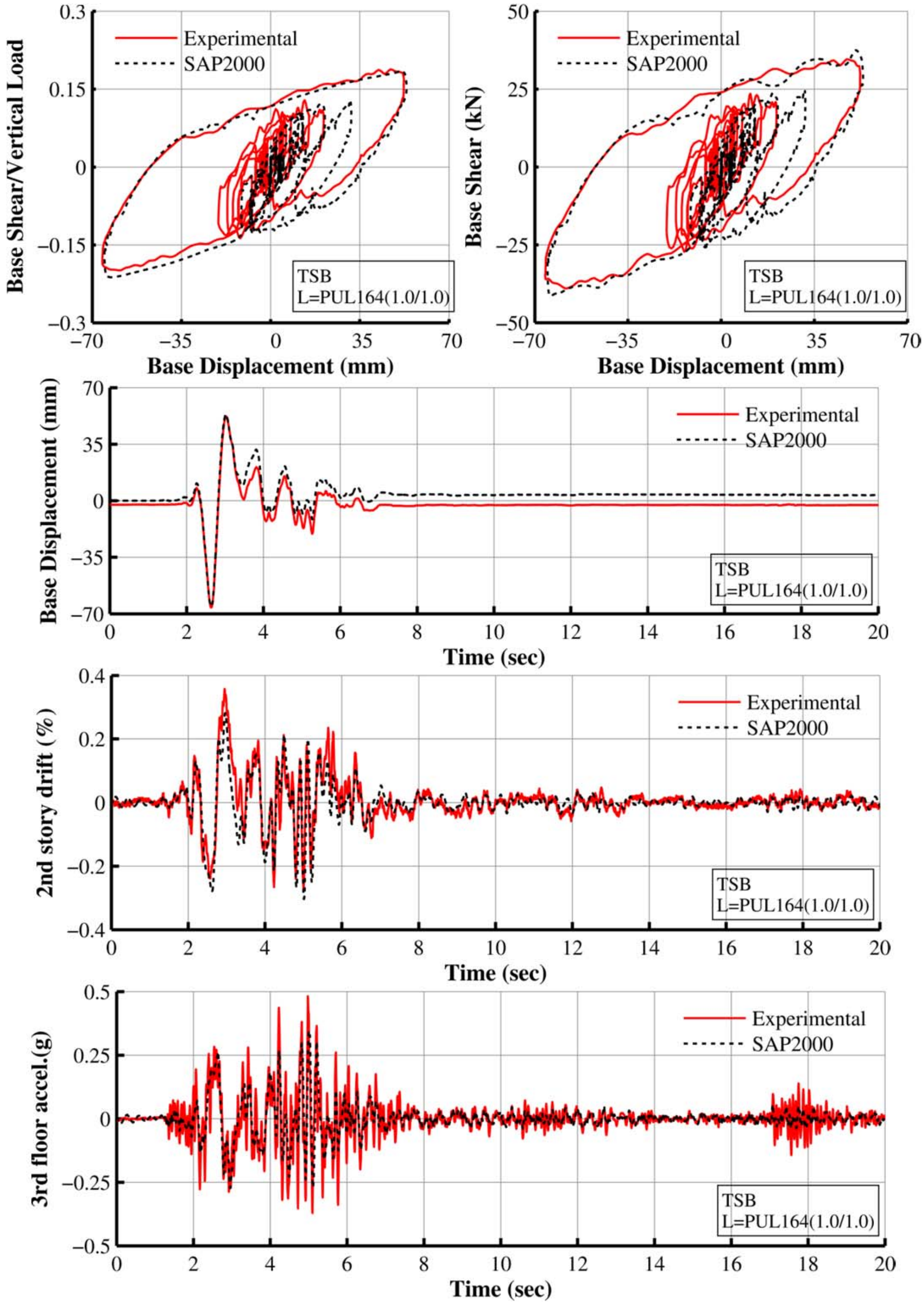
Experimental
SAP2000
Base Shear/Vertical Load
0.3
0.15
0
−0.15
−0.3
−70
−35
0
35
70
Base Displacement (mm)
TSB
L=PUL164(1.0/1.0)
Experimental
SAP2000
Base Shear (kN)
50
25
0
−25
−50
−70
−35
0
35
70
Base Displacement (mm)
TSB
L=PUL164(1.0/1.0)
Experimental
SAP2000
Base Displacement (mm)
70
35
0
−35
−70
0
2
4
6
8
10
12
14
16
18
20
Time (sec)
TSB
L=PUL164(1.0/1.0)
Experimental
SAP2000
2nd story drift (%)
0.4
0.2
0
−0.2
−0.4
0
2
4
6
8
10
12
14
16
18
20
Time (sec)
TSB
L=PUL164(1.0/1.0)
Experimental
SAP2000
3rd floor accel.(g)
0.5
0.25
0
−0.25
−0.5
0
2
4
6
8
10
12
14
16
18
20
Time (sec)
TSB
L=PUL164(1.0/1.0)

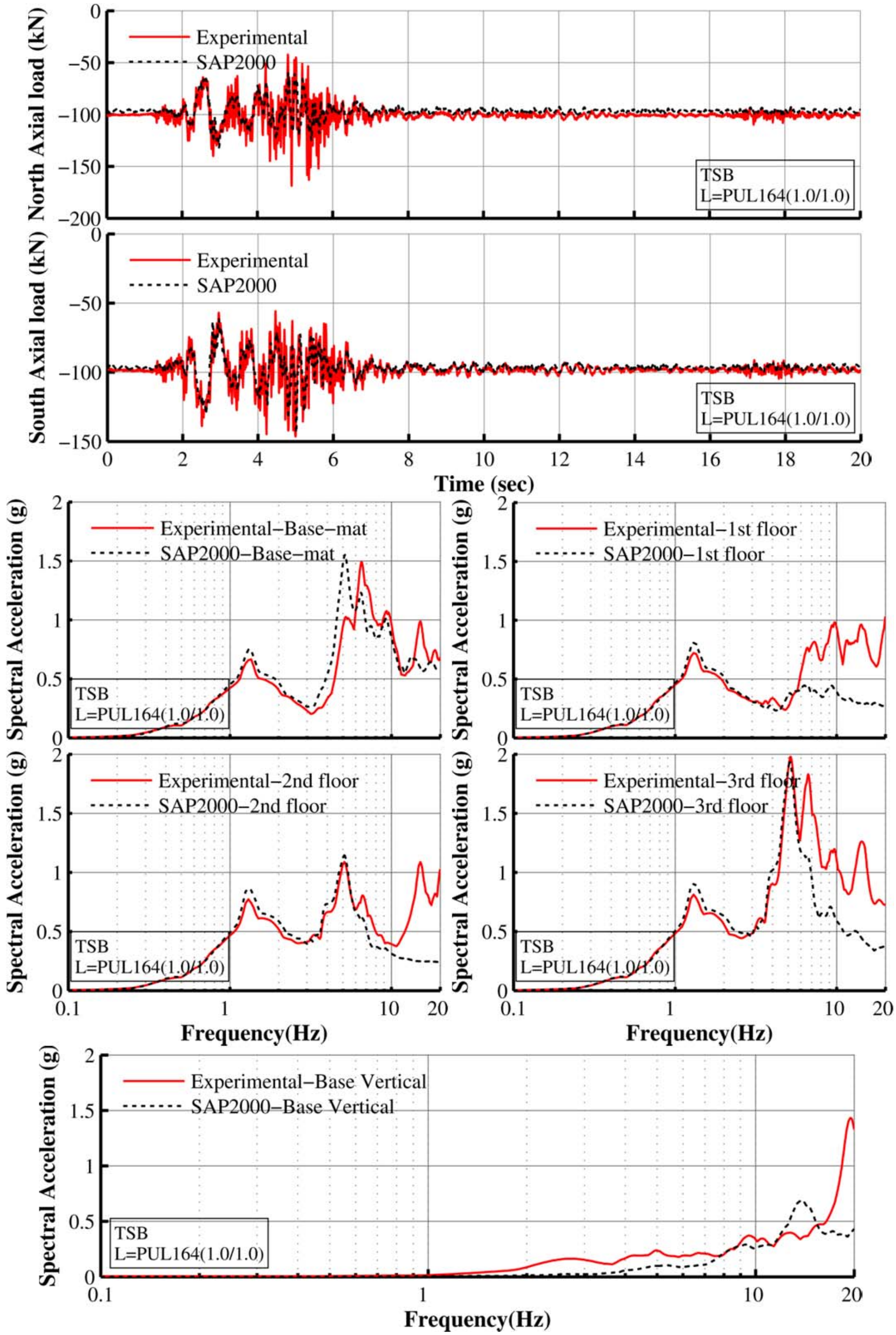

North Axial load (kN)
South Axial load (kN)
Experimental
SAP2000
TSB
L=PUL164(1.0/1.0)
Time (sec)
Spectral Acceleration (g)
Experimental−Base−mat
SAP2000−Base−mat
Experimental−1st floor
SAP2000−1st floor
Experimental−2nd floor
SAP2000−2nd floor
Experimental−3rd floor
SAP2000−3rd floor
Experimental−Base Vertical
SAP2000−Base Vertical
Frequency(Hz)

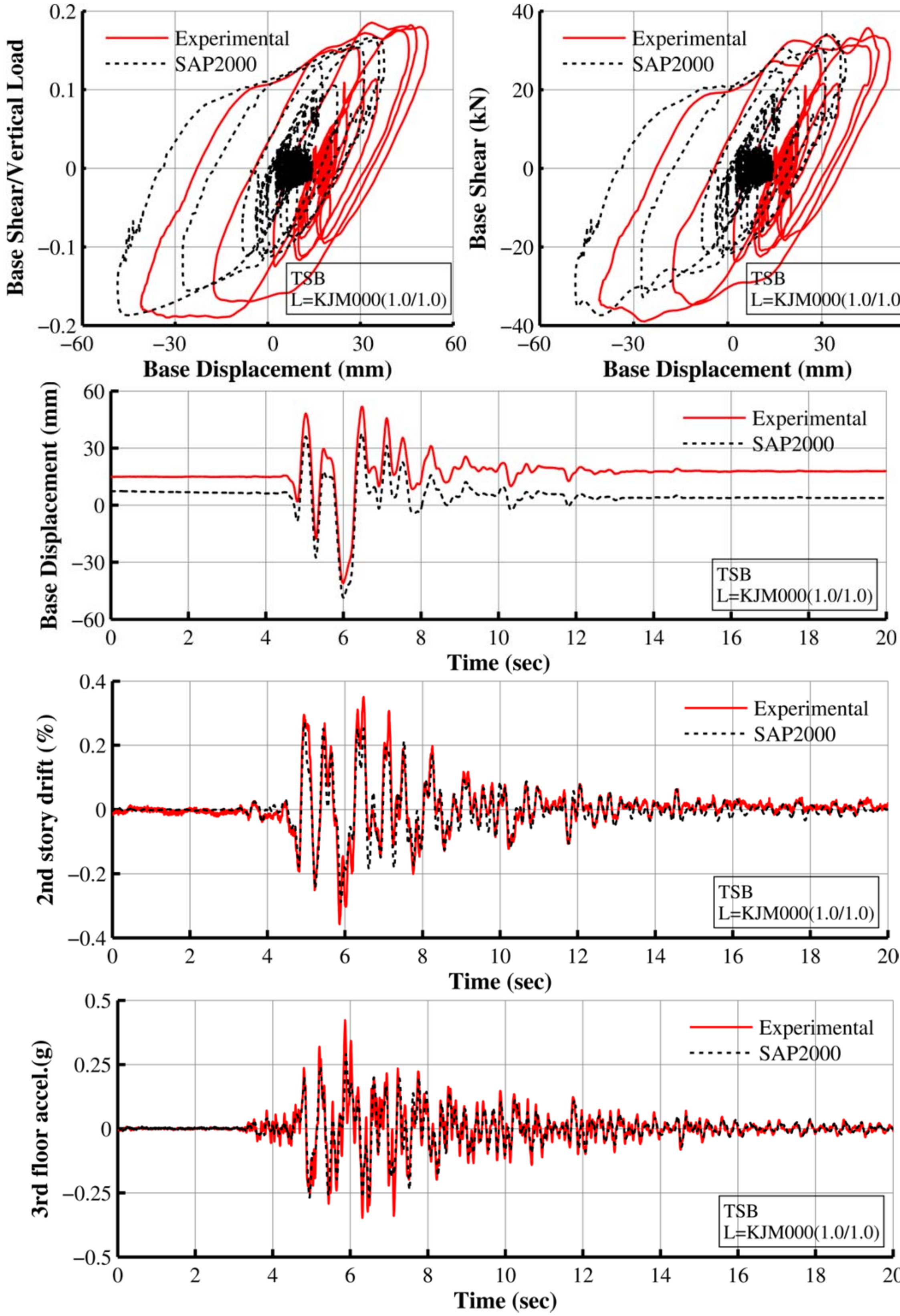
Experimental
SAP2000
TSB
L=KJM000(1.0/1.0)
Base Shear/Vertical Load
Base Displacement (mm)
Base Shear (kN)
Base Displacement (mm)
Time (sec)
2nd story drift (%)
3rd floor accel.(g)

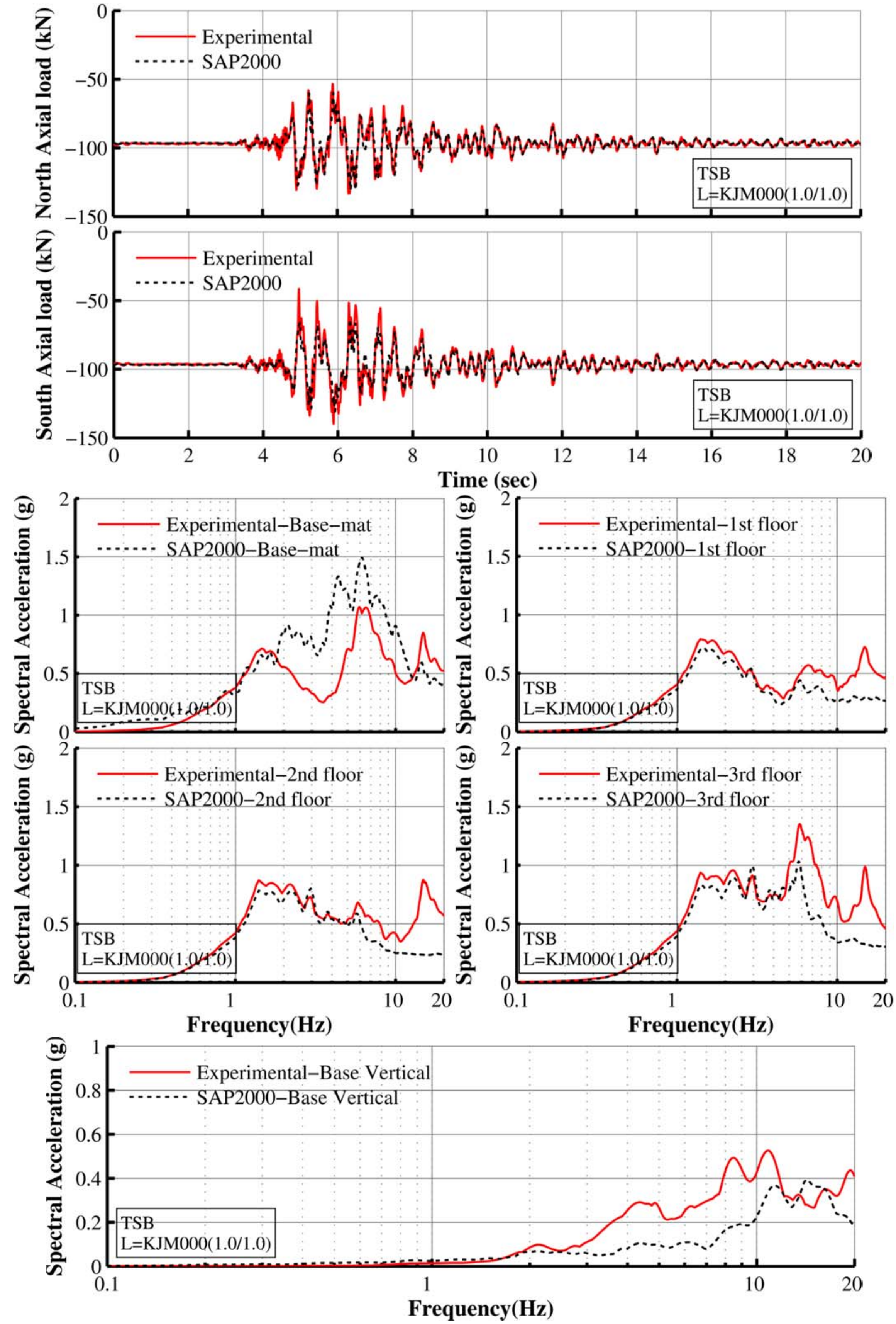

Experimental
SAP2000
North Axial load (kN)
TSB
L=KJM000(1.0/1.0)
South Axial load (kN)
Time (sec)
Experimental−Base−mat
SAP2000−Base−mat
Experimental−1st floor
SAP2000−1st floor
Experimental−2nd floor
SAP2000−2nd floor
Experimental−3rd floor
SAP2000−3rd floor
Spectral Acceleration (g)
Frequency(Hz)
Experimental−Base Vertical
SAP2000−Base Vertical

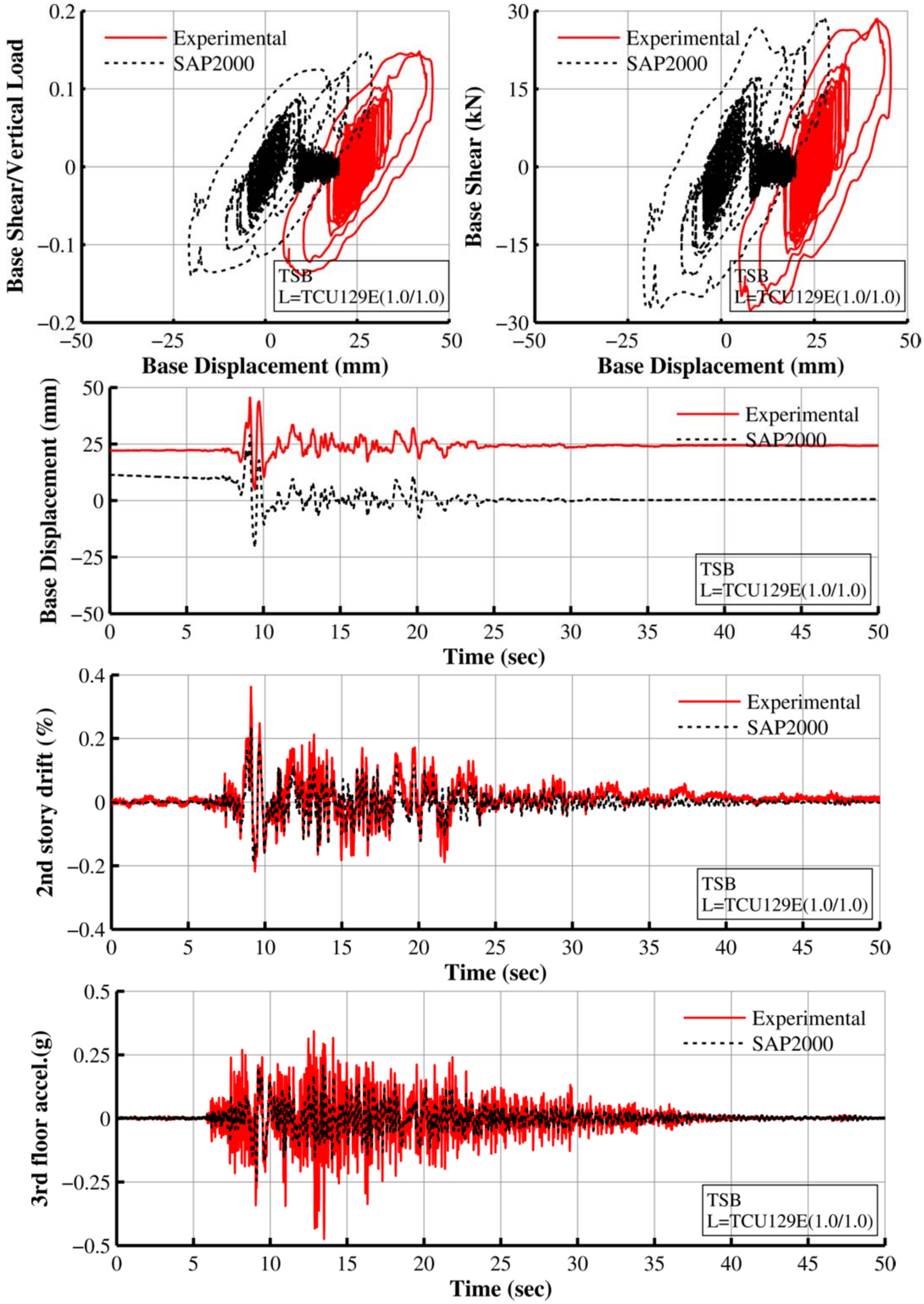
Base Shear/Vertical Load
Base Displacement (mm)
Experimental
SAP2000
TSB
L=TCU129E(1.0/1.0)
Base Shear (kN)
Base Displacement (mm)
Base Displacement (mm)
Time (sec)
2nd story drift (%)
Time (sec)
3rd floor accel.(g)
Time (sec)

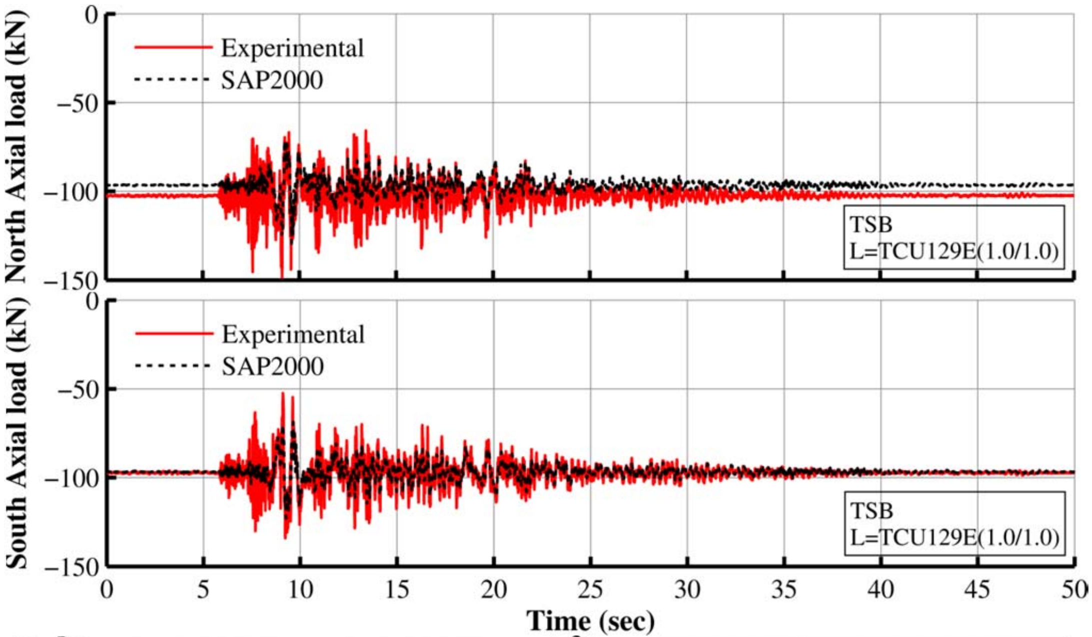
North Axial load (kN)
South Axial load (kN)
Experimental
SAP2000
TSB
L=TCU129E(1.0/1.0)
Time (sec)

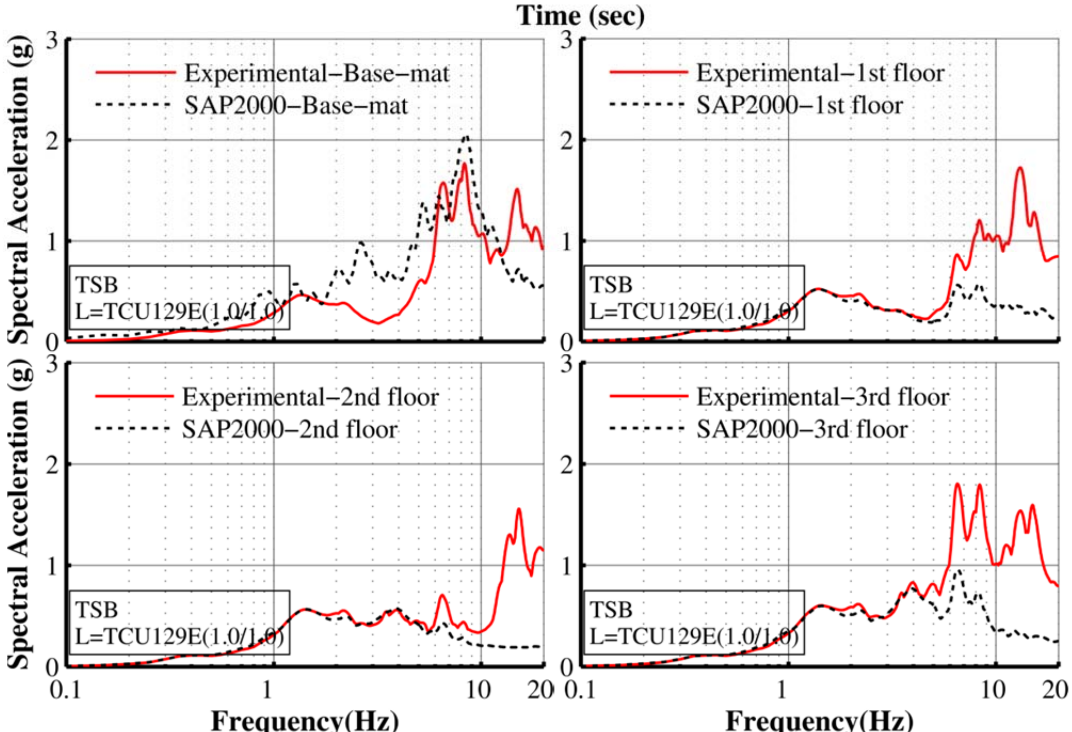
Spectral Acceleration (g)
Experimental−Base−mat
SAP2000−Base−mat
Experimental−1st floor
SAP2000−1st floor
Experimental−2nd floor
SAP2000−2nd floor
Experimental−3rd floor
SAP2000−3rd floor
TSB
L=TCU129E(1.0/1.0)
Frequency(Hz)

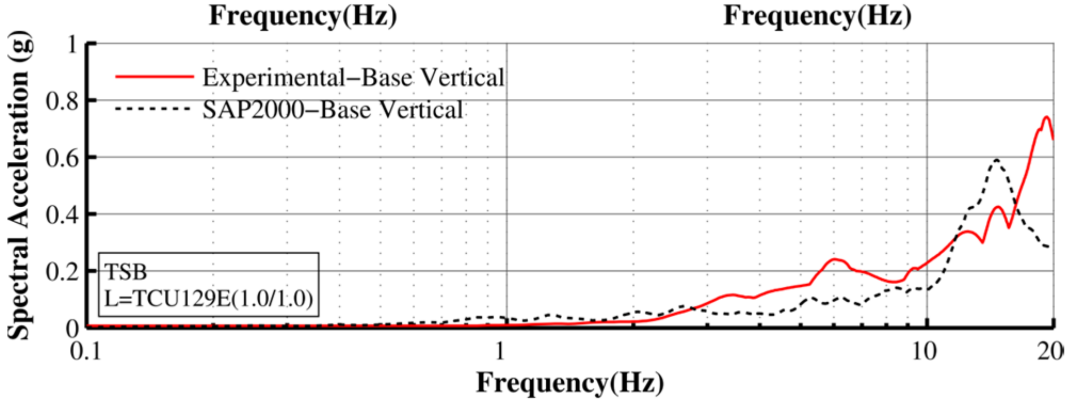
Spectral Acceleration (g)
Experimental−Base Vertical
SAP2000−Base Vertical
TSB
L=TCU129E(1.0/1.0)
Frequency(Hz)

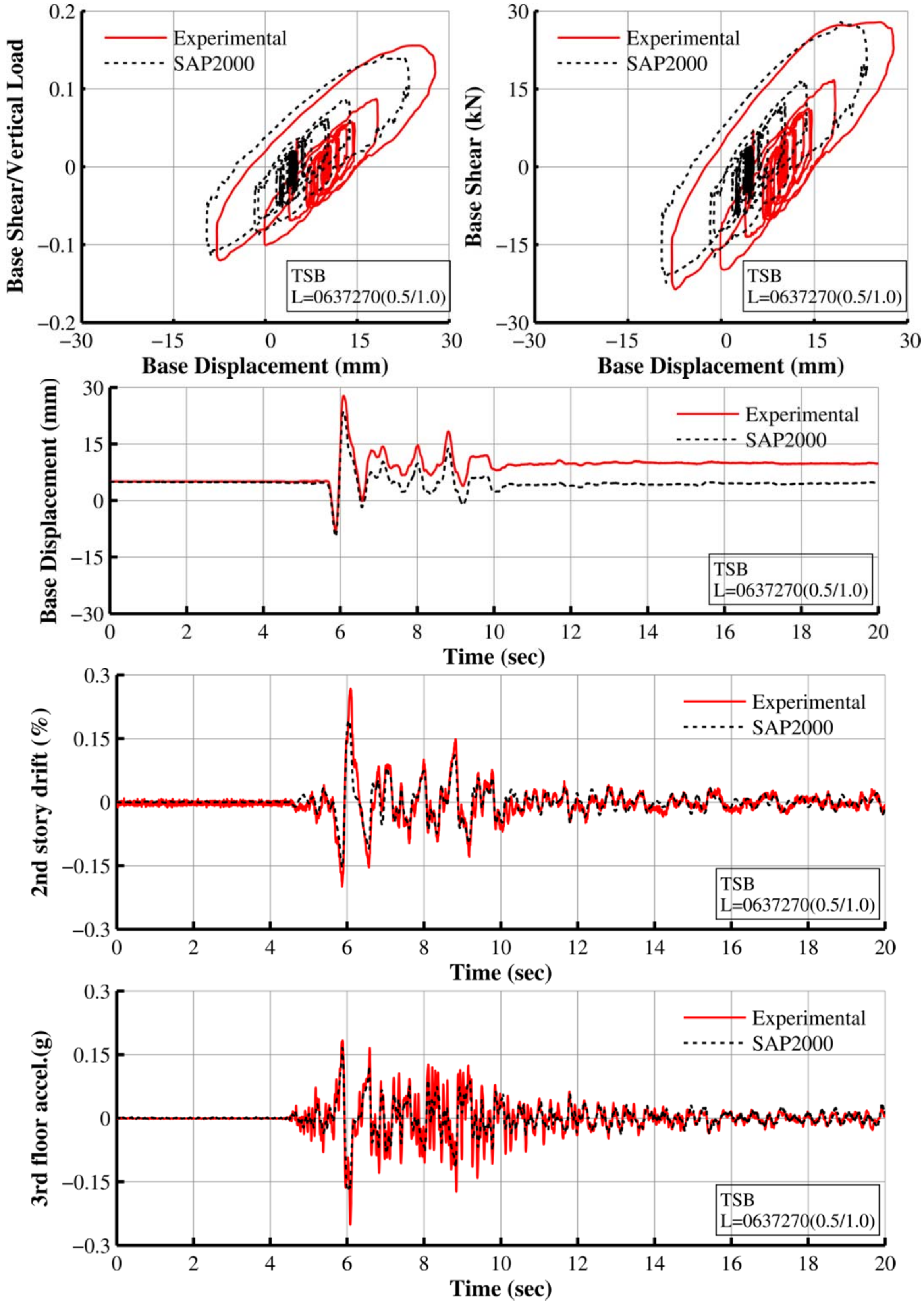
Base Shear/Vertical Load
Base Displacement (mm)
Base Shear (kN)
Base Displacement (mm)
Experimental
SAP2000
TSB
L=0637270(0.5/1.0)
Base Displacement (mm)
Time (sec)
2nd story drift (%)
Time (sec)
3rd floor accel.(g)
Time (sec)

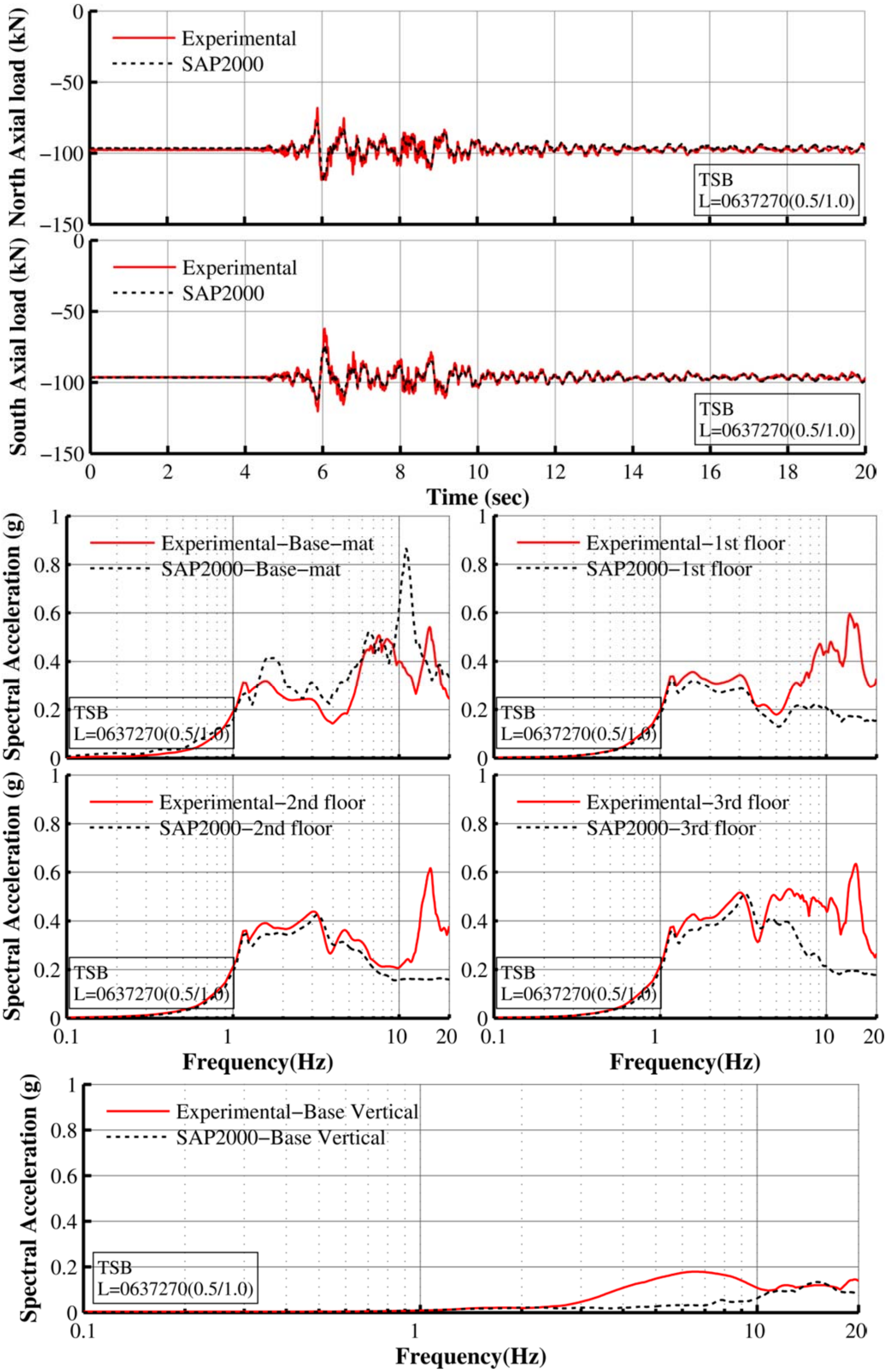

Experimental
SAP2000
North Axial load (kN)
TSB
L=0637270(0.5/1.0)
South Axial load (kN)
Time (sec)
Experimental−Base−mat
SAP2000−Base−mat
Experimental−1st floor
SAP2000−1st floor
Experimental−2nd floor
SAP2000−2nd floor
Experimental−3rd floor
SAP2000−3rd floor
Spectral Acceleration (g)
Frequency(Hz)
Experimental−Base Vertical
SAP2000−Base Vertical

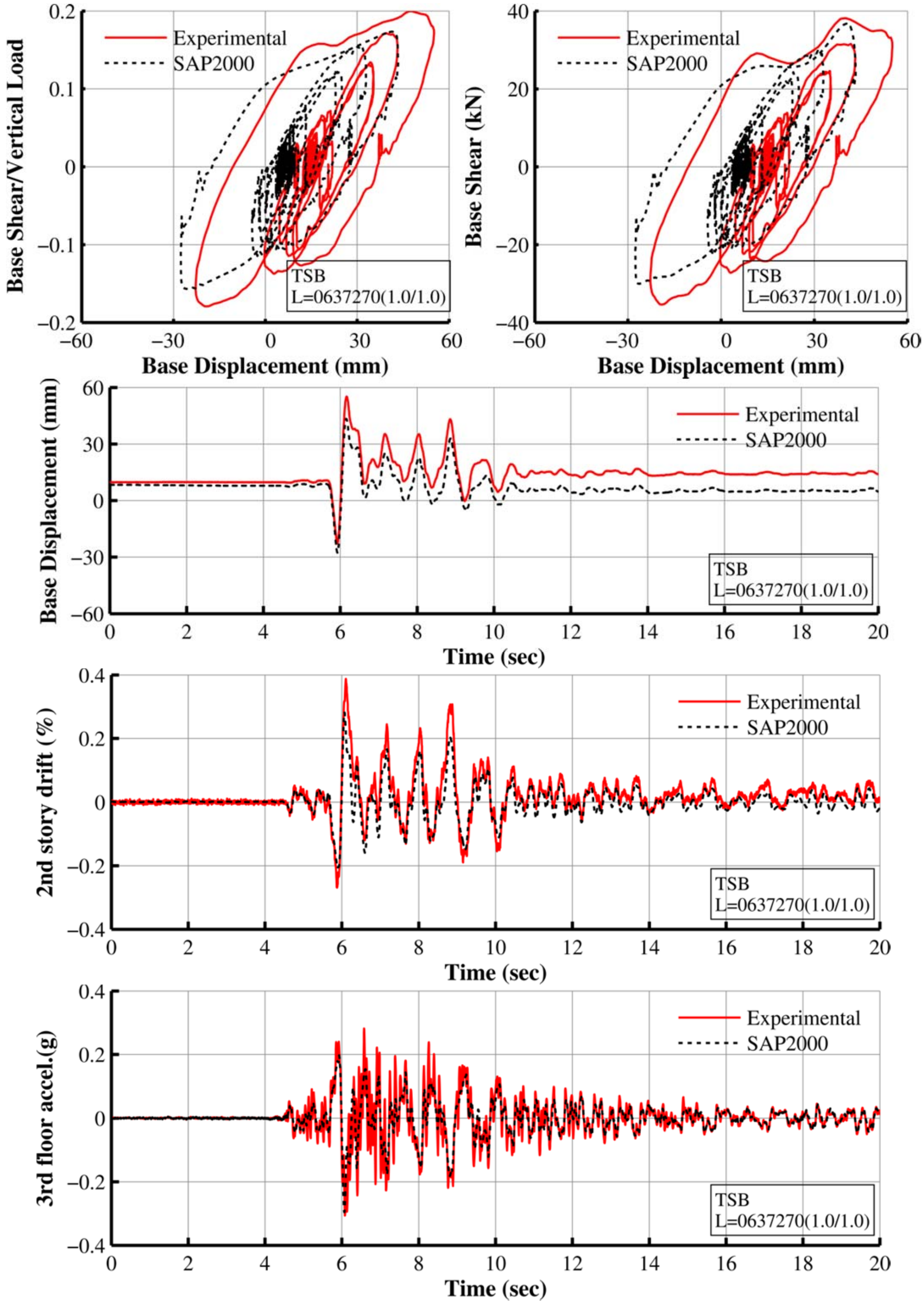

Base Shear/Vertical Load
Base Shear (kN)
Base Displacement (mm)
Base Displacement (mm)
Base Displacement (mm)
Time (sec)
2nd story drift (%)
Time (sec)
3rd floor accel.(g)
Time (sec)
Experimental
SAP2000
TSB
L=0637270(1.0/1.0)

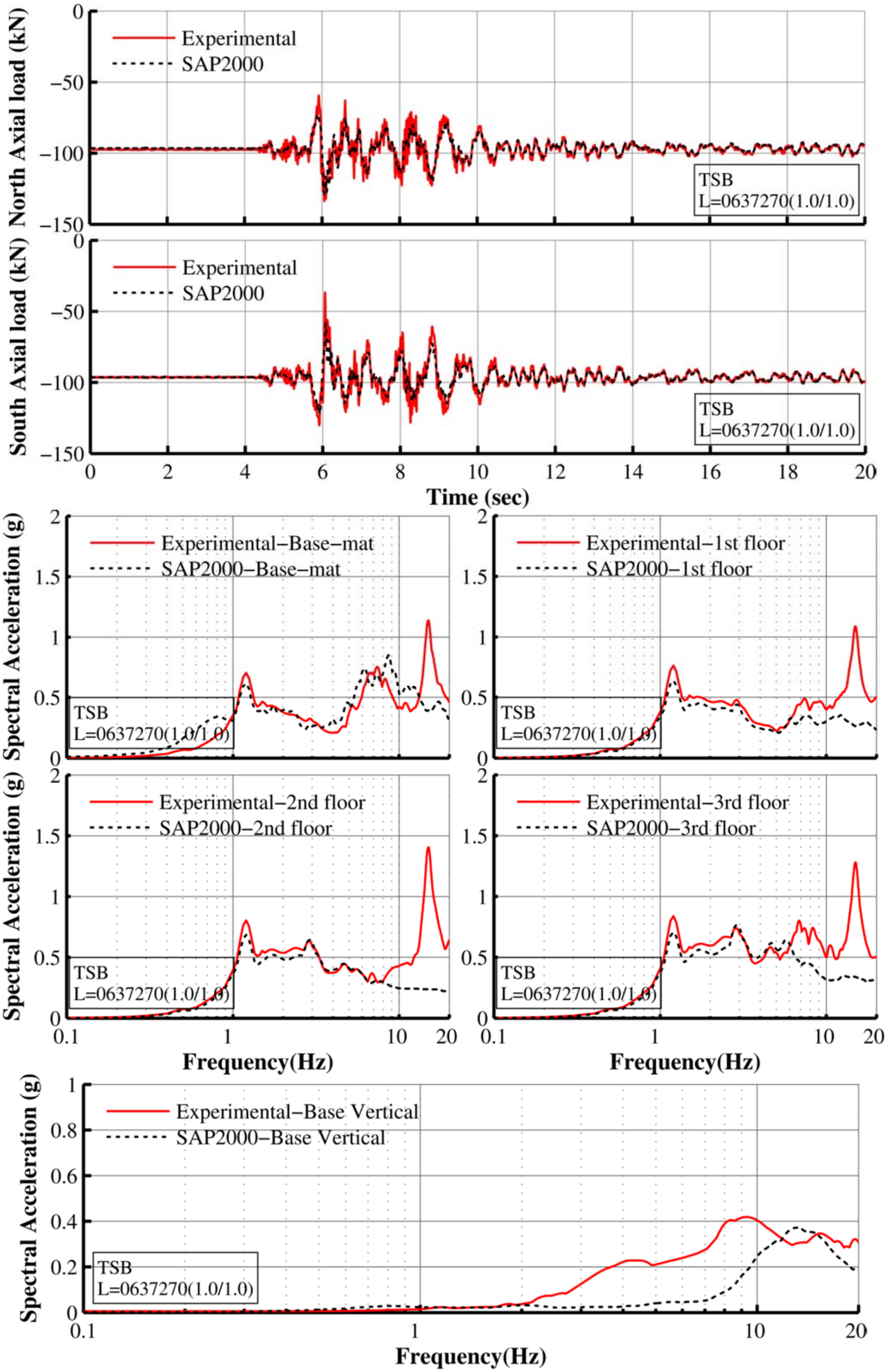

North Axial load (kN)
South Axial load (kN)
Experimental
SAP2000
TSB
L=0637270(1.0/1.0)
Time (sec)
Spectral Acceleration (g)
Experimental−Base−mat
SAP2000−Base−mat
Experimental−1st floor
SAP2000−1st floor
Experimental−2nd floor
SAP2000−2nd floor
Experimental−3rd floor
SAP2000−3rd floor
Experimental−Base Vertical
SAP2000−Base Vertical
Frequency(Hz)

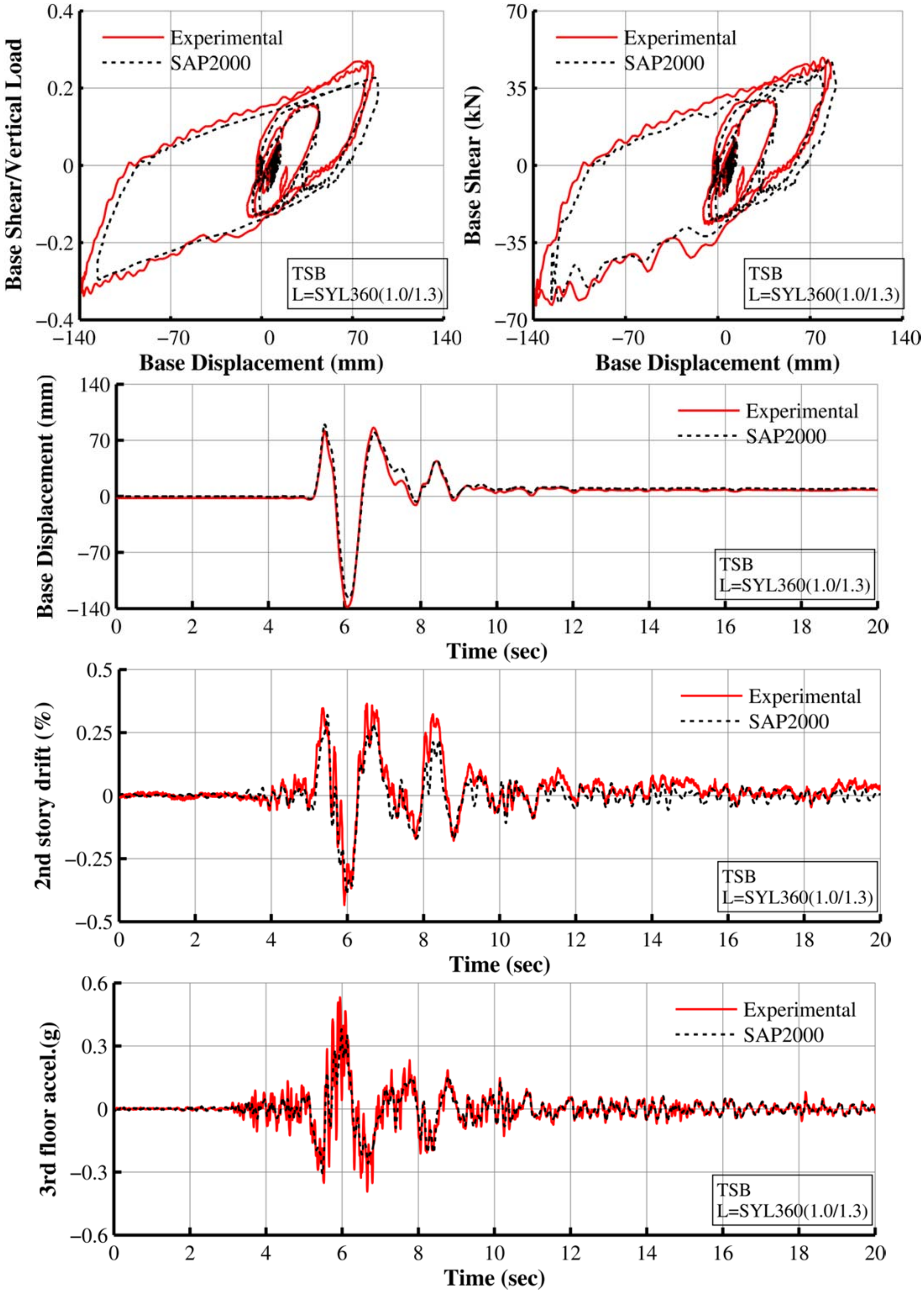

Experimental
SAP2000
TSB
L=SYL360(1.0/1.3)
Base Shear/Vertical Load
Base Displacement (mm)
Base Shear (kN)
Base Displacement (mm)
Time (sec)
2nd story drift (%)
3rd floor accel.(g)

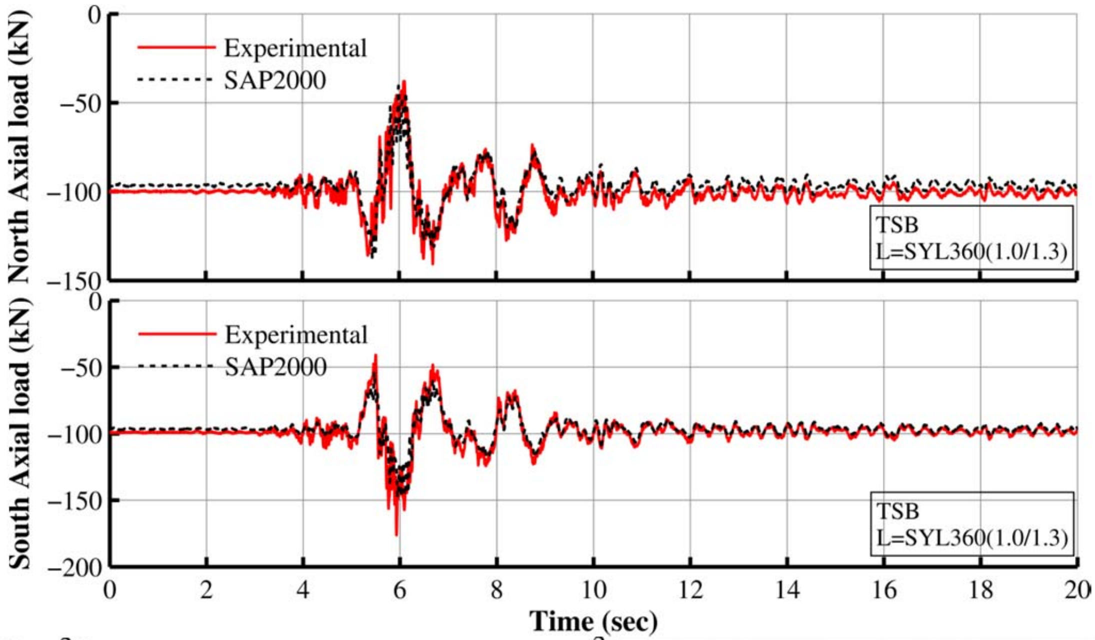
North Axial load (kN)
South Axial load (kN)
Experimental
SAP2000
TSB
L=SYL360(1.0/1.3)
Time (sec)

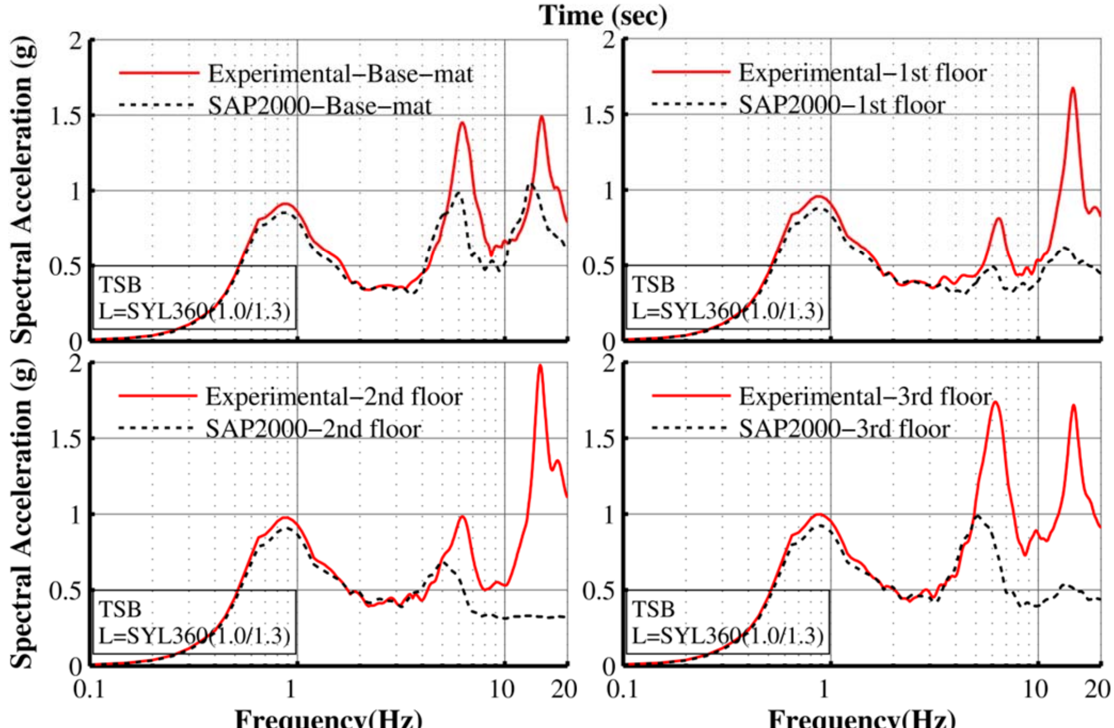
Spectral Acceleration (g)
Experimental−Base−mat
SAP2000−Base−mat
Experimental−1st floor
SAP2000−1st floor
Experimental−2nd floor
SAP2000−2nd floor
Experimental−3rd floor
SAP2000−3rd floor
TSB
L=SYL360(1.0/1.3)
Frequency(Hz)

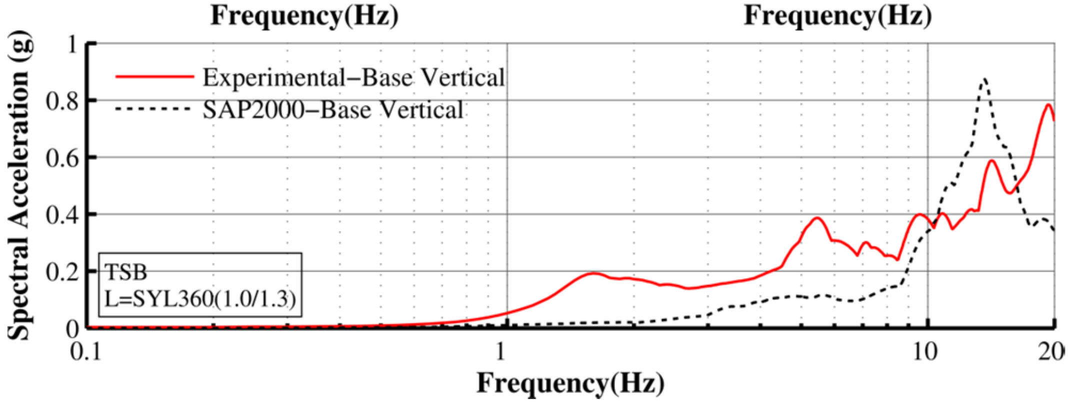
Spectral Acceleration (g)
Experimental−Base Vertical
SAP2000−Base Vertical
TSB
L=SYL360(1.0/1.3)
Frequency(Hz)

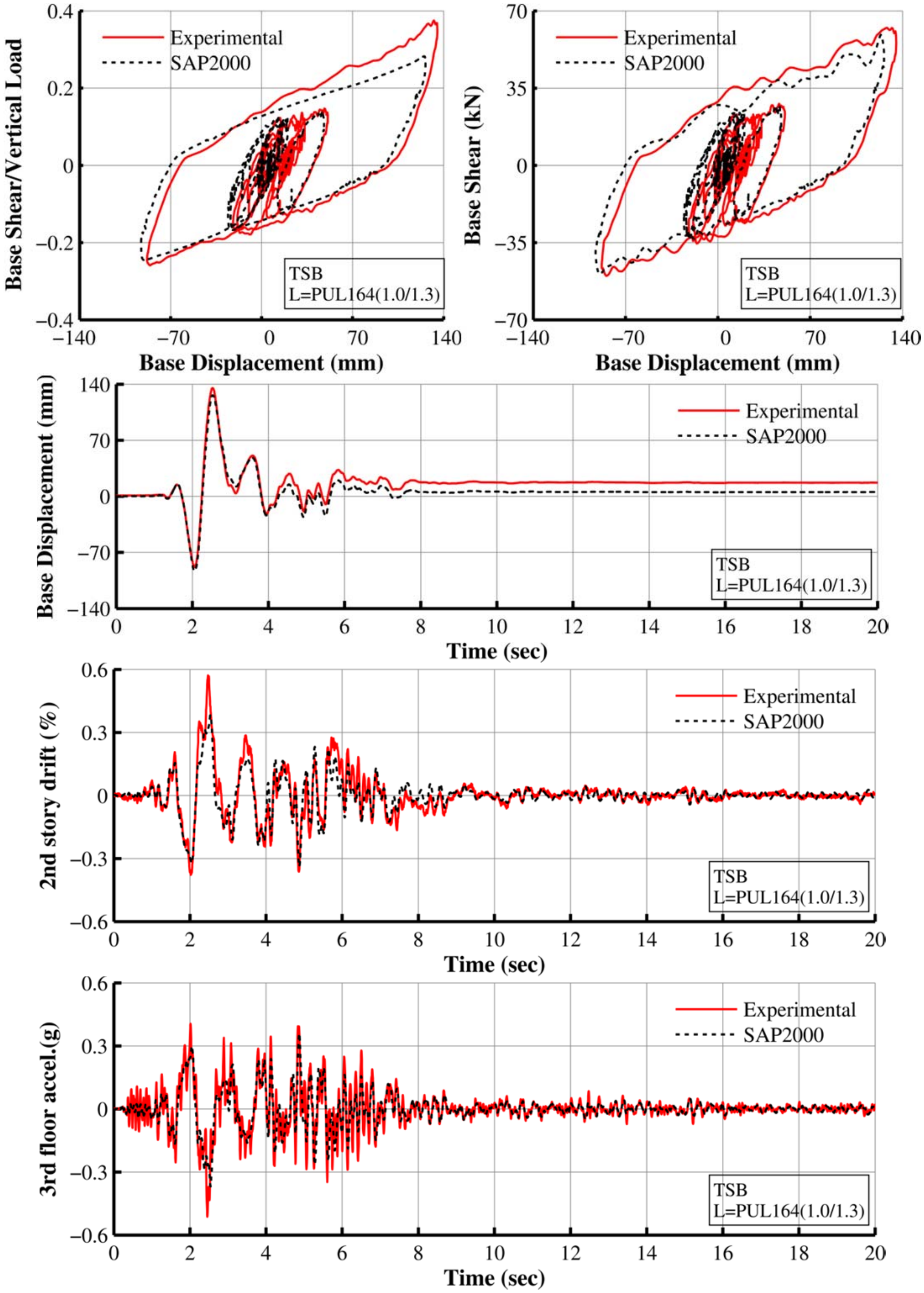
Base Shear/Vertical Load
Base Displacement (mm)
Experimental
SAP2000
TSB
L=PUL164(1.0/1.3)
Base Shear (kN)
Base Displacement (mm)
Experimental
SAP2000
TSB
L=PUL164(1.0/1.3)
Base Displacement (mm)
Time (sec)
Experimental
SAP2000
TSB
L=PUL164(1.0/1.3)
2nd story drift (%)
Time (sec)
Experimental
SAP2000
TSB
L=PUL164(1.0/1.3)
3rd floor accel.(g)
Time (sec)
Experimental
SAP2000
TSB
L=PUL164(1.0/1.3)

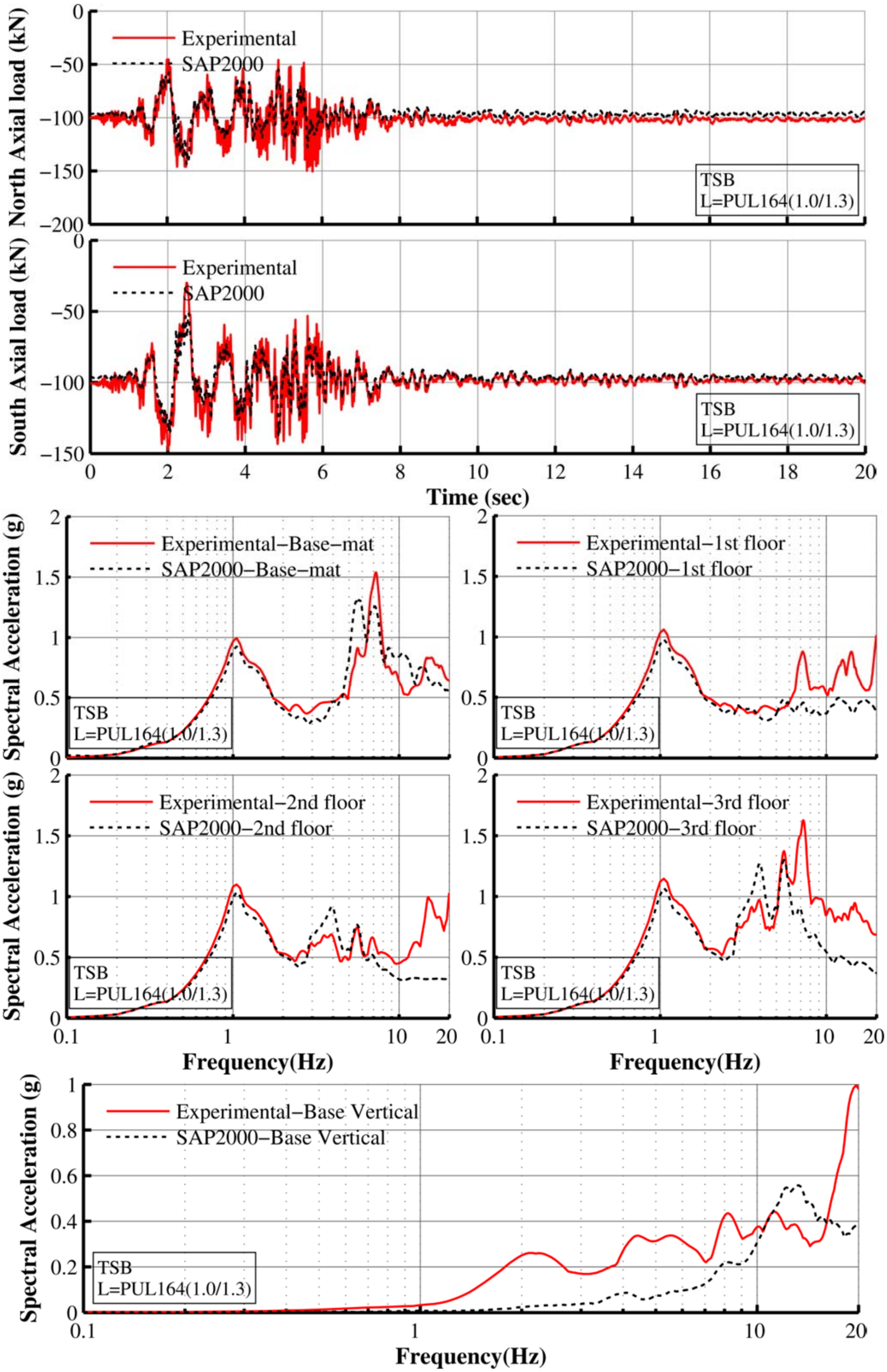
Experimental
SAP2000
TSB
L=PUL164(1.0/1.3)
North Axial load (kN)
South Axial load (kN)
Time (sec)
Experimental−Base−mat
SAP2000−Base−mat
Experimental−1st floor
SAP2000−1st floor
Experimental−2nd floor
SAP2000−2nd floor
Experimental−3rd floor
SAP2000−3rd floor
Spectral Acceleration (g)
Frequency(Hz)
Experimental−Base Vertical
SAP2000−Base Vertical

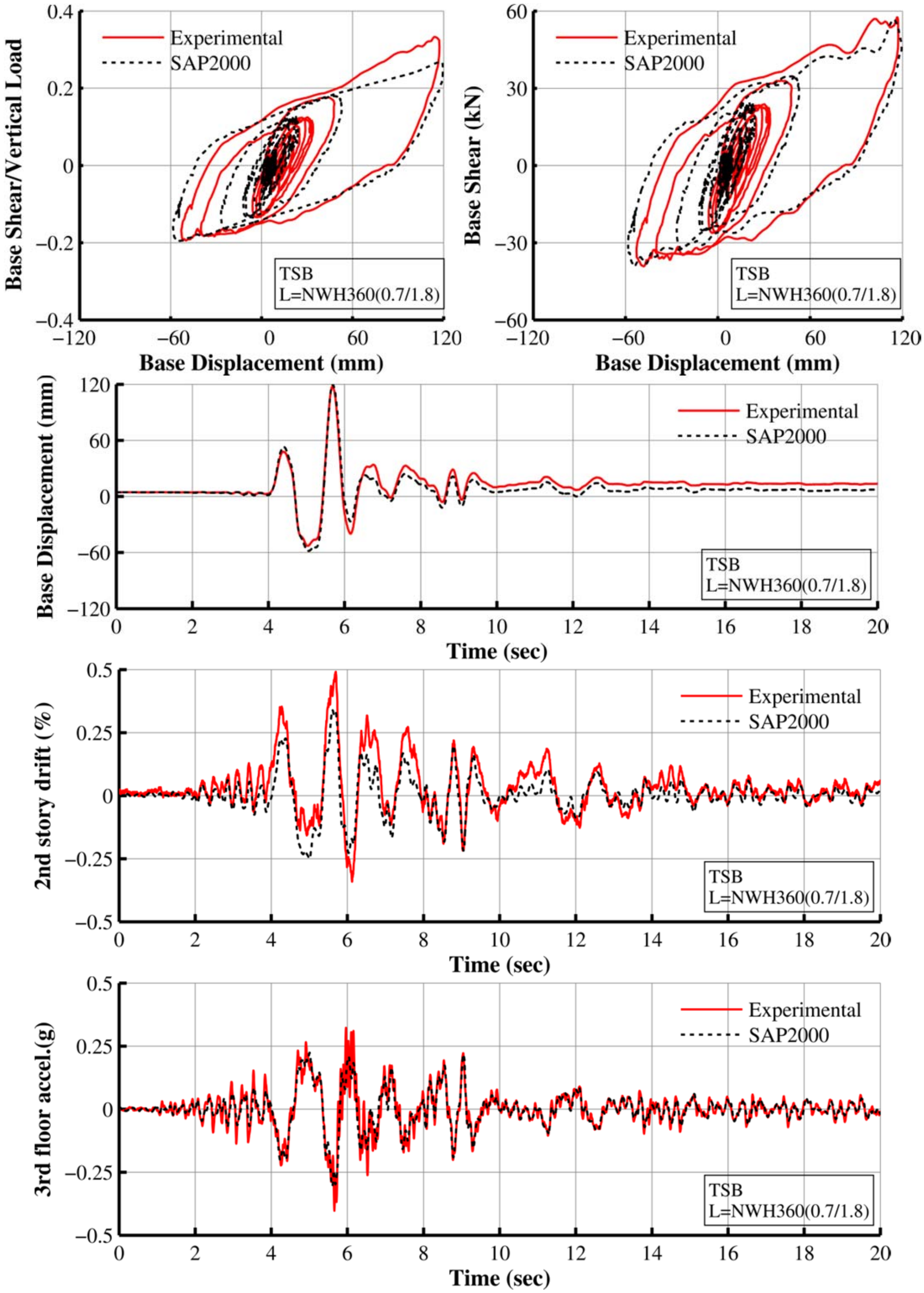

Experimental
SAP2000
TSB
L=NWH360(0.7/1.8)
Base Shear/Vertical Load
Base Displacement (mm)
Base Shear (kN)
Base Displacement (mm)
Time (sec)
2nd story drift (%)
3rd floor accel.(g)

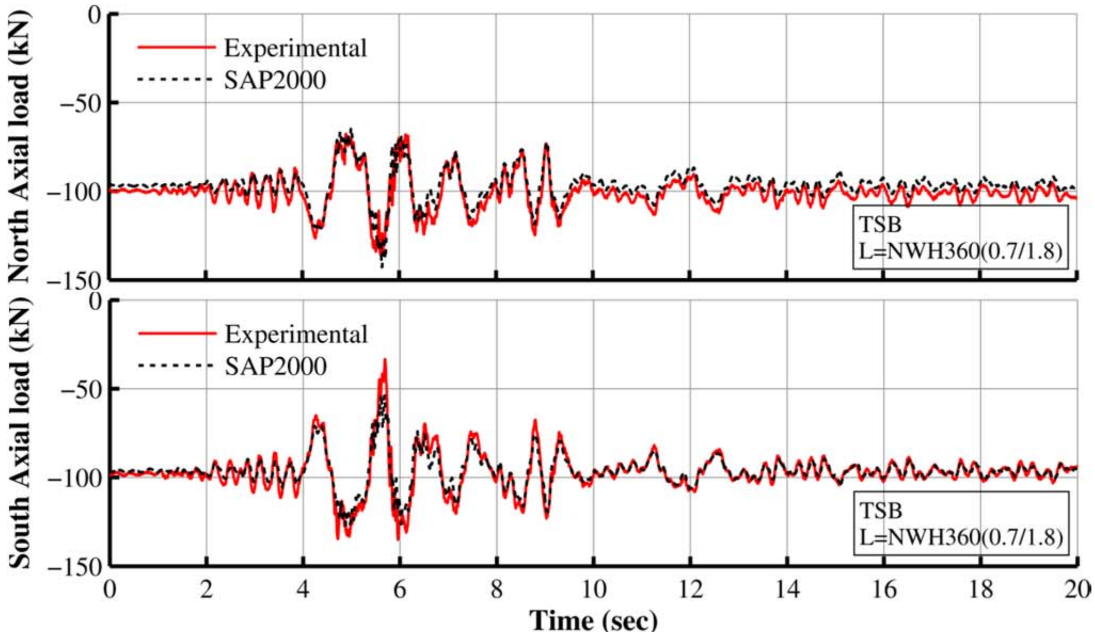
North Axial load (kN)
South Axial load (kN)
Experimental
SAP2000
TSB
L=NWH360(0.7/1.8)
Time (sec)

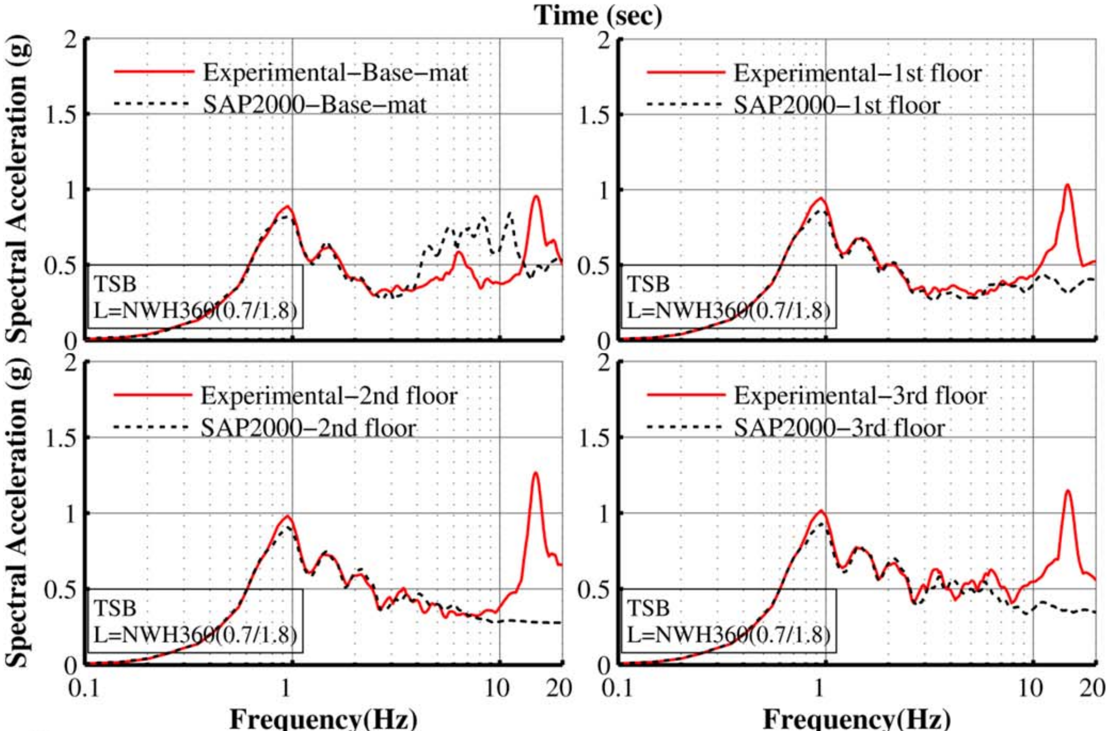
Spectral Acceleration (g)
Experimental−Base−mat
SAP2000−Base−mat
Experimental−1st floor
SAP2000−1st floor
Experimental−2nd floor
SAP2000−2nd floor
Experimental−3rd floor
SAP2000−3rd floor
TSB
L=NWH360(0.7/1.8)
Frequency(Hz)

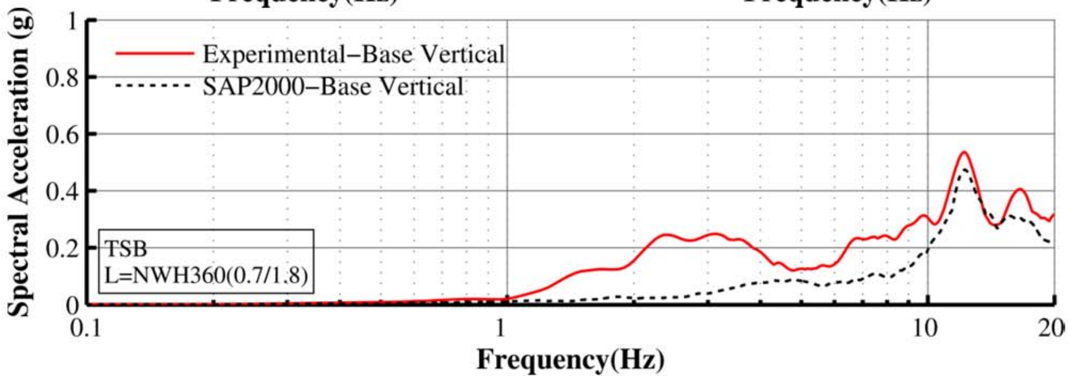
Spectral Acceleration (g)
Experimental−Base Vertical
SAP2000−Base Vertical
TSB
L=NWH360(0.7/1.8)
Frequency(Hz)

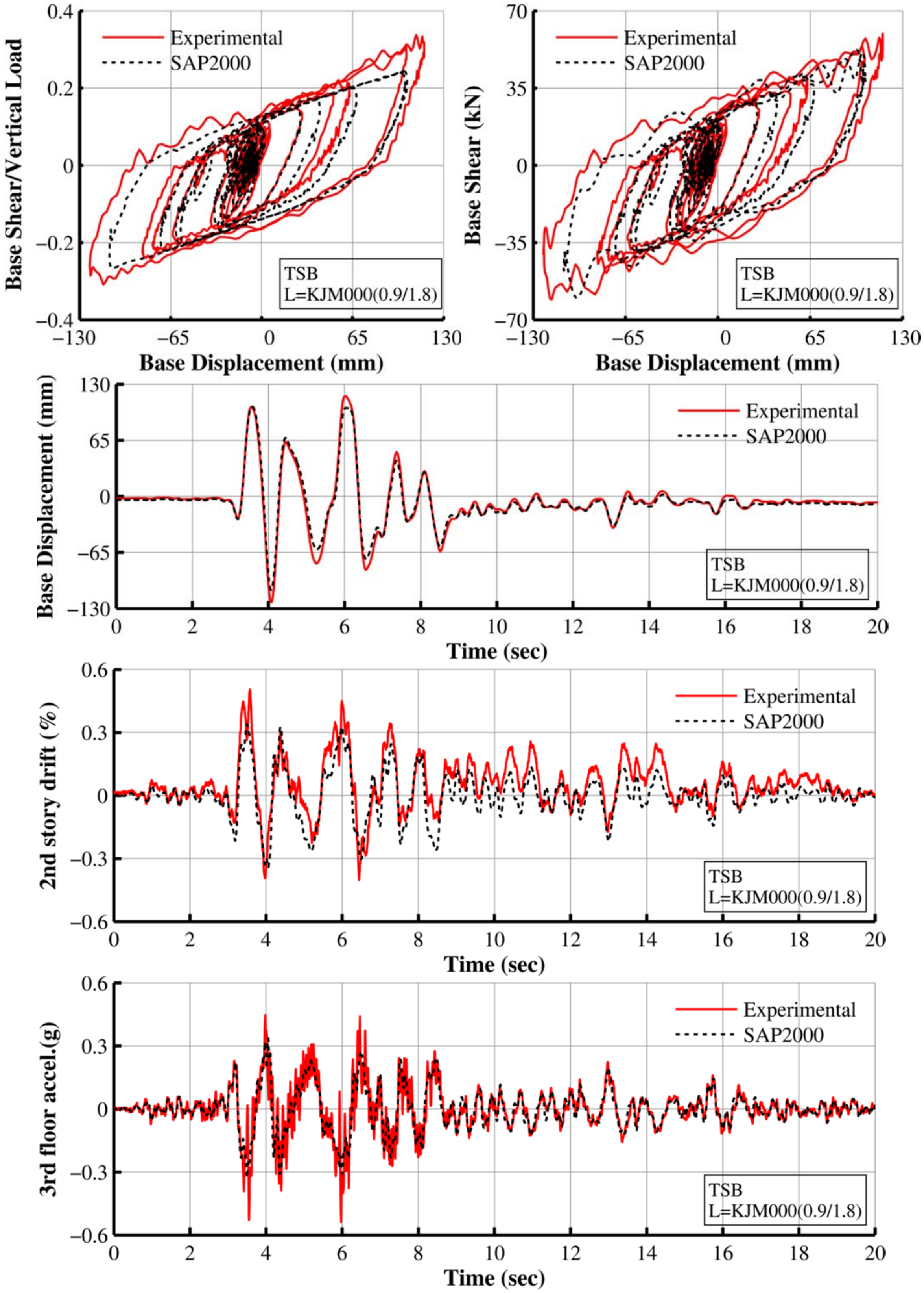
Base Shear/Vertical Load
Base Displacement (mm)
Experimental
SAP2000
TSB
L=KJM000(0.9/1.8)
Base Shear (kN)
Base Displacement (mm)
Experimental
SAP2000
TSB
L=KJM000(0.9/1.8)
Base Displacement (mm)
Time (sec)
Experimental
SAP2000
TSB
L=KJM000(0.9/1.8)
2nd story drift (%)
Time (sec)
Experimental
SAP2000
TSB
L=KJM000(0.9/1.8)
3rd floor accel.(g)
Time (sec)
Experimental
SAP2000
TSB
L=KJM000(0.9/1.8)

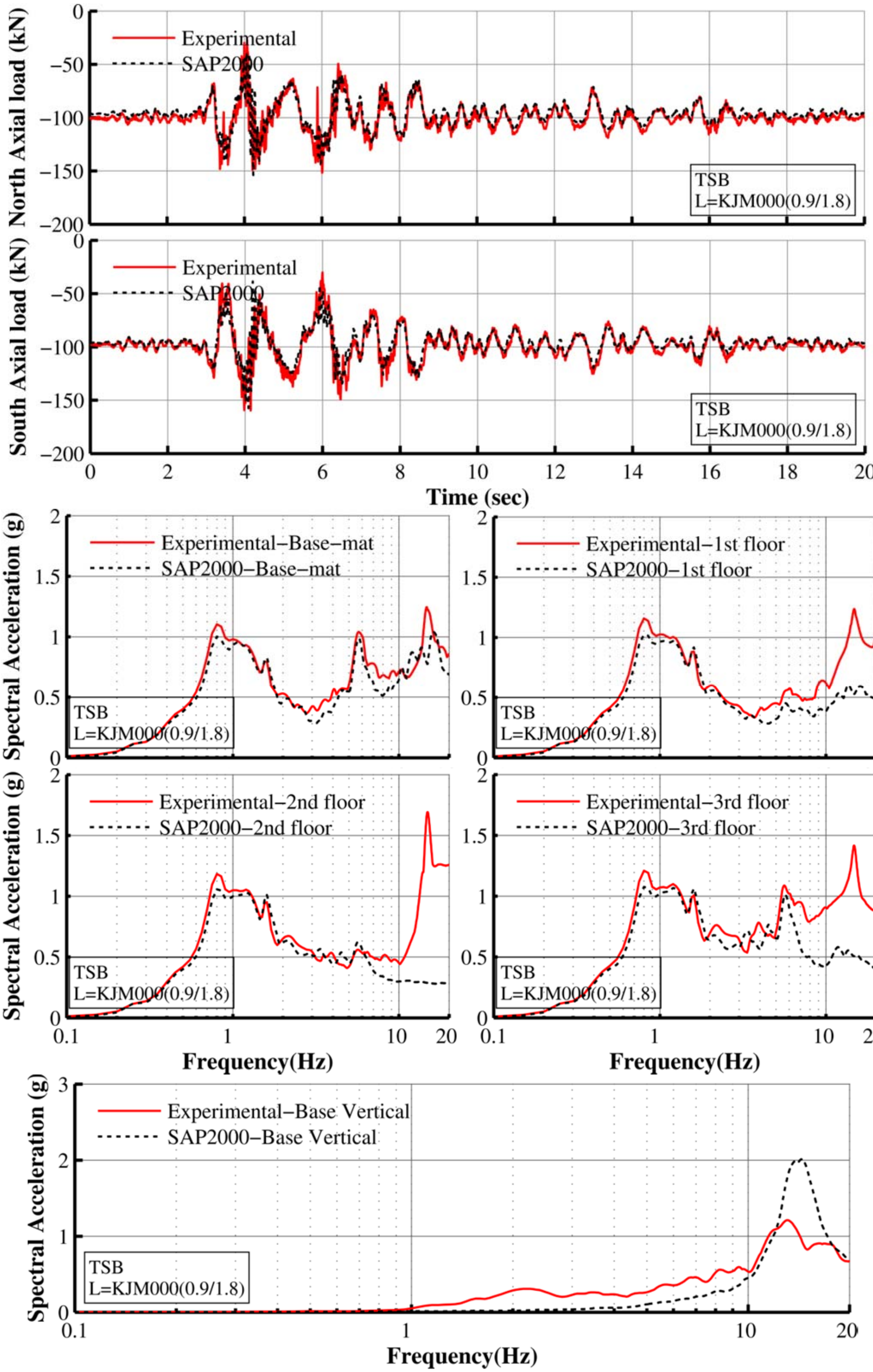

North Axial load (kN)
South Axial load (kN)
Experimental
SAP2000
TSB
L=KJM000(0.9/1.8)
Time (sec)
Spectral Acceleration (g)
Experimental−Base−mat
SAP2000−Base−mat
Experimental−1st floor
SAP2000−1st floor
Experimental−2nd floor
SAP2000−2nd floor
Experimental−3rd floor
SAP2000−3rd floor
Experimental−Base Vertical
SAP2000−Base Vertical
Frequency(Hz)

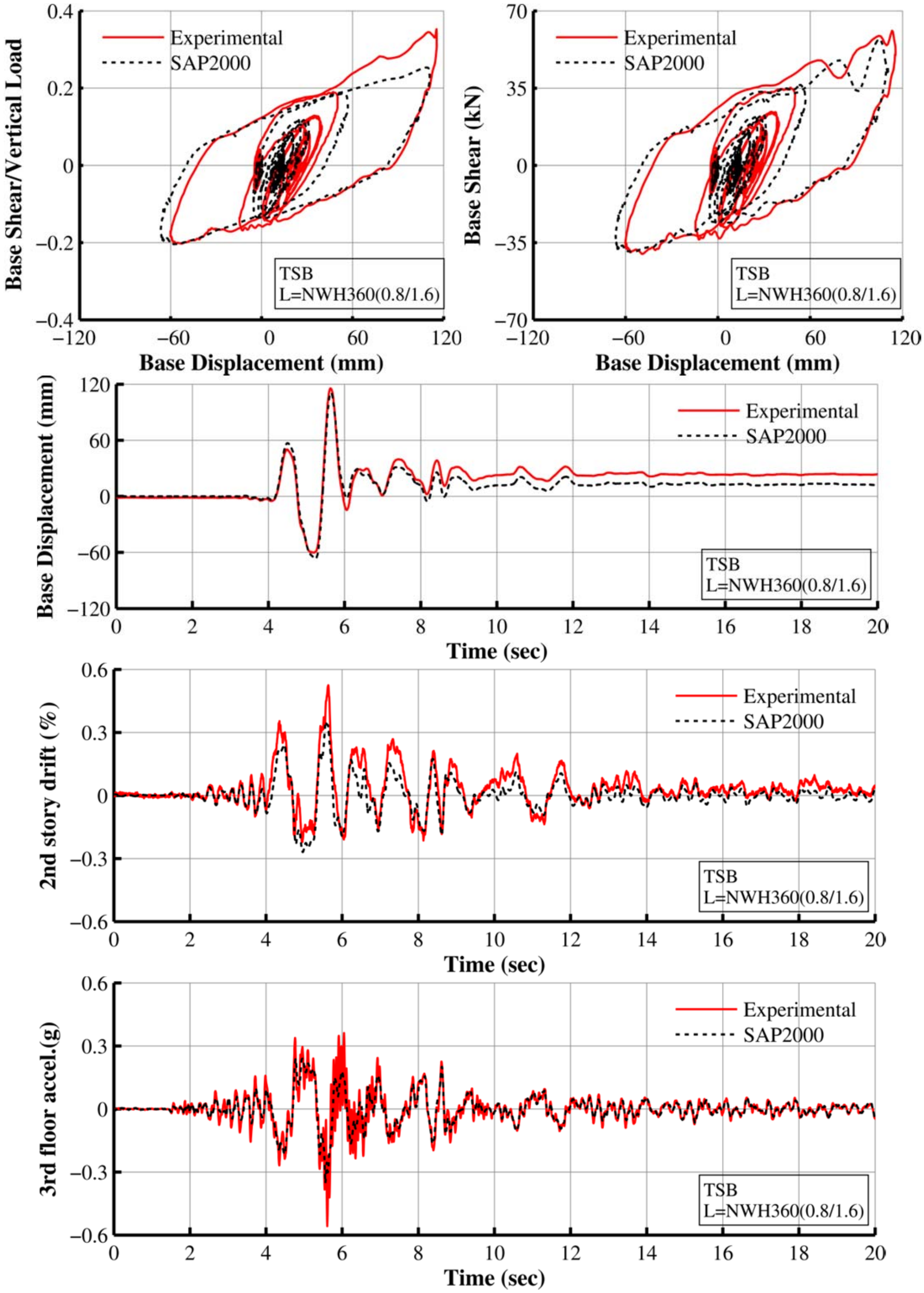
Experimental
SAP2000
Base Shear/Vertical Load
Base Displacement (mm)
TSB
L=NWH360(0.8/1.6)
Experimental
SAP2000
Base Shear (kN)
Base Displacement (mm)
TSB
L=NWH360(0.8/1.6)
Experimental
SAP2000
Base Displacement (mm)
Time (sec)
TSB
L=NWH360(0.8/1.6)
Experimental
SAP2000
2nd story drift (%)
Time (sec)
TSB
L=NWH360(0.8/1.6)
Experimental
SAP2000
3rd floor accel.(g)
Time (sec)
TSB
L=NWH360(0.8/1.6)

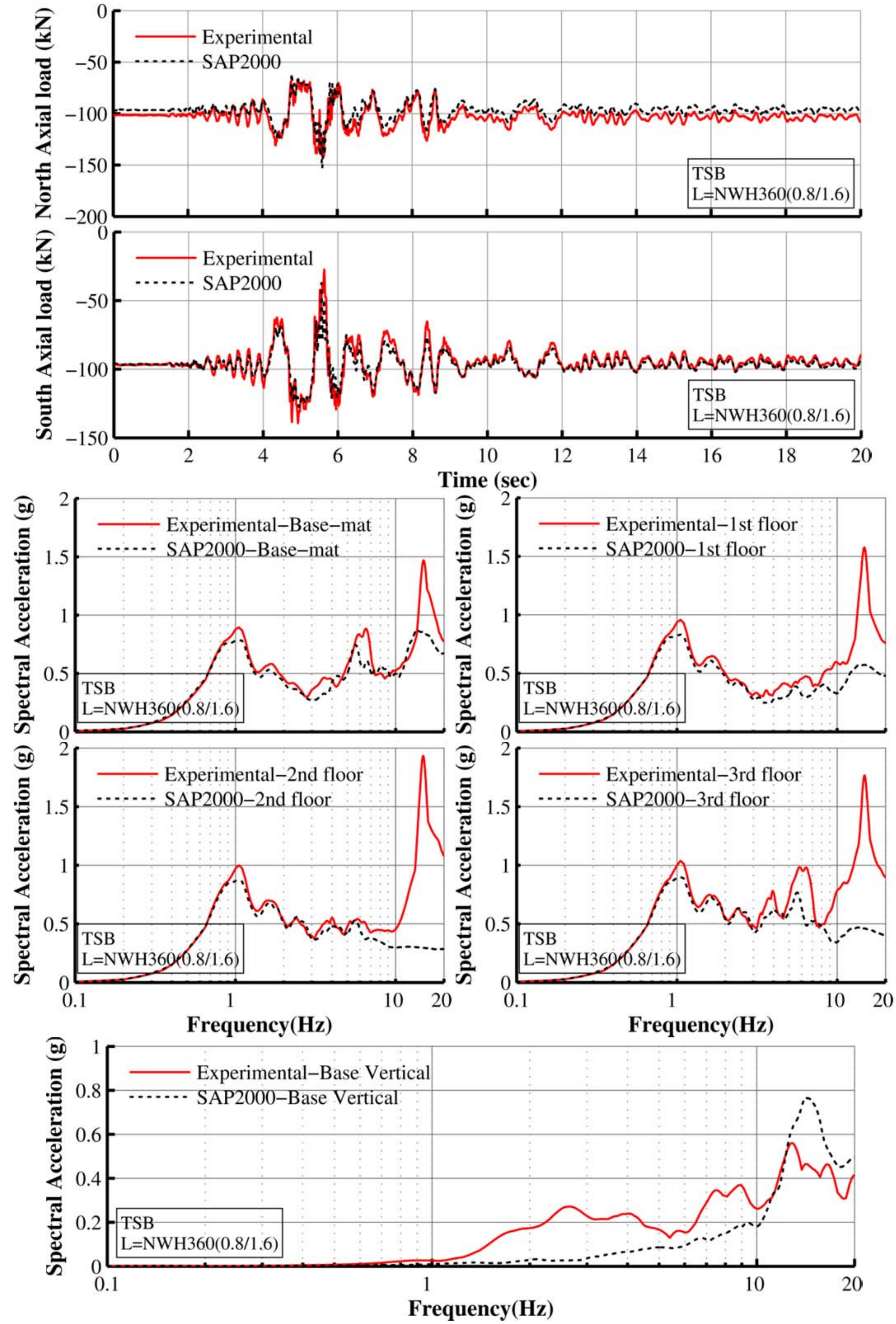
North Axial load (kN)
Experimental
SAP2000
TSB
L=NWH360(0.8/1.6)
South Axial load (kN)
Experimental
SAP2000
TSB
L=NWH360(0.8/1.6)
Time (sec)
Spectral Acceleration (g)
Experimental−Base−mat
SAP2000−Base−mat
Experimental−1st floor
SAP2000−1st floor
Experimental−2nd floor
SAP2000−2nd floor
Experimental−3rd floor
SAP2000−3rd floor
Frequency(Hz)
Experimental−Base Vertical
SAP2000−Base Vertical
TSB
L=NWH360(0.8/1.6)
Frequency(Hz)

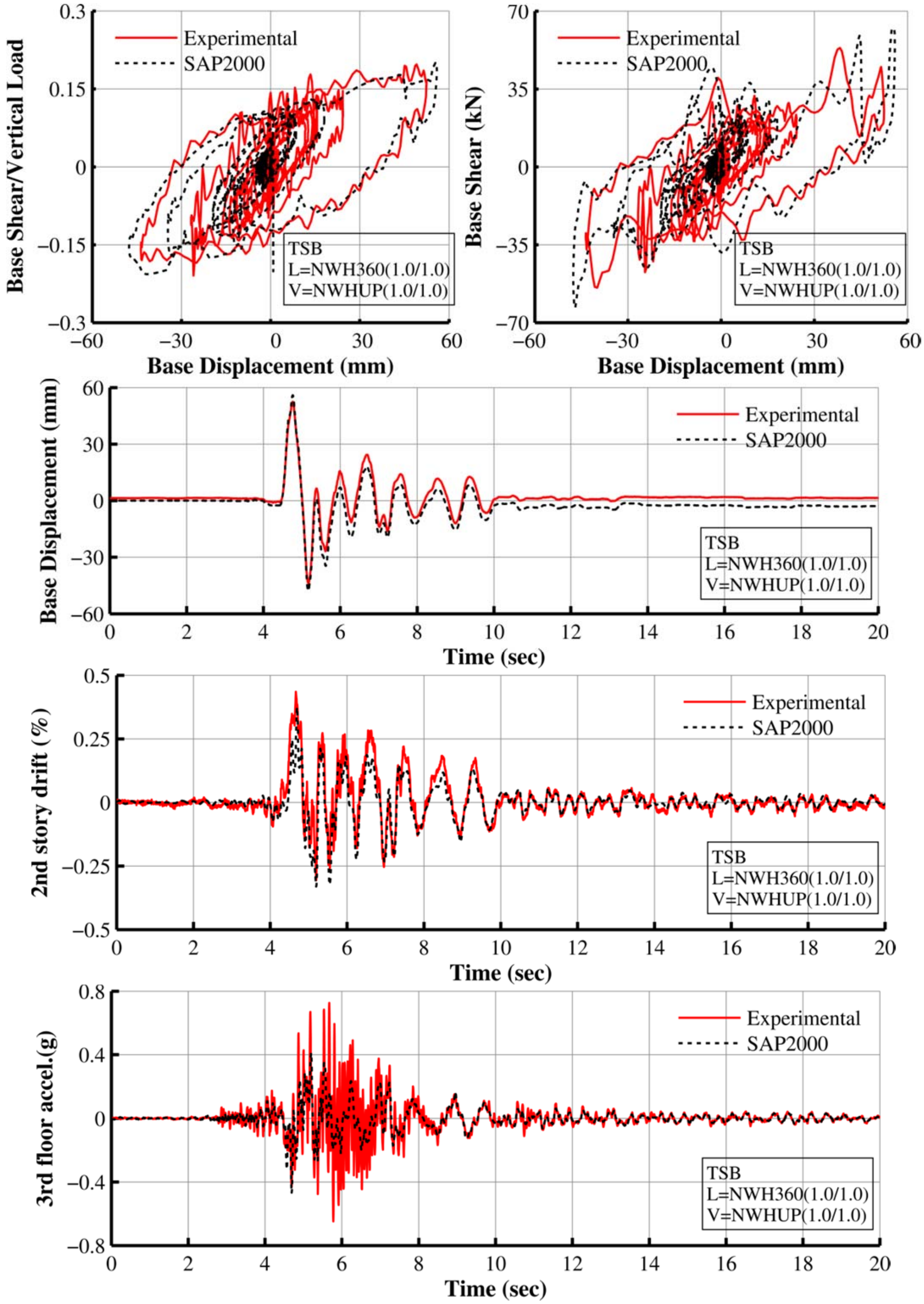
Base Shear/Vertical Load
Base Displacement (mm)
Base Shear (kN)
Base Displacement (mm)
Time (sec)
2nd story drift (%)
3rd floor accel.(g)
Experimental
SAP2000
TSB
L=NWH360(1.0/1.0)
V=NWHUP(1.0/1.0)

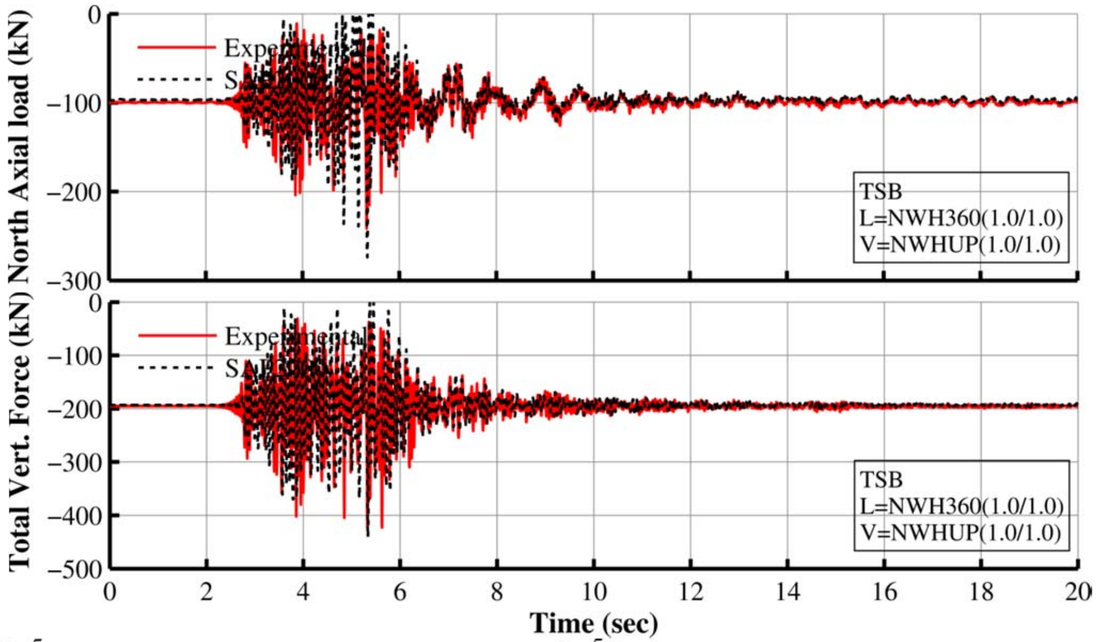
North Axial load (kN)
Total Vert. Force (kN)
Experimental
SAP2000
TSB
L=NWH360(1.0/1.0)
V=NWHUP(1.0/1.0)
Time (sec)

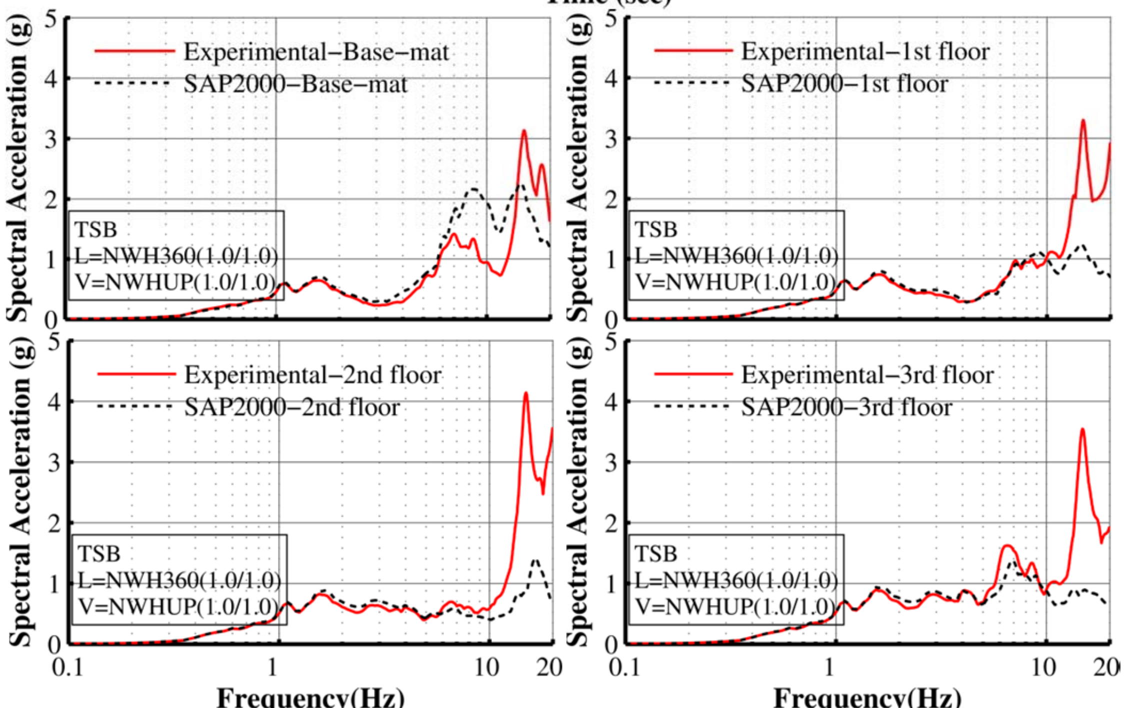
Spectral Acceleration (g)
Experimental−Base−mat
SAP2000−Base−mat
Experimental−1st floor
SAP2000−1st floor
Experimental−2nd floor
SAP2000−2nd floor
Experimental−3rd floor
SAP2000−3rd floor
TSB
L=NWH360(1.0/1.0)
V=NWHUP(1.0/1.0)
Frequency(Hz)

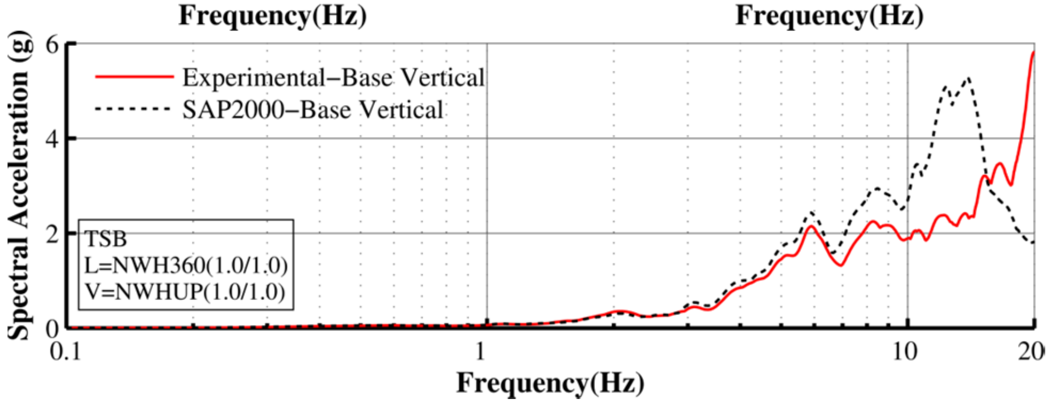
Spectral Acceleration (g)
Experimental−Base Vertical
SAP2000−Base Vertical
TSB
L=NWH360(1.0/1.0)
V=NWHUP(1.0/1.0)
Frequency(Hz)

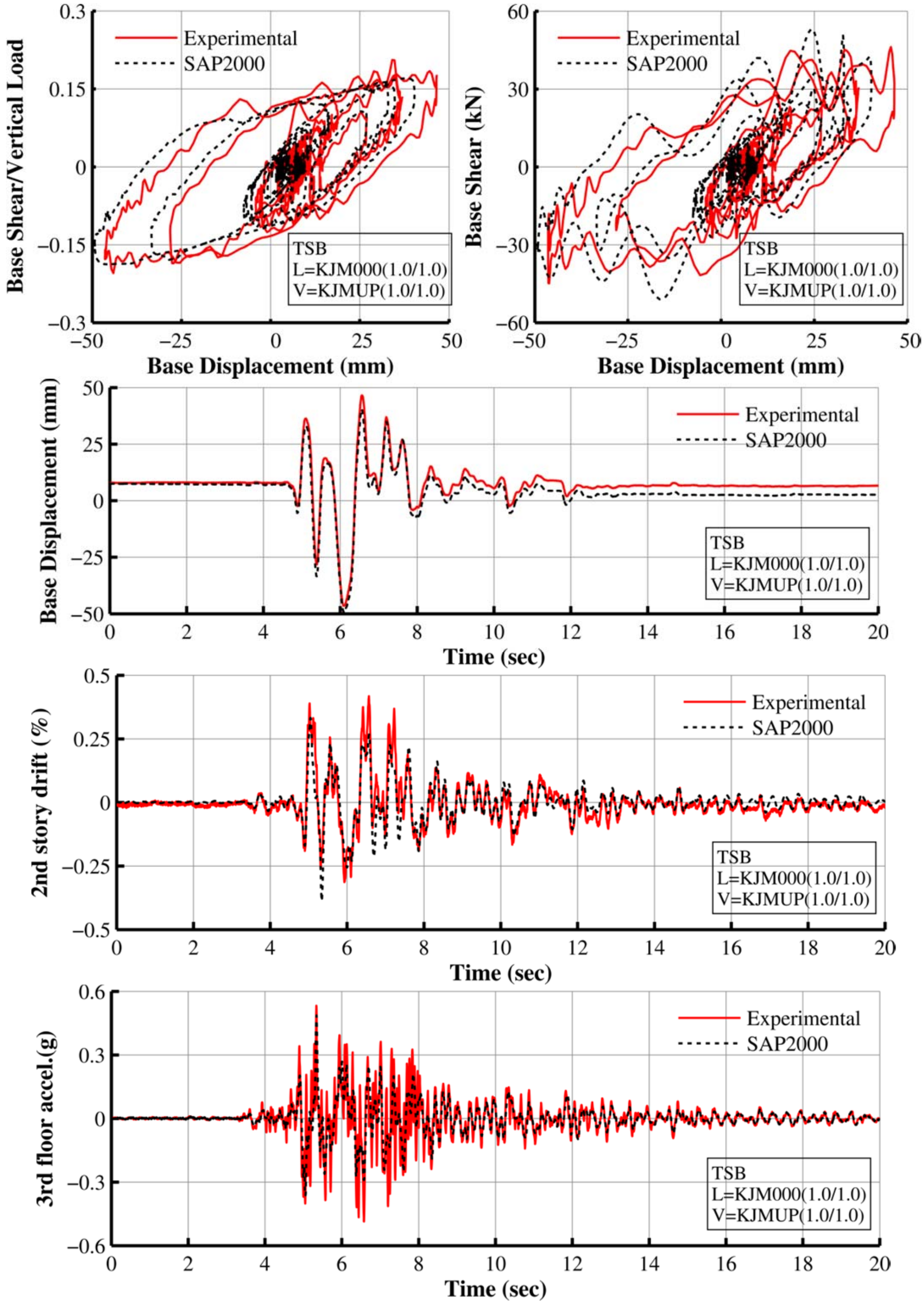

Experimental
SAP2000
TSB
L=KJM000(1.0/1.0)
V=KJMUP(1.0/1.0)
Base Shear/Vertical Load
Base Shear (kN)
Base Displacement (mm)
Base Displacement (mm)
Time (sec)
2nd story drift (%)
3rd floor accel.(g)

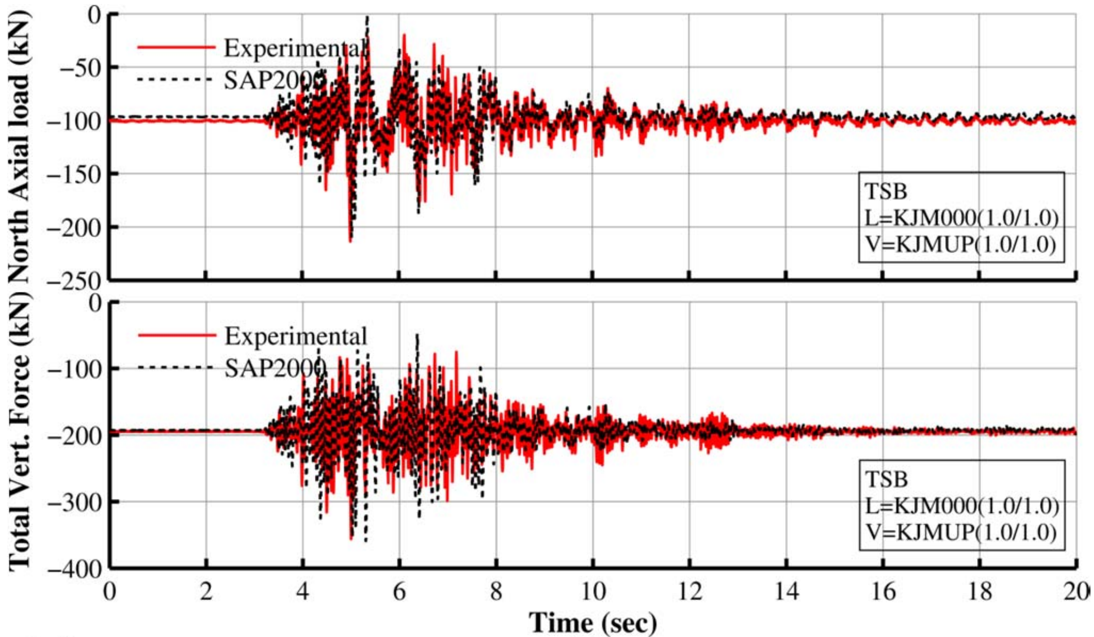
North Axial load (kN)
Total Vert. Force (kN)
Experimental
SAP2000
TSB
L=KJM000(1.0/1.0)
V=KJMUP(1.0/1.0)
Time (sec)

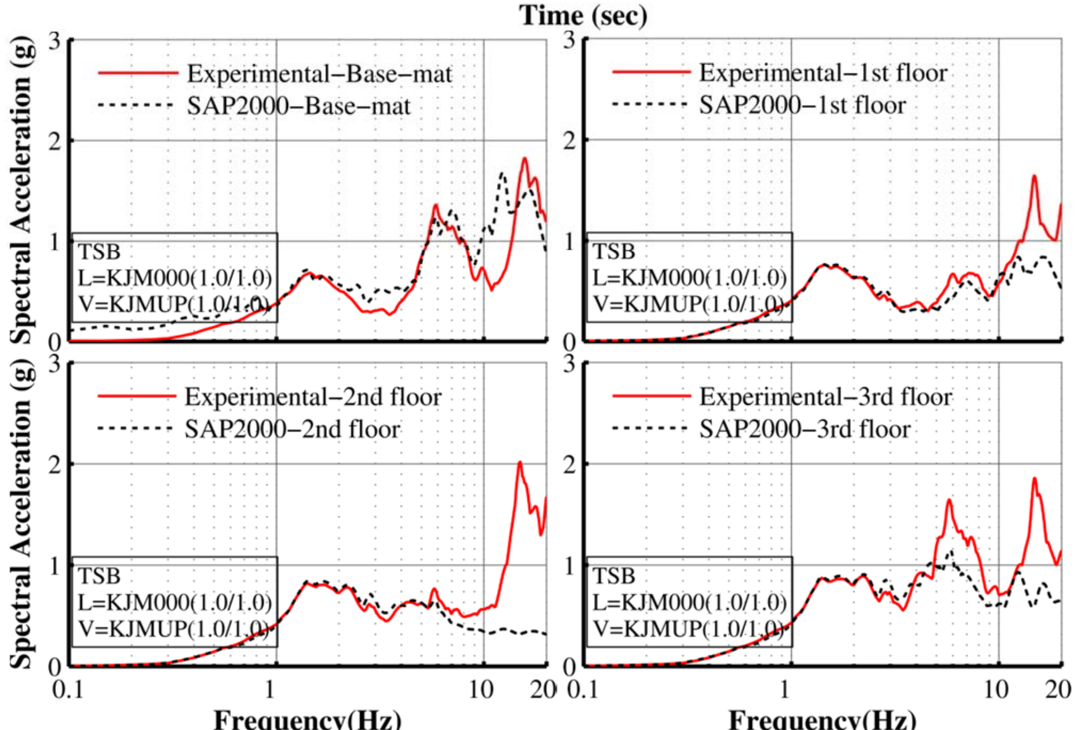
Spectral Acceleration (g)
Experimental−Base−mat
SAP2000−Base−mat
Experimental−1st floor
SAP2000−1st floor
Experimental−2nd floor
SAP2000−2nd floor
Experimental−3rd floor
SAP2000−3rd floor
TSB
L=KJM000(1.0/1.0)
V=KJMUP(1.0/1.0)
Frequency(Hz)

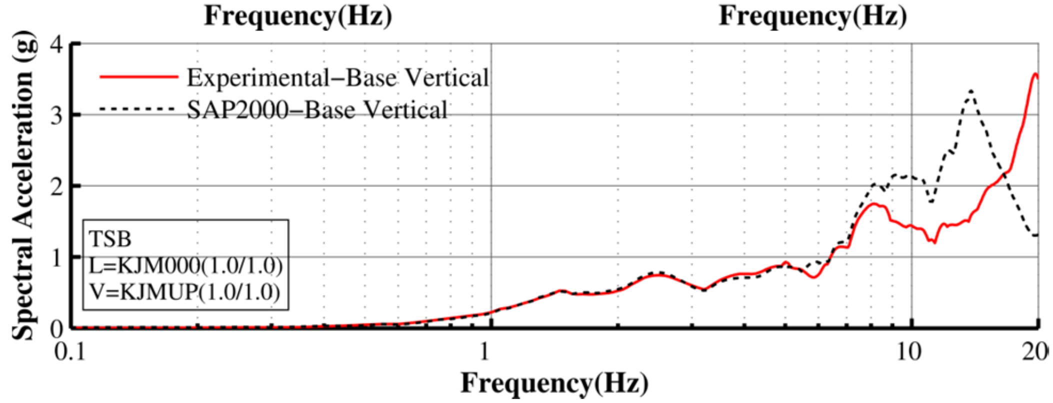
Spectral Acceleration (g)
Experimental−Base Vertical
SAP2000−Base Vertical
TSB
L=KJM000(1.0/1.0)
V=KJMUP(1.0/1.0)
Frequency(Hz)

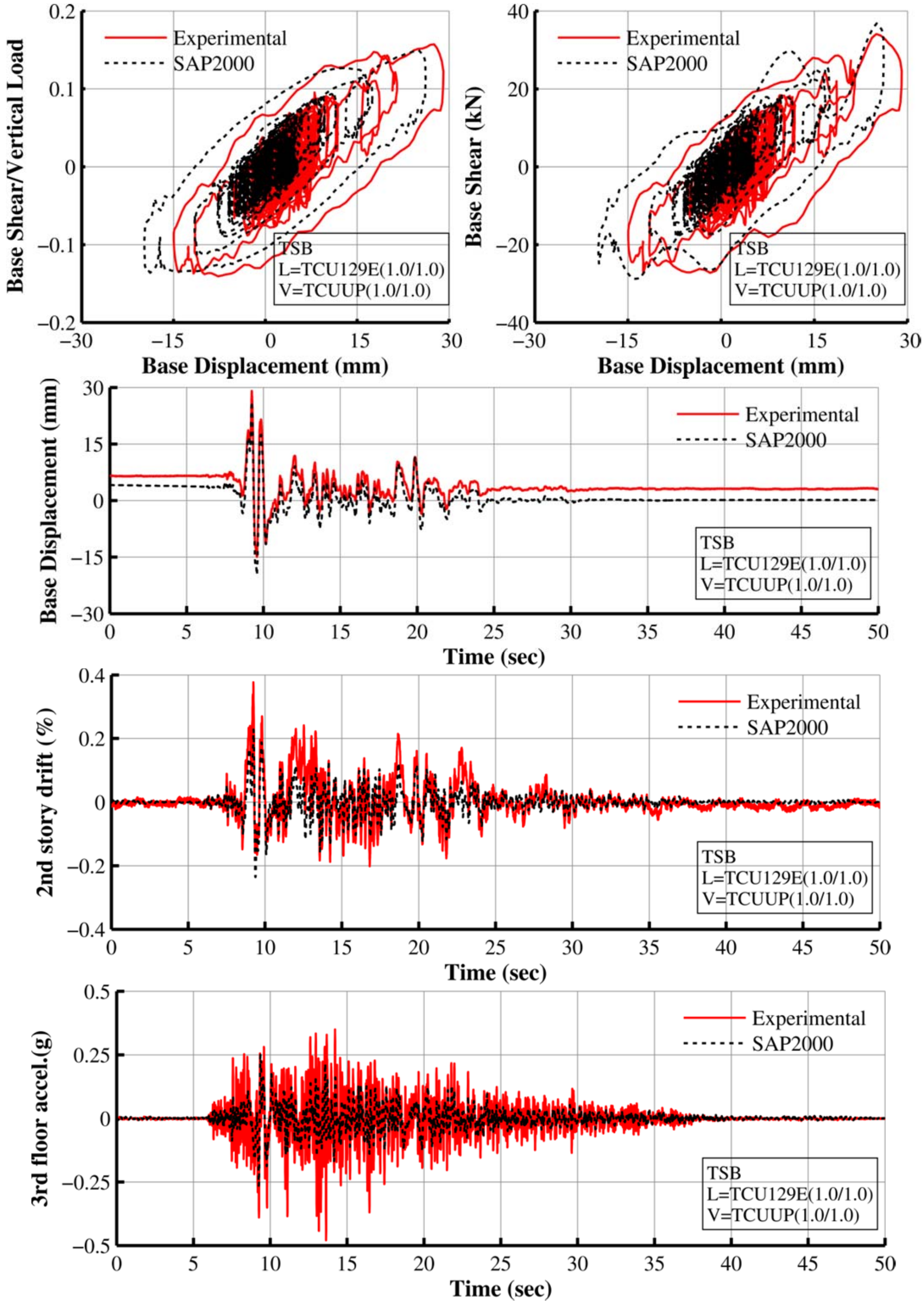
Experimental
SAP2000
TSB
L=TCU129E(1.0/1.0)
V=TCUUP(1.0/1.0)
Base Shear/Vertical Load
Base Displacement (mm)
Base Shear (kN)
Base Displacement (mm)
Time (sec)
2nd story drift (%)
3rd floor accel.(g)

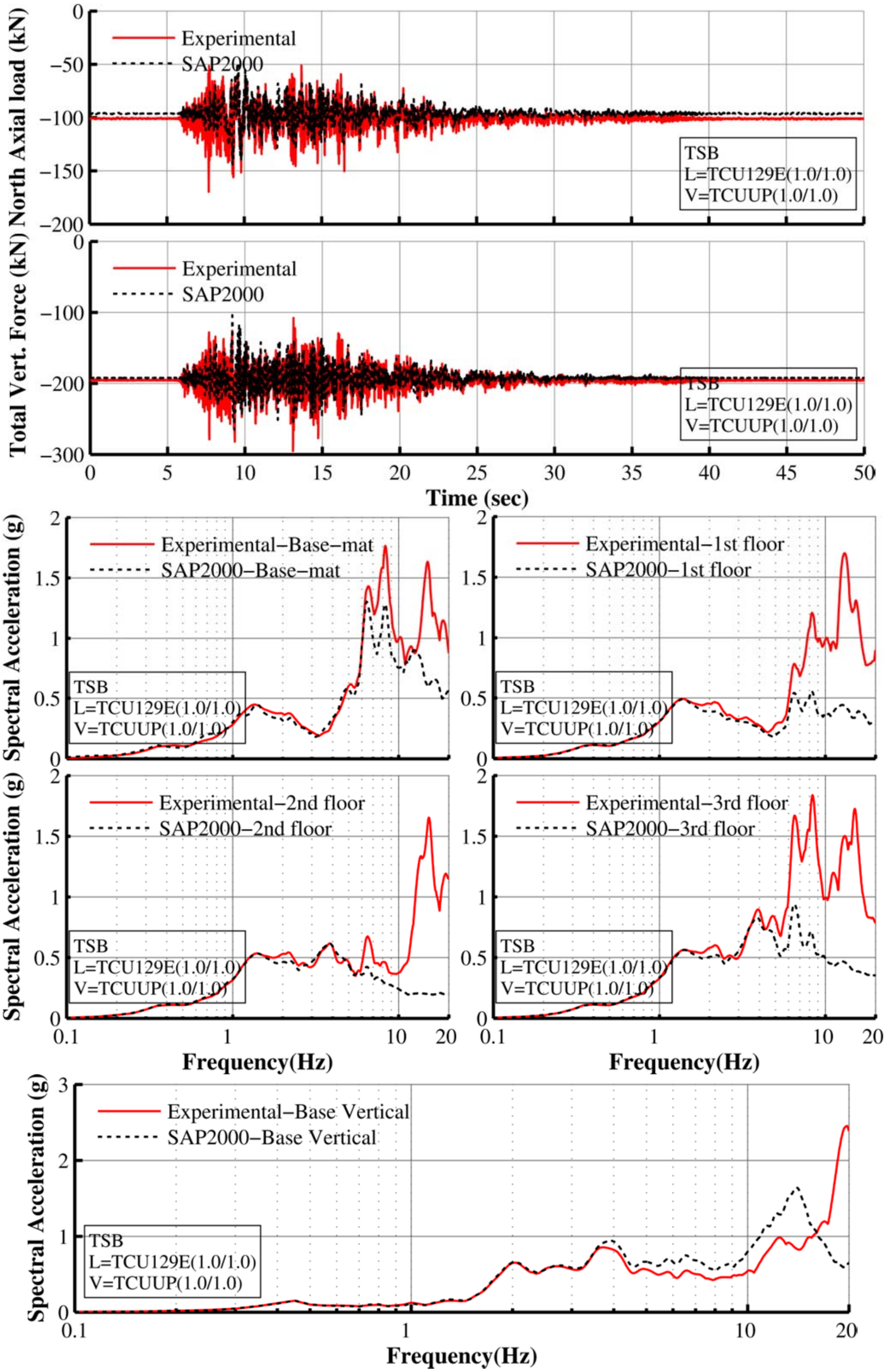
North Axial load (kN)
Experimental
SAP2000
TSB
L=TCU129E(1.0/1.0)
V=TCUUP(1.0/1.0)
Total Vert. Force (kN)
Experimental
SAP2000
TSB
L=TCU129E(1.0/1.0)
V=TCUUP(1.0/1.0)
Time (sec)
Spectral Acceleration (g)
Experimental−Base−mat
SAP2000−Base−mat
Experimental−1st floor
SAP2000−1st floor
Experimental−2nd floor
SAP2000−2nd floor
Experimental−3rd floor
SAP2000−3rd floor
Frequency(Hz)
Experimental−Base Vertical
SAP2000−Base Vertical
Frequency(Hz)

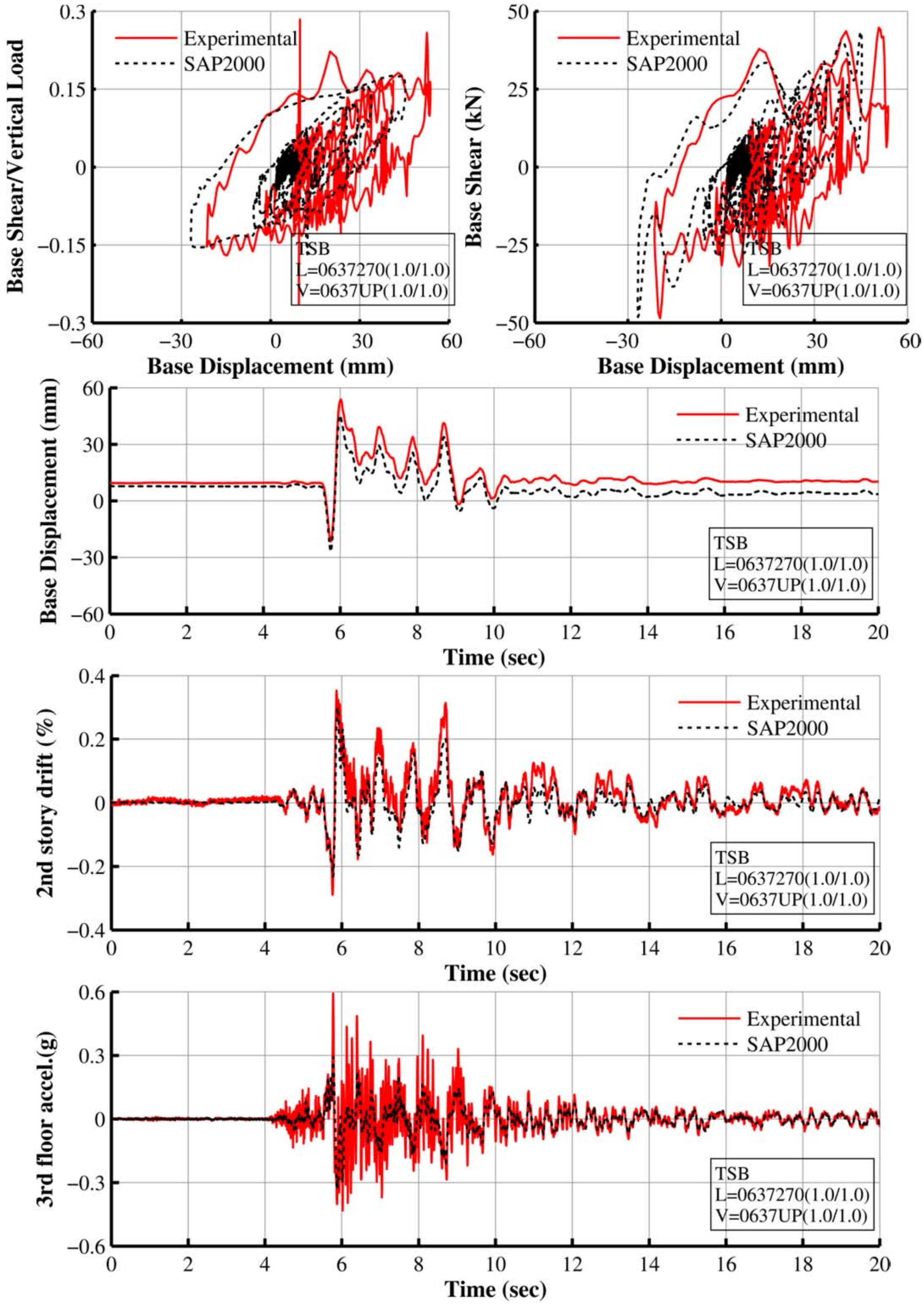
Experimental
SAP2000
TSB
L=0637270(1.0/1.0)
V=0637UP(1.0/1.0)
Base Shear/Vertical Load
Base Displacement (mm)
Base Shear (kN)
Base Displacement (mm)
2nd story drift (%)
3rd floor accel.(g)
Time (sec)

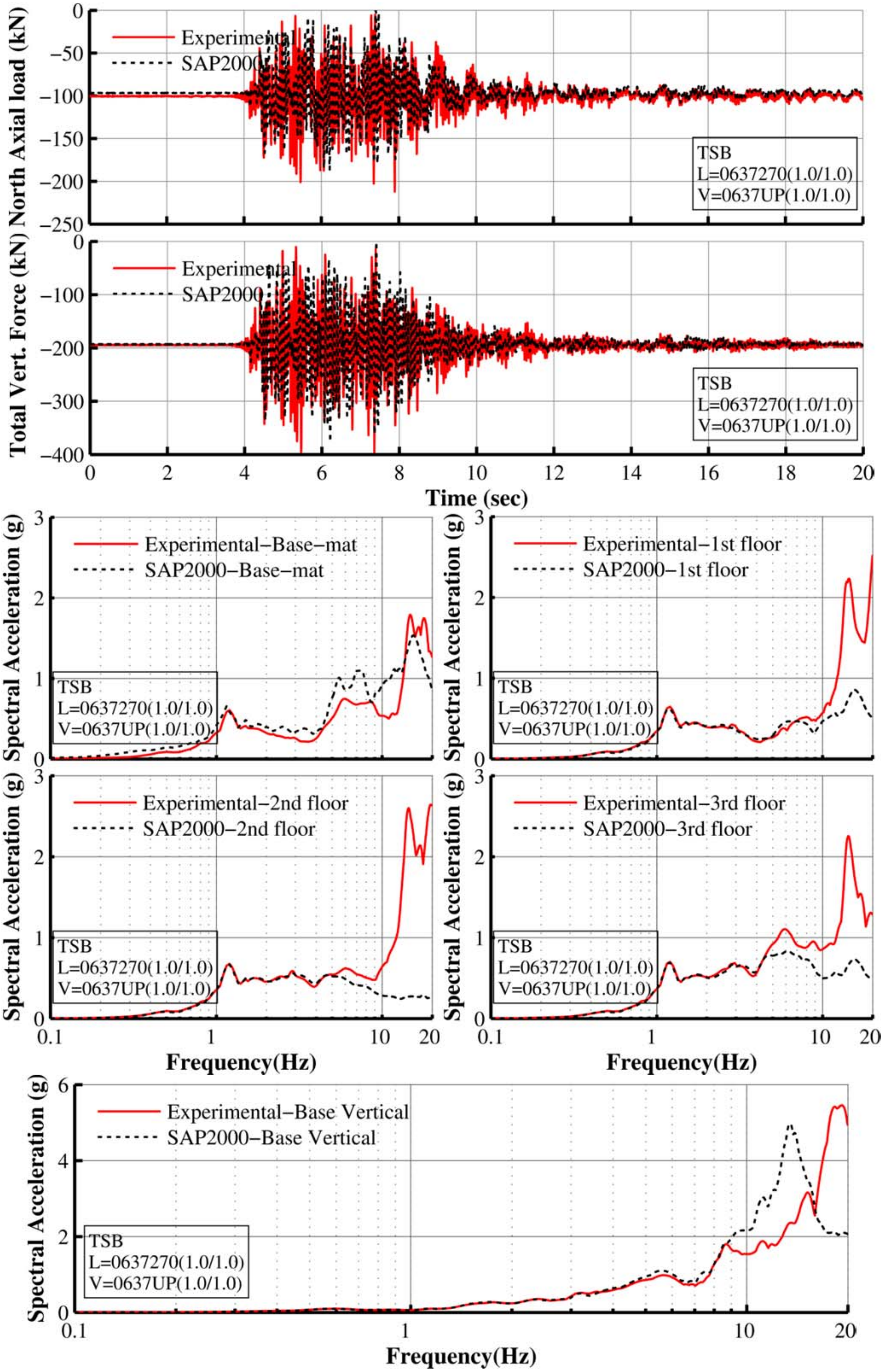
North Axial load (kN)
Experimental
SAP2000
TSB
L=0637270(1.0/1.0)
V=0637UP(1.0/1.0)
Total Vert. Force (kN)
Experimental
SAP2000
TSB
L=0637270(1.0/1.0)
V=0637UP(1.0/1.0)
Time (sec)
Spectral Acceleration (g)
Experimental−Base−mat
SAP2000−Base−mat
Experimental−1st floor
SAP2000−1st floor
Experimental−2nd floor
SAP2000−2nd floor
Experimental−3rd floor
SAP2000−3rd floor
Frequency(Hz)
Experimental−Base Vertical
SAP2000−Base Vertical
TSB
L=0637270(1.0/1.0)
V=0637UP(1.0/1.0)
Frequency(Hz)

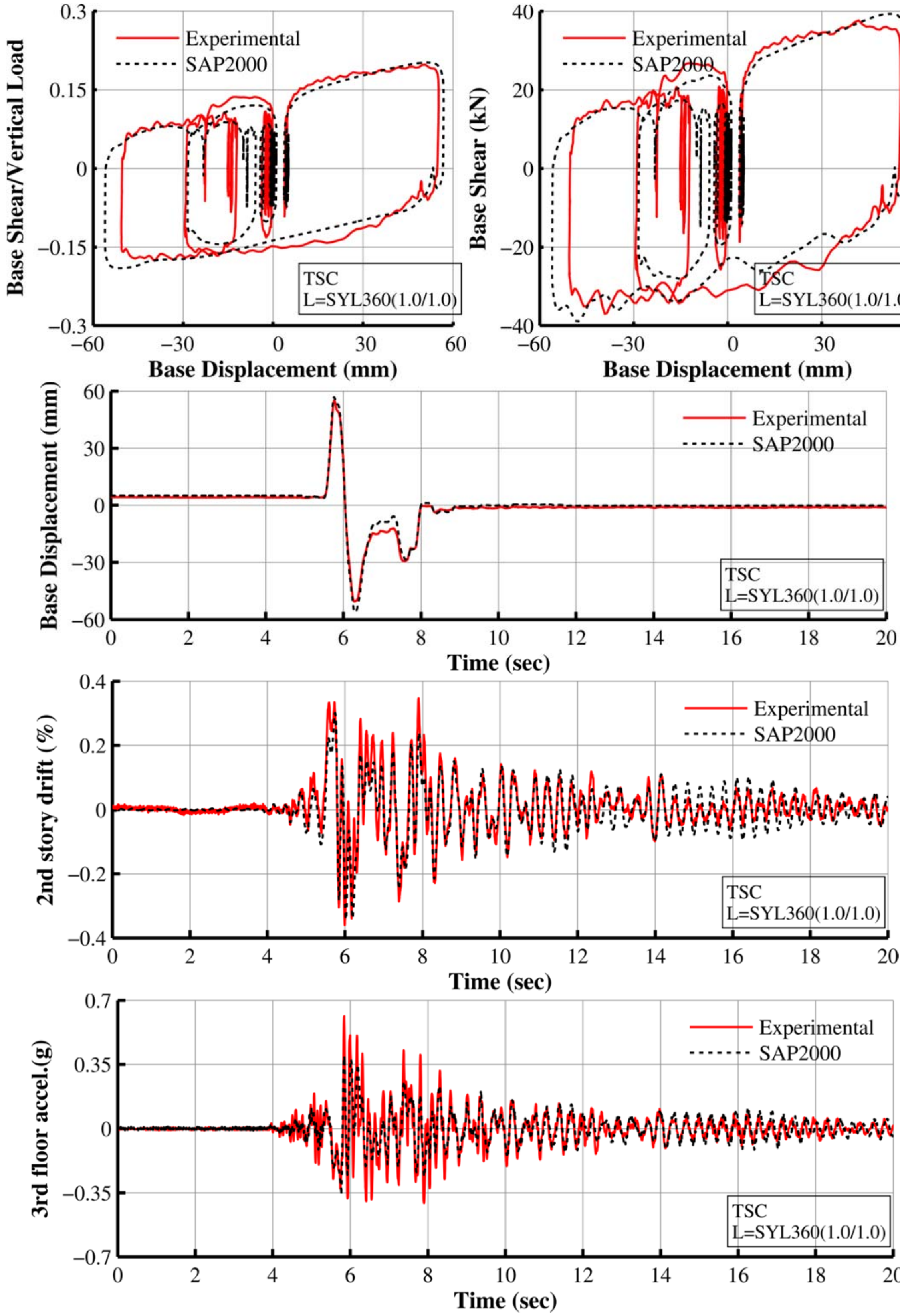
Base Shear/Vertical Load
Base Displacement (mm)
Experimental
SAP2000
TSC
L=SYL360(1.0/1.0)
Base Shear (kN)
Base Displacement (mm)
Base Displacement (mm)
Time (sec)
2nd story drift (%)
Time (sec)
3rd floor accel.(g)
Time (sec)

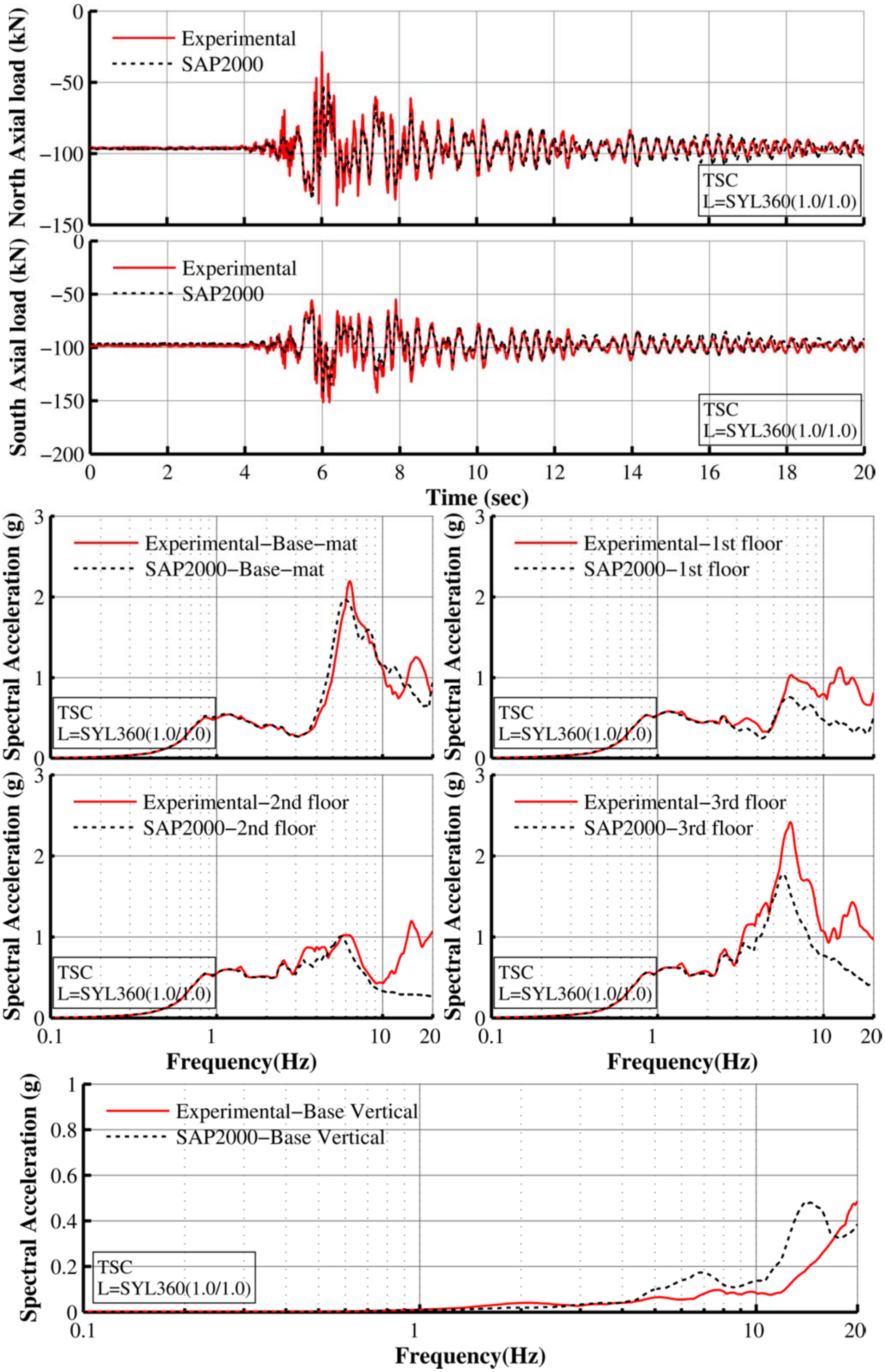
North Axial load (kN)
South Axial load (kN)
Experimental
SAP2000
TSC
L=SYL360(1.0/1.0)
Time (sec)
Spectral Acceleration (g)
Experimental−Base−mat
SAP2000−Base−mat
Experimental−1st floor
SAP2000−1st floor
Experimental−2nd floor
SAP2000−2nd floor
Experimental−3rd floor
SAP2000−3rd floor
Experimental−Base Vertical
SAP2000−Base Vertical
Frequency(Hz)

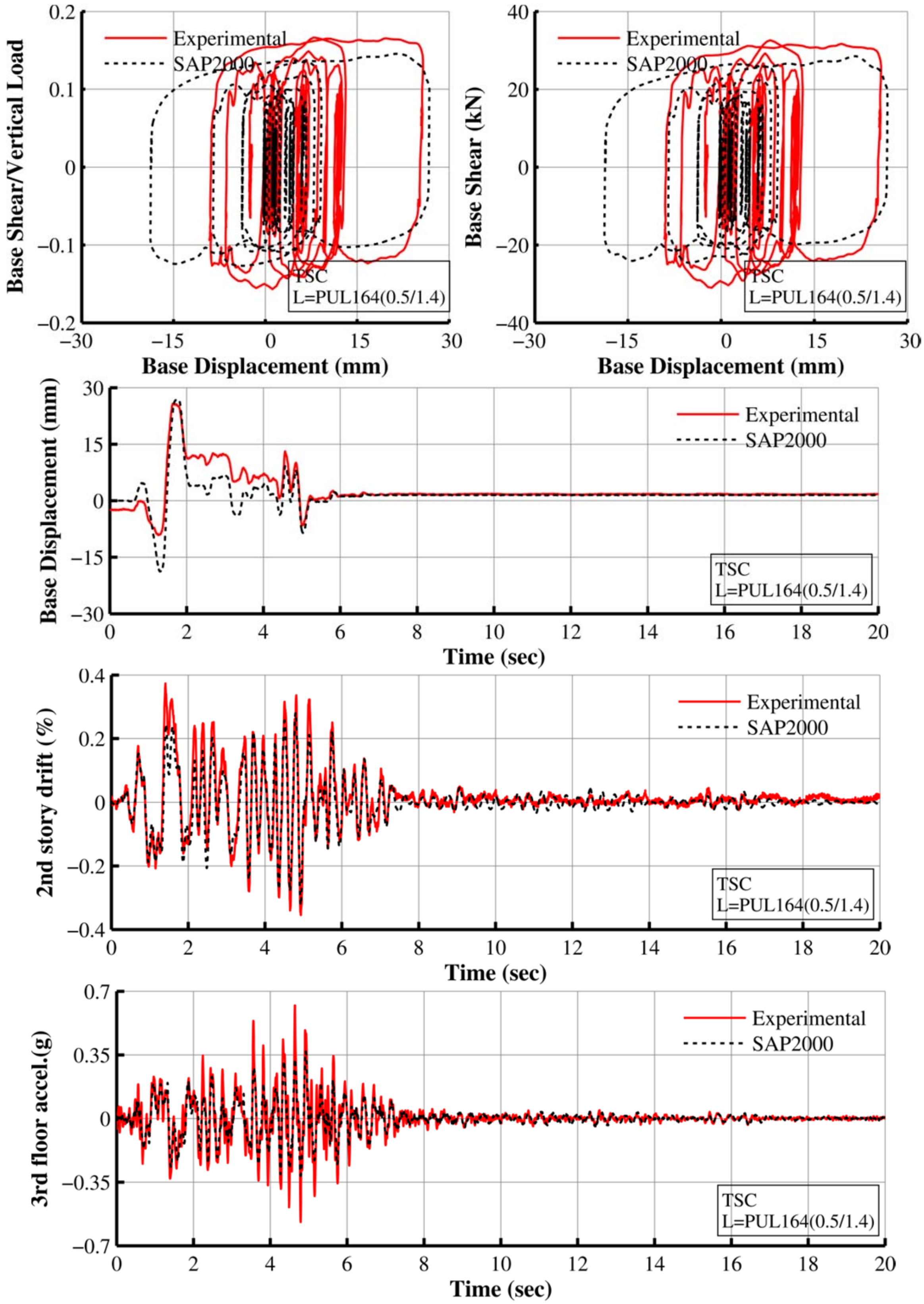
Base Shear/Vertical Load
Base Displacement (mm)
Base Shear (kN)
Base Displacement (mm)
Base Displacement (mm)
Time (sec)
2nd story drift (%)
Time (sec)
3rd floor accel.(g)
Time (sec)
Experimental
SAP2000
TSC
L=PUL164(0.5/1.4)

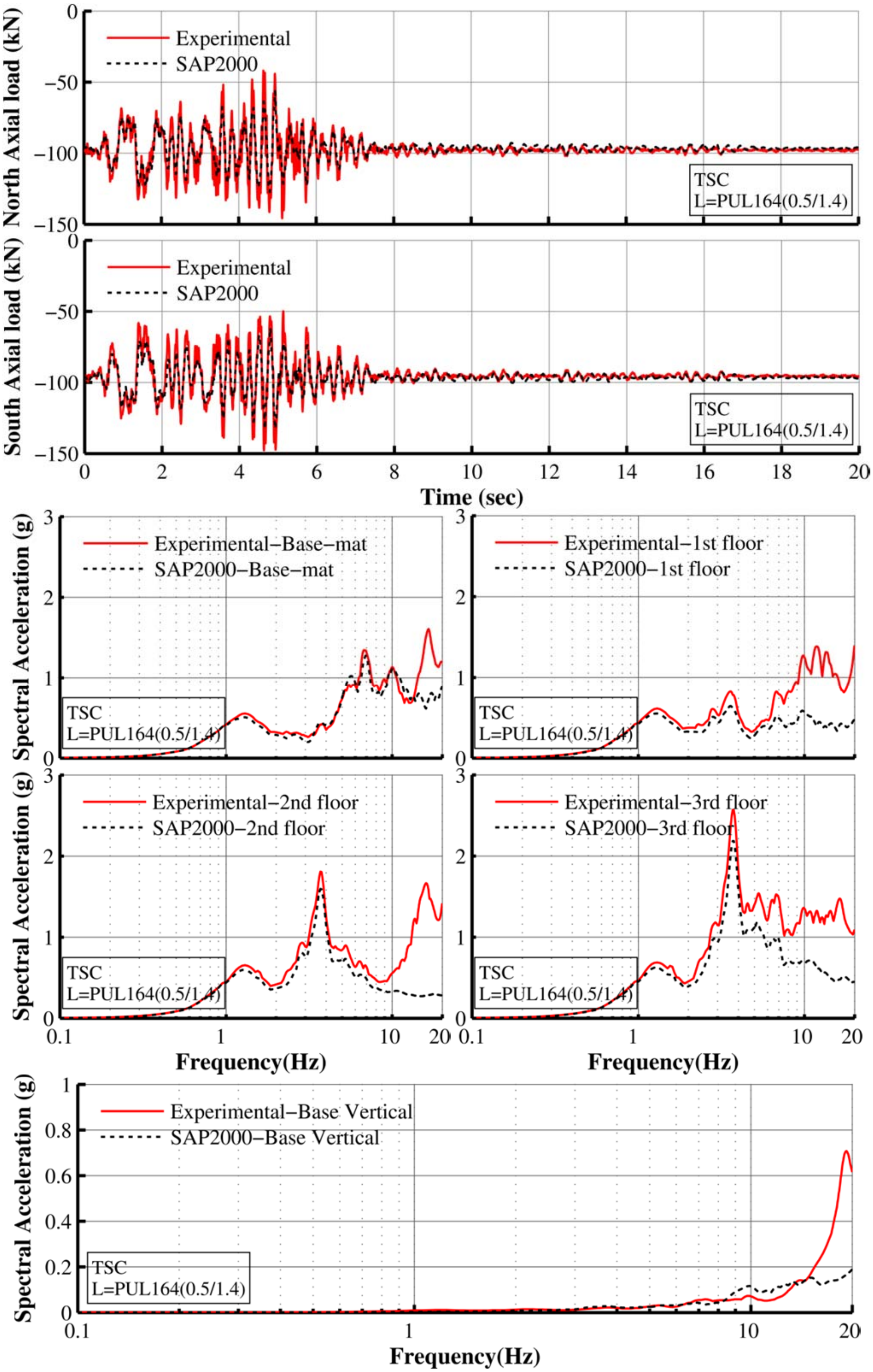
North Axial load (kN)
Experimental
SAP2000
TSC
L=PUL164(0.5/1.4)
South Axial load (kN)
Experimental
SAP2000
TSC
L=PUL164(0.5/1.4)
Time (sec)
Spectral Acceleration (g)
Experimental−Base−mat
SAP2000−Base−mat
Experimental−1st floor
SAP2000−1st floor
Experimental−2nd floor
SAP2000−2nd floor
Experimental−3rd floor
SAP2000−3rd floor
TSC
L=PUL164(0.5/1.4)
Frequency(Hz)
Frequency(Hz)
Spectral Acceleration (g)
Experimental−Base Vertical
SAP2000−Base Vertical
TSC
L=PUL164(0.5/1.4)
Frequency(Hz)

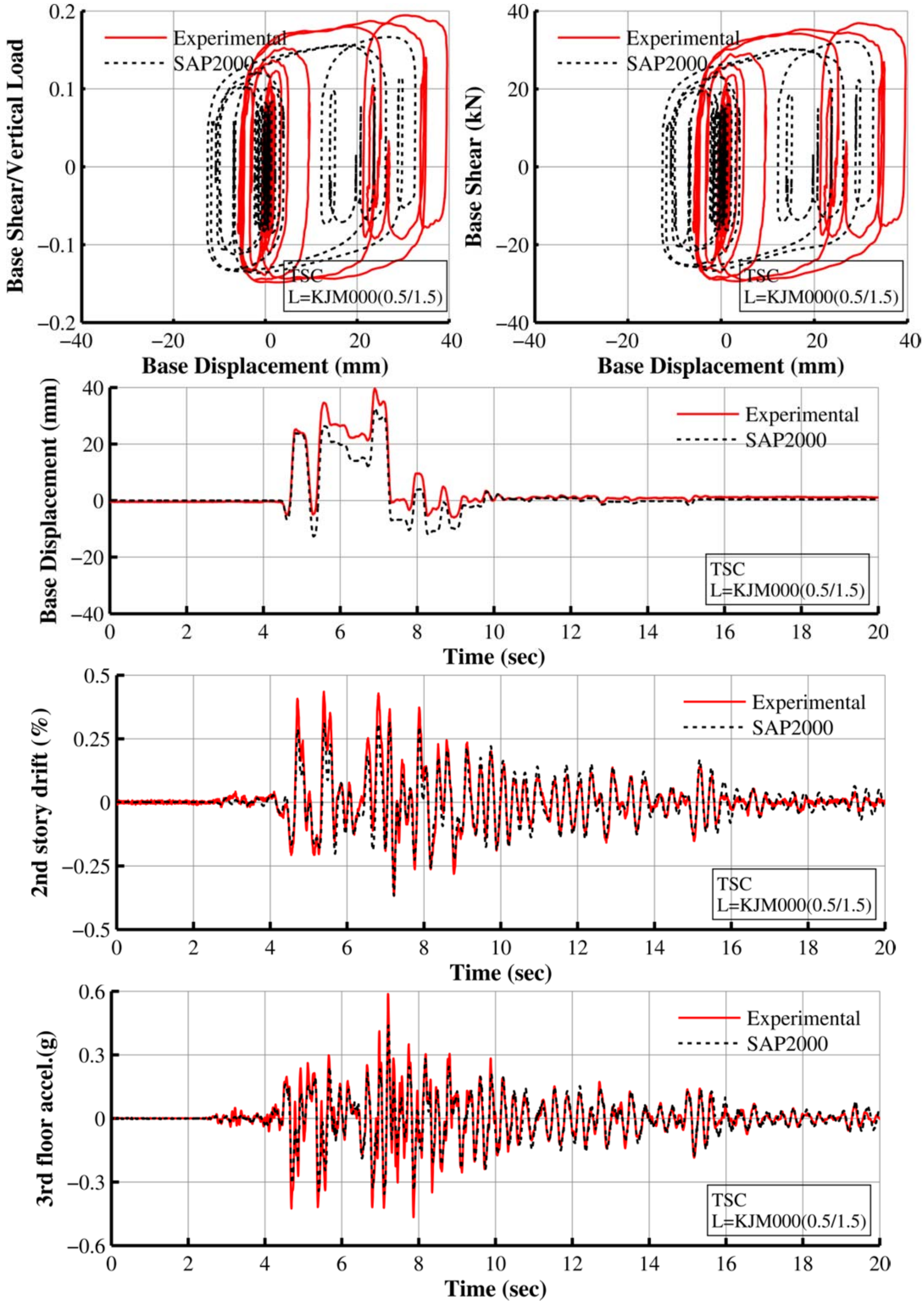
Experimental
SAP2000
TSC
L=KJM000(0.5/1.5)
Base Shear/Vertical Load
Base Displacement (mm)
Experimental
SAP2000
TSC
L=KJM000(0.5/1.5)
Base Shear (kN)
Base Displacement (mm)
Experimental
SAP2000
TSC
L=KJM000(0.5/1.5)
Base Displacement (mm)
Time (sec)
Experimental
SAP2000
TSC
L=KJM000(0.5/1.5)
2nd story drift (%)
Time (sec)
Experimental
SAP2000
TSC
L=KJM000(0.5/1.5)
3rd floor accel.(g)
Time (sec)

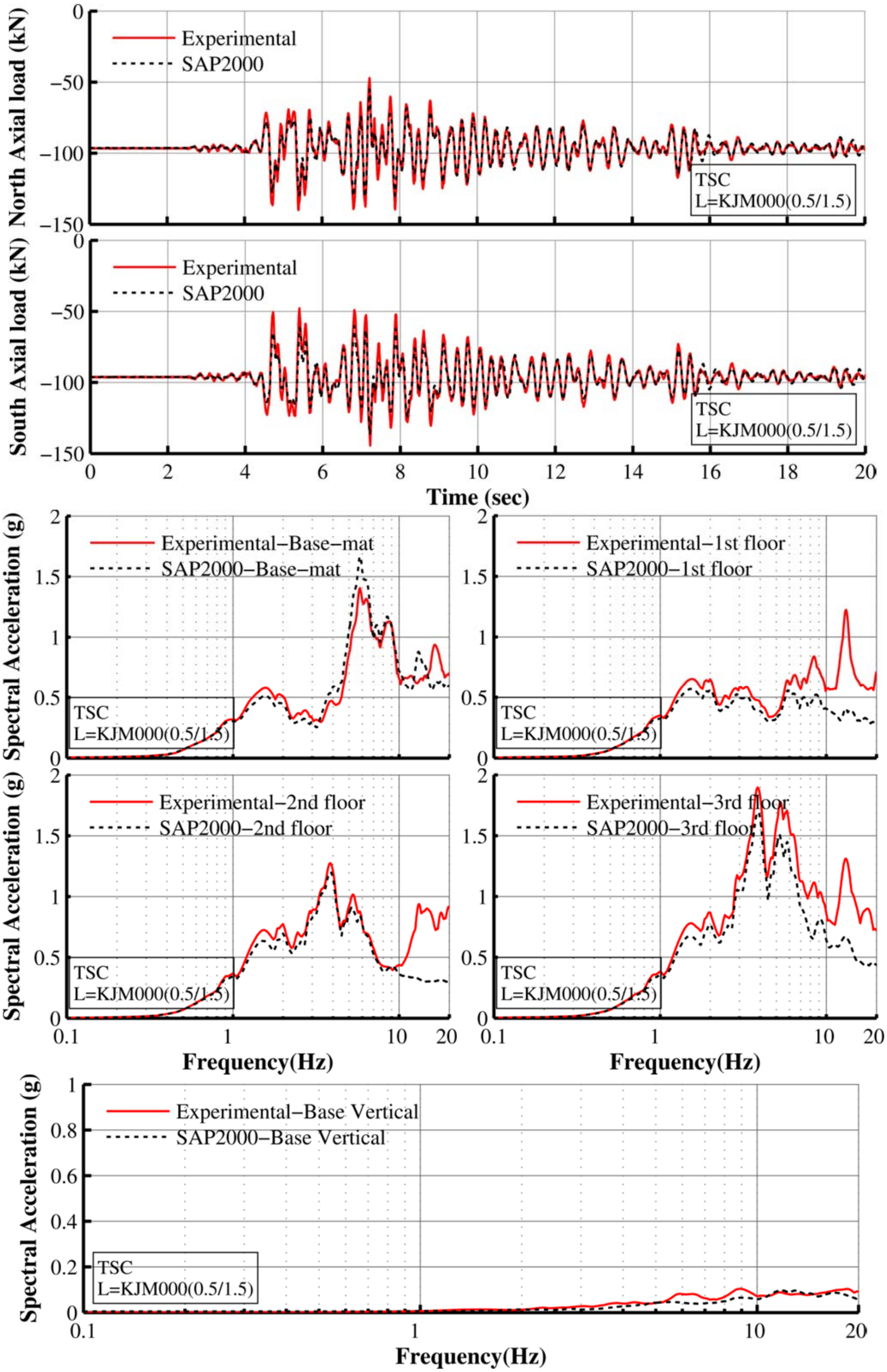
North Axial load (kN)
South Axial load (kN)
Experimental
SAP2000
TSC
L=KJM000(0.5/1.5)
Time (sec)
Spectral Acceleration (g)
Experimental−Base−mat
SAP2000−Base−mat
Experimental−1st floor
SAP2000−1st floor
Experimental−2nd floor
SAP2000−2nd floor
Experimental−3rd floor
SAP2000−3rd floor
Frequency(Hz)
Experimental−Base Vertical
SAP2000−Base Vertical

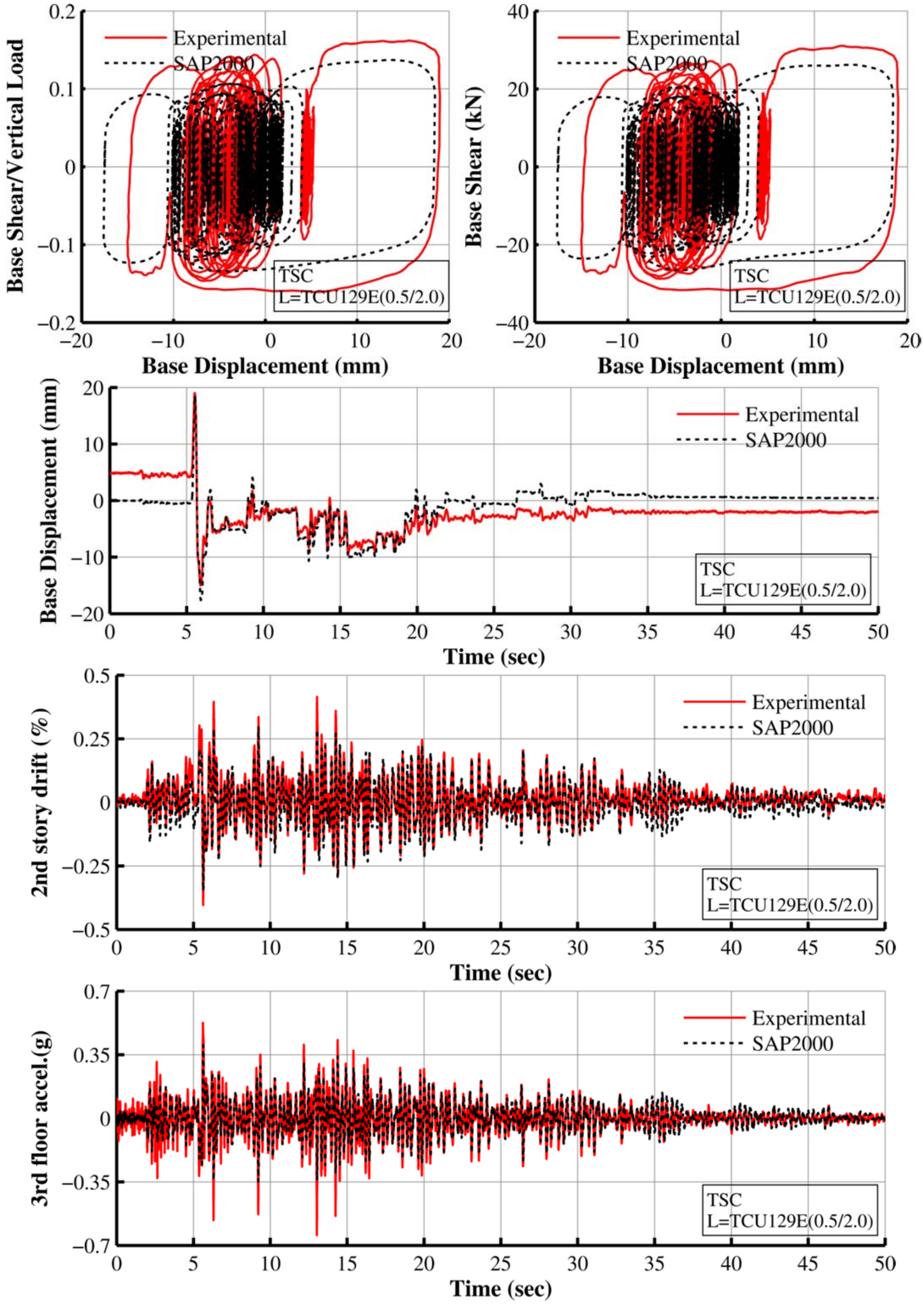
Experimental
SAP2000
TSC
L=TCU129E(0.5/2.0)
Base Shear/Vertical Load
Base Shear (kN)
Base Displacement (mm)
Time (sec)
2nd story drift (%)
3rd floor accel.(g)

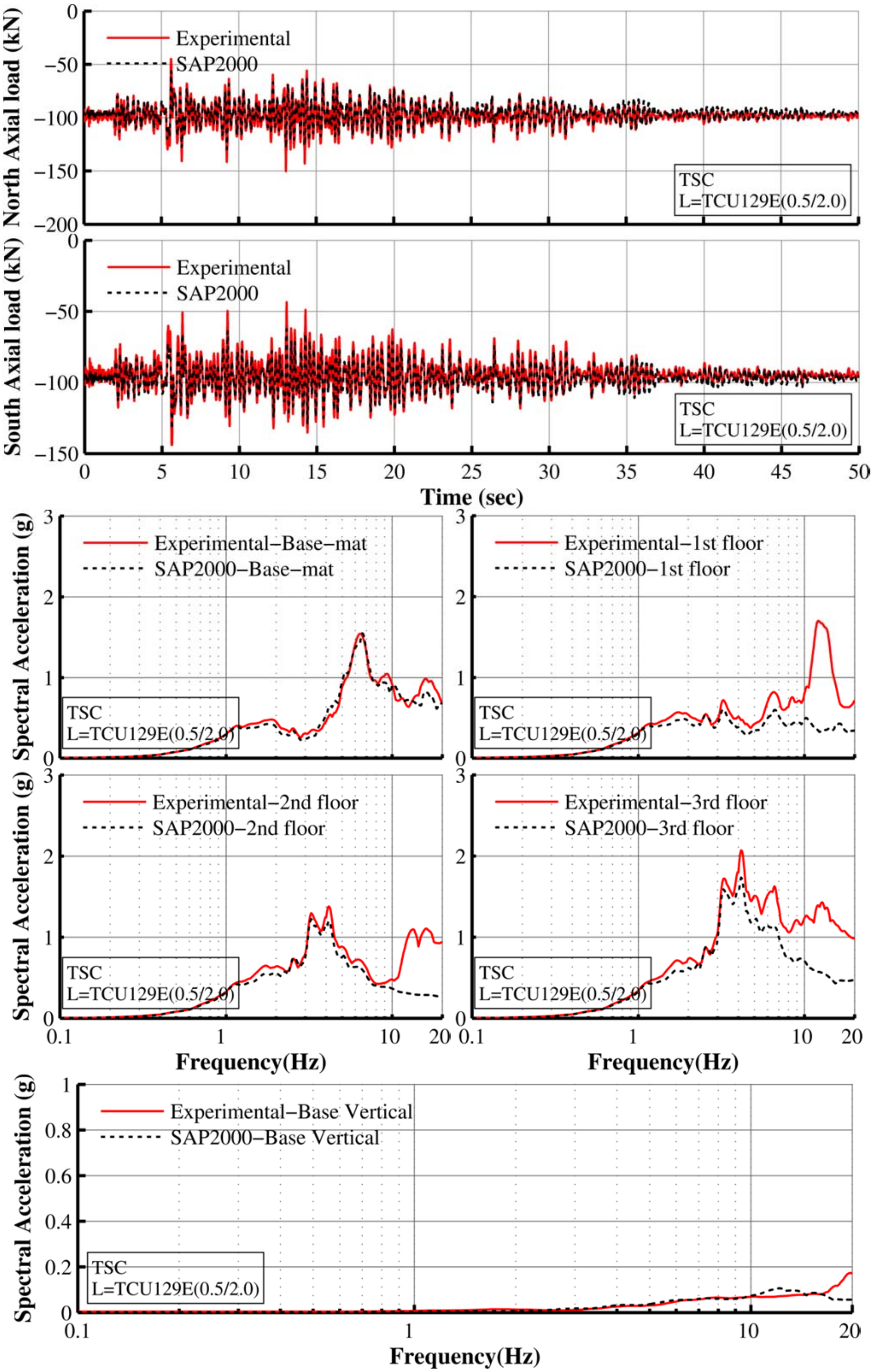
Experimental
SAP2000
North Axial load (kN)
TSC
L=TCU129E(0.5/2.0)
South Axial load (kN)
Time (sec)
Experimental−Base−mat
SAP2000−Base−mat
Experimental−1st floor
SAP2000−1st floor
Experimental−2nd floor
SAP2000−2nd floor
Experimental−3rd floor
SAP2000−3rd floor
Spectral Acceleration (g)
Frequency(Hz)
Experimental−Base Vertical
SAP2000−Base Vertical

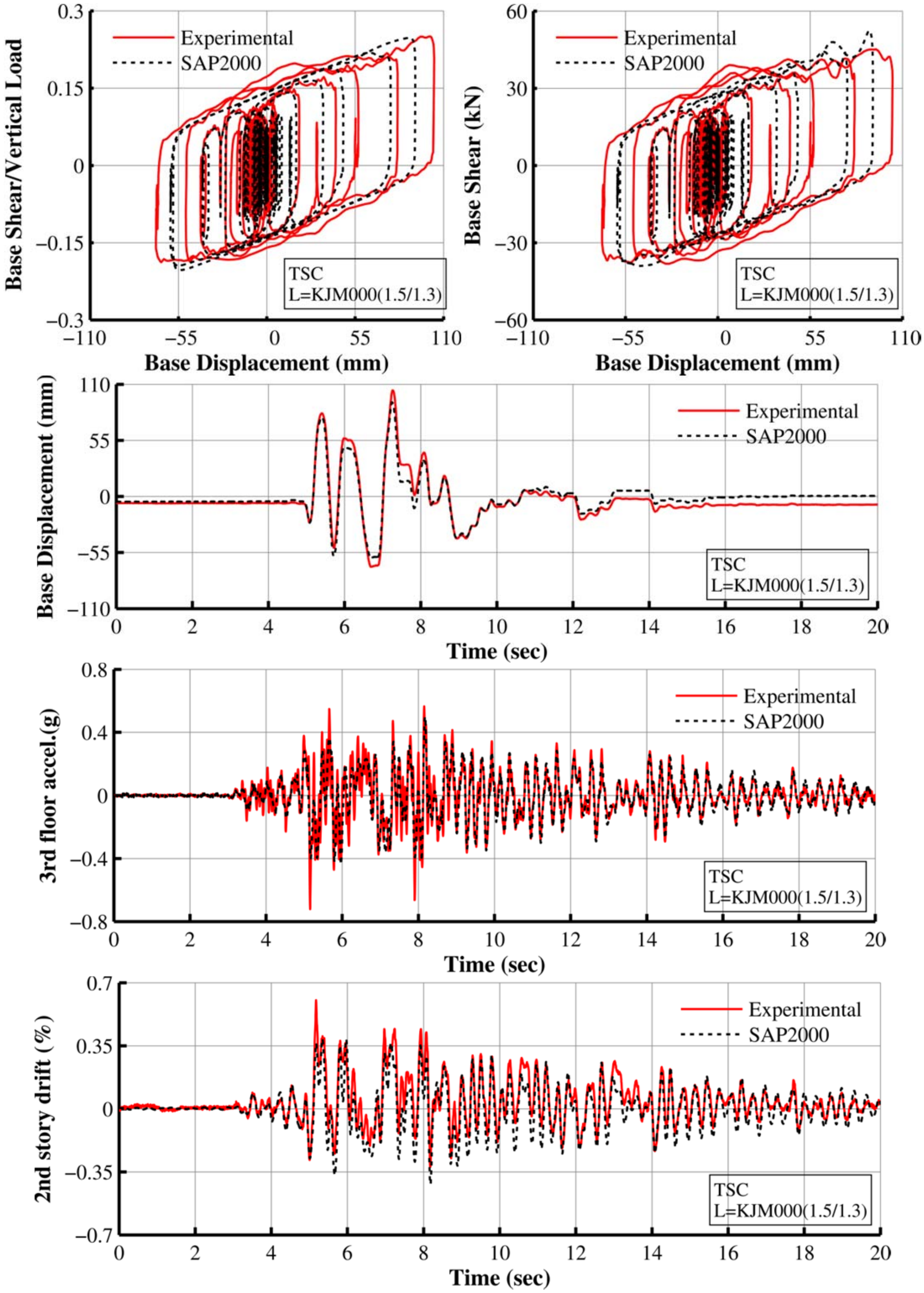
Experimental
SAP2000
TSC
L=KJM000(1.5/1.3)
Base Shear/Vertical Load
Base Displacement (mm)
Base Shear (kN)
Base Displacement (mm)
Time (sec)
3rd floor accel.(g)
2nd story drift (%)

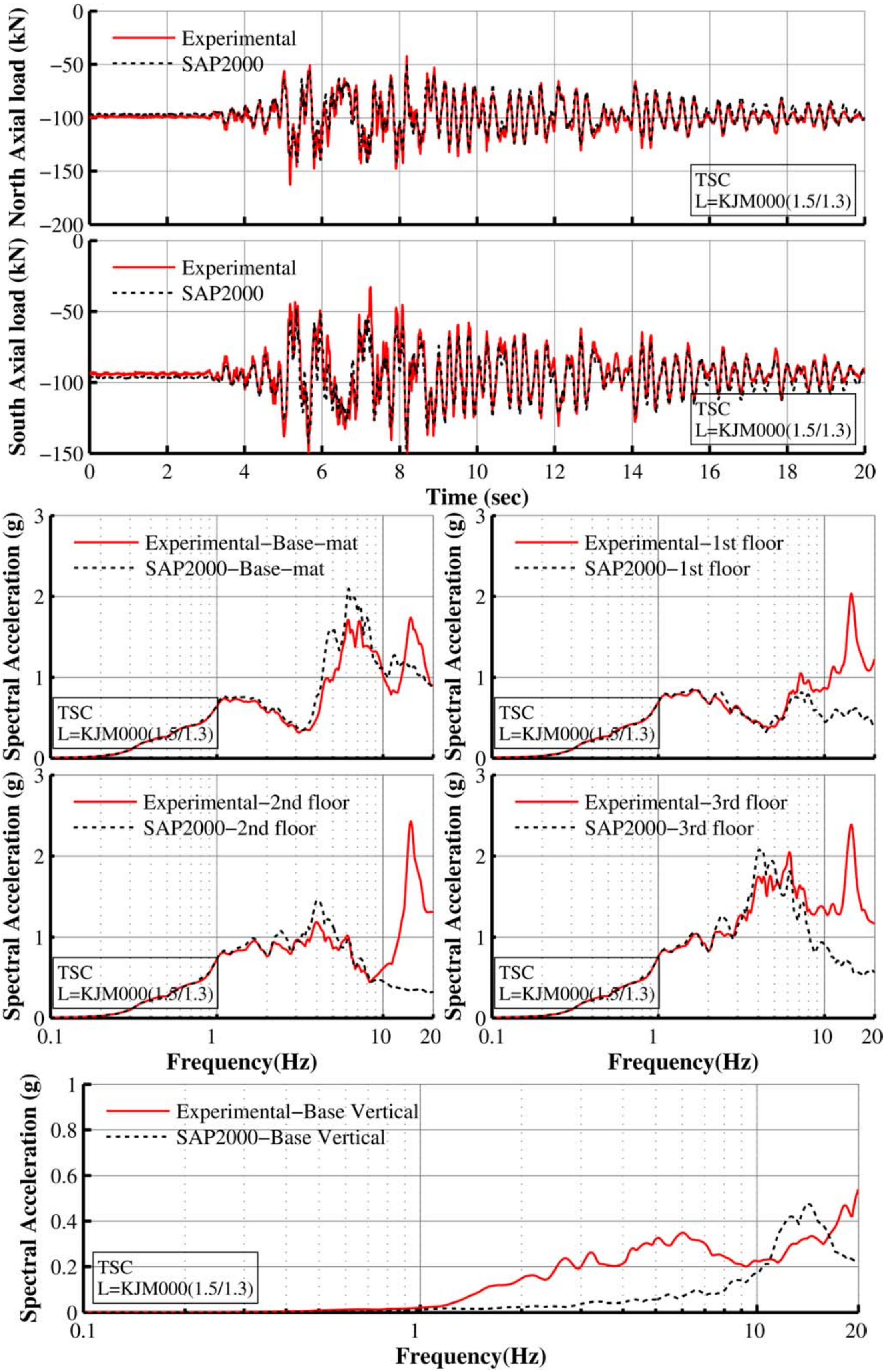

North Axial load (kN)
Experimental
SAP2000
TSC
L=KJM000(1.5/1.3)
South Axial load (kN)
Experimental
SAP2000
TSC
L=KJM000(1.5/1.3)
Time (sec)
Spectral Acceleration (g)
Experimental−Base−mat
SAP2000−Base−mat
TSC
L=KJM000(1.5/1.3)
Experimental−1st floor
SAP2000−1st floor
TSC
L=KJM000(1.5/1.3)
Experimental−2nd floor
SAP2000−2nd floor
TSC
L=KJM000(1.5/1.3)
Experimental−3rd floor
SAP2000−3rd floor
TSC
L=KJM000(1.5/1.3)
Frequency(Hz)
Frequency(Hz)
Experimental−Base Vertical
SAP2000−Base Vertical
TSC
L=KJM000(1.5/1.3)
Frequency(Hz)

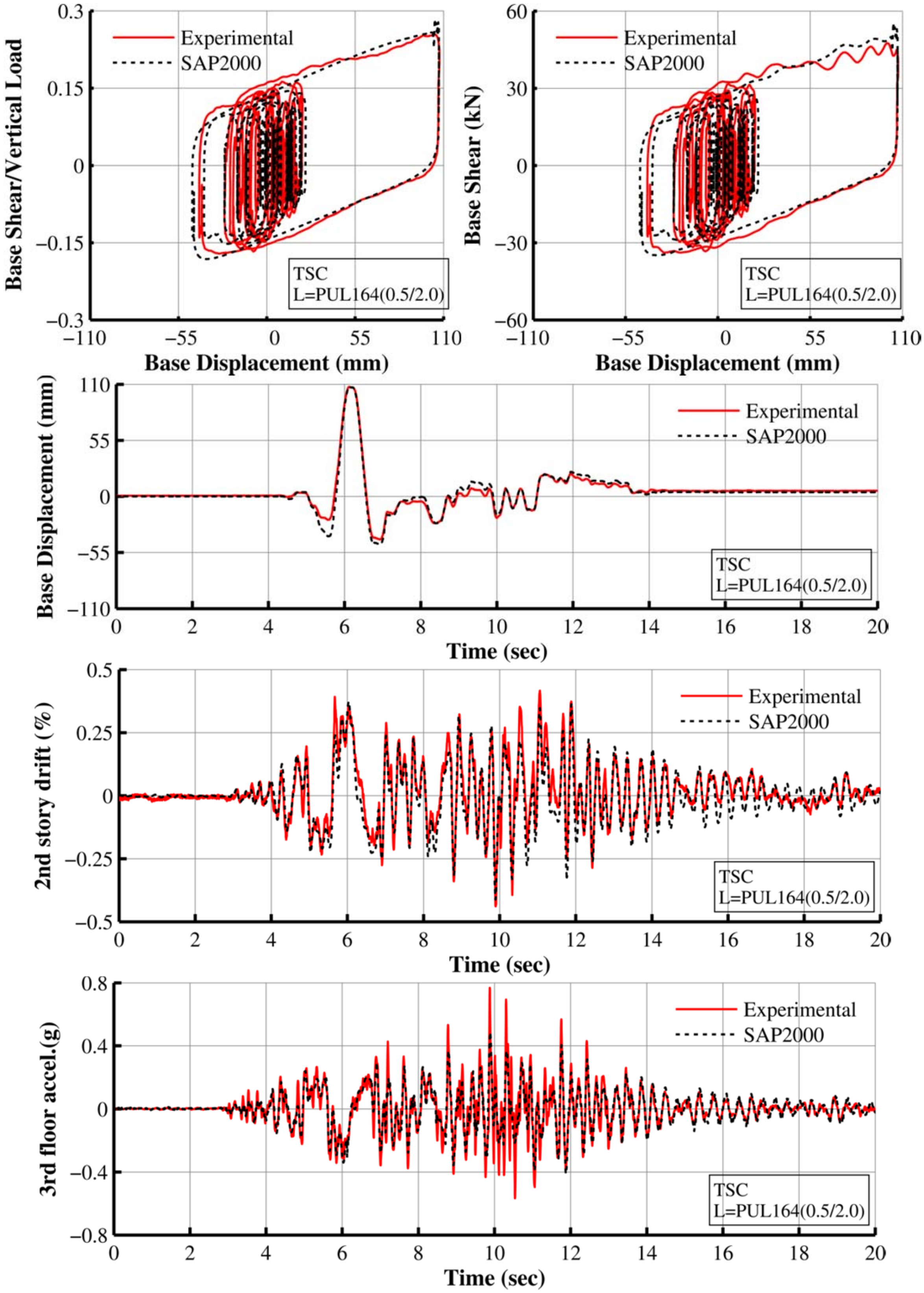

Base Shear/Vertical Load
Base Displacement (mm)
Experimental
SAP2000
TSC
L=PUL164(0.5/2.0)
Base Shear (kN)
Base Displacement (mm)
Experimental
SAP2000
TSC
L=PUL164(0.5/2.0)
Base Displacement (mm)
Time (sec)
Experimental
SAP2000
TSC
L=PUL164(0.5/2.0)
2nd story drift (%)
Time (sec)
Experimental
SAP2000
TSC
L=PUL164(0.5/2.0)
3rd floor accel.(g)
Time (sec)
Experimental
SAP2000
TSC
L=PUL164(0.5/2.0)

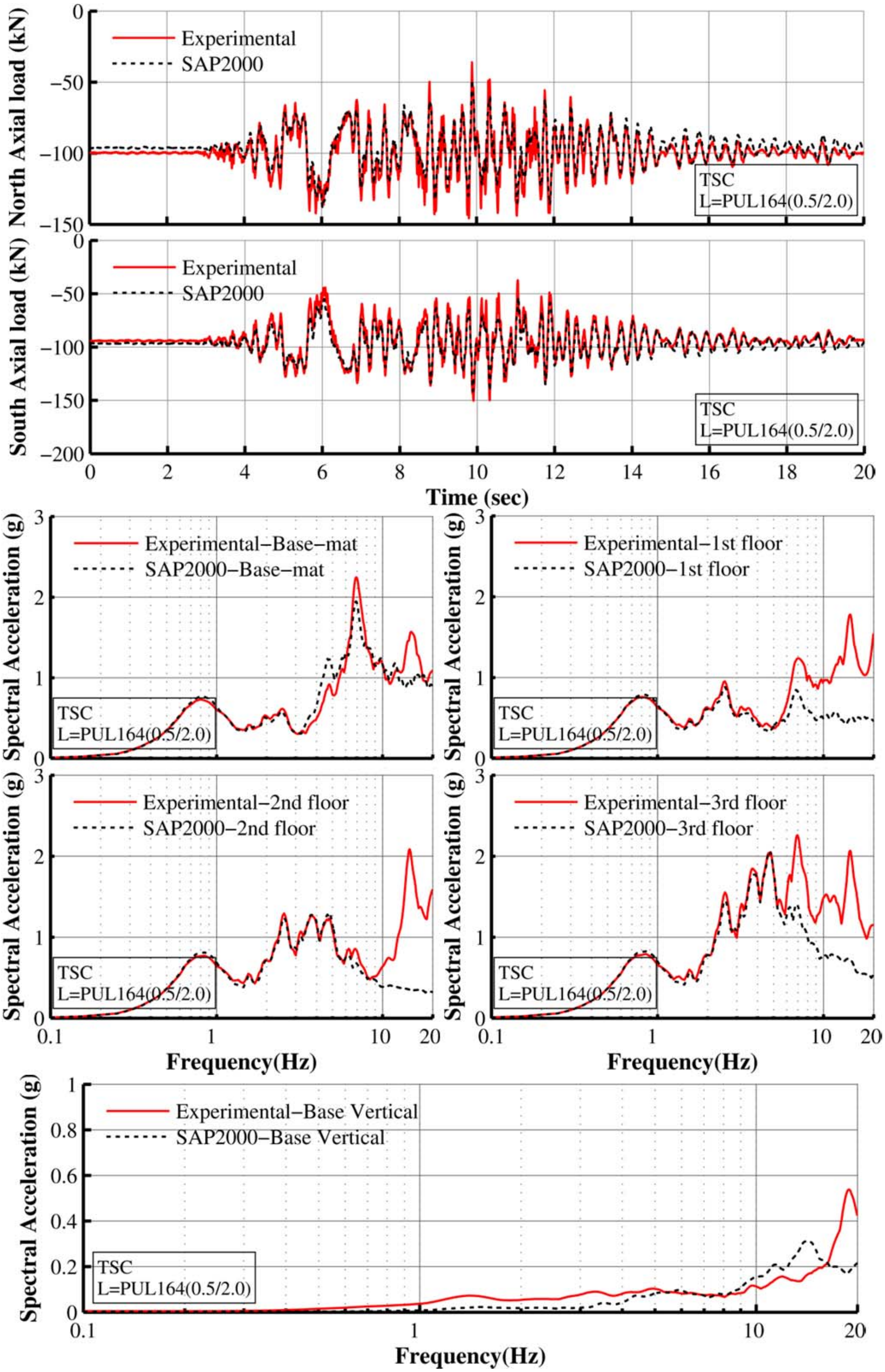

North Axial load (kN)
Experimental
SAP2000
TSC
L=PUL164(0.5/2.0)
South Axial load (kN)
Experimental
SAP2000
TSC
L=PUL164(0.5/2.0)
Time (sec)
Spectral Acceleration (g)
Experimental−Base−mat
SAP2000−Base−mat
TSC
L=PUL164(0.5/2.0)
Experimental−1st floor
SAP2000−1st floor
TSC
L=PUL164(0.5/2.0)
Experimental−2nd floor
SAP2000−2nd floor
TSC
L=PUL164(0.5/2.0)
Experimental−3rd floor
SAP2000−3rd floor
TSC
L=PUL164(0.5/2.0)
Frequency(Hz)
Frequency(Hz)
Experimental−Base Vertical
SAP2000−Base Vertical
TSC
L=PUL164(0.5/2.0)
Frequency(Hz)

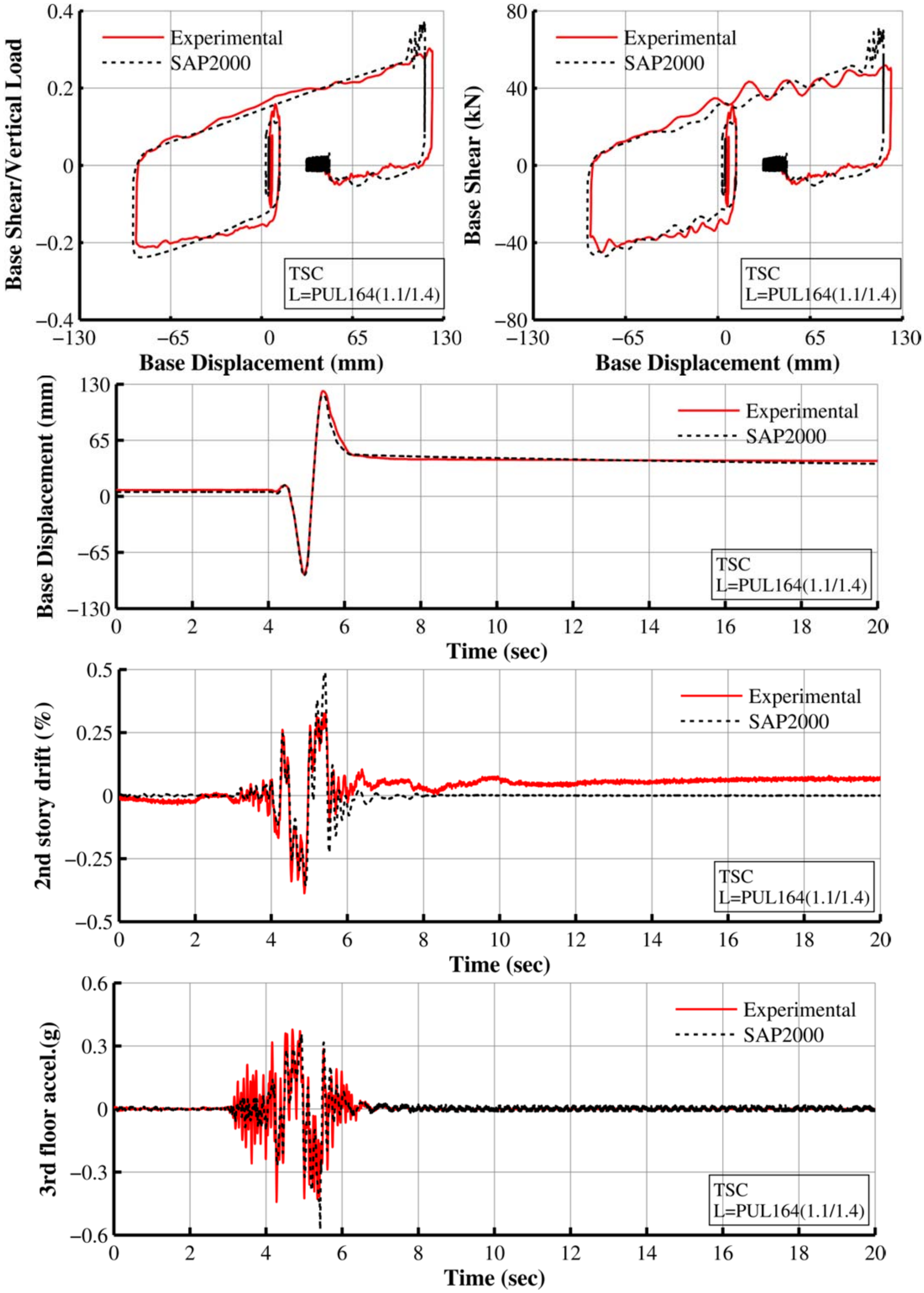
Base Shear/Vertical Load
Base Displacement (mm)
Base Shear (kN)
Base Displacement (mm)
Time (sec)
2nd story drift (%)
3rd floor accel.(g)
Experimental
SAP2000
TSC
L=PUL164(1.1/1.4)
0.4
0.2
0
−0.2
−0.4
80
40
−40
−80
−130
−65
65
130
0.5
0.25
−0.25
−0.5
0.6
0.3
−0.3
−0.6
2
4
6
8
10
12
14
16
18
20

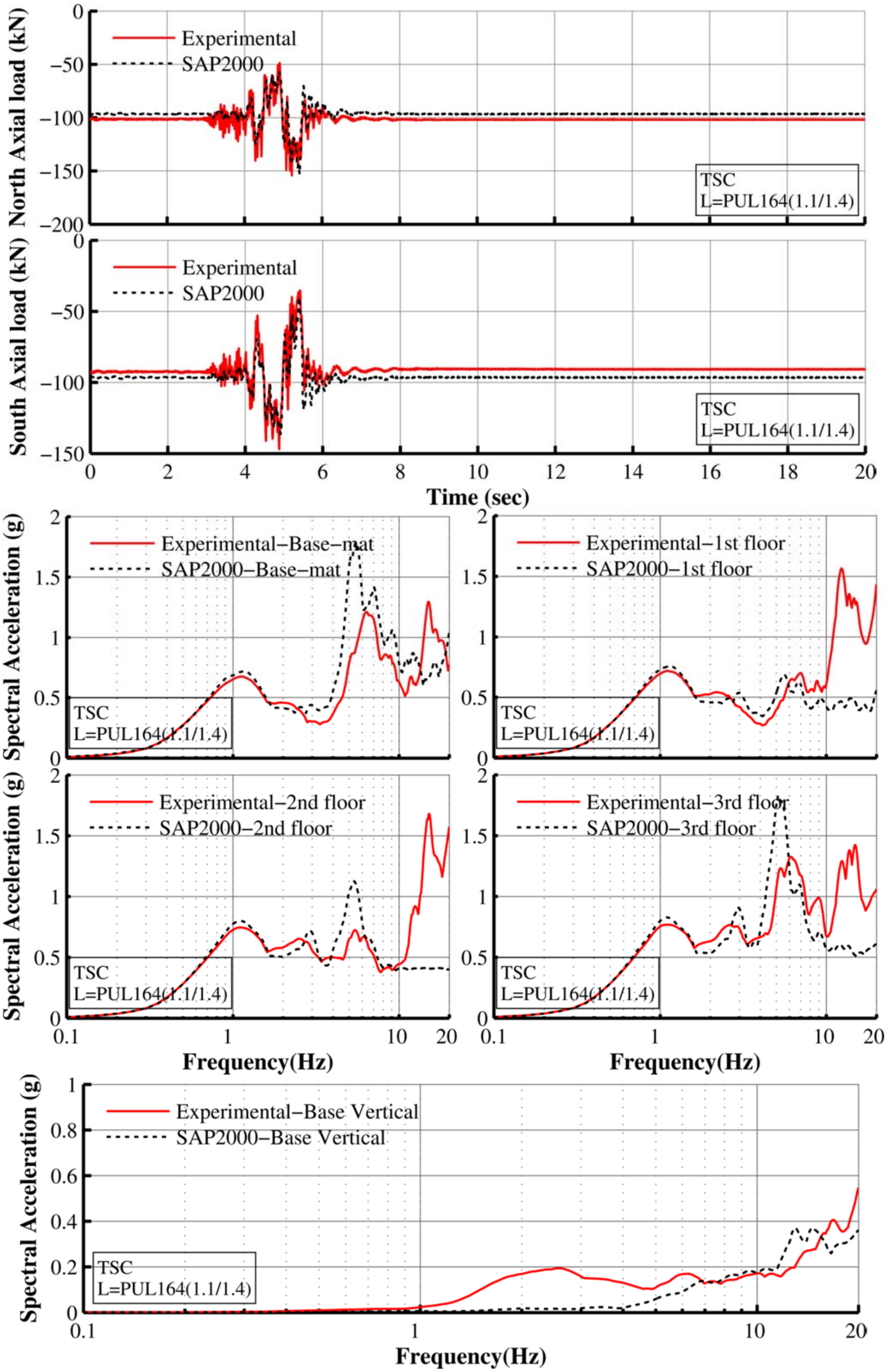
North Axial load (kN)
Experimental
SAP2000
TSC
L=PUL164(1.1/1.4)
South Axial load (kN)
Experimental
SAP2000
TSC
L=PUL164(1.1/1.4)
Time (sec)
Spectral Acceleration (g)
Experimental−Base−mat
SAP2000−Base−mat
Experimental−1st floor
SAP2000−1st floor
Experimental−2nd floor
SAP2000−2nd floor
Experimental−3rd floor
SAP2000−3rd floor
TSC
L=PUL164(1.1/1.4)
Frequency(Hz)
Spectral Acceleration (g)
Experimental−Base Vertical
SAP2000−Base Vertical
TSC
L=PUL164(1.1/1.4)
Frequency(Hz)

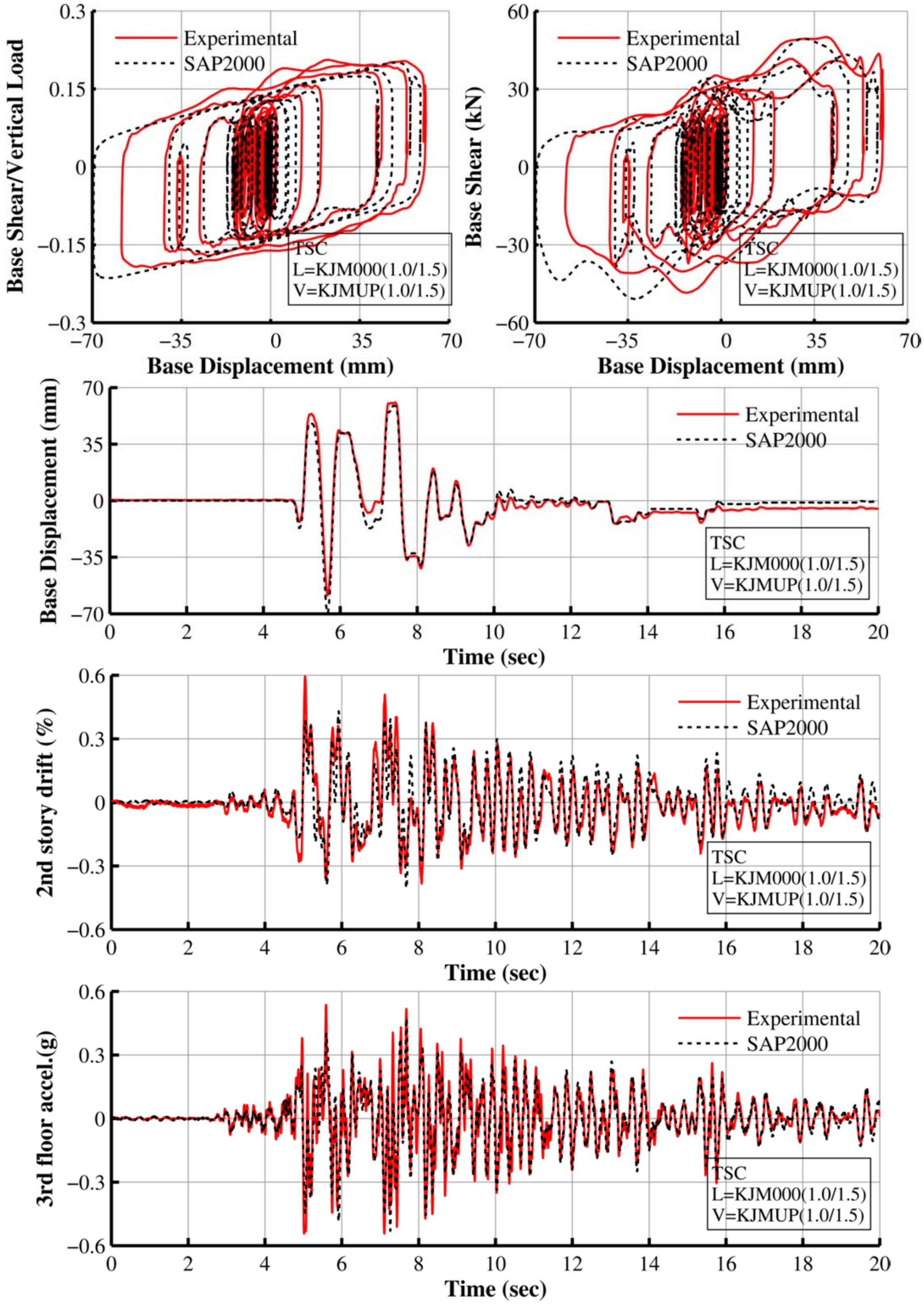
Base Shear/Vertical Load
Base Displacement (mm)
Experimental
SAP2000
TSC
L=KJM000(1.0/1.5)
V=KJMUP(1.0/1.5)
Base Shear (kN)
Base Displacement (mm)
Experimental
SAP2000
TSC
L=KJM000(1.0/1.5)
V=KJMUP(1.0/1.5)
Base Displacement (mm)
Time (sec)
Experimental
SAP2000
TSC
L=KJM000(1.0/1.5)
V=KJMUP(1.0/1.5)
2nd story drift (%)
Time (sec)
Experimental
SAP2000
TSC
L=KJM000(1.0/1.5)
V=KJMUP(1.0/1.5)
3rd floor accel.(g)
Time (sec)
Experimental
SAP2000
TSC
L=KJM000(1.0/1.5)
V=KJMUP(1.0/1.5)

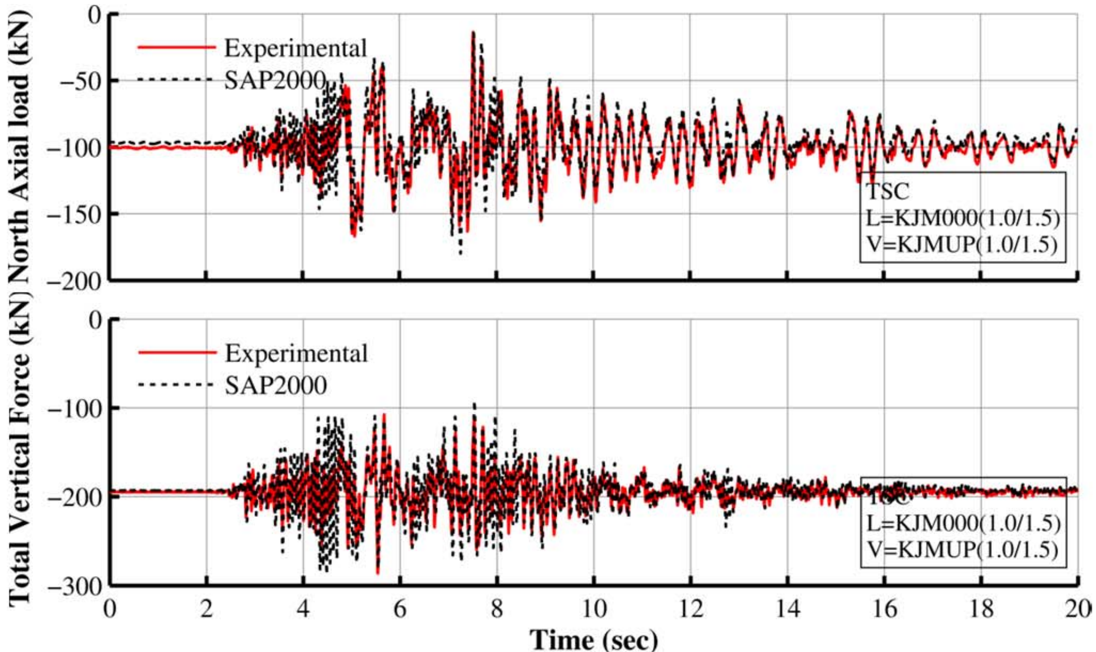
North Axial load (kN)
Experimental
SAP2000
TSC
L=KJM000(1.0/1.5)
V=KJMUP(1.0/1.5)
Total Vertical Force (kN)
Experimental
SAP2000
TSC
L=KJM000(1.0/1.5)
V=KJMUP(1.0/1.5)
Time (sec)

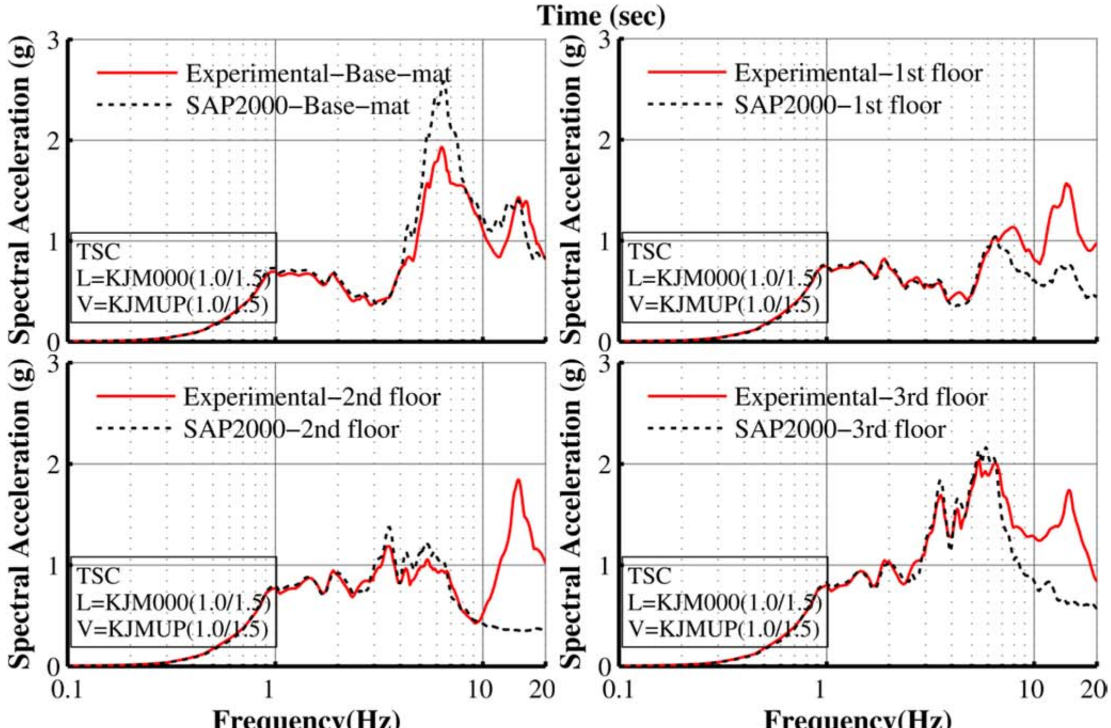
Spectral Acceleration (g)
Experimental−Base−mat
SAP2000−Base−mat
Experimental−1st floor
SAP2000−1st floor
Experimental−2nd floor
SAP2000−2nd floor
Experimental−3rd floor
SAP2000−3rd floor
TSC
L=KJM000(1.0/1.5)
V=KJMUP(1.0/1.5)
Frequency(Hz)

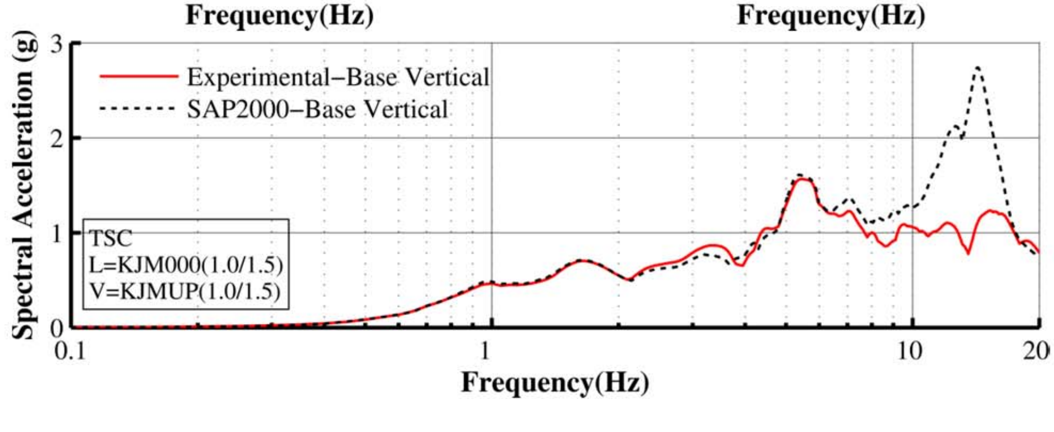
Spectral Acceleration (g)
Experimental−Base Vertical
SAP2000−Base Vertical
TSC
L=KJM000(1.0/1.5)
V=KJMUP(1.0/1.5)
Frequency(Hz)

MCEER
EARTHQUAKE ENGINEERING TO EXTREME EVENTS
University at Buffalo, The State University of New York
133A Ketter Hall ▪ Buffalo, New York 14260-4300
Phone: (716) 645-3391 ▪ Fax: (716) 645-3399
Email: *mceer@buffalo.edu* ▪ Web: *http://mceer.buffalo.edu*
University at Buffalo *The State University of New York*

ISSN 1520-295X